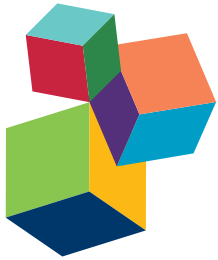


LINKING OPTICAL AND CHEMICAL PROPERTIES OF DISSOLVED ORGANIC MATTER IN NATURAL WATERS

EDITED BY: Christopher L. Osburn and Thomas S. Bianchi

PUBLISHED IN: Frontiers in Marine Science, Frontiers in Earth Science
and Frontiers in Chemistry



frontiers

Frontiers Copyright Statement

© Copyright 2007-2017 Frontiers Media SA. All rights reserved.

All content included on this site, such as text, graphics, logos, button icons, images, video/audio clips, downloads, data compilations and software, is the property of or is licensed to Frontiers Media SA ("Frontiers") or its licensees and/or subcontractors. The copyright in the text of individual articles is the property of their respective authors, subject to a license granted to Frontiers.

The compilation of articles constituting this e-book, wherever published, as well as the compilation of all other content on this site, is the exclusive property of Frontiers. For the conditions for downloading and copying of e-books from Frontiers' website, please see the Terms for Website Use. If purchasing Frontiers e-books from other websites or sources, the conditions of the website concerned apply.

Images and graphics not forming part of user-contributed materials may not be downloaded or copied without permission.

Individual articles may be downloaded and reproduced in accordance with the principles of the CC-BY licence subject to any copyright or other notices. They may not be re-sold as an e-book.

As author or other contributor you grant a CC-BY licence to others to reproduce your articles, including any graphics and third-party materials supplied by you, in accordance with the Conditions for Website Use and subject to any copyright notices which you include in connection with your articles and materials.

All copyright, and all rights therein, are protected by national and international copyright laws.

The above represents a summary only. For the full conditions see the Conditions for Authors and the Conditions for Website Use.

ISSN 1664-8714

ISBN 978-2-88945-081-7

DOI 10.3389/978-2-88945-081-7

About Frontiers

Frontiers is more than just an open-access publisher of scholarly articles: it is a pioneering approach to the world of academia, radically improving the way scholarly research is managed. The grand vision of Frontiers is a world where all people have an equal opportunity to seek, share and generate knowledge. Frontiers provides immediate and permanent online open access to all its publications, but this alone is not enough to realize our grand goals.

Frontiers Journal Series

The Frontiers Journal Series is a multi-tier and interdisciplinary set of open-access, online journals, promising a paradigm shift from the current review, selection and dissemination processes in academic publishing. All Frontiers journals are driven by researchers for researchers; therefore, they constitute a service to the scholarly community. At the same time, the Frontiers Journal Series operates on a revolutionary invention, the tiered publishing system, initially addressing specific communities of scholars, and gradually climbing up to broader public understanding, thus serving the interests of the lay society, too.

Dedication to Quality

Each Frontiers article is a landmark of the highest quality, thanks to genuinely collaborative interactions between authors and review editors, who include some of the world's best academicians. Research must be certified by peers before entering a stream of knowledge that may eventually reach the public - and shape society; therefore, Frontiers only applies the most rigorous and unbiased reviews.

Frontiers revolutionizes research publishing by freely delivering the most outstanding research, evaluated with no bias from both the academic and social point of view.

By applying the most advanced information technologies, Frontiers is catapulting scholarly publishing into a new generation.

What are Frontiers Research Topics?

Frontiers Research Topics are very popular trademarks of the Frontiers Journals Series: they are collections of at least ten articles, all centered on a particular subject. With their unique mix of varied contributions from Original Research to Review Articles, Frontiers Research Topics unify the most influential researchers, the latest key findings and historical advances in a hot research area! Find out more on how to host your own Frontiers Research Topic or contribute to one as an author by contacting the Frontiers Editorial Office: researchtopics@frontiersin.org

LINKING OPTICAL AND CHEMICAL PROPERTIES OF DISSOLVED ORGANIC MATTER IN NATURAL WATERS

Topic Editors:

Christopher L. Osburn, North Carolina State University, USA

Thomas S. Bianchi, University of Florida, USA



Satellite image of the North Carolina coast after passage of Hurricane Matthew.

Image credit: NASA Worldview
(<http://go.nasa.gov/2gVqhMN>)

A substantial increase in the number of studies using the optical properties (absorbance and fluorescence) of dissolved organic matter (DOM) as a proxy for its chemical properties in estuaries and the coastal and open ocean has occurred during the last decade. We are making progress on finding the actual chemical compounds or phenomena responsible for DOM's optical properties. Ultrahigh resolution mass spectrometry, in particular, has made important progress in making the key connections between optics and chemistry. But serious questions remain and the last major special issue on DOM optics and chemistry occurred nearly 10 years ago. Controversies remain from the non-specific optical properties of DOM that are not linked to discrete sources, and sometimes provide conflicting information. The use of optics, which is relatively easier to employ in synoptic and high resolution sampling to determine chemistry, is a critical connection to make and can lead to major advances in our understanding of organic matter cycling in all aquatic ecosystems.

The contentions and controversies raised by our poor understanding of the linkages between optics and chemistry of DOM are bottlenecks that need to be addressed and overcome.

Citation: Osburn, C. L., Bianchi, T. S., eds. (2017). Linking Optical and Chemical Properties of Dissolved Organic Matter in Natural Waters. Lausanne: Frontiers Media.
doi: 10.3389/978-2-88945-081-7

Table of Contents

- 05 Editorial: Linking Optical and Chemical Properties of Dissolved Organic Matter in Natural Waters**
Christopher L. Osburn and Thomas S. Bianchi
- 08 Optical Signatures of Dissolved Organic Matter Transformation in the Global Ocean**
Norman B. Nelson and Julia M. Gauglitz
- 23 From Fresh to Marine Waters: Characterization and Fate of Dissolved Organic Matter in the Lena River Delta Region, Siberia**
Rafael Gonçalves-Araujo, Colin A. Stedmon, Birgit Heim, Ivan Dubinenkov, Alexandra Kraberg, Denis Moiseev and Astrid Bracher
- 36 Variation in Riverine Inputs Affect Dissolved Organic Matter Characteristics throughout the Estuarine Gradient**
Eero Asmala, Hermanni Kaartokallio, Jacob Carstensen and David N. Thomas
- 51 Variability in dissolved organic matter optical properties in surface waters in the Amerasian Basin**
Céline Guéguen, Motoyo Itoh, Takashi Kikuchi, Jane Eert and William J. Williams
- 60 Pan-Arctic Trends in Terrestrial Dissolved Organic Matter from Optical Measurements**
Paul J. Mann, Robert G. M. Spencer, Peter J. Hernes, Johan Six, George R. Aiken, Suzanne E. Tank, James W. McClelland, Kenna D. Butler, Rachael Y. Dyda and Robert M. Holmes
- 78 Predicting Dissolved Lignin Phenol Concentrations in the Coastal Ocean from Chromophoric Dissolved Organic Matter (CDOM) Absorption Coefficients**
Cédric G. Fichot, Ronald Benner, Karl Kaiser, Yuan Shen, Rainer M. W. Amon, Hiroshi Ogawa and Chia-Jung Lu
- 93 Optical Proxies for Terrestrial Dissolved Organic Matter in Estuaries and Coastal Waters**
Christopher L. Osburn, Thomas J. Boyd, Michael T. Montgomery, Thomas S. Bianchi, Richard B. Coffin and Hans W. Paerl
- 108 Linkages among fluorescent dissolved organic matter, dissolved amino acids and lignin-derived phenols in a river-influenced ocean margin**
Youhei Yamashita, Cédric G. Fichot, Yuan Shen, Rudolf Jaffé and Ronald Benner
- 122 Utilizing colored dissolved organic matter to derive dissolved black carbon export by arctic rivers**
Aron Stubbins, Robert G. M. Spencer, Paul J. Mann, R. Max Holmes, James W. McClelland, Jutta Niggemann and Thorsten Dittmar

- 133 Are Extracted Materials Truly Representative of Original Samples? Impact of C18 Extraction on CDOM Optical and Chemical Properties**
Andrea A. Andrew, Rossana Del Vecchio, Yi Zhang, Ajit Subramaniam and Neil V. Blough
- 145 Mass and UV-visible spectral fingerprints of dissolved organic matter: sources and reactivity**
Heather E. Reader, Colin A. Stedmon, Nikoline J. Nielsen and Emma S. Kritzberg
- 155 Associations Between the Molecular and Optical Properties of Dissolved Organic Matter in the Florida Everglades, a Model Coastal Wetland System**
Sasha Wagner, Rudolf Jaffé, Kaelin Cawley, Thorsten Dittmar and Aron Stubbins
- 169 Fluorescence Quantum Yields of Natural Organic Matter and Organic Compounds: Implications for the Fluorescence-based Interpretation of Organic Matter Composition**
Urban J. Wünsch, Kathleen R. Murphy and Colin A. Stedmon
- 184 Corrigendum: Fluorescence Quantum Yields of Natural Organic Matter and Organic Compounds: Implications for the Fluorescence-based Interpretation of Organic Matter Composition**
Urban J. Wünsch, Kathleen R. Murphy and Colin A. Stedmon
- 195 Studies on Hydroxyl Radical Formation and Correlated Photoflocculation Process Using Degraded Wood Leachate as a CDOM Source**
Luni Sun and Kenneth Mopper
- 204 Depth-dependent photodegradation of marine dissolved organic matter**
Stephen A. Timko, Anastasia Maydanov, Sandra L. Pittelli, Maureen H. Conte, William J. Cooper, Boris P. Koch, Philippe Schmitt-Kopplin and Michael Gonsior
- 217 Linking Heterotrophic Microbial Activities with Particle Characteristics in Waters of the Mississippi River Delta in the Aftermath of Hurricane Isaac**
Kai Zier vogel, Christopher Osburn, Adeline Brym, Jessica Battles, Samantha Joye, Nigel D'souza, Joseph Montoya, Uta Passow and Carol Arnosti
- 229 Microbially-Mediated Fluorescent Organic Matter Transformations in the Deep Ocean. Do the Chemical Precursors Matter?**
Fran L. Aparicio, Mar Nieto-Cid, Encarna Borrull, Estela Romero, Colin A. Stedmon, Maria M. Sala, Josep M. Gasol, Aida F. Ríos and Cèlia Marrasé



Editorial: Linking Optical and Chemical Properties of Dissolved Organic Matter in Natural Waters

Christopher L. Osburn^{1*} and Thomas S. Bianchi²

¹ Department of Marine, Earth, and Atmospheric Sciences, North Carolina State University, Raleigh, NC, USA, ² Department of Geological Sciences, University of Florida, Gainesville, FL, USA

Keywords: CDOM, DOC, absorbance, fluorescence, biomarkers, stable isotopes, photochemistry

Editorial on the Research Topic

Linking Optical and Chemical Properties of Dissolved Organic Matter in Natural Waters

Dissolved organic matter (DOM) represents the largest reservoir of exchangeable reduced carbon in the ocean. The dynamics of this reservoir are partly due to riverine and coastal inputs but also due to primary production in the sea surface and export to depth (e.g., Bauer and Bianchi, 2011). Forming the basis of the microbial loop, DOM is an active and integral part of marine ecosystems and a critical component of the Earth's carbon cycle. The fraction of DOM that absorb light is termed chromophoric or colored DOM: CDOM. First described as "gelbstoff" or the yellow color in coastal waters, CDOM plays a key role in the ocean's carbon cycle through its absorption of sunlight, which results in an alteration of the underwater light field via contributing to light attenuation in the water column as well the potential for a variety of photochemical reactions to occur which can influence the redox chemistry of seawater and—via photooxidation—lead to the generation of carbon dioxide (CO_2) from DOM (Coble, 2007). The latter constitutes an important feedback loop for Earth's climate.

However, the light absorbing properties of CDOM also make it an important means of quantifying this pool of DOM. Ultraviolet-visible spectroscopy is used to quantify "amounts" of CDOM absorbance at specific wavelengths and the slope coefficient of models describing the absorption change with wavelength (spectral slopes or S values) inform on DOM quality (Stedmon and Markager, 2003; Helms et al., 2008). A fraction of CDOM emits light as fluorescence and fluorescence spectra often contain more structure hence more information. Multiple emission spectra measured at discrete wavelengths are concatenated into 3D excitation-emission matrices (EEMs), which for a sample may be easily visualized as a contour plot. In these plots certain classical peaks have been used to represent DOM sources and chemistry: A, C (terrestrial humic-like fluorescence), M (microbially-produced humic fluorescence), and T (protein-like fluorescence) (Coble, 1996, 2007). Uncertainty in the peak-selection technique lead to utilizing chemometrics to decompose arrays of EEMs into the underlying components via parallel factor analysis (PARAFAC) (Stedmon et al., 2003).

The global view of CDOM absorbance and fluorescence in the oceans was given by Nelson and Gauglitz. Distributions of classical EEM peaks show that intensities of humic-like fluorescence increase with depth in pelagic ocean. Correlations between apparent oxygen utilization (AOU), which increase with DOM mineralization, and EEM peaks were variable across major ocean basins with peak T exhibiting overall weakest correlations. Production of humic fluorescence in the deep ocean appeared to coincide with remineralization of particles in accordance with the microbial carbon pump hypothesis (Jiao et al., 2010). Thus, CDOM absorbance and fluorescence are tracers

OPEN ACCESS

Edited and reviewed by:

Eric P. Achterberg,

GEOMAR Helmholtz Centre for Ocean Research Kiel (HZ), Germany

*Correspondence:

Christopher L. Osburn
closburn@ncsu.edu

Specialty section:

This article was submitted to

Marine Biogeochemistry,
a section of the journal
Frontiers in Marine Science

Received: 10 October 2016

Accepted: 26 October 2016

Published: 16 November 2016

Citation:

Osburn CL and Bianchi TS (2016) Editorial: Linking Optical and Chemical Properties of Dissolved Organic Matter in Natural Waters. *Front. Mar. Sci.* 3:223.
doi: 10.3389/fmars.2016.00223

of active DOM cycling and have the potential to identify so-called labile, semi-labile, and refractory components (Hansell, 2013).

In major ocean basins of the Arctic, Guégan et al. use PARAFAC components to separate mixing of water from the Makarov Basin, enriched in humic fluorescence, with water from the Canada basin depleted in such terrestrial DOM. Looking specifically at the Lena River plume and Laptev Sea, Gonçalves-Araujo et al. examined PARAFAC fluorescence results and concluded that hydrographic processes, controlled by river flow, influence the distributions of components, while photodegradation and flocculation exert secondary controls on DOM fate.

Indeed, observations from tidal rivers to the coastal ocean demonstrate very close correspondence between DOC and CDOM that is principally driven by export of terrestrial DOM into the ocean. A key example of this linkage is the high correlation between CDOM and DOC and, especially CDOM and the terrestrial biomarker lignin. Large river systems, especially in the Arctic, reflect these linkages most directly. Mann et al. demonstrate high correlations between DOC and CDOM absorption at 350 nm (a_{350}) ($R^2 = 0.81$; $N = 301$), with even higher correlations between dissolved lignin (Σ_8) and a_{350} ($R^2 = 0.93$; $N = 31$). Lignin composition was modeled with a combination of CDOM absorption coefficient and slope values. Developing this analysis in coastal shelves, Fichot et al. explore relationships between lignin reactivity and identify key lignin-phenol groups responsible for largest variability, but also note lignin is one of many terrestrial and planktonic sources of CDOM absorbance in natural waters. Establishing such high correlations are important because they allow CDOM, which can be measured with greater rapidity and ease, to estimate DOC concentrations and fluxes. For example, a highly linear relationship between lignin and a_{400} can be utilized with remote sensing models to measure lignin concentrations from space (Fichot et al.). Stubbins et al. extend the linkage beyond the lignin biomarkers to dissolved black carbon (DBC). Using highly correlated relationships between a_{254} and DBC concentration coupled with hydrologic model, they estimated that nearly 10% of Arctic DOC export could be in the form of DBC.

Fluorescence provides more information than absorbance about biochemical classes of DOM and hence its reactivity. In the Northern Gulf of Mexico, Yamashita et al. examined linkages between CDOM and lignin but also CDOM and total dissolved amino acids (TDAA) using PARAFAC components. Lignin was best correlated with terrestrial, fulvic-acid like fluorescence, while protein-like fluorescence, resembling tryptophan, was best correlated to TDAA.

Estuaries represent the terrestrial-aquatic interface in which variable riverine inputs, long residence times, and complex mixing dynamics complicate the strong linkage between DOM's optical and chemical properties. Biological and chemical processes may "overprint" clear terrestrial-marine gradients, continuously altering DOM's biogeochemical properties, and result in a continuum of optical properties associated with its changing chemistry expressed in lignin, but also in its elemental (C:N) and stable carbon isotope ($\delta^{13}\text{C}$) properties (Asmala et al.; Osburn et al.). Seasonal variation in riverine inputs to estuaries

resulted in marked changes in regression models between optics and chemistry (Osburn et al.). In fact, CDOM performed better as a predictor of lignin concentration than of DOC in estuarine environments given the dynamics of continual supply, removal, and transformation of organic matter.

Underlying the linkages between observed optical and chemical properties of DOM across the terrestrial to marine continuum are sophisticated molecular level processes expressed at the macro level in measurements of CDOM light absorption, fluorescence, and geochemical markers. It is important that wet chemical techniques used to isolate biomarkers and/or to concentrate DOM for mass spectral analysis represent the whole of DOM. Andrew et al. examined optical properties of C₁₈ extracts compared to whole waters and found a preferential selection of high molecular weight material. This was evidenced by lower spectral slope values. This effect was more pronounced for riverine waters and diminished offshore. Optical reactivity (quantum yields for fluorescence and wavelength dependence of fluorescence emission) indicated that this extraction procedure serves as a good representative of the whole water CDOM. Wünsch et al. make a considerable step forward in developing a PARAFAC-based model which allows users to explore the biochemical composition of DOM using fluorescence quantum yields.

Molecular size and weight variations in DOM appear to strongly influence its optical properties and attendant relationships to bulk chemical parameters (Asmala et al.). Reader et al. show the power of optical properties in explaining much of DOM's composition and reactivity when absorption spectra are linked to mass spectral data. Employing principle component analysis (PCA), results from coastal riverine DOM exhibited discrete absorbance spectral features statistically related to discrete molecular mass ranges. Further, DOM photoreactivity resulted in loss of absorbance clearly related to decreases molecular mass.

In the coastal Florida Everglades, Wagner et al. have undertaken study of DOM's optical properties and mass spectral properties using state-of-the-art Fourier-transform ion cyclotron resonance mass spectrometry (FT-ICR-MS) and linking this high resolution chemical information to PARAFAC fluorescence components. Across this terrestrial-marine interface comprised of riverine, wetland, and marine DOM sources, optics are confirmed to be appropriate proxies for DOM chemistry, as Spearman rank correlations of results were consistent with prior source assignments and elucidated rather complex mixing dynamics observed in estuarine environments. These results match well with black carbon being an important component of DOC export from rivers (Stubbins et al.).

Optical-chemical linkages in DOM's chemistry is manifestly expressed in its reactivity. Sun and Mopper conducted a process-based study of DOM leached from wood in a coastal wetland in which substantial flocculation of material was induced via addition of iron, which also increased production of hydroxyl radicals that lead to photooxidation of DOM. Thus DOM processing and degradation are inextricably linked to elemental cycles such as iron. Timko et al. further investigate the role of photodegradation in the open ocean as a producer

of fluorescence signal and potential role in formation of recalcitrant DOM. Ultra-high resolution mass spectrometry was again employed to suggest that DOM molecules resistant to photodegradation are aliphatic in nature. Polyphenolic aromatic structures were prevalent in photoreactive deep waters, implicating their removal in surface waters during overturning circulation and also further indicating their formation via the microbial carbon pump.

Linkages between optics and chemistry of bathypelagic DOM which may be forged by the microbial carbon pump further emphasize our need to understand means by which deep ocean fluorescent, photoreactive material is formed. DOM's role in the microbial loop adds complexity to the linkages between optical and chemical properties of DOM in the surface ocean. Recent discoveries of base-extractable DOM from particulate organic matter (BEPOM) exhibits fluorescence patterns consistent with biochemical sources from phytoplankton and bacterioplankton confirm autochthonous processes in shaping DOM's optical properties (Osburn et al., 2012; Nelson and Siegel, 2013; Brym et al., 2014). Aparicio et al. investigated the importance of the microbial degradation in leading to potential "recalcitrance" of DOM by exposing bathypelagic Atlantic Ocean bacteria to simple substrates (sugars, amino acids) and to humic acid. Fluorescence was generated most in treatments with humic precursors while protein-like fluorescence decreased most when fresh amino acids were added. This result suggests that

marine humification processes indeed persist in the ocean and underlying mechanisms remain poorly known. Zier vogel et al. discovered in coastal waters of the Gulf of Mexico that, after Hurricane Isaac, close linkage between BEPOM fluorescence and bacterial activities, indicating how quality of organic matter in particle-rich environments is driving much of the bacterial activity. Nutrient regimes and the formation of flocculant particles ("marine snow") may be unrealized factors controlling formation of optically-active and recalcitrant DOM.

In summary, this research topic offers a globally-relevant picture of the linkage between optical and chemical properties of DOM, showing the many recent advancements in observations and techniques that will continue to improve our understanding of the organic carbon cycle. Using harmonized approaches linking optics and chemistry can provide a framework for understanding remaining knowledge gaps. These include the significant and still poorly understood biogeochemistry across the terrestrial-marine continuum that leads to export of reactive material onto coastal shelves, as well as the linkages between production of organic matter in surface waters and transformation into recalcitrant DOM fractions during transport to the bathypelagic ocean.

AUTHOR CONTRIBUTIONS

CO and TB both contributed to the writing of this editorial.

REFERENCES

- Bauer, J., and Bianchi, T. S. (2011). "Dissolved organic carbon cycling and transformation," in *Treatise on Estuarine and Coastal Science*, Vol. 5, eds E. Wolanski and D. S. McLusky (Waltham: Academic Press), 7–67.
- Brym, A., Paerl, H. W., Montgomery, M. T., Handsel, L. T., Zier vogel, K., and Osburn, C. L. (2014). Optical and chemical characterization of base-extracted particulate organic matter in coastal marine environments. *Mar. Chem.* 162, 96–113. doi: 10.1016/j.marchem.2014.03.006
- Coble, P. G. (1996). Characterization of marine and terrestrial DOM in seawater using excitation-emission matrix spectroscopy. *Mar. Chem.* 51, 325–346. doi: 10.1016/0304-4203(95)00062-3
- Coble, P. G. (2007). Marine optical biogeochemistry: the chemistry of ocean color. *Chem. Rev.* 107, 402–418. doi: 10.1021/cr050350+
- Hansell, D. A. (2013). Recalcitrant dissolved organic carbon fractions. *Ann. Rev. Mar. Sci.* 5, 421–445. doi: 10.1146/annurev-marine-120710-100757
- Helms, J. R., Stubbins, A., Ritchie, J. D., Minor, E. C., Kieber, D. J., and Mopper, K. (2008). Absorption spectral slopes and slope ratios as indicators of molecular weight, source, and photobleaching of chromophoric dissolved organic matter. *Limnol. Oceanogr.* 53, 955–969. doi: 10.4319/lo.2008.53.3.0955
- Jiao, N., Herndl, G. J., Hansell, D. A., Benner, R., Kattner, G., Wilhelm, S. W., et al. (2010). Microbial production of recalcitrant dissolved organic matter: long-term carbon storage in the global ocean. *Nat. Rev. Microbiol.* 8, 593–599. doi: 10.1038/nrmicro2386
- Nelson, N. B., and Siegel, D. A. (2013). The global distribution and dynamics of chromophoric dissolved organic matter. *Annu. Rev. Mar. Sci.* 5, 447–476. doi: 10.1146/annurev-marine-120710-100751
- Osburn, C. L., Handsel, L. T., Mikan, M. P., Paerl, H. W., and Montgomery, M. T. (2012). Fluorescence tracking of dissolved and particulate organic matter quality in a river-dominated estuary. *Environ. Sci. Technol.* 46, 8628–8636. doi: 10.1021/es3007723
- Stedmon, C. A., and Markager, S. (2003). Behaviour of the optical properties of coloured dissolved organic matter under conservative mixing. *Estuar. Coastal Shelf Sci.* 57, 973–979. doi: 10.1016/S0272-7714(03)00003-9
- Stedmon, C. A., Markager, S., and Bro, R. (2003). Tracing dissolved organic matter in aquatic environments using a new approach to fluorescence spectroscopy. *Mar. Chem.* 82, 239–254. doi: 10.1016/S0304-4203(03)00072-0

Conflict of Interest Statement: The authors declare that the research was conducted in the absence of any commercial or financial relationships that could be construed as a potential conflict of interest.

Copyright © 2016 Osburn and Bianchi. This is an open-access article distributed under the terms of the Creative Commons Attribution License (CC BY). The use, distribution or reproduction in other forums is permitted, provided the original author(s) or licensor are credited and that the original publication in this journal is cited, in accordance with accepted academic practice. No use, distribution or reproduction is permitted which does not comply with these terms.



Optical Signatures of Dissolved Organic Matter Transformation in the Global Ocean

Norman B. Nelson * and Julia M. Gauglitz †

Earth Research Institute, University of California, Santa Barbara, Santa Barbara, CA, USA

OPEN ACCESS

Edited by:

Christopher Osburn,
North Carolina State University, USA

Reviewed by:

John Robert Helms,
Morningside College, USA
X. Antón Álvarez-Salgado,
Consejo Superior de Investigaciones
Científicas, Spain

***Correspondence:**

Norman B. Nelson
norm@eri.ucsb.edu

†Present Address:

Julia M. Gauglitz,
Marine Chemistry and Geochemistry,
Woods Hole Oceanographic
Institution, Woods Hole, MA, USA

Specialty section:

This article was submitted to
Marine Biogeochemistry,
a section of the journal
Frontiers in Marine Science

Received: 30 September 2015

Accepted: 14 December 2015

Published: 07 January 2016

Citation:

Nelson NB and Gauglitz JM (2016)
Optical Signatures of Dissolved
Organic Matter Transformation in the
Global Ocean. *Front. Mar. Sci.* 2:118.
doi: 10.3389/fmars.2015.00118

Characterization of dissolved organic matter (DOM) in terms of its composition and optical properties, with an eye toward ultimately understanding its deep ocean dynamics, is the currently active frontier in DOM research. We used UV-visible absorption spectroscopy and fluorescence excitation-emission matrix (EEM) spectroscopy to characterize DOM in the open ocean along sections of the U.S. CO₂/CLIVAR Repeat Hydrography Project located in all the major ocean basins outside the Arctic. Despite large differences in fluorescence intensity between ocean basins, some variability patterns were similar throughout the global ocean, suggesting similar processes controlling the composition of the DOM. We find that commercially available single channel CDOM sensors are sensitive to the fluorescence of humic materials in the deep ocean and thermocline but not to the UVA-fluorescing and absorbing materials that characterize freshly produced CDOM in surface waters, revealing fundamental diversity in the DOM profile. In surface waters, UVA fluorescence and absorption signatures indicate the presence of freshly produced material and the process of bleaching removal, but in the upper mesopelagic and in the main thermocline these optical signatures are replaced by those of humic materials, with distribution patterns correlated to apparent oxygen utilization (AOU) and other signatures of remineralization. Empirical orthogonal function analysis (EOF) of the EEM data suggests the presence of two (unidentified) processes which convert “fresh” DOM to humic materials: one located in the surface ocean (shallower than 500 m) and one located in the main thermocline. These inferred humification processes represent less than 5% of the overall variability in oceanic humic DOM fluorescence, which appears to be dominated by terrestrial input and solar bleaching of humic materials.

Keywords: CDOM, FDOM, humic material, oceanic CDOM cycling, fluorescence analysis

INTRODUCTION

Dissolved organic matter (DOM) represents one of the largest pools of carbon in the global biosphere (Hansell, 2013; Hansell and Carlson, 2015). It is well understood that DOM in the ocean gradually remineralizes over time, but it is unclear what governs the rates of remineralization, particularly in the deep ocean (Arístegui et al., 2002; Carlson and Hansell, 2015). The structural transformations that occur during remineralization are not well understood, however the characterization of the composition of organic matter with an eye toward determining how to

detect and quantify the more labile and refractory components of DOM is critical for understanding the physico-chemical properties and residence time of the DOM pool. Optical properties of DOM, including UV-visible absorption spectra and fluorescence spectra, provide one means of characterizing the composition of DOM without subjecting the samples to concentration processes that can be selective (Green et al., 2014).

Our previous work has quantified the distribution of chromophoric DOM (CDOM) in the global ocean using UV-Visible absorption spectroscopy (Nelson and Siegel, 2013). We have postulated new production of CDOM in the surface (Nelson et al., 1998) and deep ocean (Nelson et al., 2010). Diagenesis-related changes in absorption properties of CDOM have also been documented (Nelson et al., 2007), and the relationship between CDOM and DOC in the global ocean suggests that CDOM absorption in the deep ocean represents a refractory component of the DOM (Nelson et al., 2010). In the present study, the optical properties of DOM are characterized in order to further our understanding of the different sub-pools of DOM and how they are transformed by remineralization or photodegradation (Jaffe et al., 2008; Carlson and Hansell, 2015). The present analysis is focused on distributions and processes in the open ocean, away from the input of terrestrial material on the annual scale, as this represents the majority of the global surface and deep ocean.

Distribution of CDOM (as quantified as the UV absorption coefficient of filtered seawater in the solar waveband) is characterized by surface minima, particularly in the stratified subtropics, due to solar bleaching (Nelson et al., 1998, 2010; Swan et al., 2012). At the base of the mixed layer *in situ* production can overcome bleaching, resulting in a local maximum in the CDOM profile (Nelson et al., 1998, 2010). Below the euphotic zone there can be a local minimum in the intermediate or subtropical mode waters followed by an increase in the CDOM absorption coefficient in the main thermocline (Nelson et al., 2007, 2010). Local surface maxima can occur in regions of high primary productivity (Nelson et al., 2007). Regional differences in the surface distribution of CDOM reflect upwelling zones, major river inputs, and much greater CDOM absorption coefficients in the mid to high latitudes in the northern hemisphere (Siegel et al., 2002). In the main thermocline and below, CDOM is strongly correlated with apparent oxygen utilization (AOU), except in the Atlantic, where CDOM abundance varies little over the range of AOUs present, and CDOM is much more abundant at low AOUs than in the Pacific or Indian Ocean basins (Nelson and Siegel, 2013). The pattern in the Atlantic is linked to more rapid overturning circulation and input of preformed CDOM via the Arctic (Nelson et al., 2010; Jørgensen et al., 2011).

CDOM in the ocean changes its optical properties over time. Previous work has observed increases in DOC-specific absorption coefficient and the exponential slope parameter in “older” water masses, as assessed by CFC-12 ventilation age (Nelson et al., 2007) and AOUs (Nelson et al., 2010). The distribution patterns of CDOM light absorption reflect balances between the production of CDOM and its degradation by solar bleaching, modulated by overturning circulation and the presence of preformed CDOM (Nelson et al., 2010; Nelson and Siegel, 2013). This interpretation implies that there are

two autochthonous sources of CDOM, one located in the surface productive layer (Nelson et al., 2004), and one located primarily in the main thermocline (Nelson et al., 2010). The CDOM produced by these two local sources may have significantly different composition, which is not readily revealed by absorption properties alone. Studies of “new” CDOM production in the laboratory have identified DOM with discrete peaks in UV absorbance (Steinberg et al., 2004) that do not resemble the canonical CDOM absorption spectra that resemble terrestrial humic material absorption spectra (Del Vecchio and Blough, 2004), suggesting the existence of processes that “humify” freshly produced DOM. Microbial cultures have been found to produce labile UV absorbing or fluorescing CDOM (Rochelle-Newall and Fisher, 2002; Nelson et al., 2004; Nieto-Cid et al., 2006), and long-lived, visible fluorescing material (Jørgensen et al., 2014), further suggesting a microbial link to transformation of DOM *in situ*.

In the present study, we are taking a multiparameter approach toward optical characterization by using absorption and fluorescence properties to examine patterns of variability related to transformations of organic matter in the open ocean. Fluorescence of CDOM has also been used to assess the distribution of chromophoric compounds in the ocean (Chen and Bada, 1992; Determann et al., 1996; Yamashita and Tanoue, 2009; Andrew et al., 2013). While fluorescent substances are a subset of the chromophores in DOM (Stedmon and Nelson, 2015), fluorescence spectroscopy, in particular excitation-emission matrix spectroscopy (EEM; Coble, 2007) can be used to characterize aspects of the chemical composition of CDOM over and above the light absorption spectra.

Fluorescence analysis identifies essentially two major categories of dissolved organic material in the ocean: materials that have fluorescence emission maxima in the UVA that are similar to aromatic amino acids (T, N, and B regions, **Table 1**, Yamashita and Tanoue, 2003), and humic-like materials that have fluorescent emission maxima in the visible (A, C, and M regions, (**Table 1**, Stedmon and Nelson, 2015)). According to this paradigm, depth distribution of fluorescence parameters reflects freshly produced material near the surface, and humic material at depth that represents aged terrestrial or marine-origin material (Jørgensen et al., 2011; Catalá et al., 2015). Experimental results have highlighted the UV absorption characteristics of freshly

TABLE 1 | Central locations for the canonical fluorescence regions modified from Coble (2007) by Stedmon and Nelson (2015).

Region	Type	Excitation (nm)	Emission (nm)
A	Humic (Visible, UVB Excitation)	260	400–460
T	Protein-like (UVA)	275	340
M	Humic (Visible, UVA Excitation)	290–310	370–410
C	Humic (Visible, UVA Excitation)	320–360	420–460
B	Protein-like (UVA)	275	305
N	Protein-like (UVA)	280	370
W	ECO CDOM Fluorometer	380	420

Also included is the center wavelength for the single channel WETLabs ECO CDOM fluorometer deployed on the CTD on selected sections.

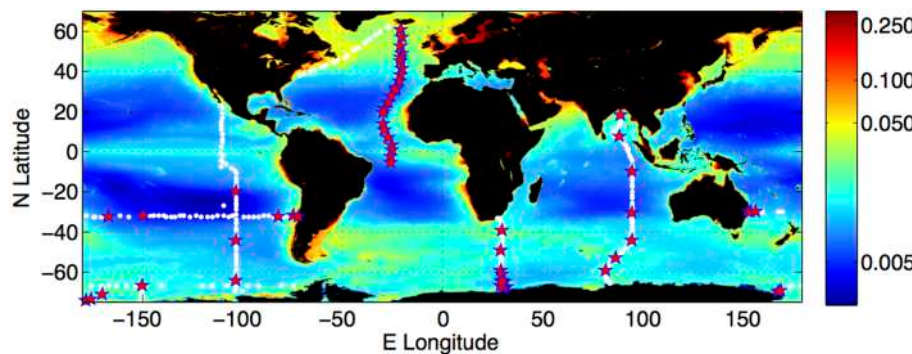


FIGURE 1 | Distribution of the climatology of surface water colored dissolved and detrital material (CDM) from ocean color observation, and locations of the field observations used in the present study. CDM is quantified as the sum of the absorption coefficient (m^{-1}) of CDOM and the absorption coefficient of non-phytoplankton (detrital) particles (m^{-1}) at 443 nm. The surface CDM field was derived from the SeaWiFS mission mean of the Garver-Siegel-Maritorena algorithm CDM product (Maritorena et al., 2002; Siegel et al., 2002). Field observations were collected on meridional transects A16N (Iceland to Brazil, 2013), P18 (Baja California to the ice edge, 2007/2008), I8S/I9N (Southern and Indian Oceans near 90°E, Feb–Apr 2007, I6 (Cape Town to the ice edge, 2009), and zonal transects S4P (Ross Sea to Bellingshausen Sea, 2011), and P6 (Brisbane—Valparaiso, 2009/2010). White dots indicate all locations at which hydrographic data were collected; red stars indicate locations at which EEMs were measured from water samples.

produced CDOM of microbial or other heterotroph origin as well (e.g., Steinberg et al., 2004; Suksomjit et al., 2009). Strong links between UV absorption or fluorescence properties, and remineralization-related variables such as AOU suggest a link between microbial degradation of DOM in the thermocline and deep ocean, and production of chromophoric DOM (Murphy et al., 2008; Yamashita and Tanoue, 2008; Nelson et al., 2010; Jørgensen et al., 2011; Catalá et al., 2015; Lonborg et al., 2015).

In the present study we build upon previous work on CDOM absorption properties in the open ocean along the Repeat Hydrography sections (Nelson et al., 2007, 2010; Swan et al., 2009) by adding fluorescence characterization to the parameters measured, using approaches analogous to those used by Jørgensen et al. (2011) and Catalá et al. (2015). Fluorescence EEM spectroscopy provides another dimension to CDOM analysis by identifying one or more fluorophores that may absorb light in a single waveband. In particular we are attempting to identify the nature and location in the water column of processes that produce long-lived chromophores in the ocean. Our sampling area excludes the continental shelves and areas directly influenced by terrestrial input, which we believe gives us the best chance at identifying autochthonous processes.

METHODS AND MATERIALS

Hydrographic Data and Sampling

We collected samples on six sections of the U.S. CO₂/CLIVAR Repeat Hydrography Project (Feely et al., 2005) between 2008 and 2013, spanning the Indian, Pacific, Southern and Atlantic Oceans (Figure 1). Our typical sampling frequency for CDOM was once daily (ca. 1° of latitude on meridional sections), with samples collected throughout the whole water column (Nelson et al., 2010). The hydrographic parameters sampled by other researchers included CTD temperature, salinity, dissolved oxygen, primary nutrients (NO₃, PO₄, and SiO₄), inorganic carbon concentrations (nominally pCO₂ and DIC), CFC species

(CFC-11, CFC-12, and CFC-13), and dissolved organic carbon (DOC) concentrations (Feely et al., 2004). WOCE standard protocols were used for all hydrographic measurements. Details of the measurement protocols, cruise narratives and data sets are available at the Repeat Hydrography Program website (<http://cchdo.ucsd.edu/>). Computations of neutral density and AOU were performed using Ocean Data View (Schlitzer, 2008).

Sample Preparation and Storage

Water samples were prepared for spectrophotometric analysis according to established methods (Nelson et al., 1998, 2004). Samples were drawn from Niskin bottles into acid-washed and ultrapure water-rinsed amber glass vials with Teflon liner caps. The samples were then filtered using 0.2 µm Nuclepore polycarbonate membrane filters that had been rinsed with ultrapure water to remove any possible absorbing contaminants. Samples for EEM analysis were shipped on ice to UCSB and kept sealed, refrigerated at 4°C, and in the dark until processing (Nelson et al., 2007). Time until processing ranged from several months to 2 years. Stability of CDOM samples has been assessed by long term storage (results for absorption properties reported in Swan et al., 2009). Some samples proved to have contamination issues related to storage and were discarded (see below).

CDOM Absorption Spectroscopy

CDOM absorption was quantified as the absorption coefficient at 325 nm of the dissolved materials as determined using a WPI UltraPath liquid waveguide spectrophotometer (Miller et al., 2002) following previously developed methods (Nelson et al., 2007; Swan et al., 2009). Absorption spectra of the filtered seawater samples equilibrated to room temperature were recorded against MilliQ water (Millipore) in the 1.984 m liquid waveguide spectrophotometer. Absorption spectra were corrected for refractive index differences between samples and ultrapure water using an empirical method based on salinity (Nelson et al., 2007). The absorption

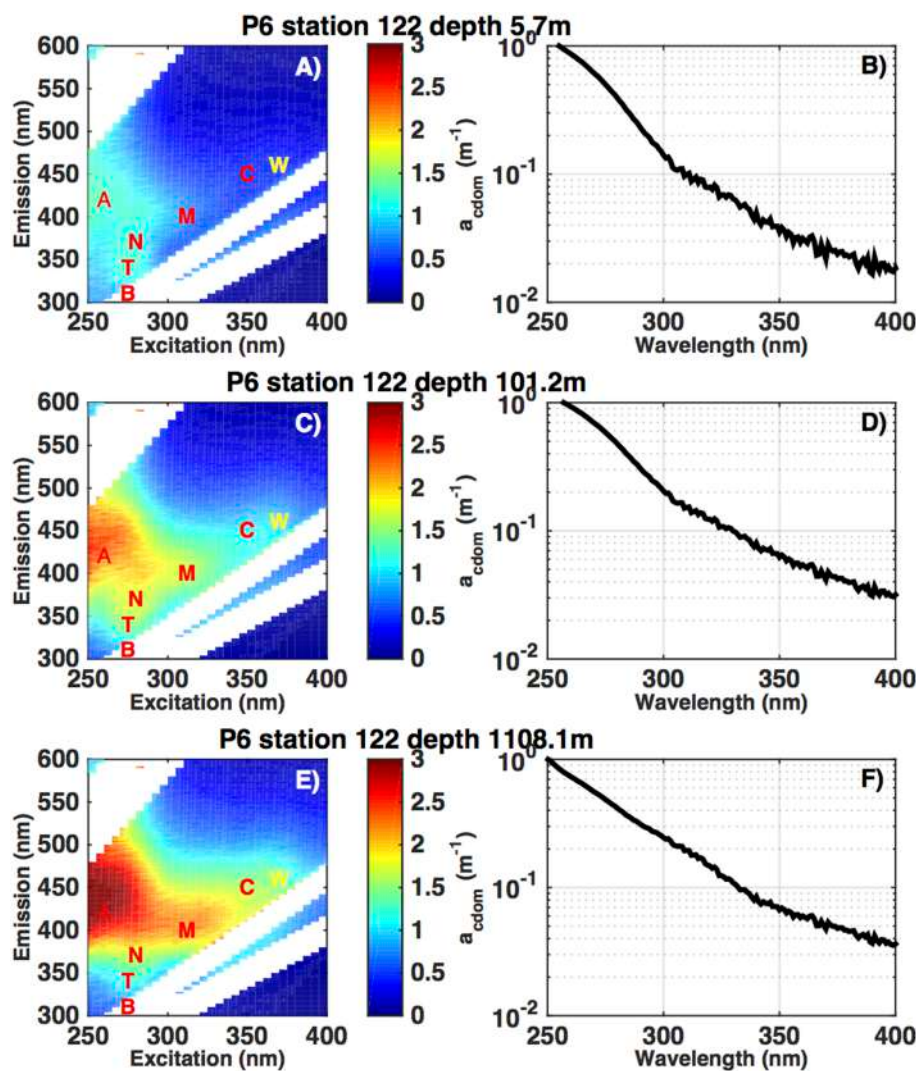


FIGURE 2 | Excitation-Emission Matrix (EEM) fluorescence spectra (ppb QSE) and absorption spectra (m^{-1}) from a depth profile in the subtropical South Pacific (32S, 149W), on the CLIVAR P6 section in December 2009. The letters in panels (A,C,E) refer to the excitation-emission coordinates of defined fluorescence regions. A, M, and C are defined by their position as humic-like fluorescence and T and B are amino acid-like fluorescence signatures (Coble 1996). The CTD ECO fluorometer measures fluorescence in a small defined band, near the C region, indicated by the W. The colorbar refers to increasing fluorescence (ppb QSE) from blue to red. Panels (B,D,F) show the corresponding CDOM absorbance spectra at 325 nm, from 250 to 400 nm.

coefficient at 325 nm (calculated as absorbance divided by path length, multiplied by 2.303 to convert to natural log units) operationally represents CDOM abundance. Duplicate samples collected from the same Niskin on the I8S/I9N sections showed root mean square differences of <4% at 325 nm.

CDOM absorption spectra typically exhibit logarithmic-scale decline with wavelength (Figures 2B,D,F). Spectral slope parameter (S_{snlf} , units of nm^{-1}), the parameter of an exponential equation that best fits the CDOM spectrum over a discrete wavelength interval, was computed for each spectrum over two wavelength ranges in the ultraviolet (Helms et al., 2008) using a least-squares non-linear curve fit method (Stedmon and Markager, 2001).

Fluorescence Spectral Analysis

On selected samples (profile locations shown as stars in Figure 1) we performed EEM fluorescence analysis (Coble, 1996; Nelson and Coble, 2010). This measurement is a compilation of fluorescence emission spectra run sequentially with a range of excitation wavelengths, resulting in a two dimensional dataset for each sample (Figures 2A,C,E).

Filtered seawater samples for EEM analysis were allowed to equilibrate to room temperature and subsequently analyzed in a Horiba Jobin-Yvon Fluoromax-4 fluorescence spectrophotometer in 1 cm quartz cells. Excitation and emission slit widths were set to 5 nm. Emission scans were recorded in ratio mode (fluorescence/reference intensity) from 300 to 600 nm, every 2 nm, with sequential excitation every 5 nm between 250

and 400 nm. Analysis of a single sample takes approximately 22 min. Before and after-measurements (not shown) indicated the samples warmed up less than 0.1°C during analysis, so no further temperature control was attempted. Ultrapure water blanks were run each session and were subtracted from the sample EEMs during data processing. The EEMs were corrected for detector response (both emission and reference detectors) using spectral correction factors provided by the manufacturer.

Each EEM was normalized to the equivalent fluorescence of a known concentration of quinine sulfate dissolved in sulfuric acid. Before each batch of EEM samples were run each day, the fluorescence emission spectrum (300–500 nm, excitation 348 nm) of a \sim 4–5 ppb quinine sulfate standard solution was measured. Subsequent EEM samples were normalized to the quinine sulfate fluorescence at the quinine sulfate excitation/emission maximum (348/450 nm) and the concentration of the standard, resulting in an EEM with units of ppb quinine sulfate equivalent (ppb QSE) that can be compared to other measurements.

In **Figures 2A,C,E** we provide an example of fluorescence EEMs from one profile in the subtropical South Pacific (32S, 149W). Highlighted on this graph in red letters are the nominal positions of the fluorescence regions typically highlighted in discussions of EEM data (cf. Coble, 1996). Regions A and C are thought to be most closely related to terrestrial humic materials, region M is thought to represent a combination of terrestrial and marine humic material (Murphy et al., 2008), and the T and B regions are clearly attributable to the fluorescence of aromatic amino acids (Yamashita and Tanoue, 2003; Jørgensen et al., 2011). The white areas on the EEM plots are areas where the fluorescence of the sample is overwhelmed by Raman or Rayleigh scattering (Zepp et al., 2004). With the instrument and bandwidth settings used in the present study we could not resolve the B region due to Raman scattering, so we do not treat this area separately. We found the T and N regions highly correlated so we only present results from the T region in comparison plots. **Figure 2** clearly shows the decline in fluorescence intensity from the deep ocean to the surface that is typical of subtropical CDOM fluorescence or absorption profiles (Nelson et al., 2010), and the relative importance of the T region can be seen to be higher at 100 m and near the surface than at depth.

We analyzed a total of 730 samples using EEM spectroscopy, representing 69 discrete stations, on the six CLIVAR cruises occupied as part of this study. EEM spectra were subjected to additional quality control mainly involving inspecting the collected data for artifacts that usually resulted from bubbles on the cuvette windows. Other samples exhibited fluorescence in the T-B region (**Figure 2**) that exceeded reasonable values based on other samples in the profile. These samples were judged to be contaminated and were discarded. Samples failing these tests were excluded from EOF analysis (see below) and from fluorescent region intensity analysis if the part of the EEM affected by bubbles was in the region. This resulted in a data set of over 500 samples for each comparison (see Results).

WETLabs CDOM Fluorometer

On the I8S/I9N, P6, and A16N sections we deployed a WETLabs ECO CDOM fluorometer (6000 m rated) on the main CTD rosette. This instrument is a single channel fluorometer with excitation at 380 ± 10 nm and emission detection at 420 ± 20 nm, closest to the C region of the EEM (**Table 1**). Data were recorded in volts. Sensitivity of the instrument varied with gain settings and calibration drift. To facilitate comparison with the EEM data, we devised a linear transfer function for each cruise (over which gain and calibration were assumed to be constant) to transfer the quinine-sulfate scaled EEM data (ppb QSE) from the W region (**Figure 2**) to the ECO fluorometer data. The fluorescence of EEM samples averaged over the excitation/emission region of the ECO fluorometer were regressed against the fluorometer voltage at the depth of the sample, averaged over 2 m depth. The resulting slope average was applied to the fluorometer data on a cruise-by-cruise basis to result in calibrated (ppb QSE) fluorescence data that can be compared between cruises and with EEM data. For the purpose of discussion, these single channel data will be referred to as " F_{cdom} ".

Analysis of EEM Data by Empirical Orthogonal Functions

We used the technique of empirical orthogonal function (EOF) analysis (e.g., Preisendorfer and Mobley, 1988) to examine the variability of fluorescence EEM data. EOF analysis is a purely empirical process that decomposes the variance of a dataset into a discrete number of constant eigenvectors (basis functions or "modes") that have the same dimensions as a single example of the data, and variable expansion coefficients or "amplitudes" which are one-dimensional. An individual data "point" (i.e., an EEM) can be reconstructed as the sum of the products of the modes, their corresponding amplitudes, and an eigenvalue for each mode that represents the total variance in the data set accounted for by the mode. The fractional contribution to the total variance of the dataset represented by each mode can be computed, and is generally used to discriminate between significant and insignificant modes of variability. We implemented the EOF analysis in Matlab by reshaping the three-dimensional matrix of multiple EEMs to a two dimensional field, and computing the largest eigenvalues and eigenvectors of the covariance matrix using the built-in Matlab function `eigs()`. Contribution of each eigenvector to the total variance was calculated as the eigenvalues divided by the sum of the eigenvalues. In the present study we only consider modes of variability that account for more than 1% of the total variance of the dataset, which corresponded to the first three eigenvectors computed.

RESULTS

Distribution of CDOM and Fluorescence Properties

The samples collected for this study came from a latitude range spanning 60N–60S (**Figure 1**), and depth ranges from the surface to over 5000 m at the ocean floor. We here present data from

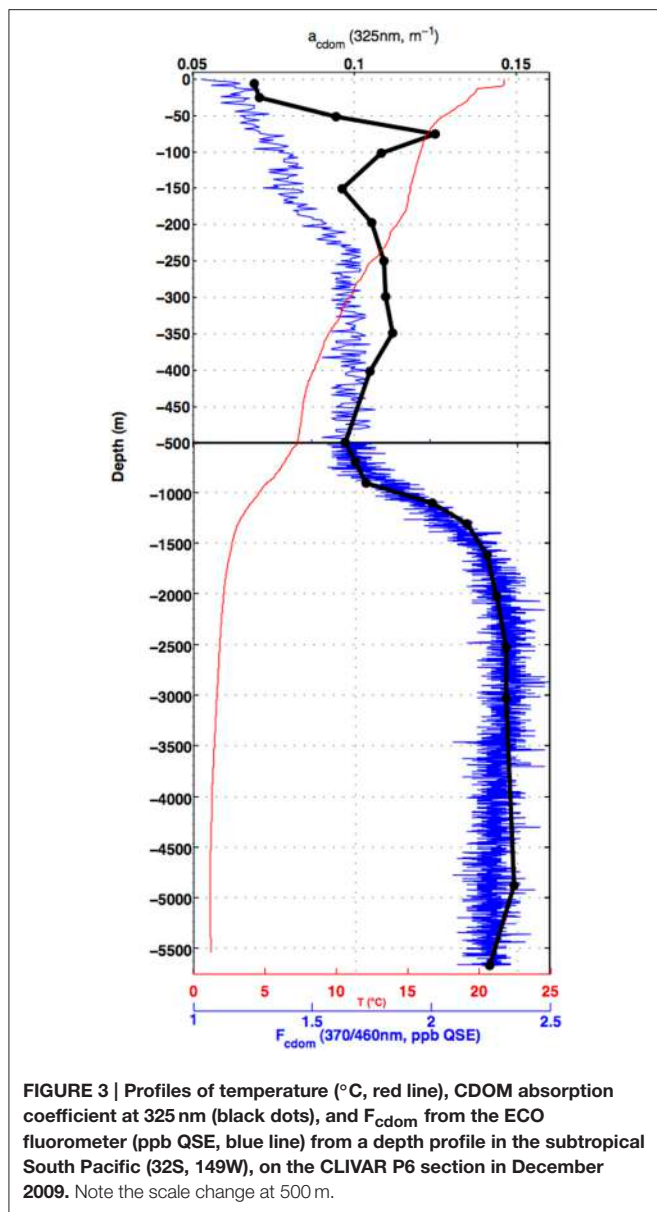


FIGURE 3 | Profiles of temperature (°C, red line), CDOM absorption coefficient at 325 nm (black dots), and F_{cdom} from the ECO fluorometer (ppb QSE, blue line) from a depth profile in the subtropical South Pacific (32S, 149W), on the CLIVAR P6 section in December 2009. Note the scale change at 500 m.

all of the major ocean basins away from the continental shelves excepting the North Pacific and the Arctic Oceans. Despite the range of locations and ecosystems sampled there were some factors common to most profiles that are highlighted first.

An example of CDOM and F_{cdom} profiles is given in **Figure 3**. This profile is from the same station from which the **Figure 2** example EEMs and absorption spectra were taken. In this picture, discrete bottle sample CDOM absorption at 325 nm (black dots) are compared to the vertical profile of temperature (red line) and F_{cdom} (blue line). In the main thermocline (~500–1500 m at this station) and below, visible light fluorescence measured by the CDOM fluorometer (F_{cdom}) is well correlated with CDOM UV absorption $a_g(325 \text{ nm})$. Between 500 and 250 m F_{cdom} remains roughly constant, then decreases monotonically toward the surface. The CDOM UV absorption profile instead shows two maxima in the depth range between 500 m and the surface: a

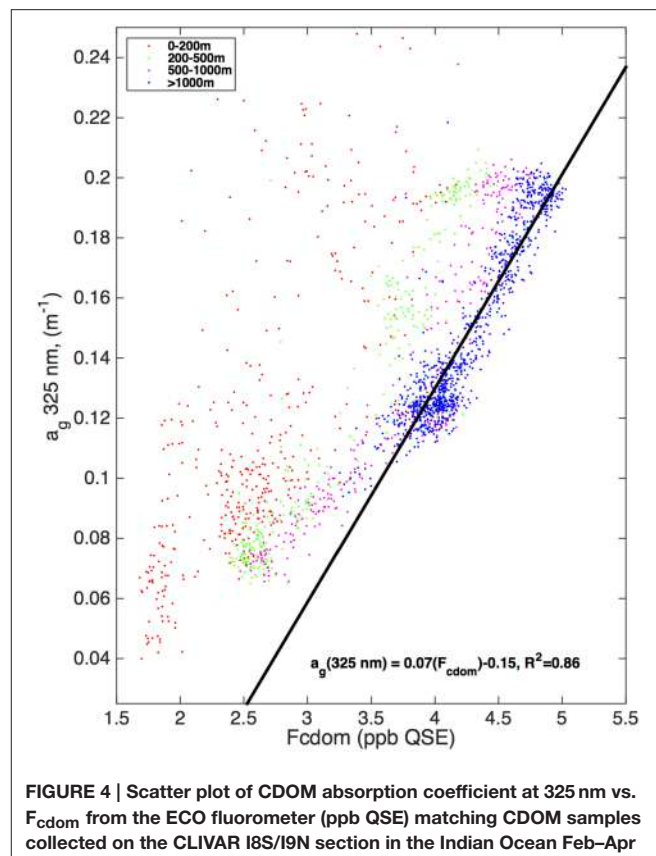


FIGURE 4 | Scatter plot of CDOM absorption coefficient at 325 nm vs. F_{cdom} from the ECO fluorometer (ppb QSE) matching CDOM samples collected on the CLIVAR I8S/I9N section in the Indian Ocean Feb–Apr 2007. Samples are color coded by depth range (see legend). Regression line and correlation coefficient are shown for the samples collected at or below 1000 m depth along the transect line.

broad shallow maximum centered near 350 m and a sharper maximum near 75 m. The surface mixed layer has the lowest CDOM absorption and fluorescence due to solar bleaching.

This pattern with a local subsurface CDOM maximum that does not correlate with F_{cdom} present was common to most open ocean areas covered in this study. **Figure 4** shows a scatter plot of F_{cdom} vs. $a_g(325 \text{ nm})$ from samples collected on the I8S/I9N section in the Indian Ocean, covering the ice edge to the Bay of Bengal (**Figure 1**). Color codes show the depth range of the samples. Samples collected in and below the main thermocline (blue dots) exhibit a strong linear relationship between F_{cdom} and $a_g(325 \text{ nm})$ ($R^2 = 0.86$), but this pattern breaks down shallower in the water column with a very weak relationship in the top 200 m where the $a_g(325 \text{ nm})$ profile has the subsurface maximum peak highlighted in **Figure 3**. Similar scatter plots for other ocean basins (not shown) reveal similar patterns, with the closest relationship between $a_g(325 \text{ nm})$ and F_{cdom} found in the main thermocline.

Nelson et al. (1998, 2010) have interpreted the absorption profile features as representing a balance between surface bleaching and water column production of UV-absorbing CDOM in the euphotic zone, with ventilation processes (e.g., subtropical or subantarctic mode water formation) affecting the profile between the euphotic zone and the main thermocline. The contrast seen with the fluorescence profile shows that for

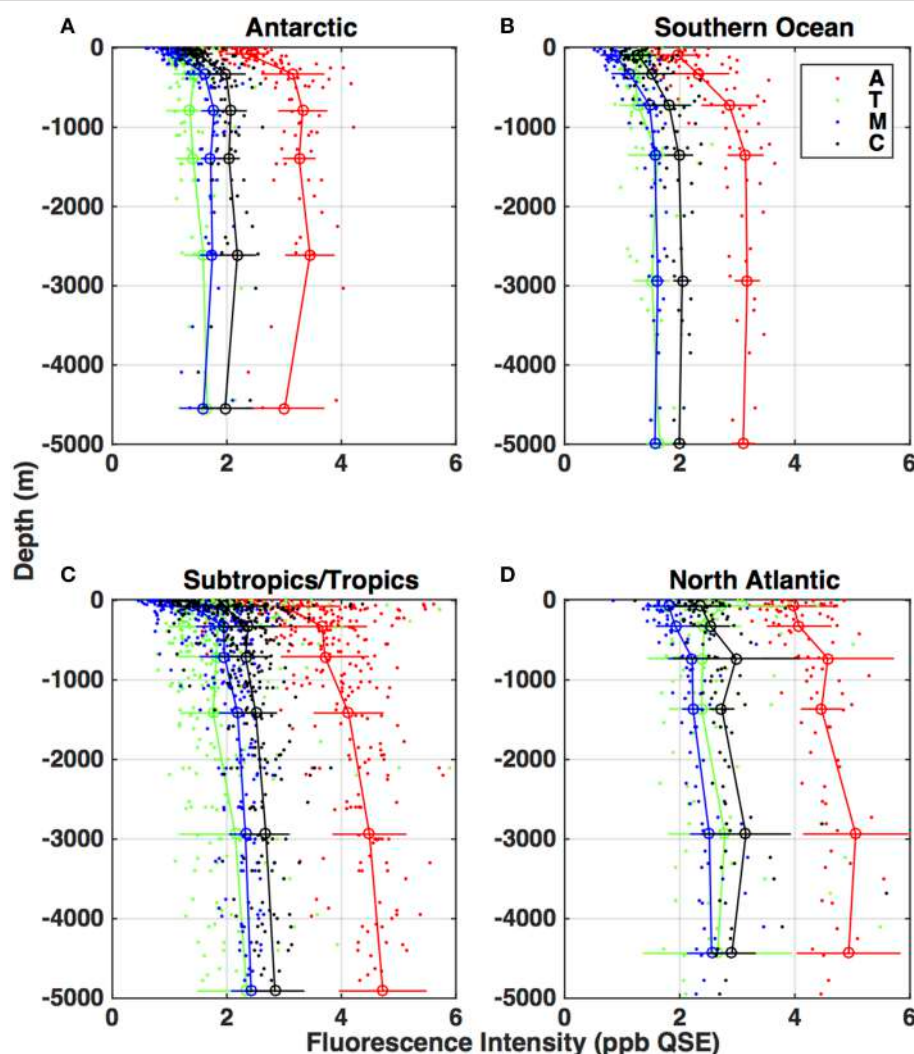


FIGURE 5 | Depth distributions of CDOM fluorescence (ppb QSE) in the characteristic EEM regions (as denoted in Figure 2), for four latitude-bounded regions of the global ocean: (A) North Atlantic ($>40^{\circ}$ N), (B) subtropical/tropical regions of all oceans (40° N– 40° S), (C) Southern Ocean (40° S– 55° S), (D) Antarctic (below 55° S). Red symbols: region A. Green symbols: region T. Black symbols: region C. Blue symbols: region M. Small dots are the individual measurements, connected circles with error bars are means and standard deviations for depth ranges 0–200, 200–500, 500–1000, 1000–2000, 2000–4000, and greater than 4000 m. The depth given for each mean value is the mean depth of the samples in the bin, so this varies slightly from panel to panel.

at least the subset of fluorescent CDOM that absorbs and fluoresces at the longest wavelengths, the production processes that affect UV-absorbing CDOM are absent or only weakly present.

Distribution of fluorescence EEM features (as represented by the A, T, M, and C regions of the EEM) also exhibited consistent patterns from basin to basin. **Figure 5** shows vertical profiles of the fluorescence intensity for each region, divided up into different ocean regions based on latitude: North Atlantic ($>40^{\circ}$ N), subtropical/tropical (40° N– 40° S), Southern Ocean (40° S– 55° S), and Antarctic (south of 55° S). In all regions the humic region A exhibited the highest fluorescence intensity. The humic A, M, and C regions were highly correlated to each other ($R^2 > 0.92$) and exhibited similar profiles, increasing from the surface into the main thermocline and remaining

roughly constant into the abyssal. In all profiles the humic region C had higher fluorescence intensity than the humic region M.

The T fluorescence profiles exhibited more variability, but on average in each basin T region fluorescence intensity was higher in or near the euphotic zone (to 500 m), declined with depth into the intermediate waters (to 1000 m), and increased again in the main thermocline. T values were weakly correlated to the humic fluorescence regions (A, M, and C; $R^2 < 0.43$) because of the relatively large scatter in the T profiles and the differences between T and the humics in the top 500 m.

The North Atlantic samples (**Figure 5A**) exhibited on average the highest fluorescence in all regions, while the Southern Ocean (**Figure 5C**) and Antarctic (**Figure 5D**) samples had the lowest. The subtropical/tropical (**Figure 5B**) and North Atlantic

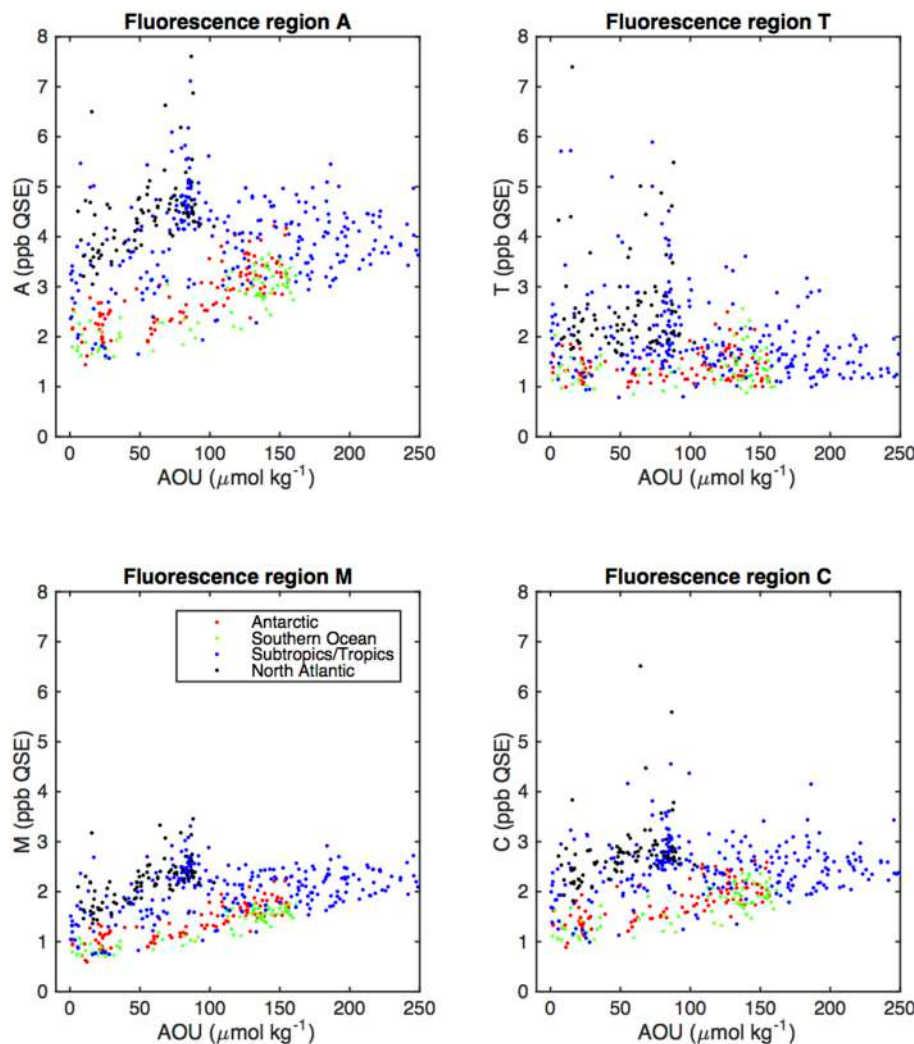


FIGURE 6 | Scatter plots of fluorescent region intensities (Figure 2) vs. AOU (colors representing the different oceanic areas as defined in Figure 5).

humic fluorescence (A, M, and C) profiles were similar in magnitude below the thermocline but the North Atlantic sample fluorescence was higher at the surface.

The distribution of fluorescent components we report here is consistent with results of prior studies using fluorescence intensity (Chen and Bada, 1992; Determann et al., 1996; Yamashita and Tanoue, 2009), and in components derived from PARAFAC analysis of EEM components (Jørgensen et al., 2011; Catalá et al., 2015). The average increase in T values in the deep ocean we observed below the thermocline was not seen by Jørgensen et al. (2011) but is consistent with the long residence times of B-related components (adjacent to the T region) elucidated by Catalá et al. (2015).

We compared fluorescence intensities of the humic regions (A, M, and C) with AOU, which is for a given sample the difference between *in situ* oxygen concentration and the theoretical atmospheric equilibrated concentration of oxygen at *in situ* temperature, salinity, and pressure. Positive values of

AOU in the ocean represent consumption of oxygen by the microbial community, and are closely linked to remineralization (Feely et al., 2004). Selected CDOM and FDOM components in the main thermocline have been seen as linearly related to AOU with high correlation (UV absorption, Nelson et al., 2010; and visible fluorescence components, Yamashita and Tanoue, 2008; Jørgensen et al., 2011), with the notable exception of the North Atlantic, where UV absorption or visible fluorescence components were much higher at low AOU (Nelson et al., 2010; Jørgensen et al., 2011). In the present study, correlation between fluorescence intensities in the canonical fluorescence regions and AOU varied between region and geographical area (Table 2).

UVA fluorescence in the T region was uncorrelated to AOU in all geographical regions.

Correlation between the visible (humic) fluorescence emission regions A and C and AOU was high in the Antarctic and Southern Ocean, but low in the North Atlantic and subtropics. Correlation between AOU and region M fluorescence was also

TABLE 2 | Correlation coefficients (R^2) for AOU ($\mu\text{mol kg}^{-1}$) vs. fluorescence region heights (ppb QSE) for the main fluorescence regions, divided into ocean basins (as in Figure 5).

Region	Antarctic	Southern ocean	Subtropics/Tropics	North Atlantic
A	0.62	0.70	0.03	0.20
T	0.01	0.03	0.11	0.00
M	0.73	0.82	0.16	0.39
C	0.56	0.61	0.02	0.14

higher in the North Atlantic. Low correlation between UVA fluorescence and AOU is consistent with previous results, and reflects the fact that higher values of T are generally found near the surface (Figure 5) and that UV absorption and the humic fluorescence regions increase as well as AOU in the main thermocline. The higher correlation we observed between M fluorescence and AOU in the North Atlantic is an exception to the general high correlation between A, C, and M fluorescence that we observed, and suggests differing dynamics between the components that give rise to A/C fluorescence and those that result in increases in M region fluorescence. The strongest correlations between fluorescent intensity and AOU in all basins were for the M region. This further suggests a link between remineralization and the formation of humic materials. Lack of correlation between T region fluorescence and AOU is most likely due to the more biolabile material represented by T fluorescence being remineralized in surface waters that are near to equilibrium with the atmosphere and thus have low and not consistently varying AOU.

We also compared fluorescence intensities in the different regions to the anthropogenic ventilation tracer CFC-12 (not shown). Correlations between the fluorescence intensity in the A, M, and C regions and CFC-12 were negative, indicating increasing humic material with increasing time since ventilation. As with AOU, fluorescence intensities in the T region were not correlated to CFC-12.

Analysis of Fluorescence Spectra Variability

We chose to use EOF analysis rather than the analogous and more commonly used parallel factors analysis (PARAFAC, Stedmon et al., 2003) to analyze the variance in fluorescence EEM data. Both EOF and PARAFAC methods decompose variability in three dimensional data sets (multiple EEMs) into two dimensional patterns and corresponding scalars that represent the contribution of each pattern to each sample. These analysis techniques allow for elucidation of variability patterns that are not immediately obvious from the fluorescence intensity data, such as assessment of the contributing factors to the M region, which includes both autochthonous and allochthonous components (Murphy et al., 2008), and for correlations between spectral regions that are not immediately apparent from inspecting the data.

The PARAFAC approach has been used successfully to discriminate between terrestrial and autochthonous CDOM

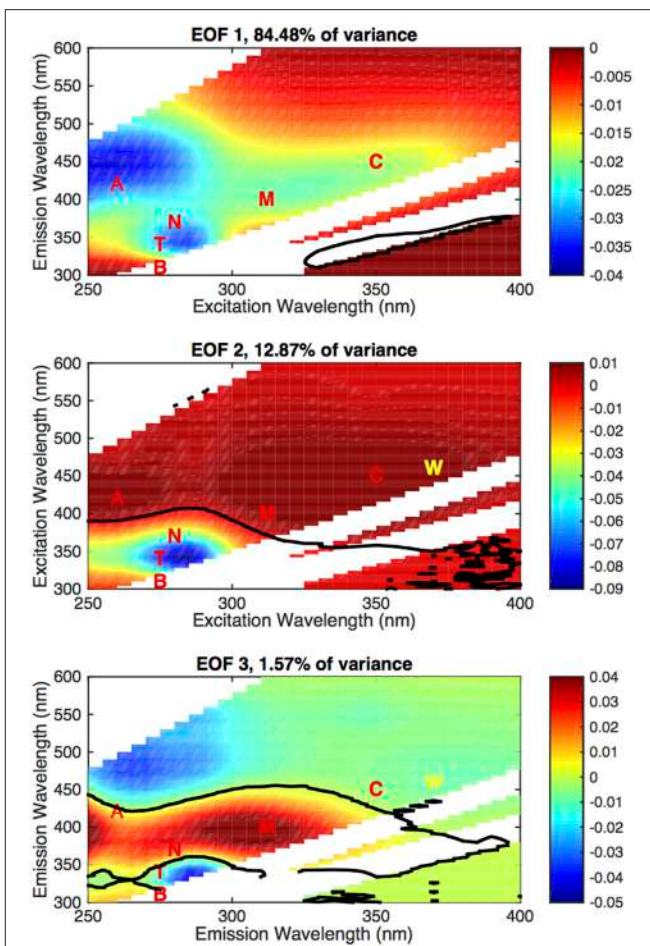


FIGURE 7 | EOF basis functions (non-dimensional) computed from the EOF data, first three modes (annotated with nominal region locations and the F_{dom} wavelength pair). The solid black line denotes where the EOF mode is zero. As in Figure 2, the white areas are masks where Rayleigh and Raman scattering obscure the sample fluorescence and are disregarded. The zero contour is interpolated when passing through this area and should not be considered significant.

fractions (Murphy et al., 2008), and to quantify characteristic components of EEM fluorescence that can be related to environmental variables, such as salinity, AOU, or amino acid concentration (Jørgensen et al., 2011). Typical PARAFAC implementations have modes which are exclusively positive values, so they better reflect components making up the EEM and their distribution. In the present study we are interested in the possibility of identifying transformations *between* components of the fluorescent material, so the ability of the EOF approach to have positive and negative regions in the modes is important.

For this data set, we identified three modes that each contributed more than 1% of the total variance (Figure 7), which we have designated EOF 1 (84.48%), EOF 2 (12.87%), and EOF 3 (1.57%). We have highlighted the nominal location of the main fluorescent regions (A, T, C, M) and the WETLabs fluorometer range (W). Distribution of the amplitudes for each mode is

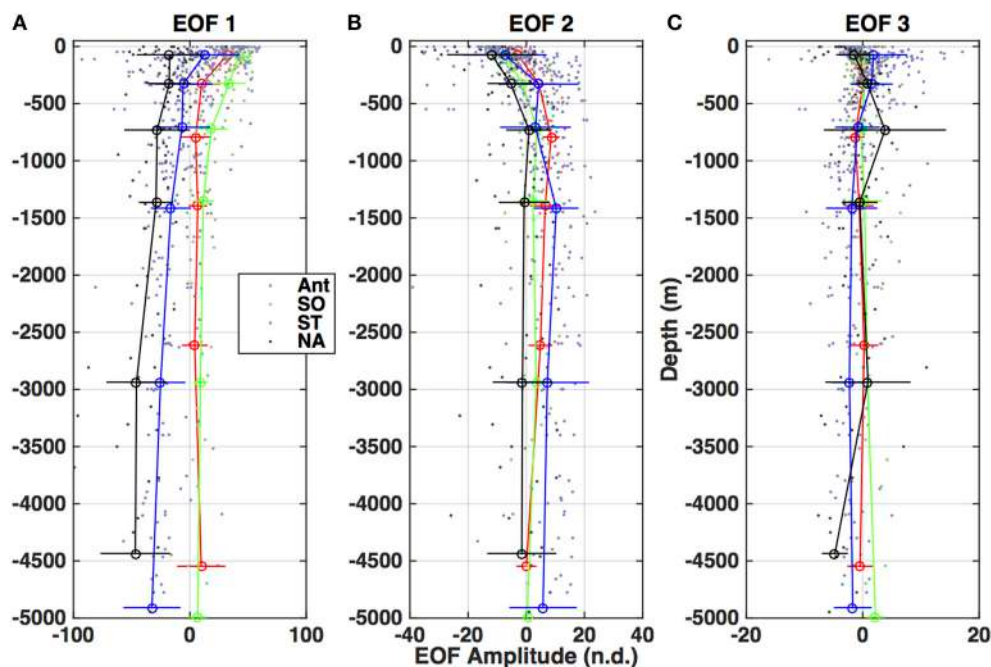


FIGURE 8 | Depth profiles of the amplitudes for each of the three EOF modes (Figure 7) divided by basin (as in Figure 5). **(A)** Amplitude of EOF 1. **(B)** Amplitude of EOF 2. **(C)** Amplitude of EOF 3.

TABLE 3 | Correlation coefficients (R^2) between AOU and the amplitudes of the first three EOF modes, with regions defined as in Table 2.

EOF Mode	Antarctic	Southern ocean	Subtropics/ Tropics	North Atlantic
EOF 1	0.61	0.69	0.14	0.14
EOF 2	0.66	0.68	0.43	0.15
EOF 3	0.00	0.00	0.01	0.00

shown in **Figure 8** as depth profiles (regions and depth averaging bins as in **Figure 5**).

The first and dominant mode, EOF 1, exhibits all the features of the EEM (A, T/N, C, and M regions are identifiable, as in **Figure 2C**) and is below zero in the entire mode (**Figure 7A**), indicating a below-the-average contribution to the EEM when the corresponding amplitude is positive. The amplitude for this mode also covered the largest range of values and on average displayed two distinct profile patterns. In the subtropics and tropics and in the North Atlantic (**Figure 8A**), the amplitudes were strongly negative in the deep ocean (indicating a strong contribution of the inverse of this mode to the EEM), and increased steadily to the surface, where the average was slightly negative in the North Atlantic and slightly positive in the tropics and subtropics. In the Southern Ocean and the Antarctic, the Mode 1 amplitude was positive in the deep ocean and increased by a factor of ~ 8 from the main thermocline to the surface. This pattern reflects the differences in overall fluorescence intensity, or abundance of fluorescent material, in the global ocean.

The secondary modes, EOF 2 and EOF 3, both exhibited strong negative and positive areas (**Figures 7B,C**). EOF 2 (12.9% of the variance) features a strong negative peak in the UVA fluorescence region near the T and N locations, with positive peaks in the A and C regions (**Figure 7B**). The profiles of the amplitude of EOF 2 (**Figure 8**) increased in each ocean basin from below zero to zero or positive values near the top of the main thermocline (750–1000 m), then declined to near zero with increasing depth in the deep ocean. Increasing amplitudes of EOF 2 indicate a decreasing contribution of UVA fluorescence and an increase in the contribution of the humic fluorescence regions with depth from the euphotic zone to the mesopelagic.

EOF 3 (1.6% of the variance) has a distribution with a strong negative in UVA fluorescence and a strong positive near the M region (**Figure 7C**). The average profile of the EOF 3 amplitude showed slightly positive values near the euphotic zone (**Figures 8A,C,D**) or upper mesopelagic (**Figure 8B**), but was very close to zero in the deep ocean. This distribution suggests removal of UVA fluorescence balanced by increases in M fluorescence occurring in the euphotic zone and the upper mesopelagic.

EEM variability patterns in the first two EOF modes also exhibited correlation to indices of remineralization. **Figure 9** shows scatter plots of AOU ($\mu\text{mol kg}^{-1}$) vs. EOF amplitude, color-coded by ocean basin. The first EOF mode (**Figure 9A**) shows a slight negative linear correlation with AOU, with the North Atlantic standing out as having a higher contribution from EOF 1 than the trend. The second EOF mode shows a strong correlation to AOU (**Figure 9B**) and the third EOF shows no correlation with AOU (**Figure 9C**), because on average

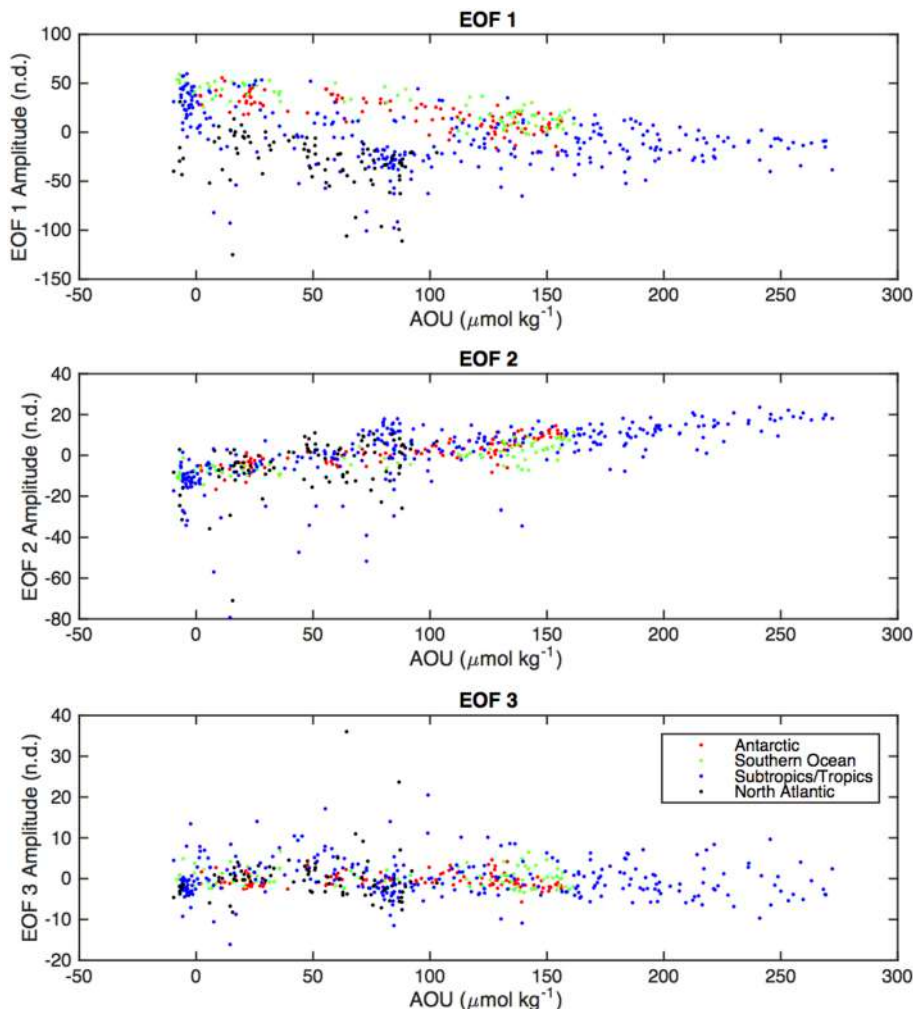


FIGURE 9 | Scatter plots of EOF amplitudes (corresponding to EOF modes shown in Figure 7) vs. AOU (colors representing the different oceanic areas as in Figures 5, 6).

positive values of EOF 3 occur only near the surface where AOU values are near zero (**Figure 8**). Similar results were obtained for correlations between EOF amplitudes and other indices of remineralization such as total CO₂ and inorganic nutrients (not shown). As with fluorescence intensities (**Table 2**), correlation of the EOF amplitudes with AOU varied by basin (**Table 3**). Correlations between AOU and EOF 1 and 2 amplitudes, were lowest in the North Atlantic and highest in the Antarctic and Southern Ocean areas. Similar lack of correlation was observed for EOF 1 in the subtropics and tropics (**Table 3**).

The amplitude of EOFs 1 and 2 were also correlated to CFC-12 concentration (**Table 4**). Water of increasing ventilation age as assessed by CFC-12 concentration has been linked to increased CDOM UV absorption and decreased spectral slope in the North Atlantic interior (Nelson et al., 2007). The amplitude of EOF 1 showed a positive linear relationship with CFC-12 concentration in all basins. The amplitude of EOF 2 showed a negative linear relationship with CFC-12 that was significant in all basins except

TABLE 4 | Correlation coefficients (R^2) between CFC-12 concentration and the amplitudes of the first three EOF modes, with regions defined as in Table 2.

EOF Mode	Antarctic	Southern ocean	Subtropics/ Tropics	North Atlantic
EOF 1	0.59	0.62	0.25	0.23
EOF 2	0.53	0.64	0.29	0.01
EOF 3	0.00	0.00	0.15	0.02

for the North Atlantic. This result qualitatively indicates that water of increasing ventilation age has an increased relative contribution of humic material and a decreased contribution of the humification process described by EOF 2. The lack of correlation between EOF 2 and CFC-12 in the North Atlantic is driven by a number of outliers of very low EOF 2 amplitude (not shown) at intermediate CFC-12 concentrations.

DISCUSSION

Characterization of Chromophoric DOM

Our results highlight the divergence between assessments of chromophoric DOM using absorption and fluorescence techniques. Comparative profiles of UV absorption and visible fluorescence (**Figure 3**) indicate that UV absorption represents a combination of UV absorbing and fluorescent material that originates in or near the euphotic zone (Nelson et al., 1998, 2010; Jørgensen et al., 2011; Yamashita et al., 2015), but also reflects the abundance of humic material in the main thermocline and deep ocean (**Figure 4**). This result further implies a diversity of chromophores in the DOM profile that can be further characterized using fluorescence EEM analysis. It is important to note that single-channel CDOM fluorometers only respond to a portion of potential fluorescent material in the ocean, and the data should be interpreted accordingly (e.g., Yamashita et al., 2015). In the case of the WETLabs ECO CDOM fluorometer, the fluorescence channel chosen responds to visible fluorescence near the C region, meaning it can be used to assess some forms of humic material but not the UVA fluorescing material found in freshly produced chromophoric DOM. Comparison of single channel visible fluorescence data with absorption data or EEM data can furnish insight into the location of remineralization processes that can increase CDOM abundance in the environment.

We attempted to use the absorption spectrum slope ratio parameter (Helms et al., 2008) to relate properties of the CDOM absorption spectrum to fluorescence properties and environmental variables. Slope ratio values in all ocean basins (not shown) ranged from 0.25 to 4 (n.d.) and exhibited a clear average depth profile with the highest values at the surface, and a deep ocean average of about 1.5, with considerable scatter. No relationships were found between the slope ratio and fluorescence region heights, nor were there correlations with the three main EOF amplitudes. We find that the slope ratio relates to increasing solar bleaching (high values) and increasing contribution of humic material (gradient to low values), as was postulated by Helms et al. (2008), but it does not directly relate to the presence or dynamics of fluorescent components.

Our results are largely consistent with the interpretation of fluorescent EEMs as reflecting a limited number of independent components (Stedmon and Nelson, 2015). In our results, the UVA fluorescing regions (T, B, and N) and the visible fluorescing regions (A, C, and M) were highly correlated to each other and only weakly correlated between groups. Nevertheless, we found some differences in the distribution of fluorescent components that suggest some diversity in processes controlling fluorescent materials, as we discuss below.

Origin and Dynamics of Humic Material in the Global Ocean

We interpret the patterns of fluorescence variability revealed by the EOF analysis as revealing *transformation processes* common to the whole ocean. The dominant mode of variability (EOF 1, **Figure 7A**) contains elements of all the fluorescence features of the EEM (cf. **Figure 2**) and we interpret the amplitude of

EOF 1 as an overall index of fluorescent material abundance, as controlled by terrestrial material abundance or autochthonous production (increasing negative amplitude), and removal via bleaching (increasing positive amplitude). The profiles of EOF 1 amplitude differ significantly between the North Atlantic and subtropics (**Figures 8A,B**) and the Southern Ocean and Antarctic (**Figures 8C,D**). All profiles reflect the increasing contribution of EOF 1 with depth, but the North Atlantic and (sub)tropical profiles start at a higher level. The similarity between North Atlantic and subtropical/tropical profiles further suggests that the higher contribution of terrestrial material to the DOM found in the North Atlantic (Jørgensen et al., 2011; Catalá et al., 2015) is transported rapidly into the lower latitudes via meridional overturning circulation (Nelson et al., 2007).

EOF modes 2 and 3 appear to reveal removal of fresh DOM and production of humic material, as reflected in depth profiles (EOF 2 and 3, **Figure 8**) and correlation with AOU (EOF 2, **Figure 9**). In both cases these processes appear to be located in the upper ocean, in or near the euphotic zone (EOF 3) and above and within the main thermocline (EOF 2). This result is consistent with our observations of the single-channel visible fluorescence profiles vs. UV absorption profiles (**Figure 3**), which diverge above the main thermocline. The amplitude of EOF 2 is correlated to AOU and CFC-12, suggesting a connection to remineralization processes that occur over a significant length of time. The amplitude of EOF 3 is not correlated to AOU, but this is probably because this process appears to occur in the ventilated surface waters where AOU remains near zero.

The amount of variability contained in these remineralization-linked modes is small (<15%), implying that the primary source of gradients in fluorescent DOM in the global ocean is not autochthonous input of new fluorophores. Instead the distribution of fluorescence appears to be related to the removal of allochthonous fluorescent DOM by solar bleaching at the surface. This interpretation explains the higher CDOM/FDOM to AOU relationships observed in the North Atlantic (Nelson et al., 2010; Jørgensen et al., 2011) as being driven by high terrestrial preformed chromophoric DOM entering from the Arctic via the surface and North Atlantic Deep Water formation (Hernes and Benner, 1996; Granskog et al., 2012), and being removed at the surface via upwelling processes and solar bleaching (Nelson et al., 2010). In this interpretation the strong link between UV absorption, certain fluorescent components, and AOU (Nelson et al., 2010; Jørgensen et al., 2011) is partially coincidental. Increase of AOU is related to microbial consumption of POC and semi-labile DOC in the main thermocline, but the gradient in CDOM and FDOM in the main thermocline is essentially driven by removal in the upper ocean and supply of autochthonous CDOM from the thermohaline circulation.

These results are nevertheless consistent with the results of Catalá et al. (2015), who computed long (>350 years) lifetimes for fluorescent components in the deep ocean, which is longer than the oceanic turnover time. The difference between the ocean turnover time and the lifetimes of the fluorescent components is explained by the slow addition of new fluorescent material that we identify here. Our results indicate

that these processes occur near the ocean surface and the main thermocline.

The processes that result in the patterns revealed by EOF 2 and 3 can include transformation of DOM, or removal of fresh DOM and production of humic DOM from colorless DOM and/or particles, as is implied by the microbial carbon pump hypothesis (Jiao et al., 2011). The general pattern of DOC distribution in the ocean (Hansell, 2002; Hansell and Carlson, 2015) suggests that the labile/semi-labile DOM is being remineralized, and it's possible some of this is transformed into humic material (Ogawa et al., 2001; Murphy et al., 2008). It is likely that remineralization of particles results in humic material formation, with perhaps "fresh" DOM as an intermediate step. Zooplankton excretion contain DOM that has distinct absorption spectra that do not resemble the canonical CDOM absorption spectra (Steinberg et al., 2004). Furthermore, the difference in the two EOF modes implies there is more than one process that converts "fresh" fluorescent DOM into two kinds of long-lived "humic" fluorescent DOM. Interestingly, in contrast to previous similar studies, we found that the average amount of fluorescence in the T region also increases slightly in the thermocline to the deep ocean (**Figure 5**). The increased T region fluorescence could represent newly produced UVA absorbing or fluorescing CDOM from microbial or heterotrophic processes (Nelson et al., 2004; Steinberg et al., 2004; Stedmon and Markager, 2005; Shimotori et al., 2009; Suksomjit et al., 2009) or material directly released via particle dissociation related to zooplankton grazing (Urban-Rich et al., 1996). This process could also be one source of UVA fluorescence in surface waters. The minimum in the T fluorescence profile can be explained by the processes described by EOFs 2 and 3 removing materials related to the T fluorescence and replacing them with humic materials.

As stated above, the results from the EOF analysis imply the presence of processes that convert fresh, UVA absorbing/fluorescing DOM into long-lived humic-like CDOM. These processes result in the apparent transfer of fluorescence from the T, B, and N region (where aromatic amino acids fluoresce) to the humic A and C regions (EOF 2) or the humic M region (EOF 3). One candidate for the sort of reaction that could underlie this process is a peptide-catalyzed aldol condensation reaction (Dziedzic et al., 2006) which is thought to give rise to visible-light absorbing oligomers that resemble humic material in marine aerosols (Nozière et al., 2007). There is also a photochemical condensation mechanism that can give rise to compounds with fulvic and humic acid-like absorption and fluorescence (Bianco et al., 2014; Gonsior et al., 2014), and the production of a visible light absorbing substance in the presence of nitrate was observed by Swan et al. (2012) in photochemical bleaching experiments. These processes are essentially abiotic, which is not consistent with the idea that the humification process is directly linked to remineralization. However, it is also

likely, given the connections to AOU, that there are microbially mediated processes that perform similar functions that remain to be identified (Jørgensen et al., 2014). Aerosols as a source of new humic material to the global surface ocean should be considered as well, but solar bleaching is likely to give the material a short lifetime.

In summary, we conducted a global scale survey of chromophoric DOM in the ocean away from immediate terrestrial influence that included absorption and fluorescence properties. Our results partitioned chromophoric DOM into freshly created, UVA-absorbing-and-fluorescing material in the surface ocean, and long-lived, humic-like, visible-fluorescing material in the deep ocean. The main variability in humic material in the open ocean interior appears to result from introduction of allochthonous CDOM via the North Atlantic Deep Water, and removal of CDOM via solar bleaching of upwelled material. These results are consistent with previous global scale studies of fluorescent DOM (Jørgensen et al., 2011; Catalá et al., 2015). Furthermore, using EOF analysis of EEM data we identified two variability patterns that appear to reflect conversion of freshly produced material into humic material and localized these processes to the euphotic zone and the upper part of the main thermocline. Our results point to a need to identify the differences between terrestrial and marine humic materials and the reactions that "humify" DOM in the ocean.

AUTHOR CONTRIBUTIONS

NN is the principal investigator and initiated the project. Both NN and JG contributed to the analysis, data processing, and quality control of the data. Both authors participated in writing the manuscript and interpreting the results.

ACKNOWLEDGMENTS

This research was supported by grants from NASA (grants NAG5-13277 and NNX14AG24G) and NSF (OCE-0241614 and OCE-0648541) to NN and D. A. Siegel. We would like to acknowledge the ongoing support of the U.S. CO₂/CLIVAR/GO-SHIP Repeat Hydrography Program (Dick Feely, Lynne Talley, Rik Wanninkhof, Rana Fine), and the crews and support staff of the research vessels *Revelle*, *Ronald H. Brown*, *Melville*, and *Nathaniel B. Palmer*. Aimee Neeley, Stan Hooker, and Joaquin Chaves of NASA GSFC, collected samples for us on the I6S and S4P sections. Chantal Swan, Jamie Creason, Erica Aguilera, and Michelle Higgins conducted spectroscopic analysis in our lab, and our field teams included Dave Menzies, Chantal Swan, Ellie Halewood, Meg Murphy, KG Fairbarn, Erik Stassinos, and Eli Aghassi. Thanks also to Teresa Catalá for helpful discussions on EEM analysis and interpretation, and two anonymous reviewers for comments on the manuscript.

REFERENCES

- Andrew, A., Blough, N. V., Subramaniam, A., and Del Vecchio, R. (2013). Chromophoric dissolved organic matter (CDOM) in the Equatorial Atlantic Ocean: optical properties and their relation to CDOM structure and source. *Mar. Chem.* 148, 33–43. doi: 10.1016/j.marchem.2012.11.001
- Aristegui, J., Duarte, C. M., Agustí, S., Doval, M., Álvarez-Salgado, X. A., and Hansell, D. A. (2002). Dissolved organic carbon support of respiration in the dark ocean. *Science* 298:1967. doi: 10.1126/science.1076746
- Bianco, A., Minella, M., De Laurentiis, E., Maurino, V., Minero, C., and Vione, D. (2014). Photochemical generation of photoactive compounds with fulvic-like and humic-like fluorescence in aqueous solution. *Chemosphere* 111, 529–536. doi: 10.1016/j.chemosphere.2014.04.035
- Carlson, C. A., and Hansell, D. A. (2015). “DOM sources, sinks, reactivity, and budgets,” in *Biogeochemistry of Marine Dissolved Organic Matter*, 2nd Edn, eds D. A. Hansell and C. A. Carlson (San Diego, CA, Academic Press), 66–127.
- Catalá, T. S., Reche, I., Fuentes-Lema, A., Romera-Castillo, C., Nieto-Cid, M., Ortega-Retuerta, E., et al. (2015). Turnover time of fluorescent dissolved organic matter in the dark global ocean. *Nat. Commun.* 6:5986. doi: 10.1038/ncomms6986
- Chen, R. F., and Bada, J. L. (1992). The fluorescence of dissolved organic matter in seawater. *Mar. Chem.* 37, 191–221.
- Coble, P. G. (1996). Characterization of marine and terrestrial DOM in seawater using excitation–emission matrix spectroscopy. *Mar. Chem.* 51, 325–346.
- Coble, P. G. (2007). Marine optical biogeochemistry: the chemistry of ocean color. *Chem. Rev.* 107, 402–418. doi: 10.1021/cr050350+
- Del Vecchio, R., and Blough, N. V. (2004). On the origin of the optical properties of humic substances. *Environ. Sci. Technol.* 38, 3885–3891. doi: 10.1021/es049912h
- Determann, S., Reuter, R., and Wilkomm, R. (1996). Fluorescent matter in the eastern Atlantic Ocean. 2. Vertical profiles and relation to water masses. *Deep Sea Res. I* 43, 345–360.
- Dziedzic, P., Zou, W., Häfren, J., and Córdova, A. (2006). The small peptide-catalyzed direct asymmetric aldol reaction in water. *Org. Biomol. Chem.* 4, 38–40. doi: 10.1039/B515880J
- Feely, R. A., Sabine, C., Schlitzer, R., Bullister, J. L., Mecking, S., and Greeley, D. (2004). Oxygen utilization and organic carbon remineralization in the upper water column of the Pacific Ocean. *J. Oceanogr.* 60, 45–52. doi: 10.1023/B:JOCE.0000038317.01279.aa
- Feely, R. A., Talley, L. D., Johnson, G. C., Sabine, C. L., and Wanninkhof, R. (2005). Repeat hydrography cruises reveal chemical changes in the North Atlantic. *EOS Trans. Am. Geophys. Union* 86, 404–405. doi: 10.1029/2005EO420003
- Gonsior, M., Hertkorn, N., Conte, M. H., Cooper, W. J., Bastviken, D., Druffel, E., et al. (2014). Photochemical production of polyols arising from significant photo-transformation of dissolved organic matter in the oligotrophic surface ocean. *Mar. Chem.* 163, 10–18. doi: 10.1016/j.marchem.2014.04.002
- Granskog, M. A., Stedmon, C. A., Dodd, P. A., Amon, R. M. W., Pavlov, A. K., de Steur, L., et al. (2012). Characteristics of colored dissolved organic matter (CDOM) in the Arctic outflow in the Fram Strait: assessing the changes and fate of terrigenous CDOM in the Arctic Ocean. *J. Geophys. Res.* 117, C12021. doi: 10.1029/2012JC008075
- Green, N. W., Perdue, E. M., Aiken, G. R., Butler, K. D., Chen, H., Dittmar, T., et al. (2014). An intercomparison of three methods for the large-scale isolation of oceanic dissolved organic matter. *Mar. Chem.* 161, 14–19. doi: 10.1016/j.marchem.2014.01.012
- Hansell, D. A. (2002). “DOC in the global ocean carbon cycle,” in *Biogeochemistry of Marine Dissolved Organic Matter*, eds D. A. Hansell and C. A. Carlson (San Diego, CA: Academic Press), 685–715.
- Hansell, D. A. (2013). Recalcitrant dissolved organic carbon fractions. *Annu. Rev. Mar. Sci.* 5, 421–445. doi: 10.1146/annurev-marine-120710-100757
- Hansell, D. A., and Carlson, C. A. (2015). *Biogeochemistry of Marine Dissolved Organic Matter*, 2nd Edn. San Diego, CA, Academic Press.
- Helms, J. R., Stubbins, A., Ritchie, J. C., Minor, E. C., Kieber, D. J., and Mopper, K. (2008). Absorption spectral slopes and slope ratios as indicators of molecular weight, source, and photobleaching of chromophoric dissolved organic matter. *Limnol. Oceanogr.* 53, 955–969. doi: 10.4319/lo.2008.53.3.0955
- Hernes, P. J., and Benner, R. (1996). Terrigenous organic matter sources and reactivity in the North Atlantic Ocean and a comparison to the Arctic and Pacific oceans. *Mar. Chem.* 100, 66–79.
- Jaffe, R., McKnight, D., Maie, N., Cory, R., McDowell, W. H., and Campbell, J. L. (2008). Spatial and temporal variations in DOM composition in ecosystems: the importance of long-term monitoring of optical properties. *J. Geophys. Res.* 113:G04032. doi: 10.1029/2008JG000683
- Jiao, N., Azam, F., and Sanders, S. (eds.). (2011). *Microbial Carbon Pump in the Ocean*. Washington, DC: AAAS.
- Jørgensen, L., Stedmon, C. A., Granskog, M. A., and Middelboe, M. (2014). Tracing the long-term microbial production of recalcitrant fluorescent dissolved organic matter in seawater. *Geophys. Res. Lett.* 41, 2481–2488. doi: 10.1002/2014GL059428
- Jørgensen, L., Stedmon, C. A., Tragh, T., Markager, S., Middleboe, M., and Sondergaard, M. (2011). Global trends in the fluorescence characteristics and distribution of marine dissolved organic matter. *Mar. Chem.* 126, 139–148. doi: 10.1016/j.marchem.2011.05.002
- Lonborg, C., Yokokawa, T., Herndl, G. J., and Alvarez-Salgado, X. A. (2015). Production and degradation of fluorescent dissolved organic matter in surface waters of the eastern north Atlantic ocean. *Deep Sea Res. I* 96, 28–37. doi: 10.1016/j.dsr.2014.11.001
- Maritorena, S., Siegel, D. A., and Peterson, A. R. (2002). Optimization of a semianalytical ocean color model for global-scale applications. *Appl. Optics* 41, 2705–2714. doi: 10.1364/AO.41.002705
- Miller, R. L., Belz, M., Del Castillo, C., and Trzaska, R. (2002). Determining CDOM absorption spectra in diverse coastal environments using a multiple pathlength, liquid core waveguide system. *Continental Shelf Res.* 22, 1301–1310. doi: 10.1016/S0278-4343(02)00009-2
- Murphy, K. R., Stedmon, C. A., Waite, T. D., and Ruiz, G. M. (2008). Distinguishing between terrestrial and autochthonous organic matter sources in marine environments using fluorescence spectroscopy. *Mar. Chem.* 108, 40–58. doi: 10.1016/j.marchem.2007.10.003
- Nelson, N. B., Carlson, C. A., and Steinberg, D. K. (2004). Production of chromophoric dissolved organic matter by Sargasso Sea microbes. *Mar. Chem.* 89, 273–287. doi: 10.1016/j.marchem.2004.02.017
- Nelson, N. B., and Coble, P. G. (2010). “Optical analysis of chromophoric dissolved organic matter,” in *Practical Guidelines for the Analysis of Seawater*, ed O. Wurl (Boca Raton, FL: CRC), 79–96.
- Nelson, N. B., and Siegel, D. A. (2013). The global distribution and dynamics of chromophoric dissolved organic matter. *Annu. Rev. Mar. Sci.* 5, 447–476. doi: 10.1146/annurev-marine-120710-100751
- Nelson, N. B., Siegel, D. A., Carlson, C. A., and Swan, C. M. (2010). Tracing global biogeochemical cycles and meridional overturning circulation using chromophoric dissolved organic matter, *Geophys. Res. Lett.* 37, L03610. doi: 10.1029/2009GL042325
- Nelson, N. B., Siegel, D. A., Carlson, C. A., Swan, C., Smethie, W. M. Jr., and Khatiwala, S. (2007). Hydrography of chromophoric dissolved organic matter in the North Atlantic. *Deep Sea Res. I* 54, 710–731. doi: 10.1016/j.dsr.2007.02.006
- Nelson, N. B., Siegel, D. A., and Michaels, A. F. (1998). Seasonal dynamics of colored dissolved material in the Sargasso Sea. *Deep Sea Res. I* 45, 931–957.
- Nieto-Cid, M., Alvarez-Salgado, X. A., and Pérez, F. F. (2006). Microbial and photochemical reactivity of fluorescent dissolved organic matter in a coastal upwelling system. *Limnol. Oceanogr.* 51, 1391–1400. doi: 10.4319/lo.2006.51.3.1391
- Nozière, B., Dziedzic, P., and Córdova, A. (2007). Formation of secondary light-absorbing “fulvic-like” oligomers: a common process in aqueous and ionic atmospheric particles? *Geophys. Res. Lett.* 34, L21812. doi: 10.1029/2007gl031300
- Ogawa, H., Amagai, Y., Koike, I., Kaiser, K., and Benner, R. (2001). Production of refractory DOC by bacteria. *Science* 292, 917–920. doi: 10.1126/science.1057627
- Preisendorfer, R. W., and Mobley, C. D. (1988). *Principal Component Analysis in Meteorology and Oceanography*. San Diego, CA: Elsevier.
- Rochelle-Newall, E. J., and Fisher, T. R. (2002). Production of chromophoric dissolved organic matter fluorescence in marine and estuarine environments: an investigation into the role of phytoplankton. *Mar. Chem.* 77, 7–21. doi: 10.1016/S0304-4203(01)00072-X
- Schlitzer, R. (2008). *Ocean Data View*. Available online at: <http://odv.awi.de/>

- Shimotori, K., Omori, Y., and Hama, T. (2009). Bacterial production of marine humic-like fluorescent dissolved organic matter and its biogeochemical importance. *Aquat. Microb. Ecol.* 58, 55–66. doi: 10.3354/ame01350
- Siegel, D. A., Maritorena, S., Nelson, N. B., Hansell, D. A., and Lorenzi-Kayser, M. (2002). Global distribution and dynamics of colored dissolved and detrital organic materials. *J. Geophys. Res.* 107, 3228. doi: 10.1029/2001jc000965
- Stedmon, C. A., and Markager, S. (2001). The optics of chromophoric dissolved organic matter (CDOM) in the Greenland Sea: An algorithm for differentiation between marine and terrestrially derived organic matter. *Limnol. Oceanogr.* 46, 2087–2093. doi: 10.4319/lo.2001.46.8.2087
- Stedmon, C. A., and Markager, S. (2005). Tracing the production and degradation of autochthonous fractions of dissolved organic matter by fluorescence analysis. *Limnol. Oceanogr.* 50, 1415–1426. doi: 10.4319/lo.2005.50.5.1415
- Stedmon, C. A., Markager, S., and Bro, R. (2003). Tracing dissolved organic matter in aquatic environments using a new approach to fluorescence spectroscopy. *Mar. Chem.* 82, 239–254. doi: 10.1016/S0304-4203(03)00072-0
- Stedmon, C. A., and Nelson, N. B. (2015). “The optical properties of DOM in the ocean,” in *Biogeochemistry of Marine Dissolved Organic Matter*, 2nd Edn, eds D. A. Hansell and C. A. Carlson (San Diego, CA, Academic Press), 481–508.
- Steinberg, D. K., Nelson, N., Carlson, C. A., and Prusak, A. C. (2004). Production of chromophoric dissolved organic matter (CDOM) in the open ocean by zooplankton and the colonial cyanobacterium *Trichodesmium* spp. *Mar. Ecol. Prog. Ser.* 267, 45–56. doi: 10.1016/j.dsr.2012.01.008
- Suksomjit, M., Nagao, S., Ichimi, K., Yamada, T., and Tada, K. (2009). Variation of dissolved organic matter and fluorescence characteristics before, during and after Phytoplankton Bloom. *J. Oceanogr.* 65, 835–846. doi: 10.1007/s10872-009-0069-x
- Swan, C. M., Nelson, N. B., and Siegel, D. A. (2012). The effect of surface irradiance on the absorption spectrum of chromophoric dissolved organic matter in the global ocean. *Deep Sea Res. I* 63, 52–64. doi: 10.1016/j.dsr.2012.01.008
- Swan, C. M., Siegel, D. A., Nelson, N. B., Carlson, C. A., and Nasir, E. (2009). Biogeochemical and hydrographic controls on chromophoric dissolved organic matter in the Pacific Ocean. *Deep Sea Res. I* 56, 2172–2192. doi: 10.1016/j.dsr.2009.09.002
- Urban-Rich, J., McCarty, J. T., Fernandez, D., and Acuna, J. L. (1996). Larvaceans and copepods excrete fluorescent dissolved organic matter (FDOM). *J. Exp. Mar. Biol. Ecol.* 332, 96–105.
- Yamashita, Y., Lu, C.-J., Ogawa, H., Nishioka, J., Obata, H., and Saito, H. (2015). Application of an *in situ* fluorometer to determine the distribution of fluorescent organic matter in the open ocean. *Mar. Chem.* 177, 298–305. doi: 10.1016/j.marchem.2015.06.025
- Yamashita, Y., and Tanoue, E. (2003). Chemical characterization of protein-like fluorophores in DOM in relation to aromatic amino acids. *Mar. Chem.* 82, 255–271. doi: 10.1016/S0304-4203(03)00073-2
- Yamashita, Y., and Tanoue, E. (2008). Production of bio-refractory fluorescent dissolved organic matter in the ocean interior. *Nat. Geosci.* 1, 579–582. doi: 10.1038/ngeo279
- Yamashita, Y., and Tanoue, E. (2009). Basin scale distribution of chromophoric dissolved organic matter in the Pacific Ocean. *Limnol. Oceanogr.* 54, 598–609. doi: 10.4319/lo.2009.54.2.0598
- Zepp, R., Sheldon, W. M., and Moran, M. A. (2004). Dissolved organic fluorophores in southeastern US coastal waters: correction method for eliminating Rayleigh and Raleigh scattering peaks in excitation – emission matrices. *Mar. Chem.* 89, 15–36. doi: 10.1016/j.marchem.2004.02.006

Conflict of Interest Statement: The authors declare that the research was conducted in the absence of any commercial or financial relationships that could be construed as a potential conflict of interest.

Copyright © 2016 Nelson and Gauglitz. This is an open-access article distributed under the terms of the Creative Commons Attribution License (CC BY). The use, distribution or reproduction in other forums is permitted, provided the original author(s) or licensor are credited and that the original publication in this journal is cited, in accordance with accepted academic practice. No use, distribution or reproduction is permitted which does not comply with these terms.



From Fresh to Marine Waters: Characterization and Fate of Dissolved Organic Matter in the Lena River Delta Region, Siberia

Rafael Gonçalves-Araujo^{1,2*}, Colin A. Stedmon³, Birgit Heim⁴, Ivan Dubinenkov^{2,5},
Alexandra Kraberg⁶, Denis Moiseev⁷ and Astrid Bracher^{1,8}

¹ PHYTOOPTICS Group, Physical Oceanography of Polar Seas, Climate Sciences, Alfred Wegener Institute for Polar and Marine Research, Bremerhaven, Germany, ² Faculty of Biology and Chemistry (FB-2), University of Bremen, Bremen, Germany, ³ Section for Marine Ecology and Oceanography, National Institute for Aquatic Resources, Technical University of Denmark, Charlottenlund, Denmark, ⁴ Periglacial Research, Geosciences, Alfred Wegener Institute for Polar and Marine Research, Potsdam, Germany, ⁵ Ecological Chemistry, Biosciences, Alfred Wegener Institute for Polar and Marine Research, Bremerhaven, Germany, ⁶ Shelf Sea System Ecology, Biosciences, Biologische Anstalt Helgoland, Alfred Wegener Institute for Polar and Marine Research, Helgoland, Germany, ⁷ Murmansk Marine Biological Institute of Kola Science Centre, Russian Academy of Sciences, Murmansk, Russia, ⁸ Institute of Environmental Physics, University of Bremen, Bremen, Germany

OPEN ACCESS

Edited by:

Christopher Osburn,
North Carolina State University, USA

Reviewed by:

Karin M. Björkman,
University of Hawaii, USA
John Robert Helms,
Morningside College, USA

*Correspondence:

Rafael Gonçalves-Araujo
rafael.goncalves.araujo@awi.de;
rafaelgoncalvesaraudo@gmail.com

Specialty section:

This article was submitted to
Marine Biogeochemistry,
a section of the journal
Frontiers in Marine Science

Received: 30 September 2015

Accepted: 23 November 2015

Published: 16 December 2015

Citation:

Gonçalves-Araujo R, Stedmon CA,
Heim B, Dubinenkov I, Kraberg A,
Moiseev D and Bracher A (2015) From

Fresh to Marine Waters:
Characterization and Fate of Dissolved
Organic Matter in the Lena River Delta
Region, Siberia.

Front. Mar. Sci. 2:108.
doi: 10.3389/fmars.2015.00108

Connectivity between the terrestrial and marine environment in the Arctic is changing as a result of climate change, influencing both freshwater budgets, and the supply of carbon to the sea. This study characterizes the optical properties of dissolved organic matter (DOM) within the Lena Delta region and evaluates the behavior of DOM across the fresh water-marine gradient. Six fluorescent components (four humic-like; one marine humic-like; one protein-like) were identified by Parallel Factor Analysis (PARAFAC) with a clear dominance of allochthonous humic-like signals. Colored DOM (CDOM) and dissolved organic carbon (DOC) were highly correlated and had their distribution coupled with hydrographical conditions. Higher DOM concentration and degree of humification were associated with the low salinity waters of the Lena River. Values decreased toward the higher salinity Laptev Sea shelf waters. Results demonstrate different responses of DOM mixing in relation to the vertical structure of the water column, as reflecting the hydrographical dynamics in the region. Two mixing curves for DOM were apparent. In surface waters above the pycnocline there was a sharper decrease in DOM concentration in relation to salinity indicating removal. In the bottom water layer the DOM decrease within salinity was less. We propose there is a removal of DOM occurring primarily at the surface layer, which is likely driven by photodegradation and flocculation.

Keywords: DOC, CDOM, FDOM, PARAFAC, optical indices, hydrography, Laptev Sea, Arctic

INTRODUCTION

Colored or chromophoric dissolved organic matter (CDOM) is the fraction of DOM that absorbs light and it is one of the dominant components influencing the underwater light field in coastal and inner-shelf waters (Siegel et al., 2002; Nelson and Siegel, 2013). CDOM absorbs light in the ultraviolet (UV) and visible wavelength ranges and thus it is able to shield aquatic biota from harmful UV radiation (Arrigo and Brown, 1996) and can be detected by ocean color remote sensing

(Siegel et al., 2002, 2005). As a result of its UV absorbing properties, CDOM is susceptible to photodegradation, which either induces direct mineralization or produces microbiologically labile low molecular weight compounds, which are subsequently utilized by bacteria (Mopper and Kieber, 2002). Fluorescent DOM (FDOM), which is the part of CDOM able to fluoresce, can be used to trace the supply, mixing, and removal of different fractions of DOM (Yamashita and Tanoue, 2003, 2004; Coble, 2007; Chari et al., 2013; Fukuzaki et al., 2014). With the recent adaptation of the Parallel Factor Analysis (PARAFAC) for analysis of DOM, a more holistic analysis of excitation-emission matrices (EEMs) allows for the differentiation of wider range of underlying DOM components (Stedmon and Bro, 2008). A recent study showed significant associations between molecular groups and PARAFAC-derived DOM components (Stubbins et al., 2014). For instance, the humic-like fluorescent peak A (e.g., Coble, 2007) is associated with high molecular weight compounds with little nitrogen, whereas the humic-like peak C correlated to lignin-derived phenols and the amino acid-like peak T was associated to low molecular weight and aromatic content compounds, such as hydrolysable amino acids (Stubbins et al., 2014).

By applying the EEMs/PARAFAC technique, the distribution and dynamics of fluorescent DOM have been studied in a wide range of environments varying from lakes (Zhang et al., 2009), estuaries (Stedmon and Markager, 2005; Singh et al., 2010), coastal and shelf (Murphy et al., 2008; Kowalcuk et al., 2010; Para et al., 2010) to pelagic waters (Yamashita et al., 2010; Jørgensen et al., 2011; Kowalcuk et al., 2013). In coastal regions, especially in areas close to river outflows, the riverine input, and its mixing with marine waters are the major factors controlling the distribution and composition of DOM (Stedmon and Markager, 2003; Guo et al., 2007; Alling et al., 2010). In these waters processes such as photobleaching (Opsahl and Benner, 1998; Stubbins et al., 2006; Helms et al., 2008, 2014; Porcal et al., 2013, 2015), sorption to sediments, flocculation (Uher et al., 2001; Shank et al., 2005; Guo et al., 2007; von Wachenfeldt et al., 2008; Asmala et al., 2014), biological uptake (Boyd and Osburn, 2004), biological release (Romera-Castillo et al., 2010), and photo-production of DOM (Helms et al., 2014) can also play a crucial role in controlling the amount, composition, and reactivity of DOM in these environments.

The Arctic Ocean receives considerable input of terrigenous carbon mobilized from high latitude carbon-rich soils and peatlands (Opsahl et al., 1999; Benner et al., 2004). This terrigenous material is supplied by Arctic rivers, which account for more than 10% of the total riverine and terrestrial organic carbon into the global ocean waters (Opsahl et al., 1999; Benner et al., 2004). Among those rivers, the Lena River (eastern Siberia) accounts for the highest annual DOM discharge into the Arctic Ocean (Raymond et al., 2007; Stedmon et al., 2011), with a peak discharge in June (Amon et al., 2012; Fedorova et al., 2015). It contributes approximately 20% to the total fresh water discharge into the Arctic Ocean through its delta into the Laptev Sea (Cauwet and Sidorov, 1996). The Lena Delta and the Laptev Sea inner shelf encompass a large, shallow environment characterized by pronounced physical-chemical gradients (Bauch et al., 2009;

Fofanova et al., 2014) and considerable amounts of sediments, dissolved, and particulate organic matter over the water column (Semiletov et al., 2011; Vonk et al., 2012, 2014; Wegner et al., 2013; Heim et al., 2014; Sánchez-García et al., 2014). Eastern Siberia (including the Lena River and its delta) is known to be affected by global warming with a thawing permafrost (Yang et al., 2002; Schuur et al., 2008), which subsequently affects the fresh water discharge, the production of DOM in river catchments and the riverine transport of organic material input into the shelf seas (Frey and McClelland, 2009; Lyon and Destouni, 2010; Semiletov et al., 2012, 2013; Vonk et al., 2012, 2014; Sánchez-García et al., 2014; Fedorova et al., 2015).

The Lena Delta region and Laptev Sea have high DOC concentrations ($>500 \mu\text{M}$) and high CDOM associated with low salinity waters (Alling et al., 2010; Stedmon et al., 2011; Semiletov et al., 2013; Walker et al., 2013; Heim et al., 2014; Dubinenkov et al., 2015a), decreasing toward higher salinities through conservative mixing (Cauwet and Sidorov, 1996; Kattner et al., 1999). This is a characteristic also thought to be shared by other Arctic rivers (Dittmar and Kattner, 2003). However, a recent study has indicated non-conservative mixing of DOC within the Lena Delta region, with average losses of 30–50% during mixing along the shelf (Alling et al., 2010). These authors also identified additional sources of DOC in the region (such as primary production and coastal erosion), and pointed out photodegradation, flocculation, sedimentation, and microbial activity as possible processes to be responsible for the removal of DOC and humic substances, although currently poorly resolved. Rectifying this is difficult due to not only the remoteness of the location but also because there is a lack of information on the composition, amount, reactivity, and fate of DOM in these waters. Despite the recent techniques applied for DOM analysis and the advances in the knowledge of the dynamics and composition of DOM in some aquatic environments, there is still a considerable lack of information on this important component of the global carbon pool. This is particularly compounded when accounting for the composition and processes modulating the distribution and reactivity of DOM in the Arctic regions. Hence, further studies addressing these issues are essential for a better understanding of the role of DOM in the carbon cycle within the aquatic environments, especially the Arctic Ocean.

In this study DOM characteristics within the Lena Delta region based on fluorescent properties was investigated. The distribution and transformation of the DOM along the fresh water-marine gradient were investigated, using samples collected in September 2013 at the Lena Delta region in the southern Laptev Sea. The findings provide an insight into the fate of Arctic riverine DOM while it is mixed at the shelf with the waters from the Laptev Sea.

MATERIALS AND METHODS

Sampling

The Lena Expedition was conducted in late summer 2013 (1–7 September) on board the Russian R/V “*Dalnie Zelentsy*” of the Murmansk Marine Biological Institute, in the surrounding

areas of the Lena River Delta region, Laptev Sea, Siberia. A total of 18 oceanographic stations were occupied and split into four transects (**Figure 1A**). The hydrographic characteristics of the water column were assessed from vertical profiles acquired with a CTD-profiler SEACAT SBE 19+. Prior to the cruise, temperature, conductivity, and pressure sensors were calibrated at laboratories of the All-Russia D. I. Mendeleyev Scientific and Research Institute for Metrology. Water samples were taken using Niskin bottles at surface and discrete depths chosen based on CTD profiles. The amount of samples per profile and station varied according to the local depth, ranging from two samples at shallow water (<5 m) and six samples at deeper water stations (e.g., 20–35 m). The full data set used to compose this work is available online in two published datasets (Dubinenkov et al., 2015b; Gonçalves-Araujo et al., 2015a).

Water Column Structure Assessment

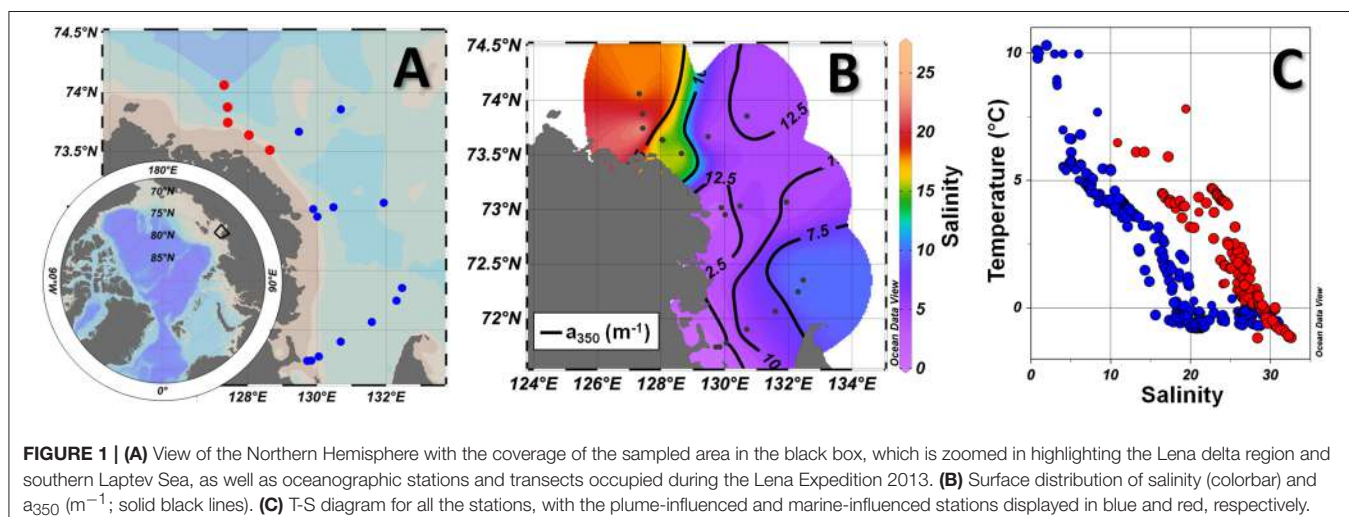
To assess the structure of the water column, vertical profiles of temperature and salinity from the CTD casts were used to obtain potential water density (ρ) profiles. The depth where variations in density were equal or greater than 0.125 kg m^{-3} over a 5-m depth interval was considered the upper mixed layer depth (UMLD), as adapted from Levitus (1982) and Kara et al. (2000a). The bottom depth was adopted as UMLD for inner shelf stations with vertically mixed profiles. The water column stability parameter (E) was obtained from vertical density variations assessed by the buoyancy or Brunt-Väisälä frequency (N^2), which is defined by $N^2 = \frac{g}{\rho} \frac{\partial \rho}{\partial z}$ (rad 2 s $^{-2}$) leading to $E = \frac{N^2}{g}$ (10 $^{-8}$ rad 2 m $^{-1}$), where g is gravity. The maximum stability immediately below the UMLD was considered to represent the strength of the pycnocline/stratification (Gonçalves-Araujo et al., 2015b; and references therein).

DOC and DOM Sample Processing and Data Analysis

Water samples for DOC analysis were filtered through 0.7 μm GF/F filters (Whatman, pre-combusted, 4 h, 450°C) and dark

stored in a freezer until further analysis in the laboratory. DOC concentrations were measured using high temperature catalytic oxidation (TOC-VCPN, Shimadzu). For external calibration of the instrument potassium hydrogen phthalate (KHP, Merck) was used. All samples were acidified (0.1 M HCl suprapur, Merck) and purged with O₂ for >5 min. Performance of the instrument was recorded by daily analysis of in-lab KHP standard solutions and reference samples (deep sea reference, DSR, Hansell research lab). The instrument blank was ~2 μM C and quality of analysis was monitored continuously based on results of DSR reference samples.

The samples for CDOM analysis were immediately syringe-filtered after sampling with Whatman Spartan 13 filters (0.2 μm) and then stored in amber glass bottles (100 mL) and kept cooled in the fridge (4°C) until further analysis. Before analysis, the samples were mixed and filtered once more through Whatman Spartan 13 syringe filters (0.2 μm). Fluorescence EEMs were collected using an Aqualog® fluorescence spectrometer (HORIBA Jobin Yvon, Germany). Freshly produced Milli-Q water was used as reference. Fluorescence intensity was measured across emission wavelengths 220–620 nm (resolution 1.77 nm, 4 pixel) at excitation wavelengths from 240 to 600 nm with 3 nm increments, and an integration time of 2 s. The blank-corrected absorbance spectra was converted into Napierian absorption coefficient (a) at each wavelength (λ), using the given equation: $a_{\lambda}(m^{-1}) = (2.303 \times A_{\lambda})/L$, where A_{λ} is the absorbance at specific wavelength and L is the cuvette path length in meters. The absorption coefficients in the visible (440 nm— a_{440}) and UV (350 nm— a_{350}) bands are generally adopted as indicators of CDOM magnitude. Although many studies have presented their results using the absorption coefficient at 440 nm (a_{440}) due to its application to ocean color remote sensing (e.g., Siegel et al., 2005; Heim et al., 2014), in this study we determined the absorption coefficients in both visible (a_{440}) and UV (a_{350}) ranges. Nevertheless, we focus our results and discussions on the a_{350} coefficient because of its correlations to DOC and lignin concentrations and to permit comparison



with earlier results (Spencer et al., 2009; Stedmon et al., 2011; Walker et al., 2013). The raw EEMs acquired with Aqualog® were corrected for inner-filter effects and for the Raman and Rayleigh scattering (Murphy et al., 2013). The different fluorescent components of DOM were isolated from combined signal by PARAFAC modeling using the “drEEM Toolbox” and following the recommendation of Murphy et al. (2013). The DOM components derived from PARAFAC modeling were compared with PARAFAC components from other studies through the OpenFluor database (Murphy et al., 2014). The complete absorption and emission spectra of the fluorescent components derived from PARAFAC are available on the OpenFluor database after publication (<http://www.openflour.org>). We have estimated the hypothetical conservative mixing of DOM (i.e., a_{350} , DOC, and fluorescence intensity of each of the PARAFAC components) by considering the average of two values of the respective parameter at the highest and at the lowest salinity extremities, respectively, as the end points of the conservative line.

DOM Modification Indices, Statistical Analyses, and Graphical Tools

Besides the determination of the magnitude and characterization of DOM components, the optical characteristics of CDOM and FDOM can also be used to assess the origin and degree of transformation of DOM through the calculation of optical indices. By applying an exponential function to the 275–295 nm spectral range it is possible to derive the spectral slope of absorption spectra ($SCDOM$, in μm^{-1}) that varies in relation to the source of CDOM. It has also been shown to be inversely correlated with the molecular weight of DOM and can be related to photobleaching (Helms et al., 2008; Fichot and Benner, 2012; Fichot et al., 2013). The specific UV absorbance (SUVA) is used as a proxy for the degree of aromaticity in CDOM samples (Weishaar et al., 2003) and it is defined by $SUVA = A_{254}/[\text{DOC}]$, where A_{254} is the absorbance at 254 nm and the concentration of DOC, $[\text{DOC}]$, is measured in mg CL^{-1} . Due to the high absorption of aromatic compounds in the UV-visible, higher SUVA values indicate higher aromaticity from allochthonous input (e.g., humic compounds), while lower SUVA values are associated to more autochthonous or modified terrestrial CDOM with lower aromaticity (Weishaar et al., 2003).

Two optical indices, that take FDOM into account, were also used to investigate both the degree of humification and biological degradation of the DOM. The humification index (HIX) estimates the degree of maturation of DOM (Zsolnay et al., 1999; Zsolnay, 2003), considering that humification is associated with an increase in the C/H ratio (Stevenson, 1982) and is thus reflected in emissions at longer wavelengths (Senesi et al., 1991). The HIX index is the ratio of the areas of two spectral wavelength regions in the emission spectra for an excitation at 254 nm and it is obtained as: $HIX = H/L$, where H is the area between 435 and 480 nm in the emission spectra and L is the area in the emission spectra between 300 and 345 nm (Zsolnay et al., 1999). An increase in the degree of aromaticity (humification) leads to a red shift in the emission spectrum, which will be associated with higher HIX values. The biological/autochthonous index (BIX) is

used to assess the biological modification of DOM based on UV fluorescence. The BIX index is obtained by calculating the ratio of the emission at 380 and 430 nm, excited at 310 nm: $BIX = I_{Em380}/I_{Em430}$ (Huguet et al., 2009). High BIX values correspond to autochthonous origin of DOM, i.e., freshly released DOM, whereas low BIX values indicate allochthonous DOM (Huguet et al., 2009).

The relationships between all pairs of variables were investigated using Spearman correlation coefficients. To compare the variables among themselves or among different groups of samples, Kruskal–Wallis H tests were applied, after performing normality tests. Furthermore, the relationship between each pair of variables was determined based on linear regressions.

RESULTS

Hydrography and Water Column Structure

Pronounced environmental variability was observed within the studied region, with sampling varying from fresh to marine waters, as demonstrated by the noticeable hydrographical gradients in the T-S diagram (Figure 1C). Salinity varied between 0.90 and 32.63, with the lowest values associated with fresh water input from the Lena River and plume (Figures 1B,C). Temperature ranged from -1.2 to 10.3°C, with higher values related to the warmer and fresher Lena river plume and the lowest values attributed to the presence of the colder and saltier Laptev Sea shelf waters. In addition, a strong horizontal frontal zone was found within the NW portion of the study area, with the isohaline of 10 depicting the surface limit between two hydrographic provinces observed: the sites under direct influence of fresher Lena River plume and the sites under influence of the saltier waters from the Laptev Sea shelf (Figures 1A,B), hereafter named as plume- and marine-influenced stations. Note that, although named marine-influenced stations, those sites were still under influence of the continental fresh water input, however less than the plume-influenced ones, given the still low salinity observed at surface (varying from 13.21 to 25.60; Figure 1B).

A low salinity surface layer generated by the influence of the fresh waters from the Lena River was observed along the entire sampled area (Figure 1). The occupation of the surface layer by the river plume leads to the establishment of an upper mixed layer of ~10 m and a pronounced vertical gradient of density. Nevertheless, a few shallower stations (<5 m deep) close to the main outflows of the Lena River (Bykovskaya and Trofimovskaya) were characterized by vertically mixed profiles with very low salinity (<3) waters from the Lena plume. The stability parameter (E) was obtained for all the stations where a vertical stratification was observed. The strength of the pycnocline was inversely related to the surface salinity ($r^2 = 0.82$; $p < 0.01$). Thus, the plume-influenced stations exhibited a greater stratification in comparison to the marine-influenced ones, with averaged E -values of about $7.01 \pm 2.84 \times 10^{-8}$, $4.32 \pm 1.79 \times 10^{-8}$, and $3.98 \pm 1.80 \times 10^{-8} \text{ rad}^2 \text{ m}^{-1}$ for stations located at the inner-plume (surface salinity<5), outer-plume (5<surface salinity<10) and marine-influenced stations (surface salinity>10), respectively).

CDOM and DOC Spatial Variability

CDOM displayed a distribution tightly coupled with salinity (see Figures 1B, 2). a_{350} ranged from 0.9 to 15.7 m^{-1} (Figure 2) and showed a significant negative correlation with salinity [$a_{350} = -0.377(\text{salinity}) + 12.774$; $r^2 = 0.96$; $p < 0.0001$]. The highest a_{350} values were observed within the fresher waters under the influence of the Lena plume with a decrease in a_{350} toward the saltier waters from the Laptev Sea. DOC ranged from 110 to $732 \mu\text{M}$ and was highly correlated to a_{350} [DOC = $38.529(a_{350}) + 106.889$; $r^2 = 0.99$; $p < 0.0001$], exhibiting a very similar behavior as CDOM across the salinity gradient [DOC = $-14.878(\text{salinity}) + 605.236$; $r^2 = 0.96$; $p < 0.0001$] (Figure 2). Additionally, a_{440} varied between 0.12 and 2.97 m^{-1} and it was significantly highly correlated to a_{350} [$a_{350} = 5.188(a_{440}) + 0.361$; $r^2 = 0.99$; $p < 0.0001$] and DOC [DOC = $199.057(a_{440}) + 121.760$; $r^2 = 0.98$; $p < 0.0001$].

When taking into account the relationship between DOM and salinity for each of the hydrographic provinces separately, some features/patterns become clear (Figures 2, 3): a higher DOM amount is associated to the plume-influenced sites; a steeper curve is exhibited by samples above the pycnocline in relation to the samples below it; and there is low variability in DOM along the pycnocline itself. In addition, the a_{350} vs. salinity curve above the pycnocline displayed by the plume-influenced sites was even steeper than the same curve for the marine-influenced sites (Figure 3). Overall, a non-conservative behavior

is observed in the low salinity, surface layer (given the deviation in relation to the hypothetical conservative mixing line) with an indication of removal of DOM (deviating up to 56% from the hypothetical conservative mixing line). That deviation decreases at the underlying layer, suggesting a conservative mixing of DOM in those waters (see Figures 2, 3).

FDOM Components by PARAFAC

Six fluorescent components (C1-C6) were identified by the PARAFAC model (Figure 4). Four components had broad emission and excitation spectra, with emission maxima at visible wavelengths typical of humic-like material (C1, C2, C4, and C5). C3 and C6 had comparably narrow UVA emission maxima. The fluorescence intensity of the components differed greatly, with C1 having the greatest values (reaching up to 2.08 nm^{-1}) and C6 the lowest (up to 0.18 nm^{-1} ; Figure 4). The humic-like components C1 and C2 were the dominant fluorescent signals, accounting for more than 50% of total FDOM in all the samples. The humic-like contribution to total FDOM reached up to 86% at low salinity (see colorbar in Figure 5), and was inversely related to salinity ($p < 0.0001$). C1, C2, C3, and C4 presented a similar scattered pattern in relation to salinity. A steeper curve at low salinity (< 10) suggests removal in that layer, whereas a less steep curve fit at high salinity (> 10) indicates the presence of a conservative mixing (Figure 4, right panel). Although being likewise inversely correlated with salinity, C5 and C6 presented distinct patterns

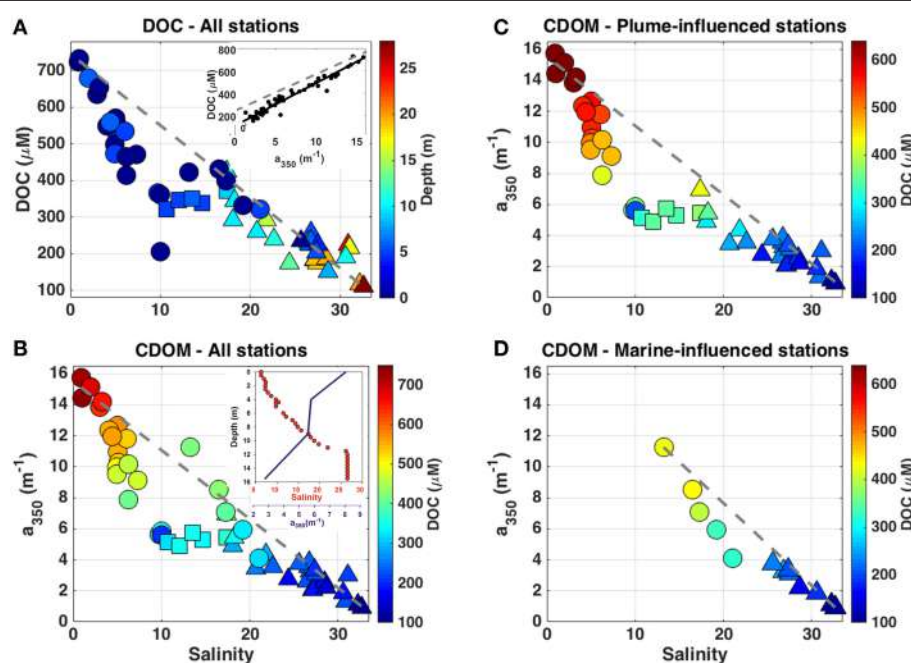


FIGURE 2 | (A) DOC (μM) against salinity and depth for all the samples related to this study (m; colorbar). **(B)** a_{350} (m^{-1}) against salinity and DOC for the entire dataset used in this study (μM ; colorbar), which was split into two subsets regard to the hydrographical conditions: the plume-influenced stations **(C)** and the marine-influenced stations **(D)** that are plotted against salinity and DOC (μM ; colorbar). In all the plots, samples above the pycnocline are displayed as circles, samples at the pycnocline as squares, and samples below the pycnocline are displayed as triangles. Gray dashed-lines indicate the hypothetical conservative mixing line between DOM (or DOC) and salinity. Inset graph in **(A)** shows the relationship between a_{350} (m^{-1}) and DOC (μM) and the dashed line shows the fit exhibited for the coastal Canadian Arctic (Walker et al., 2009). Inset graph in **(B)** exhibits vertical distribution of salinity (red dots) and a_{350} (m^{-1} ; blue line) for one typical plume-influenced station.

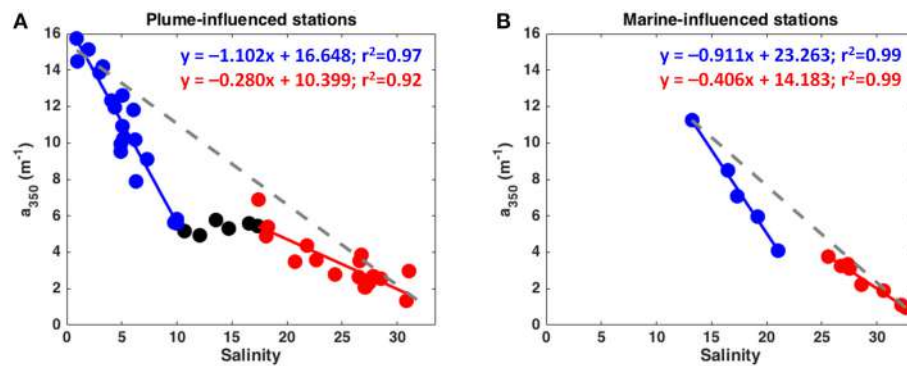


FIGURE 3 | a_{350} against salinity plot for the Plume-influenced (A) and Marine-influenced (B) stations. Samples above the pycnocline are displayed in blue whereas the ones below it are presented in red. Samples located at the pycnocline are displayed in black. All the fits presented in this figure are significant ($p < 0.0001$). Gray dashed-lines indicate the hypothetical conservative mixing line between DOM and salinity for each of the plots.

when compared to the other components (Figure 4). Both components exhibited a non-conservative mixing, however with indication of release/production during the transit from the river to the outer shelf (Figure 4, right panel).

Optical Indices of DOM Modification

Different optical indices including S_{CDOM} , SUVA, HIX, and BIX indices (in Figure 5 shown in relation to salinity), as well as the slope ratio (S_{Ratio} ; Helms et al., 2008) and the fluorescence index (FI; McKnight et al., 2001; not shown) were evaluated within all samples. All indices, except S_{Ratio} ($p > 0.05$), were significantly correlated with salinity, a_{350} , DOC and FDOM, and by that also to each other ($p < 0.0001$). Although it was not significantly correlated to salinity ($p > 0.05$), the S_{Ratio} indicated a dominance of terrigenous signal over the entire sample area, given that most of the samples (~93%) presented S_{Ratio} values below 1 (Figure 5E). In addition, the lack of significance between S_{Ratio} and salinity might be due to an increase in the signal-to-noise ratio for the absorbance spectra at wavelengths longer than 350 nm observed in samples at higher salinity that, in turn, presented the greatest variability in S_{Ratio} values. S_{CDOM} ranged from 15.5 to $21.4 \mu\text{m}^{-1}$ and was directly related to salinity (Figure 5A), suggesting a decrease in the molecular weight with increased salinity (Helms et al., 2008). The values observed for the SUVA index were high, ranging from 1.33 to $4.80 \text{ m}^2 \text{ g}^{-1}$, and was inversely related to salinity ($p < 0.0001$), evidencing a decrease in the aromaticity of the molecules toward high salinity (Figure 5B). The HIX index values ranged from 3.4 to 16.6, and the BIX index values were lower than 0.73 (Figures 5C,D, respectively), indicating a high degree of humification and low autochthonous contribution within our sample set, respectively. Moreover, HIX and BIX showed a decrease (increase) in the degree of humification (DOM from biological activity) with increase in salinity, given the significant relationship ($p < 0.0001$) displayed by those indices and salinity (Figures 5C,D). FI presented values below 1.3 and was inversely related ($p < 0.0001$) to salinity (not shown), indicating a consistent predominance of terrestrial sources of DOM to the region.

DISCUSSION

Characterization and Transformation of DOM

The results characterize the DOM composition (here using the EEM/PAFARAC approach and optical indices of DOM modification) along the fresh water-marine gradient within the Lena delta region and Laptev Sea. Four of the six fluorescent components identified by PARAFAC analysis, three humic-like (C1, C2, and C5) and one protein-like (C6; see Figure 4-center), were already reported in the Lena River and in other large Arctic rivers (Walker et al., 2013). In addition, a recent study reported the presence of three of those components (C1, C2, and C6) in the Amerasian basin (Guéguen et al., 2015), which seem to be common components of the Arctic DOM pool. Although, our sampling was carried out during a period of mid discharge flow (Stedmon et al., 2011), C1 and C2 presented similar fluorescence intensities to the average observed for the Lena River during the discharge peak (~1.6 and 0.9 nm^{-1} , respectively; Walker et al., 2013). C5 and C6, on the other hand, presented intensities close to the average observed in the Lena during the mid discharge flow (see Figure 4-right column; Walker et al., 2013). Our results demonstrate that the FDOM composition in the Lena Delta region was mainly characterized by the dominance of riverine humic-like compounds. This is evidenced by the high contribution of the allochthonous humic-like components with fluorescence in the visible range (C1, C2, C4, and C5) observed in relation to the total FDOM (Figure 4), as well as by the optical indices of DOM modification (Figure 5). A recent study has identified PARAFAC components similar to our humic-like C1 (also referred in the literature as the classical peak C) and C4, which presented strong correlation to lignin phenol concentrations (Yamashita et al., 2015). Dominance of humic-like compounds has been already reported in the Lena Delta in late summer 1995, when high concentrations of lignin, and high contribution of terrigenous DOC (about 60% of total DOC) were observed (Kattner et al., 1999). The humic-like component 1 is a dominant component of the FDOM signal not only in the Lena River and Delta, but it has also been found to be

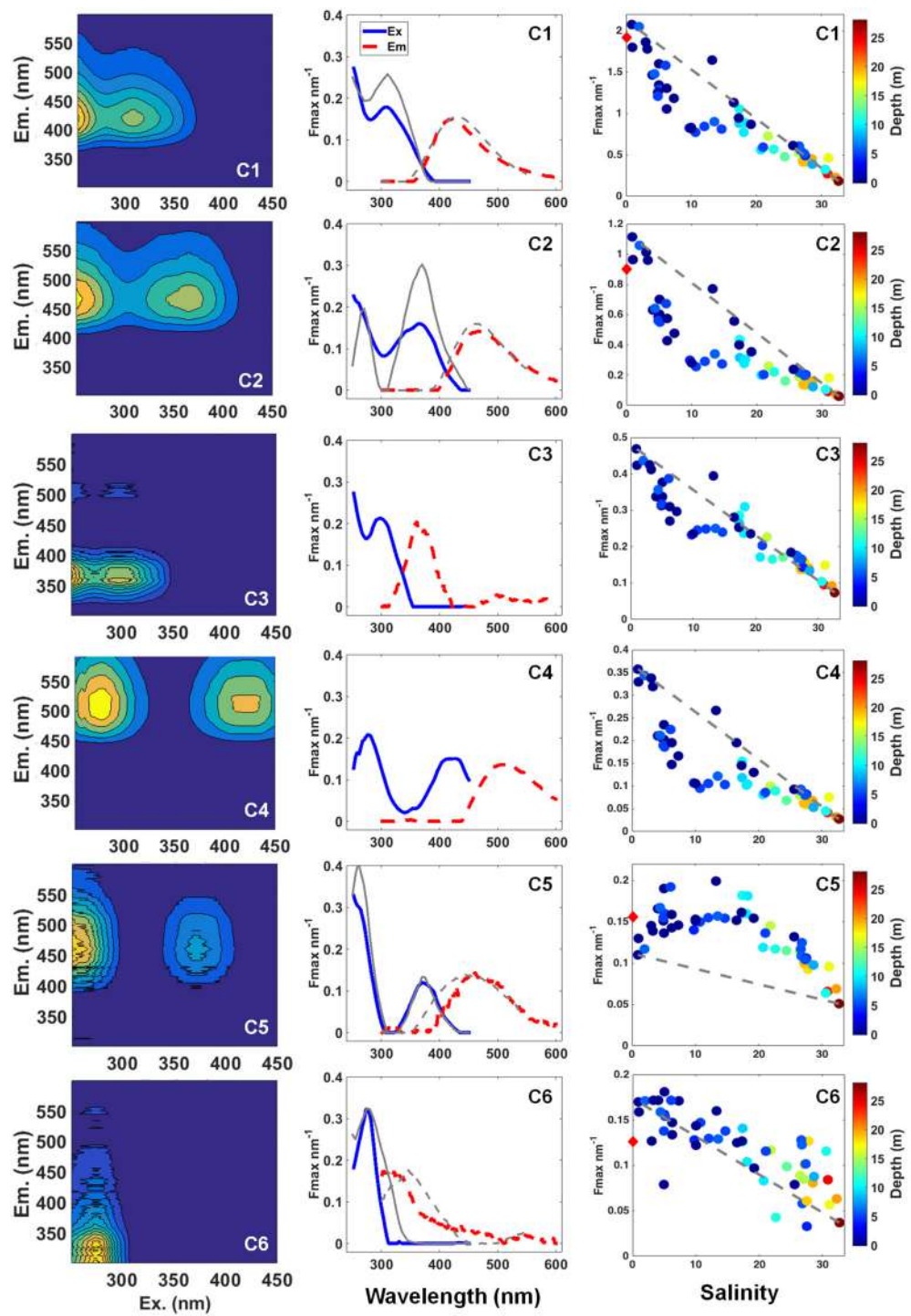


FIGURE 4 | Three-dimensional fluorescence landscapes (left), the excitation (solid line) and emission (dashed line) spectra (center), and F_{max} (nm^{-1}) against salinity and depth (m; right) for each of the six fluorescent components identified by PARAFAC model for all the samples. Gray lines displayed in components spectra graphs (center) show the spectra for components previously found in the major Arctic Rivers (Walker et al., 2013). Gray dashed-lines in F_{max} against salinity plots (right) indicate the hypothetical conservative mixing line between each of the components and salinity. Red diamonds in y-axis indicate averaged F_{max} values for similar components found in the Lena River during periods of peak discharge (for C1 and C2) and mid flow (for C5 and C6; Walker et al., 2013).

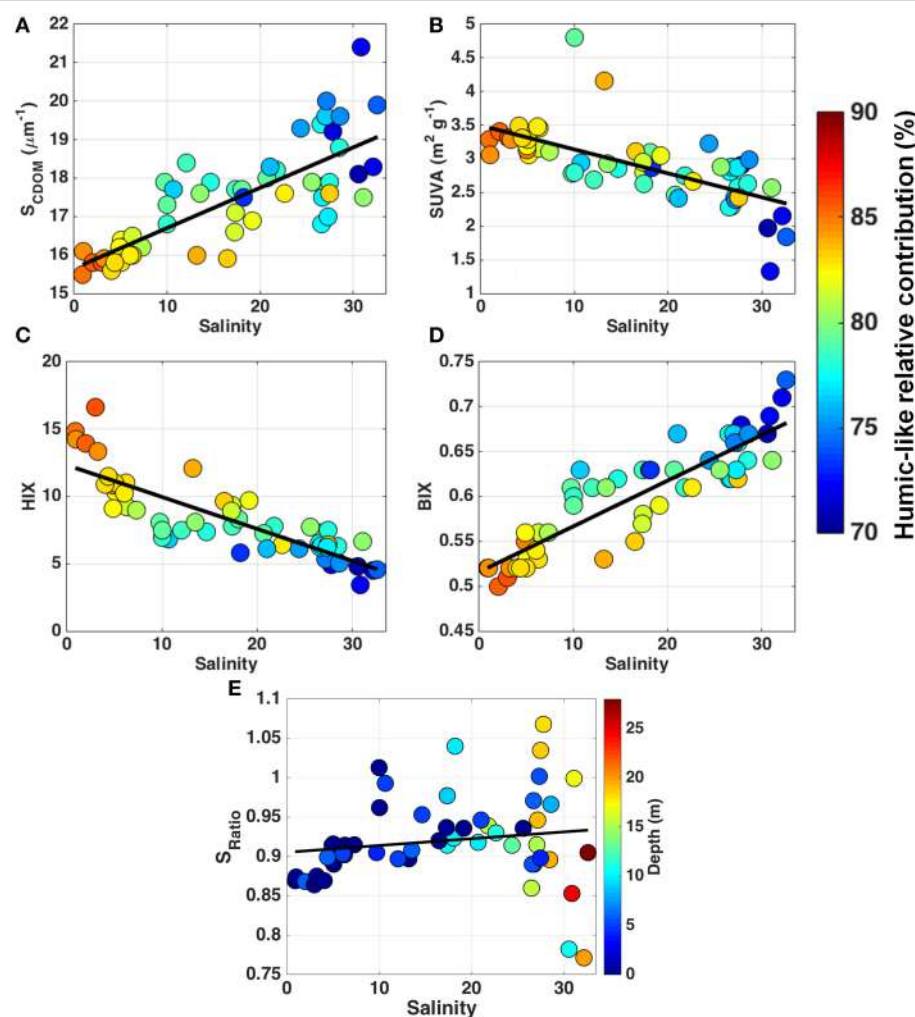


FIGURE 5 | The relationship between the optical indices of DOM modification and salinity for all the samples: S_{CDOM} (μm^{-1}) (A); SUVA ($\text{m}^2 \text{g}^{-1}$) (B); HIX (C); BIX (D); Slope ratio (E). Colorbar indicates the relative contribution (%) of the humic-like signal (C1+C2+C4+C5) to the total FDOM (A–D) and depth (m; E). Black lines indicate the regression lines between each parameter and salinity.

dominant in other Arctic rivers such as Mackenzie, Kolyma, Ob, and Yenisei (Walker et al., 2009, 2013), in the Amerasian basin (Guéguen et al., 2015) and in shelf waters in the North Atlantic (Kowalcuk et al., 2009; Yamashita et al., 2013). In accordance to the results obtained with the EEM/PARAFAC approach, the optical indices of DOM modification have also pointed to a dominance of humic-like compounds within the samples (see Figure 5).

Despite the dominance of allochthonous humic-like components over the entire sampled area, autochthonous components (such as the marine-humic like C3 and the protein-like C6) have their relative contribution (to total FDOM signal) enhanced toward high salinity (see colorbar in Figure 5). Increased relative contribution of C6 was also observed during the base flow of the Lena River, when the terrestrial input is reduced (Walker et al., 2013). In addition, the component C6, also referred in other studies as tryptophan-like, seems

to be a useful indicator of bioavailability of DOM, given the strong correlation showed by it and total dissolved amino acids concentrations (Yamashita et al., 2015). The increase observed in the relative contribution of autochthonous compounds toward the high salinity waters of the Laptev Sea shelf region was also evident when observing the ranges presented by the optical indices of DOM modification (see Figure 5). Furthermore, those indices can provide more information on the transformation of the DOM during the transit from the river to the outer shelf. The use of optical indices has been successfully applied to assess the transformation of DOM along wide salinity ranges in some estuary regions worldwide (Benner and Opsahl, 2001; Helms et al., 2008, 2014; Huguet et al., 2009; Asmala et al., 2014). The values obtained for the optical indices at low salinity in our study are in agreement with previous studies conducted in the Lena River. For instance, those studies have reported S_{CDOM} , SUVA, and BIX values around $16 \mu\text{m}^{-1}$, $2.8 \text{ m}^2 \text{ g}^{-1}$ and 0.52,

respectively (Stedmon et al., 2011; Walker et al., 2013). All the optical indices taken into account in this study demonstrated that the DOM in the Lena delta region experiences an evident transformation along the riverine-marine transition. This is supported by the reduction on the molecular weight, aromaticity and humification degree of DOM observed toward high salinity, with the more photochemically reactive compounds associated to the surface (with lower salinity) layer and components with more refractory character being associated to the high salinity-Laptev Sea shelf waters (**Figure 5**). The possible mechanisms driving the observed transformation in DOM are discussed in the following section.

Dynamics and Fate of DOM in the Lena Delta Region

The hydrographic observations during our campaign revealed strong gradients, with noticeable northward propagation of the Lena River plume along the study region. This generated a shallow, low salinity surface mixed layer with strong stratification, which separates the surface layer from the underlying high salinity layer with Laptev Sea shelf water (see **Figure 1**). The propagation of the plume along the Laptev Sea shelf has also induced the establishment of a strong frontal system in the NW part of our study area (see **Figure 1**). Such hydrographic characteristics were previously described as offshore wind conditions, when the predominant winds from the continent drive the offshore propagation of the Lena waters generating a strong stratification and a frontal system NW of the Lena Delta region (Bauch et al., 2009; Wegner et al., 2013). Thus, we have identified the presence of two hydrographic provinces within the sampled area: the plume- and marine-influenced sites (see **Figure 1**).

The noticeable variability in hydrographic conditions due to the dynamics between fresh water input from the Lena River and the Laptev Sea shelf waters were also reflected in the striking differences of the amount and composition of DOM (**Figures 2, 3**). The association of the highest DOM concentrations with the low salinity waters of the Lena outflow decreasing toward the high salinity Laptev Sea shelf waters (see **Figure 2**) re-emphasizes the importance of the Lena River as a major source of DOM to the Laptev Sea. Such inverse relationship has previously been indicated for this region (Cauwet and Sidorov, 1996; Kattner et al., 1999; Alling et al., 2010; Semiletov et al., 2013; Heim et al., 2014) and it is the case for many other estuarine regions (Benner and Opsahl, 2001; Guo et al., 2007; Huguet et al., 2009). Both CDOM and DOC were highly correlated, displaying a similar relationship as found for the coastal Canadian Arctic (Walker et al., 2009; see **Figure 2**), although with a higher a_{350} relative to DOC in the Lena delta waters. The presented values are comparable to other studies previously conducted in this region, with a_{350} (a_{440}) values of about 15 m^{-1} (2.9 m^{-1}) at low salinity and DOC concentrations ranging from $500\text{--}700$ to $100\text{ }\mu\text{M}$ at low and high salinity, respectively (Alling et al., 2010; Stedmon et al., 2011; Semiletov et al., 2013; Walker et al., 2013; Heim et al., 2014; Dubinenkov et al., 2015a).

Our results show a coupled relationship between DOM and the two hydrographic provinces identified in this work. Plume-influenced stations presented higher DOM concentrations at surface as compared to marine-influenced stations ($p < 0.001$; see **Figure 1**). Despite these differences within the surface layers, both hydrographic provinces exhibited similar patterns regarding the relationship between DOM and salinity. Distinct DOM mixing patterns (in relation to salinity) were observed for samples above and below the pycnocline, i.e., the low and high salinity layers, respectively (**Figure 6**). The mixing curves derived from samples above the pycnocline exhibited higher slope than the ones below it (see **Figures 2, 3, 6**). The same pattern is observed when looking at the results from an expedition conducted at the Lena Delta region in September 2005 (see Figure 9 in Semiletov et al., 2013); however, the possible causes of this pattern were not addressed in that study. We suggest that such an increase in the slope of the relationship can be interpreted as a non-conservative decrease in DOM concentration along with the surface layer. This DOM removal in the surface (lower salinity) layer occurred despite the short residence time (of about 2 months) the Lena River plume waters in the Laptev Sea (Alling et al., 2010). Release/production of the components C5 and C6 was observed along the entire riverine-marine transition (see **Figure 4**, right panel). The autochthonous protein-like C6 is known to be released by microbial metabolism (Romera-Castillo et al., 2010; Fukuzaki et al., 2014) and its release in our sampling area can be related to the microbial community presented within the region. On the other hand, the humic-like C5 could have had its release associated with photoproduction, given that some humic-like components, such as alkyl, have been shown to be produced via that process (Helms et al., 2014). Although the components C5 and C6 presented indication of release/production along the riverine-marine transition, the contribution of those components to the total fluorescence signal was small (less than 20%). Thus, the overall DOM mixing curve mirrored the curves displayed by C1-C4 (accounting for more than 80% of the total FDOM signal), with a removal of DOM at low salinities and a conservative mixing behavior related to the saltier Laptev Sea shelf waters. Non-conservative mixing characterized by removal at low salinities seems to be a characteristic shared by other estuarine regions in the Baltic Sea (Kowalczuk et al., 2010; Asmala et al., 2014).

Given the strong stratification observed within the sampled area, we assume that exchanges between surface and underneath layer are limited (Kara et al., 2000b) compared to well-mixed conditions. As a result, the humic-like-dominated, highly photo-reactive DOM (Helms et al., 2014; Timko et al., 2015) is exposed longer to photochemical degradation (Fichot and Miller, 2010). This process is evidenced by the relationship between S_{Ratio} and salinity (**Figure 5E**), with high S_{Ratio} values (>0.95) observed in intermediate salinity (10–20). Furthermore, the influence of particulate matter and sediments in coastal and shelf environments has to be taken into account given their influence on DOM removal through the process of sorption and flocculation (Uher et al., 2001; Shank et al., 2005; Guo et al., 2007; Asmala et al., 2014). The flocculation process, in turn, can be increased either due to the presence of the salt in the

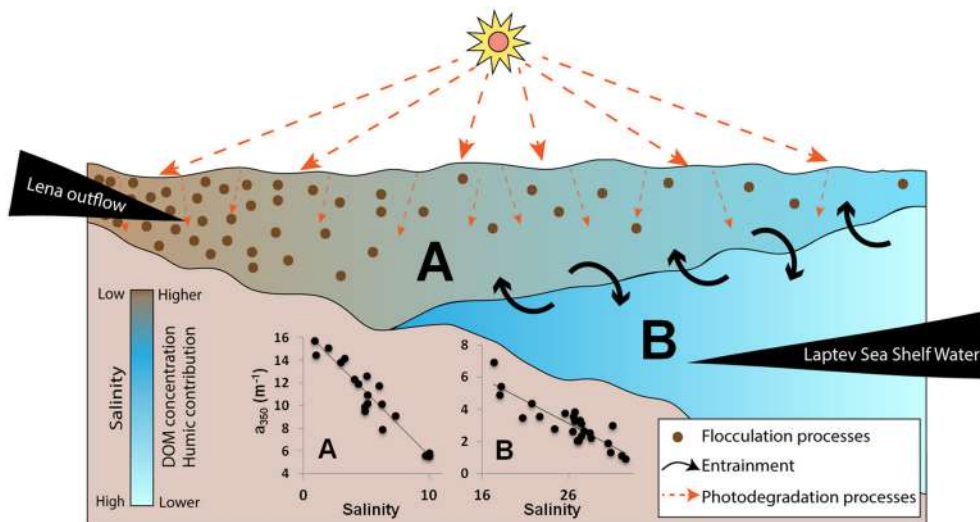


FIGURE 6 | Schematic diagram showing the complex interactions occurring in the Laptev Sea continental shelf, close to the Lena River delta region.

The vertical distribution of the two water masses found within the region (Lena River plume and Laptev Sea Shelf waters) is presented. A strong gradient between the two water masses with limited exchanges between them is depicted. Salinity, DOM concentration and the humic-like contribution are shown in the colorbar. The main removal processes within the surface layer (photodegradation and flocculation) are demonstrated by the symbols presented in the inset legend. Inset graphs show the DOM (a_{350} ; m^{-1}) against salinity plots for the Lena plume (A) and Laptev Sea shelf Waters (B).

marine water (Asmala et al., 2014, and references therein) and to the exposition to high light intensities that, together with photochemical processes, can synergistically enhance the DOM removal from the dissolved phase (von Wachenfeldt et al., 2008; Porcal et al., 2013, 2015). A sharp decrease in POC concentrations at low salinity has been reported in the Lena delta region and was attributed to sinking of particles (Cauwet and Sidorov, 1996). We speculate that the main drivers on the apparent removal of highly humic content DOM observed within the surface layer are the photodegradation and flocculation, given the high susceptibility of those aromatic carbons to those processes (von Wachenfeldt et al., 2008; Porcal et al., 2013, 2015; Asmala et al., 2014; Helms et al., 2014). Those processes have also been indicated to modulate the non-conservative mixing behavior in other estuaries such as the Mississippi delta (Benner and Opsahl, 2001). Our findings from late summer 2013 corroborate the indication of DOM removal within the region as observed in late summer 2008 (Alling et al., 2010); however, with a more refined spatial coverage, we have demonstrated that the removal of DOM occurs mostly in the low salinity surface layer (Figure 6).

Considering that the impact of temperature increases to the Arctic and Siberian environments, an increase in permafrost thawing rates, changes in the freshwater budget, catchment vegetation and hydrology, and subsequent DOM discharge into the Arctic Ocean are expected (Peterson et al., 2002; McClelland et al., 2004; Frey and McClelland, 2009). As a consequence, changes in concentration and composition of DOM are expected, given the release of ancient DOM trapped in the permafrost layer due to its thaw (Aiken et al., 2014; O'Donnell et al., 2014), and given the variability of DOM composition in response to variations in river discharge (Walker

et al., 2013). Subsequently, with an enhanced input of DOM (especially CDOM) into the Arctic Ocean, changes in the radiant heating in the upper meters of the ocean as well as a possible increase in the sea-ice melt rates might be foreseen (Granskog et al., 2015). Furthermore, the characteristics of DOM have been shown to be a powerful proxy for tracing organic substances with permafrost origin (Aiken et al., 2014; O'Donnell et al., 2014; Dubinenkov et al., 2015a). Moreover, long-term studies concerning the quantification, composition and dynamics of DOM, from fresh to marine waters in the main rivers flowing into the Arctic Ocean, are needed to improve the understanding of DOM dynamics, its role in the carbon cycle pathways. Thus, a better comprehension of DOM composition and its fate, as presented in this study, can be used as baseline for further monitoring of the sources, biogeochemical implications and export of riverine DOM with regard to climate change effects in northern Siberian environments and Arctic Ocean.

SUMMARY

This study brings new insights on the composition, transformation and fate of DOM in the Lena Delta region. DOM composition evaluated through PARAFAC modeling showed dominance of strong humic-like signal over the entire sampled area. We have demonstrated that the dynamics between the Lena River outflow and Laptev Sea shelf waters is the main driver controlling the hydrographical conditions and, consequently, the DOM behavior within the region. Higher DOM concentrations (also with higher humic-like content) were associated to the low salinity waters of the Lena River that showed to be the main DOM source for the region. The concentration of

DOM, as well as its humic-like content and reactivity, decreased along the fresh water-marine gradient toward high salinity. Although being limited by sampling within a synoptic scale, we have identified different mixing behaviors of DOM coupled with the dynamics between the Lena River plume and the Laptev Sea shelf waters, which were expressed through the vertical structure of the water column: a sharper decrease in DOM concentration in relation to salinity is observed in waters above the pycnocline, under influence of the low salinity waters from the continental runoff. This indicates that different processes modulating the distribution, composition, and reactivity of DOM occur within the two layers and that there is evidence of removal of DOM in the surface mixed layer. Thus, we suggest photodegradation and flocculation as the main drivers on modulating the removal of highly humified DOM within the surface layer of the Lena Delta region.

ACKNOWLEDGMENTS

The authors acknowledge the Captain and the crew of the R/V "Dalmie Zelentsy" and the researchers E. Druzhkova and

K. Bobrov for their assistance during the field sampling. We are thankful to the logistics department of the Alfred Wegener Institute (AWI) particularly Waldemar Schneider for the support, and to Sonja Wiegmann for the work in the laboratory. This work was funded by the Helmholtz Impulse Fond (HGF Young Investigators Group Phytooptics), and by the Presidium of Russian Academy of Sciences program "Prospecting fundamental research in the interest of the Russian Arctic Zone development in 2014–2015" through the project "Biological resources of the Russian Arctic Seas: current state, influence of natural changes and anthropogenic impacts, scientific principles, and perspectives of use." RG is funded by a Ph.D. fellowship from the Coordination for the Improvement of Higher Level Personnel (CAPES–Brazil) in collaboration with the German Academic Exchange Service (DAAD), and a visiting fellowship from the Helmholtz Graduate School for Polar and Marine Research (POLMAR–AWI). CS acknowledges funding from Danish Research Council for Independent Research (DFF 1323-00336). BH acknowledges grants from the German Science Foundation (DFG 4575) and the Helmholtz Climate Initiative REKLIM.

REFERENCES

- Aiken, G. R., Sepner, R. G. M., Striegl, R. G., Schuster, P. F., and Raymond, P. A. (2014). Influences of glacier melt and permafrost thaw on the age of dissolved organic carbon in the Yukon River basin. *Global Biogeochem. Cycles* 28, 525–537. doi: 10.1002/2013GB004764
- Alling, V., Sanchez-Garcia, L., Porcelli, D., Pugach, S., Vonk, J. E., van Dongen, B., et al. (2010). Nonconservative behavior of dissolved organic carbon across the Laptev and East Siberian seas. *Global Biogeochem. Cycles* 24, GB4033. doi: 10.1029/2010GB003834
- Amon, R. M. V., Rinehart, A. J., Duan, S., Louchoourn, P., Prokushkin, A., Guggenberger, G., et al. (2012). Dissolved organic matter sources in large Arctic rivers. *Geochim. Cosmochim. Acta* 94, 217–237. doi: 10.1016/j.gca.2012.07.015
- Arrigo, K. R., and Brown, C. W. (1996). Impact of chromophoric dissolved organic matter on UV inhibition of primary productivity in the Sea. *Mar. Ecol. Prog. Ser.* 140, 207–216. doi: 10.3354/meps140207
- Asmala, E., Bowers, D. G., Autio, R., Kaartokallio, H., and Thomas, D. N. (2014). Qualitative changes of riverine dissolved organic matter at low salinities due to flocculation. *J. Geophys. Res. Biogeosci.* 119, 1919–1933. doi: 10.1002/2014jg002722
- Bauch, D., Dmitrenko, I. A., Wegner, C., Hölemann, J., Kirilov, S. A., Timokhov, L. A., et al. (2009). Exchange of Laptev Sea and Arctic Ocean halocline waters in response to atmospheric forcing. *J. Geophys. Res.* 114, C05008. doi: 10.1029/2008jc005062
- Benner, R., Benitez-Nelson, B., Kaiser, K., and Amon, R. M. W. (2004). Export of young terrigenous dissolved organic carbon from rivers to the Arctic Ocean. *Geophys. Res. Lett.* 31, L05305. doi: 10.1029/2003gl019251
- Benner, R., and Opsahl, S. (2001). Molecular indicators of the sources and transformations of dissolved organic matter in the Mississippi river plume. *Org. Geochem.* 32, 597–611. doi: 10.1016/S0146-6380(00)00197-2
- Boyd, T. J., and Osburn, C. L. (2004). Changes in CDOM fluorescence from allochthonous and autochthonous sources during tidal mixing and bacterial degradation in two coastal estuaries. *Mar. Chem.* 89, 189–210. doi: 10.1016/j.marchem.2004.02.012
- Cauwet, G., and Sidorov, I. S. (1996). The biogeochemistry of Lena river: organic carbon and nutrient distribution. *Mar. Chem.* 53, 211–227. doi: 10.1016/0304-4203(95)00090-9
- Chari, N. V. H. K., Keerthi, S., Sarma, N. S., Rao Pandi, S., Chiranjeevulu, G., Kiran, R., et al. (2013). Fluorescence and absorption characteristics of dissolved organic matter excreted by phytoplankton species of western Bay of Bengal under axenic laboratory condition. *J. Exp. Mar. Biol. Ecol.* 445, 148–155. doi: 10.1016/j.jembe.2013.03.015
- Coble, P. G. (2007). Marine optical biogeochemistry: the chemistry of ocean color. *Chem. Rev.* 107, 402–418. doi: 10.1021/cr050350+
- Dittmar, T., and Kattner, G. (2003). The biogeochemistry of the river and shelf ecosystem of the Arctic Ocean: a review. *Mar. Chem.* 83, 103–120. doi: 10.1016/S0304-4203(03)00105-1
- Dubinenkov, I., Flerus, R., Schmitt-Kopplin, P., Kattner, G., and Koch, B. P. (2015a). Origin-specific molecular signatures of dissolved organic matter in the Lena Delta. *Biogeochemistry* 123, 1–14. doi: 10.1007/s10533-014-0049-0
- Dubinenkov, I., Kraberg, A., Bussmann, I., Kattner, G., and Koch, B. P. (2015b). *Data from: Physical Oceanography and Dissolved Organic Matter in the Coastal Laptev SEA in 2013*. PANGAEA. Available online at: <http://doi.pangaea.de/10.1594/PANGAEA.842221>
- Fedorova, I., Chetverova, A., Bolshiyanov, D., Makarov, A., Boike, J., Heim, B., et al. (2015). Lena Delta hydrology and geochemistry: long-term hydrological data and recent field observations. *Biogeosciences* 12, 345–363. doi: 10.5194/bg-12-345-2015
- Fichot, C. G., and Benner, R. (2012). The spectral slope coefficient of chromophoric dissolved organic matter ($S_{275-295}$) as a tracer of terrigenous dissolved organic carbon in river-influenced ocean margins. *Limnol. Oceanogr.* 57, 1453–1466. doi: 10.4319/lo.2012.57.5.1453
- Fichot, C. G., Kaiser, K., Hooker, S. B., Amon, R. M. W., Babin, M., Bélanger, S., et al. (2013). Pan-Arctic distributions of continental runoff in the Arctic Ocean. *Sci. Rep.* 3:1053. doi: 10.1038/srep01053
- Fichot, C. G., and Miller, W. L. (2010). An approach to quantify depth-resolved marine photochemical fluxes using remote sensing: application to carbon monoxide (CO) photoproduction. *Remote Sens. Environ.* 114, 1363–1377. doi: 10.1016/j.rse.2010.01.019
- Fofanova, V., Androsov, A., Danilov, S., Janout, M., Sofina, E., and Wiltshire, K. (2014). Semidiurnal tides in the Laptev Sea Shelf zone in the summer season. *Cont. Shelf Res.* 73, 119–132. doi: 10.1016/j.csr.2013.11.010
- Frey, K. E., and McClelland, J. W. (2009). Impacts of permafrost degradation on arctic river biogeochemistry. *Hydrol. Process.* 23, 169–182. doi: 10.1002/hyp.7196
- Fukuzaki, K., Imai, I., Fukushima, K., Ishii, K.-I., Sawayama, S., and Yoshioka, T. (2014). Fluorescent characteristics of dissolved organic matter produced by bloom-forming coastal phytoplankton. *J. Plankton Res.* 36, 685–694. doi: 10.1093/plankt/fbu015
- Gonçalves-Araujo, R., de Souza, M. S., Tavano, V. M., and Garcia, C. A. E. (2015b). Influence of oceanographic features on spatial and interannual variability of

- phytoplankton in the Bransfield Strait, Antarctica. *J. Mar. Syst.* 142, 1–15. doi: 10.1016/j.jmarsys.2014.09.007
- Gonçalves-Araujo, R., Stedmon, C. A., Heim, B., Dubinenkov, I., Kraberg, A., Moiseev, D., et al. (2015a). Data from: Dissolved Organic Matter in the Lena River Delta Region, Siberia, Russia. PANGAEA. Available online at: <http://doi.pangaea.de/10.1594/PANGAEA.844928>
- Granskog, M., Pavlov, A. K., Sagan, S., Kowalcuk, P., Raczkowska, A., and Stedmon, C. A. (2015). Effect of sea-ice melt on inherent optical properties and vertical distribution of solar radiant heating in Arctic surface waters. *J. Geophys. Res. Oceans* 120, 7028–7039. doi: 10.1002/2015jc011087
- Guégan, C., Itoh, M., Kikuchi, T., Eert, J., and Williams, W. J. (2015). Variability in dissolved organic matter optical properties in surface waters in the Amerasian Basin. *Front. Mar. Sci.* 2:78. doi: 10.3389/fmars.2015.00078
- Guo, W., Stedmon, C. A., Han, Y., Wu, F., Yu, X., and Hu, M. (2007). The conservative and non-conservative behavior of chromophoric dissolved organic matter in Chinese estuarine waters. *Mar. Chem.* 107, 357–366. doi: 10.1016/j.marchem.2007.03.006
- Heim, B., Abramova, E., Doerffer, R., Günther, F., Hölemann, J., Kraberg, A., et al. (2014). Ocean colour remote sensing in the southern Laptev Sea: evaluation and applications. *Biogeosciences* 11, 4191–4210. doi: 10.5194/bg-11-4191-2014
- Helms, J. R., Mao, J., Stubbins, A., Schmidt-Rohr, K., Spencer, R. G. M., Hernes, P. J., et al. (2014). Loss of optical and molecular indicators of terrigenous dissolved organic matter during long-term photobleaching. *Aquat. Sci.* 76, 353–373. doi: 10.1007/s00027-014-0340-0
- Helms, J. R., Stubbins, A., Ritchie, J. D., Minor, E. C., Kieber, D. J., and Mopper, K. (2008). Absorption spectral slopes and slope ratios as indicators of molecular weight, source, and photobleaching of chromophoric dissolved organic matter. *Limnol. Oceanogr.* 53, 955–969. doi: 10.4319/lo.2008.53.3.0955
- Huguet, A., Vacher, L., Relexans, S., Saubusse, S., Froidefond, J. M., and Parlanti, E. (2009). Properties of fluorescent dissolved organic matter in the Gironde Estuary. *Org. Geochem.* 40, 706–719. doi: 10.1016/j.orggeochem.2009.03.002
- Jørgensen, L., Stedmon, C. A., Kragh, T., Markager, S., Middelboe, M., and Søndergaard, M. (2011). Global trends in the fluorescence characteristics and distribution of marine dissolved organic matter. *Mar. Chem.* 126, 139–148. doi: 10.1016/j.marchem.2011.05.002
- Kara, A. B., Rochford, P. A., and Hurlburt, H. E. (2000a). An optimal definition for ocean mixed layer depth. *J. Geophys. Res.* 105, 16803–16821. doi: 10.1029/2000JC000072
- Kara, A. B., Rochford, P. A., and Hurlburt, H. E. (2000b). Mixed layer depth variability and barrier layer formation over the North Pacific Ocean. *J. Geophys. Res.* 105, 16783–16801. doi: 10.1029/2000JC000071
- Kattner, G., Lobbes, J. M., Fitznar, H. P., Engbrodt, R., Nöthig, E.-M., and Lara, R. J. (1999). Tracing dissolved organic substances and nutrients from the Lena River through Laptev Sea (Arctic). *Mar. Chem.* 65, 25–39. doi: 10.1016/S0304-4203(99)00008-0
- Kowalcuk, P. M., Durako, J., Young, H., Kahn, A. E., Cooper, W. J., Gonsior, M., et al. (2009). Characterization of dissolved organic matter fluorescence in the South Atlantic Bight with use of PARAFAC model: interannual variability. *Mar. Chem.* 113, 182–196. doi: 10.1016/j.marchem.2009.01.015
- Kowalcuk, P. M., Zablocka, S., Sagan, and Kulniński, K. (2010). Fluorescence measured *in situ* as a proxy of CDOM absorption and DOC concentration in the Baltic Sea. *Oceanologia* 52, 431–471. doi: 10.5697/oc.52-3.431
- Kowalcuk, P., Tilstone, G. H., Zablocka, M., Röttgers, R., and Thomas, R. (2013). Composition of dissolved organic matter along an Atlantic Meridional transect from fluorescence spectroscopy and parallel factor analysis. *Mar. Chem.* 157, 170–184. doi: 10.1016/j.marchem.2013.10.004
- Levitus, S. (1982). *Climatological Atlas of the World Ocean*. NOAA Professional Paper 13. Washington, DC: U.S. Govt. Print. Off.
- Lyon, S. W., and Destouni, G. (2010). Changes in catchment-scale recession flow properties in response to permafrost thawing in the Yukon River basin. *Int. J. Climatol.* 30, 2138–2145. doi: 10.1002/joc.1993
- McClelland, J. W., Holmes, R. M., Peterson, B. J., and Stieglitz, M. (2004). Increasing river discharge in the Eurasian Arctic: consideration of dams, permafrost thaw, and fires as potential agents of change. *J. Geophys. Res.* 109, D18102. doi: 10.1029/2004jd004583
- McKnight, D. M., Boyer, E. W., Westerhoff, P. K., Doran, P. T., Kulbe, T., and Andersen, D. T. (2001). Spectrofluorometric characterization of dissolved organic matter for indication of precursor organic material and aromaticity. *Limnol. Oceanogr.* 46, 38–48. doi: 10.4319/lo.2001.46.1.00038
- Mopper, K., and Kieber, D. J. (2002). "Photochemistry and the cycling of carbon, sulfur, nitrogen and phosphorus" in *Biogeochemistry of Marine Dissolved Organic Matter*, eds C. Carlson and D. Hansell (San Diego, CA: Academic Press), 455–508.
- Murphy, K. R., Stedmon, C. A., Graeber, D., and Bro, R. (2013). Fluorescence spectroscopy and multi-way techniques. *PARAFAC. Anal. Methods* 5, 6557–6566. doi: 10.1039/c3ay41160e
- Murphy, K. R., Stedmon, C. A., Waite, T. D., and Ruiz, G. M. (2008). Distinguishing between terrestrial and autochthonous organic matter sources in marine environments using fluorescence spectroscopy. *Mar. Chem.* 108, 40–58. doi: 10.1016/j.marchem.2007.10.003
- Murphy, K. R., Stedmon, C. A., Wenig, P., and Bro, R. (2014). OpenFluor – an online spectral library for auto-fluorescence by organic compounds in the environment. *Anal. Methods* 6, 658–661. doi: 10.1039/C3AY41935E
- Nelson, N. B., and Siegel, D. A. (2013). The global distribution and dynamics of chromophoric dissolved organic matter. *Annu. Rev. Mar. Sci.* 5, 447–476. doi: 10.1146/annurev-marine-120710-100751
- O'Donnell, J. O., Aiken, G. R., Walvoord, M. A., Raymond, P. A., Butler, K. D., Dornblaser, M. M., et al. (2014). Using dissolved organic matter age and composition to detect permafrost thaw in boreal watersheds of interior Alaska. *J. Geophys. Res. Biogeosci.* 119, 2155–2170. doi: 10.1002/2014JG002695
- Opsahl, S., and Benner, R. (1998). Photochemical reactivity of dissolved lignin in river and ocean waters. *Limnol. Oceanogr.* 43, 1297–1304. doi: 10.4319/lo.1998.43.6.1297
- Opsahl, S., Benner, R., and Amon, R. M. W. (1999). Major flux of terrigenous organic matter through the Arctic Ocean. *Limnol. Oceanogr.* 44, 2017–2023. doi: 10.4319/lo.1999.44.8.2017
- Para, J., Coble, P. G., Charrière, B., Tedetti, M., Fontana, C., and Sempére, R. (2010). Fluorescence and absorption properties of chromophoric dissolved organic matter (CDOM) in coastal surface waters of the northwestern Mediterranean Sea, influence of the Rhône River. *Biogeosciences* 7, 4083–4103. doi: 10.5194/bg-7-4083-2010
- Peterson, B. J., Holmes, R. M., McClelland, J. W., Vörösmarty, C. J., Lammers, R. B., Shiklomanov, I. A., et al. (2002). Increasing river discharge to the Arctic Ocean. *Science* 298, 2171–2173. doi: 10.1126/science.1077445
- Porcal, P., Dillon, P. J., and Molot, L. A. (2013). Photochemical production and decomposition of particulate organic carbon in a freshwater stream. *Aquat. Sci.* 73, 469–482. doi: 10.1007/s00027-013-0293-8
- Porcal, P., Dillon, P. J., and Molot, L. A. (2015). Temperature dependence of photodegradation of dissolved organic matter to dissolved inorganic carbon and particulate organic carbon. *PLoS ONE* 10:e0128884. doi: 10.1371/journal.pone.0128884
- Raymond, P. A., McClelland, J. W., Holmes, R. M., Zhulidov, A. V., Mull, K., Peterson, B. J., et al. (2007). Flux and age of dissolved organic carbon exported to the Arctic Ocean: a carbon isotopic study of the five largest arctic rivers. *Global Biogeochem. Cycles* 21, GB4011. doi: 10.1029/2007GB002934
- Romera-Castillo, C., Sarmento, H., Álvarez-Salgado, X. A., Gasol, J. M., and Marrasé, C. (2010). Production of chromophoric dissolved organic matter by marine phytoplankton. *Limnol. Oceanogr.* 55, 446–454. doi: 10.4319/lo.2010.55.1.00446
- Sánchez-García, L., Vonk, J. E., Charkin, A., Kosmach, D., Dudarev, O., Semiletov, I., et al. (2014). Characterisation of three regimes of collapsing Arctic ice complex deposits on the SE Laptev Sea coast using biomarkers and dual carbon isotopes. *Permafrost Periglacial Process.* 25, 172–183. doi: 10.1002/ppp.1815
- Schlitzer, R. (2015). *Ocean Data View*. Available online at: <http://odv.awi.de>
- Schuur, E. A. G., Bockheim, J., Canadell, J. G., Euskirchen, E., Field, C. B., Goryachkin, S. V., et al. (2008). Vulnerability of permafrost carbon to climate change: implications for the global carbon cycle. *Bioscience* 58, 701–714. doi: 10.1641/B580807
- Semiletov, I. P., Pipko, I. I., Shakhova, N. E., Dudarev, O. V., Pugach, S. P., Charkin, A. N., et al. (2011). Carbon transport by the Lena River from its headwaters to the Arctic Ocean, with emphasis on fluvial input of terrestrial particulate organic carbon vs. carbon transport by coastal erosion. *Biogeosciences* 8, 2407–2426. doi: 10.5194/bg-8-2407-2011

- Semiletov, I. P., Shakhova, N. E., Pugach, S. P., Charkin, A. N., Dudarev, O. V., Kosmach, D. A., et al. (2013). Space-time dynamics of carbon and environmental parameters related to carbon dioxide emissions in the Buor-Khaya Bay and adjacent part of the Laptev Sea. *Biogeosciences* 10, 5977–5996. doi: 10.5194/bg-10-5977-2013
- Semiletov, I. P., Shakhova, N. E., Sergienko, V. I., Pipko, I. I., and Dudarev, O. V. (2012). On carbon transport and fate in the East Siberian Arctic land-shelf-atmosphere system. *Environ. Res. Lett.* 7, 015201. doi: 10.1088/1748-9326/7/1/015201
- Senesi, N., Miano, N. T., Provenzano, M. R., and Brunetti, G. (1991). Characterization, differentiation and classification of humic substances by fluorescence spectroscopy. *Soil Sci.* 152, 259–271. doi: 10.1097/00010694-199110000-00004
- Shank, G. C., Zepp, R. G., Whitehead, R. F., and Moran, M. A. (2005). Variations in the spectral properties of freshwater and estuarine CDOM caused by partitioning onto river and estuarine sediments. *Estuar. Coast. Shelf Sci.* 65, 289–301. doi: 10.1016/j.ecss.2005.06.009
- Siegel, D. A., Maritorena, S., Nelson, N. B., Behrenfeld, M. J., and McClain, R. (2005). Colored dissolved organic matter and its influence on the satellite-based characterization of the ocean biosphere. *Geophys. Res. Lett.* 32, L20605. doi: 10.1029/2005gl024310
- Siegel, D. A., Maritorena, S., Nelson, N. B., Hansell, D. A., and Lorenz-Kayser, M. (2002). Global distribution and dynamics of colored dissolved and detrital organic materials. *J. Geophys. Res.* 107, 3228. doi: 10.1029/2001jc00965
- Singh, S., D'Sa, E. J., and Sweson, E. M. (2010). Chromophoric dissolved organic matter (CDOM) variability in Barataria Basin using excitation-emission matrix (EEM) fluorescence and parallel factor analysis (PARAFAC). *Sci. Total Environ.* 408, 3211–3222. doi: 10.1016/j.scitotenv.2010.03.044
- Spencer, R. G. M., Aiken, G. R., Butler, K. D., Dornblaser, M. M., Striegl, R. G., and Hernes, P. J. (2009). Utilizing chromophoric dissolved organic matter measurements to derive export and reactivity of dissolved organic carbon exported to the Arctic Ocean: a case study of the Yukon River, Alaska. *Geophys. Res. Lett.* 36, L06401. doi: 10.1029/2008gl036831
- Stedmon, C. A., Amon, R. M. W., Rinehart, A. J., and Walker, S. A. (2011). The supply and characteristics of colored dissolved organic matter (CDOM) in the Arctic Ocean: par Arctic trends and differences. *Mar. Chem.* 124, 108–118. doi: 10.1016/j.marchem.2010.12.007
- Stedmon, C. A., and Bro, R. (2008). Characterizing dissolved organic matter fluorescence with parallel factor analysis: a tutorial. *Limnol. Oceanogr.* 6, 572–579. doi: 10.4319/lom.2008.6.5.572
- Stedmon, C. A., and Markager, S. (2003). Behaviour of the optical properties of coloured dissolved organic matter under conservative mixing. *Est. Cost. Shelf Sci.* 57, 1–7. doi: 10.1016/s0272-7714(03)00003-9
- Stedmon, C. A., and Markager, S. (2005). Resolving the variability in dissolved organic matter fluorescence in a temperate estuary and its catchment using PARAFAC analysis. *Limnol. Oceanogr.* 50, 686–697. doi: 10.4319/lo.2005.50.2.00686
- Stevenson, F. J. (1982). *Humus Chemistry*. New York, NY: Genesis, Composition, Reactions, Wiley-Interscience.
- Stubbins, A., Lapierre, J.-F., Berggren, M., Prairia, Y. T., Dittmar, T., and del Giorgio, P. A. (2014). What's in an EEM? Molecular signatures associated with dissolved organic fluorescence in boreal Canada. *Environ. Sci. Technol.* 48, 10598–10606. doi: 10.1021/es502086e
- Stubbins, A., Uher, G., Law, C. S., Mopper, K., Robinson, C., and Upstill-Goddard, R. C. (2006). Open-ocean carbon monoxide photoproduction. *Deep Sea Res. II* 53, 1695–1705. doi: 10.1016/j.dsr2.2006.05.011
- Timko, S. A., Maydanov, A., Pittelli, S. L., Conte, M. H., Cooper, W. J., Koch, B. P., et al. (2015). Depth-dependent photodegradation of marine dissolved organic matter. *Front. Mar. Sci.* 2:66. doi: 10.3389/fmars.2015.00066
- Uher, G., Hughes, C., Henry, G., and Upstill-Goddard, R. C. (2001). Non-conservative mixing behavior of colored dissolved organic matter in a humic-rich, turbid estuary. *Geophys. Res. Lett.* 28, 3309–3312. doi: 10.1029/2000GL012509
- von Wachenfeldt, E., Sobek, S., Batsviken, D., and Tranvik, L. J. (2008). Linking allochthonous dissolved organic matter and boreal lake sediment carbon sequestration: the role of light-mediated flocculation. *Limnol. Oceanogr.* 53, 2416–2426. doi: 10.4319/lo.2008.53.6.2416
- Vonk, J. E., Sánchez-García, L., van Dongen, B. E., Alling, V., Kosmach, D., Charkin, A., et al. (2012). Activation of old carbon by erosion of coastal and subsea permafrost in Arctic Siberia. *Nature* 489, 137–140. doi: 10.1038/nature11392
- Vonk, J. E., Semiletov, I., Dudarev, O., Eglington, T., Andersson, A., Shakhova, N., et al. (2014). Preferential burial of permafrost-derived organic carbon in Siberian-Arctic shelf waters. *J. Geophys. Res.* 119, 8410–8421. doi: 10.1002/2014JC010261
- Walker, S. A., Amon, R. M. W., and Stedmon, C. A. (2013). Variations in high-latitude riverine fluorescent dissolved organic matter: a comparison of large Arctic rivers. *J. Geophys. Res. Biogeosci.* 118, 1689–1702. doi: 10.1002/2013jg002320
- Walker, S. A., Amon, R. M. W., Stedmon, C., Duan, S., and Loucheourn, P. (2009). The use of PARAFAC modeling to trace terrestrial dissolved organic matter and fingerprint water masses in coastal Canadian Arctic surface waters. *J. Geophys. Res.* 114, G00F06. doi: 10.1029/2009jg000990
- Wegner, C., Bauch, D., Hölemann, J. A., Janout, M. A., Heim, B., Novikhin, A., et al. (2013). Interannual variability of surface and bottom sediment transport on Laptev Sea shelf during summer. *Biogeosciences* 10, 1117–1129. doi: 10.5194/bg-10-1117-2013
- Weishaar, J. L., Aiken, G. R., Bergamaschi, B. A., Fram, M. S., Fujii, R., and Mopper, K. (2003). Evaluation of specific ultraviolet absorbance as an indicator of the chemical composition and reactivity of dissolved organic carbon. *Environ. Sci. Technol.* 37, 4702–4708. doi: 10.1021/es030360x
- Yamashita, Y., Boyer, J. N., and Jaffé, R. (2013). Evaluating the distribution of terrestrial dissolved organic matter in a complex coastal ecosystem using fluorescence spectroscopy. *Cont. Shelf Res.* 66, 136–144. doi: 10.1016/j.csr.2013.06.010
- Yamashita, Y., Cory, R. M., Nishioka, J., Kuma, K., Tanoue, E., and Jaffé, R. (2010). Fluorescence characteristics of dissolved organic matter in the deep waters of the Okhotsk Sea and the northwestern North Pacific Ocean. *Deep Sea Res. II* 57, 1478–1485. doi: 10.1016/j.dsr2.2010.02.016
- Yamashita, Y., Fichot, C. G., Shen, Y., Jaffé, R., and Benner, R. (2015). Linkages among fluorescent dissolved organic matter, dissolved amino acids and lignin-derived phenols in a river-influenced ocean margin. *Front. Mar. Sci.* 2:92. doi: 10.3389/fmars.2015.00092
- Yamashita, Y., and Tanoue, E. (2003). Chemical characterization of protein-like fluorophores in DOM in relation to aromatic amino acids. *Mar. Chem.* 82, 255–271. doi: 10.1016/S0304-4203(03)00073-2
- Yamashita, Y., and Tanoue, E. (2004). Chemical characteristics of amino acid-containing dissolved organic matter in seawater. *Org. Chem.* 35, 679–692. doi: 10.1016/j.orggeochem.2004.02.007
- Yang, D., Kane, D. L., Hinzman, L. D., Zhang, X., Zhang, T., and Ye, H. (2002). Siberia Lena River hydrologic regime and recent change. *J. Geophys. Res.* 107, 4694. doi: 10.1029/2002JD002542
- Zhang, Y., van Dijk, M. A., Liu, M., Zhu, G., and Qin, B. (2009). The contribution of phytoplankton degradation to chromophoric dissolved organic matter (CDOM) in eutrophic shallow lakes: field and experimental evidence. *Water Res.* 43, 4685–4697. doi: 10.1016/j.watres.2009.07.024
- Zsolnay, Á., Baigär, E., Jimenez, E., Steinweg, B., and Saccomandi, F. (1999). Differentiating with fluorescence spectroscopy the source of dissolved organic matter in soils subjected to drying. *Chemosphere* 38, 45–50. doi: 10.1016/S0045-6535(98)00166-0
- Zsolnay, Á. (2003). Dissolved organic matter: artefacts, definitions and functions. *Geoderma* 113, 187–209. doi: 10.1016/S0016-7061(02)00361-0
- Conflict of Interest Statement:** The authors declare that the research was conducted in the absence of any commercial or financial relationships that could be construed as a potential conflict of interest.
- Copyright © 2015 Gonçalves-Araujo, Stedmon, Heim, Dubinenkov, Kraberg, Moiseev and Bracher. This is an open-access article distributed under the terms of the Creative Commons Attribution License (CC BY). The use, distribution or reproduction in other forums is permitted, provided the original author(s) or licensor are credited and that the original publication in this journal is cited, in accordance with accepted academic practice. No use, distribution or reproduction is permitted which does not comply with these terms.



Variation in Riverine Inputs Affect Dissolved Organic Matter Characteristics throughout the Estuarine Gradient

Eero Asmala^{1,2*}, Hermanni Kaartokallio², Jacob Carstensen¹ and David N. Thomas^{2,3}

¹ Department of Bioscience, Aarhus University, Roskilde, Denmark, ² Marine Research Centre, Finnish Environment Institute (SYKE), Helsinki, Finland, ³ School of Ocean Sciences, Bangor University, Menai Bridge, UK

Highlights

OPEN ACCESS

Edited by:

Christopher Osburn,
North Carolina State University, USA

Reviewed by:

Mar Nieto-Cid,
Consejo Superior de Investigaciones

Científicas - Instituto de
Investigaciones Marinas, Spain
Gene Brooks Avery,
University of North Carolina at
Wilmington, USA

*Correspondence:

Eero Asmala
eear@bios.au.dk

Specialty section:

This article was submitted to
Marine Biogeochemistry,
a section of the journal
Frontiers in Marine Science

Received: 15 October 2015

Accepted: 23 December 2015

Published: 12 January 2016

Citation:

Asmala E, Kaartokallio H,
Carstensen J and Thomas DN (2016)
*Variation in Riverine Inputs Affect
Dissolved Organic Matter
Characteristics throughout the
Estuarine Gradient.*
Front. Mar. Sci. 2:125.
doi: 10.3389/fmars.2015.00125

- DOM quality characteristics are highly correlated, indicating common transformations along the salinity continuum
- variability in freshwater end-member adds complexity to the analysis of conservative mixing
- residence time alone cannot explain deviations from conservative mixing.

Terrestrial dissolved organic matter (DOM) undergoes significant changes during the estuarine transport from river mouths to the open sea. These include transformations and degradation by biological and chemical processes, but also the production of fresh organic matter. Since many of these processes occur simultaneously, properties of the DOM pool represent the net changes during the passage along the hydrological path. We examined changes in multiple DOM characteristics across three Finnish estuarine gradients during spring, summer and autumn: Dissolved organic carbon (DOC) concentration, colored DOM absorbance and fluorescence, stable carbon isotope signal of DOC, and molecular size distribution. Changes in these DOM characteristics with salinity were analyzed in relation to residence time (i.e., freshwater transit time), since increased residence time is likely to enhance DOM degradation while stimulating autochthonous DOM production at the same time. Our results show that the investigated DOM characteristics are highly correlated, indicating common physico-chemical transformations along the salinity continuum. Residence time did not explain variations in the DOM characteristics any better than salinity. Due to large variations in DOM characteristics at the river end-member, conservative mixing models do not seem to be able to accurately describe the occurrence and extent of deviations in DOM properties in the estuaries we investigated.

Keywords: freshwater residence time, colored dissolved organic matter, conservative mixing, DOM quality, organic matter cycling

INTRODUCTION

Organic matter (OM) in aquatic systems originates from two distinct sources; autochthonous OM from within the system and allochthonous OM from outside of the system, which in most cases is from terrestrial sources (Peterson et al., 1994). Autochthonous OM dominates in systems with low terrestrial influence, or systems with high nutrient loadings that stimulate high primary production (e.g., eutrophic lakes and coastal areas). Allochthonous OM dominates in systems where there is significant terrestrial influence and moderate nutrient loadings limiting the growth of aquatic primary producers. Most of the aquatic organic matter is in dissolved form (dissolved organic matter; DOM). The DOM pool is highly heterogeneous, and the quality of DOM may vary significantly regardless of quantity. The quality of DOM determines its cycling, bioavailability and reactivity in the environment, i.e., the fate of terrestrial DOM in coastal systems.

During the transport along the hydrological path from a terrestrial source to the open sea, terrestrially-derived DOM is transformed and removed from the water column by various processes. These processes include salt-induced flocculation (Sholkovitz, 1976; Forsgren et al., 1996; Asmala et al., 2014), photo mineralization (Moran and Zepp, 1997; Aarnos et al., 2012), and microbial uptake and degradation (Raymond and Bauer, 2000; Kirchman et al., 2004). These processes may remineralize DOM compounds partially or completely, incorporate organic material in biomass or cause sedimentation of aggregated DOM molecules; effectively changing and decreasing the DOM pool. However, the DOM pool is replenished by autochthonous production in the estuarine environment, for example by exudates from phytoplankton and macro-vegetation (Brylinsky, 1977; Wiebe and Smith, 1977; Romera-Castillo et al., 2010). All these processes combine so that the DOM pool is gradually changing from terrestrial to marine DOM (Koch et al., 2005). In general, there is a continuum from more reactive terrestrial ("young") DOM to less reactive marine ("old") DOM, which accumulates in the ocean interior (Jiao et al., 2010).

The quality of the highly heterogeneous DOM pool can be analyzed with multiple analytical approaches (Leenheer and Croué, 2003; Sulzberger and Durisch-Kaiser, 2009; Nebbioso and Piccolo, 2013). Individual quality parameters of bulk DOM have been linked to the chemical properties or biogeochemical reactivity, and these proxies have been widely used in aquatic biogeochemistry. For instance, the spectral slope of colored DOM (CDOM) absorption between wavelengths 275 and 295 nm is a good proxy for the average molecular size of the DOM pool (Helms et al., 2008). Molecular size in turn has been linked to the bioavailability and reactivity of DOM (Tranvik, 1990; Amon and Benner, 1996). Stable carbon isotope ratios of dissolved organic carbon (DOC) can be linked to its origin, as the signal from terrestrial and aquatic primary producers can be differentiated (Peterson et al., 1994; McCallister et al., 2004). DOC-specific absorbance in UV wavelengths (CDOM absorption) and visible light emission from UV excitation (CDOM fluorescence) indicate humic-like properties of the bulk DOM (Coble, 1996; Weishaar et al., 2003).

The role of freshwater residence time in the estuarine studies has been studied, especially in relation to nutrient retention processes (Borum, 1996; Josefson and Rasmussen, 2000; McGlathery et al., 2007). Increasing residence time in estuaries typically increases the biological processing of nutrients, and thus decreases the amount of nutrients reaching the open sea (Church, 1986). However, biological processes within an estuary can transform, decrease or increase DOM along the salinity gradient. The effect of residence time on DOM transformation is not well known. Traditionally, the extent to which biogeochemical processes alter the DOM pool along the estuarine salinity gradient has been analyzed by quantifying deviations from conservative mixing (Officer, 1979). Employing this method, the DOM properties of interest (e.g., DOC concentration) for two salinity end-members of the system are connected with a mixing line and DOM characteristics for intermediate salinities are analyzed to assess if biogeochemical processes, in addition to mixing, significantly affect these observations (Sholkovitz, 1976; Guo et al., 2007; Markager et al., 2011; Asmala et al., 2014). These biogeochemical processes (degradation, production, and transformation of DOM) are all, to some degree, enhanced by increasing residence time.

Even though changes in the DOM pool along estuarine gradients have been studied extensively, most studies have not successfully separated removal, production, and transformation processes from conservative mixing (Mantoura and Woodward, 1983; Abril et al., 2002; Köhler et al., 2003; Bowers et al., 2004; Guo et al., 2007; Spencer et al., 2007a). On the other hand, some studies have been able to show significant non-conservative dynamics in the DOM pool (Uher et al., 2001; Huguet et al., 2009; Markager et al., 2011; Asmala et al., 2014). It is evident that some system- or compound-specific properties determine whether the DOM pool follows conservative mixing in estuaries. As the effect of residence time on DOM dynamics along the estuarine mixing has not been thoroughly studied yet, our objective was to add a new perspective to estuarine changes in DOM, by calculating the freshwater residence time for all our sampling points and analysing its potential influence on DOM properties. Further, our aim was to characterize DOM pool with different analytical approaches and link these to get a synchronized view of the DOM properties along the gradients of salinity and freshwater age. We hypothesize that (1) the freshwater residence time is a valuable predictor of the changes in the DOM pool along the estuarine gradient alongside salinity; (2) changes in the DOM pool are unidirectional and can be measured with different analytical approaches; (3) analysis of the freshwater residence time combined with the multiparametric DOM characterization improves the applicability and accuracy of traditional conservative mixing models.

MATERIALS AND METHODS

Field Sampling

Our field data comes from transect samplings conducted in three Finnish rivers draining to the Baltic Sea: Karjaanjoki, Kyrönjoki, and Kiiminkijoki, sampled in the spring, summer, and autumn of 2010 and 2011 (**Figure 1**). Each transect consisted of five to six

horizontal sampling points from surface layer and below the river water lens, typically at 5 or 10 m depth. There were 18 transect datasets with $n = 187$ observations in total.

The three catchments have different land-use and consequently the river water properties differ significantly (Asmala et al., 2013, 2014; Kaartokallio et al., in press). Kiiminkijoki and Kyrönjoki have a characteristic spring peak in freshwater runoff due to melting of snow and ice in the catchment, whereas discharges from Karjaanjoki in southern Finland were more evenly distributed over the year (Figure 1). The Karjaanjoki estuary is the longest of the three estuaries with a distance between river and sea end-member of 38 km, and the salinities of the coastal waters were on average 6.3 ± 0.5 . In the Kyrönjoki and Kiiminkijoki estuaries the distances between end-members are 36 and 21 km and salinities of the coastal waters were 2.7 ± 1.1 and 2.3 ± 0.1 , respectively. Majority of DOM loading in these estuaries originates from the rivers: 15.5% in Karjaanjoki, 0.7% in Kyrönjoki, and 0.0% in Kiiminkijoki (Räike et al., 2012).

In all estuaries surface waters were sampled from the main channels with a small boat or coastal vessel using either a Limnos-type water sampler or polyethylene bucket. The water samples were immediately transferred to 30 L polyethylene canisters, and were stored cool and dark until filtration in laboratory (within 24 h). For analysis of DOM properties, sampled water was filtered through pre-combusted (450°C for 4 h) GF/F (Whatman) filters.

Pre-combustion of GF/F filters decrease their nominal pore size so that the effective filtering cut-off is comparable to filters with a nominal pore size of $0.2 \mu\text{m}$ for freshwater and estuarine bacteria (Nayar and Chou, 2003).

A subset of the filtered samples for colored dissolved organic matter (CDOM) and fluorescent dissolved organic matter (FDOM) were stored in acid-washed, pre-combusted (4 h at 450°C) glass vials at 4°C until absorbance and fluorescence measurements were made within 2 weeks from sampling. Filtered DOM samples stored refrigerated have shown negligible changes in both spectral CDOM absorption and humic-like fluorescence characteristics during storage periods of up to 5 months (Boyd and Osburn, 2004; Chen and Gardner, 2004; Retamal et al., 2007; Gueguen et al., 2015). Samples for size-exclusion chromatography (SEC) measurement were stored in acid-washed, pre-combusted glass vials at -20°C until analysis. A subset for DOC analyses were acidified with H_3PO_4 and stored frozen at -20°C until measurement. DOC concentration does not change in filtered and acidified samples when stored frozen for up to 1 year (Benner and Opsahl, 2001; Dittmar et al., 2006; Norman and Thomas, 2014). For stable carbon isotope analysis ($\delta^{13}\text{C}_{\text{DOC}}$), 500 mL water samples were filtered through pre-combusted GF/F and acidified with HCl to pH 2 to transform all carbonates to CO_2 . The acidified samples were frozen and subsequently freeze-dried to attain solid samples.

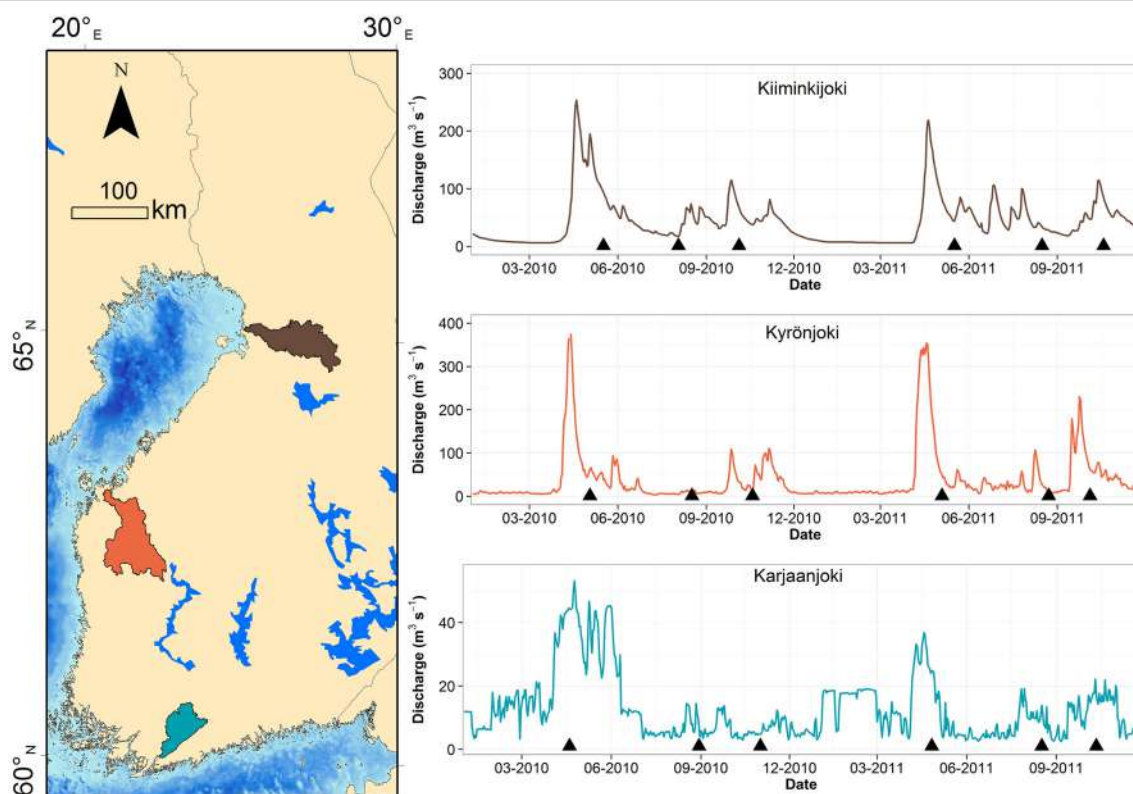


FIGURE 1 | Map of study estuaries and river discharges during the study period. Sampling occasions are marked with triangle symbol. Catchment of each river is colored with respective color as in discharge graph.

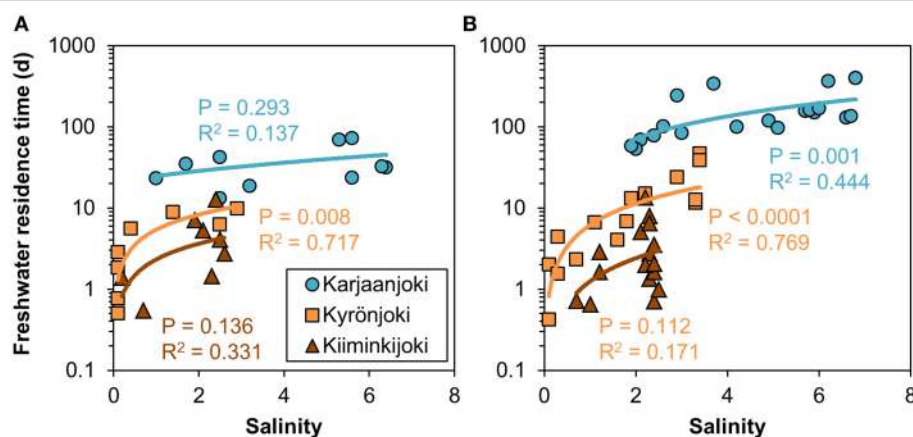


FIGURE 2 | Relationships between freshwater residence time and salinity in the three study estuaries during (A) high (spring) and (B) low (summer and autumn) river discharge conditions. Non-linear power regression models were fitted to data.

Analytical Procedures Used

DOC concentrations were analyzed by high temperature combustion on a MQ1000 TOC analyser according to Qian and Mopper (1996). Analysis integrity was tested daily on certified reference material [University of Miami, Consensus Reference Materials, Florida Strait seawater (lot #05–10: 41 to 44 $\mu\text{mol C L}^{-1}$)]. The method yielded an average DOC concentration of this material of 42 ± 7 (SD) $\mu\text{mol C L}^{-1}$ ($n = 213$). Dissolved organic nitrogen (DON) was calculated by subtracting the combined inorganic nitrogen (NH_4^+ , NO_2^- and NO_3^-) from the total dissolved nitrogen (TDN; from the filtered fraction). The inorganic nutrient analyses were carried out according to Grasshoff et al. (1983), where the NH_4^+ analyses were done manually and for the NO_2^- and NO_3^- analyses an automated flow injection analyser was used (Lachat QC 8000). TDN was determined following alkaline persulfate oxidation (Koroleff et al., 1977; Grasshoff et al., 1999) followed by automated analysis.

Spectrophotometric analyses of CDOM samples were performed using PerkinElmer Lambda 650 UV/VIS spectrophotometer with 1 cm quartz cuvette over the spectral range from 200 to 800 nm with 1 nm intervals. Milli-Q (Millipore) water was used as the reference for all samples. Absorbance measurements were transformed to absorption coefficients by multiplying by 2.303 and dividing by the path length (0.01 m). The spectral slope ($S_{275-295} \mu\text{m}^{-1}$) has been derived from CDOM absorption spectra by fitting the absorption data to the equation: $a_\lambda = a_{\lambda_{\text{ref}}} e^{-S(\lambda - \lambda_{\text{ref}})}$ where a = Napierian absorption coefficient (m^{-1}), λ = wavelength (nm), and λ_{ref} = reference wavelength (nm). The resulting slope coefficient was multiplied by 1000 to convert unit from nm^{-1} to μm^{-1} . SUVA₂₅₄ values were determined by dividing the UV absorbance measured at 254 nm by the DOC concentration and are reported in the units of square meters per gram carbon.

Excitation/emission matrices of fluorescence were measured for DOM samples in 1 cm quartz cuvette in a Varian Cary Eclipse fluorometer (Agilent). Bandwidths were set to 5 nm for excitation and 4 nm for emission. A series of emission scans

(280–600 nm) were collected over excitation wavelengths ranging from 220 to 450 nm by 5 nm increments. Fluorescence spectra were corrected for inner filter effects, which accounted for the absorption of both excitation and emission light by the sample in the cuvette (Mobed et al., 1996). This was done following the methods of Murphy et al. (2010). The fluorescence spectra (excitation and emission) were also corrected for instrument biases using an excitation correction spectrum derived from a concentrated solution of Oxazine 1 and an emission correction spectrum derived using a ground quartz diffuser. Fluorescence spectra were Raman calibrated by normalizing to the area under the Raman scatter peak (excitation wavelength of 350 nm) of a Milli-Q water sample, run on the same session as the samples. To remove the Raman signal, a Raman normalized Milli-Q excitation-emission matrix (EEM) was subtracted from the sample data. As the measured signal was normalized to the Raman peak and excitation and emission correction spectra were used, all the instrument specific biases were effectively removed (Murphy et al., 2010). Rayleigh scatter effects were removed from the data set by not including any emission measurements made at wavelengths = excitation wavelength +20 nm. Most likely due to the high heterogeneity of the samples in relation to number of observations, parallel factor analysis (PARAFAC) was not successful in extracting relevant information from the dataset. Instead, we used the classical peak-picking method, and fluorescence peaks C, A, M, and T were extracted from the EEM data (Coble, 1996). Peak A is a primary fluorescence peak from dissolved humic substances; peak C is a secondary humic substance peak characteristic of terrestrially derived DOM; peak M is a secondary humic substance peak characteristic of microbial DOM; peak T is a peak attributable to fluorescence from the aromatic amino acid tryptophan (Coble, 1996). Being a proxy for humic-like, typically terrestrially derived material, we chose to use only peak A for further analysis.

We analyzed the molecular size of DOM with SEC. The SEC analyser consisted of an integrated autosampler and pump module (GPCmax, Viscotek Corp.), a linear type column [TSK G2000SW_{XL} column (7.8 × 300 mm, 5 μm particle size, Tosoh

Bioscience GmbH)], a guard column (Tosoh Bioscience GmbH) and a UV detector (Waters 486 Tunable Absorbance Detector) set to 254 nm. The flow rate was 0.8 ml min⁻¹ and the injection volume 100 µL. The columns were thermo-regulated in a column oven (Croco-cil 100-040-220P, Cluzeau Info Labo) at 25°C. The data were collected with OmniSEC 4.5 software (Viscotek Corp.). The eluent was 0.01 M acetate buffer at a pH of 7.00 (Vartiainen et al., 1987). Prior to injection, the samples were filtered through a 0.2 µm PTFE syringe filter. The system was calibrated using a combination of standards, as follows: acetone, ethylene glycol, salicylic acid, polystyrene sulphonate (PSS) 3.5 kDa and PSS 6.5 kDa (58, 100, 138, 3610, and 6530 Da, respectively). The calibration curve was linear ($R^2 = 0.99$) over the apparent molecular weight (AMW) range tested. Comparison between SEC method and absorbance measurements [$a_{(CDOM254)}$] yielded a linear correlation coefficient of 0.92, indicating high qualitative recovery of (C)DOM with the SEC method, as measured from integrated signal from SEC chromatogram. From integrated signal we calculated the weighted average apparent molecular weight (AMW_w).

For stable carbon isotope analysis, acidified and freeze-dried DOM was packed to foil cups and analyzed at the Stable Isotope Facility at UC Davis (USA). There, samples were analyzed for $\delta^{13}\text{C}$ using a PDZ Europa ANCA-GSL elemental analyser interfaced to a PDZ Europa 20-20 isotope ratio mass spectrometer (Sercon Ltd., Cheshire, UK). The resulting carbon delta values are expressed relative to international standard Vienna PeeDee Belemnite. Reported standard deviation for this method is $\pm 0.2\text{\textperthousand}$. $\delta^{13}\text{C}$ was only measured for samples taken in 2011.

Calculation of Freshwater Residence Time

We calculated the freshwater residence time for our surface water samples using measured river discharge, surface salinity, and a volume estimate for each upstream segment to a sampling point, totalling 3 or 4 segments for each of the three river estuaries. This approach can be described as the freshwater transit time, which is the average amount of the water parcel (and its dissolved constituents) spend in the estuary between entrance (river end-member) and exit (sea end-member; Zimmerman, 1976; Sheldon and Alber, 2002). The volume of the upper mixed layer in each segment was determined using the bathymetry and the stratification depth. Area of the polygon bounding each segment was determined using publicly available version of the Google Earth (www.google.com/earth/) service and open Earth Point polygon area tool (<http://www.earthpoint.us/>) and approximate mean depth using high-resolution nautical maps. The mixed layer depth in each segment was determined from the conductivity-temperature-depth (CTD) profiles taken at each sampling occasion. For one of the spring sampling transects no CTD data was available and corresponding mixed layer depth from previous year's sampling was used.

Using the estimated volume of the upper mixed layer or whole segment, measured surface water salinity at each sampling station and known salinities of seawater and river end-members, a freshwater fraction in each segment was

calculated using salinity as a tracer. The freshwater fraction and segment volume were then used to estimate the amount of freshwater in each segment and subsequently the time needed to replace the fresh water in a segment was calculated by using the 10-day average river discharge preceding each sampling occasion. Cumulative age of the freshwater in each segment was calculated by assuming homogeneous mixing and zero lateral exchange between segments, i.e., freshwater in each segment to be completely replaced before entering the next segment downstream the estuary. In estuaries tidal mixing is often limiting the usability of approach described above, however, in the Baltic Sea, tidal variation in water level is virtually absent, allowing us to reliably use this simple estimation.

Statistical Analyses

First, we investigated mixing curves for changes in DOC concentration with salinity to test if end-member concentrations and mixing between these two were constant or varied over time. Linear regressions of DOC versus salinity for each sampling transect (six for each estuary, 18 regressions in total) were fitted, and in contrast to ordinary linear regressions, the residual variation around the regression lines was also allowed to vary with salinity by formulating a linear model for the standard deviation (Carstensen and Weydmann, 2012). Through this modeling approach variations in conservative mixing specific to each transect and potential heteroscedasticity were analyzed for each estuary separately. Due to the low number of observations in each transect, it was not possible to investigate heteroscedasticity for individual transects.

Second, we analyzed if measurements of DOM quality changed consistently with DOC along the estuarine gradients. The investigated DOM quality measurements were SUVA₂₅₄, S_{275–295}, peak A, $\delta^{13}\text{C}_{\text{DOC}}$, AMW_w, and the DOC:DON ratios. If these DOM components were processed in the estuaries in a similar way as DOC, relationships between the DOM components and DOC would be linear, whereas significant deviations from linear relationships would indicate that the DOM components were degraded, produced, or transformed at a different rate than DOC along the estuarine gradient. Generalized additive models (GAM) were employed to examine if there were significant departures from linearity in the relationships between DOM quality variables and DOC. The GAM also included a categorical seasonal factor to account for additive differences in the relationships to DOC between spring, summer and autumn transects. If the non-linear component of the GAM was not significant then the relationship was reduced to linearity. Hence, the GAM included two parametric components (slope and seasonal variation) and one non-parametric component (departure from linearity in the DOM quality versus DOC relationship).

Third, we examined interrelationships between DOM quality measurements for the three estuaries separately using a principal component analysis (PCA) for five of the six quality variables. The stable carbon isotope ($\delta^{13}\text{C}_{\text{DOC}}$) was not included in this analysis, since it was only measured during the second year of sampling. The first two principal components, expressing the most significant changes in the DOM composition, were

investigated in relation to salinity, DOC and residence time using GAM.

Finally, we analyzed if the relatively inexpensive DOM quality measurement $S_{275-295}$ could be used for predicting other DOM components and if such relationships were uniform across the three estuaries. Further, we were interested in the precision of such relationships. For the general applicability of the approach, parametric models were employed. Exponential relationships for SUVA₂₅₄, peak A, $\delta^{13}\text{C}_{\text{DOC}}$, AMW_W, and DOC:DON versus $S_{275-295}$ were fitted to describe the general curvature in the scatter plots with parameters specific to each estuary. Tests for common intercepts and exponential slopes across the three estuaries were carried out, and the models were reduced when significant differences were not present.

The statistical analyses were carried out in SAS 9.3 using PROC MODEL, PROC GAM, and PROC PRINCOMP.

RESULTS

Relationship between Freshwater Residence Time and Salinity

The calculated freshwater residence time in the studied estuaries varied greatly from 0 days at the river mouth to 395 days in the outer Karjaanjoki estuary. In Kyrönjoki and Kiiminkijoki estuaries the longest residence times were 47 and 13 days, respectively. The relationships between freshwater residence time and salinity were highly variable, as for example freshwater residence time varied from a few days to a few months at salinity around 2 (**Figure 2**). Freshwater residence time increased sharply at low salinity and gradually flattened toward the seaward end-member. The relationships varied between estuaries and flow regimes: The long and relatively deep Karjaanjoki estuary, which also receives the lowest river discharges, had the highest freshwater residence times in general and the increase of residence time with increasing salinity was the highest in Karjaanjoki estuary. Kyrönjoki and Kiiminkijoki estuaries had higher freshwater discharges, and lower surface volumes, resulting in considerably lower residence times. During seasons with high river flow, the freshwater residence time was generally lower along the salinity gradient as compared to the periods of low river discharge (**Figure 2**).

Besides freshwater residence time, the quantity and quality of DOM varied between the three estuaries (**Table 1**). DOM originating from rivers Kiiminkijoki and Kyrönjoki had a higher DOC concentration, more pronounced humic-like signal and relatively larger average molecular size compared to DOM entering the Karjaanjoki estuary. Differences among these estuaries and effects on the DOM characteristics have been discussed in Asmala et al. (2013).

Changes in Dom Pool along the Salinity Gradient

In order to analyse the variation of DOM quantity and quality along the estuarine salinity gradient, we modeled the conservative mixing of DOC between the two end-members for each sampling transect separately (**Figures 3A–C**). There

TABLE 1 | Salinity and DOM characteristics for the river and sea end-members in the three studied estuaries (KA = Karjaanjoki, KI = Kiiminkijoki, and KY = Kyrönjoki).

River	End member	Salinity	DOC ($\mu\text{mol L}^{-1}$)	SUVA ₂₅₄ ($\text{m}^2 \text{ g C}^{-1}$)	$S_{275-295}(\mu\text{m}^{-1})$	Peak A (R.U.)	$\delta^{13}\text{C}_{\text{DOC}}\text{‰}$	AMW _W (Da)	DOC:DON
KA	River	0	654 (545–801)	3.5 (2.9–4.2)	17.3 (14.7–18.8)	1.00 (0.86–1.18)	-28.1 (-28.4 to -27.9)	654 (2192–2523)	23.2 (18.6–29.4)
	Sea	6.2 (5.6–6.8)	341 (310–364)	2.3 (2.2–2.6)	24.4 (23.2–26.1)	0.33 (0.29–0.35)	-26.9 (-27.6 to -26.2)	341 (1672–1797)	16.2 (13.0–18.2)
KI	River	0	1368 (919–1822)	5.0 (3.5–7.0)	12.0 (11.6–12.3)	1.95 (1.53–2.35)	-28.6 (-28.7 to -28.4)	1368 (2598–3208)	44.8 (31.0–57.1)
	Sea	2.3 (1.9–2.4)	399 (254–547)	4.1 (2.8–5.6)	17.5 (15.8–19.2)	0.59 (0.55–0.62)	-27.4 (-27.7 to -27.2)	399 (2063–2241)	24.1 (17.7–30.1)
KY	River	0	1575 (949–2233)	4.4 (3.5–4.9)	13.5 (12.7–14.6)	2.84 (1.82–3.36)	-28.0 (-28.2 to -27.8)	1575 (2205–2997)	31.2 (21.5–45.6)
	Sea	3.0 (1.4–3.4)	489 (264–827)	3.0 (2.1–4.1)	18.5 (13.9–22.2)	0.68 (0.37–1.48)	-27.2 (-27.5 to -26.8)	489 (1899–2304)	27.4 (17.9–38.9)

Mean value and range (in parentheses) of each variable are presented. DOC, dissolved organic carbon; SUVA₂₅₄, DOC-specific UV absorbance at 254 nm; $S_{275-295}$, slope of CDOM absorbance between 275 and 295 nm; Peak A, DOM fluorescence in ex/em range 260/400–460/460 nm; $\delta^{13}\text{C}_{\text{Doc}}$, stable carbon isotope ratio of DOC; AMW_W, weight-averaged molecular weight; and DOC:DON ratio (mol/mol).

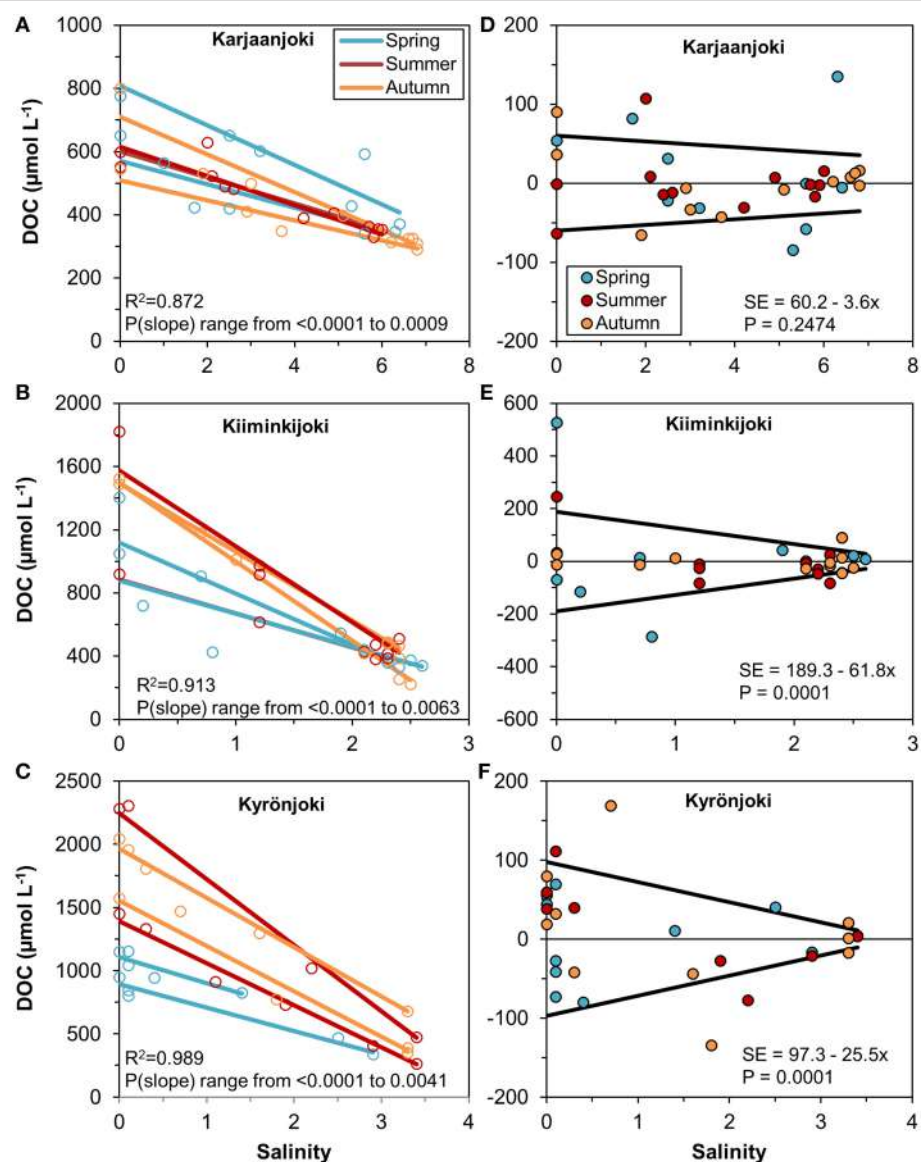


FIGURE 3 | (A–C) Linear regressions between DOC concentration and salinity for each sampling transect, estuary, and season. Observations are shown with open symbols. All slopes are significant ($P < 0.05$) and the R^2 is for all regressions within the estuary. **(D–F)** Residuals from the regression models and the estimated models for the residual standard error for the three estuaries.

was a considerable variation between the regression lines, particularly for the Kiiminkijoki and Kyrönjoki estuaries, and a pronounced seasonal tendency for mixing of lower DOC concentrations in the two northern estuaries in spring, where freshwater discharge is strongly influenced by snowmelt. Even within seasons the conservative mixing lines varied substantially. Furthermore, we used the residuals from the regression models to quantify the variability of DOC around the mixing line (**Figures 3D–F**). In essence, the higher the residual the larger is the deviation from conservative mixing. In the Kiiminkijoki and Kyrönjoki estuaries, DOC variability around the mixing line was significantly higher in the freshwater end of the

salinity gradient and decreased with increasing salinity, whereas variability around the mixing line was generally smaller in the Karjaanjoki estuary and did not change significantly with salinity.

We chose six DOM quality variables for this investigation, which are analytically diverse and provide a broad range of the DOM pool properties: Two variables were measured directly with CDOM spectroscopy ($S_{275-295}$ and fluorescence peak A), one with mass spectrometry ($\delta^{13}\text{C}_{\text{DOC}}$), and three with combination of analyses (SUVA₂₅₄, AMW_W, DOC:DON). Even though the six variables represent different characteristics and have been measured with different methods, the DOM variables correlated strongly. The selected DOM variables are quality characteristics,

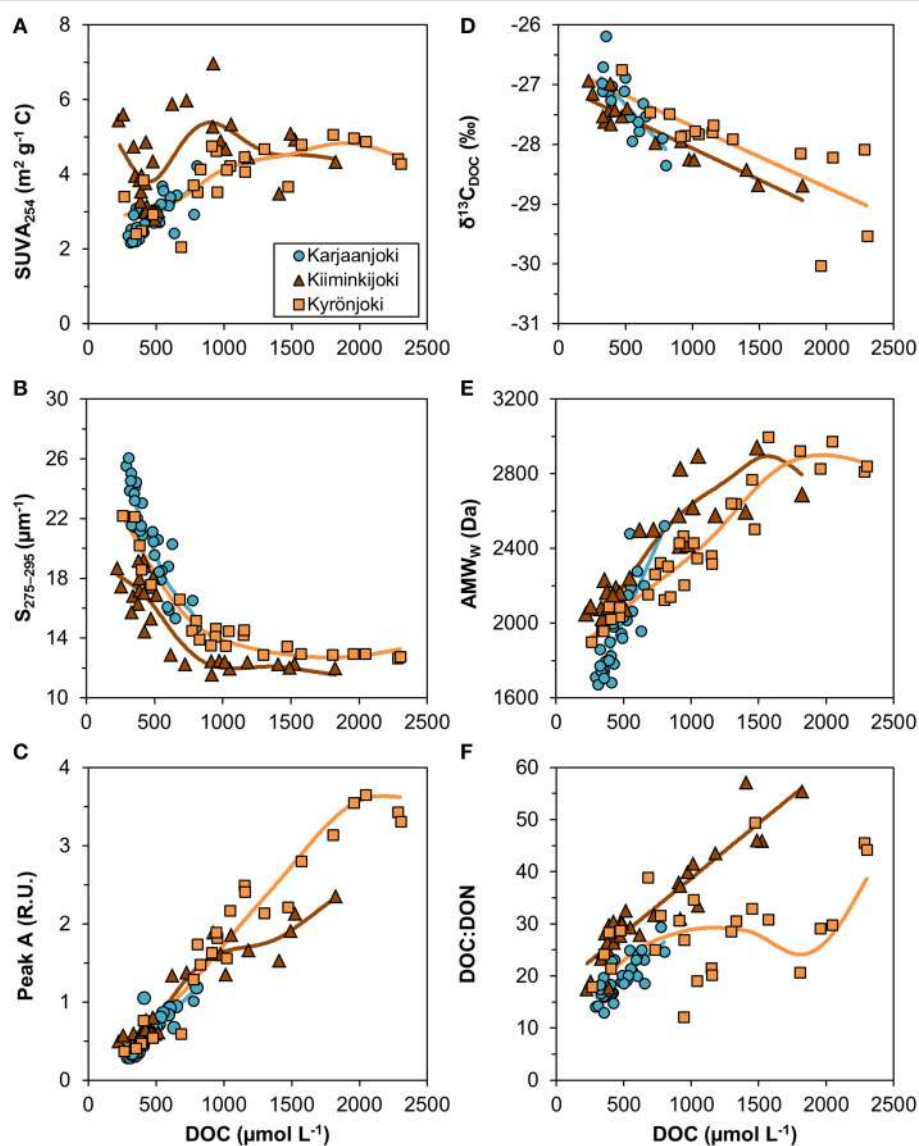


FIGURE 4 | Relationships between DOM quality variables and DOC concentration. (A) SUVA₂₅₄ = DOC-specific UV absorbance at 254 nm, **(B)** $S_{275-295}$ = slope of CDOM absorbance between 275 and 295 nm, **(C)** peak A = DOM fluorescence in ex/em range 260/400–460 nm, **(D)** $\delta^{13}\text{C}_{\text{DOC}}$ = stable carbon isotope ratio of DOC, **(E)** AMW_w = weight-averaged molecular weight, and **(F)** DOC:DON ratio (mol/mol). Generalized additive models (GAM) are fitted to data (solid lines). The GAM relationships are shown as linear regressions if the non-linear component was not significant (Table 2).

and not directly derived from the DOC concentration with the exception of SUVA₂₅₄ and DOC:DON. However, the two latter express ratios between CDOM and DOC, and C and N in the DOM pool and therefore characterize the quality rather than quantity of DOM.

Variable relationships with DOC concentration were observed (Figure 4) and many of them had significant departures from linearity (Table 2). All DOM quality variables had a significant linear GAM component, except for SUVA₂₅₄ in Kiiminkijoki that displayed an oscillating pattern without any clear tendency to change with DOC (Figure 4A). $S_{275-295}$ had significant non-linear relationships for all three estuaries, decreasing with DOC in an exponential manner (Figure 4B). Peak A had an

apparent linear relationship with DOC concentrations below 1000 $\mu\text{mol L}^{-1}$ with significant departures near the river mouths in Kiiminkijoki and Kyrönjoki estuaries (Figure 4C). On the other hand, the stable carbon isotope signature of DOC ($\delta^{13}\text{C}_{\text{DOC}}$) changed linearly with DOC throughout the entire scale (Figure 4D). In Kiiminkijoki and Kyrönjoki estuaries changes in AMW_w were small near the river mouths followed by larger, almost linear, declines with DOC (Figure 4E). The DOC:DON ratio increased linearly with DOC in Karjaanjoki and Kiiminkijoki estuaries, whereas the relationship in Kyrönjoki was more complex (Figure 4F). Overall, in Karjaanjoki the DOM quality changed consistently with DOC across the salinity gradient, whereas there were pronounced non-linearities in

the relationships with DOC near the freshwater sources in Kiiminkijoki and Kyrönjoki estuaries.

In addition to the changes with DOC, there were weak seasonal patterns in the DOM quality variables, except in Kyrönjoki where spring samples generally had higher values of $S_{275-295}$ and Peak A, and lower DOC:DON values (**Table 2**; **Figure S1**). However, the other DOM quality variables did not show any significant seasonal pattern in Kyrönjoki estuary.

The five DOM quality variables in the PCA were strongly inter-correlated, and the first principal component (PC1) explained between 71 and 82% of variation across the three estuaries (**Figure 5**). PC1 represented a weighted average of the five DOM quality variables with almost equal weight to each of them, except for DOC:DON in Kyrönjoki estuary that had a slightly lower weight. The second principal component (PC2) explained 10% of the variation in Karjaanjoki, whereas it was more important in the two other estuaries accounting for 20–22% of variation. In all three estuaries, the second component represented a difference between DOC:DON and SUVA₂₅₄.

We examined the information contained in PC1 and PC2 in relation to salinity, DOC concentration and freshwater residence time (**Figure 6**). PC1 had a strong, mostly linear relationship with both salinity and DOC concentration (**Figures 6A,B**), whereas the relationship between PC1 and freshwater residence time was non-linear (**Figure 6C**). The strongest relationships for PC1 were salinity in Karjaanjoki and DOC in Kiiminkijoki and Kyrönjoki. PC2 was related neither to salinity nor freshwater residence time (**Figures 6D,F**), whereas a weak coupling to DOC was observed in Kiiminkijoki (**Figure 6E**). Nevertheless, no general pattern was found using salinity, DOC and freshwater residence time as explanatory variables for the variations in PC2. We have labeled PC1 as “Mixing” and PC2 as “Processing” for clarity, and the justification of this is presented in Section Discussion.

$S_{275-295}$ could be used as predictor for the other DOM quality variables with a reasonable precision (**Figure 7**). Although the relationships estimated for the three estuaries were significantly different (either intercepts or exponential slopes or both were different), the nature of the relationships was similar. For all other five DOM variables the relationship to $S_{275-295}$ had an exponential form.

DISCUSSION

In order to improve our understanding about the role of DOM processing along the estuarine passage from the river mouth to the open sea, we calculated the residence time for our study estuaries (**Figure 2**). We observed significant variation in freshwater residence time along the salinity gradient. This variation reveals that at a given salinity on the estuarine gradient the “age” of the freshwater fraction may vary considerably, which has further implications on the associated nutrient and organic matter pool. The calculated freshwater residence time at the sea end-member ranged from 2 to 396 days, depending on the estuary and the flow regime (**Table 1**). This range covers the reported residence times in different estuarine systems: 0.8–2.7 days (Childs and Quashnet estuaries, USA; Geyer, 1997), 2–210 days (Childs, Columbia, Parker, Satilla and Susquehanna

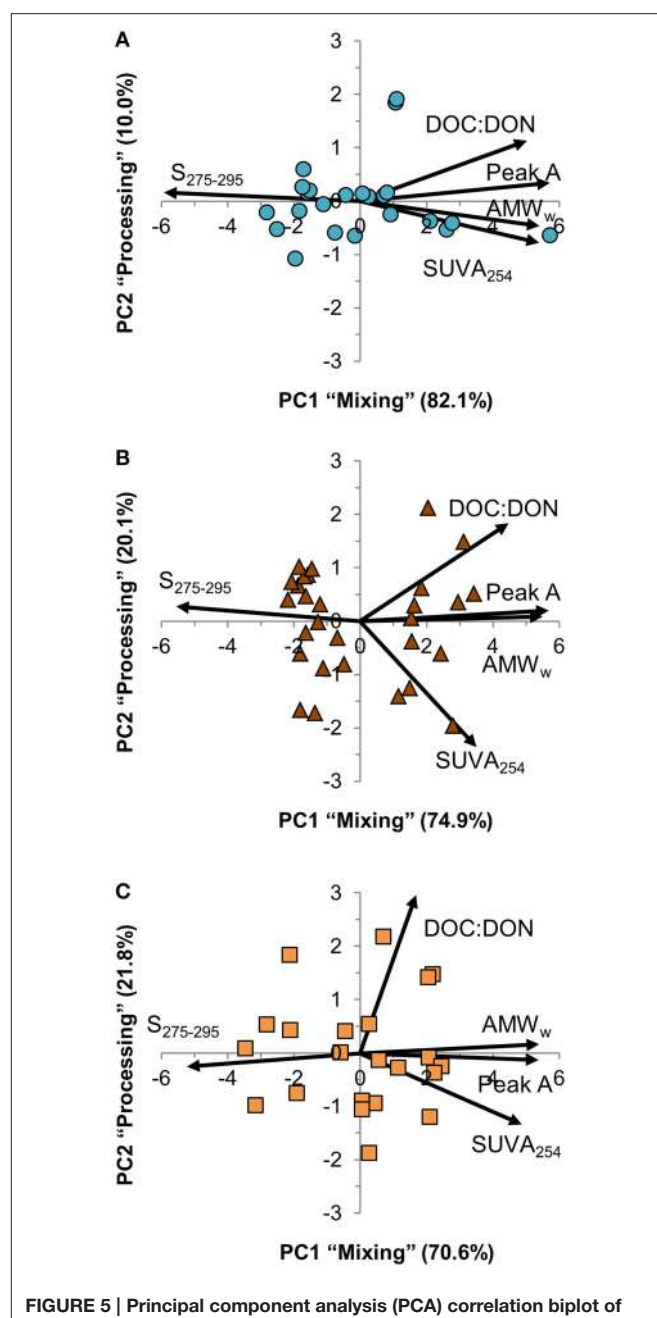


FIGURE 5 | Principal component analysis (PCA) correlation biplot of the two first principal components (PC1 and PC2). Samples are shown as symbols and the contribution of the DOM quality variables to the principal components as vectors. The proportion of variation explained by both principal components is included with the axes titles. **(A)** Karjaanjoki, **(B)** Kiiminkijoki, and **(C)** Kyrönjoki estuary.

estuaries, USA; Hopkinson et al., 1998), 20–180 days (Choptank and Pocomoke estuaries, USA; Bouvier and del Giorgio, 2002), 4–36 days (Bangpakong estuary, Thailand; Buranapratheprat et al., 2002), and 2–100 days (Fourleague Bay; Perez et al., 2011). Our aim was to use calculated residence time to detect patterns in freshwater dynamics in the estuaries, possibly explaining the variation in DOM quantity and quality.

TABLE 2 | Significance of the three GAM components for explaining variations in DOM quality variables in the three estuaries.

DOM variable	Karjaanjoki			Kiiminkijoki			Kyrönjoki		
	Season	Linear	Spline	Season	Linear	Spline	Season	Linear	Spline
SUVA ₂₅₄	0.3101	<0.0001	0.4033	0.5514	0.0807	0.0002	0.0501	<0.0001	0.0019
S _{275–295}	0.0513	<0.0001	0.0199	0.0169	<0.0001	<0.0001	0.0050	<0.0001	<0.0001
Peak A	0.0665	<0.0001	0.0657	0.2059	<0.0001	<0.0001	0.0024	<0.0001	0.0013
δ ¹³ C _{DOC}	0.4247	0.0027	0.4717	0.2287	<0.0001	0.2759	0.8734	0.0127	0.7683
AMW _W	0.1184	<0.0001	0.2074	0.3970	<0.0001	0.0085	0.0821	<0.0001	0.0005
DOC:DON	0.2932	<0.0001	0.7050	0.6773	<0.0001	0.1129	0.0165	0.0088	0.0096

Season describes additive differences between spring, summer, and autumn. The relationship with DOC is modeled with a linear component and a non-parametric spline function. Components significant at the $P < 0.05$ level are highlighted in bold.

We were able to identify two distinct freshwater discharge patterns in our dataset; low and high flow conditions. During the low flow, less freshwater enters the estuarine system and the inferred freshwater residence time increases compared to high flow conditions. Essentially, during low flow conditions, freshwater residence time is higher at a given salinity compared to high flow conditions. Low flow conditions occur in summer and autumn, simultaneously with significant autochthonous OM production and high photo-oxidation (Vodacek et al., 1997; Lønborg et al., 2009), potentially changing the DOM pool. To quantify the variation in DOC concentration along the estuarine gradient, we used a linear regression model for each sampling transects separately (Figure 3). Variation in DOC concentration was high in freshwater end-member, from $\pm 60 \mu\text{mol L}^{-1}$ in Karjaanjoki to $\pm 190 \mu\text{mol L}^{-1}$ in Kiiminkijoki. Variation decreased rapidly when moving along the salinity gradient, reflecting the stability of the coastal sea end-member. This is not surprising, as the freshwater discharge in riverine systems typically fluctuates on seasonal and even diel timescales (Spencer et al., 2007b; Holmes et al., 2012). Most of the DOC in these estuaries originates from the respective river, and not from external point sources (Räike et al., 2012). So it can be argued that the changes in DOM characteristics are in major part due to the alterations of the initial DOM entering the estuary (as opposed to being an artifact of DOM additions within the estuary). Further, in the catchment area different biological processes and human activities cause changes in hydrological conditions and organic matter fluxes from the terrestrial system (Jickells, 1998; Sachse et al., 2005; Asmala et al., 2013). Thus, the combination of changes in discharge and changes in organic matter loading from catchment create large temporal variations in the DOM pool entering the estuaries.

We observed that different DOM quality variables changed differently in relation to DOC concentration (Figure 4). For instance, the stable carbon isotope signature of DOC and humic-like fluorescence had almost linear relationships with DOC concentration, meaning that processes changing the quantity of DOM change these quality indices in similar proportion. On the other hand, SUVA₂₅₄ shows no clear pattern along the measured DOC concentration range, whereas both S_{275–295} and molecular weight had coherent, non-linear relationships. The patterns of the slopes and the

molecular weight versus DOC in Kyrönjoki and Kiiminkijoki estuaries suggests that part of the DOM pool remains unchanged even though the DOC concentration decreases. In other words, there are components in the DOM pool that persist after the first phases of the degradation processes in the estuarine transport, such as flocculation and microbial degradation.

The analyzed DOM quality characteristics were highly correlated (Figure 5), even though different analytical methods to characterize DOM were used. We argue that the observed high correlation between different quality parameters of the bulk DOM is an indication that common transformations have occurred along the salinity gradients. Also, the changes along the salinity gradient were unidirectional with the expected changes according to the reactivity continuum concept (Amon and Benner, 1996). Our results suggest, that mixing and processing together cause molecules in the DOM pool to decrease in size, lose aromaticity and have a lighter carbon isotope composition when moving down the reactivity (salinity) continuum. PCA was used to examine the relationships between the DOM quality variables (Figure 5). Further, we compared the results of PCA to salinity, DOC concentration and freshwater residence time for a better understanding of DOM processing during the estuarine transport (Figure 6). From the strong correlation between the first principal component (PC1) and both salinity and DOC concentration (Figures 6A,B), it is evident that PC1 actually describes mixing of the two end-members, and is labeled in Results Section accordingly. The second principal component (PC2) on the other hand, does not correlate with salinity, DOC concentration or freshwater residence time, indicating some DOM transformation processes not explained by mixing, DOC concentration or residence time. PC2 was labeled as processing to cover all changes in DOM properties that cannot be attributed to mixing. The weak link between PC2 (processing) and DOC concentration suggests that changes in quantity and quality of DOM are to some extent decoupled.

We used multiple analytical methods in this study to characterize the DOM pool, but still only some components or fractions of the DOM pool were measured, a bias which might have implications when interpreting the results. Specifically, with spectroscopic analyses the non-colored DOM was not detected by most of our methods. This non-colored pool of DOM

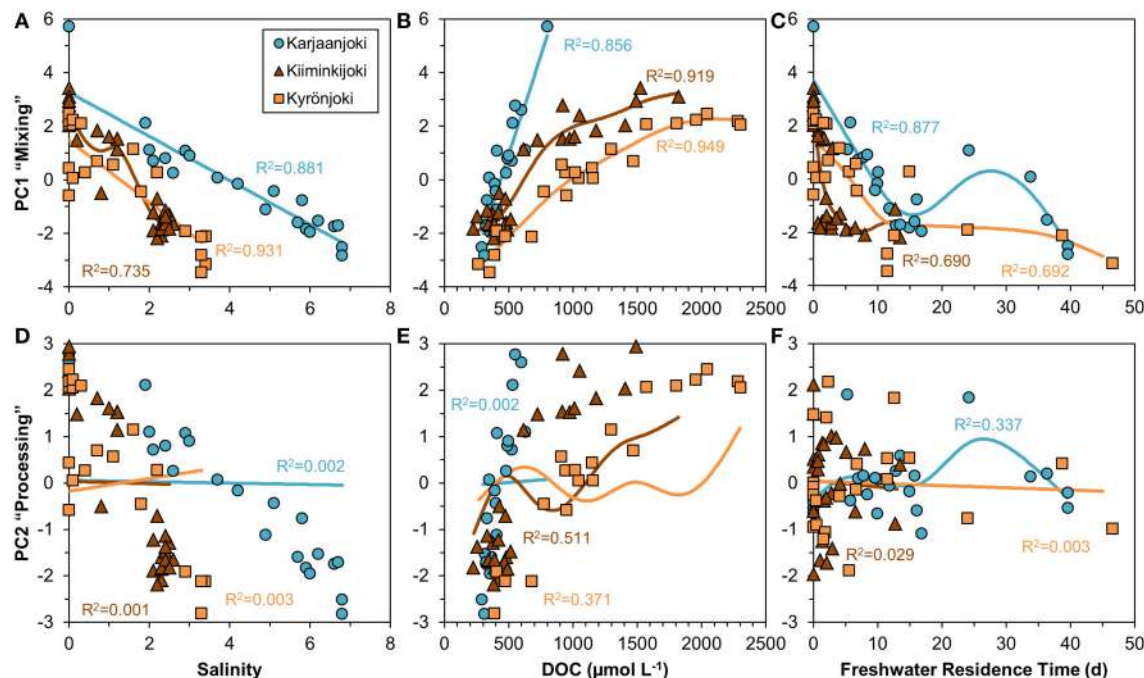


FIGURE 6 | Relationships of the two first principal components versus salinity, DOC concentration and freshwater residence time investigated by a non-parametric GAM (solid line). (A–C) Principal component 1 (“Mixing”). (D–F) Principal component 2 (“Processing”). Freshwater residence time in the Karjaanjoki estuary is divided by 10 for the figure to allow comparison with other two estuaries.

might be biogeochemically highly relevant, containing such reactive components as amino acids or simple carbohydrates (Vodacek et al., 1997; Sulzberger and Durisch-Kaiser, 2009). The selectivity of DOM analyses is ubiquitous; virtually all methods used to characterize DOM leave parts of the whole pool undetected. From an analytical perspective, the UV absorption slope ($S_{275-295}$) proved to be a useful predictor for other DOM variables (Figure 7). The applicability of this slope has been shown in previous studies (e.g., Helms et al., 2008; Fichot and Benner, 2012), and because of its relatively easy and inexpensive analysis, it is highly recommended to continue to use this spectral region as a standard biogeochemical marker in monitoring the DOM-related processes in aquatic environments.

Typically, conservative mixing models have been used to analyse the extent of allochthonous DOM processing in estuarine systems (e.g., Stedmon and Markager, 2003; Boyd and Osburn, 2004). Our data suggests that the variation in DOM quantity and quality occurring in relatively short timescale (days–weeks) poses significant challenges for drawing conclusions from conservative mixing models (Figure 3). The range of the variation in the end-members ultimately determines the applicability of conservative mixing model. Previous studies where non-conservative behavior of DOM has been observed, typically include multiple quantitative and qualitative variables, which show that some parameters deviate from conservative mixing while others do not (Bowers et al., 2004; Markager et al., 2011; Asmala et al., 2014). These qualitative changes can be attributed to simultaneous production and removal of DOM,

which may leave the concentration in seemingly steady state, but in fact the DOM pool is subject to continuous dynamic processes.

In this study, we emphasize the importance of taking the variation in freshwater end-member into account in the analysis of DOM processes along the estuarine gradient (Figures 3D–F). Quantification of this variation is especially important when using conservative mixing models to study the DOM transformation, removal and production processes in estuaries, as a relatively large variation on the other end will cause instability throughout the observation range. In coastal systems, the sea end-member is typically relatively stable compared to the freshwater end-member (Fleming-Lehtinen et al., 2014). The results of this study are also supported by long-term time series from the study estuaries, where the measured total organic carbon concentrations range fourfold in Karjaanjoki and Kyrönjoki, and five-fold in Kiiminkijoki (Figure 8). Also, the amount of variation is changing between estuaries, making the predictions about a “typical” situation even more difficult. Without knowledge of the amount and drivers of end-member variations in estuarine studies, analyses based on conservative mixing models will be evidently inadequate as the large variation in the river end-member is carried over throughout the estuarine gradient, thus introducing source of error in conservative mixing models. And as this pattern of variation is evident for DOM quantity, it is highly likely that similar system- and season-specific variations can be observed for DOM quality characteristics as well.

Residence time in the studied systems is likely not long enough to allow biogeochemical processes to significantly alter

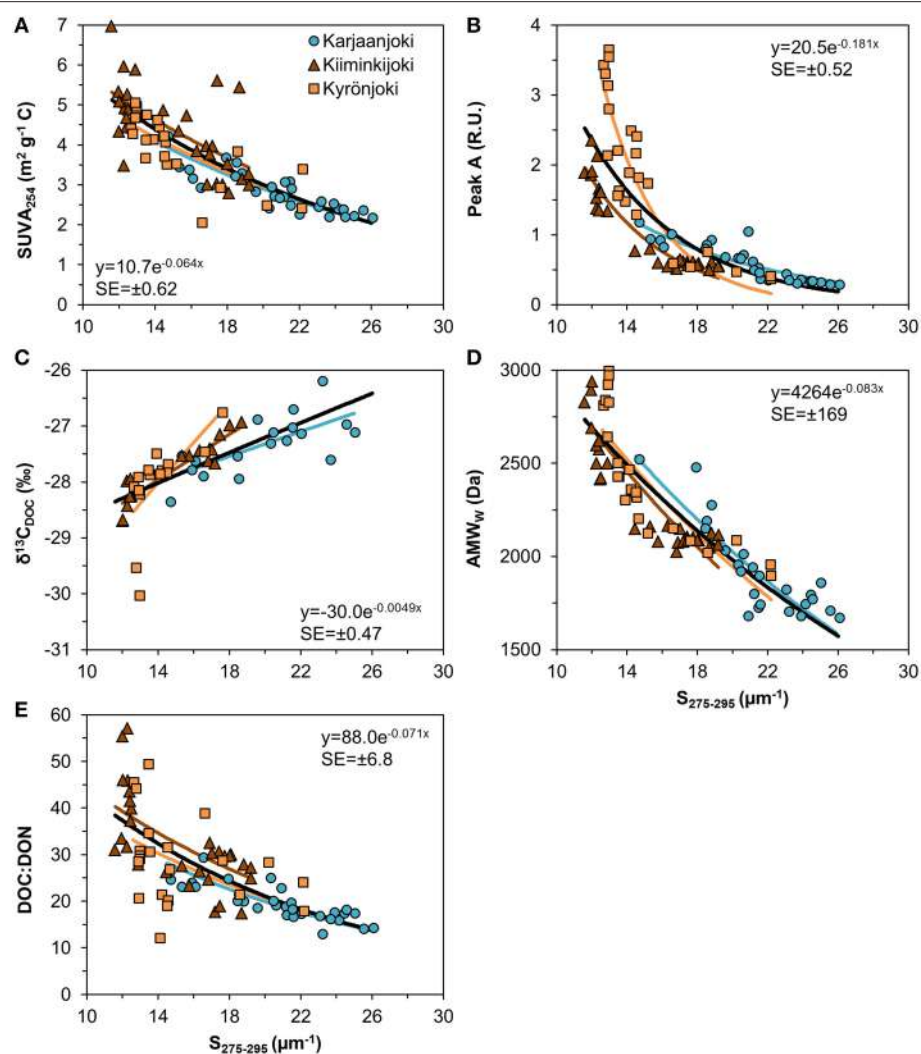


FIGURE 7 | Relationship between UV slope ($S_{275-295}$) and other DOM quality variables used in this study. (A) $SUVA_{254}$; **(B)** Fluorescence peak A; **(C)** $\delta^{13}\text{C}_{\text{DOC}}$; **(D)** AMW_W ; **(E)** DOC:DON ratio. Exponential models were fitted to data for each estuary after testing for common intercepts and exponential slopes. A common model (black line) was fitted to all data with the formula and the residual standard error (SE) inserted in the plots.

the major, refractory part of the DOM pool, especially in the two northernmost estuaries (Figure 2). However, this approach is significantly altered if we do not assume that the terrestrial signal of the DOM pool is refractory, but instead assume that the estuarine DOM pool is being constantly replenished, depleted and transformed. These changes in the DOM pool result as a dynamic state where the balance between various processes determines the resulting characteristics of the bulk DOM. For these particular estuaries, flocculation and bacterial degradation of DOM have been reported (Asmala et al., 2013, 2014), and high rates of photodegradation have been measured in the coastal Baltic Sea (Aarnos et al., 2012). Further, production of DOM by the marine primary producers is evident (Romera-Castillo et al., 2010). Also, heterotrophic bacteria may produce CDOM from non-colored DOM, thus changing the quality of the DOM pool (Nelson et al., 2004; Shimotori et al., 2010). The highly dynamic

nature of these processes and the inherent variability in the river end-member pose significant challenges for identification of deviations from conservative mixing in estuaries. In order to analyse the estuarine conservative mixing in a given system, the biogeochemical processes that affect the DOM pool along the estuarine gradient should be identified and quantified, alongside detailed hydrologic measurements.

In conclusion, we surprisingly found that the residence time in these systems did not explain variation any better than salinity. Increasing freshwater residence time in estuaries typically increases the nutrient retention, which can be analyzed with simple mass balance calculations, as production of nutrients within estuary is insignificant compared to the magnitude of nutrient removal processes. With organic matter the biogeochemical cycling is much more complex and dynamic, and transformation, degradation, and production of DOM

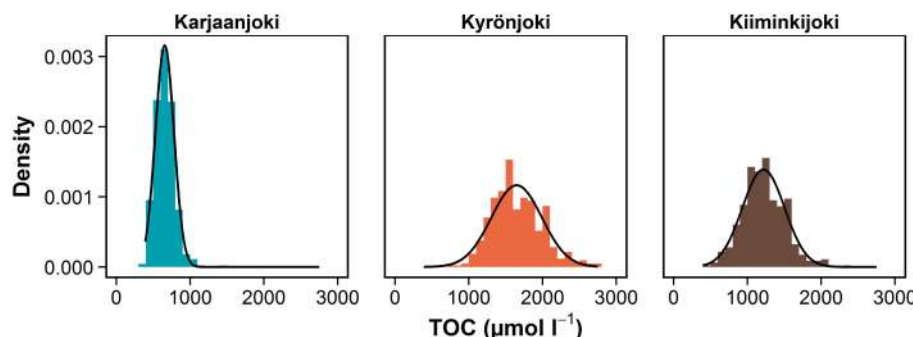


FIGURE 8 | Density of observed TOC concentrations in river end-members of study estuaries between 1975 and 2014. Mean values, standard deviation and range: Karjaanjoki ($n = 442$) 655 (126, 392–1417), Kyrönjoki ($n = 425$) 1648(342, 758–2750), and Kiiminkijoki ($n = 463$) 1217(287, 467–2333) $\mu\text{mol L}^{-1}$. More than 90% of TOC is in dissolved form (DOC) in these systems (Mattsson et al., 2005). Data source: Räike et al. (2012). Normal distribution curve is fitted over each density histogram.

occur continuously. Our results show that mixing is the major factor governing the characteristics of the DOM pool along the estuarine gradient. Further, we show that variations in DOM pool at the freshwater end-member can introduce substantial departures from linear mixing, but the quality of the DOM pool is not altered consistently with the DOM quantity. Therefore, mixing can only partially account for changes in the DOM pool along the estuarine gradient and more research on the various transformation processes is needed to understand the variability of DOM quality at the land-sea interface.

AUTHOR CONTRIBUTIONS

EA participated in the experiment design, performed most of the field samplings, conducted most of the laboratory analyses, participated in data analyses and was responsible for the manuscript preparation. HK participated in the experiment design, field samplings, and the laboratory analyses, was responsible for the residence time calculation and participated in manuscript preparation. JC was responsible of principal component analysis and general additive model, and participated in manuscript preparation. DT led the experiment design, and participated field samplings and the laboratory analyses, and participated in manuscript preparation.

REFERENCES

- Aarnos, H., Ylöstalo, P., and Vähätalo, A. V. (2012). Seasonal phototransformation of dissolved organic matter to ammonium, dissolved inorganic carbon, and labile substrates supporting bacterial biomass across the Baltic Sea. *J. Geophys. Res. Biogeosci.* 117:G01004. doi: 10.1029/2010jg001633
- Abrial, G., Nogueira, M., Etcheber, H., Cabeçadas, G., Lemaire, E., and Brogueira, M. J. (2002). Behaviour of organic carbon in nine contrasting European estuaries. *Estuar. Coast. Shelf Sci.* 54, 241–262. doi: 10.1006/ecss.2001.0844
- Amon, R. M., and Benner, R. (1996). Bacterial utilization of different size classes of dissolved organic matter. *Limnol. Oceanogr.* 41, 41–51. doi: 10.4319/lo.1996.41.1.0041
- Asmala, E., Autio, R., Kaartokallio, H., Pitkänen, L., Stedmon, C., and Thomas, D. N. (2013). Bioavailability of riverine dissolved organic matter in three Baltic Sea estuaries and the effect of catchment land use. *Biogeosciences* 10, 6969–6986. doi: 10.5194/bg-10-6969-2013
- Asmala, E., Bowers, D. G., Autio, R., Kaartokallio, H., and Thomas, D. N. (2014). Qualitative changes of riverine dissolved organic matter at low salinities due to flocculation. *J. Geophys. Res. Biogeosci.* 119, 1919–1933. doi: 10.1002/2014jg002722
- Benner, R., and Opsahl, S. (2001). Molecular indicators of the sources and transformations of dissolved organic matter in the Mississippi river plume. *Org. Geochem.* 32, 597–611. doi: 10.1016/S0146-6380(00)00197-2

ACKNOWLEDGMENTS

This study was supported by the Academy of Finland (Finland Distinguished Professor Programme, project no. 127097), Walter and Andrée de Nottbeck Foundation and the BONUS COCOA project (grant agreement 2112932-1), funded jointly by the EU and Danish Research Council. The authors would like to thank Riitta Autio, Chris Hulatt, Anne-Mari Luhtanen, and Johanna Oja, for field and laboratory support. Support for sampling was also given by staff from the Tärminne Zoological Station, South Ostrobothnia and North Ostrobothnia Centres for Economic Development, Transport and the Environment, and Kiviniemi Association of Finnish Lifeboat Institution.

SUPPLEMENTARY MATERIAL

The Supplementary Material for this article can be found online at: <http://journal.frontiersin.org/article/10.3389/fmars.2015.00125>

Figure S1 | Seasonal patterns of DOM quality predicted for average DOC in the different estuaries (Karjaanjoki 465, Kiiminkijoki 688, and Kyrönjoki 1026 $\mu\text{mol L}^{-1}$). (A) SUVA₂₅₄; (B) Slope 275–295 nm; (C) Fluorescence peak A; (D) $\delta_{13}\text{C}_{\text{DOC}}$; (E) AMW_W; (F) DOC:DON ratio. Error bars indicate SE of the seasonal means. Asterisks indicate significance level (cf. **Table 2**) with * <0.05 and ** <0.01 .

- Borum, J. (1996). "Shallow waters and land/sea boundaries," in *Eutrophication in Coastal Marine Ecosystems*, eds B. B. Jorgensen and K. Richardson (Washington, DC: American Geophysical Union). doi: 10.1029/CE052p0179
- Bouvier, T. C., and del Giorgio, P. A. (2002). Compositional changes in free-living bacterial communities along a salinity gradient in two temperate estuaries. *Limnol. Oceanogr.* 47, 453–470. doi: 10.4319/lo.2002.47.2.0453
- Bowers, D. G., Evans, D., Thomas, D. N., Ellis, K., and Williams, P. L. B. (2004). Interpreting the colour of an estuary. *Estuar. Coast. Shelf Sci.* 59, 13–20. doi: 10.1016/j.ecss.2003.06.001
- Boyd, T. J., and Osburn, C. L. (2004). Changes in CDOM fluorescence from allochthonous and autochthonous sources during tidal mixing and bacterial degradation in two coastal estuaries. *Mar. Chem.* 89, 189–210. doi: 10.1016/j.marchem.2004.02.012
- Brylinsky, M. (1977). Release of dissolved organic matter by some marine macrophytes. *Mar. Biol.* 39, 213–220. doi: 10.1007/BF00390995
- Buranapratheprat, A., Yanagi, T., Boonphakdee, T., and Sawangwong, P. (2002). Seasonal variations in inorganic nutrient budgets of the Bangpakong Estuary, Thailand. *J. Oceanogr.* 58, 557–564. doi: 10.1023/A:1021214726762
- Carstensen, J., and Weydmann, A. (2012). Tipping points in the Arctic: Eyeballing or statistical significance? *Ambio* 41, 34–43. doi: 10.1007/s13280-011-0223-8
- Chen, R. F., and Gardner, G. B. (2004). High-resolution measurements of chromophoric dissolved organic matter in the Mississippi and Atchafalaya River plume regions. *Mar. Chem.* 89, 103–125. doi: 10.1016/j.marchem.2004.02.026
- Church, T. M. (1986). Biogeochemical factors influencing the residence time of microconstituents in a large tidal estuary, Delaware Bay. *Mar. Chem.* 18, 393–406. doi: 10.1016/0304-4203(86)90020-4
- Coble, P. G. (1996). Characterization of marine and terrestrial DOM in seawater using excitation-emission matrix spectroscopy. *Mar. Chem.* 51, 325–346. doi: 10.1016/0304-4203(95)00062-3
- Dittmar, T., Hertkorn, N., Kattner, G., and Lara, R. J. (2006). Mangroves, a major source of dissolved organic carbon to the oceans. *Global Biogeochem. Cycles* 20:GB1012. doi: 10.1029/2005GB002570
- Fichot, C. G., and Benner, R. (2012). The spectral slope coefficient of chromophoric dissolved organic matter (S275–295) as a tracer of terrigenous dissolved organic carbon in river-influenced ocean margins. *Limnol. Oceanogr.* 57, 1453–1466. doi: 10.4319/lo.2012.57.5.1453
- Fleming-Lehtinen, V., Räike, A., Kortelainen, P., Kauppila, P., and Thomas, D. N. (2014). Organic carbon concentration in the northern coastal Baltic Sea between 1975 and 2011. *Estuaries Coasts* 38, 466–481. doi: 10.1007/s12237-014-9829-y
- Forsgren, G., Jansson, M., and Nilsson, P. (1996). Aggregation and sedimentation of iron, phosphorus and organic carbon in experimental mixtures of freshwater and estuarine water. *Estuar. Coast. Shelf Sci.* 43, 259–268. doi: 10.1006/ecss.1996.0068
- Geyer, W. R. (1997). Influence of wind on dynamics and flushing of shallow estuaries. *Estuar. Coast. Shelf Sci.* 44, 713–722. doi: 10.1006/ecss.1996.0140
- Grasshoff, K., Ehrhardt, M., and Kremling, K. (1983). *Methods of Seawater Analysis*. Weinheim: Verlag Chemie.
- Grasshoff, K., Kremling, K., and Ehrhardt, M. (1999). *Methods of Seawater Analysis*. Weinheim: Verlag Chemie.
- Gueguen, C., Itoh, M., Kikuchi, T., Eert, J., and Williams, W. J. (2015). Variability in dissolved organic matter optical properties in surface waters in the Amerasian Basin. *Front. Mar. Sci.* 2:78. doi: 10.3389/fmars.2015.00078
- Guo, W., Stedmon, C. A., Han, Y., Wu, F., Yu, X., and Hu, M. (2007). The conservative and non-conservative behavior of chromophoric dissolved organic matter in Chinese estuarine waters. *Mar. Chem.* 107, 357–366. doi: 10.1016/j.marchem.2007.03.006
- Helms, J. R., Stubbins, A., Ritchie, J. D., Minor, E. C., Kieber, D. J., and Mopper, K. (2008). Absorption spectral slopes and slope ratios as indicators of molecular weight, source, and photobleaching of chromophoric dissolved organic matter. *Limnol. Oceanogr.* 53, 955. doi: 10.4319/lo.2008.53.3.0955
- Holmes, R. M., McClelland, J. W., Peterson, B. J., Tank, S. E., Bulygina, E., Eglington, T. I., et al. (2012). Seasonal and annual fluxes of nutrients and organic matter from large rivers to the Arctic Ocean and surrounding seas. *Estuaries Coasts* 35, 369–382. doi: 10.1007/s12237-011-9386-6
- Hopkinson, C. S., Buffam, I., Hobbie, J., Vallino, J., Perdue, M., Eversmeyer, B., et al. (1998). Terrestrial inputs of organic matter to coastal ecosystems: an intercomparison of chemical characteristics and bioavailability. *Biogeochemistry* 43, 211–234. doi: 10.1023/A:1006016030299
- Huguet, A., Vacher, L., Relexans, S., Saubusse, S., Froidefond, J. M., and Parlant, E. (2009). Properties of fluorescent dissolved organic matter in the Gironde Estuary. *Org. Geochem.* 40, 706–719. doi: 10.1016/j.orggeochem.2009.03.002
- Jiao, N., Herndl, G. J., Hansell, D. A., Benner, R., Kattner, G., Wilhelm, S. W., et al. (2010). Microbial production of recalcitrant dissolved organic matter: long-term carbon storage in the global ocean. *Nat. Rev. Microbiol.* 8, 593–599. doi: 10.1038/nrmicro2386
- Jickells, T. D. (1998). Nutrient biogeochemistry of the coastal zone. *Science* 281, 217–222.
- Josefson, A. B., and Rasmussen, B. (2000). Nutrient retention by benthic macrofaunal biomass of Danish estuaries: importance of nutrient load and residence time. *Estuar. Coast. Shelf Sci.* 50, 205–216. doi: 10.1006/ecss.1999.0562
- Kaartokallio, H., Asmala, E., Autio, R., and Thomas, D. N. (in press). Bacterial production, abundance and cell properties in boreal estuaries: relation to dissolved organic matter quantity and quality. *Aquat. Sci.* doi: 10.1007/s00027-015-0449-9
- Kirchman, D. L., Dittel, A. I., Findlay, S. E., and Fischer, D. (2004). Changes in bacterial activity and community structure in response to dissolved organic matter in the Hudson River, New York. *Aquat. Microb. Ecol.* 35, 243–257. doi: 10.3354/ame035243
- Koch, B. P., Witt, M., Engbrodt, R., Dittmar, T., and Kattner, G. (2005). Molecular formulae of marine and terrigenous dissolved organic matter detected by electrospray ionization Fourier transform ion cyclotron resonance mass spectrometry. *Geochim. Cosmochim. Acta* 69, 3299–3308. doi: 10.1016/j.gca.2005.02.027
- Köhler, H., Meon, B., Gordeev, V. V., Spitz, A., and Amon, R. M. W. (2003). Dissolved organic matter (DOM) in the estuaries of Ob and Yenisei and the adjacent Kara-Sea, Russia. *Proc. Mar. Sci.* 6, 281–309.
- Koroleff, F., Palmork, K. H., Oe, U., and Gieskes, J. M. (1977). *The international Intercalibration Exercise for Nutrient Methods*. Cooperative Research Report (Charlottenlund), 67.
- Leenheer, J. A., and Croué, J. P. (2003). Peer reviewed: characterizing aquatic dissolved organic matter. *Environ. Sci. Technol.* 37, 18A–26A. doi: 10.1021/es032333c
- Lønborg, C., Davidson, K., Álvarez-Salgado, X. A., and Miller, A. E. (2009). Bioavailability and bacterial degradation rates of dissolved organic matter in a temperate coastal area during an annual cycle. *Mar. Chem.* 113, 219–226. doi: 10.1016/j.marchem.2009.02.003
- Mantoura, R. F. C., and Woodward, E. M. S. (1983). Conservative behaviour of riverine dissolved organic carbon in the Severn Estuary: chemical and geochemical implications. *Geochim. Cosmochim. Acta* 47, 1293–1309. doi: 10.1016/0016-7037(83)90069-8
- Markager, S., Stedmon, C. A., and Søndergaard, M. (2011). Seasonal dynamics and conservative mixing of dissolved organic matter in the temperate eutrophic estuary Horsens Fjord. *Estuar. Coast. Shelf Sci.* 92, 376–388. doi: 10.1016/j.ecss.2011.01.014
- Mattsson, T., Kortelainen, P., and Räike, A. (2005). Export of DOM from boreal catchments: impacts of land use cover and climate. *Biogeochemistry* 76, 373–394. doi: 10.1007/s10533-005-6897-x
- McCallister, S. L., Bauer, J. E., Cherrier, J. E., and Ducklow, H. W. (2004). Assessing sources and ages of organic matter supporting river and estuarine bacterial production: a multiple-isotope ($\Delta^{14}\text{C}$, $\delta^{13}\text{C}$, and $\delta^{15}\text{N}$) approach. *Limnol. Oceanogr.* 49, 1687–1702. doi: 10.4319/lo.2004.49.5.1687
- McGlathery, K. J., Sundback, K., and Anderson, I. C. (2007). Eutrophication in shallow coastal bays and lagoons: the role of plants in the coastal filter. *Mar. Ecol. Prog. Ser.* 348, 1–18. doi: 10.3354/meps07132
- Mobed, J. J., Hemmingsen, S. L., Autry, J. L., and McGown, L. B. (1996). Fluorescence characterization of IHSS humic substances: total luminescence spectra with absorbance correction. *Environ. Sci. Technol.* 30, 3061–3065. doi: 10.1021/es960132l
- Moran, M. A., and Zepp, R. G. (1997). Role of photoreactions in the formation of biologically labile compounds from dissolved organic matter. *Limnol. Oceanogr.* 42, 1307–1316. doi: 10.4319/lo.1997.42.6.1307
- Murphy, K. R., Butler, K. D., Spencer, R. G., Stedmon, C. A., Boehme, J. R., and Aiken, G. R. (2010). Measurement of dissolved organic matter fluorescence in

- aquatic environments: an interlaboratory comparison. *Environ. Sci. Technol.* 44, 9405–9412. doi: 10.1021/es102362t
- Nayar, S., and Chou, L. M. (2003). Relative efficiencies of different filters in retaining phytoplankton for pigment and productivity studies. *Estuar. Coast. Shelf Sci.* 58, 241–248. doi: 10.1016/S0272-7714(03)00075-1
- Nebbiuso, A., and Piccolo, A. (2013). Molecular characterization of dissolved organic matter (DOM): a critical review. *Anal. Bioanal. Chem.* 405, 109–124. doi: 10.1007/s00216-012-6363-2
- Nelson, N. B., Carlson, C. A., and Steinberg, D. K. (2004). Production of chromophoric dissolved organic matter by Sargasso Sea microbes. *Mar. Chem.* 89, 273–287. doi: 10.1016/j.marchem.2004.02.017
- Norman, L., and Thomas, D. N. (2014). *Long-Term Storage of Riverine Dissolved Organic Carbon*. Technical note, Researchgate. doi: 10.13140/2.1.3331.5200
- Officer, C. B. (1979). Discussion of the behaviour of nonconservative dissolved constituents in estuaries. *Estuar. Coast. Mar. Sci.* 9, 91–94. doi: 10.1016/0302-3524(79)90009-4
- Perez, B. C., Day, J. W. Jr., Justic, D., Lane, R. R., and Twilley, R. R. (2011). Nutrient stoichiometry, freshwater residence time, and nutrient retention in a river-dominated estuary in the Mississippi Delta. *Hydrobiologia* 658, 41–54. doi: 10.1007/s10750-010-0472-8
- Peterson, B., Fry, B., Hullar, M., Saupe, S., and Wright, R. (1994). The distribution and stable carbon isotopic composition of dissolved organic carbon in estuaries. *Estuaries* 17, 111–121. doi: 10.2307/1352560
- Qian, J., and Mopper, K. (1996). Automated high-performance, high-temperature combustion total organic carbon analyzer. *Anal. Chem.* 68, 3090–3097. doi: 10.1021/ac960370z
- Räike, A., Kortelainen, P., Mattsson, T., and Thomas, D. N. (2012). 36year trends in dissolved organic carbon export from Finnish rivers to the Baltic Sea. *Sci. Tot. Environ.* 435, 188–201. doi: 10.1016/j.scitotenv.2012.06.111
- Raymond, P. A., and Bauer, J. E. (2000). Bacterial consumption of DOC during transport through a temperate estuary. *Aquat. Microb. Ecol.* 22, 1–12. doi: 10.3354/ame022001
- Retamal, L., Vincent, W. F., Martineau, C., and Osburn, C. L. (2007). Comparison of the optical properties of dissolved organic matter in two river-influenced coastal regions of the Canadian Arctic. *Estuar. Coast. Shelf Sci.* 72, 261–272. doi: 10.1016/j.ecss.2006.10.022
- Romera-Castillo, C., Sarmiento, H., Alvarez-Salgado, X. A., Gasol, J. M., and Marraséa, C. (2010). Production of chromophoric dissolved organic matter by marine phytoplankton. *Limnol. Oceanogr.* 55, 446–454. doi: 10.4319/lo.2010.55.1.00446
- Sachse, A., Henrion, R., Gelbrecht, J., and Steinberg, C. E. W. (2005). Classification of dissolved organic carbon (DOC) in river systems: influence of catchment characteristics and autochthonous processes. *Org. Geochem.* 36, 923–935. doi: 10.1016/j.orggeochem.2004.12.008
- Sheldon, J. E., and Alber, M. (2002). A comparison of residence time calculations using simple compartment models of the Altamaha River Estuary, Georgia. *Estuaries* 25, 1304–1317. doi: 10.1007/BF02692226
- Shimotori, K., Omori, Y., and Hama, T. (2010). Bacterial production of marine humic-like fluorescent dissolved organic matter and its biogeochemical importance. *Aquat. Microb. Ecol.* 58, 55. doi: 10.3354/ame01350
- Sholkovitz, E. R. (1976). Flocculation of dissolved organic and inorganic matter during the mixing of river water and seawater. *Geochim. Cosmochim. Acta* 40, 831–845. doi: 10.1016/0016-7037(76)90035-1
- Spencer, R. G., Ahad, J. M., Baker, A., Cowie, G. L., Ganeshram, R., Upstill-Goddard, R. C., et al. (2007a). The estuarine mixing behaviour of peatland derived dissolved organic carbon and its relationship to chromophoric dissolved organic matter in two North Sea estuaries (UK). *Estuar. Coast. Shelf Sci.* 74, 131–144. doi: 10.1016/j.ecss.2007.03.032
- Spencer, R. G., Pellerin, B. A., Bergamaschi, B. A., Downing, B. D., Kraus, T. E., Smart, D. R., et al. (2007b). Diurnal variability in riverine dissolved organic matter composition determined by in situ optical measurement in the San Joaquin River (California, USA). *Hydrol. Process.* 21, 3181–3189. doi: 10.1002/hyp.6887
- Stedmon, C. A., and Markager, S. (2003). Behaviour of the optical properties of colored dissolved organic matter under conservative mixing. *Estuar. Coast. Shelf Sci.* 57, 973–979. doi: 10.1016/S0272-7714(03)00003-9
- Sulzberger, B., and Durisch-Kaiser, E. (2009). Chemical characterization of dissolved organic matter (DOM): a prerequisite for understanding UV-induced changes of DOM absorption properties and bioavailability. *Aquat. Sci.* 71, 104–126. doi: 10.1007/s00027-008-8082-5
- Tranvik, L. J. (1990). Bacterioplankton growth on fractions of dissolved organic carbon of different molecular weights from humic and clear waters. *Appl. Environ. Microbiol.* 56, 1672–1677.
- Uher, G., Hughes, C., Henry, G., and Upstill-Goddard, R. C. (2001). Non-conservative mixing behavior of colored dissolved organic matter in a humic-rich, turbid estuary. *Geophys. Res. Lett.* 28, 3309–3312. doi: 10.1029/2000GL012509
- Vartiainen, T., Liimatainen, A., and Kauranen, P. (1987). The use of TSK size exclusion columns in determination of the quality and quantity of humus in raw waters and drinking waters. *Sci. Tot. Environ.* 62, 75–84. doi: 10.1016/0048-9697(87)90484-0
- Vodacek, A., Blough, N. V., DeGrandpre, M. D., and Nelson, R. K. (1997). Seasonal variation of CDOM and DOC in the Middle Atlantic Bight: terrestrial inputs and photooxidation. *Limnol. Oceanogr.* 42, 674–686. doi: 10.4319/lo.1997.42.4.00674
- Weishaar, J. L., Aiken, G. R., Bergamaschi, B. A., Fram, M. S., Fujii, R., and Mopper, K. (2003). Evaluation of specific ultraviolet absorbance as an indicator of the chemical composition and reactivity of dissolved organic carbon. *Environ. Sci. Technol.* 37, 4702–4708. doi: 10.1021/es030360x
- Wiebe, W. J., and Smith, D. F. (1977). Direct measurement of dissolved organic carbon release by phytoplankton and incorporation by microheterotrophs. *Mar. Biol.* 42, 213–223. doi: 10.1007/BF00397745
- Zimmerman, J. T. F. (1976). Mixing and flushing of tidal embayments in the western Dutch Wadden Sea part I: distribution of salinity and calculation of mixing time scales. *Neth. J. Sea Res.* 10, 149–191. doi: 10.1016/0077-7579(76)90013-2

Conflict of Interest Statement: The authors declare that the research was conducted in the absence of any commercial or financial relationships that could be construed as a potential conflict of interest.

Copyright © 2016 Asmala, Kaartokallio, Carstensen and Thomas. This is an open-access article distributed under the terms of the Creative Commons Attribution License (CC BY). The use, distribution or reproduction in other forums is permitted, provided the original author(s) or licensor are credited and that the original publication in this journal is cited, in accordance with accepted academic practice. No use, distribution or reproduction is permitted which does not comply with these terms.



Variability in dissolved organic matter optical properties in surface waters in the Amerasian Basin

Céline Guéguel^{1*}, Motoyo Itoh², Takashi Kikuchi², Jane Eert³ and William J. Williams³

¹ Department of Chemistry, Trent University, Peterborough, ON, Canada, ² Research Institute for Global Change, Japan Agency for Marine-Earth Science and Technology, Yokosuka, Japan, ³ Department of Fisheries and Ocean, Institute of Ocean Sciences, Sidney, BC, Canada

OPEN ACCESS

Edited by:

Christopher Osburn,
North Carolina State University, USA

Reviewed by:

Mukesh Gupta,
Environment Canada, Canada
Mar Nieto-Cid,
CSIC - Instituto de Investigaciones
Marinas, Spain

*Correspondence:

Céline Guéguel,
Department of Chemistry, Trent
University, 1600 West Bank Drive,
Peterborough, ON K9J 7B8, Canada
celinegueguen@trentu.ca

Specialty section:

This article was submitted to
Marine Biogeochemistry,
a section of the journal
Frontiers in Marine Science

Received: 10 July 2015

Accepted: 18 September 2015

Published: 29 October 2015

Citation:

Guéguel C, Itoh M, Kikuchi T, Eert J and Williams WJ (2015) Variability in dissolved organic matter optical properties in surface waters in the Amerasian Basin. *Front. Mar. Sci.* 2:78.
doi: 10.3389/fmars.2015.00078

Surface absorption and fluorescence measurements of Dissolved Organic Matter (DOM) were conducted along with hydrographic parameters in the Amerasian and Makarov Basins. Parallel factor analysis of DOM fluorescence identified four humic-like and one protein-like component in all 107 surface samples. Based on strong negative trends observed between the spectral slope in the 275–295 nm range and absorption at 370 nm, and four humic-like components C1–4, the DOM character was found to be basin-dependent. The Makarov Basin surface DOM was largely dominated by high molecular weight and humic-rich material whereas the Canada Basin surface DOM was more heterogeneous with a marked influence of *in situ* production. This study highlights that absorbing and fluorescing measurements can be used successfully to trace and differentiate DOM from diverse sources and across frontal zones, and as such can be convenient and complementary tools for the better understanding of marine biogeochemical cycling of carbon.

Keywords: CDOM, FDOM, Makarov Basin, Canada Basin, frontal zone, ice cover

Introduction

Colored dissolved organic matter (CDOM) is one of the major light attenuating components of natural waters: it is responsible for much of the ultraviolet and visible light attenuation in the water column (Hansell and Carlson, 2002). CDOM also plays an important role in the solubility of essential elements such as iron and copper in natural waters (e.g., Chen et al., 2013; Heller et al., 2013; Uchida et al., 2013). The optical properties of CDOM have been previously used to discriminate between terrestrial and marine DOM sources (Blough and Del Vecchio, 2002; and references therein) and to trace the mixing of terrestrially derived DOM in oceanic waters (e.g., Amon et al., 2003; Guéguel et al., 2011; Stedmon et al., 2011; Fichot et al., 2013). For example, the absorbance properties of CDOM have been used to differentiate the surface to 300 m waters of the Canada and Eurasian Basins (Stedmon et al., 2011). More recently the application of fluorescence excitation emission matrices (EEMs) with a multivariate statistical analysis such as parallel factor analysis (PARAFAC; Stedmon and Bro, 2008) allowed us to discriminate the main fluorescing components in the fluorescing DOM (FDOM) pool and to assess their dynamics in marine waters (Ishii and Boyer, 2007; Stedmon et al., 2007; Murphy et al., 2008; Walker et al., 2009; Yamashita et al., 2010; Jørgensen et al., 2011; Guéguel et al., 2011, 2012; Dainard and Guéguel, 2013).

The Arctic Ocean basin represents ~4% of global ocean area and receives approximately 2.5 times more inflow per unit area than the world average. This disproportionate share of global

river discharge into the Arctic Ocean and the high dissolved organic carbon concentrations in arctic rivers (up to 1600 μM ; Stedmon et al., 2011; Amon et al., 2012) highlight the importance of freshwater and terrestrial organic matter in the biogeochemical cycles of the Arctic Ocean. However, there is a limited amount of data available on how this allochthonous DOM mixes with autochthonous marine DOM.

The general circulation in surface oceanic waters in the western Arctic Ocean is dominated by two main water masses: saline Atlantic water, entering through eastern Fram Strait and the Barents Sea, flows eastward following the Arctic continental margin where Eurasian river runoff is incorporated; and fresher Pacific-derived waters entering through Bering Strait and modified in the Chukchi Sea and Mackenzie River-influenced Beaufort shelves. The Pacific-Atlantic boundary in the Arctic Ocean delineates the extent of the Pacific-origin water, and thus where the saltier Atlantic-origin water must subduct beneath the Pacific Water. Eurasian river water has been reported in the Beaufort Gyre (Yamamoto-Kawai et al., 2009) and Pacific-origin water has recently been found in the surface layer of the North Pole (Alkire et al., 2007, 2010). Historically, this boundary lies along the Lomonosov Ridge, at the boundary between the Eurasian and Amerasian Basins of the Arctic Ocean (Jones and Anderson, 1986; Anderson et al., 1994), but recent studies have showed Atlantic character in the Makarov Basin that lies in the northern Amerasian Basin (i.e., Makarov and Canada Basins) between the Lomonosov Ridge and the Alpha-Mendeleyev Ridge (Guay et al., 1999; Nishino et al., 2008, 2013; Guéguen et al., 2012). This part of the ocean is largely under-sampled which makes difficult to assess the presence of such a barrier that constrains transfer of heat, solutes, and plankton (Guéguen and Kowalczuk, 2013; and references therein).

Here we report spectral absorbance and fluorescence properties of surface water samples collected along transects from waters in the Amundsen Gulf across the Canada Basin to the Makarov Basin and back again. Our aim is to provide insight on sources and mixing of CDOM and FDOM in surface waters (i.e., terrestrial, marine and *in-situ* production) and thus improve our understanding of the biogeochemical cycling of carbon in the ocean.

Materials and Methods

Sample Collection

Surface water samples were collected from 107 sites located between the Canadian Arctic coast and the Lomonosov Ridge during August 21–September 27, 2011, on board the icebreaker Canadian Coast Guard Ship Louis S. St-Laurent (**Figure 1**) during the Natural Resources Canada expedition to assess sovereignty rights in the deep Arctic Ocean as required by the United Nations Convention on the Law of the Sea (UNCLOS). Samples were collected from the water intake line (depth ~ 10 m) every 6 h when steaming. *In-situ* measurements of temperature and conductivity were obtained by a Seabird electronics SBE-21 probe mounted on the sampling line inside the icebreaker. *In situ* fluorescence chlorophyll Chla (WETStar fluorometer) and FDOM (WETLabs ECOFLD 370 nm excitation, 460 nm

emission; Guéguen et al., 2012) sensors were also mounted on the intake line. *In-situ* measurements were conducted every 5 s and 1-min-averaged during post-processing. Samples collected for absorbance and fluorescence analysis were immediately stored in pre-combusted amber-glass vials with little to no headspace at 4°C until the analysis is performed. All samples were measured within 6 months of collection. The preservation and storage conditions used in this study may have favored microbial activities (Spencer and Coble, 2014; and reference therein). For example, Baker et al. (2007) reported a significant decrease (mean 58%) in protein-like fluorescence when samples were not filtered. The *in situ* FDOM sensor was linearly correlated with a_{370} , and humic like components C2 and C3 (described below) measured in discrete samples ($r^2 = 0.80, 0.66$, and 0.67, respectively; $n = 107$). Additionally, the survey was augmented by expendable CTD (XCTD; Lockheed-Martin-Sippican) deployment.

Absorbance Analysis

CDOM absorbance measurements of the collected water samples were made on a Shimadzu UV 2550 spectrophotometer over a wavelength region of 260–700 nm with a 10-cm quartz cuvette using Milli-Q water as a reference. In order to correct for instrumental drift and light scattering, an offset correction was applied by subtracting the average absorbance between 650 and 700 nm from the Milli-Q absorbance spectrum (Green and Blough, 1994; Guéguen et al., 2006, 2012). The measured absorbance at wavelength λ was converted to the absorption coefficient a (m^{-1}) according to the relationship:

$$a_\lambda = 2.303 \cdot A_\lambda / L,$$

where A_λ is the absorbance and L is the path-length of the optical cell in meters (here 0.1 m). The slope parameter S , a proxy for molecular weight (Helms et al., 2008), was calculated over a range of 275–295 nm ($S_{275-295}$; Helms et al., 2008) using non-linear least squares fitting procedures in Matlab. An increase in $S_{275-295}$ is indicative of decreasing aromaticity and molecular weight of the CDOM (Helms et al., 2008). S calculated over the 300–650 nm range ($S_{300-650}$; Stedmon and Markager, 2001; Retamal et al., 2007; Hancke et al., 2014) was used to compare previous mixing models (Stedmon and Markager, 2001; Hancke et al., 2014).

Fluorescence Analysis

Samples were warmed to room temperature and then analyzed with a Horiba Jobin-Yvon fluorometer (FluoroMax4) using a 1-cm quartz cuvette with excitation and emission slit widths each set to 5 nm. The quartz cuvette was checked for cleanliness between each sample at excitation wavelengths of 270 and 350 nm. The excitation-emission matrix (EEM) of each sample was recorded in signal-to-noise mode by collecting a series of emission wavelengths ranging from 250 to 600 nm at excitation wavelengths ranging from 300 to 450 nm, both in 5-nm increments. The post processing steps included: correction of instrument bias using the correction files provided by the manufacturer, subtraction of the EEM of Milli-Q water, and finally the fluorescence intensity was corrected to the area under the Milli-Q water Raman peak (excitation 350 nm) run

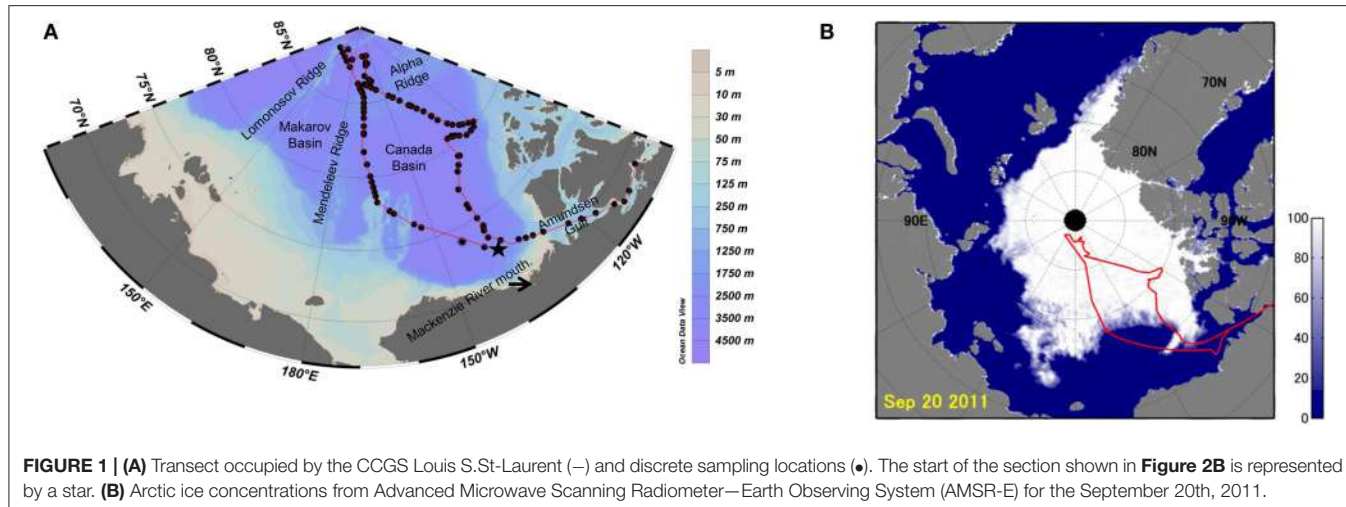


FIGURE 1 | (A) Transect occupied by the CCGS Louis S.St-Laurent (—) and discrete sampling locations (●). The start of the section shown in **Figure 2B** is represented by a star. **(B)** Arctic ice concentrations from Advanced Microwave Scanning Radiometer—Earth Observing System (AMSR-E) for the September 20th, 2011.

daily (Lawaetz and Stedmon, 2009). No significant variation in the integral of the Raman peak was observed during the investigation (1.2%). The fluorescence intensity was reported in equivalent water Raman units (r.u.). The Raman normalization is independent of the instrument design (Nelson and Coble, 2009; and references therein), allowing comparison with other studies.

PARAFAC decomposes the complex mixtures of FDOM fluorophores into their main components (Stedmon et al., 2003). PARAFAC analysis was carried out in Matlab using the DOMFluor toolbox (Stedmon and Bro, 2008), and outlier identification was performed using the OutlierTest function included therein. No samples with extreme leverage were found, indicating no extreme, and potentially outlying, EEMs in the dataset. Determination of the most suitable number of components was achieved by the split-half analysis and random initialization (Stedmon et al., 2003) whereby both halves were successfully validated. The model was constrained to non-negative values, and no systematic residual was found in the modeled EEMs. The spectra of the cross validated PARAFAC components were compared with those reported in earlier studies through online repository of published PARAFAC components (Murphy et al., 2014). The similarity of components was statistically identified as having Tucker congruence exceeding 0.95 (Murphy et al., 2014). The percent contribution of a given component was calculated as the ratio of the given component fluorescence intensity to the total humic component fluorescence intensity [i.e., $C1\% = C1/(C1 + C2 + C3 + C4)$].

Results and Discussion

Salinity, Temperature, *in situ* FDOM, and CDOM Distributions

A marked frontal zone characterized by significant changes in physical and chemical characteristics was observed at latitude around 83°N (Figures 2, 3), coinciding with the latitude of the Alpha-Mendeleev Ridge that separates the Makarov and Canada Basins. Intrusion of warm Pacific Summer Waters around 50 m

and halo-stad around 50–125 m due to Pacific Summer and Winter Waters were found in the southern part of the UNCLOS area (<83°N; Figure 2). In contrast, higher latitude waters (>83°N) were ice covered ($98.9 \pm 1.8\%$; Figure 1A), colder ($<-1.5^{\circ}\text{C}$) and saltier (>30 ; Figure 2), indicative of a stronger influence of Atlantic-origin water. The front at 83°N seems to be related to boundary of Atlantic and Pacific waters.

Surface distribution of salinity, temperature, FDOM_{WETLabs}, a_{370} $S_{275-295}$ and Chla (Figure 3) showed contrasting characteristics across the frontal zone. The higher salinity (30.8 ± 0.3) observed north of 83°N suggest source waters of Atlantic origin while the high FDOM_{WETLabs} signal (0.14 ± 0.01 V), high a_{370} values ($0.70 \pm 0.15 \text{ m}^{-1}$) and low $S_{275-295}$ ($0.0215 \pm 0.001 \text{ nm}^{-1}$) reflect contribution from Eurasian Arctic rivers (Guay et al., 1999). Indeed, river influenced waters are typically enriched in larger molecular weight (low $S_{275-295}$; Helms et al., 2008) and humic-rich DOM (higher a_{370}). The near freezing temperature ($-0.75 \pm 0.53^{\circ}\text{C}$) north of 83°N reflects the presence of sea ice (Figure 1B). The >83°N region was also characterized by high Chla levels ($>0.5 \text{ mg/m}^3$). Nishino et al. (2013) have reported higher Chla in the Makarov Basin than in the Canadian Basin, likely due to sea ice retreat and shallower nutricline. On the other hand, the lower salinities were observed south of 83°N in the Canada Basin and the lowest salinities (as low as 24) were found in the central Canada Basin. These low salinities reflecting the contribution of sea ice melt and river inflow (Carmack, 1990; Yamamoto-Kawai et al., 2009). The highest $S_{275-295}$ values ($0.025\text{--}0.034 \text{ nm}^{-1}$) coupled with lower FDOM_{WETLabs} (~ 0.8 V) and a_{370} values ($0.07\text{--}0.17 \text{ m}^{-1}$) were found in the central Canada Basin (latitudes 72–83°N). The presence of lower molecular weight (high $S_{275-295}$) and less humified DOM is expected to primarily be the result of dilution of allochthonous CDOM (Granskog, 2012). Similar $S_{275-295}$ ranges were previously measured in the Arctic Ocean (Dainard and Guéguen, 2013; Fichot et al., 2013). The warmer ($>0^{\circ}\text{C}$) and saltier waters (Salinity ~28) encountered in Amundsen Gulf were also characterized by low FDOM_{WETLabs} values, medium to high a_{370} values and low $S_{275-295}$. These values are indicative

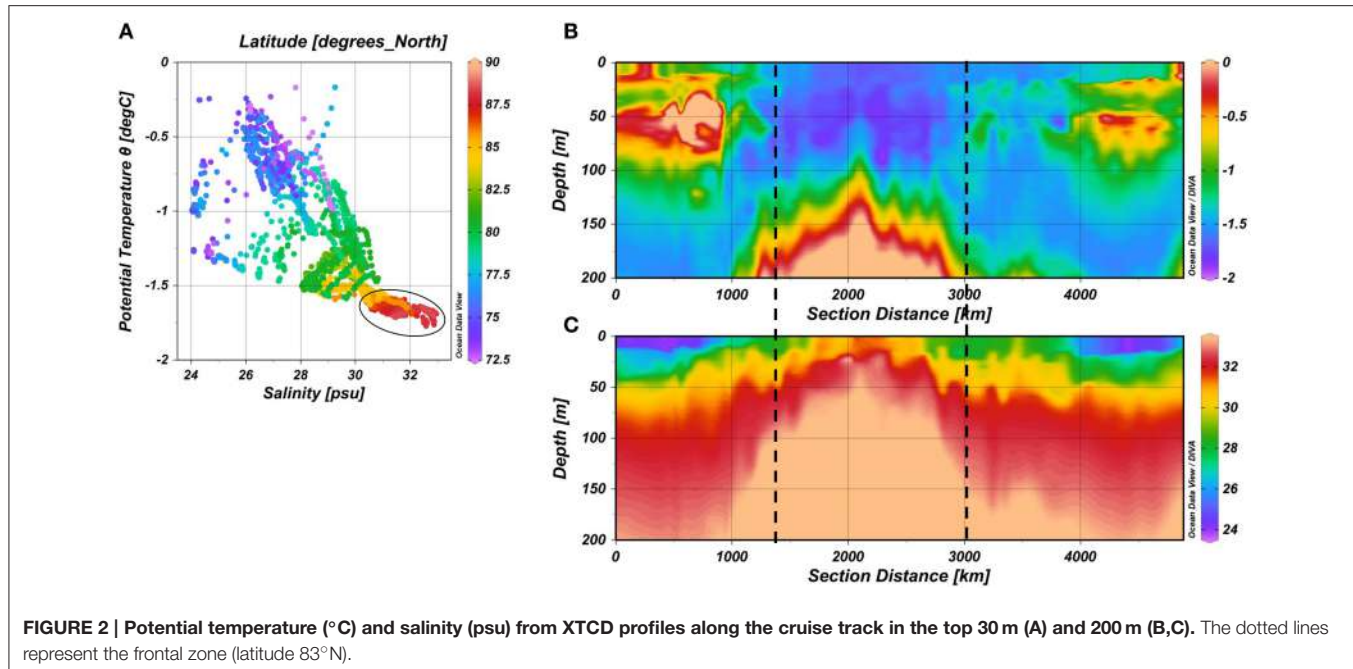


FIGURE 2 | Potential temperature ($^{\circ}$ C) and salinity (psu) from XTCD profiles along the cruise track in the top 30 m (A) and 200 m (B,C). The dotted lines represent the frontal zone (latitude 83 $^{\circ}$ N).

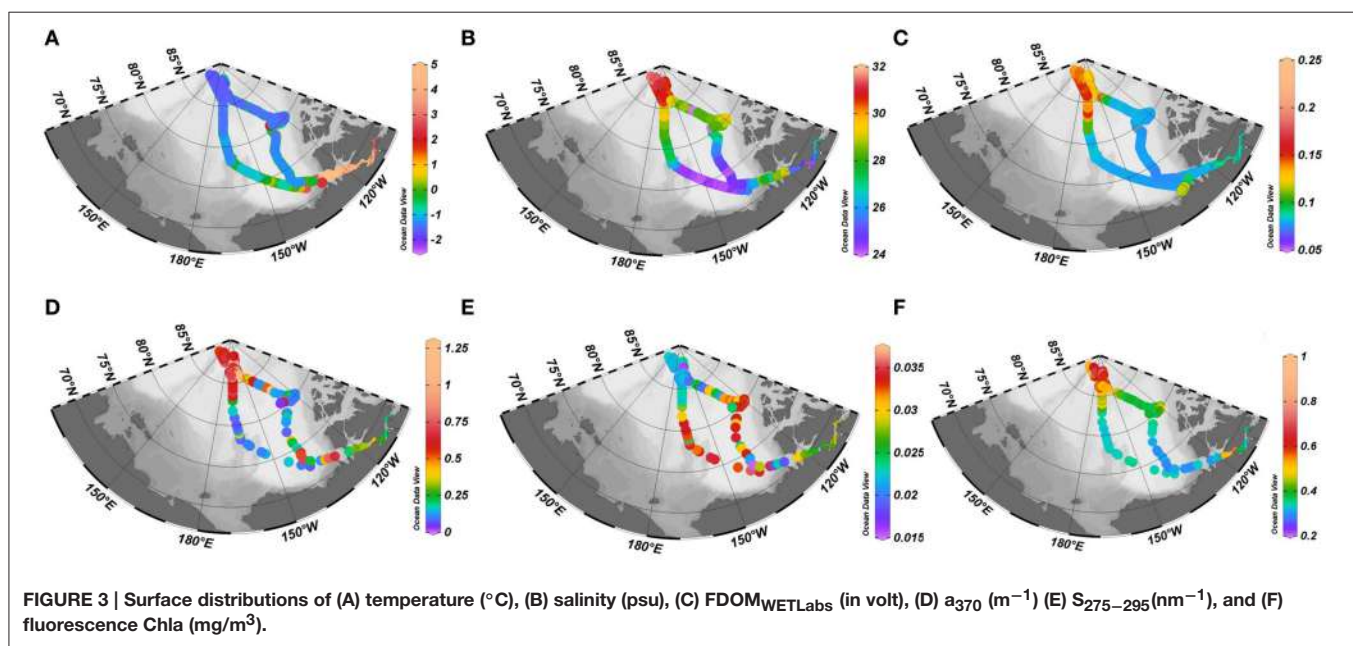


FIGURE 3 | Surface distributions of (A) temperature ($^{\circ}$ C), (B) salinity (psu), (C) FDOM_{WETLabs} (in volt), (D) a_{370} (m^{-1}) (E) $S_{275-295}$ (nm^{-1}), and (F) fluorescence Chla (mg/m^3).

of river influence, but this will not be the Mackenzie River in 2011 as winds were easterly for the entire summer and fall which pushes the Mackenzie River water toward the west and offshore into the central Canada Basin (Yamamoto-Kawai et al., 2010).

FDOM Characterization and Distribution

Based on the PARAFAC modeling of EEM, five independent fluorescent components (C1–C5) were successfully validated. Their spectral characteristics were similar to components identified in previous studies (Figure 4; Figure S1). Components C1–C4 were characterized as humic-like, as they displayed an

emission maximum around and above 400 nm. Components C1 and C4 showed an intensive peak at 285–305 nm excitation and 390–415 nm emission which was similar to the marine humic-like peak M traditionally defined (Coble, 1996). In recent studies, peak M has also been shown to be evident in DOM that has been altered by microbial reprocessing (Stedmon and Markager, 2005; Yamashita et al., 2008). Similar components were found in coastal and marine waters (Søndergaard et al., 2003; Yamashita et al., 2011; Dainard et al., 2015; Figure S1). The spectral features of C2 were similar to a component reported as humic-like peak A + M (Coble, 1996). Component C3 was assigned as the traditional

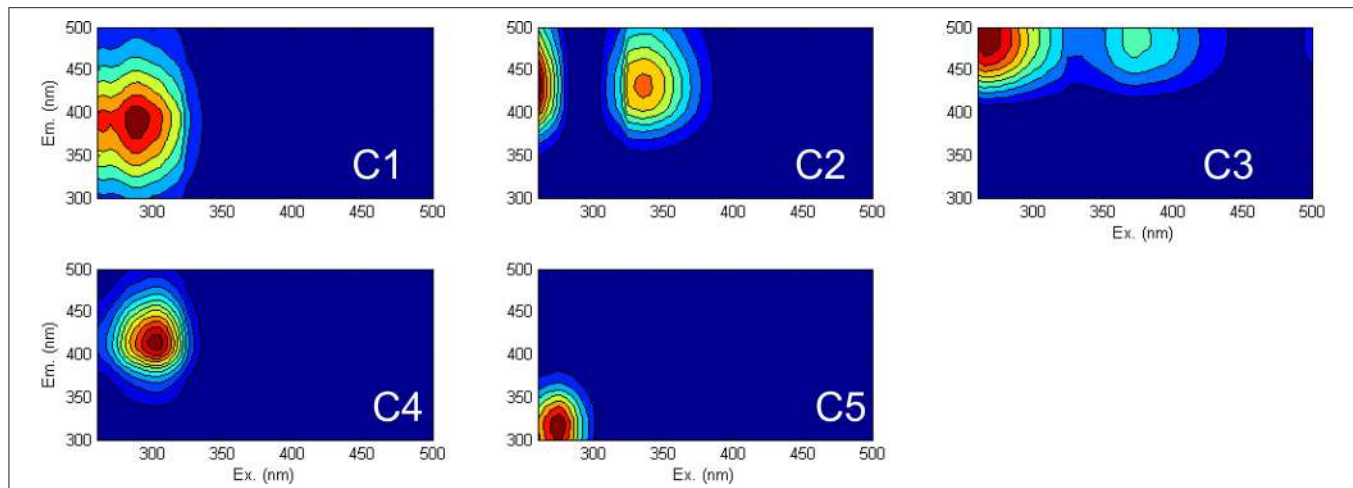


FIGURE 4 | Spectral characteristics of 5-component model for surface arctic water dataset ($N = 107$). The greatest intensities are shown in red.

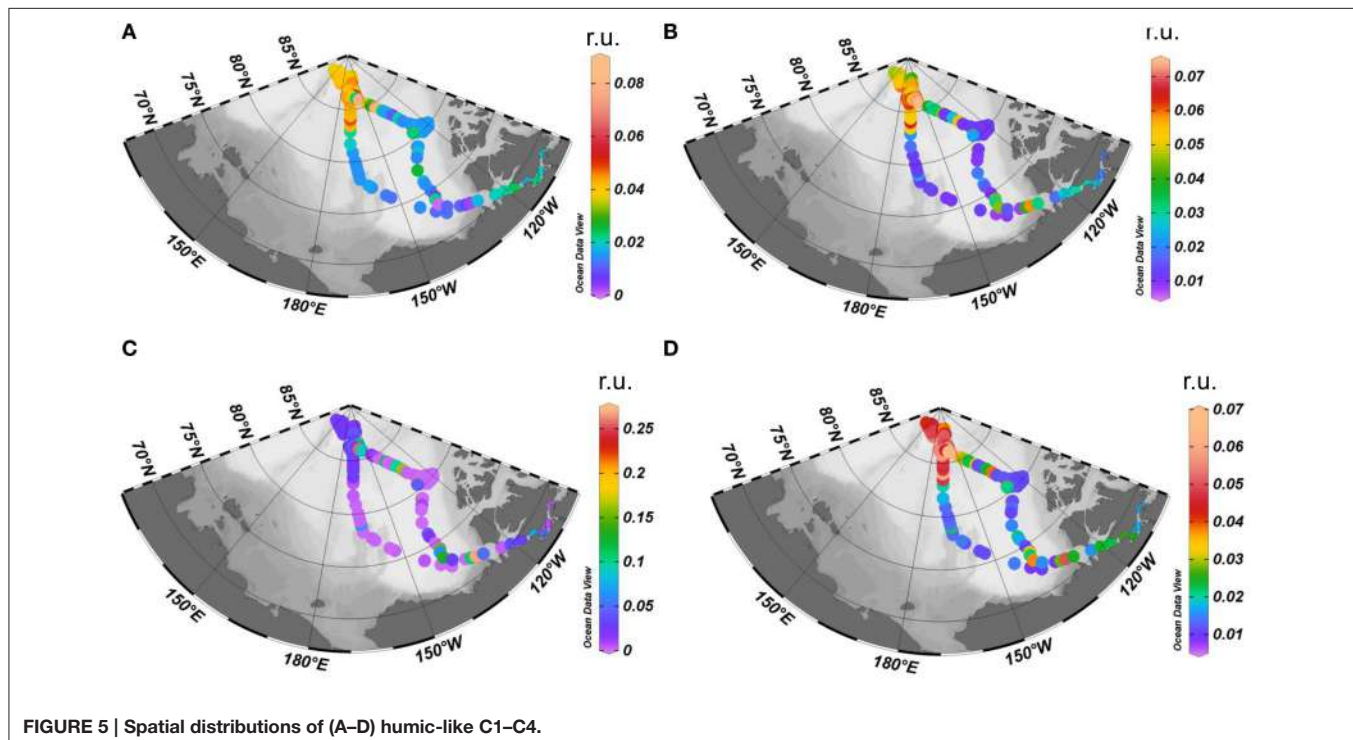


FIGURE 5 | Spatial distributions of (A–D) humic-like C1–C4.

humic-like peak A + C (Coble, 1996) which is usually considered to be representative of fluorophores in terrestrial environments (Ishii and Boyer, 2007) and found in ocean waters (Søndergaard et al., 2003; Stedmon and Markager, 2005; Murphy et al., 2006, 2008; Stedmon et al., 2007; Walker et al., 2009; Kowalcuk et al., 2013; Brym et al., 2014). Component C5 was classified as protein-like since it displayed an emission maximum below 400 nm. This component was similar to those of a tyrosine-like component found in previous PARAFAC studies (Stedmon et al., 2007; Walker et al., 2009; Osburn and Stedmon, 2011; Cawley et al., 2012; Yamashita et al., 2013; Bianchi et al., 2014; Dainard

et al., 2015; Figure S1). As the samples were unfiltered, microbes could have altered the protein-like fluorescence via consumption of the original labile DOM and/or production of new protein-like fluorescence. Therefore, only results from the humic like components (C1–C4) were used for further data analysis in this study.

Strong humic-like C1–C4 signals were associated with the $>83^{\circ}\text{N}$ region (Figure 5). In terms of compositional distribution, microbially derived humic-like C1 was more abundant at intermediate latitudes in ice-edge (Figure 1B) and productive (Chla $\sim 0.4 \text{ mg.m}^{-3}$; Figure 3F) waters ($75\text{--}83^{\circ}\text{N}$)

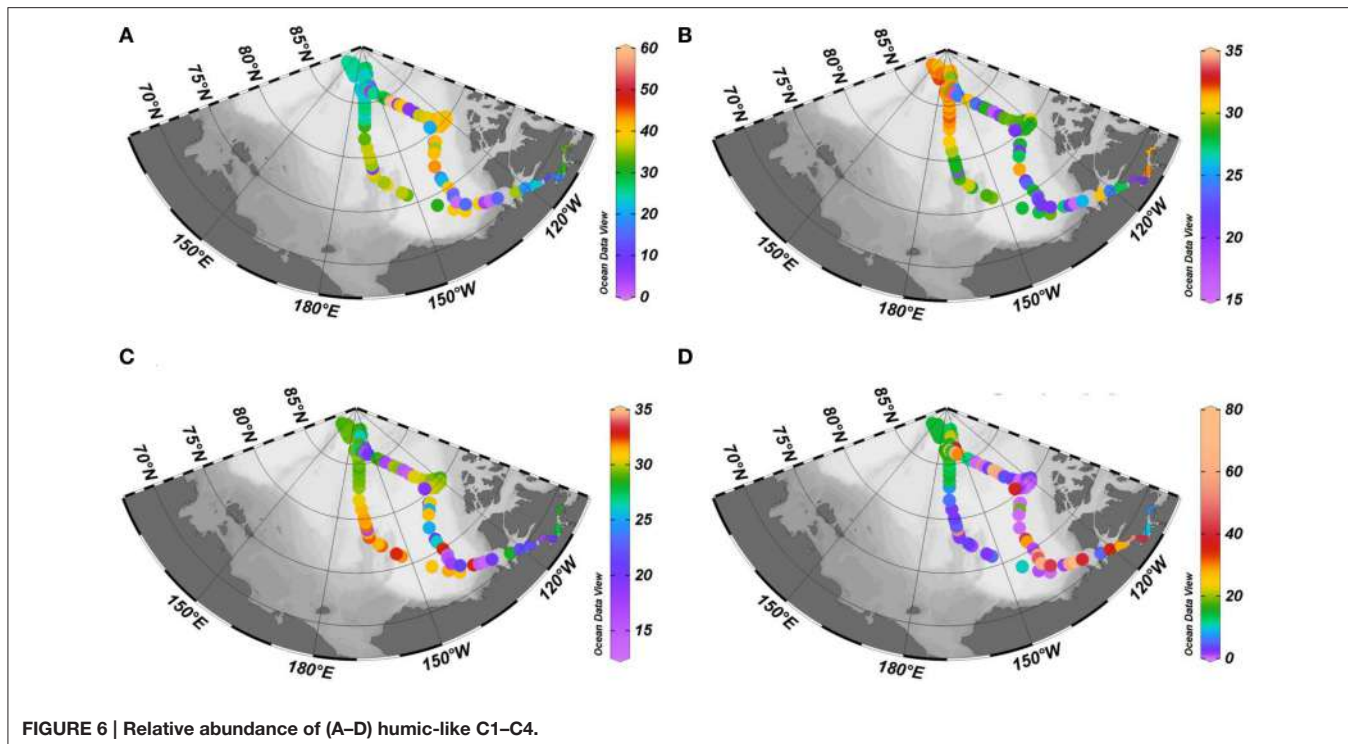
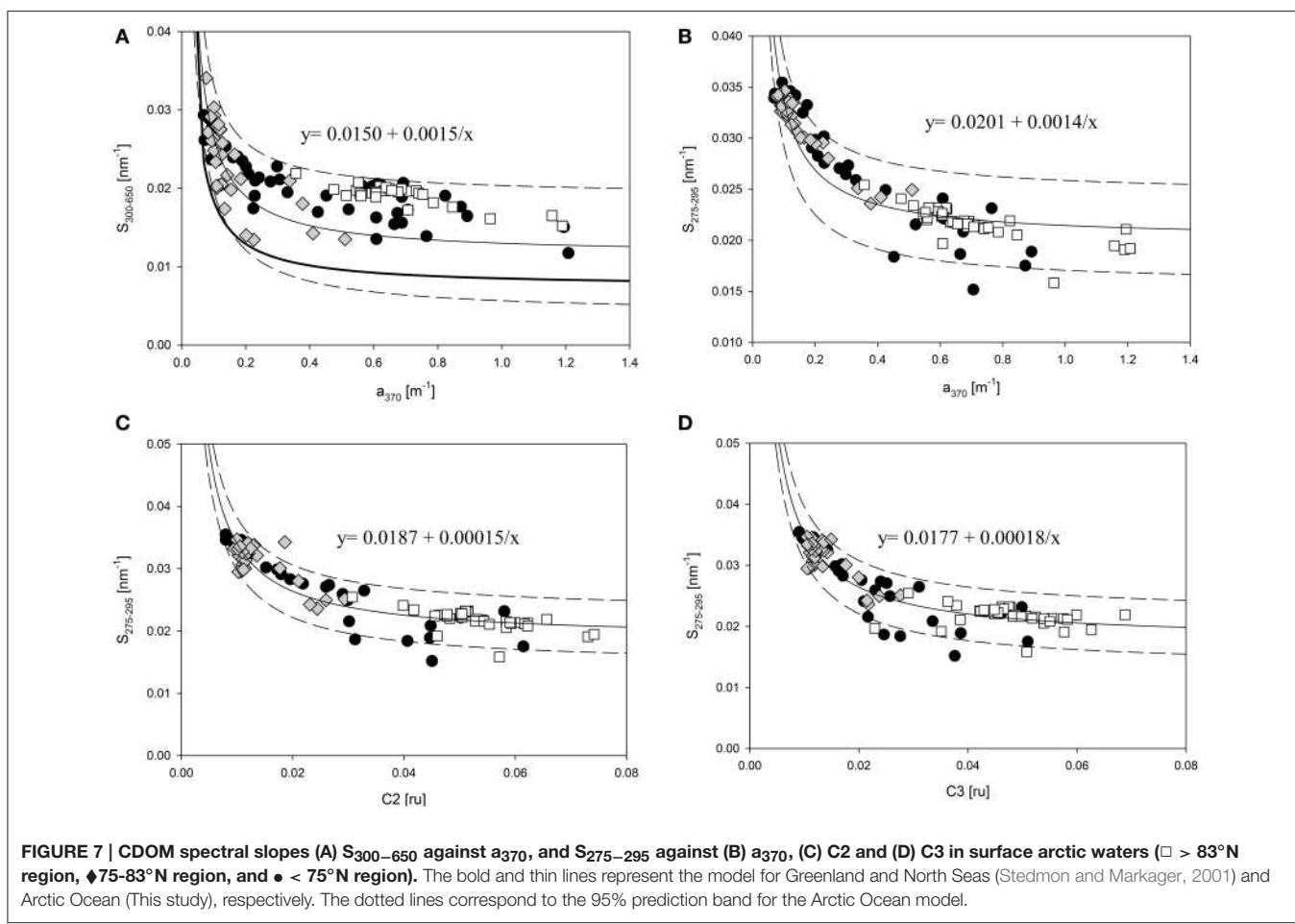


FIGURE 6 | Relative abundance of (A–D) humic-like C1–C4.

FIGURE 7 | CDOM spectral slopes (A) $S_{300-650}$ against a_{370} , and (B) $S_{275-295}$ against (B) a_{370} , (C) C2 and (D) C3 in surface arctic waters ($\square > 83^{\circ}\text{N}$ region, $\blacklozenge 75-83^{\circ}\text{N}$ region, and $\bullet < 75^{\circ}\text{N}$ region). The bold and thin lines represent the model for Greenland and North Seas (Stedmon and Markager, 2001) and Arctic Ocean (This study), respectively. The dotted lines correspond to the 95% prediction band for the Arctic Ocean model.

than in the $>83^{\circ}\text{N}$ region (32.4 ± 11.3 vs. $25.4 \pm 8.7\%$; **Figure 6A**). Greater abundance of microbially derived C1 agrees well with a more efficient microbial loop in the ice-edge bloom regions (Stanley et al., 2015). This contrasts with microbially derived C4 which was abundantly found in the $>83^{\circ}\text{N}$ region (15–20%; **Figure 6D**) and near the Mackenzie coast and in the Amundsen Gulf (>40%; **Figure 6D**). Unlike the $>83^{\circ}\text{N}$ region, the coastal region (i.e., Mackenzie coast and Amundsen Gulf) was however not associated with high chla (**Figure 3F**), suggesting that C4 was not always derived from freshly produced DOM. Humic-like C2–C3 (**Figures 6B,C**) showed higher abundances in the $>83^{\circ}\text{N}$ region (~15–32%) and along the western transect (~20–32%).

Mixing Processes

In marine environment, autochthonous CDOM can be discriminated from allochthonous CDOM by the relationship between spectral slope parameter and absorption coefficient (Stedmon and Markager, 2001). In our study, a significant inverse relationship was apparent between $S_{300-650}$ and a_{370} (**Figure 7A**), congruent with previous studies in the Arctic Ocean (>100 m of depth; Stedmon et al., 2011), the Fram Strait (Granskog et al., 2012), and the Greenland and North Seas (Stedmon and Markager, 2001; Hancke et al., 2014). This contrasts with coastal waters (i.e., high terrestrial input) where S was shown to be independent of CDOM absorption coefficient (Babin et al., 2003). The majority of the points from $>83^{\circ}\text{N}$ waters had $S_{300-650}$ values around 0.019 nm^{-1} and deviated from the Stedmon and Markager (2001) model (thick line), likely the result of differences in DOM characteristics between Greenland/North Seas and western Arctic Ocean. $S_{275-295}$ was also used instead of $S_{300-650}$ as a better precision can be obtained in oceanic waters over the wavelength range 275–295 nm (Helms et al., 2008). A stronger relationship of $S_{275-295}$ vs. a_{370} ($r^2 = 0.85$ vs. 0.65 , $n = 107$). However, this study, for the first time, reports a strong relationship between $S_{275-295}$ and FDOM (i.e., C2, $r^2 = 0.86$; C3, $r^2 = 0.85$; **Figures 7C,D**), suggesting mixing processes affecting C2 and C3 intensities in surface water.

References

- Alkire, M. B., Falkner, K. K., Morison, J., Collier, R. W., Guay, C. K., Desiderio, R. A., et al. (2010). Sensor-based profiles of the NO parameter in the central Arctic and southern Canada Basin: new insights regarding the cold halocline. *Deep Sea Res. I*, 57, 1432–1443. doi: 10.1016/j.dsr.2010.07.011
- Alkire, M. B., Falkner, K. K., Rigor, I. G., Steele, M., and Morison, J. (2007). The return of Pacific waters to the upper layers of the central Arctic Ocean. *Deep Sea Res. I*, 54, 1509–1529. doi: 10.1016/j.dsr.2007.06.004
- Amon, R. M. W., Budeus, G., and Meon, B. (2003). Dissolved organic carbon distribution and origin in the Nordic Seas: exchanges with the Arctic Ocean and the North Atlantic. *J. Geophys. Res. Oceans* 108, 14-1–14-17. doi: 10.1029/2002jc001594
- Amon, R. M. W., Rinehart, A. J., Duan, S., Louchevare, P., Prokushkin, A., Guggenberger, G., et al. (2012). Dissolved organic matter sources in large Arctic rivers. *Geochim. Cosmochim. Acta* 94, 217–237. doi: 10.1016/j.gca.2012.07.015
- Anderson, L. G., Bjork, G., Holby, O., Jones, E. P., Kattner, G., Koltermann, K. P., et al. (1994). Water masses and circulation in the Eurasian Basin: results from the Oden 91Expedition. *J. Geophys. Res.* 99, 3273–3283. doi: 10.1029/93JC02977
- Babin, M., Stramski, D., Ferrari, G. M., Claustre, H., Bricaud, A., Obolensky, G., et al. (2003). Variations in the light absorption coefficients of phytoplankton, nonalgal particles, and dissolved organic matter in coastal waters around Europe. *J. Geophys. Res.* 108, 3211. doi: 10.1029/2001JC000882
- Baker, A., Elliott, S., and Lead, J. R. (2007). Effects of filtration and pH perturbation on freshwater organic matter fluorescence. *Chemosphere* 67, 2035–2043. doi: 10.1016/j.chemosphere.2006.11.024
- Bianchi, T. S., Osburn, C., Shields, M. R., Yvon-Lewis, S., Young, J., Guo, L., et al. (2014). Deepwater horizon oil in Gulf of Mexico Waters after 2 years: transformation into the dissolved organic matter pool. *Environ. Sci. Technol.* 48, 9288–9297. doi: 10.1021/es501547b
- Blough, N. V., and Del Vecchio, R. (2002). “Chromophoric DOM in the coastal environment,” in *Biogeochemistry of Marine Dissolved Organic Matter*, eds D. Hansell and C. Carlson (New York, NY: Academic Press), 509–546. doi: 10.1016/b978-012323841-2/50012-9

The behavior of CDOM and humic-like C2 and C3 was successfully modeled. Using **Figure 7**, one can clearly identify two different CDOM and FDOM pools: DOM from $>83^{\circ}\text{N}$, with an invariant S-value pool ($S_{275-295} = 0.0216 \pm 0.0017 \text{ nm}^{-1}$), mixing with central Canada Basin waters (75 – 83°N) with mean $S_{275-295}$ of $0.0312 \pm 0.0031 \text{ nm}^{-1}$. Together these results show that the surface waters in the Canada and Makarov Basins differ significantly in composition.

Summary

This study shows that the combination of absorbance and fluorescence spectroscopies and multivariate statistics (i.e., PARAFAC) can be used to examine the source and mixing processes of DOM in the Canada and Makarov Basins. The presence of a frontal zone at latitude $\sim 83^{\circ}\text{N}$ was evidenced by marked changes in $S_{275-295}$ and a_{370} values and intensity and contribution of four humic-like PARAFAC components. High molecular weight (i.e., low $S_{275-295}$) DOM, dominated by terrestrially derived humic-like material, in the Makarov Basin was replaced by lower molecular weight DOM, with a reduced terrestrial character, in the Canada Basin. The CDOM and FDOM pools were concluded to be the result of mixing of two dominant sources (i.e., Eurasian and Central Canada Basins).

Acknowledgments

Funding for this study was provided by the Canada Research Chairs program and the Natural Sciences and Engineering Research Council of Canada (CG). We would like to acknowledge Baptiste Marcere for assistance in the sample analysis. We are also grateful to the Captain, crew and scientists from the CCGS *Louis S. St-Laurent* during UNCLOS2011 for their help with sampling.

Supplementary Material

The Supplementary Material for this article can be found online at: <http://journal.frontiersin.org/article/10.3389/fmars.2015.00078>

- Brym, A., Paerl, H. W., Montgomery, M. T., Handsel, L. T., Zier vogel, K., and Osburn, C. L. (2014). Optical and chemical characterization of base-extracted particulate organic matter in coastal marine environments. *Mar. Chem.* 162, 96–113. doi: 10.1016/j.marchem.2014.03.006
- Carmack, E. C. (1990). "Large scale physical oceanography of polar oceans," in *Polar Oceanography. Part A: Physical Science*, ed W. O. Smith (San Diego, CA: Academic Press), 171–222.
- Cawley, K. M., Butler, K. D., Aiken, G. R., Larsen, L. G., Huntington, T. G., and McKnight, D. M. (2012). Identifying fluorescent pulp mill effluent in the Gulf of Maine and its watershed. *Mar. Pollut. Bull.* 64, 1678–1687. doi: 10.1016/j.marpolbul.2012.05.040
- Chen, W., Smith, D. S., and Guéguen, C. (2013). Influence of water chemistry and dissolved organic matter molecular size on copper and mercury binding determined by multiresponse fluorescence quenching. *Chemosphere* 92, 351–359. doi: 10.1016/j.chemosphere.2012.12.075
- Coble, P. G. (1996). Characterization of marine and terrestrial DOM in seawater using excitation-emission matrix spectroscopy. *Mar. Chem.* 51, 325–346. doi: 10.1016/0304-4203(95)00062-3
- Dainard, P. G., and Guéguen, C. (2013). Distribution of PARAFAC modeled CDOM components in the North Pacific ocean, Bering, Chukchi and Beaufort seas. *Mar. Chem.* 157, 216–223. doi: 10.1016/j.marchem.2013.10.007
- Dainard, P. G., Guéguen, C., McDonald, N., and Williams, W. (2015). Photobleaching of fluorescent dissolved organic matter in Beaufort Sea and North Atlantic Subtropical Gyre. *Mar. Chem.*
- Fichot, C. G., Kaiser, K., Hooker, S. B., Amon, R. M. W., Babin, M., Bélanger, S., et al. (2013). Pan-Arctic distributions of continental runoff in the Arctic Ocean. *Sci. Rep.* 3:1053. doi: 10.1038/srep01053
- Granskog, M. A. (2012). Changes in spectral slopes of dissolved organic matter absorption with mixing and removal in a terrestrially dominated marine system (Hudson Bay, Canada). *Mar. Chem.* 134–135, 10–17. doi: 10.1016/j.marchem.2012.02.008
- Granskog, M. A., Stedmon, C. A., Dodd, P. A., Amon, R. M. W., Pavlov, A. K., de Steur, L., et al. (2012). Characteristics of colored dissolved organic matter (CDOM) in the Arctic outflow in the Fram Strait: assessing the changes and fate of terrigenous CDOM in the Arctic Ocean. *J. Geophys. Res.* 117, C12021. doi: 10.1029/2012jc008075
- Green, S. A., and Blough, N. V. (1994). Optical absorption and fluorescence properties of chromophoric dissolved organic matter in natural waters. *Limnol. Oceanogr.* 39, 1903–1916. doi: 10.4319/lo.1994.39.8.1903
- Guay, C. K., Klinkhammer, G. P., Falkner, K. K., Benner, R., Coble, P. G., Whittlestone, T. E., et al. (1999). High-resolution measurements of dissolved organic carbon in the Arctic Ocean by *in situ* fiber-optic spectrometry. *Geophys. Res. Lett.* 26, 1007–1010. doi: 10.1029/1999GL900130
- Guéguen, C., Granskog, M. A., McCullough, G., and Barber, D. G. (2011). Characterization of colored dissolved organic matter in Hudson Bay and Hudson Strait using Parallel Factor Analysis. *J. Mar. Syst.* 88, 423–433. doi: 10.1016/j.jmarsys.2010.12.001
- Guéguen, C., Guo, L., Wang, D., Tanaka, N., Hung, C.-C. (2006). Chemical characteristics and origin of dissolved organic matter in the Yukon River. *Biogeochemistry* 77, 139–155. doi: 10.1007/s10533-005-0806-1
- Guéguen, C., and Kowalcuk, P. (2013). "Colored dissolved organic matter in frontal zones," in *Chemical Oceanography of Frontal Zones*, ed I. Belkin (Berlin: Springer-Verlag).
- Guéguen, C., McLaughlin, F. A., Carmack, E. C., Itoh, M., Narita, H., and Nishino, S. (2012). The nature of colored dissolved organic matter in the southern Canada Basin and East Siberian Sea. *Deep Sea Res. II*, 81–84, 102–113. doi: 10.1016/j.dsr2.2011.05.004
- Hancke, K., Hovland, E. K., Volent, Z., Pettersen, R., Johnsen, G., Moline, M., et al. (2014). Optical properties of CDOM across the Polar Front in the Barents Sea: origin, distribution and significance. *J. Mar. Syst.* 130, 219–227. doi: 10.1016/j.jmarsys.2012.06.006
- Hansell, D. A., and Carlson, C. A. (2002). *Biogeochemistry of Marine Dissolved Organic Matter*. San Diego, CA: Academic Press.
- Heller, M. I., Gaiero, D. M., and Croot, P. L. (2013). Basin scale survey of marine humic fluorescence in the Atlantic: relationship to rion solubility and H_2O_2 . *Glob. Biogeochem. Cycle* 27, 88–100. doi: 10.1029/2012GB004427
- Helms, J. R., Stubbins, A., Ritchie, J. D., Minor, E. C., Kieber, D. J., and Mopper, K. (2008). Absorption spectral slopes and slope ratios as indicators of molecular weight, source and photobleaching of chromophoric dissolved organic matter. *Limnol. Oceanogr.* 53, 955–969. doi: 10.4319/lo.2008.53.3.0955
- Ishii, S. K. L., and Boyer, T. H. (2007). Behavior of reoccurring PARAFAC components in fluorescent dissolved organic matter in natural and engineered systems: a critical review. *Environ. Sci. Technol.* 41, 2006–2017. doi: 10.1021/es043504
- Jones, E. P., and Anderson, L. G. (1986). On the origin of the chemical properties of the Arctic Ocean halocline. *J. Geophys. Res.* 91, 10759–10767. doi: 10.1029/JC091iC09p10759
- Jørgensen, L., Stedmon, C. A., Kragh, T., Markager, S., Middleboe, M., and Sondergaard, M. (2011). Global trends in the fluorescence characteristics and distribution of marine dissolved organic matter. *Mar. Chem.* 126, 139–148. doi: 10.1016/j.marchem.2011.05.002
- Kowalcuk, P., Tilstone, G. H., Zablocka, M., Röttgers, R., and Thomas, R. (2013). Composition of dissolved organic matter along an Atlantic Meridional transect from fluorescence spectroscopy and parallel factor analysis. *Mar. Chem.* 157, 170–184. doi: 10.1016/j.marchem.2013.10.004
- Lawaetz, A. J., and Stedmon, C. A. (2009). Fluorescence intensity calibration using the Raman scatter peak of water. *Appl. Spectrosc.* 63, 936–940. doi: 10.1366/000370209788964548
- Murphy, K. R., Ruiz, G. M., Dunsmuir, W. T. M., and Waite, T. D. (2006). Optimized parameters for fluorescence-based verification of ballast water exchange by ships. *Environ. Sci. Technol.* 40, 2357–2362. doi: 10.1021/es0519381
- Murphy, K. R., Stedmon, C. A., Waite, T. D., and Ruiz, G. M. (2008). Distinguishing between terrestrial and autochthonous organic matter sources in marine environments using fluorescence spectroscopy. *Mar. Chem.* 108, 40–58. doi: 10.1016/j.marchem.2007.10.003
- Murphy, K. R., Stedmon, C. A., Wenig, P., and Bro, R. (2014). OpenFluor—an online spectral library of auto-fluorescence by organic compounds in the environment. *Anal. Methods* 6, 658–661. doi: 10.1039/C3AY41935E
- Nelson, N. B., and Coble, P. G. (2009). "Optical analysis of chromophoric dissolved organic matter," in *Practical Guidelines for the Analysis of Seawater*, ed O. Wurl (Boca Raton, NJ: CRC Press), 79–96.
- Nishino, S., Itoh, M., Williams, W. J., and Semiletov, I. (2013). Shoaling of the nutricline with an increase in near-freezing temperature water in the Makarov Basin. *J. Geophys. Res. Oceans* 118, 635–649. doi: 10.1029/2012JC008234
- Nishino, S., Shimada, S., Itoh, M., Yamamoto-Kawai, M., and Chiba, S. (2008). East-west differences in water mass, nutrient, and chlorophyll a distributions in the sea ice reduction region of the western Arctic Ocean. *J. Geophys. Res.* 113, C00A01. doi: 10.1029/2007jc004666
- Osburn, C. L., and Stedmon, C. A. (2011). Linking the chemical and optical properties of dissolved organic matter in the Baltic-North Sea transition zone to differentiate three allochthonous inputs. *Mar. Chem.* 126, 281–294. doi: 10.1016/j.marchem.2011.06.007
- Retamal, L., Vincent, W. F., Martineau, C., and Osburn, C. L. (2007). Comparison of the optical properties of dissolved organic matter in two river-influenced coastal regions of the Canadian Arctic. *Estuar. Coast. Shelf Sci.* 72, 261–272. doi: 10.1016/j.ecss.2006.10.022
- Søndergaard, M., Borch, N. H., and Stedmon, C. A. (2003). Fate of terrigenous dissolved organic matter (DOM) in estuaries: aggregation and bioavailability. *Ophelia* 57, 161–176. doi: 10.1080/00785236.2003.10409512
- Spencer, R. G. M., and Coble, P. G. (2014). "Sampling design for organic matter fluorescence analysis," in *Aquatic Organic Matter Fluorescence*, eds P. G. Coble, J. Lead, D. M. Reynolds, and R. G. M. Spencer (New York, NY: Cambridge Press), 125–146.
- Stanley, R. H. R., Sandwith, Z. O., and Williams, W. J. (2015). Rates of summertime biological productivity in the Beaufort Gyre: a comparison between the low and record-low ice conditions of August 2011 and 2012. *J. Mar. Syst.* 147, 29–44. doi: 10.1016/j.jmarsys.2014.04.006
- Stedmon, C. A., Amon, R. M. W., Rinehart, A. J., and Walker, S. A. (2011). The supply and characteristics of colored dissolved organic matter (CDOM) in the Arctic Ocean: Pan Arctic trends and differences. *Mar. Chem.* 124, 108–118. doi: 10.1016/j.marchem.2010.12.007
- Stedmon, C. A., and Bro, R. (2008). Characterizing dissolved organic matter fluorescence with parallel factor analysis: a tutorial. *Limnol. Oceanogr. Methods* 6, 572–579. doi: 10.4319/lom.2008.6.572

- Stedmon, C. A., and Markager, S. (2001). The optics of chromophoric dissolved organic matter (CDOM) in the Greenland Sea: an algorithm for differentiation between marine and terrestrially derived organic matter. *Limnol. Oceanogr.* 46, 2087–2093. doi: 10.4319/lo.2001.46.8.2087
- Stedmon, C. A., Markager, S., and Bro, R. (2003). Tracing dissolved organic matter in aquatic environments using a new approach to fluorescence spectroscopy. *Mar. Chem.* 82, 239–254. doi: 10.1016/S0304-4203(03)00072-0
- Stedmon, C. A., Markager, S., Tranvik, L., Kronberg, L., Slatis, T., and Martinsen, W. (2007). Photochemical production of ammonium and transformation of dissolved organic matter in the Baltic Sea. *Mar. Chem.* 104, 227–240. doi: 10.1016/j.marchem.2006.11.005
- Stedmon, C. A., and Markager, S. (2005). Resolving the variability in dissolved organic matter fluorescence in a temperate estuary and its catchment using PARAFAC analysis. *Limnol. Oceanogr.* 50, 686–697. doi: 10.4319/lo.2005.50.2.0686
- Uchida, R., Kuma, K., Omata, A., Ishikawa, S., Hioki, N., Ueno, H., et al. (2013). Water column iron dynamics in the subarctic North Pacific Ocean and the Bering Sea. *J. Geophys. Res.* 118, 1257–1271. doi: 10.1002/jgrc.20097
- Walker, S. A., Amon, R. M. W., Stedmon, C., Duan, S., and Louchoourn, P. (2009). The use of PARAFAC modeling to trace terrestrial dissolved organic matter and fingerprint water masses in coastal Canadian Arctic surface waters. *J. Geophys. Res.* 114, G00F06. doi: 10.1029/2009JG000990
- Yamamoto-Kawai, M., Carmack, E. C., McLaughlin, F. A., and Falkner, K. K. (2010). Oxygen isotope ratio, barium and salinity in waters around the North American coast from the Pacific to the Atlantic: implications for freshwater sourced to the Arctic throughflow. *J. Mar. Syst.* 68, 97–117. doi: 10.1357/002224010793078988
- Yamamoto-Kawai, M., McLaughlin, F. A., Carmack, E. C., Nishino, S., Shimada, K., and Kurita, N. (2009). Surface freshening of the Canada Basin, 2003–2007: river runoff versus sea ice meltwater. *J. Geophys. Res. Oceans* 114:C00A05. doi: 10.1029/2008jc005000
- Yamashita, Y., Boyer, J. N., and Jaffé, R. (2013). Evaluating the distribution of terrestrial dissolved organic matter in a complex coastal ecosystem using fluorescence spectroscopy. *Cont. Shelf Res.* 66, 136–144. doi: 10.1016/j.csr.2013.06.010
- Yamashita, Y., Cory, R. M., Nishioka, J., Kuma, K., Tanoue, E., and Jaffé, R. (2010). Fluorescence characteristics of dissolved organic matter in the deep waters of the Okhotsk Sea and the northwestern North Pacific Ocean. *Deep-Sea Res. II*, 57, 1478–1485. doi: 10.1016/j.dsr2.2010.02.016
- Yamashita, Y., Jaffé, R., Maie, N., and Tanoue, E. (2008). Assessing the dynamics of dissolved organic matter (DOM) in coastal environments by excitation-emission matrix fluorescence and parallel factor analysis (EEM-PARAFAC). *Limnol. Oceanogr.* 53, 1900–1908. doi: 10.4319/lo.2008.53.5.1900
- Yamashita, Y., Panton, A., Mahaffey, C., and Jaffé, R. (2011). Assessing the spatial and temporal variability of dissolved organic matter in Liverpool Bay using excitation_emission matrix fluorescence and parallel factor analysis. *Ocean Dyn.* 61, 569–579. doi: 10.1007/s10236-010-0365-4

Conflict of Interest Statement: The authors declare that the research was conducted in the absence of any commercial or financial relationships that could be construed as a potential conflict of interest.

Copyright © 2015 Guéguen, Itoh, Kikuchi, Eert and Williams. This is an open-access article distributed under the terms of the Creative Commons Attribution License (CC BY). The use, distribution or reproduction in other forums is permitted, provided the original author(s) or licensor are credited and that the original publication in this journal is cited, in accordance with accepted academic practice. No use, distribution or reproduction is permitted which does not comply with these terms.



Pan-Arctic Trends in Terrestrial Dissolved Organic Matter from Optical Measurements

Paul J. Mann^{1*}, Robert G. M. Spencer², Peter J. Hernes³, Johan Six⁴, George R. Aiken⁵, Suzanne E. Tank⁶, James W. McClelland⁷, Kenna D. Butler⁵, Rachael Y. Dyda³ and Robert M. Holmes⁸

¹ Department of Geography, Northumbria University, Newcastle-Upon-Tyne, UK, ² Department of Earth, Ocean and Atmospheric Science, Florida State University, Tallahassee, FL, USA, ³ Department of Land, Air, and Water Resources, University of California, Davis, Davis, CA, USA, ⁴ Department of Environmental Systems Science, ETH-Zurich, Zurich, Switzerland, ⁵ United States Geological Survey, Boulder, CO, USA, ⁶ Department of Biological Sciences, University of Alberta, Edmonton, AB, Canada, ⁷ Marine Science Institute, University of Texas, Port Aransas, TX, USA, ⁸ Woods Hole Research Center, Falmouth, MA, USA

OPEN ACCESS

Edited by:

Christopher Osburn,
North Carolina State University, USA

Reviewed by:

Rudolf Jaffe,
Florida International University, USA
Jean-Francois Lapierre,
Michigan State University, USA

*Correspondence:

Paul J. Mann
paul.mann@northumbria.ac.uk

Specialty section:

This article was submitted to
Marine Biogeochemistry,
a section of the journal
Frontiers in Earth Science

Received: 05 October 2015

Accepted: 23 February 2016

Published: 17 March 2016

Citation:

Mann PJ, Spencer RGM, Hernes PJ,
Six J, Aiken GR, Tank SE,
McClelland JW, Butler KD, Dyda RY
and Holmes RM (2016) Pan-Arctic
Trends in Terrestrial Dissolved Organic
Matter from Optical Measurements.
Front. Earth Sci. 4:25.
doi: 10.3389/feart.2016.00025

Climate change is causing extensive warming across Arctic regions resulting in permafrost degradation, alterations to regional hydrology and shifting amounts and composition of dissolved organic matter (DOM) transported by streams and rivers. Here, we characterize the DOM composition and optical properties of the six largest Arctic rivers draining into the Arctic Ocean to examine the ability of optical measurements to provide meaningful insights into terrigenous carbon export patterns and biogeochemical cycling. The chemical composition of aquatic DOM varied with season, spring months were typified by highest lignin phenol and dissolved organic carbon (DOC) concentrations with greater hydrophobic acid content, and lower proportions of hydrophilic compounds, relative to summer and winter months. Chromophoric DOM (CDOM) spectral slope ($S_{275-295}$) tracked seasonal shifts in DOM composition across river basins. Fluorescence and parallel factor analysis identified seven components across the six Arctic rivers. The ratios of “terrestrial humic-like” vs. “marine humic-like” fluorescent components co-varied with lignin monomer ratios over summer and winter months, suggesting fluorescence may provide information on the age and degradation state of riverine DOM. CDOM absorbance (a_{350}) proved a sensitive proxy for lignin phenol concentrations across all six river basins and over the hydrograph, enabling for the first time the development of a single pan-arctic relationship between a_{350} and terrigenous DOC ($R^2 = 0.93$). Combining this lignin proxy with high-resolution monitoring of a_{350} , pan-arctic estimates of annual lignin flux were calculated to range from 156 to 185 Gg, resulting in shorter and more constrained estimates of terrigenous DOM residence times in the Arctic Ocean (spanning 7 months to 2½ years). Furthermore, multiple linear regression models incorporating both absorbance and fluorescence variables proved capable of explaining much of the variability in lignin composition across rivers and seasons. Our findings suggest that synoptic, high-resolution optical measurements can provide improved understanding of northern high-latitude organic matter cycling and flux, and prove an important technique for capturing future climate-driven changes.

Keywords: carbon cycle, Arctic, lignin, colored dissolved organic matter (CDOM), parallel factor analysis (PARAFAC), DOC, climate change, hydrology

INTRODUCTION

Northern high-latitude regions contain substantial quantities of organic carbon in perennially and seasonally frozen soils, comprising more than half the entire global carbon soil stock (Tarnocai et al., 2009). Large Arctic rivers play an increasingly recognized role in regional carbon cycling by transporting a proportion of this terrigenous material from land to the ocean, whilst also acting as sites for active carbon metabolism and transformation (Striegl et al., 2005; Holmes et al., 2012; Mann et al., 2015; Spencer et al., 2015). Arctic riverine export is substantial enough ($\sim 10\%$ of the global freshwater discharge) that it imparts estuarine-like water quality characteristics throughout the Arctic Ocean, influencing coastal salinity structure on a localized basis (Aagaard and Carmack, 1989; Serreze et al., 2006; McClelland et al., 2011). Furthermore, significant quantities of dissolved organic matter (DOM) accompany this freshwater flux causing higher than average dissolved organic carbon (DOC) concentrations in the Arctic Ocean relative to other ocean basins (Opsahl et al., 1999; Mathis et al., 2005; Hernes and Benner, 2006). Six major Arctic rivers account for the majority of freshwater flux, each draining vast watersheds on the Eurasian (Kolyma, Ob', Lena, Yenisey) or North American (Mackenzie, Yukon) continents, combined delivering $\sim 64\%$ of the total freshwater supplied to the Arctic Ocean (Holmes et al., 2012).

Arctic rivers are characterized by their strong seasonality and large intra-annual variability in runoff, driven by extreme fluctuations in snow cover and air temperatures. Discharge rapidly peaks with the onset of snow melt and ice-breakup, resulting in dramatic spring freshet events and rapid transport of terrigenous DOM offshore (Stedmon et al., 2011a; Amon et al., 2012; Mann et al., 2012). By contrast, winter months are distinguished by low discharge and DOC concentrations, with DOM exhibiting lower average aromaticity and molecular weight (Spencer et al., 2008; O'Donnell et al., 2012). Future changes in the fluxes and composition of terrigenous DOM released to and exported from Arctic rivers are likely. River discharge across much of the pan-arctic watershed is increasing, particularly during winter months (Peterson, 2002; McClelland et al., 2006; Smith et al., 2007; Déry et al., 2009; Rawlins et al., 2010). Deepening of the seasonally thawed active layer will also result in leaching of deeper soil and permafrost horizons altering the amount and type of DOM liberated to inland waters (Romanovsky et al., 2010). Changes in the quality of DOM affect the reactivity and fate of terrigenous DOM, influencing carbon turnover rates and regional carbon budgets (Holmes et al., 2008; Mann et al., 2012, 2014; Wickland et al., 2012). Tracing future alterations in the composition as well as concentration of riverine DOM is therefore crucial for understanding the effects of climate change.

Lignin phenols are unique biomarkers of vascular plant material and therefore act as sensitive indicators for the terrigenous component of aquatic DOM. As well as providing pertinent information on DOM source, lignin phenols also have the capacity to capture degradative processing and source information (Opsahl and Benner, 1995; Hernes et al., 2007;

Spencer et al., 2010a). DOM source and composition has also been assessed via separation of the DOM pool using XAD fractionation techniques. DOC fractionation has been used to differentiate between high molecular weight, aromatic dominated carbon DOM fractions, primarily sourced from allochthonous materials, and those dominated by microbially-derived or photodegraded DOM (e.g., Aiken et al., 1992; Spencer et al., 2012). Despite providing critical information, both lignin phenol and XAD fractionation techniques are costly and extremely time consuming to conduct, limiting their applicability for high-resolution monitoring. The remote nature of Arctic watersheds and the rapid shifts in hydrology make effective sampling and observation of these regions incredibly challenging. Despite far greater understanding of constituent fluxes and biogeochemical cycles across Arctic river systems, much garnered from international sampling campaigns (e.g., PARTNERS, Arctic-GRO), insufficient temporal and spatial resolution in measurements still limits our ability to capture changes in terrigenous DOM supply and examine how it may alter under future scenarios. For example, the Arctic Great Rivers Observatory (Arctic-GRO) captures the major seasonal patterns in river chemistry and freshwater discharge across the six major Arctic rivers, ensuring identical sampling and analytical protocols yet is limited with respect to the number of samples that can be feasibly collected. The use of optical measurements, which can be rapidly collected and measured, remotely derived or determined *in-situ* is one pathway that can help to address these problems.

A number of studies have investigated the ability of optical measurements to capture changes in DOM composition occurring across rivers or over the hydrograph, or to relate optical and lignin-based proxies to improve estimates of terrigenous DOM residence times in the Arctic Ocean (Spencer et al., 2009; Stedmon et al., 2011a; Walker et al., 2013). Recently, chromophoric DOM (CDOM) absorbance measurements from 30 unique US watersheds were shown to correlate to DOM composition, as derived via XAD fractionation, highlighting the potential of optical measurements to improve our understanding of DOM dynamics in fluvial systems (Spencer et al., 2012). Additionally, CDOM absorbance-lignin relationships have been developed for the Yukon River and then scaled to the pan-arctic, assuming similar relative loads of lignin in freshwater fluxes across all Arctic rivers (Spencer et al., 2009). Using this approach, Spencer et al. (2009) found that terrigenous DOM export to the Arctic Ocean was higher than previously thought, and thus concluded that a greater proportion must either be modified during transit through estuaries, or removal processes in the Arctic Ocean are greater than previously thought. CDOM fluorescence measurements have also shown to be potentially useful proxies for lignin phenol concentration and composition in freshwaters (Hernes et al., 2009; Walker et al., 2013). Successful relationships have been reported between CDOM fluorescence, collected as excitation-emission matrices (EEMs) and decomposed using parallel factor analysis (PARAFAC), and lignin measurements across individual Arctic rivers, yet pan-arctic relationships remain elusive (Walker et al., 2013). In particular, no studies have attempted to develop relationships

between DOM optical properties from across all six Arctic rivers and DOC fractionation measurements (XAD), or with vascular plant biomarkers (lignin phenols) as rapid proxies for terrestrial DOC export and composition across the Arctic. Additionally, no studies have examined the utility of combining absorbance and fluorescence techniques to develop Arctic proxies for terrigenous DOM export.

Here, we characterize the DOM optical properties and composition (XAD and lignin phenol) of the six largest Arctic rivers to examine the ability of optical measurements to provide meaningful insights into terrigenous carbon export patterns and biogeochemical cycling across broad spatial scales in the Arctic. Specifically, we attempt to identify common optical indices that trace DOC and lignin phenol concentration and compositional information across all six Arctic rivers. Further, we examine the utility of using a combination of absorbance and fluorescence measurements to predict trends in DOC and lignin phenol biomarkers. Finally, we develop, for the first time, a pan-arctic optical proxy for estimating terrestrial OC flux from Arctic rivers to the Arctic Ocean and apply our findings to high-resolution optical measurements to improve terrigenous DOC export estimates.

MATERIALS AND METHODS

Study Areas and Sample Collection

Samples from each of the six largest Arctic rivers were collected as part of the Arctic Great Rivers Observatory (Arctic-GRO; www.arcticgreatrivers.org; **Figure 1**). Each of the six rivers was sampled five times per year in 2009 and 2010 (except for 2009 on the Yukon with six samples) using a standardized collection method as detailed elsewhere (Raymond et al., 2007; McClelland et al., 2008; Holmes et al., 2012). Depth and width integrated samples were collected from near the mouth of each river (above tidal influence) across the hydrograph, incorporating baseflow, spring melt, and summer conditions. Near-daily surface sampling (0.5 m) was also conducted over the spring freshet hydrographs on each of the six Arctic rivers during both years to provide high-resolution optical measurements for this period ($n = 241$).

Samples collected for DOC concentration, optical properties and lignin analyses were filtered within a few hours of collection into pre-cleaned high-density polyethylene bottles through pre-rinsed 0.45 μm capsule filters (Geotech or Pall Aquaprep 600) and measured on unfractionated waters.

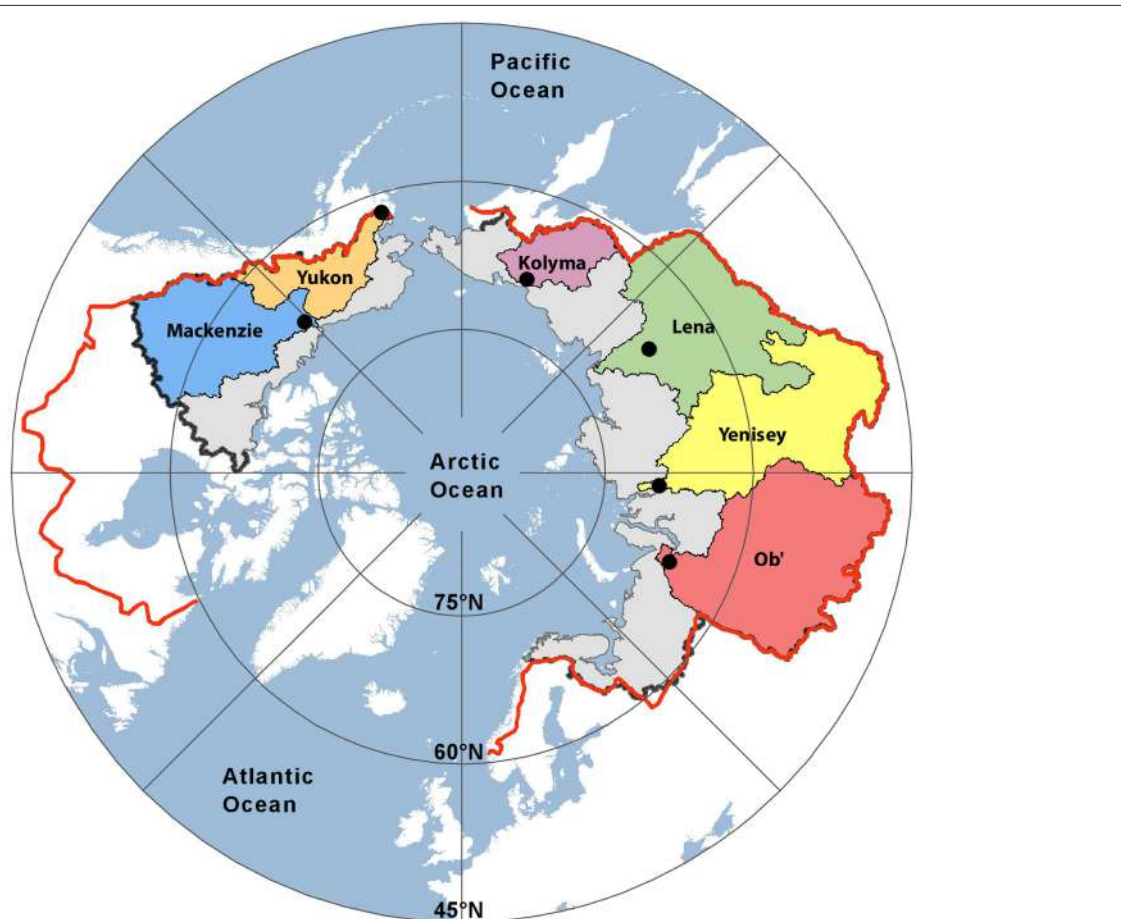


FIGURE 1 | Map showing the six Arctic river catchments sampled. Black dots indicate sampling locations. The black (PA1) and red lines (PA2) represent two estimates of the total pan-arctic watershed area ($16.8 \times 10^6 \text{ km}^2$ and $20.5 \times 10^6 \text{ km}^2$, respectively).

Samples for DOC fractionation were filtered as above and acidified to pH 2.

Dissolved Organic Carbon and XAD Fractionation

Dissolved organic carbon (DOC) measurements were performed on a Shimadzu (TOC-V) organic carbon analyzer as the mean of 3–5 replicate injections where the coefficient of variance was <2% (Mann et al., 2012). River water DOC samples were chromatographically separated into operationally defined hydrophobic organic acid (HPOA), hydrophobic neutral (HPON), low molecular weight hydrophilic (HPI) and transphilic organic acid (TPIA) fractions using XAD-8 and XAD-4 resins and established methodologies (Aiken et al., 1992). The amount of organic matter within each fraction is expressed as a percentage of the total DOC concentration and the sample mass of each fraction. The HPOA fraction typically contains more aromatic humic and fulvic acids and the HPI fraction less aromatic and more aliphatic forms of carbon, providing information on DOC composition.

Lignin Phenol Biomarkers

Lignin phenols were measured via the CuO oxidation method described by Hedges and Ertel (1982), with modifications as outlined by Spencer et al. (2010b). In brief, filtered whole waters were acidified to pH 2 with 12N HCl, rotary evaporated to ~3 mL and the concentrate transferred to Monel reaction vessels (Prime Focus, Inc.) and dried under vacuum centrifugation. All samples were alkaline oxidized at 155°C in a stoichiometric excess of CuO, followed by acidification (pH = 1 with 12 N H₂SO₄) and extracted three times with ethyl acetate, passed through Na₂SO₄ drying columns and taken to dryness under a gentle stream of ultrapure nitrogen. After redissolution in pyridine, lignin phenols were silylated (BSTFA) and quantified on a GC-MS (Agilent 6890 gas chromatograph equipped with an Agilent 5973 mass selective detector and a DB5-MS capillary column; 30 m, 0.25 mm inner diameter, Agilent) using cinnamic acid as an internal standard and a five-point calibration scheme. Eight lignin phenols were quantified for all samples, including three vanillyl phenols (vanillin, acetovanillone, vanillic acid), three syringyl phenols (syringaldehyde, acetosyringone, syringic acid), and two cinnamyl phenols (p-coumaric acid, ferulic acid). One blank was run for every ten-sample oxidations and all samples were blank corrected. Blank concentrations of lignin phenols were low (30–40 ng) and consequently never exceeded 5% of the total lignin phenols in a sample. Lignin phenol concentrations are reported as the sum of the cinnamyl, syringyl and vanillyl phenols (Σ_8). Additionally, the carbon normalized sum of the lignin phenols (Λ_8) were calculated.

DOM Absorbance and Fluorescence

UV-visible absorbance was measured in a 1 cm quartz cuvette across 200–800 nm at room temperature (20°C) with a dual beam Shimadzu UV-1800 spectrophotometer. Measurements were recorded in triplicate at 1 nm wavelength intervals and referenced against Milli-Q water blanks. Absorbance values were converted to Napierian absorption coefficients by multiplying

raw absorbance values by 2.303 and dividing by the pathlength (m) (Hu et al., 2002). The slope (S) of the absorbance spectra was calculated from wavelength ranges spanning 275–295, 290–350, and 350–400 nm and the slope ratio (S_R) determined (Helms et al., 2008). Slope coefficients can provide information pertaining to CDOM composition and source, with steeper values and increasing S_R indicative of lower molecular weight and decreasing DOM aromaticity (Blough and Green, 1995; Blough and Del Vecchio, 2002; Helms et al., 2008). Specific UV absorbance (SUVA₂₅₄) was calculated by dividing the decadal UV absorbance at 254 nm by the DOC concentration (Weishaar et al., 2003). The specific UV absorbance (SUVA₂₅₄) has been shown to be positively correlated to percent aromaticity within DOM (Weishaar et al., 2003).

Fluorescence was analyzed using a Horiba Fluoromax-4 spectrofluorometer (Jobin-Yvon). Excitation-emission matrices (EEMs) were collected at 20°C in ratio (S/R) mode over excitation and emission wavelengths of 250–450 and 320–550 nm, in 5 and 2 nm increments respectively. Measurements were performed with 0.1s integration times and 5 nm slit widths on the excitation and emission monochromators. Instrument specific correction files were applied before further analyses. Fluorescence EEMs were blank corrected from at least daily Milli-Q blanks collected identically to samples. Daily water Raman scans were collected at Ex = 350 nm (e.g., Lawaetz and Stedmon, 2009). Raman and Rayleigh-Tyndall scatter were removed and interpolated using the *smootheem* function and absorbance measurements were used to correct EEMs for inner filter effects according to the method of Lakowicz (2006), within the drEEM toolbox (Murphy et al., 2013). The fluorescence index (FI) was also calculated as the ratio of emission at 470 to 520 nm, at an excitation wavelength of 370 nm (McKnight et al., 2001; Cory et al., 2010).

PARAFAC and Statistical Analyses

Exploratory analysis of fluorescence EEM data was conducted using parallel factor analysis (PARAFAC) to decompose the number, shape and amounts of underlying spectral components among samples. PARAFAC was conducted using the drEEM (version 2.0) and N-way (version 3.20) toolbox (Murphy et al., 2013) within the MATLAB R2013a environment.

To aid decomposition and provide greater variance within the dataset, additional EEMs (total $n = 645$) collected across a wide range of stream and river environments from the Kolyma River Basin were included and analyzed alongside the Arctic-GRO fluorescence dataset. PARAFAC modeling was performed after normalizing each EEM to its total signal (to unit norm) by dividing by the sum of the squared values of all variables in the sample, and imposing non-negativity constraints, thus negating problems caused by large concentration gradients apparent in seasonal samples (Murphy et al., 2013). The number of components within the model was validated using all of the techniques recommended in Murphy et al. (2013), including examination of systematic variation in the dataset, visualization of spectral loadings and split half analysis. The final model was successfully validated using four splits of the data and three validation tests across six

different dataset halves ($S_4C_6T_3$) (Harshman and Lundy, 1994; Murphy et al., 2013). Fluorescence loadings were calculated after normalizing the dataset ensuring unscaled model scores were recovered.

Principle component analysis (PCA; nonrotated solutions) was employed to explore relationships between optical properties, DOC and lignin phenol concentration and composition using the PLS_Toolbox (Eigenvector, Inc., Seattle, WA v. 8.0) within MATLAB (R2013a). Autoscaling was used on variables measured prior to PCA. Multiple linear regression models were developed using a forward stepwise approach minimizing the Akaike Information Criterion, and were conducted in SPSS v22 (IBM).

Constituent Flux Calculations

Constituent fluxes were estimated using the USGS LoadEstimator software (LOADEST) within the LoadRunner software interface (Runkel et al., 2004; Booth et al., 2007). LOADEST calculates daily constituent flux estimates by generating relationships between measured discharge and element concentrations and was run as in Holmes et al. (2012). Daily discharge data were obtained from US Geological Survey (Yukon), Water Survey of Canada (Mackenzie) and Roshydromet (Kolyma, Lena, Ob' and Yenisey), and are freely available from <http://arcticgreatrivers.org/data.html> and the Water Survey of Canada http://wateroffice.ec.gc.ca/mainmenu/historical_data_index_e.html.

Corrections were applied to allow for the distance between the discharge measurement station and sample location as has been previously described (Holmes et al., 2012). Any gaps in the discharge data were filled by interpolation, however there were no gaps during peak flow on any river.

RESULTS

Spatial and Temporal Patterns in Chemical Fractions of DOC

Total DOC concentrations ranged over the study period from 2.6 to 17.5 mg L^{-1} . Highest average DOC concentrations were measured in the Lena river ($15.7 \pm 0.9\text{ mg L}^{-1}$, \pm SE) during spring, and lowest during winter in the Yukon river (2.9 mg L^{-1} , $n = 1$; **Table 1**). DOC concentrations from all six rivers were correlated with runoff ($\text{m}^3 \text{ km}^{-2} \text{ d}^{-1}$; $R^2 = 0.44$, not shown). Riverine DOC was mainly comprised of high contributions from the HPOA fraction, averaging $53 \pm 1\%$ across the six Arctic rivers (**Table 1**). Eurasian rivers contained higher average proportions of the HPOA fraction over the year (54 to $56 \pm 2\%$) relative to the North American Yukon ($50 \pm 2\%$) and Mackenzie rivers ($45 \pm 2\%$, *t*-test $p < 0.001$). HPI and TPIA fractions contributed a smaller proportion to bulk DOC, averaging 19 ± 0

TABLE 1 | Total dissolved organic carbon concentrations (DOC) and major chemical fractions of DOC and fraction-specific ultraviolet absorbance (SUVA₂₅₄) across the six great Arctic rivers (mean \pm standard error) during Spring (May and June), Summer (July through to October) and Winter (November through to April).

Site	Season	Total DOC (mg C^{-1})	Total SUVA ₂₅₄ ($\text{L mg C}^{-1} \text{ m}^{-1}$)	HPOA (%)	HPOA SUVA ₂₅₄ ($\text{L mg C}^{-1} \text{ m}^{-1}$)	TPIA (%)	TPIA SUVA ₂₅₄ ($\text{L mg C}^{-1} \text{ m}^{-1}$)	HPI (%)	HPI SUVA ₂₅₄ ($\text{L mg C}^{-1} \text{ m}^{-1}$)
Kolyma	Spring	10.8 ± 1.7	2.9 ± 0.1	54 ± 2	3.9 ± 0.1	16 ± 1	2.4 ± 0.0	21 ± 1	1.5 ± 0.2
	Summer	3.7 ± 0.2	2.5 ± 0.0	56 ± 7	3.4 ± 0.2	18 ± 0	2.2 ± 0.0	20 ± 2	1.7 ± 0.2
	Winter	4.3 ± 1.7	2.0 ± 0.1	50 ± 7	2.9 ± 0.1	18 ± 0	2.0	20	2.1
Lena	Spring	15.7 ± 0.9	3.7 ± 0.0	57 ± 1	4.3 ± 0.0	17 ± 0	2.9 ± 0.0	17 ± 0	1.7 ± 0.0
	Summer	7.4 ± 0.6	2.8 ± 0.4	52 ± 3	4.0 ± 0.4	16 ± 1	2.5 ± 0.1	18 ± 0	1.5 ± 0.1
	Winter	9.7 ± 2.0	2.6 ± 0.3	53 ± 1	3.7 ± 0.1	17 ± 1	2.6 ± 0.1	16 ± 0	1.7 ± 0.2
Mackenzie	Spring	4.7 ± 0.3	2.5 ± 0.6	47 ± 1	3.6 ± 0.2	19 ± 0	2.4 ± 0.1	20 ± 1	1.4 ± 0.1
	Summer	5.4 ± 0.5	2.3 ± 0.1	46 ± 2	3.8 ± 0.2	20 ± 1	2.4 ± 0.1	20 ± 1	1.3 ± 0.0
	Winter	5.1	1.5	40	3.2	16	2.2	24	1.2
Ob'	Spring	9.0 ± 0.4	3.4 ± 0.0	57 ± 1	4.1 ± 0.0	15 ± 1	2.8 ± 0.1	18 ± 1	1.8 ± 0.1
	Summer	11.4 ± 0.9	3.1 ± 0.4	56 ± 1	4.2 ± 0.1	16 ± 1	2.8 ± 0.2	17 ± 1	–
	Winter	9.2 ± 1.9	3.0 ± 0.1	55 ± 3	4.0 ± 0.0	17 ± 1	2.8 ± 0.2	16 ± 1	–
Yenisey	Spring	10.1 ± 0.2	3.9 ± 0.0	60 ± 2	4.4 ± 0.1	16 ± 1	3.1 ± 0.1	16 ± 0	1.7 ± 0.0
	Summer	7.4 ± 1.8	2.8 ± 0.2	49 ± 3	4.2 ± 0.1	17 ± 1	2.6 ± 0.0	22 ± 2	1.5
	Winter	4.7 ± 0.7	2.6 ± 0.2	49 ± 6	3.9 ± 0.2	18 ± 1	2.5 ± 0.1	23 ± 3	2.3
Yukon	Spring	9.8 ± 2.3	3.2 ± 0.1	53 ± 1	4.2 ± 0.1	15 ± 0	2.8 ± 0.0	19 ± 1	2.2 ± 0.2
	Summer	7.1 ± 1.5	2.5 ± 0.2	50 ± 2	4.0 ± 0.4	19 ± 1	2.6 ± 0.1	21 ± 2	1.9 ± 0.2
	Winter	2.9	2	43	3.3	18	2.1	22	2.2

Hydrophobic acids (HPOA), transphilic acids (TPI), and hydrophilic organic matter (HPI) presented as percentage of total DOC concentrations and the sample mass of each fraction (HPON comprises the remaining $<10\%$ of the DOC pool).

and $17 \pm 0\%$ respectively. The average HPI and TPIA fractions were less variable than HPOA, ranging from 17 to 21 and 16 to 19% respectively across all sites and seasons (**Table 1**). HPON fractions generally contributed <10% to bulk DOC across rivers and were thus omitted from further study.

The composition of DOC was further characterized by calculating specific UV-visible absorbance (SUVA₂₅₄) of DOC and its major chemical fractions (**Table 1**). Mean SUVA₂₅₄ values of total DOC varied considerably among rivers with lowest values measured in the Mackenzie River ($2.5 \text{ L mgC}^{-1} \text{ m}^{-1}$) and highest in the Yenisey River ($3.4 \text{ L mgC}^{-1} \text{ m}^{-1}$). Mean SUVA₂₅₄ values of the HPOA fraction also varied among rivers with lowest values observed in the Kolyma River ($3.6 \text{ L mgC}^{-1} \text{ m}^{-1}$) and highest in the Yenisey ($4.3 \text{ L mgC}^{-1} \text{ m}^{-1}$), and were consistently higher than bulk DOC highlighting the greater number of highly aromatic compounds represented by this fraction. The SUVA₂₅₄ values of the HPI (1.2 to $2.3 \text{ L mgC}^{-1} \text{ m}^{-1}$) and TPIA (2.0 to $3.1 \text{ L mgC}^{-1} \text{ m}^{-1}$) fractions were less variable across rivers, and lower than bulk DOC, indicating the presence of a lower relative number of aromatic moieties (**Table 1**).

The contribution of HPOA to the total DOC pool was generally highest during spring months with maximum contributions varying considerably between rivers (47–60%; **Table 1**). Percent contributions of the HPOA fraction were typically lowest during winter flow periods. No clear seasonal differences in the fraction of HPOA present were observed in the Ob' River (55 ± 3 to $57 \pm 1\%$). Mean SUVA₂₅₄ values of total DOC were consistently highest across all rivers during spring months, intermediate during summer months (2.3 to $3.1 \text{ L mgC}^{-1} \text{ m}^{-1}$) and lowest in winter across all rivers (1.5 to $3.0 \text{ L mgC}^{-1} \text{ m}^{-1}$; **Table 1**). SUVA₂₅₄ values of the HPOA fraction followed similar seasonal trends as total DOC. TPIA and HPI SUVA₂₅₄ values displayed less clear seasonal patterns (**Table 1**).

Spatial and Temporal Patterns in Lignin Phenols

Mean lignin phenol concentrations (Σ_8) varied significantly among the six rivers, with lowest concentrations observed in the Mackenzie River ($9.5 \mu\text{g L}^{-1}$) and highest in the Lena River ($70.0 \mu\text{g L}^{-1}$; **Table 2**). Highest carbon normalized lignin yields (Λ_8) were observed in the Yenisey River, mostly due to lower mean DOC concentrations relative to the Lena River (**Table 2**). Lowest mean Λ_8 values were measured in the Mackenzie River [$0.19 (\text{mg}(100 \text{ mg OC}))^{-1}$]. Lignin values measured in this study were consistent with prior measurements in the Yukon and Russian Arctic rivers (Lobbes et al., 2000; Spencer et al., 2009) but notably lower than lignin measurements from the earlier PARTNERS project (Amon et al., 2012).

The Lena and Yenisey rivers displayed lowest mean cinnamyl (C) to vanillyl (V) phenol ratios (C/V), indicative of greater contributions of woody versus non-woody sources to bulk DOM of these rivers (Hedges and Mann, 1979). Highest C/V ratios were measured in the Mackenzie and Ob' Rivers (**Table 2**). Spatial variability in syringyl (S) to vanillyl ratios (S/V) mainly mirrored those of C/V, except for higher S/V values in the Yukon River as

compared to the Mackenzie River (**Table 2**). Higher S/V ratios are indicative of greater proportions of angiosperm vs. gymnosperm sources to DOM (Hedges and Mann, 1979).

Acid to aldehyde ratios (Ad/Al) have been suggested to provide evidence of the relative degree of DOM degradation, with higher ratios indicating greater degradation of plant tissues (Hedges et al., 1988; Opsahl and Benner, 1995; Hernes and Benner, 2003). Mean ratios of vanillic acid to vanillin (Ad/Al)_v ranged from 1.07 in the Mackenzie River to 1.48 in the Yukon River (**Table 2**). Ratios of syringic acid to syringaldehyde (Ad/Al)_s varied from 0.84 in the Yenisey to 1.06 in the Mackenzie River.

Σ_8 values among rivers were strongly linearly related to runoff ($R^2 = 0.69$, not shown) suggesting terrigenous DOM export dynamics were largely controlled by hydrology. Accordingly, highest Σ_8 concentrations were recorded across all rivers during the spring freshet and lowest concentrations during base flow winter conditions. Highest individual Σ_8 values were measured in the Lena River ($120 \mu\text{g L}^{-1}$) and lowest in the Kolyma and Yukon Rivers ($3.8 \mu\text{g L}^{-1}$). During the freshet, Λ_8 yields were between 2.6 and 4.8 times higher than winter Λ_8 values across sites, the Yenisey River displaying the least variability and the Yukon the greatest (**Table 2**).

C/V and S/V ratios generally declined with increasing runoff across all rivers (**Table 2**). Acid aldehyde ratios (Al/Ad) were highly variable among rivers, generally increasing with greater runoff, yet in some cases (e.g., Lena River) demonstrated opposing patterns. Highest Ad/Al ratios during the spring freshet may represent the export of greater quantities of largely “fresh” microbially unprocessed DOM relative to later in the year (Hernes et al., 2007; Spencer et al., 2008; Amon et al., 2012).

Chromophoric and Fluorescence DOM of Arctic Rivers

The absorbance coefficient of CDOM at 350 nm (a_{350}) ranged from 2.3 to 42.6 m^{-1} among rivers and seasons, and similar to DOC and Σ_8 concentrations, generally increased with greater freshwater runoff ($R^2 = 0.57$, $p < 0.001$, $n = 60$; Supplemental Table 1). Spectral slope values ($S_{275-295}$, $S_{290-350}$, $S_{350-400}$) steepened with decreasing runoff, in good agreement with previous studies (Spencer et al., 2009; Stedmon et al., 2011a), indicating the export of lower molecular weight material, or DOM with decreasing aromaticity as discharge rates decline (Blough and Green, 1995; Blough and Del Vecchio, 2002). The slope ratio (S_R) showed an opposing pattern to spectral slopes, declining at higher runoff rates thus confirming an increase in DOM molecular weight during the spring freshet and reduction during winter baseflow months (Helms et al., 2008; Spencer et al., 2010a, 2012).

Fluorescence index (FI) values were similar across rivers and averaged 1.34 ± 0.01 across all sites and sampling dates reflecting DOM from a mixture of terrigenous and microbial sources (McKnight et al., 2001). Highest FI values were measured across all rivers during winter months (mean 1.41 ± 0.03), reflecting a potentially higher contribution of microbial derived or lower aromaticity DOM during this period. Lowest FI values among

TABLE 2 | Sampling location and date of dissolved organic carbon (DOC) and lignin phenol concentration (Σ_8), carbon normalized sum of lignin yields (Λ_8), lignin ratios (C/V and S/V), and acid aldehyde ratios (Ad/AI) measurements. Site-normalized discharge (Q) is also presented.

River	Date	Q ($\text{m}^3 \text{s}^{-1}$)	DOC (mgC L^{-1})	Σ_8 ($\mu\text{g L}^{-1}$)	Λ_8 [$\text{mg(100 mg OC)}^{-1}$]	C/V	S/V	(Ad/AI)v	(Ad/AI)s
Kolyma	05 Jun 2009	12,800	10.7	54.2	0.51	0.16	0.51	1.58	1.14
Kolyma	12 Jun 2009	11,100	9.1	45.1	0.50	0.18	0.58	1.42	1.00
Kolyma	21 Jun 2009	8270	5.5	16.8	0.31	0.18	0.41	1.29	1.06
Kolyma	09 Sep 2009	8390	3.9	17.0	0.44	0.19	0.64	1.51	1.08
Kolyma	08 Nov 2009	3850	2.6	3.8	0.15	0.24	0.47	1.41	1.02
Lena	31 May 2009	68,328	17.5	120.0	0.69	0.04	0.17	1.28	0.98
Lena	05 Jun 2009	128,769	16.7	107.2	0.65	0.05	0.19	1.28	0.94
Lena	11 Jun 2009	83,800	12.9	85.2	0.66	0.07	0.25	1.30	0.96
Lena	22 Aug 2009	33,400	6.8	20.9	0.31	0.14	0.28	1.36	1.05
Lena	18 Nov 2009	4102	7.7	16.5	0.22	0.12	0.30	1.34	1.09
Mackenzie	11 Jun 2009	24,300	4.3	16.2	0.38	0.17	0.34	1.01	0.81
Mackenzie	30 Jun 2009	20,900	5.3	9.3	0.18	0.28	0.50	1.24	1.38
Mackenzie	02 Jul 2009	21,100	6.6	8.3	0.13	0.19	0.43	0.98	0.89
Mackenzie	08 Sep 2009	13,800	5.0	8.0	0.16	0.18	0.37	1.06	1.00
Mackenzie	25 Mar 2010	4380	5.1	5.5	0.11	0.32	0.51	1.09	1.13
Ob'	02 Jun 2009	36,300	8.1	55.5	0.69	0.23	0.61	1.39	0.93
Ob'	07 Jun 2009	36,100	8.5	40.4	0.48	0.19	0.58	1.39	0.89
Ob'	13 Jun 2009	35,400	7.7	55.7	0.73	0.19	0.59	1.38	0.88
Ob'	25 Aug 2009	13,500	10.5	22.4	0.22	0.20	0.46	0.93	0.90
Ob'	01 Dec 2009	5152	7.3	17.2	0.24	0.31	0.68	0.97	0.75
Yenisey	17 Jun 2009	85,400	9.8	71.2	0.73	0.07	0.29	1.39	0.91
Yenisey	21 Jun 2009	67,200	9.5	74.7	0.79	0.08	0.29	1.40	0.86
Yenisey	27 Jun 2009	45,600	9.6	57.6	0.60	0.07	0.26	1.17	0.77
Yenisey	08 Aug 2009	15,200	5.6	18.7	0.33	0.15	0.37	0.99	0.80
Yenisey	30 Nov 2009	11,167	4.0	12.2	0.31	0.18	0.35	0.84	0.88
Yukon	14 May 2009	11,836	5.2	17.2	0.34	0.10	0.57	1.70	1.05
Yukon	20 May 2009	10,874	13.0	62.1	0.48	0.11	0.48	1.90	1.03
Yukon	26 May 2009	26,901	15.0	95.5	0.64	0.13	0.54	1.79	1.28
Yukon	07 Jul 2009	15,008	5.6	11.5	0.21	0.15	0.46	0.99	0.77
Yukon	18 Aug 2009	7759	2.6	4.2	0.16	0.27	0.51	1.02	0.77
Yukon	12 Jan 2010	1869	2.9	3.8	0.13	0.33	0.63	1.10	1.14

rivers (mean 1.31 ± 0.01), indicative of greatest terrigenous and aromatic DOM supply, were observed during the high discharge spring freshet.

Parallel Factor Analysis (PARAFAC)

The PARAFAC analysis of DOM excitation-emission scans collected from all six Arctic rivers over the hydrograph identified seven unique components (Figure 2; Supplemental Figure 1). The spectra of each component identified were compared with the open fluorescence database (openfluor.org) containing spectra from previous studies (currently 53 studies) detailing PARAFAC models. All seven components (AG1-7) closely matched (tucker congruence coefficient, TCC > 0.95 ; Tucker, 1951) the excitation and emission spectra of previously identified components from 37 independent studies (Table 3).

Four of the seven AG components were very closely related (TCC ≥ 0.97) to those reported in the five-component Horsens catchment model (Murphy et al., 2014). For each of the seven

components identified here, at least three independent studies had previously identified statistically similar spectra, except for component AG3 for which there was only a single match. Table 3 provides information and a description of the seven components identified.

AG3 was closely related (TCC = 0.97) to C1 in Murphy et al. (2014) where it was identified as displaying an emission spectrum identical to syringaldehyde, a product of lignin breakdown. The AG model shared two components with a five-component PARAFAC model explaining fluorescence DOM collected from five of the major Arctic rivers sampled here over 2004–2005 (Walker et al., 2013). AG6 was similar (TCC > 0.95) to C1 from this model (Walker et al., 2013), while AG7 was identical to C5, which can be described as tryptophan-like and has been commonly associated with biological production in surface waters (Determann et al., 1994).

Two AG model components were also highly related to components previously reported in sea ice. AG1 was comparable

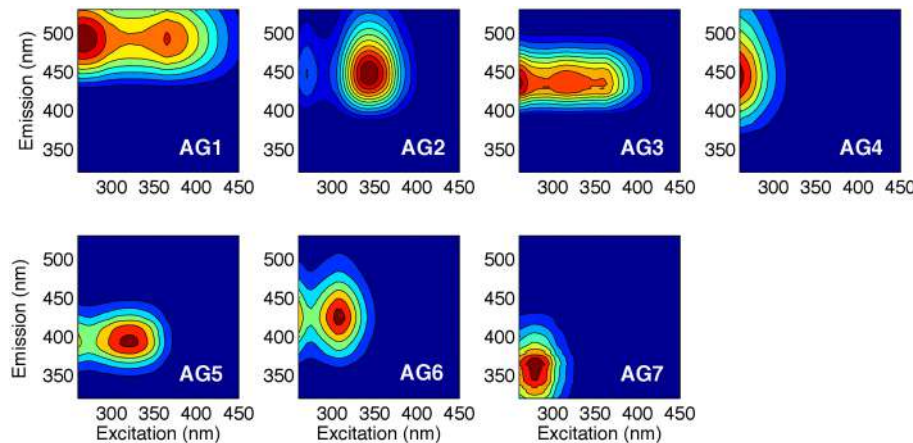


FIGURE 2 | Seven independent fluorescent components (AG1-7) identified using PARAFAC analysis of 645 excitation-emission matrices. Excitation and emission peak positions are reported alongside descriptions in **Table 3**.

TABLE 3 | Excitation and emission maxima (Ex_{max}/Em_{max}) of the seven components identified using parallel factor analysis of DOM fluorescence (Figure 2).

Component	Ex_{max} (nm)	Em_{max} (nm)	Comparable study ID* (component with TCC > 0.95)	Description
AG1	265	492	7(C3), 8(C2), 28(C2), 31(C4), 37(C3), 44(C2), 48(C2), 54(C2)	Humic-like fluorophore, terrigenous or autochthonous source, fulvic acid-like, present in all environments; Positively related to agriculture and bacterial production. Identified in many models and possibly formed as intermediate during photochemical degradation. Susceptible to microbial degradation.
AG2	270	448	29(C5), 31(C3), 69(C4)	Similar to classical "C peak". Terrigenous component identified across a range of environments.
AG3	315	434	8(C1)	Humic-like, emission spectrum identical to syringaldehyde (produced in breakdown of lignin) associated with waters containing high DOM loadings.
AG4	365	444	22(C3), 34(C1), 41(C2), 47(C2), 53(C5), 55(C3)	Similar to classical "A peak". Terrigenous humic-like substances, refractory in nature.
AG5	320	392	8(C4), 22(C2), 26(C6), 32(C4), 47(C3), 68(C2)	Similar to classical "M peak". Marine and terrigenous humic material source, possibly derived from microbial reprocessing.
AG6	305	424	9(C1), 28(C3), 35(C1), 44(C3), 48(C1), 54(C3), 64(C1)	Humic-like fluorophore, terrigenous; not correlated with land use or bacterial production.
AG7	280	364	8(C5), 9(C7), 33(C5), 34(C7), 35(C5), 39(C5), 64(C5)	Tryptophan-like associated with biological production in surface waters. Also a region known to be associated with phenolic fluorescence.

Description of previously identified components displaying similar optical properties (TCC > 0.95; see text for details). *ID number refers to assigned study number in OpenFluor (<http://www.openfluo.org>). ⁷(Murphy et al., 2006), ⁸(Murphy et al., 2014), ⁹(Murphy et al., 2008), ²²(Kothawala et al., 2012), ²⁶(Stedmon et al., 2011b), ²⁸(Stedmon et al., 2007), ²⁹(Stedmon and Markager, 2005), ³¹(Søndergaard et al., 2003), ³²(Jørgensen et al., 2011), ³³(Stedmon et al., 2003), ³⁴(Stedmon and Markager, 2005), ³⁵(Osburn and Stedmon, 2011), ³⁷(Walker et al., 2009), ³⁹(Yamashita et al., 2011), ⁴¹(Yamashita et al., 2010a), ⁴⁴(Yamashita et al., 2010b), ⁴⁷(Kowalcuk et al., 2009), ⁴⁸(Graeber et al., 2012), ⁵³(Kothawala et al., 2013), ⁵⁴(Osburn et al., 2012), ⁵⁵(Osburn et al., 2011), ⁶⁴(Walker et al., 2013), ⁶⁸(Tanaka et al., 2014), ⁶⁹(Lapierre and del Giorgio, 2014).

to the terrestrially-derived component C2 found within Baltic sea ice (Stedmon et al., 2007). AG1 was also identical to C3 in coastal Canadian Arctic waters, which proved to be highly positively correlated with Σ_8 (Walker et al., 2009). AG5 was identical to C6 in a study of Antarctic sea ice brines (Stedmon et al., 2011b), and is similar to the commonly described "M" peak across a wide range of environments (Coble, 1996, 2007; Fellman et al., 2010).

Component AG4 contributed the greatest ($23.4 \pm 0.6\%$) and AG7 the lowest percentage ($5.1 \pm 0.3\%$) toward total fluorescence across all rivers and seasons. In contrast to previous studies, no consistent pan-arctic seasonal or spatial patterns were apparent in the fluorescence loadings or percent contribution of any of the seven components (Walker et al., 2009). Individual patterns in

fluorescence were however observed across rivers and seasons. Component AG1 contributed a significantly higher proportion of total fluorescence during the summer months in the Kolyma ($20.5 \pm 0.1\%$) and Lena Rivers ($20.6 \pm 0.6\%$) relative to each of the other rivers (16.8 to 17.7%), yet comprised similar amounts during the rest of the year. Similarly, the proportion of AG3 was significantly higher in the Kolyma ($23.2 \pm 0.8\%$) and Lena ($19.1 \pm 1.4\%$) Rivers relative to the others (11.3 to 17.6%) during the summer months alone. Opposing patterns were observed in AG6, with significantly lower proportions in the Kolyma ($4.4 \pm 0.1\%$) and Lena Rivers ($5.3 \pm 0.6\%$) relative to the others, in particular the Yenisey ($9.7 \pm 1.2\%$) and Ob' Rivers ($8.4 \pm 1.8\%$). The Mackenzie River contained high proportions of AG7 during

the summer months ($6.7 \pm 1.1\%$) relative to all other rivers (3.9 to 5.2%).

DISCUSSION

Optical Measurements, DOC

Concentration and DOM Composition

CDOM absorption (a_{350}) correlated strongly with DOC concentration across all rivers during the standard Arctic-GRO sampling over 2009 and 2010 ($R^2 = 0.89; p < 0.001; n = 60$). This strong positive linear relationship persisted when DOC concentration and a_{350} values from the additional high-resolution measurements collected over the freshet period were included ($R^2 = 0.81; p < 0.001; n = 301$; Figure 3A). Despite this robust pan-arctic relationship however, when rivers were analyzed independently significant differences in the slopes and intercepts for the DOC to a_{350} relationships were observed (Table 4). This indicates that the relative amount of non-chromophoric DOM varies across Arctic rivers, and suggests that the proportion of DOC per unit CDOM within individual river basins should in future be separately determined (Table 4). Interestingly, we also find that the variability in river-specific slope and intercepts were well-explained by total annual river discharge, with increasing discharge resulting in higher DOC: a_{350} intercepts ($R^2 = 0.58; p < 0.05$, not shown) and shallower slopes ($R^2 = 0.72, p < 0.05$, not shown). The relationship between annual discharge and DOC: a_{350} intercepts improved significantly ($R^2 = 0.98; p < 0.01$) with the exclusion of the Mackenzie River. Thus, greater dilution of DOM and export of non-chromophoric organics occurs with increasing total discharge. The different relationship observed in the Mackenzie may be due to its relatively low DOM yield, high abundance of suspended sediments as well as high proportion of lakes relative to other watersheds (Stedmon et al., 2011a).

HPOA fraction was closely related to $S_{275-295}$ across rivers, with the relative proportion of HPOA decreasing with steepening slope ($R^2 = 0.65; p < 0.001, n = 58$), as previously reported across five of these rivers in 2004–2005 (Walker et al., 2013). This suggests that average DOM molecular weight and aromaticity decreases as the proportion of HPOA declines, in good agreement with a number of previous studies (Neff et al., 2006; Striegl et al., 2007; O'Donnell et al., 2012; Spencer et al., 2012). This was further supported by a positive linear relationship between average HPOA and SUVA₂₅₄ across rivers ($R^2 = 0.56, p < 0.01$, Supplemental Figure 2). The DOM composition of winter flow has been shown to contain lower proportions of the HPOA fraction as compared to HPI, with lower SUVA₂₅₄ values relative to summer and spring months in the Yukon River (O'Donnell et al., 2012). The aromaticity of the HPOA fraction (HPOA-SUVA₂₅₄), was negatively correlated with FI ($R^2 = 0.32, p < 0.001, n = 47$), confirming the role of terrigenous supply on delivering increased proportions of aromatic organics to the exported DOM pool.

No pan-arctic relationships were observed between any of the fluorescence component loadings and DOC concentration

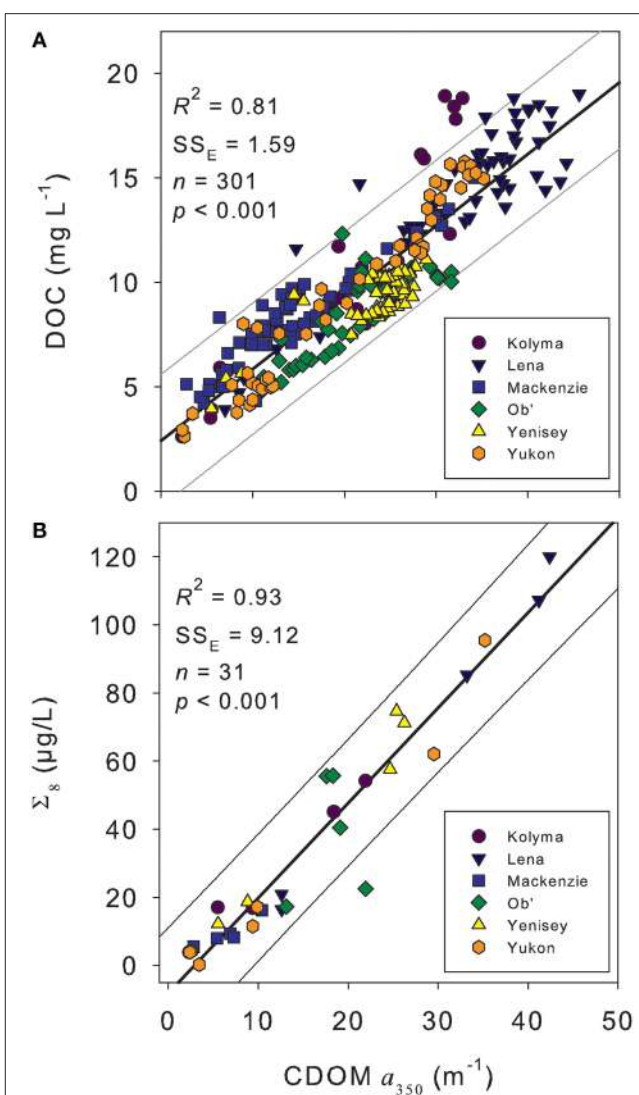


FIGURE 3 | (A) Dissolved organic carbon (DOC) concentration vs. the CDOM absorbance coefficient at 350 nm (a_{350}) from across the hydrograph of the six Arctic rivers. **(B)** Lignin phenol concentration (Σ_g) vs. a_{350} from across the hydrographs of the six Arctic rivers. Thick black line represents the linear regression of the data. Thin gray lines represent the extent of the prediction of fit (95% confidence limit). SS_E indicates the error of estimate providing an indication of variation around the fit.

or composition (Supplemental Tables 2 and 3). However, weak yet significant relationships were observed between the relative proportions of components AG3 and AG4 to total fluorescence, and DOC concentrations across all six rivers ($R^2 = 0.15$ and 0.16 respectively, $p < 0.01$). AG3 proportions generally decreased with increasing DOC concentrations, where AG4 proportions increased with greater DOC concentrations. These relationships were largely driven by particularly strong relationships across the Kolyma and Lena Rivers (AG3 $R^2 = 0.70$; AG4 $R^2 = 0.70, p < 0.001$). The relatively weak pan-arctic relationships we observe here contrasts with the findings of Walker et al. (2013), whom report strong correlations between DOC concentration and fluorescence loadings. These conflicting

TABLE 4 | Linear regression fits for relationships between dissolved organic carbon concentration (DOC) and absorbance coefficient (a_{350}) determined for each river.

River	n	R^2	slope	intercept	SE _E (%)	Discharge ^a (km ³ year ⁻¹)
Kolyma	23	0.84	0.478 ± 0.045	0.845 ± 1.022	2.0	111
Lena	57	0.83	0.333 ± 0.020	3.429 ± 0.666	1.5	581
Mackenzie	60	0.86	0.310 ± 0.017	3.871 ± 0.256	0.9	298
Ob'	54	0.74	0.295 ± 0.024	2.240 ± 0.531	1.0	427
Yenisey	58	0.66	0.231 ± 0.022	3.793 ± 0.528	0.8	636
Yukon	49	0.95	0.405 ± 0.014	1.346 ± 0.310	1.0	208
ALL	301	0.81	0.343 ± 0.009	2.414 ± 0.229	1.6	2261

n, represents number of measurements; R^2 , the coefficient of determination; and SE_E, the standard error of estimate. ^aAnnual average discharge from each river from Holmes et al. (2012).

findings may have been due to the additional normalization step we applied to scale each EEM to its total signal, thus ensuring the model focused entirely on compositional rather than concentration gradients. Alternately, the addition of a significant number of EEMs from upstream sources may have resulted in the validation of different components during PARAFAC decomposition. The latter seems unlikely however, as two of the seven components were spectrally identical ($TCC > 0.95$) to the PARAFAC model used by Walker et al. (2013), including component AG6 which was spectrally indistinguishable from a component (C1) identified as most closely tracing DOC and Σ_8 concentrations. Other potential causes include differences in the treatment of inner filter effects. We applied a commonly employed *post-hoc* method by Lakowicz (2006) to correct our EEMs for inner filter effects using parallel CDOM absorbance measurements, whereas samples in Walker et al. (2013) were diluted prior to measurement. Our method more closely reflects direct measurement of field samples and is similar to information that could be derived from *in-situ* instruments. Our findings suggest that loadings derived from fluorescence EEMs decomposed using PARAFAC may not always be useful when tracing DOC concentration.

Optical Measurements and Lignin Concentration and Composition

CDOM (a_{350}) measurements were highly correlated to Σ_8 across all six rivers basins ($R^2 = 0.92$; $p < 0.001$; $n = 31$; **Figure 3B**). This represents the first pan-arctic relationship to be reported between a_{350} and Σ_8 across all six major rivers. The observed linear relationship [$\Sigma_8 = -8.06 \pm 2.71 + (2.80 \pm 0.14 a_{350})$] was similar to, yet displayed a slightly higher slope, than reported in Spencer et al. (2008) for the Yukon River Basin only [$\Sigma_8 = -6.67 \pm 2.88 + (2.21 \pm 0.11 a_{350})$]. Previous studies have reported a much steeper linear relationship between a_{350} and Σ_8 , with the Mackenzie and Ob' Rivers grouping separately from the Kolyma, Lena, and Yenisey (Walker et al., 2013). The steeper slope of the previously reported relationship is caused by the substantially higher (often greater than double) lignin concentrations (Σ_8) reported in Amon et al. (2012) and used in Walker et al.

(2013) relative to those presented here. The differences in Σ_8 concentrations may be due to methodological differences, as suggested by Walker et al. (2013), and raises concern over future potential in comparing datasets. For example, comparison of data from Spencer et al. (2008) in Walker et al. (2013) suggested low relative lignin concentrations in DOM from the Yukon, whereas we identify a similar Σ_8 to a_{350} relationship across all six major Arctic rivers.

Carbon normalized lignin (Λ_8) yields decreased exponentially with steepening $S_{275-295}$ values across all rivers and seasons ($R^2 = 0.80$; $p < 0.01$, $n = 31$). Steepening $S_{275-295}$ values were associated with decreasing runoff rates, thus Λ_8 yields typically increased as DOM average molecular weight and aromaticity increased, and during spring and summer months in response to greater allochthonous DOM supply.

Lignin phenols have been shown to comprise a major component of the HPOA fraction (Templier et al., 2005; Spencer et al., 2008, 2010a). This was confirmed by a significant positive correlation between proportion HPOA and Λ_8 yields ($R^2 = 0.71$, $p < 0.001$, $n = 29$; not shown). Lignin phenol biomarkers thus appear capable of providing information on the biogeochemical cycling of the entire hydrophobic DOM pool, which comprises up to two-thirds of aquatic DOM.

Lignin phenol C/V ratios increased with steepening $S_{275-295}$ values ($R^2 = 0.54$; $p < 0.001$, $n = 31$) and declining total SUVA₂₅₄ values ($R^2 = 0.48$; $p < 0.001$, $n = 31$). The overall decline in C/V ratios with increasing freshwater runoff appears to represent increased contributions of lignin from litter and surface soil layers alongside greater proportions of aromatic and higher molecular weight DOM export (Hedges and Mann, 1979). These findings however appear counterintuitive relative to what we currently understand about hydrologic flowpaths and sources of DOM to aquatic systems. Non-woody litter tissues associated with surficial, predominantly overland flow paths are expected to impart higher C/V ratios and lower degradative alteration than observed in DOM exported during deeper baseflow conditions. Physical processes, such as leaching and sorption, can however also influence lignin phenol ratios (Hernes et al., 2007, 2008) and may therefore be responsible for the observed trends. S/V and acid to aldehyde ratios did not correlate closely with spectral slope, SUVA₂₅₄ or SR values. The overall trends in lignin phenol composition we report are similar to those previously shown across Arctic rivers (Spencer et al., 2008, 2009; Amon et al., 2012), and demonstrate a shift from predominantly modern surface-derived and lignin-rich DOM during the spring freshet to older, less lignin-rich DOM under baseflow winter conditions.

No pan-arctic relationships were observed between fluorescent PARAFAC component loadings and lignin phenol concentration or composition measures. A weak yet significant relationship was however found between the %AG4 and Σ_8 concentration ($R^2 = 0.18$; $p < 0.02$) but again was significantly stronger across the Kolyma and Lena Rivers in particular ($R^2 = 0.79$; $p < 0.001$). FI values positively correlated with increasing C/V ratios ($R^2 = 0.48$, $p < 0.001$, $n = 30$) confirming losses in the proportion of woody tissues with increased autochthonous or less aromatic DOM supply.

Linking Optical Properties to Arctic River DOM Composition

Underlying patterns and relationships between optical DOM parameters, DOC and lignin were further explored using principle component analysis (PCA), which can identify the structure of data that best explains the variance within the dataset. The optical properties of DOM varied with season across all rivers, as demonstrated by PCA plots containing PARAFAC fluorescence components (percent contribution) and spectral slope information. The addition of FI and S_R values added little additional information to the PCA analyses. Furthermore, SUVA₂₅₄ followed identical patterns to each of the spectral slope parameters and its inclusion led to similar PCA plots. These indices were therefore omitted from the final PCA model for clarity. Three principle components (PCs; eigenvalue > 1) were identified that together explained 80% of the total variance in the optical data (PCopt 1–3). PC1opt was related to increasing fluorescence contributions from AG3, AG1 and AG5, but decreasing contributions from AG6, AG4 and AG2 (Figure 4). Components AG1, 3 and 5 represent DOM fluorescence signatures that have all previously

been reported to be susceptible to microbial processing, or to be a byproduct of vascular material degradation (Table 3 and references herein). These fluorescence signatures may therefore represent indicators of “degraded” or processed humic-like components. In contrast, components AG 2, 4, and 6 appear to represent more unreactive and stable components, previously being described as refractory in nature and shown not to co-vary with bacterial production (Table 3). PC1opt may therefore reflect potential reactivity or be an indicator of prior DOM processing. PC2opt appeared to be related to the shifting molecular weight of DOM, as indicated by strong relationships with changes in all spectral slopes (and SUVA₂₅₄, not shown), whereas PC3opt was positively related to increased protein-like or phenolic DOM (AG7) and decreasing contributions from humic-like DOM (AG2 and AG1). PCA models ran with only PARAFAC components contained two principle components, each indistinguishable from PC1opt and PC3opt, demonstrating that information on DOM potential reactivity and the relative contribution of protein-like versus humic-like could be obtained from fluorescence measurements alone.

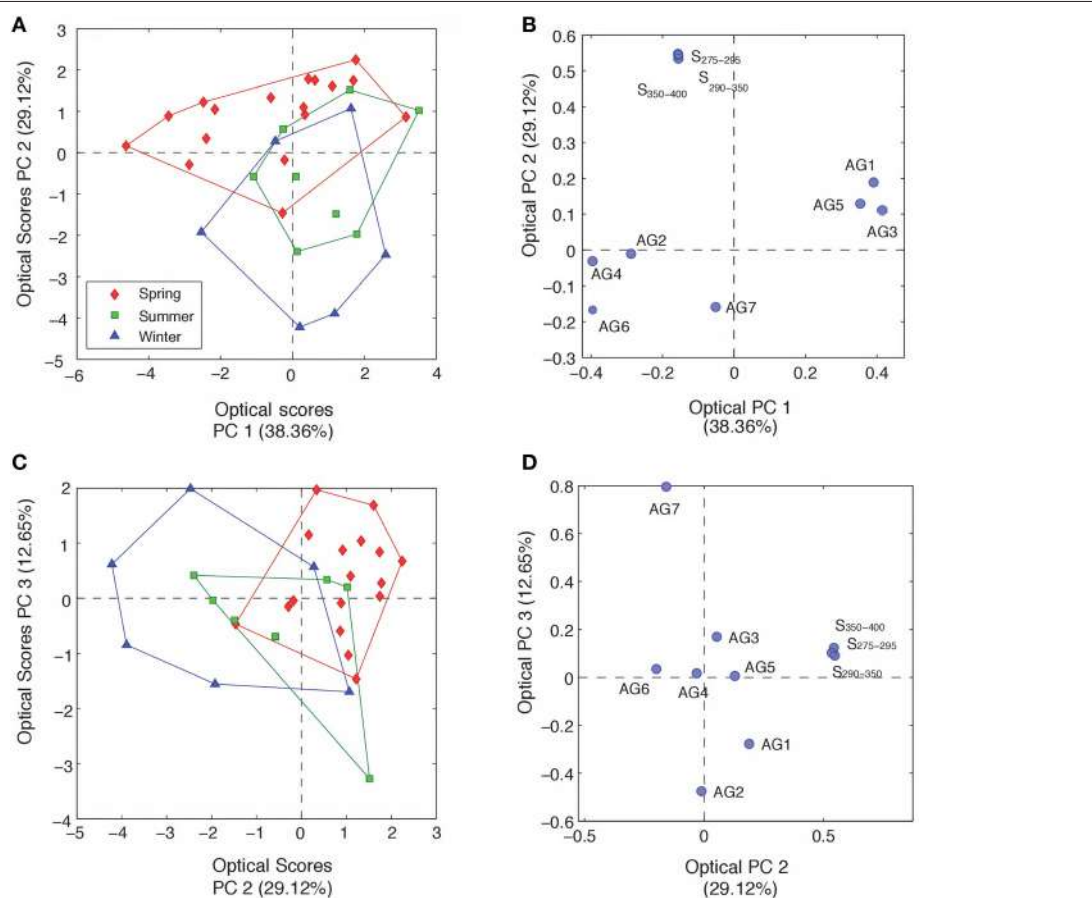


FIGURE 4 | (A) Principle component scores across PC1opt and PC2opt for all optical samples labeled by season. **(B)** PC scores of each optical parameter across PC1opt and PC2opt. **(C)** Principle component scores across PC2opt and PC3opt for all optical samples labeled by season. **(D)** PC scores of each optical parameter across PC2opt and PC3opt. FI and SUVA₂₅₄ values were not included in the final optical PCA, see text for details.

Seasonal changes in DOM composition across all six rivers were most clearly separated along the PC2opt axis, with spring waters containing higher molecular weight material with shallower spectral slopes than summer and winter month waters. Positive scores on PC3opt during spring and winter months, relative to summer, suggest greater contributions of protein-like or phenolic material (as inferred by the proportion of component AG7), potentially representing reductions in allochthonous supply or increased export of fresh organics from surface layers, respectively. No clear separation among the six different rivers was apparent with optical properties alone across any of the PC axes.

To examine if the observed trends in DOM optical properties were related to geochemical changes in organic matter we conducted a separate PCA incorporating all lignin phenol and DOC fractionation variables. We subsequently compared the identified PCs with those extracted from optical measurements alone. Two PCs (PCmol 1–2) were identified, in combination explaining 67% of the total variance

in geochemical composition (Figure 5). PC1mol positively related to increasing HPOA, Σ_8 and Λ_8 contributions and negatively with C/V ratio and proportions of the hydrophobic neutral and hydrophilic fractions. The axis therefore primarily separates seasonal variability observed in DOC, with spring months delivering greater proportions of HPOA with high concentrations of Σ_8 and Λ_8 values. PC2mol most strongly correlated to (Ad/Al) ratios suggesting it represented changing proportions of DOM degradation state. S/V ratio was also positively related with PC2mol, indicating that shifts in the relative proportions of sources waters may also be represented by this axis or similar processes (e.g., leaching and sorption) may be driving the observed S/V and (Ad/Al) ratios.

Comparing separate PCs from both optical and geochemical PCAs across all sites and sampling dates, only a single significant positive correlation was observed between PC2opt extracted from optical characteristics and PC1mol from DOC and lignin composition ($R^2 = 0.65$, $p < 0.001$, $n = 30$; Figure 5).

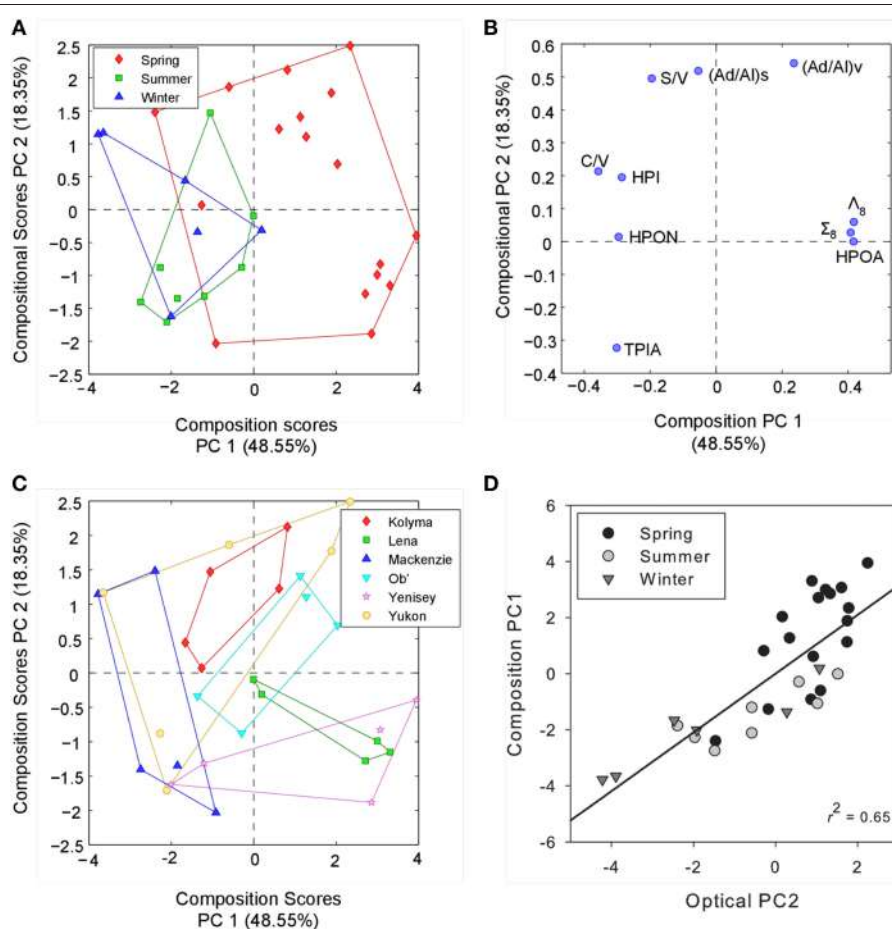


FIGURE 5 | (A) Principle component scores across PC1mol and PC2mol for all compositional measurements labeled by season. **(B)** PC scores of each compositional parameter across PC1mol and PC2mol. **(C)** Principle component scores across PC1mol and PC2mol for all compositional measurements labeled by river. **(D)** Relationship between PC2opt derived from optical data alone and PC1mol explaining compositional measurements. Black line represents the linear regression ($R^2 = 0.65$, $p < 0.001$).

Thus, seasonal variability in DOC composition was explained by relatively simple CDOM slope (and SUVA₂₅₄) metrics. Separating over seasons, PC1opt correlated significantly with PC2mol during the summer ($R^2 = 0.85, p < 0.05, n = 8$) and winter months ($R^2 = 0.65, p = 0.06, n = 6$), but not over spring periods across all six rivers. This further suggests that shifts in the relative proportions of PARAFAC components reflect shifts in the relative degradation signature of DOC inferred from acid:aldehyde ratios during certain periods of the year. Information pertaining to the source (S/V ratios) of DOM may therefore also be contained in the relative ratio of more or less reactive or degraded PARAFAC components. Interestingly, (Ad/Al)_v ratios have also been shown to correlate with the average ¹⁴C age of DOC within these Arctic Rivers (Amon et al., 2012). Fluorescence measurements may therefore provide information pertaining to both the age and degradation history of DOM across Arctic systems. Broad patterns in the temporal variability of DOM composition over pan-arctic scales therefore appear best captured using simple CDOM spectral slope and SUVA₂₅₄ measurements. Information on DOM processing, source and age may instead be contained within CDOM

fluorescence spectra and the relative contributions of PARAFAC components.

Modeling Terrestrial Biomarkers with Optical Measurements

We ran a series of multiple linear regression models with the aim of predicting Λ_8 , C/V, S/V, (Ad/Al)s, and (Ad/Al)_v across all sampling dates and rivers. Incorporating absorbance (a_{350} , slope ratios, SUVA₂₅₄), and fluorescence optical measurements (FI, % PARAFAC component contributions) as potential parameters, Λ_8 ($R^2 = 0.76$; **Figure 6A**), C/V ($R^2 = 0.70$; **Figure 6B**) and S/V values ($R^2 = 0.68$, **Figure 6C**) could be successfully predicted by model fits (all $p < 0.001; n = 31$). Modeled values for (Ad/Al)_v were also strongly correlated with observed values ($p < 0.001$), but predictive capability was low ($R^2 = 0.49$, not shown). Model fits failed to accurately predict the variability in the (Ad/Al)s ratios ($p > 0.05$).

The optical parameters providing the greatest predictive power varied between each lignin parameter. Models predicting Λ_8 only incorporated S_{275–295} and a_{350} values [$\Lambda_8 = 1.136 \pm$

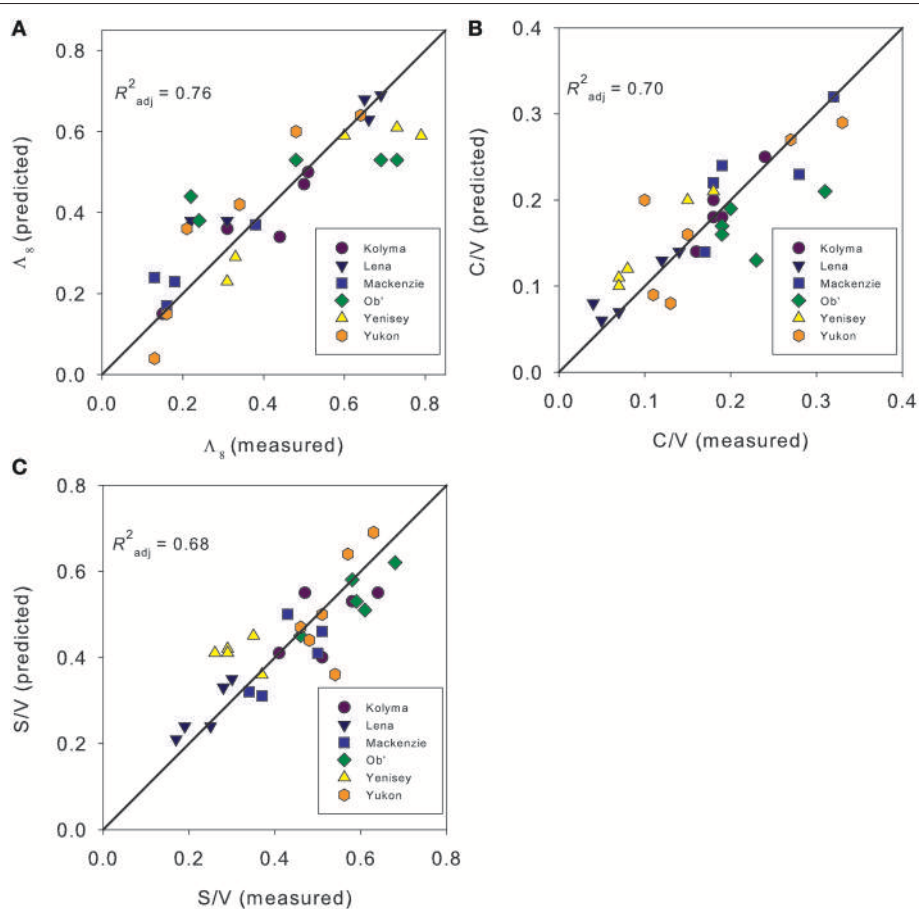


FIGURE 6 | Model predicted values against observed measurements of (A). Carbon normalized sum of the lignin phenols [$\Lambda_8; \text{mg (100 mg OC)}^{-1}$], **(B)** Cinnamyl to vanillyl phenol ratios (C/V), and **(C)** Syringyl to vanillyl phenol ratios (S/V).

$0.250 + (55.742 \pm 14.152 * S_{275-295}) + (0.006 \pm 0.003 * a_{350})$. Modeling C/V values also used $S_{275-295}$ and a_{350} values (alone explaining 58% of the variance), but improved with inclusion of %AG7 and $S_{290-350}$ values [$C/V = -0.153 \pm 0.127 - (57.265 \pm 17.921 * S_{275-295}) + (0.040 \pm 0.015 * \%AG7) + (45.225 \pm 18.604 * S_{290-350}) - (0.002 * a_{350})$]. Models explaining S/V values incorporated $S_{290-350}$, a_{350} , %AG7 and FI ($S/V = -2.704 \pm 0.827 + (64.131 \pm 14.843 * S_{290-350}) + (2.896 \pm 0.695 * FI) - (0.009 \pm 0.002 * a_{350}) + (0.074 \pm 0.027 * \%AG7)$). S/V could not be explained with absorbance measurements alone. The ability to predict lignin composition as well as concentration using fluorescence measurements has previously been reported using partial least squares model of samples collected over a 2 year period on the Sacramento River/San Joaquin River Delta, California (Hernes et al., 2009). The authors demonstrated that the most significant predictive capability for lignin was within the commonly referred to protein-like fluorescence region (similar to our component AG7). Fluorescence of propylphenol monomers, that structurally comprise lignin, can generate fluorescence signatures in a similar region to amino acids and in the region known as “protein-like,” thus our results may indicate information obtained from changes in dissolved phenolics rather than amino acid or proteins (Hernes et al., 2009). Therefore, it seems that rapid, inexpensive optical measurements may be capable of acting as a proxy for dissolved lignin compositional parameters as well as concentration across pan-arctic scales and catchments. The combination of absorbance and fluorescence metrics can also add predictive power when attempting to predict shifts in the composition of terrigenous DOC.

Improving Terrigenous OC Export Estimates

The absorbance coefficient at 350 nm (a_{350}) has previously been shown to be a sensitive and inexpensive proxy for lignin phenol concentration across a range of freshwater environments within Arctic river basins (Spencer et al., 2008, 2009; Stedmon et al., 2011a). Furthermore, increased sampling frequency of Arctic rivers has led to significantly higher and better constrained DOC export estimates, particularly after the inclusion of samples from across the spring freshet period (e.g., Köhler et al., 2003; Striegl et al., 2005; Holmes et al., 2012). Here, we investigate if the combination of a lignin proxy with high-resolution monitoring of a_{350} over Arctic river hydrographs may be used to develop improved estimates of pan-arctic terrigenous DOC export, hereby refining land-to-ocean carbon flux estimates.

CDOM-derived lignin phenol concentrations (lignin_{350}) were calculated using the linear regression of Σ_8 and a_{350} (Figure 3B). lignin_{350} values were derived from a_{350} measurements taken from waters collected over the main Arctic-GRO sampling campaign and additional high-resolution samples taken over the freshet hydrographs. Inclusion of near-daily absorbance measurements collected over the peak discharge period alongside measurements spanning the entire year was crucial in adequately constraining fluxes during the spring freshet, when the majority of annual lignin export is expected (Spencer et al., 2008; Amon et al., 2012). lignin_{350} concentrations calculated for samples with

TABLE 5 | Total annual mean fluxes of CDOM-derived lignin (lignin_{350}) and DOC calculated using LOADEST.

River/region	Watershed Area (10^6 km^2)	Discharge ($\text{km}^3 \text{ year}^{-1}$)	Lignin $_{350}$ (Gg year^{-1})		
			2009	2010	1999–2010
Kolyma	0.65	132	3.6	3.2	5.0 ± 1.2
Lena	2.4	591	50.5	36.2	43.1 ± 8.6
Mackenzie	1.75	319	5.2	3.5	4.0 ± 1.0
Ob'	2.95	421	15.5	16.2	18.6 ± 4.8
Yenisey	2.56	671	20.9	21.9	22.3 ± 2.3
Yukon	0.83	207	4.6	6.3	$5.4 \pm 1.7^\#$
Arctic-GRO	11.14	2342	100.3	87.3	98.4
Pan-arctic1 (PA1)	16.8	3700	158.5	137.9	155.5
Pan-arctic2 (PA2)	20.5	4410	188.9	164.4	185.3

Arctic-GRO refers to the sum of all 6 rivers studied, and pan-arctic1 and 2 are the regions delineated in Figure 1. Mean annual discharge is calculated for the 1999–2010 period.
#Averaged over 2001–2010.

concurrent Σ_8 measurements were highly correlated across all Arctic rivers ($R^2 = 0.92$, $p < 0.01$, $n = 31$, Standard error of estimate, $\text{SE}_E = 8.8\%$) demonstrating the robust nature of this approach.

Daily model loads (mass d^{-1}) of Σ_8 in each river were calculated using a hydrologic load estimation model (LOADEST) integrating the lignin_{350} concentrations and 12 years of daily discharge data ranging from 1999 to 2010 (see Materials and Methods). Estimated lignin loads varied from 4.0 Gg year^{-1} in the Mackenzie to $43.1 \text{ Gg year}^{-1}$ in the Lena River (Table 5). The Lena, Yenisey and Ob' Rivers export $>85\%$ of the total annual lignin discharge from the six largest Arctic rivers, a proportion that is very similar to that found by Amon et al. (2012). Flux estimates using lignin phenol concentrations measured using identical methods and approaches compared well. Our mean annual Yukon River lignin flux derived for 2001–2009 ($5.4 \pm 1.7 \text{ Gg year}^{-1}$; Table 5) is similar to previous estimates of $5.3 \pm 1.3 \text{ Gg year}^{-1}$ independently derived from measurements from 2004 to 2005 (Spencer et al., 2009), confirming the modeling approach is reproducible and robust. Our estimated lignin loads from all six major Arctic rivers ($98.4 \text{ Gg year}^{-1}$) were however almost half of the $192.0 \text{ Gg year}^{-1}$ reported by Amon et al. (2012) for the same rivers from 2003 to 2007. These differences were primarily due to the significantly higher lignin concentrations (Σ_8) reported by Amon et al. (2012) versus those of Spencer et al. (2009) and reported here, demonstrating the necessity for more standardization and intercomparison across lignin phenol measurements to ensure comparable datasets across studies.

Freshwater fluxes were scaled to the unsampled proportion of the Arctic using two published estimates of total Arctic Ocean watershed area. The smallest estimate (PA1; black line Figure 1) spans an area of $16.8 \times 10^6 \text{ km}^2$, where the largest (PA2; red line; Figure 1) encompassing Hudson Bay drainage covers an area of $20.5 \times 10^6 \text{ km}^2$ (Hernes et al., 2014). Pan-arctic lignin fluxes were estimated to span between $155.5 \text{ Gg year}^{-1}$ (PA1) and $185.3 \text{ Gg year}^{-1}$ (PA2; Table 5) across these two geographic regions.

Dissolved lignin concentrations have previously been applied as a tracer of terrigenous DOM to the Arctic Ocean (Opsahl et al., 1999; Benner et al., 2005; Fichot et al., 2013) and used to estimate turnover rates of terrigenous DOC in the ocean (Opsahl et al., 1999; Hernes and Benner, 2006). Applying our pan-arctic flux (derived using our lignin₃₅₀ proxy) and assuming Arctic Ocean lignin concentrations ranging between 84 and 320 ng L⁻¹ (Opsahl et al., 1999), we calculate the residence time of terrigenous DOC in polar surface waters to be in the order of 7 months to 2.5 years. This compares well, yet slightly shorter than residence time estimates of <1 to 4 years calculated with comparable freshwater fluxes but scaled from the Yukon River alone (Spencer et al., 2009). Assuming the export of lignin phenol concentrations twice as high, similar to those reported by Amon et al. (2012), would result in even faster residence time estimates of <4 months to 1 year. Overall, the short timeframes identified by these studies indicate either rapid losses of terrigenous DOC, via microbial, photochemical, or flocculation processes, or faster physical transport from Arctic Ocean waters to the North Atlantic than previously thought.

CONCLUSIONS

Employing optical techniques can increase the temporal and spatial coverage of DOM measurements across Arctic river systems, shedding light on future changes in the composition and concentration of exported DOM, and help to more accurately estimate the amount and timing of terrigenous DOC flux. Here, river-specific relationships between a_{350} and DOC concentrations are presented and attributed to the export of varying proportions of non-chromophoric DOM from Arctic catchments. We show that simple absorbance proxies (a_{350} , $S_{275-295}$), which can be measured with *in-situ* techniques, are capable of tracing dissolved lignin concentrations (Σ_8) and seasonal changes in geochemical DOM composition (e.g., Δ_8 and percent HPOA) occurring across the six major Arctic rivers. Furthermore, we demonstrate that lignin phenol biomarkers appear capable of providing information on the biogeochemical cycling of the hydrophobic DOC fraction, thus knowledge on a major proportion of the aquatic DOM pool. More complex fluorescence DOM measurements followed by PARAFAC decomposition provided few direct pan-arctic proxies of DOM concentration or composition. However, the proportion of fluorescence signatures previously attributed to microbial processing or suggested to be by-products of vascular material degradation co-varied with lignin monomer ratios over much of the year, suggesting these optical measurements may be capable of offering insights into changing DOM degradation

state and source. Combining fluorescence and absorbance indices further strengthened our ability to predict DOM composition, in particular inclusion of fluorescence index and protein-like contributions with absorbance coefficient and spectral slope measurements enabled predictive models of lignin ratios; suggesting potential to distinguish DOM source characteristics. Finally, we combine our pan-arctic relationship between a_{350} and Σ_8 with high resolution monitoring of a_{350} to develop more accurately constrained residence times for terrigenous DOC in the Arctic Ocean of between 7 months to 2½ years. Optical measurements can provide key insights into the flux and biogeochemical cycling of terrigenous DOC in the Arctic which will prove critical for understanding how carbon budgets and fluxes alter under future climate change scenarios.

AUTHOR CONTRIBUTIONS

All authors contributed to the design of the study. PH, KB, and RD analyzed samples for XAD fractionation and lignin phenol analyses. PM, RS, and ST conducted modeling studies. All authors contributed to the interpretation of data and writing of the manuscript.

ACKNOWLEDGMENTS

This work was supported by grants from the National Science Foundation for the Global Rivers Project (0851101), the PARTNERS Project (0229302), the Arctic Great Rivers Observatory I & II (0732522 and 1107774), Detecting the Signature of Permafrost Thaw in Arctic Rivers (1203885 and 1500169) and the US Geological Survey's National Research Program. This work was aided by an NSF equipment grant to upgrade the analytical facilities at the North-East Science Station (0938254). We thank Alexander Shiklomanov for providing additional river discharge data, and the field staff of the USGS Alaska Science Center for their sample collection efforts. Special thanks to Ekaterina Bulygina and Lydia Russell-Roy for help running laboratory analyses. Also thanks to Greg Fiske for production of Figure 1. Any use of trade, firm, or product names is for descriptive purposes only and does not imply endorsement by the U.S. Government.

SUPPLEMENTARY MATERIAL

The Supplementary Material for this article can be found online at: <http://journal.frontiersin.org/article/10.3389/feart.2016.00025>

REFERENCES

- Aagaard, K., and Carmack, E. C. (1989). The role of sea ice and other fresh water in the Arctic circulation. *J. Geophys. Res. Atmosph.* 94, 14485–14498. doi: 10.1029/JC094iC10p14485
- Aiken, G. R., McKnight, D. M., Thorn, K. A., and Thurman, E. M. (1992). Isolation of hydrophilic organic acids from water using nonionic macroporous resins. *Org. Geochem.* 18, 567–573. doi: 10.1016/0146-6380(92)90119-I

- Amon, R. M. W., Rinehart, A. J., Duan, S., Loucheurn, P., Prokushkin, A., Guggenberger, G., et al. (2012). Dissolved organic matter sources in large Arctic rivers. *Geochim. Cosmochim. Acta* 94, 217–237. doi: 10.1016/j.gca.2012.07.015
- Benner, R., Loucheurn, P., and Amon, R. M. W. (2005). Terrigenous dissolved organic matter in the Arctic Ocean and its transport to surface and deep waters of the North Atlantic. *Global Biogeochem. Cycles* 19, GB2025. doi: 10.1029/2004GB002398

- Blough, N. V., and Del Vecchio, R. (2002). "Chromophoric DOM in the coastal environment," in *Biogeochemistry of Marine Dissolved Organic Matter*, eds D. A. Hansell and C. A. Carlson (San Diego, CA: Academic Press), 509–546.
- Blough, N. V., and Green, S. A. (1995). "Spectroscopic characterization and remote sensing of non-living organic matter," in *The Role of Non-Living Organic Matter on the Earth's Carbon Cycle*, eds R. G. Zepp and C. Sonntag (Chichester, UK: Wiley), 23–45.
- Booth, G. P., Raymond, P. A., and Oh, N. H. (2007). *LoadRunner. Software and Website*. New Haven, CT: Yale University.
- Coble, P. G. (1996). Characterization of marine and terrestrial DOM in seawater using excitation-emission matrix spectroscopy. *Mar. Chem.* 51, 325–346. doi: 10.1016/0304-4203(95)00062-3
- Coble, P. G. (2007). Marine optical biogeochemistry: the chemistry of ocean color. *Chem. Rev.* 107, 402–418. doi: 10.1021/cr050350
- Cory, R. M., Miller, M. P., and McKnight, D. M. (2010). Effect of instrument-specific response on the analysis of fulvic acid fluorescence spectra. *Limnol. Oceanogr. Methods* 8, 67–78. doi: 10.4319/lom.2010.8.67
- Déry, S. J., Stahl, K., Moore, R. D., Whitfield, P. H., Menounos, B., and Burford, J. E. (2009). Detection of runoff timing changes in pluvial, nival, and glacial rivers of western Canada. *Water Resour. Res.* 45, W04426. doi: 10.1029/2008WR006975
- Determann, S., Reuter, R., Wagner, P., and Willkomm, R. (1994). Fluorescent matter in the eastern Atlantic Ocean. Part 1: method of measurement and near-surface distribution. *Deep Sea Res. Part I Oceanogr. Res. Papers* 41, 659–675.
- Fellman, J. B., Hood, E., and Spencer, R. G. M. (2010). Fluorescence spectroscopy opens new windows into dissolved organic matter dynamics in freshwater ecosystems: a review. *Limnol. Oceanogr.* 55, 2452–2462. doi: 10.4319/lo.2010.55.6.2452
- Fichot, C. G., Kaiser, K., Hooker, S. B., Amon, R. M. W., Babin, M., Bélanger, S., et al. (2013). Pan-Arctic distributions of continental runoff in the Arctic Ocean. *Sci. Rep.* 3:1053. doi: 10.1038/srep01053
- Graeber, D., Gelbrecht, J., Pusch, M. T., Anlanger, C., and von Schiller, D. (2012). Agriculture has changed the amount and composition of dissolved organic matter in Central European headwater streams. *Sci. Total Environ.* 438, 435–446. doi: 10.1016/j.scitotenv.2012.08.087
- Harshman, R. A., and Lundy, M. E. (1994). PARAFAC: parallel factor analysis. *Comput. Stat. Data Anal.* 18, 39–72. doi: 10.1016/0167-9473(94)90132-5
- Hedges, J. I., Clark, W. A., and Cowie, G. L. (1988). Organic matter sources to the water column and surficial sediments of a marine bay. *Limnol. Oceanogr.* 33, 1116–1136. doi: 10.4319/lo.1988.33.5.1116
- Hedges, J. I., and Ertel, J. R. (1982). Characterization of lignin by gas capillary chromatography of cupric oxide oxidation products. *Anal. Chem.* 54, 174–178. doi: 10.1021/ac00239a007
- Hedges, J. I., and Mann, D. C. (1979). The characterization of plant tissues by their lignin oxidation products. *Geochim. Cosmochim. Acta* 43, 1803–1807.
- Helms, J. R., Stubbins, A., and Ritchie, J. D. (2008). Absorption spectral slopes and slope ratios as indicators of molecular weight, source, and photobleaching of chromophoric dissolved organic matter. *Limnol. Oceanogr. Methods* 53, 955–969. doi: 10.4319/lo.2008.53.3.0955
- Hernes, P. J., and Benner, R. (2003). Photochemical and microbial degradation of dissolved lignin phenols: implications for the fate of terrigenous dissolved organic matter in marine environments. *J. Geophys. Res.* 108, 3291. doi: 10.1029/2002JC001421
- Hernes, P. J., and Benner, R. (2006). Terrigenous organic matter sources and reactivity in the North Atlantic Ocean and a comparison to the Arctic and Pacific oceans. *Mar. Chem.* 100, 66–79. doi: 10.1016/j.marchem.2005.11.003
- Hernes, P. J., Bergamaschi, B. A., Eckard, R. S., and Spencer, R. G. M. (2009). Fluorescence-based proxies for lignin in freshwater dissolved organic matter. *J. Geophys. Res.* 114, G00F03–G00F10. doi: 10.1029/2009JG000938
- Hernes, P. J., Holmes, R. M., Raymond, P. A., Spencer, R. G. M., and Tank, S. E. (2014). "Fluxes, processing, and fate of riverine organic and inorganic carbon in the Arctic Ocean," in *Biogeochemical Dynamics at Major River-Coastal Interfaces: Linkages with Global Change*, eds T. S. Bianchi, M. A. Allison, and W.-J. Cai (Cambridge, UK: Cambridge University Press), 530–553.
- Hernes, P. J., Robinson, A. C., and Aufdenkampe, A. K. (2007). Fractionation of lignin during leaching and sorption and implications for organic matter "freshness." *Geophys. Res. Lett.* 34, L17401–L17406. doi: 10.1029/2007GL031017
- Hernes, P. J., Spencer, R. G. M., Dyda, R. Y., Pellerin, B. A., Bachand, P. A. M., and Bergamaschi, B. A. (2008). The role of hydrologic regimes on dissolved organic carbon composition in an agricultural watershed. *Geochim. Cosmochim. Acta* 72, 5266–5277. doi: 10.1016/j.gca.2008.07.031
- Holmes, R. M., McClelland, J. W., Peterson, B. J., Tank, S. E., Bulygina, E., Eglington, T. I., et al. (2012). Seasonal and annual fluxes of nutrients and organic matter from Large Rivers to the Arctic Ocean and Surrounding Seas. *Estuar. Coasts* 35, 369–382. doi: 10.1007/s12237-011-9386-6
- Holmes, R. M., McClelland, J. W., Raymond, P. A., Frazer, B. B., Peterson, B. J., and Stieglitz, M. (2008). Lability of DOC transported by Alaskan rivers to the Arctic Ocean. *Geophys. Res. Lett.* 35, L03402–L03405. doi: 10.1029/2007GL032837
- Hu, C., Muller-Karger, F. E., and Zepp, R. G. (2002). Absorbance, absorption coefficient, and apparent quantum yield: a comment on common ambiguity in the use of these optical concepts. *Limnol. Oceanogr.* 47, 1261–1267. doi: 10.4319/lo.2002.47.4.1261
- Jørgensen, L., Stedmon, C. A., Kragh, T., Markager, S., Middelboe, M., and Søndergaard, M. (2011). Global trends in the fluorescence characteristics and distribution of marine dissolved organic matter. *Mar. Chem.* 126, 139–148. doi: 10.1016/j.marchem.2011.05.002
- Köhler, H., Meon, B., Gordeev, V. V., Spitz, A., and Amon, R. M. W. (2003). "Dissolved organic matter (DOM) in the estuaries of Ob and Yenisei and the adjacent Kara Sea, Russia," in *Siberian River Run-Off in the Kara Sea*, eds R. Stein, K. Fahl, D. K. Fütterer, E. M. Galimov, and O. V. Stepanets (Amsterdam: Elsevier Science B.V.), 281–308.
- Kothawala, D. N., von Wachenfeldt, E., Koehler, B., and Tranvik, L. J. (2012). Selective loss and preservation of lake water dissolved organic matter fluorescence during long-term dark incubations. *Sci. Total Environ.* 433, 238–246. doi: 10.1016/j.scitotenv.2012.06.029
- Kothawala, D. N., Stedmon, C. A., Müller, R. A., Weyhenmeyer, G. A., Köhler, S. J., and Tranvik, L. J. (2013). Controls of dissolved organic matter quality: evidence from a large-scale boreal lake survey. *Global Change Biol.* 20, 1101–1114. doi: 10.1111/gcb.12488
- Kowalcuk, P., Durako, M. J., Young, H., Kahn, A. E., Cooper, W. J., and Gonsior, M. (2009). Characterization of dissolved organic matter fluorescence in the South Atlantic Bight with use of PARAFAC model: Interannual variability. *Mar. Chem.* 113, 182–196. doi: 10.1016/j.marchem.2009.01.015
- Lakowicz, J. R. (2006). *Principles of Fluorescence Spectroscopy*, 3rd Edn. Kolkata: Springer. doi: 10.1007/978-0-387-46312-4
- Lapierre, J.-F., and del Giorgio, P. A. (2014). Partial coupling and differential regulation of biologically and photochemically labile dissolved organic carbon across boreal aquatic networks. *Biogeosciences* 11, 5969–5985. doi: 10.5194/bg-11-5969-2014
- Lawaetz, A. J., and Stedmon, C. A. (2009). Fluorescence intensity calibration using the Raman scatter peak of water. *Appl. Spectrosc.* 63, 936–940. doi: 10.1366/000370209788964548
- Lobbes, J. M., Fitznar, H. P., and Kattner, G. (2000). Biogeochemical characteristics of dissolved and particulate organic matter in Russian rivers entering the Arctic Ocean. *Geochim. Cosmochim. Acta* 64, 2973–2983. doi: 10.1016/S0016-7037(00)00409-9
- Mann, P. J., Davydova, A., Zimov, N., Spencer, R. G. M., Davydov, S., Bulygina, E., et al. (2012). Controls on the composition and lability of dissolved organic matter in Siberia's Kolyma River basin. *J. Geophys. Res.* 117, G01028. doi: 10.1029/2011jg001798
- Mann, P. J., Eglington, T. I., McIntyre, C. P., Zimov, N., Davydova, A., Vonk, J. E., et al. (2015). Utilization of ancient permafrost carbon in headwaters of Arctic fluvial networks. *Nat. Commun.* 6, 7856. doi: 10.1038/ncomms8856
- Mann, P. J., Spencer, R. G. M., Dinga, B. J., Poulsen, J. R., Hernes, P. J., Fiske, G., et al. (2014). The biogeochemistry of carbon across a gradient of streams and rivers within the Congo Basin. *J. Geophys. Res. Biogeosci.* 119, 687–702. doi: 10.1002/(ISSN)2169-8961
- Mathis, J. T., Hansell, D. A., and Bates, N. R. (2005). Strong hydrographic controls on spatial and seasonal variability of dissolved organic carbon in the Chukchi Sea. *Deep Sea Res. Part II Topic Stud. Oceanogr.* 52, 3245–3258. doi: 10.1016/j.dsr2.2005.10.002
- McClelland, J. W., Déry, S. J., Peterson, B. J., Holmes, R. M., and Wood, E. F. (2006). A pan-arctic evaluation of changes in river discharge during the

- latter half of the 20th century. *Geophys. Res. Lett.* 33, L06715–L06714. doi: 10.1029/2006GL025753
- McClelland, J. W., Holmes, R. M., Dunton, K. H., and Macdonald, R. W. (2011). The Arctic Ocean Estuary. *Estuar. Coasts* 35, 353–368. doi: 10.1007/s12237-010-9357-3
- McClelland, J. W., Holmes, R. M., Peterson, B. J., Amon, R. M. W., Brabets, T., Cooper, L. W., et al. (2008). Development of a Pan-Arctic database for river chemistry. *Eos* 89, 217–218. doi: 10.1029/2005JG000031
- McKnight, D. M., Boyer, E. W., Westerhoff, P. K., Doran, P. T., Kulbe, T., and Andersen, D. T. (2001). Spectrofluorometric characterization of dissolved organic matter for indication of precursor organic material and aromaticity. *Limnol. Oceangr.* 46, 38–48. doi: 10.4319/lo.2001.46.1.00038
- Murphy, K. R., Bro, R., and Stedmon, C. A. (2014). “Chemometric analysis of organic matter fluorescence,” in *Aquatic Organic Matter Fluorescence*, eds P. Coble, J. Lead, A. Baker, D. Reynolds, and R. G. M. Spencer (Cambridge, UK: Cambridge University Press), 339–375. doi: 10.13140/2.1.2595.8080
- Murphy, K. R., Ruiz, G. M., Dunsmuir, W. T. M., and Waite, T. D. (2006). Optimized parameters for fluorescence-based verification of ballast water exchange by ships. *Environ. Sci. Technol.* 40, 2357–2362. doi: 10.1021/es0519381
- Murphy, K. R., Stedmon, C. A., Graeber, D., and Bro, R. (2013). Fluorescence spectroscopy and multi-way techniques. *PARAFAC. Anal. Methods* 5, 6557–6566. doi: 10.1039/c3ay41160e
- Murphy, K. R., Stedmon, C. A., Waite, T. D., and Ruiz, G. M. (2008). Distinguishing between terrestrial and autochthonous organic matter sources in marine environments using fluorescence spectroscopy. *Mar. Chem.* 108, 40–58. doi: 10.1016/j.marchem.2007.10.003
- Neff, J. C., Finlay, J. C., Zimov, S. A., Davydov, S. P., Carrasco, J. J., Schuur, E. A. G., et al. (2006). Seasonal changes in the age and structure of dissolved organic carbon in Siberian rivers and streams. *Geophys. Res. Lett.* 33, L23401. doi: 10.1029/2006GL028222
- O'Donnell, J. A., Aiken, G. R., Walvoord, M. A., and Butler, K. D. (2012). Dissolved organic matter composition of winter flow in the Yukon River basin: implications of permafrost thaw and increased groundwater discharge. *Global Biogeochem. Cycles* 26, 4. doi: 10.1029/2012GB004341
- Opsahl, S., and Benner, R. (1995). Early diagenesis of vascular plant tissues: Lignin and cutin decomposition and biogeochemical implications. *Geochim. Cosmochim. Acta* 59, 4889–4904. doi: 10.1016/0016-7037(95)00348-7
- Opsahl, S., Benner, R., and Amon, R. M. W. (1999). Major flux of terrigenous dissolved organic matter through the Arctic Ocean. *Limnol. Oceangr.* 44, 2017–2023. doi: 10.4319/lo.1999.44.8.2017
- Osburn, C. L., Handsel, L. T., Mikan, M. P., Paerl, H. W., and Montgomery, M. T. (2012). Fluorescence tracking of dissolved and particulate organic matter quality in a river-dominated estuary. *Environ. Sci. Technol.* 46, 8628–8636. doi: 10.1021/es3007723
- Osburn, C. L., and Stedmon, C. A. (2011). Linking the chemical and optical properties of dissolved organic matter in the Baltic–North Sea transition zone to differentiate three allochthonous inputs. *Mar. Chem.* 126, 281–294. doi: 10.1016/j.marchem.2011.06.007
- Osburn, C. L., Wigdahl, C. R., Fritz, S. C., and Saros, J. E. (2011). Dissolved organic matter composition and photoreactivity in prairie lakes of the U.S. Great Plains. *Limnol. Oceangr.* 56, 2371–2390. doi: 10.4319/lo.2011.56.6.2371
- Peterson, B. J. (2002). Increasing River Discharge to the Arctic Ocean. *Science* 298, 2171–2173. doi: 10.1126/science.1077445
- Rawlins, M. A., Steele, M., Holland, M. M., Adam, J. C., Cherry, J. E., Francis, J. A., et al. (2010). Analysis of the Arctic System for freshwater cycle intensification: observations and expectations. *J. Climate* 23, 5715–5737. doi: 10.1175/2010JCLI3421.1
- Raymond, P. A., McClelland, J. W., Holmes, R. M., Zhulidov, A. V., Mull, K., Peterson, B. J., et al. (2007). Flux and age of dissolved organic carbon exported to the Arctic Ocean: a carbon isotopic study of the five largest arctic rivers. *Global Biogeochem. Cycles* 21:4. doi: 10.1029/2007GB002934
- Romanovsky, V. E., Drozdov, D. S., Oberman, N. G., Malkova, G. V., Kholodov, A. L., Marchenko, S. S., et al. (2010). Thermal state of permafrost in Russia. *Permafrost Periglac. Process.* 21, 136–155. doi: 10.1002/pp.683
- Runkel, R. L., Crawford, C. G., and Cohn, T. A. (2004). *Load Estimator (LOADEST): A FORTRAN Program for Estimating Constituent Loads in Streams and Rivers: U.S. Geological Survey Techniques and Methods Book 4, Chapter A5*. CreateSpace Independent Publishing Platform.
- Serreze, M. C., Barrett, A. P., Slater, A. G., Woodgate, R. A., Aagaard, K., Lammers, R. B., et al. (2006). The large-scale freshwater cycle of the Arctic. *J. Geophys. Res.* 111, C11010–C11019. doi: 10.1029/2005JC003424
- Smith, L. C., Pavelsky, T. M., MacDonald, G. M., Shiklomanov, A. I., and Lammers, R. B. (2007). Rising minimum daily flows in northern Eurasian rivers: a growing influence of groundwater in the high-latitude hydrologic cycle. *J. Geophys. Res.* 112, S47. doi: 10.1029/2006JG000327
- Søndergaard, M., Stedmon, C. A., and Borch, N. H. (2003). Fate of terrigenous dissolved organic matter (DOM) in estuaries: aggregation and bioavailability. *Ophelia* 57, 161–176. doi: 10.1080/00785236.2003.10409512
- Spencer, R. G. M., Aiken, G. R., Butler, K. D., Dornblaser, M. M., Striegl, R. G., and Hernes, P. J. (2009). Utilizing chromophoric dissolved organic matter measurements to derive export and reactivity of dissolved organic carbon exported to the Arctic Ocean: a case study of the Yukon River, Alaska. *Geophys. Res. Lett.* 36, L06401–L06406. doi: 10.1029/2008GL036831
- Spencer, R. G. M., Aiken, G. R., Dyda, R. Y., Butler, K. D., Bergamaschi, B. A., and Hernes, P. J. (2010b). Comparison of XAD with other dissolved lignin isolation techniques and a compilation of analytical improvements for the analysis of lignin in aquatic settings. *Org. Geochem.* 41, 445–453. doi: 10.1016/j.orggeochem.2010.02.004
- Spencer, R. G. M., Aiken, G. R., Wickland, K. P., Striegl, R. G., and Hernes, P. J. (2008). Seasonal and spatial variability in dissolved organic matter quantity and composition from the Yukon River basin, Alaska. *Global Biogeochem. Cycles* 22, 4. doi: 10.1029/2008GB003231
- Spencer, R. G. M., Butler, K. D., and Aiken, G. R. (2012). Dissolved organic carbon and chromophoric dissolved organic matter properties of rivers in the USA. *J. Geophys. Res.* 117, G03001–G03014. doi: 10.1029/2011JG001928
- Spencer, R. G. M., Hernes, P. J., Ruf, R., Baker, A., Dyda, R. Y., Stubbins, A., et al. (2010a). Temporal controls on dissolved organic matter and lignin biogeochemistry in a pristine tropical river, Democratic Republic of Congo. *J. Geophys. Res.* 115, G03013. doi: 10.1029/2009JG001180
- Spencer, R. G. M., Mann, P. J., Dittmar, T., Eglinton, T. I., McIntyre, C., Holmes, R. M., et al. (2015). Detecting the signature of permafrost thaw in Arctic rivers. *Geophys. Res. Lett.* 42, 2830–2835. doi: 10.1002/2015GL063498
- Stedmon, C. A., Amon, R., Rinehart, A. J., and Walker, S. A. (2011a). The supply and characteristics of colored dissolved organic mater (CDOM) in the Arctic Ocean: pan Arctic trends and differences. *Mar. Chem.* 124, 108–118. doi: 10.1016/j.marchem.2010.12.007
- Stedmon, C. A., and Markager, S. (2005). Resolving the variability in dissolved organic matter fluorescence in a temperate estuary and its catchment using PARAFAC analysis. *Limnol. Oceangr.* 50, 686–697. doi: 10.4319/lo.2005.50.2.00686
- Stedmon, C. A., Markager, S., and Bro, R. (2003). Tracing dissolved organic matter in aquatic environments using a new approach to fluorescence spectroscopy. *Mar. Chem.* 82, 239–254. doi: 10.1016/S0304-4203(03)00072-0
- Stedmon, C. A., Thomas, D. N., Granskog, M., Kaartokallio, H., Papadimitriou, S., and Kuosa, H. (2007). Characteristics of dissolved organic matter in Baltic Coastal Sea Ice: Allochthonous or Autochthonous Origins? *Environ. Sci. Technol.* 41, 7273–7279. doi: 10.1012/es071210f
- Stedmon, C. A., Thomas, D. N., Papadimitriou, S., Granskog, M. A., and Dieckmann, G. S. (2011b). Using fluorescence to characterize dissolved organic matter in Antarctic sea ice brines. *J. Geophys. Res.* 116, G03027–G03029. doi: 10.1029/2011JG001716
- Striegl, R. G., Aiken, G. R., Dornblaser, M. M., Raymond, P. A., and Wickland, K. P. (2005). A decrease in discharge-normalized DOC export by the Yukon River during summer through autumn. *Geophys. Res. Lett.* 32, L21413. doi: 10.1029/2005GL024413
- Striegl, R. G., Dornblaser, M. M., Aiken, G. R., Wickland, K. P., and Raymond, P. A. (2007). Carbon export and cycling by the Yukon, Tanana, and Porcupine rivers, Alaska, 2001–2005. *Water Resour. Res.* 43, 2. doi: 10.1029/2006WR005201
- Tanaka, K., Kuma, K., Hamasaki, K., and Yamashita, Y. (2014). Accumulation of humic-like fluorescent dissolved organic matter in the Japan Sea. *Sci. Rep.* 4, 1–7. doi: 10.1038/srep05292

- Tarnocai, C., Canadell, J. G., Schuur, E. A. G., Kuhry, P., Mazhitova, G., and Zimov, S. (2009). Soil organic carbon pools in the northern circumpolar permafrost region. *Global Biogeochem. Cycles* 23, 2. doi: 10.1029/2008GB003327
- Templer, J., Derenne, S., Croué, J.-P., and Largeau, C. (2005). Comparative study of two fractions of riverine dissolved organic matter using various analytical pyrolytic methods and a ^{13}C CP/MAS NMR approach. *Org. Geochem.* 36, 1418–1442. doi: 10.1016/j.orggeochem.2005.05.003
- Tucker, L. R. (1951). *A Method for Synthesis of Factor Analysis Studies* (Personnel Research Section Report No. 984). Washington, DC: Department of the Army.
- Walker, S. A., Amon, R. M. W., and Stedmon, C. A. (2013). Variations in high-latitude riverine fluorescent dissolved organic matter: a comparison of large Arctic rivers. *J. Geophys. Res. Biogeosci.* 118, 1689–1702. doi: 10.1002/2013JG002320
- Walker, S. A., Amon, R. M. W., Stedmon, C. A., Duan, S., and Loucheouarn, P. (2009). The use of PARAFAC modeling to trace terrestrial dissolved organic matter and fingerprint water masses in coastal Canadian Arctic surface waters. *J. Geophys. Res.* 114, G00F06–G00F012. doi: 10.1029/2009JG000990
- Weishaar, J. L., Aiken, G. R., Bergamaschi, B. A., Fram, M. S., Fujii, R., and Mopper, K. (2003). Evaluation of Specific Ultraviolet Absorbance as an Indicator of the Chemical Composition and Reactivity of Dissolved Organic Carbon. *Environ. Sci. Technol.* 37, 4702–4708. doi: 10.1021/es030360x
- Wickland, K. P., Aiken, G. R., Butler, K., Dornblaser, M. M., Spencer, R. G. M., and Striegl, R. G. (2012). Biodegradability of dissolved organic carbon in the Yukon River and its tributaries: seasonality and importance of inorganic nitrogen. *Global Biogeochem. Cycles* 26, 4. doi: 10.1029/2012GB004342
- Yamashita, Y., Kloepel, B. D., Knoepp, J., Zausen, G. L., and Jaffé, R. (2011). Effects of watershed history on dissolved organic matter characteristics in headwater streams. *Ecosystems* 14, 1110–1122. doi: 10.1007/s10021-011-9469-z
- Yamashita, Y., Maie, N., Briceño, H., and Jaffé, R. (2010b). Optical characterization of dissolved organic matter in tropical rivers of the Guayana Shield, Venezuela. *J. Geophys. Res.* 115, G00F10–G00F15. doi: 10.1029/2009JG000987
- Yamashita, Y., Scinto, L. J., Maie, N., and Jaffé, R. (2010a). Dissolved organic matter characteristics across a subtropical wetland's landscape: application of optical properties in the assessment of environmental dynamics. *Ecosystems* 13, 1006–1019. doi: 10.1007/s10021-010-9370-1

Conflict of Interest Statement: The authors declare that the research was conducted in the absence of any commercial or financial relationships that could be construed as a potential conflict of interest.

Copyright © 2016 Mann, Spencer, Hernes, Six, Aiken, Tank, McClelland, Butler, Dyda and Holmes. This is an open-access article distributed under the terms of the Creative Commons Attribution License (CC BY). The use, distribution or reproduction in other forums is permitted, provided the original author(s) or licensor are credited and that the original publication in this journal is cited, in accordance with accepted academic practice. No use, distribution or reproduction is permitted which does not comply with these terms.



Predicting Dissolved Lignin Phenol Concentrations in the Coastal Ocean from Chromophoric Dissolved Organic Matter (CDOM) Absorption Coefficients

Cédric G. Fichot^{1*†}, Ronald Benner^{1,2}, Karl Kaiser^{1,3}, Yuan Shen¹, Rainer M. W. Amon³, Hiroshi Ogawa⁴ and Chia-Jung Lu⁴

¹ Marine Science Program, University of South Carolina, Columbia, SC, USA, ² Department of Biological Sciences, University of South Carolina, Columbia, SC, USA, ³ Departments of Marine Sciences and Oceanography, Texas A&M University, Galveston, TX, USA, ⁴ Atmosphere and Ocean Research Institute, The University of Tokyo, Kashiwa, Japan

OPEN ACCESS

Edited by:

Christopher Osburn,
North Carolina State University, USA

Reviewed by:

Paul James Mann,
Northumbria University Newcastle, UK
Rossana Del Vecchio,
University of Maryland, USA

*Correspondence:

Cédric G. Fichot
cgfichot@gmail.com

†Present Address:

Cédric G. Fichot,
Jet Propulsion Laboratory, California
Institute of Technology, Pasadena, CA,
USA

Specialty section:

This article was submitted to
Marine Biogeochemistry,
a section of the journal
Frontiers in Marine Science

Received: 01 October 2015

Accepted: 21 January 2016

Published: 18 February 2016

Citation:

Fichot CG, Benner R, Kaiser K, Shen Y, Amon RMW, Ogawa H and Lu C-J (2016) Predicting Dissolved Lignin Phenol Concentrations in the Coastal Ocean from Chromophoric Dissolved Organic Matter (CDOM) Absorption Coefficients. *Front. Mar. Sci.* 3:7.
doi: 10.3389/fmars.2016.00007

Dissolved lignin is a well-established biomarker of terrigenous dissolved organic matter (DOM) in the ocean, and a chromophoric component of DOM. Although evidence suggests there is a strong linkage between lignin concentrations and chromophoric dissolved organic matter (CDOM) absorption coefficients in coastal waters, the characteristics of this linkage and the existence of a relationship that is applicable across coastal oceans remain unclear. Here, 421 paired measurements of dissolved lignin concentrations (sum of nine lignin phenols) and CDOM absorption coefficients [$a_g(\lambda)$] were used to examine their relationship along the river-ocean continuum (0–37 salinity) and across contrasting coastal oceans (sub-tropical, temperate, high-latitude). Overall, lignin concentrations spanned four orders of magnitude and revealed a strong, non-linear relationship with $a_g(\lambda)$. The characteristics of the relationship (shape, wavelength dependency, lignin-composition dependency) and evidence from degradation indicators were all consistent with lignin being an important driver of CDOM variability in coastal oceans, and suggested physical mixing and long-term photodegradation were important in shaping the relationship. These observations were used to develop two simple empirical models for estimating lignin concentrations from $a_g(\lambda)$ with a $\pm 20\%$ error relative to measured values. The models are expected to be applicable in most coastal oceans influenced by terrigenous inputs.

Keywords: chromophoric dissolved organic matter, lignin, lignin-derived phenols, chromophore, absorption coefficient, coastal ocean, degradation indicators, photodegradation

INTRODUCTION

Lignin is a major biochemical component of vascular plant tissues, and a well-established biomarker of terrigenous organic matter in the ocean. Lignin is a complex aromatic heteropolymer that binds cellulose and hemicellulose microfibrils in the secondary cell wall of xylem tissues, and provides biomechanical support to stems in vascular plants. Lignin is exclusively produced on land by vascular plants, with the exception of an intertidal red seaweed *Calliarthron cheilosporioides*

(Martone et al., 2009). During decomposition of plant matter by microorganisms in litter and soils, some lignin is mobilized in particulate or dissolved form to nearby streams and rivers (Aiken et al., 1985; Aiken and Cotsaris, 1995; Eriksson, 2010). Lignin eventually reaches the ocean, where its vascular-plant origin makes it an unambiguous biomarker of terrigenous organic matter (Hedges et al., 1997). As a result, lignin extracted from seawater and marine sediments has long been used to derive qualitative and quantitative information about the origins, transformations, and fates of terrigenous organic matter in the ocean (Opsahl and Benner, 1997; Hernes and Benner, 2006; Goni et al., 2008; Amon et al., 2012; Fichot and Benner, 2014; Tesi et al., 2014; Medeiros et al., 2015).

Dissolved lignin molecules are also chromophores, and evidence suggests they contribute significantly to the optical properties of chromophoric dissolved organic matter (CDOM) in natural waters. Lignin is an aromatic macromolecule, and is therefore an efficient absorber of ultraviolet radiation in natural waters (Chin et al., 1994; Weishaar and Aiken, 2001; Schmidt, 2010). The complex macromolecular structure of lignin is also thought to promote a continuum of intramolecular charge-transfer interactions that extend the absorption properties of lignin well into the visible region of the solar spectrum (Furman and Lonsky, 1988a,b; Del Vecchio and Blough, 2004; Boyle et al., 2009). As a result, strong linear relationships between dissolved lignin concentrations and absorption and fluorescence properties of CDOM have been observed in various estuarine and coastal environments (Hernes and Benner, 2003; Spencer et al., 2008; Hernes et al., 2009; Walker et al., 2009; Osburn and Stedmon, 2011; Fichot and Benner, 2012; Fichot et al., 2013; Yamashita et al., 2015). The ubiquity of correlations between CDOM and dissolved lignin in river-influenced ocean margins suggests lignin could be an important driver of the variability of CDOM optical properties in such systems. This strong linkage also suggests CDOM optical properties could serve as practical optical proxies for the concentration of this terrigenous biomarker in the ocean.

The utility of CDOM as a proxy for lignin concentration hinges strongly on the existence of relationships that are applicable to most river-influenced environments, and on an understanding of the factors driving and impacting these relationships. Despite the various reports of linkages between CDOM and dissolved lignin, the general characteristics of the CDOM-lignin relationship and of its drivers along the river-ocean continuums of the coastal ocean remains poorly known. Differences in the origin and alteration of CDOM and lignin, or the occurrence of non-lignin and non-covarying components of CDOM are examples of factors that can impact the lignin-CDOM relationship and jeopardize the utility of the proxy. Here, we investigated the relationship between dissolved lignin and CDOM absorption coefficients in the ultraviolet range (250–400 nm) using a large and fairly comprehensive data set ($n = 421$) that spanned the full salinity gradient and multiple types of coastal systems in the global ocean. The objectives of this study were to reveal the characteristics of the relationship between CDOM absorption and dissolved lignin concentration in the ocean, provide insights about the factors driving and affecting the relationship, and provide simple models for predicting dissolved

lignin concentration from CDOM absorption coefficients that are widely applicable in terrestrially-influenced coastal systems.

MATERIALS AND METHODS

Field Sampling Overview and Study Regions

Field samples were collected from a wide variety of rivers, estuaries, and coastal waters across the northern hemisphere (Figure 1 and Table 1). A total of 421 paired water samples for CDOM and dissolved lignin analyses were collected as part of different research projects between September 2005 and October 2013. Nine different coastal-ocean areas off North America and Asia were sampled and encompassed subtropical, temperate, and arctic environments. A majority of samples was collected in waters from or influenced by rivers that contrast in terms of discharge dynamics and drainage-basin vegetation (e.g., Mississippi, Atchafalaya, Delaware, Susquehanna, Hudson, Connecticut, Mackenzie, Ob, Yukon, Noatak, Lena, and Yenisey). Two study regions stood out: (1) the Chukchi Sea was an area of high biological productivity that received less riverine inputs compared to the other regions (Cota et al., 1996; Grebmeier, 2012; Shen et al., 2012a; Palmer et al., 2013), and (2) the Otsuchi Bay was influenced by rivers with small drainage basins, steep slopes, and short residence times (Fukuda et al., 2007). Some samples in this data set (e.g., northern Gulf of Mexico, South Carolina Coast, Middle Atlantic Bight) were also collected in waters influenced by coastal wetlands and marshes. Finally, a significant number of samples were also representative

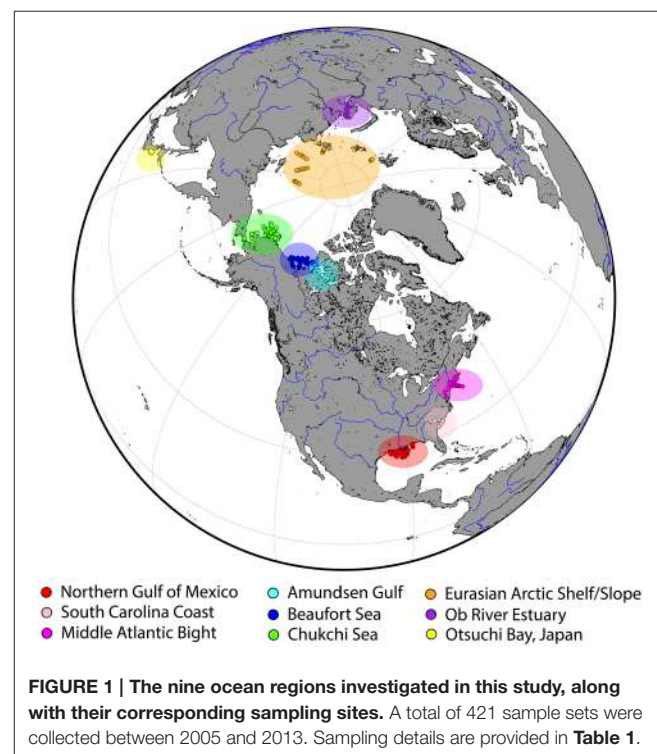


TABLE 1 | General sampling information.

	Research project*	Sampling period	Number of samples	Salinity range	Sample depth range	Related publications†
Gulf of Ob	–	September 2005	9	0–17.61	Surface	Fichot et al., 2013
Amundsen Gulf	CFL	July–August 2008	38	4.40–34.85	Surface–500 m	Fichot et al., 2013
Eurasian Arctic Shelf and Slope	NABOS	November 2008	54	27.53–34.97	Surface–700 m	Fichot et al., 2013
Northern Gulf of Mexico	GulfCarbon	January 2009	17	0–36.39	Surface	Fichot and Benner, 2011
		April 2009	22	0–36.95	Surface	Shen et al., 2012b
		July 2009	21	0–36.59	Surface	Fichot and Benner, 2012
		October–November 2009	22	0–36.55	Surface	Fichot et al., 2013
		March 2010	20	0–32.16	Surface	Fichot et al., 2014
Beaufort Sea	Malina	September 2009	80	0–34.87	Surface–1000 m	Fichot and Benner, 2014
Chukchi Sea	ICESCAPE	June–July 2010	74	29.07–33.99	Surface–200 m	Fichot et al., 2013
South Carolina coast	–	Aug–November 2011	6	0–35.10	Surface	Fichot and Benner, 2014
Otsuchi Bay, Japan	TEAMS	September 2012	6	31.96–32.72	Surface	–
US Mid-Atlantic Bight	UNOLS Chief Scientist Training Cruise	November 2012	7	0–33.67	Surface	–
		October 2013	45	0–35.95	Surface–2800 m	–
Total			421	0–36.95	Surface–2800 m	

The corresponding sampling areas and sites are shown in **Figure 1**. A total of 160 measurements were acquired below the surface (i.e., sample depth >20 m).

*CFL, Circumpolar Flaw Lead; NABOS, Nansen and Amundsen Basin Observational System; ICESCAPE, Impacts of Climate on the Eco-Systems and Chemistry of the Arctic Pacific Environment; TEAMS, Tohoku Ecosystem-Associated Marine Science; UNOLS, University-National Oceanographic Laboratory System.

†Peer-reviewed publication(s) in which part or all of the research project's data [TDLP_g and $a_g(\lambda)$] has previously been used.

of oligotrophic, subsurface (e.g., Arctic halocline), and deep-water environments (e.g., North Atlantic Deep Water). Overall, samples were collected during different seasons from waters spanning salinities ranging from 0 to 37, depths ranging from 0 to 2800 m, and water types ranging from nutrient-rich riverine waters to oligotrophic marine waters.

CDOM Sampling and Analysis

Most samples for CDOM analysis were gravity filtered from Niskin bottles using Whatman Polycap Aqueous Solution (AS) cartridges (0.2-μm pore size), collected in pre-combusted borosilicate glass vials, and stored immediately at 4°C until analysis in the laboratory. A few samples were collected using a bucket and filtered using a peristaltic pump through the Whatman Polycap Aqueous Solution (AS) cartridges. Absorbance of the samples was measured from $\lambda = 250$ –800 nm using an ultraviolet (UV)-visible dual-beam spectrophotometer (Shimadzu UV-1601 or UV-2401PC/2501PC) and 10-cm quartz cells. For riverine and low-salinity samples (salinity < 10), 5-cm quartz cells or 1-cm quartz cuvettes were used. An exponential fit of the absorbance spectrum over an optimal spectral range was used to derive an offset value that was subtracted from the absorbance spectrum (Fichot and Benner, 2011). The optimal spectral range for the fit was typically 400–700 nm, but was adjusted for each sample (e.g., 350–700, 450–700 nm) as to provide the best fit of the absorbance spectrum possible over that spectral range. Absorbance corrected for offset was then

converted to Napierian absorption coefficients, $a_g(\lambda)$ (m^{-1}). The dependence of $a_g(\lambda)$ on λ is described using Equation (1):

$$a_g(\lambda) = a_g(\lambda_0) \cdot \exp(-S(\lambda - \lambda_0)) \quad (1)$$

where $\lambda_0 < \lambda$ and S is the spectral slope coefficient in the λ_0 – λ nm spectral range. A careful examination of each $a_g(\lambda)$ spectrum demonstrated the $a_g(\lambda)$ -values (especially for $\lambda > 350$ nm) were well above the uncertainty of the measurement ($\pm 0.005\text{ m}^{-1}$ at $\lambda = 400$ nm, for a 10-cm pathlength). The spectral slope coefficient of CDOM between 275 and 295 nm, $S_{275–295}$, was calculated as the slope of the linear regression of $\ln[a_g(\lambda)]$ on λ , between $\lambda = 275$ and 295 nm (Helms et al., 2008; Fichot and Benner, 2011). The $S_{275–295}$ -values are reported in nm^{-1} .

Lignin Sampling and Analysis

Samples for lignin analysis (1–10 L) were gravity filtered from Niskin bottles using Whatman Polycap AS cartridges (0.2-μm pore size), acidified to pH = 2.5–3 with sulfuric acid, and extracted within a few hours using C-18 cartridges (Loucheouarn et al., 2000). Cartridges were stored at 4°C until elution with 30 mL of methanol (HPLC-grade). The eluent was stored in sealed, pre-combusted glass vials at –20°C until analysis. Lignin phenols were analyzed using the CuO oxidation method of Kaiser and Benner (2012). Concentrations of lignin phenols were measured as trimethylsilyl derivatives using an Agilent 7890 gas chromatograph equipped with a Varian DB5-MS capillary column and an Agilent 5975 mass selective

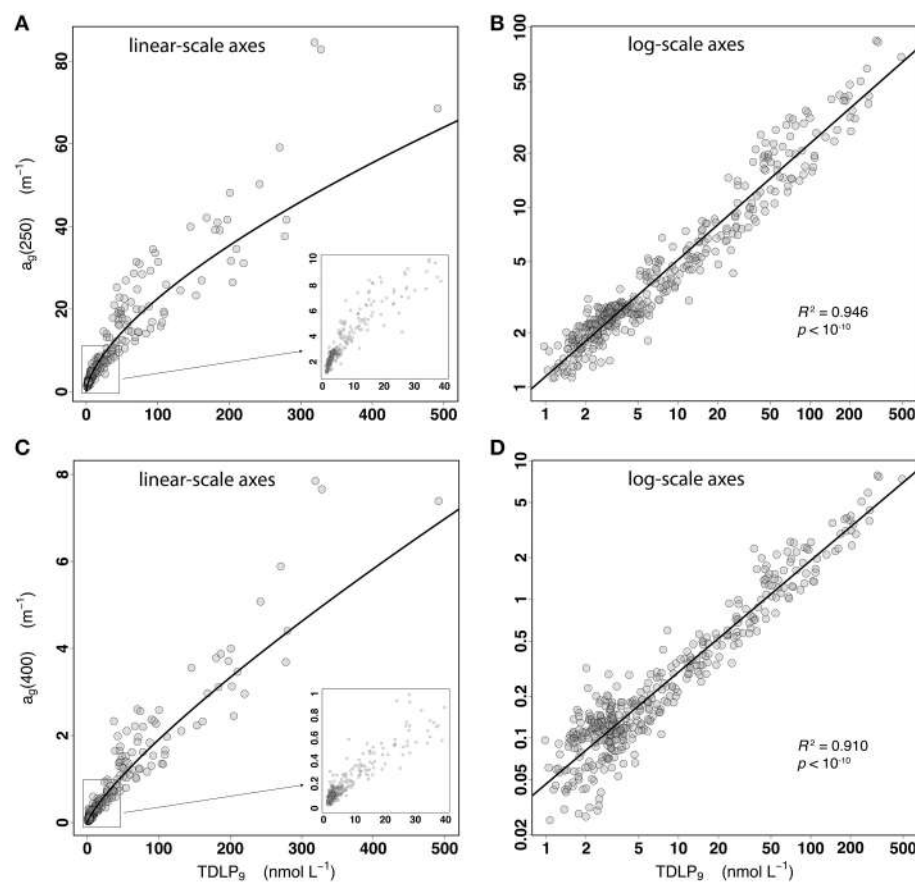


FIGURE 2 | (A,B) Scatter plots of $a_g(250)$ vs. TDLP₉ for the entire data set ($n = 421$) displayed using linear-scale and log-scale axes, respectively. The inset in (A) is a close-up of the relationship for the lower $a_g(250)$ and TDLP₉-values. The coefficient of determination (R^2) and p -value of the linear regression of $\ln[a_g(250)]$ on $\ln(\text{TDLP}_9)$ are shown in (B). **(C,D)** Same as (A,B) but for $a_g(400)$.

detector. The sum of nine lignin phenols was calculated as the total lignin phenol concentration: *p*-hydroxybenzaldehyde (PAL), *p*-hydroxyacetophenone (PON), *p*-hydroxybenzoic acid (PAD), vanillin (VAL), acetovanillone (VON), vanillic acid (VAD), syringaldehyde (SAL), acetosyringone (SON), and syringic acid (SAD). The sum of nine *p*-hydroxy, vanillyl, and syringyl lignin phenols is denoted as TDLP₉ and is reported in units of nmol L⁻¹. The sums of concentrations of the three *p*-hydroxy phenols (PAL+PON+PAD), three vanillyl phenols (VAL+VON+VAD), and three syringyl phenols (SAL+SON+SAD) were also calculated, and are denoted here as P, V, and S phenols. All values of P, V, and S phenols are reported in units of nmol L⁻¹. The P/V and S/V ratios were also calculated and are unitless.

Models

The models presented in this work for predicting dissolved lignin concentration from CDOM absorption coefficients were developed using the R environment for statistical computing and graphics and the “lm {stats}” function, obtained from the Comprehensive R Archive Network (<https://cran.r-project.org>).

RESULTS AND DISCUSSION

The Relationship between Lignin and CDOM Absorption Coefficients Across Coastal Oceans

A strong, non-linear relationship between dissolved lignin concentrations and the ultraviolet (UV) absorption coefficients of CDOM was observed over the full range of lignin concentrations measured in this study (Figures 2A,C). Dissolved lignin concentrations, TDLP₉, ranged more than 500-fold from <1 to 491 nmol L⁻¹, and the CDOM absorption coefficient, $a_g(\lambda)$, ranged 85-fold at $\lambda = 250$ nm (1.1–84.5 m⁻¹), and 300-fold at $\lambda = 400$ nm (0.025–7.8 m⁻¹). The relationship between TDLP₉ and $a_g(\lambda)$ followed a relatively well-behaved exponential over the wide range of lignin concentrations and coastal environments sampled, thereby indicating that the observed variations in CDOM UV absorption are tightly linked to changes in lignin along the river-ocean continuum (Figures 2A,C). The concave-down shape of the exponential (Figures 2A,C) further indicated that the rate of decrease of $a_g(\lambda)$ relative to that of TDLP₉ (i.e., the derivative of the fitted line) increased substantially as lignin

concentration decreased along the river-ocean continuum. At 250 nm, this rate increased about nine-fold from 0.09 to 0.75 L nmol⁻¹ m⁻¹, meaning $a_g(250)$ decreased 9 times faster in high-salinity waters than in low-salinity waters for the same 1 nmol L⁻¹ decrease in TDLP₉ along the river-ocean continuum. The exponential behavior was less accentuated at 400 nm, for which the rate increased only 3-fold from ~0.01 to 0.035 L nmol⁻¹ m⁻¹.

Linear regressions of the form shown in Equation (2) provided adequate fits for the exponential relationship between TDLP₉ and $a_g(\lambda)$ at any wavelength in the 250–400 nm range (**Figures 2B,D, 3A**).

$$\ln(a_g(\lambda)) = \alpha \cdot \ln(\text{TDLP}_9) + \beta \quad (2)$$

The relationship was stronger with $a_g(250)$ than with $a_g(400)$, as indicated by the coefficient of determination (R^2) of Equation (2) decreasing from 0.946 at 250 nm to 0.910 at 400 nm (**Figures 2B,D**). A comparison of the R^2 for every wavelength between 250 and 400 nm further indicated the overall relationship was strongest ($R^2 > 0.95$) at ~285 nm (**Figure 3A**). Despite the goodness of the regression, significant scatter around the fitted lines was evident. A close examination of the relationship between TDLP₉ and $a_g(250)$ using log-scale axes (**Figure 2B**) revealed that the scatter was relatively uniform (i.e., homoscedastic) over the entire range of lignin concentration. In contrast, the scatter around the fit was much less uniform (i.e., heteroscedastic) for $a_g(400)$, and increased substantially and progressively with decreasing lignin concentration (**Figure 2D**). The linear relationship between TDLP₉ and $a_g(400)$ was marginal ($R^2 < 0.4$) when lignin concentration was <6 nmol L⁻¹.

The strength of the relationship between dissolved lignin concentration and CDOM absorption was maximal in the UV-C region at low lignin concentrations, and shifted to the UV-A region at higher lignin concentrations (**Figure 3B**). Additional insights about the relationship were gained by comparing the R^2 of Equation (2) for two subsets of the entire data set: 1) a “low-CDOM” subset ($n = 263$) where $a_g(250) < 4 \text{ m}^{-1}$, and 2) a “high-CDOM” subset ($n = 158$) where $a_g(250) \geq 4 \text{ m}^{-1}$. The R^2 analysis using the “low-CDOM” subset (**Figure 3B**) revealed the relationship was optimal ($R^2 \sim 0.7$) at 250–275 nm (UV-C region), but weakened progressively and rapidly with wavelength to reach a minimal value ($R^2 \sim 0.35$) at 400 nm. The $a_g(263)$ was the optimal predictor of TDLP₉ for the “low-CDOM” subset. However, the $a_g(\lambda)$ in the UV-A region ($\lambda > 320 \text{ nm}$) was generally a poor predictor of lignin concentration in waters less influenced by terrigenous inputs. Interestingly, the reverse trend was observed when examining the “high-CDOM” subset. The R^2 analysis using the “high-CDOM” subset (**Figure 3B**) indicated the relationship was good at all wavelengths, but improved significantly from a minimum $R^2 = 0.87$ at 250 nm to a $R^2 \sim 0.92$ in the UV-A region (320–400 nm). As will be explained later, this shift from UV-A to UV-C is likely related to the progressive change in the molecular structure of lignin, and potentially, of other terrigenous chromophores co-varying with lignin. This shift also indicates that $a_g(\lambda)$ at a single wavelength is not an optimal predictor for lignin concentration over the range of lignin concentration found in coastal oceans.

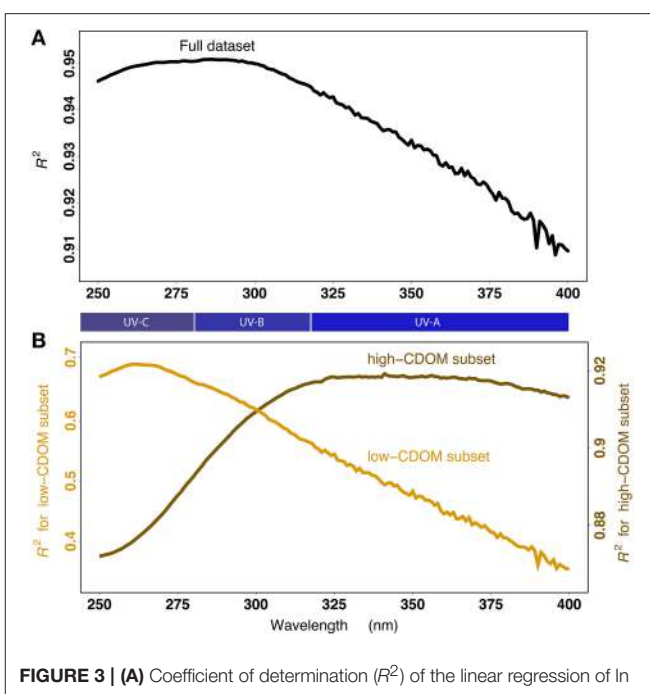


FIGURE 3 | (A) Coefficient of determination (R^2) of the linear regression of $\ln[a_g(\lambda)]$ on $\ln(\text{TDLP}_9)$ as a function of wavelength λ , and using the entire data set ($n = 421$). Note the regression lines corresponding to the R^2 at $\lambda = 250 \text{ nm}$ and 400 nm are shown in **Figures 2B,D**, respectively. **(B)** Same as in panel A but using a “low-CDOM” subset of the entire data set [$a_g(250) < 4 \text{ m}^{-1}$; $n = 263$], shown here in orange, or a “high-CDOM” subset of the entire data set [$a_g(250) \geq 4 \text{ m}^{-1}$; $n = 158$], shown here in brown. The corresponding ranges of the UV-A, UV-B, and UV-C are shown for reference.

The *p*-hydroxy phenols (P), vanillyl phenols (V), and syringyl phenols (S) that make up TDLP₉ exhibited varying degrees of correlation with the CDOM absorption coefficient (**Figure 4**). As explained earlier, the relationship between $a_g(\lambda)$ and TDLP₉ was optimal at ~285 nm for the entire range of lignin concentrations ($R^2 = 0.951$). The separation of TDLP₉ into P, V, and S phenols indicated the relationship between $a_g(285)$ and P phenols across the full range of values was even stronger ($R^2 = 0.959$) than with TDLP₉. Only samples from the Ob estuary deviated significantly from the general relationship, and were enriched in P phenols relative to $a_g(285)$. However, this enrichment in P phenols was apparent and most likely originated from elevated levels of peat-derived sphagnum acid typically found in the Ob watershed, and their subsequent conversion into P phenols during the oxidation of lignin (Amon et al., 2012; Philben et al., 2014). The relationship became progressively less robust with V phenols ($R^2 > 0.925$) and S phenols ($R^2 > 0.893$). The trend is consistent with P phenols being more resistant to degradation in natural waters than V phenols, and with S phenols being the most susceptible to degradation (Opsahl and Benner, 1995; Benner and Opsahl, 2001; Benner and Kaiser, 2011). Furthermore, lignin produced by gymnosperms is devoid of S phenols, whereas P and V phenols are ubiquitous in lignin (Hedges and Mann, 1979; Benner and Opsahl, 2001; Shen et al., 2012b). This most likely impacted the relationship between $a_g(285)$ and S phenols by making it sensitive to variations in watershed vegetation.

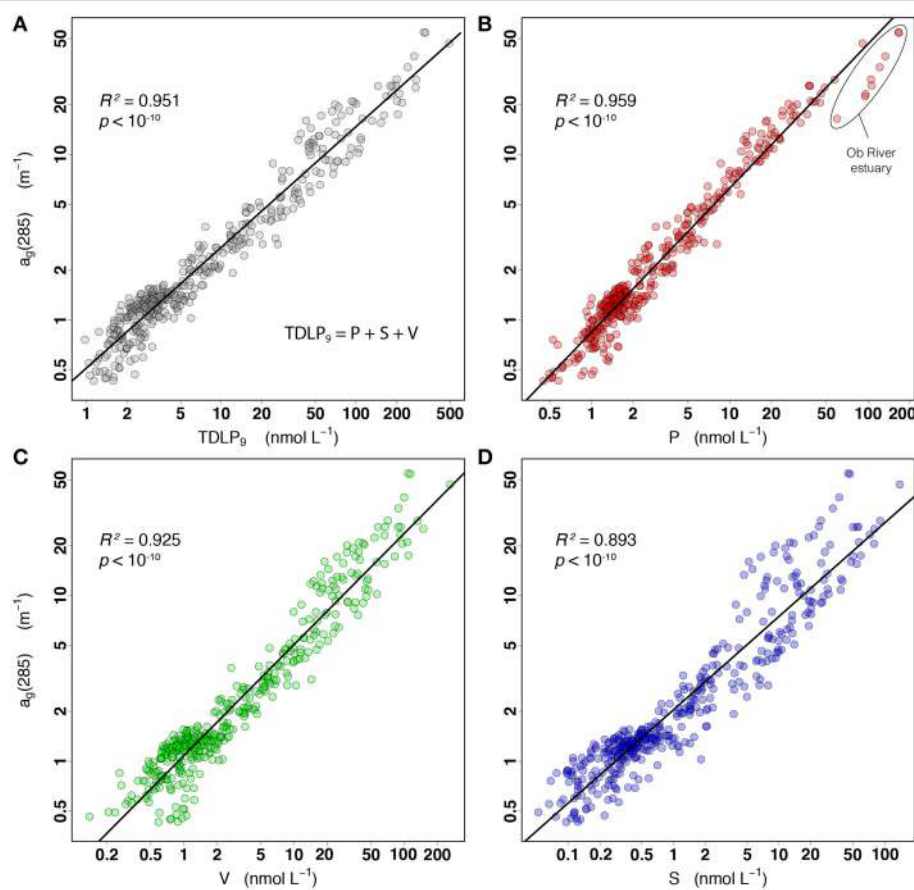


FIGURE 4 | Relationships between $a_g(285)$ and the concentrations of (A) TDLP₉, (B) *p*-hydroxy phenols, (C) vanillyl phenols, (D) and syringyl phenols.

Physical Mixing and Degradation Of Terrigenous CDOM

The decreasing trends in TDLP₉ concentrations and $a_g(285)$ along the salinity gradient confirmed the importance of physical mixing in the distribution of these two variables along the river-ocean continuum (Figure 5). As expected from the strong relationship observed between TDLP₉ and $a_g(285)$, the relationships between salinity and TDLP₉ (Figures 5A,B) and between salinity and $a_g(285)$ (Figures 5C,D) were strikingly similar. Although a large scatter in TDLP₉ and $a_g(285)$ at salinities <5 and >35 indicated important differences among riverine sources and ocean end-members, the trends observed for each region clearly indicated physical mixing of riverine and oceanic end-members played a dominant role in regulating the variability of TDLP₉ and $a_g(285)$ concentrations. Two South Carolina samples strongly influenced by salt-marsh inputs (Ashley River and Hunting Island, SC) stood out as being relatively enriched in CDOM and lignin, in agreement with previous observations that marsh-derived CDOM can be chemically and optically distinct (e.g., stronger absorption) from other estuarine CDOM (Tzortziou et al., 2008). In contrast, samples with salinities $\sim 28\text{--}33$ from the Western Arctic Ocean (Chukchi Sea, Beaufort Sea, Amundsen Gulf) stood out as being

relatively depleted in CDOM and lignin. Considering most of these samples were collected in regions experiencing extensive sea-ice melting, this relative depletion in CDOM and lignin was likely due to the presence of ice-melt water (low salinity and depleted in DOM).

Several degradation indicators further indicated the general decrease in lignin concentrations from the rivers to the oligotrophic regions of coastal oceans was accompanied by a progressive change in the degradation state of terrigenous CDOM (Figure 6). The TDLP₉-values decreased by almost four orders-of-magnitude along the river-ocean continuum. This decrease exhibited a weak, but significant and positive correlation ($r = 0.51$) with the ratio of S to V phenols (S/V), and was accompanied by exponential increases in the ratio of P to V phenols (P/V) and the spectral slope coefficient of CDOM absorption ($S_{275\text{--}295}$). These trends are consistent with similar observations along the salinity gradient of river-influenced ocean margins in previous studies, and with the physical mixing of two terrigenous CDOM end-members with different degradation states (Opsahl and Benner, 1998; Hernes and Benner, 2003; Helms et al., 2008; Fichot and Benner, 2012).

More specifically, the trends in S/V, P/V, and $S_{275\text{--}295}$ observed herein are consistent with the physical mixing of two

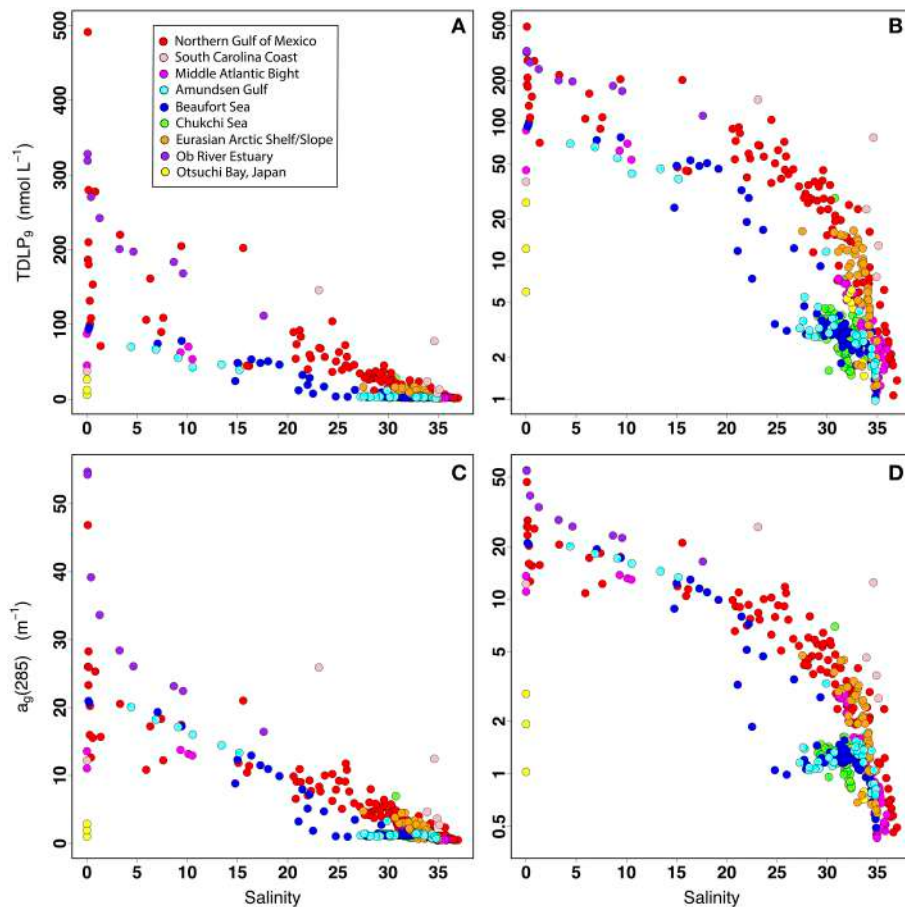


FIGURE 5 | Relationships between salinity and TDLP₉ using a linear-scale y-axis (A) and a log-scale y-axis (B), and relationships between salinity and $a_g(285)$ using a linear-scale y-axis (C) and a log-scale y-axis (D).

end-members: (1) a relatively unaltered terrigenous CDOM end-member from rivers, and (2) a photochemically altered terrigenous CDOM end-member from the oligotrophic regions of the coastal oceans (Benner and Opsahl, 2001; Hernes and Benner, 2003; Fichot and Benner, 2012). The S/V has been shown to decrease during natural sunlight photodegradation experiments and during coupled photochemical-biological degradation experiments under simulated sunlight (Opsahl and Benner, 1998; Spencer et al., 2009; Benner and Kaiser, 2011). Note that Spencer et al. (2009) actually showed an increase in S/V after extreme exposure to solar radiation, but only after an initial decrease in S/V. The P/V has also been shown to increase during photodegradation experiments (Benner and Kaiser, 2011). In addition, the S_{275–295} has been shown to increase with decreasing molecular weight of CDOM and during exposure to solar radiation (Helms et al., 2008; Fichot and Benner, 2012; Yamashita et al., 2013). The trends in S/V, P/V, and S_{275–295} observed in this data set are consistent with the effects of photodegradation, and suggest the progressive change in the degradation state of terrigenous CDOM played an important role shaping the relationship between lignin and CDOM absorption coefficients.

The relatively weak correlation ($r = 0.51$) between the S/V and TDLP₉ was not unexpected (Figure 6A). The S/V is not only affected by solar exposure, but is also a well-established indicator of the source vegetation of lignin and terrigenous DOM in natural waters (Hedges and Mann, 1979; Hedges and Ertel, 1982; Opsahl et al., 1999; Dittmar and Kattner, 2003; Shen et al., 2012b). As mentioned earlier, the S/V reflects the relative contributions of gymnosperm and angiosperm vegetation in lignin and terrigenous DOM because S phenols are not produced by gymnosperms. Lower S/V are thus typically measured in lignin that originates from gymnosperm-dominated watersheds (e.g., boreal forests), whereas higher S/V are indicative of significant contributions from angiosperms (e.g., tundra, deciduous forests). The effect of vegetation source on lignin phenol composition was evident in this data set, with low S/V values (< 0.5) measured in Arctic waters. The drainage basins of large Arctic rivers are dominated by gymnosperms, and the S/V of Arctic rivers typically range from ~0.2 to 0.45 (when calculated from nmol L⁻¹ concentrations) and exhibit some moderate variations with flow regime (Amon et al., 2012). The effect of vegetation was also evident from the high S/V values (>0.5) measured in the sub-tropical and temperate coastal oceans, which receive

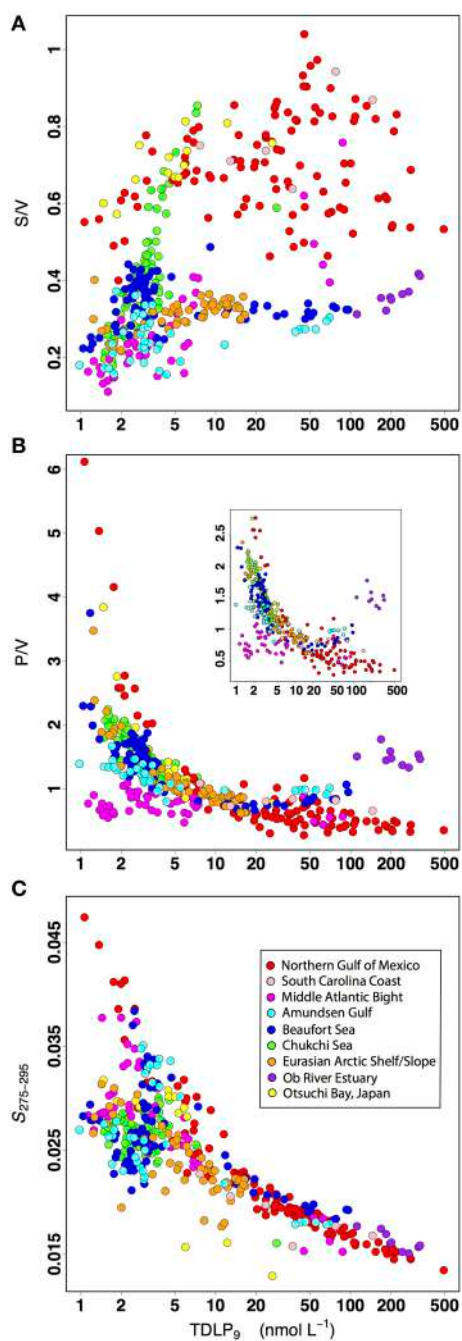


FIGURE 6 | Relationships between TDLP₉ and several degradation indicators of lignin and CDOM degradation: (A) S/V ratio of syringyl phenols to vanillyl phenols (unitless), (B) P/V ratio of *p*-hydroxy phenols to vanillyl phenols (unitless), and (C) the spectral slope coefficient of CDOM absorption coefficient spectrum between 275 and 295 nm, $S_{275-295}$ (nm^{-1}).

substantial contributions from angiosperms. Some samples from the Chukchi Sea had relatively high S/V values, but these samples were strongly influenced by Pacific Ocean water or small rivers draining tundra. Finally, a large number of samples from the Middle Atlantic Bight had comparatively low S/V values. This

was likely observed because most of the terrigenous DOM on the shelf of the Middle Atlantic Bight shelf originates from gymnosperm-dominated environments further north, and is transported southward by currents (Chapman and Beardsley, 1989; Mountain, 1991).

Evidence suggests the P/V ratio is a useful indicator of the extent of lignin degradation. Here, the P/V increased several-fold and exponentially with decreasing lignin concentrations (Figure 6B). The P/V has been shown to increase substantially after continuous or intermittent solar exposure (Benner and Kaiser, 2011), and unlike the S/V, the P/V is not as sensitive to changes in source vegetation. The P phenols are widely distributed among vascular plants. However, as mentioned earlier, inputs from peatlands can increase the P/V, most likely as a result of the conversion of sphagnum acid into P phenols during CuO oxidation. Elevated concentrations of P phenols were observed in the peatland-influenced samples from the Ob River estuary, and to a much lesser degree, from the Mackenzie River estuary. Samples influenced by sub-tropical salt marshes (e.g., Terrebonne Bay, South Carolina Coast) also have slightly elevated values of P/V. Note the P/V can also reflect changes in the flow regime of rivers and be indicative of the ¹⁴C age of terrigenous DOM immobilized (Amon et al., 2012). High P/V and lower lignin concentrations have thus been observed during base flow in Arctic Rivers, and the reverse observed during peak flow (Amon et al., 2012), suggesting that changes in river flow could contribute to the trends observed here between TDLP₉ and P/V. Finally, the highest P/V-values (>4) were observed in samples from oligotrophic eddies shed from the Loop Current and impinging on the continental shelf in the northern Gulf of Mexico (Schiller et al., 2011; Fichot et al., 2014). These high P/V were likely attributed to the long-term solar exposure and degradation in the optically clear Loop-Current waters, which originate in the Atlantic Ocean.

The exponential increase in $S_{275-295}$ with decreasing lignin concentrations was also consistent with physical mixing and the effects of photochemical degradation (Figure 6C). $S_{275-295}$ has been shown to increase during photodegradation and is a sensitive indicator of CDOM photodegradation in natural waters (Helms et al., 2008, 2013; Ortega-Retuerta et al., 2009; Fichot and Benner, 2012; Yamashita et al., 2013). Overall, the $S_{275-295}$ displayed a clear increasing trend with decreasing TDLP₉ concentrations in the present study. With the exception of a few outliers, $S_{275-295}$ increased monotonically with decreasing TDLP₉-values ranging from 500 to 10 nmol L⁻¹. When TDLP₉ was <10 nmol L⁻¹, the relationship between $S_{275-295}$ and TDLP₉ split into two groups of data: one that continued to show a strong relationship between $S_{275-295}$ and TDLP₉, and one that showed little correlation between the two. The first group consisted essentially of surface samples, whereas the second group corresponded primarily of sub-surface and deep waters, and of productive, high-latitude waters that were moderately influenced by terrigenous inputs (e.g., Chukchi Sea, Canada Basin, Amundsen Gulf). Limited solar exposure, a greater relative contribution of microbial degradation, or a more prominent influence of non-terrestrial sources of CDOM (*in situ* production) can be expected in these water types, and are

consistent with the relatively low $S_{275-295}$ -values ($\sim 0.025 \text{ nm}^{-1}$) observed. The limited solar exposure in sub-surface and deep water likely contributed to the lower $S_{275-295}$. Furthermore, previous studies reported $S_{275-295}$ -values of $\sim 0.025 \text{ nm}^{-1}$ for plankton-derived CDOM, and have provided evidence that $S_{275-295}$ decreases slightly during microbial degradation (Ortega-Retuerta et al., 2009; Fichot and Benner, 2012).

It is important to understand that the progressive changes in the degradation state of terrigenous CDOM observed along the river-ocean continuum are largely driven by the physical mixing of riverine and ocean end-members (Fichot and Benner, 2012), and that the observed change largely reflects long-term effects of photochemical degradation on the ocean end-member of terrigenous CDOM. Terrigenous CDOM, which remains relatively unaltered in rivers, mixes with photochemically altered terrigenous CDOM from oligotrophic regions of ocean margins (Benner and Opsahl, 2001; Hernes and Benner, 2003; Fichot and Benner, 2012). Solar exposure in surface waters and the extent of photochemical degradation occurring over typical residence times of river water in ocean margins (e.g., months) has been shown to be relatively moderate, even in subtropical river-influenced ocean margins (Fichot and Benner, 2014). Much of the photochemical degradation occurs beyond the shelf where the residence time of the water is much longer and solar exposure in surface waters is strongly enhanced by a sharp increase in UV penetration relative to the mixed layer depth. In some cases, the terrigenous CDOM found in the oligotrophic regions of the coastal oceans can have a very different and more distant origin, as was the case in this data set when Loop-Current oligotrophic eddies impinged on the Northern Gulf of Mexico shelf (Fichot et al., 2014). In the Arctic Ocean, solar exposure and photodegradation are less than in subtropical regions, but the ocean end-member can have a more distant origin and the terrigenous CDOM can be more chemically altered (e.g., Pacific Water in Chukchi or Beaufort Seas, or Atlantic water off Svalbard).

The concave-down shape of the exponential relationship between TDLP₉ and $a_g(\lambda)$ was consistent with mixing and long-term photodegradation playing important roles in shaping the relationship between lignin concentration and CDOM absorption coefficients. Photodegradation has been shown to lead to a decrease in the molecular weight and aromaticity of terrigenous CDOM (Kieber et al., 1989, 1990; Opsahl and Benner, 1998; Miller et al., 2002; Helms et al., 2008). The molecular weight and aromaticity of a compound is, in turn, strongly linked to its molar absorptivity (Chin et al., 1994; Weishaar and Aiken, 2001), such that a given concentration of lignin in low-molecular-weight molecules absorbs much less efficiently than the same concentration of lignin within high-molecular weight molecules. The concave-down shape of the relationship indicated there was an acceleration in the loss of $a_g(\lambda)$ relative to that of TDLP₉ as lignin concentrations decreased from riverine to oligotrophic waters. A loss of absorption strictly due to the loss of chromophoric material (i.e., without a loss of molar absorptivity) would tend to produce a linear rather than a concave-down exponential relationship. Here, the acceleration in the loss of $a_g(\lambda)$ was consistent with a progressive loss of molar

absorptivity superimposed on a loss of chromophoric material, and is consistent with previous observations of a decrease in molecular weight of both CDOM and lignin along the river-ocean continuum in ocean margins (Hernes and Benner, 2003; Helms et al., 2008).

The characteristics of the relationship between TDLP₉ and $a_g(400)$ were consistent with a progressive loss of intramolecular charge-transfer interactions in CDOM along the river-ocean continuum. Intramolecular charge-transfer interactions among chromophores in aromatic molecules such as lignin have been proposed as a mechanism to explain the exponential shape of the CDOM absorption spectrum and its absorption at wavelengths $> 350 \text{ nm}$ (Del Vecchio and Blough, 2004; Boyle et al., 2009; Sharpless and Blough, 2014). In this model, charge-transfer interactions among electron donors (e.g., phenols and/or methoxylated phenols in lignin) and electron acceptors (e.g., quinones or aromatic ketones/aldehydes in lignin) are thought to produce lower-energy optical transitions and enhance CDOM absorption at wavelengths $> 350 \text{ nm}$. The contribution of electronic interactions to the CDOM absorption is linked to the molecular weight of terrigenous molecules like lignin, because compounds with higher molecular weight have a greater potential for intramolecular charge-transfer interactions. A sharp decrease in the molecular weight of lignin along the river-ocean continuum would therefore be associated with a loss of intramolecular charge-transfer interactions, and with a weakening contribution of lignin to the CDOM absorption at wavelengths $> 350 \text{ nm}$. The worsening of the relationship between TDLP₉ and $a_g(400)$ with decreasing lignin concentrations, which eventually leads to an insignificant relationship between TDLP₉ and $a_g(400)$ in the more oligotrophic regions of the coastal oceans, is consistent with the effects of photodegradation.

On the Contribution of Lignin and other Components to CDOM Absorption

The existence of a well-behaved relationship between TDLP₉ and $a_g(\lambda)$ from the rivers to the oligotrophic regions of several contrasting coastal oceans was a strong indication that lignin is generally an important driver of the variability of CDOM absorption coefficients in coastal waters. However, the contribution of lignin to the absorption coefficient of CDOM was not uniform across the 250–400 nm spectrum. Lignin appeared an important contributor to $a_g(\lambda)$ in the UV-C ($\lambda < 280 \text{ nm}$) and UV-B ($280 < \lambda < 320 \text{ nm}$) regions over the entire range of lignin concentrations observed in this study. However, for $\lambda > 350 \text{ nm}$, lignin only seemed to contribute significantly to CDOM absorption for the upper range of TDLP₉ concentrations and $a_g(\lambda)$ values (e.g., TDLP₉ $> 10 \text{ nmol L}^{-1}$ or $a_g(250) > 4 \text{ m}^{-1}$). For this upper range, lignin appeared an even greater contributor to $a_g(\lambda)$ in the UV-A region than in the UV-B and UV-C regions. As described earlier, the spectral dependency of the relationship likely results from the change in the degradation state of terrigenous CDOM. The P phenols in lignin appeared to be the greater contributor to the absorption coefficients of CDOM, followed by the V phenols and the S phenols. A greater contribution of the P phenols to CDOM absorption is consistent

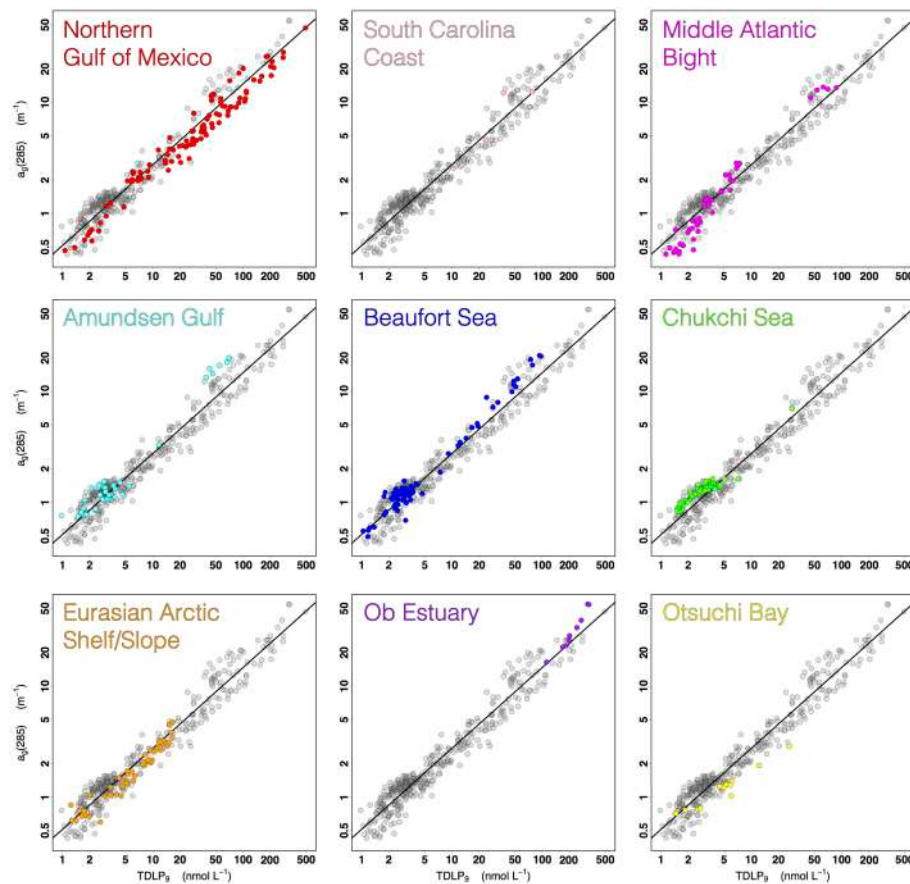


FIGURE 7 | Scatter plots of the relationship between $a_g(285)$ and TDLP₉ (log-scale axes) highlighting the data from each of the nine study regions.

with their greater resistance to photodegradation (Benner and Kaiser, 2011), and their selective preservation relative to the V and S phenols as lignin concentrations decrease along the river-ocean continuum. Although this is only speculation, it is possible the greater photochemical resistance of P phenols contributes to their preservation in higher molecular weight and more aromatic structures that have higher molar absorptivities and higher potential for intramolecular electronic interactions. The selective preservation of the P phenols is consistent with the strong relationship observed between P phenols and $a_g(\lambda)$ in the more oligotrophic regions of the coastal oceans.

A variety of other chromophoric constituents in terrigenous DOM also likely contribute to CDOM absorption and impact the relationship between lignin and CDOM. Lignin has the chemical moieties necessary to make it an important chromophore (Boyle et al., 2009; Sharpless and Blough, 2014). It is important to recognize, however, that a variety of other chromophoric components in terrigenous DOM likely co-vary strongly with lignin, and can contribute significantly to the CDOM absorption despite the strong linkage observed between CDOM and lignin. Tannins, a class of polyphenols, are components of many terrestrial plant tissues (e.g., foliage, bark) and are readily released to aquatic systems (Benner et al., 1990; Hernes et al.,

2001; Kraus et al., 2003; Maie et al., 2008). Dissolved tannins also absorb very strongly in the ultraviolet and visible region (Lawrence, 1980; Alberts, 1982; Kraus et al., 2003). However, previous studies have reported that tannin concentrations are very low in natural waters (Maie et al., 2006), and that microbial degradation, precipitation, sorption to sediments and potentially photodegradation removes tannins from aquatic systems (Benner et al., 1986; Hernes et al., 2001; Maie et al., 2008). The contribution of tannins to the CDOM absorption in coastal waters remains unclear, and more work is needed to directly assess the linkage between tannins and CDOM in coastal oceans.

Dissolved black carbon is a component of terrigenous DOM, and several studies indicate it is a potentially important component of DOC in natural waters (Kim et al., 2004; Mannino and Harvey, 2004; Ziolkowski and Druffel, 2010; Dittmar et al., 2012). Dissolved black carbon is thought to contribute up to 10% of the global riverine DOC flux to the ocean (Jaffé et al., 2013), and it contains condensed aromatic compounds that absorb strongly in the ultraviolet region (Russo et al., 2012). Stubbins et al. (2015) showed that dissolved black carbon concentration was more strongly correlated with $a_g(250)$ than with $a_g(400)$ for high-CDOM samples [$a_g(250) \sim 10\text{--}150\text{ m}^{-1}$]. Interestingly, our study revealed the reverse trend for lignin, with

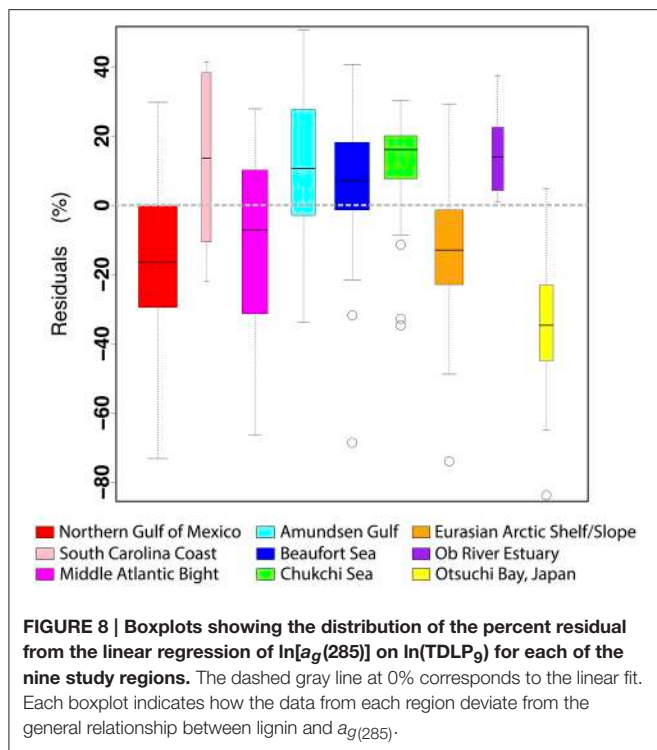


FIGURE 8 | Boxplots showing the distribution of the percent residual from the linear regression of $\ln[a_g(285)]$ on $\ln(\text{TDLP}_9)$ for each of the nine study regions. The dashed gray line at 0% corresponds to the linear fit. Each boxplot indicates how the data from each region deviate from the general relationship between lignin and $a_g(285)$.

lignin concentration being more strongly correlated with $a_g(400)$ than with $a_g(250)$ for samples from a similar range of CDOM absorption [$a_g(250) \sim 4\text{--}100 \text{ m}^{-1}$]. These opposing trends are possibly linked to differences in the molecular structures of dissolved black carbon and dissolved lignin. Black carbon contains condensed aromatic compounds that typically have very high molar absorptivities in the UV (Chin et al., 1994; Weishaar and Aiken, 2001; Russo et al., 2012), whereas partially oxidized lignin contains the moieties responsible for intramolecular charge-transfer interactions, which are particularly effective at absorbing at wavelengths $>350 \text{ nm}$ (Del Vecchio and Blough, 2004; Boyle et al., 2009; Sharpless and Blough, 2014). Soils are a major source of black carbon and lignin, suggesting these two components likely correlate strongly in river-influenced coastal areas. More work is needed to better understand the potential contribution of black carbon to the optical properties of CDOM along the river-ocean continuum.

An analysis of the percent residuals from the linear fit of the $a_g(285)$ -TDLP₉ relationship revealed some interesting variations among the different coastal oceans of this study (Figures 7, 8). Although deviations from the fitted line can occur for a variety of reasons, independent variations in the relative contributions of other, non-lignin components are likely a dominant factor. Plankton and microbes can also produce chromophoric compounds (e.g., amino acids, nucleic acids) that have variable effects on the CDOM dynamics of natural waters and will tend to contribute to the scatter in the relationship between TDLP₉ and $a_g(\lambda)$ (Rochelle-Newall and Fisher, 2002; Nelson et al., 2004; Yamashita and Tanoue, 2008; Ortega-Retuerta et al., 2009; Zhang et al., 2009; Fichot and Benner, 2012). Most of the samples from the Northern

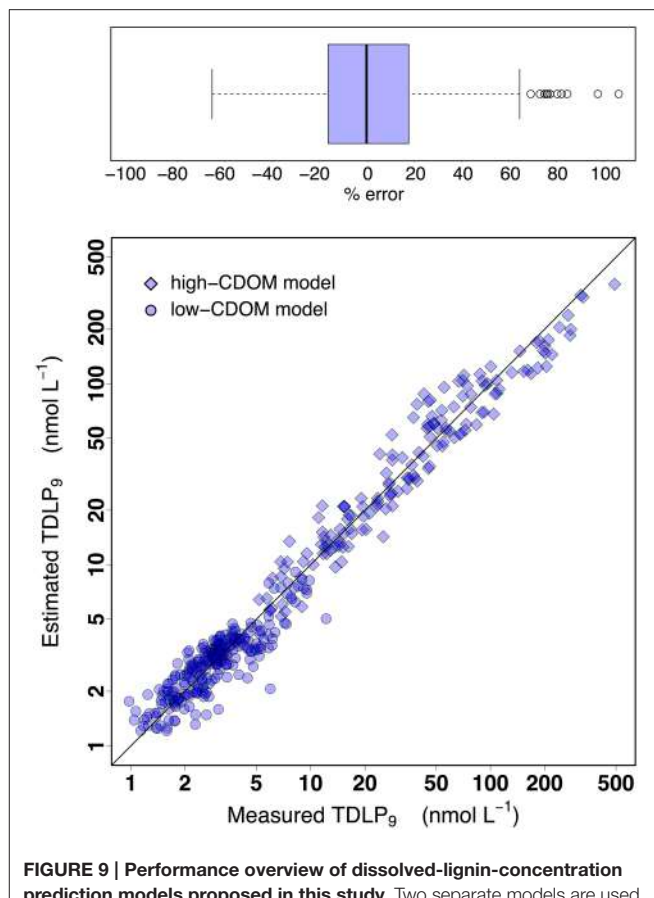


FIGURE 9 | Performance overview of dissolved-lignin-concentration prediction models proposed in this study. Two separate models are used to predict TDLP₉ from $a_g(\lambda)$, and the cutoff $a_g(250) = 4 \text{ m}^{-1}$ is used to separate the two models. For the low-CDOM model where $a_g(250) < 4 \text{ m}^{-1}$, a simple linear regression between $a_g(263)$ and TDLP₉ is used. In contrast, a multiple-linear-regression model of $\ln(\text{TDLP}_9)$ on $\ln[a_g(\lambda)]$ ($\lambda = 275, 295$, and 350 nm) is used for the high-CDOM model when $a_g(250) \geq 4 \text{ m}^{-1}$. The parameters used to implement the models are provided in Equations (3) and (4).

Gulf of Mexico, Middle Atlantic Bight, Eurasian shelf, and Otsuchi Bay, exhibited elevated TDLP₉-values relative to $a_g(285)$ (i.e., negative residuals), thereby suggesting lignin was a more dominant contributor to $a_g(285)$ in these waters. The deviation was particularly strong in the Otsuchi Bay waters, which receives inputs from short and steep rivers with short water residence times. In contrast, most samples from the Amundsen Gulf, Beaufort Sea, Chukchi Sea, Ob estuary, and South Carolina coast exhibited relatively low TDLP₉-values compared to $a_g(285)$ (i.e., positive residuals), suggesting a greater contribution of non-lignin chromophores. The positive residuals in the Chukchi Sea (all collected in summer) were potentially related to a higher background of autochthonous CDOM in these productive waters (Shen et al., 2012a), whereas those of the Ob estuary are consistent with significant contribution of non-lignin CDOM from *Sphagnum sp.* peats (Amon et al., 2012; Philben et al., 2014). The positive residuals in the South Carolina coast samples are likely related to contributions from the tidal marshes, which have been shown to have distinctive CDOM chemical and optical

properties (Tzortziou et al., 2008). Finally, many of the positive residuals were from samples collected in or near rivers during summer, and could be related to the *in situ* production of CDOM, or be related to depletion of lignin observed after the peak river flow during spring (Amon et al., 2012; Shen et al., 2012b).

Empirical Models For Estimating TDLP₉ from $a_g(\lambda)$

Exploration of lignin and CDOM relationships provided useful information for the development of two simple empirical models for the retrieval of TDLP₉ from $a_g(\lambda)$ in coastal oceans. The $a_g(285)$ was, on average, the best single-wavelength predictor of TDLP₉ over the range of absorption coefficients and lignin concentrations observed in this study. However, the spectral dependency of the relationship indicated $a_g(263)$ was the optimal single-wavelength predictor of TDLP₉ for samples where $a_g(250) < 4 \text{ m}^{-1}$, and $a_g(350)$ was the optimal single-wavelength predictor for TDLP₉ for samples where $a_g(250) \geq 4 \text{ m}^{-1}$. Furthermore, photodegradation had a strong effect on the relationship, and $S_{275-295}$ helped factor in this effect and improve the TDLP₉ predictions for high-CDOM samples, where $S_{275-295}$ and TDLP₉ were most correlated [TDLP₉ $\geq 10 \text{ nmol L}^{-1}$ or $a_g(250) \geq 4 \text{ m}^{-1}$]. These observations guided the development of two sub-models separated by the $a_g(250) = 4 \text{ m}^{-1}$ cutoff.

When $a_g(250) < 4 \text{ m}^{-1}$, a “low-CDOM” sub-model based on a simple linear regression was used,

$$\ln(\text{TDLP}_9) = 0.7672 \cdot a_g(263) - 0.3987 \quad (3)$$

When $a_g(250) \geq 4 \text{ m}^{-1}$, a “high-CDOM” sub-model based on a multiple linear regression was used,

$$\begin{aligned} \ln(\text{TDLP}_9) = & -2.282 \cdot \ln(a_g(350)) - 8.209 \cdot \ln(a_g(275)) \\ & + 11.365 \cdot \ln(a_g(295)) + 2.909 \end{aligned} \quad (4)$$

In the case of the multiple linear regression of Equation (4), all derived coefficients were significant by the *t*-test ($p < 0.0005$), thereby confirming $a_g(275)$ and $a_g(295)$ represented meaningful additions to the model. The addition of $a_g(275)$ and $a_g(295)$ also improved the adjusted R^2 of the regression (adj $R^2 = 0.936$) relative to a single regression model using only $a_g(350)$ (adj $R^2 = 0.918$). The use of $a_g(275)$ and $a_g(295)$ in Equation (4) was somewhat similar to using $S_{275-295}$ as one of the terms, but did not require the extra step of calculating $S_{275-295}$. Note the use of additional predictors in either Equation (3) or (4), or the use of partial-least-square regressions did not significantly improve the adjusted R^2 of the regressions nor the % error of the estimates relative to these simple empirical models. This indicated the useful information contained in the spectral shape of CDOM was mostly exploited. Note here, that even though the predictor terms in Equation (4) are strongly correlated, multi-collinearity does not represent an issue for predictive models. Multi-collinearity is problematic when trying to interpret the meaning of the derived parameters in the equations.

Overall, these simple empirical models provide a practical means to derive reasonably accurate estimates of TDLP₉ from CDOM absorption coefficients in coastal oceans (Figures 9, 10). A comparison of the measured and estimated TDLP₉ indicated the model retrieved TDLP₉-values that were on average within $\pm 20\%$ of the measured values (Figure 9). The % error was $< 17\%$ for half of all retrieved TDLP₉-values, and it very rarely exceeded 60%. As it is currently parameterized, the model might slightly underestimate some of the very high lignin concentrations found in rivers ($> 200 \text{ nmol L}^{-1}$). The capacity of the model to reproduce realistic distributions of TDLP₉ was also assessed for a cross-shelf section of the Middle Atlantic Bight (Figure 10). This subset of the data set was chosen because it encompassed a coastal region with a moderate gradient in TDLP₉, and included data from both surface and sub-surface waters. The

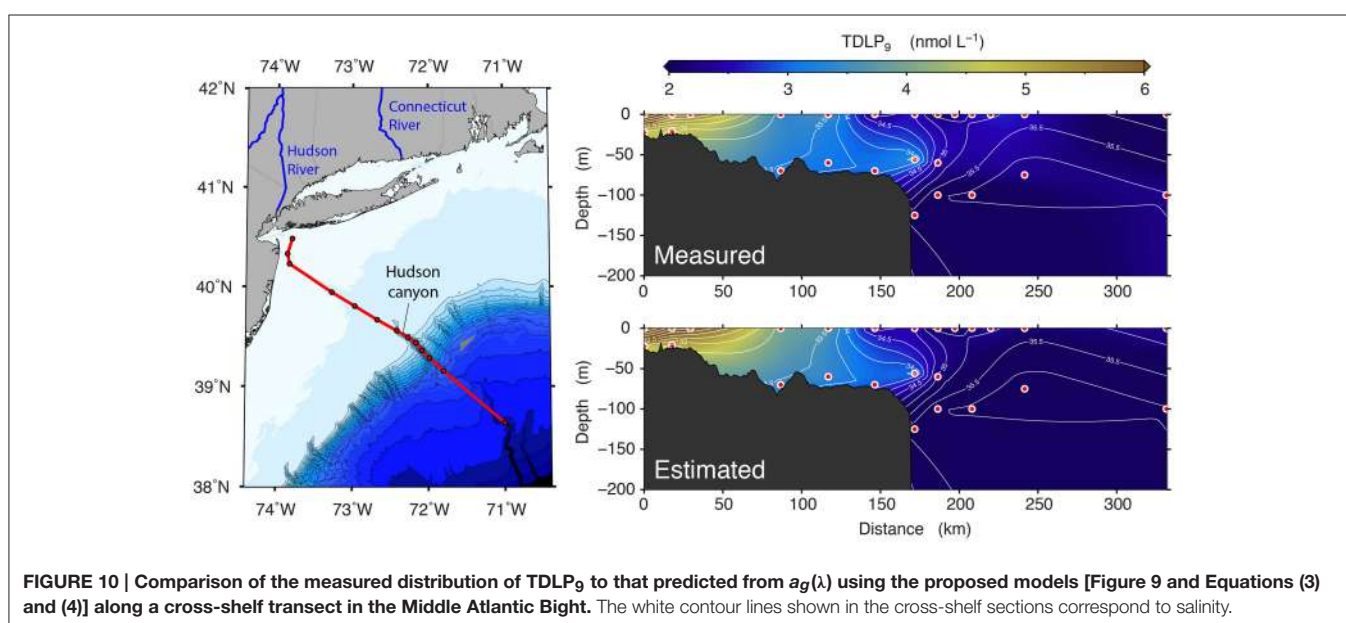


FIGURE 10 | Comparison of the measured distribution of TDLP₉ to that predicted from $a_g(\lambda)$ using the proposed models [Figure 9 and Equations (3) and (4)] along a cross-shelf transect in the Middle Atlantic Bight. The white contour lines shown in the cross-shelf sections correspond to salinity.

model adequately reproduced the most important features of the measured-TDLP₉ distribution along the salinity gradient. For instance, the cross-shelf gradient from the lignin-rich mouth of the Hudson River to the depleted open waters of the Middle Atlantic Bight was well-reproduced, just like the subsurface TDLP₉ maximum measured at the entrance of Hudson canyon. The more subtle features of the TDLP₉ distribution were less well-reproduced. The average error of $\pm 20\%$ associated with the retrievals implies that the model can only reproduce significant gradients in lignin.

The model is expected to perform similarly well in most river-influenced coastal oceans of the world, as long as the TDLP₉ predictions are made within the ranges of $a_g(\lambda)$ and TDLP₉-values used to train the model. The variety of coastal environments represented in this data set suggests the model will be suitable for most sub-tropical, temperate, and Arctic coastal oceans that receive notable inputs of terrigenous DOM. However, the performance of the model remains uncertain in coastal regions influenced by tropical rivers, as these were not represented in the training data set. More importantly, the use of the model is not recommended in major coastal upwelling systems that typically receive little terrigenous DOM inputs (e.g., California current, Benguela current). In these coastal water types, autochthonous sources of DOM are likely to exert a more dominant control on the dynamics of $a_g(\lambda)$, and the link between TDLP₉ and $a_g(\lambda)$ is likely to deviate significantly from the relationship established. Naturally, this simple model is not final, and can be very easily re-trained to improve and expand its applicability as more data become available.

AUTHOR CONTRIBUTIONS

CF, RB, KK, CL, and HO collected the *in situ* samples for CDOM and lignin analysis. CF, KK, YS, and CL processed the lignin samples, and CF, YS, CL, and RA processed the CDOM samples. CF wrote the manuscript with important discussion with RB, KK, YS, and RA and with comments from all authors.

REFERENCES

- Aiken, G. R., and Cotsaris, E. (1995). Soil and Hydrology: their effects on NOM. *J. Am. Water Work. Assoc.* 87, 36–45.
- Aiken, G. R., McKnight, D. M., Wershaw, R. L., and MacCarthy, P. (eds.). (1985). “Humic substances,” in *Soil, Sediment, and Water: Geochemistry, Isolation and Characterization* (New York, NY: John Wiley & Sons), 363–385.
- Alberts, J. J. (1982). The effect of metal ions on the ultraviolet spectra of humic acid, tannic acid and lignosulfonic acid. *Water Res.* 16, 1273–1276. doi: 10.1016/0043-1354(82)90146-4
- Amon, R. M. W., Rinehart, A. J., Duan, S., Loucheurn, P., Prokushkin, A., Guggenberger, G., et al. (2012). Dissolved organic matter sources in large Arctic rivers. *Geochim. Cosmochim. Acta* 94, 217–237. doi: 10.1016/j.gca.2012.07.015
- Benner, R., Hatcher, P. G., and Hedges, J. I. (1990). Early diagenesis of mangrove leaves in a tropical estuary: bulk chemical characterization using solid-state ¹³C NMR and elemental analyses. *Geochim. Cosmochim. Acta* 54, 2003–2013. doi: 10.1016/0016-7037(90)90268-P
- Benner, R., and Kaiser, K. (2011). Biological and photochemical transformations of amino acids and lignin phenols in riverine dissolved organic matter. *Biogeochemistry* 102, 209–222. doi: 10.1007/s10533-010-9435-4
- Benner, R., and Opsahl, S. (2001). Molecular indicators of the sources and transformations of dissolved organic matter in the Mississippi river plume. *Org. Geochem.* 32, 597–611. doi: 10.1016/S0146-6380(00)00197-2
- Benner, R., Peele, E. R., and Hodson, R. E. (1986). Microbial utilization of dissolved organic matter from leaves of the red mangrove, Rhizophora mangle, in the Fresh Creek estuary, Bahamas. *Estuar. Coast. Shelf Sci.* 23, 607–619. doi: 10.1016/0272-7714(86)90102-2
- Boyle, E. S., Guerrero, N., Thialet, A., Del Vecchio, R., and Blough, N. V. (2009). Optical properties of humic substances and CDOM: relation to structure. *Environ. Sci. Technol.* 43, 2262–2268. doi: 10.1021/es803264g
- Chapman, D. C., and Beardsley, R. C. (1989). On the origin of shelf water in the Middle Atlantic Bight. *J. Phys. Oceanogr.* 19, 384–391.

ACKNOWLEDGMENTS

Most of the data used in this study were collected during research cruises carried out as part of the following projects: (1) the Malina Scientific Program (<http://malina.obs-vlfr.fr>) funded by ANR (Agence nationale de la recherche), INSU-CNRS (Institut national des sciences de l'univers, Centre national de la recherche scientifique), CNES (Centre national d'études spatiales), and ESA (European Space Agency); (2) the Circumpolar Flaw Lead (CFL) study (http://www.ipy-api.gc.ca/pg_IPYAPI_029-eng.html) funded by the Government of Canada (IPY #96); (3) the Impacts of Climate on the Eco-Systems and Chemistry of the Arctic Pacific Environment (ICESCAPE) program (<http://www.espo.nasa.gov/icescape/>) funded by NASA (National Aeronautics and Space Administration); (4) the Nansen and Amundsen Basin Observational System (NABOS) project (<http://nabos.iarc.uaf.edu/index.php>) funded by the US-NSF (National Science Foundation), NOAA (National Oceanographic and Atmospheric Administration), the ONR (Office of Naval Research), and JAMSTEC (Japan Marine Science and Technology Center), (5) the GulfCarbon project funded by the National Science Foundation (http://ocean.otr.usm.edu/~w301130/research/gulfcarbon_new.htm), and (6) the University-National Oceanographic Laboratory System (UNOLS) 2013 chief scientist training cruise sponsored by the National Science Foundation (<https://www.unols.org/chief-scientist-training-cruise>) and supported under NSF grant OCE-1230900. The Otsuchi Bay samples were collected as part of the research program “Tohoku Ecosystem-Associated Marine Sciences” (TEAMS) of the Ministry of Education, Culture, Sports, Science and Technology (MEXT). This work was directly supported by NSF grants 0713915 and 0850653 to R.B., and NSF grants 0229302, 0425582, 0713991 to R.M.W.A. We thank the following people: the crews of the R/V Cape Hatteras, R/V Hugh Sharp, R/V Endeavor, USCGC Healy, CCGS Amundsen, and Russian icebreaker Kapitan Dranitsyn for assistance with sample collection, Dr. Jolynn Carroll for collecting the Gulf-of-Ob samples, Stephanie Smith and Sally Walker for absorbance measurements on the NABOS samples, and Steven E. Lohrenz and Wei-Jun Cai for providing berths on the GulfCarbon cruises.

- Chin, Y., Aiken, G., and O'Loughlin, E. (1994). Molecular weight, polydispersity, and spectroscopic properties of aquatic humic substances. *Environ. Sci. Technol.* 28, 1853–1858.
- Cota, G. F., Pomeroy, L. R., Harrison, W. G., Jones, E. P., Peters, F., Sheldon, W. M., et al. (1996). Nutrients, primary production and microbial heterotrophy in the southeastern Chukchi Sea: Arctic summer nutrient depletion and heterotrophy. *Mar. Ecol. Prog. Ser.* 135, 247–258. doi: 10.3354/meps135247
- Del Vecchio, R., and Blough, N. V. (2004). On the origin of the optical properties of humic substances. *Environ. Sci. Technol.* 38, 3885–3891. doi: 10.1021/es049912h
- Dittmar, T., de Rezende, C. E., Manecki, M., Niggemann, J., Coelho Ovalle, A. R., Stubbins, A., et al. (2012). Continuous flux of dissolved black carbon from a vanished tropical forest biome. *Nat. Geosci.* 5, 618–622. doi: 10.1038/ngeo1541
- Dittmar, T., and Kattner, G. (2003). The biogeochemistry of the river and shelf ecosystem of the Arctic Ocean: a review. *Mar. Chem.* 83, 103–120. doi: 10.1016/S0304-4203(03)00105-1
- Eriksson, K.-E. (2010). “Lignin Biodegradation,” in *Lignin and Lignans*, eds C. Heitner, D. R. Dimmel, and J. A. Schmidt (Boca Raton, FL: CRC Press), 495–520.
- Fichot, C. G., and Benner, R. (2011). A novel method to estimate DOC concentrations from CDOM absorption coefficients in coastal waters. *Geophys. Res. Lett.* 38:L03610. doi: 10.1029/2010gl046152
- Fichot, C. G., and Benner, R. (2012). The spectral slope coefficient of chromophoric dissolved organic matter (S275–S295) as a tracer of terrigenous dissolved organic carbon in river-influenced ocean margins. *Limnol. Oceanogr.* 57, 1453–1466. doi: 10.4319/lo.2012.57.5.1453
- Fichot, C. G., and Benner, R. (2014). The fate of terrigenous dissolved organic carbon in a river-influenced ocean margin. *Global Biogeochem. Cycles* 28, 300–318. doi: 10.1002/2013GB004670
- Fichot, C. G., Kaiser, K., Hooker, S. B., Amon, R. M. W., Babin, M., Bélanger, S., et al. (2013). Pan-Arctic distributions of continental runoff in the Arctic Ocean. *Sci. Rep.* 3, 1053. doi: 10.1038/srep01053
- Fichot, C. G., Lohrenz, S. E., and Benner, R. (2014). Pulsed, cross-shelf export of terrigenous dissolved organic carbon to the Gulf of Mexico. *J. Geophys. Res. Ocean.* 119, 1176–1194. doi: 10.1002/2013JC009424
- Fukuda, H., Ogawa, H., Sohrin, R., Yamasaki, A., and Koike, I. (2007). Sources of dissolved organic carbon and nitrogen in Otsuchi Bay on the Sanriku ria coast of Japan in the spring. *Coast. Mar. Sci.* 31, 19–29.
- Furman, G. S., and Lonsky, W. F. W. (1988a). Charge-transfer complexes in kraft lignin part 1: occurrence. *J. Wood Chem. Technol.* 8, 165–189.
- Furman, G. S., and Lonsky, W. F. W. (1988b). Charge-transfer complexes in kraft lignin part 2: contribution to color. *J. Wood Chem. Technol.* 8, 191–208.
- Goni, M. A., Monacci, N., Gisewhite, R., Crockett, J., Nittrouer, C., Ogston, A., et al. (2008). Terrigenous organic matter in sediments from the Fly River delta-clinoform system (Papua New Guinea). *J. Geophys. Res. Earth Surf.* 113. doi: 10.1029/2006jf000653
- Grebmeier, J. M. (2012). Shifting patterns of life in the Pacific Arctic and Sub-Arctic Seas. *Ann. Rev. Mar. Sci.* 4, 63–78. doi: 10.1146/annurev-marine-120710-100926
- Hedges, J. I., and Ertel, J. R. (1982). Characterization of lignin by gas capillary chromatography of cupric oxide oxidation products. *Anal. Chem.* 54, 174–178. doi: 10.1021/ac00239a007
- Hedges, J. I., Keil, R. G., and Benner, R. (1997). What happens to terrestrial organic matter in the ocean? *Org. Geochem.* 27, 195–212. doi: 10.1016/S0146-6380(97)00066-1
- Hedges, J. I., and Mann, D. C. (1979). The characterization of plant tissues by their lignin oxidation products. *Geochim. Cosmochim. Acta* 43, 1803–1807. doi: 10.1016/0016-7037(79)90028-0
- Helms, J. R., Stubbins, A., Perdue, E. M., Green, N. W., Chen, H., and Mopper, K. (2013). Photochemical bleaching of oceanic dissolved organic matter and its effect on absorption spectral slope and fluorescence. *Mar. Chem.* 155, 81–91. doi: 10.1016/j.marchem.2013.05.015
- Helms, J. R., Stubbins, A., Ritchie, J. D., Minor, E. C., Kieber, D. J., and Mopper, K. (2008). Absorption spectral slopes and slope ratios as indicators of molecular weight, source, and photobleaching of chromophoric dissolved organic matter. *Limnol. Oceanogr.* 53, 955–969. doi: 10.4319/lo.2008.53.3.0955
- Hernes, P. J., and Benner, R. (2003). Photochemical and microbial degradation of dissolved lignin phenols: Implications for the fate of terrigenous dissolved organic matter in marine environments. *J. Geophys. Res.* 108. doi: 10.1029/2002jc001421
- Hernes, P. J., and Benner, R. (2006). Terrigenous organic matter sources and reactivity in the North Atlantic Ocean and a comparison to the Arctic and Pacific oceans. *Mar. Chem.* 100, 66–79. doi: 10.1016/j.marchem.2005.11.003
- Hernes, P. J., Benner, R., Cowie, G. L., Goni, M. A., Bergamaschi, B. A., and Hedges, J. I. (2001). Tannin diagenesis in mangrove leaves from a tropical estuary: a novel molecular approach. *Geochim. Cosmochim. Acta* 65, 3109–3122. doi: 10.1016/S0016-7037(01)00641-X
- Hernes, P. J., Bergamaschi, B. A., Eckard, R. S., and Spencer, R. G. M. (2009). Fluorescence-based proxies for lignin in freshwater dissolved organic matter. *J. Geophys. Res. Biogeosci.* 114, 1–10. doi: 10.1029/2009JG000938
- Jaffé, R., Ding, Y., Niggemann, J., Vähäntalo, A. V., Stubbins, A., Spencer, R. G. M., et al. (2013). Global charcoal mobilization from soils via dissolution and riverine transport to the oceans. *Science* 340, 345–347. doi: 10.1126/science.1231476
- Kaiser, K., and Benner, R. (2012). Characterization of lignin by gas chromatography and mass spectrometry using a simplified CuO oxidation method. *Anal. Chem.* 84, 459–464. doi: 10.1021/ac202004r
- Kieber, D. J., McDaniel, J., and Mopper, K. (1989). Photochemical source of biological substrates in sea water: implications for carbon cycling. *Nature* 341, 637–639. doi: 10.1038/341637a0
- Kieber, R. J., Zhou, X., and Mopper, K. (1990). Formation of carbonyl compounds from UV-induced photodegradation of humic substances in natural waters: fate of riverine carbon in the sea. *Limnol. Oceanogr.* 35, 1503–1515. doi: 10.4319/lo.1990.35.7.1503
- Kim, S., Kaplan, L. A., Benner, R., and Hatcher, P. G. (2004). Hydrogen-deficient molecules in natural riverine water samples - Evidence for the existence of black carbon in DOM. *Mar. Chem.* 92, 225–234. doi: 10.1016/j.marchem.2004.06.042
- Kraus, T. E., Dahlgren, R. A., and Zasoski, R. J. (2003). Tannins in nutrient dynamics of forest ecosystems - a review. *Plant Soil* 256, 41–66. doi: 10.1023/A:1026206511084
- Lawrence, J. (1980). Semi-quantitative determination of fulvic acid, tannin and lignin in natural waters. *Water Res.* 14, 373–377. doi: 10.1016/0043-1354(80)90085-8
- Louchouarn, P., Opsahl, S., and Benner, R. (2000). Isolation and quantification of dissolved lignin from natural waters using solid-phase extraction and GC/MS. *Anal. Chem.* 72, 2780–2787. doi: 10.1021/ac9912552
- Maie, N., Jaffé, R., Miyoshi, T., and Childers, D. L. (2006). Quantitative and qualitative aspects of dissolved organic carbon leached from senescent plants in an oligotrophic wetland. *Biogeochemistry* 78, 285–314. doi: 10.1007/s10533-005-4329-6
- Maie, N., Pisani, O., and Jaffé, R. (2008). Mangrove tannins in aquatic ecosystems: their fate and possible influence on dissolved organic carbon and nitrogen cycling. *Limnol. Oceanogr.* 53, 160–171. doi: 10.4319/lo.2008.53.1.0160
- Mannino, A., and Harvey, H. R. (2004). Black carbon in estuarine and coastal ocean dissolved organic matter. *Limnol. Oceanogr.* 49, 735–740. doi: 10.4319/lo.2004.49.3.0735
- Martone, P. T., Estevez, J. M., Lu, F., Ruel, K., Denny, M. W., Somerville, C., et al. (2009). Discovery of lignin in seaweed reveals convergent evolution of cell-wall architecture. *Curr. Biol.* 19, 169–175. doi: 10.1016/j.cub.2008.12.031
- Medeiros, P. M., Seidel, M., Ward, N. D., Carpenter, E. J., Gomes, H. R., Niggemann, J., et al. (2015). Fate of the Amazon River dissolved organic matter in the tropical Atlantic Ocean. *Global Biogeochem. Cycles* 29:2015GB005115. doi: 10.1002/2015GB005115
- Miller, W. L., Moran, M. A., Sheldon, W. M., Zepp, R. G., and Opsahl, S. (2002). Determination of apparent quantum yield spectra for the formation of biologically labile photoproducts. *Limnol. Oceanogr.* 47, 343–352. doi: 10.4319/lo.2002.47.2.0343
- Mountain, D. G. (1991). The volume of Shelf Water in the Middle Atlantic Bight: seasonal and interannual variability, 1977–1987. *Cont. Shelf Res.* 11, 251–267. doi: 10.1016/0278-4343(91)90068-H
- Nelson, N. B., Carlson, C. A., and Steinberg, D. K. (2004). Production of chromophoric dissolved organic matter by Sargasso Sea microbes. *Mar. Chem.* 89, 273–287. doi: 10.1016/j.marchem.2004.02.017
- Opsahl, S., and Benner, R. (1995). Early diagenesis of vascular plant tissues: lignin and cutin decomposition and biogeochemical implications. *Geochim. Cosmochim. Acta* 59, 4889–4904. doi: 10.1016/0016-7037(95)00348-7

- Opsahl, S., and Benner, R. (1997). Distribution and cycling of terrigenous dissolved organic matter in the ocean. *Nature* 386, 480–482. doi: 10.1038/386480a0
- Opsahl, S., and Benner, R. (1998). Photochemical reactivity of dissolved lignin in river and ocean waters. *Limnol. Oceanogr.* 43, 1297–1304. doi: 10.4319/lo.1998.43.6.1297
- Opsahl, S., Benner, R., and Amon, R. M. W. (1999). Major flux of terrigenous dissolved organic matter through the Arctic Ocean. *Limnol. Oceanogr.* 44, 2017–2023. doi: 10.4319/lo.1999.44.8.2017
- Ortega-Retuerta, E., Frazer, T. K., Duarte, C. M., Ruiz-Halpern, S., Tovar-Sánchez, A., Arrieta, J., et al. (2009). Biogeneration of chromophoric dissolved organic matter by bacteria and krill in the Southern Ocean. *Limnol. Oceanogr.* 54, 1941–1950. doi: 10.4319/lo.2009.54.6.1941
- Osburn, C. L., and Stedmon, C. A. (2011). Linking the chemical and optical properties of dissolved organic matter in the Baltic-North Sea transition zone to differentiate three allochthonous inputs. *Mar. Chem.* 126, 281–294. doi: 10.1016/j.marchem.2011.06.007
- Palmer, M. A., van Dijken, G. L., Greg Mitchell, B., Seegers, B. J., Lowry, K. E., Mills, M. M., et al. (2013). Light and nutrient control of photosynthesis in natural phytoplankton populations from the Chukchi and Beaufort seas, Arctic Ocean. *Limnol. Oceanogr.* 58, 2185–2205. doi: 10.4319/lo.2013.58.6.2185
- Philben, M., Kaiser, K., and Benner, R. (2014). Biochemical evidence for minimal vegetation change in peatlands of the West Siberian lowland during the medieval climate anomaly and little ice age. *J. Geophys. Res. Biogeosci.* 119, 808–825. doi: 10.1002/2013JG002396
- Rochelle-Newall, E. J., and Fisher, T. R. (2002). Production of chromophoric dissolved organic matter fluorescence in marine and estuarine environments: an investigation into the role of phytoplanton. *Mar. Chem.* 77, 7–21. doi: 10.1016/S0304-4203(01)00072-X
- Russo, C., Stanziona, F., Alfè, M., Ciajolo, A., and Tregrossi, A. (2012). Spectral analysis in the UV-visible range for revealing the molecular form of combustion-generated carbonaceous species. *Combust. Sci. Technol.* 184, 1219–1231. doi: 10.1080/00102202.2012.664315
- Schiller, R. V., Kourafalou, V. H., Hogan, P., and Walker, N. D. (2011). The dynamics of the Mississippi River plume: impact of topography, wind and offshore forcing on the fate of plume waters. *J. Geophys. Res. Ocean.* 116. doi: 10.1029/2010jc006883
- Schmidt, J. (2010). “Electronic Spectroscopy of Lignins,” in *Lignin and Lignans*, eds C. Heitner, D. R. Dimmel, and J. A. Schmidt (Boca Raton, FL: CRC Press), 49–102.
- Sharpless, C. M., and Blough, N. V. (2014). The importance of charge-transfer interactions in determining chromophoric dissolved organic matter (CDOM) optical and photochemical properties. *Environ. Sci. Process. Impacts* 16, 654–671. doi: 10.1039/c3em00573a
- Shen, Y., Fichot, C. G., and Benner, R. (2012a). Dissolved organic matter composition and bioavailability reflect ecosystem productivity in the Western Arctic Ocean. *Biogeosciences* 9, 4993–5005. doi: 10.5194/bg-9-4993-2012
- Shen, Y., Fichot, C. G., and Benner, R. (2012b). Floodplain influence on dissolved organic matter composition and export from the Mississippi-Atchafalaya River system to the Gulf of Mexico. *Limnol. Oceanogr.* 57, 1149–1160. doi: 10.4319/lo.2012.57.4.1149
- Spencer, R. G. M., Aiken, G. R., Wickland, K. P., Striegl, R. G., and Hernes, P. J. (2008). Seasonal and spatial variability in dissolved organic matter quantity and composition from the Yukon River basin, Alaska. *Global Biogeochem. Cycles* 22, 1–13. doi: 10.1029/2008GB003231
- Spencer, R. G. M., Stubbins, A., Hernes, P. J., Baker, A., Mopper, K., Aufdenkampe, A. K., et al. (2009). Photochemical degradation of dissolved organic matter and dissolved lignin phenols from the Congo River. *J. Geophys. Res. Biogeosci.* 114, 1–12. doi: 10.1029/2009JG000968
- Stubbins, A., Spencer, R. G. M., Mann, P. J., Holmes, R. M., McClelland, J. W., Niggemann, J., et al. (2015). Utilizing colored dissolved organic matter to derive dissolved black carbon export by arctic rivers. *Front. Earth Sci.* 3:63. doi: 10.3389/feart.2015.00063
- Tesi, T., Semiletov, I., Hugelius, G., Dudarev, O., Kuhry, P., and Gustafsson, Ö. (2014). Composition and fate of terrigenous organic matter along the Arctic land-ocean continuum in East Siberia: insights from biomarkers and carbon isotopes. *Geochim. Cosmochim. Acta* 133, 235–256. doi: 10.1016/j.gca.2014.02.045
- Tzortziou, M., Neale, P. J., Osburn, C. L., Megonigal, J. P., Maie, N., and Jaffé, R. (2008). Tidal marshes as a source of optically and chemically distinctive colored dissolved organic matter in the Chesapeake Bay. *Limnol. Oceanogr.* 53, 148–159. doi: 10.4319/lo.2008.53.1.0148
- Walker, S. A., Amon, R. M. W., Stedmon, C., Duan, S., and Louchouarn, P. (2009). The use of PARAFAC modeling to trace terrestrial dissolved organic matter and fingerprint water masses in coastal Canadian Arctic surface waters. *J. Geophys. Res. Biogeosci.* 114, 1–12. doi: 10.1029/2009JG000990
- Weishaar, J., and Aiken, G. (2001). Evaluation of specific ultra-violet absorbance as an indicator of the chemical content of dissolved organic carbon. *Environ. Chem.* 41, 843–845. doi: 10.1021/es030360x
- Yamashita, Y., Fichot, C. G., Shen, Y., Jaffé, R., and Benner, R. (2015). Linkages among fluorescent dissolved organic matter, dissolved amino acids and lignin-derived phenols in a river-influenced ocean margin. *Front. Mar. Sci.* 2:92. doi: 10.3389/fmars.2015.00092
- Yamashita, Y., Nosaka, Y., Suzuki, K., Ogawa, H., Takahashi, K., and Saito, H. (2013). Photobleaching as a factor controlling spectral characteristics of chromophoric dissolved organic matter in open ocean. *Biogeosciences* 10, 7207–7217. doi: 10.5194/bg-10-7207-2013
- Yamashita, Y., and Tanoue, E. (2008). Production of bio-refractory fluorescent dissolved organic matter in the ocean interior. *Nat. Geosci.* 1, 579–582. doi: 10.1038/ngeo279
- Zhang, Y., van Dijk, M. A., Liu, M., Zhu, G., and Qin, B. (2009). The contribution of phytoplankton degradation to chromophoric dissolved organic matter (CDOM) in eutrophic shallow lakes: field and experimental evidence. *Water Res.* 43, 4685–4697. doi: 10.1016/j.watres.2009.07.024
- Ziolkowski, L. A., and Druffel, E. R. M. (2010). Aged black carbon identified in marine dissolved organic carbon. *Geophys. Res. Lett.* 37, 4–7. doi: 10.1029/2010GL043963

Conflict of Interest Statement: The authors declare that the research was conducted in the absence of any commercial or financial relationships that could be construed as a potential conflict of interest.

Copyright © 2016 Fichot, Benner, Kaiser, Shen, Amon, Ogawa and Lu. This is an open-access article distributed under the terms of the Creative Commons Attribution License (CC BY). The use, distribution or reproduction in other forums is permitted, provided the original author(s) or licensor are credited and that the original publication in this journal is cited, in accordance with accepted academic practice. No use, distribution or reproduction is permitted which does not comply with these terms.



Optical Proxies for Terrestrial Dissolved Organic Matter in Estuaries and Coastal Waters

Christopher L. Osburn^{1*}, Thomas J. Boyd², Michael T. Montgomery², Thomas S. Bianchi³, Richard B. Coffin⁴ and Hans W. Paerl⁵

OPEN ACCESS

Edited by:

Marta Álvarez,
Instituto Español de Oceanografía,
Spain

Reviewed by:

Claire Mahaffey,
University of Liverpool, UK
Christian Lønborg,
Australian Institute of Marine Science,
Australia
X. Antón Álvarez-Salgado,
Consejo Superior de Investigaciones
Científicas, Spain

*Correspondence:

Christopher L. Osburn
closburn@ncsu.edu

Specialty section:

This article was submitted to
Marine Biogeochemistry,
a section of the journal
Frontiers in Marine Science

Received: 04 October 2015

Accepted: 24 December 2015

Published: 20 January 2016

Citation:

Osburn CL, Boyd TJ,
Montgomery MT, Bianchi TS,
Coffin RB and Paerl HW (2016)
Optical Proxies for Terrestrial
Dissolved Organic Matter in Estuaries
and Coastal Waters.
Front. Mar. Sci. 2:127.
doi: 10.3389/fmars.2015.00127

¹ Department of Marine, Earth, and Atmospheric Sciences, North Carolina State University, Raleigh, NC, USA, ² Marine Biogeochemistry, United States Naval Research Laboratory, Washington, DC, USA, ³ Department of Geological Sciences, University of Florida, Gainesville, FL, USA, ⁴ Department of Physical and Environmental Sciences, Texas A&M University-Corpus Christi, Corpus Christi, TX, USA, ⁵ Institute of Marine Sciences, The University of North Carolina at Chapel Hill, Morehead City, NC, USA

Dissolved organic matter (DOM) absorbance and fluorescence were used as optical proxies to track terrestrial DOM fluxes through estuaries and coastal waters by comparing models developed for several coastal ecosystems. Key to using these optical properties is validating and calibrating them with chemical measurements, such as lignin-derived phenols—a proxy to quantify terrestrial DOM. Utilizing parallel factor analysis (PARAFAC), and comparing models statistically using the OpenFluor database (<http://www.openfluor.org>) we have found common, ubiquitous fluorescing components which correlate most strongly with lignin phenol concentrations in several estuarine and coastal environments. Optical proxies for lignin were computed for the following regions: Mackenzie River Estuary, Atchafalaya River Estuary (ARE), Charleston Harbor, Chesapeake Bay, and Neuse River Estuary (NRE) (all in North America). The slope of linear regression models relating CDOM absorption at 350 nm (a_{350}) to DOC and to lignin, varied 5–10-fold among systems. Where seasonal observations were available from a region, there were distinct seasonal differences in equation parameters for these optical proxies. The variability appeared to be due primarily to river flow into these estuaries and secondarily to biogeochemical cycling of DOM within them. Despite the variability, overall models using single linear regression were developed that related dissolved organic carbon (DOC) concentration to CDOM (DOC = $40 \pm 2 \times a_{350} + 138 \pm 16$; $R^2 = 0.77$; $N = 130$) and lignin (Σ_8) to CDOM ($\Sigma_8 = 2.03 \pm 0.07 \times a_{350} - 0.47 \pm 0.59$; $R^2 = 0.87$; $N = 130$). This wide variability suggested that local or regional optical models should be developed for predicting terrestrial DOM flux into coastal oceans and taken into account when upscaling to remote sensing observations and calibrations.

Keywords: CDOM absorbance, CDOM fluorescence, dissolved organic matter (DOM), lignin, carbon stable isotopes

INTRODUCTION

Terrestrial organic carbon (OC) flux from rivers and estuaries into coastal oceans is on the order of 0.2 Pg C yr^{-1} and constitutes a major part of the oceanic carbon cycle (Raymond and Spencer, 2014). Absorbing and fluorescing properties of chromophoric dissolved organic matter (CDOM) have been used to fingerprint OC sources, and often to track terrestrial DOM fluxes into the ocean (Coble, 2007). These optical properties can be used as proxies for organic matter in such instances to calibrate remote sensing observations from space and in deployed on *in situ* platforms (Mannino et al., 2008; Fichot and Benner, 2011; Etheridge et al., 2014). In particular, ultraviolet (UV) absorption has been used to quantify DOC and measure its quality (sources) (Ferrari, 2000; Stedmon et al., 2000; Helms et al., 2008; Fichot and Benner, 2011; Asmala et al., 2012).

Studies on terrestrial DOC fluxes from rivers into coastal waters rely on strong correlations between DOC and lignin (e.g., Hernes and Benner, 2003; Spencer et al., 2008; Walker et al., 2009; Fichot and Benner, 2012). In terms of estuarine and coastal ocean biogeochemistry, this work has mainly been restricted to large rivers and to delta front estuaries (Raymond and Spencer, 2014). Both CDOM and lignin have been studied widely in estuaries separately, but rarely together (e.g., Osburn and Stedmon, 2011). This paucity of information complicates an understanding of how estuarine processes modify terrestrial DOC during transport to coastal waters.

In this work, we report on an analysis of CDOM, DOC, and lignin measurements from six estuaries across North America: the Atchafalaya River, the Mackenzie River, the Chesapeake Bay, Charleston Harbor, Puget Sound, and the Neuse River Estuary (**Figure 1**). These six systems represent a wide variety of estuaries in terms of their formation, morphology, hydrology, and their geographical distributions, as well as their catchment vegetation and land use. The aim of this work is to determine efficacy of using CDOM properties to predict DOC and lignin concentration across these six estuaries. Both CDOM absorption and excitation-emission matrix (EEM) fluorescence, modeled by parallel factor analysis (PARAFAC), were evaluated. Finally, we assessed whether optical-chemical linkages that underlie coupled optics-biogeochemical models can be applied widely across different estuarine types.

METHODS

Study Sites

Six North American estuarine and coastal systems were sampled from 2003 to 2011 (**Table 1**, **Figure 1**; station coordinates, Table S1). The Atchafalaya River Estuary (ARE) is a component of the Mississippi-Atchafalaya River System (MARS) a major component of the Gulf of Mexico. This river receives diverted flow from the Mississippi River and thus reflects the Mississippi's drainage. The Chesapeake Bay (CBE) is the largest estuary in the continental United States and the largest system we studied. The CBE has multiple river inputs and is heavily impacted by urban and agricultural land use. Charleston Harbor (CHE) is a coastal plain estuary dominated by three main river inputs (Ashley, Cooper, and Wando). The Mackenzie River (MRE) is one of the

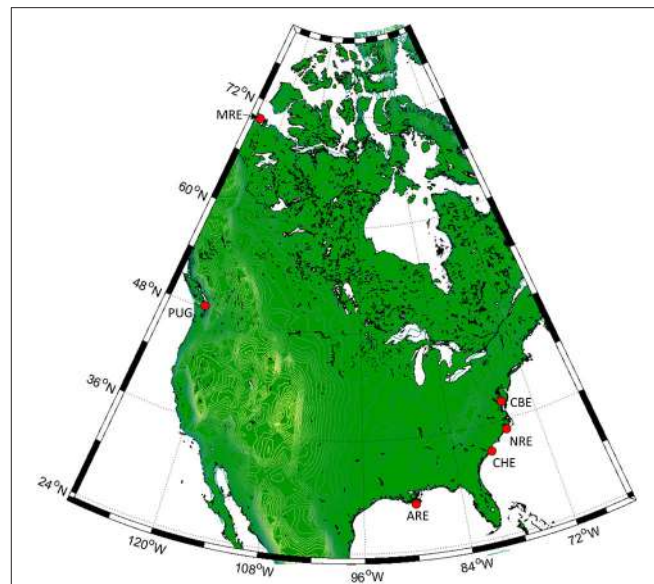


FIGURE 1 | Locations of the six North American estuaries in this study.

Clockwise from right: Chesapeake Bay (CBE), Neuse River (NRE), Charleston Harbor (CHE), Atchafalaya River (ARE), Puget Sound (PUG), and Mackenzie River (MRE).

largest rivers flowing into the Arctic Ocean and drains boreal forest and Arctic tundra. The Neuse River Estuary (NRE) drains into the largest lagoonal estuary in the United States, the Pamlico Sound. The NRE receives drainage from the lower Piedmont to Coastal Plain and, like CBE, has had chronic problems with eutrophication. Puget Sound in the Pacific Northwest region of the United States contains several deep fjords (e.g., Hood Canal) and several small rivers. In this study, we include samples from Hood Canal, the Snohomish River, and the Straits of Juan de Fuca, the latter which connect Puget Sound to the Pacific Ocean. Thus, our data set cover estuaries sampled across wide geographic and climatic regions.

There were more observations for the CBE and NRE than the other systems. Most observations came from estuarine environments although several samples came from coastal waters across the continental shelf (with the exception of Puget Sound). These seasonal samplings spanned a salinity range from 0 to 36. Thus, the data set represents a range of river influences from weak (Puget Sound) to strong (Atchafalaya and Neuse River Estuaries) and hence captures most hydrologic conditions encountered in estuaries. Only the NRE had a truly comprehensive seasonal dataset covering spring, summer, autumn, and winter. Most samples were collected from just below the water surface, though some were collected at mid-depths either by pneumatic pumps with Teflon tubing suspended at depth or by Niskin bottles. Salinity was often different for these sub-surface samples compared to their surface water counterparts so these samples were treated separately.

Two events of note for these samplings are important to mention. In July 2006, the Chesapeake Bay was sampled roughly 1 week after a period of intense summer squalls with increased freshwater discharge to the Bay. Discharge of the Bay's main tributary, the Susquehanna River, measured at Conowingo, MD,

TABLE 1 | Site description information for the estuaries and coastal waters in this study.

Location	Code	Environment	Year(s) sampled	Season	No. of samples	Notes
Atchafalaya River	ARE	Delta front estuary	2007	Spring	7	Data include the Louisiana-Texas shelf and possibly influenced by the Mississippi River
			2011	Summer	14	Data are from Bianchi et al. (2013)
Chesapeake Bay	CBE	Coastal plain estuary	2004	Spring	12	Includes observations from the Potomac River and other major river mouths in the Chesapeake Bay
				Summer	7	
			2005	Spring	15	
			2006	Summer	8	Samples collected after period of substantial rain the CBE watershed
Charleston Harbor	CHE	Coastal plain estuary	2011	Summer	4	
Mackenzie River	MRE	Delta front estuary	2003	Summer	1	CDOM and DOC data from Osburn et al. (2009)
				Autumn	1	
			2004	Spring	4	
				Summer	12	
Neuse River	NRE	Coastal plain estuary	2010	Spring	9	
				Summer	5	
				Autumn	11	
				Winter	6	
			2011	Winter	5	February only
Puget Sound	PUG	Sound	2005	Autumn	8	Data include the Snohomish River, Dabob Bay, and the Straits of Juan de Fuca

approached $11,000 \text{ m}^3 \text{ s}^{-1}$ (USGS gauge 01578310) and the Potomac River, measured near Washington, DC, approached $2300 \text{ m}^3 \text{ s}^{-1}$ (USGS gauge 01646502). Mean annual flows for each river (2000–2014) were 1184 and $346 \text{ m}^3 \text{ s}^{-1}$, respectively.

The second event occurred in the Atchafalaya River basin whereby a flooding event in May 2011 required that the Morganza Floodway near Baton Rouge, be opened for the first time in 40 years, to prevent New Orleans from being flooded. More specifically, the floodway was opened on May 14, 2011 when the Mississippi River reached a flow of over $42,000 \text{ m}^3 \text{ s}^{-1}$, the highest flow recorded since floods of 1927.

Optical Analyses

Absorbance and fluorescence were measured according to Osburn et al. (2009, 2012). Briefly, samples were filtered shipboard, refrigerated and analyzed within 3 weeks of each field effort. Absorbance (A) was measured on filtered samples, although two different filter sizes were used: $0.2 \mu\text{m}$ filters prior to 2009 and $0.7 \mu\text{m}$ filters after 2009. All samples were scanned from 200 to 800 nm against air and periodic MilliQ water blanks were scanned and subtracted from sample spectra. Samples were diluted if the absorbance in a 1-cm cell was greater than 0.4 at 240 nm. Absorbances at wavelength, λ , corrected for MilliQ water blanks were converted to Napierian absorption coefficients (a):

$$a(\lambda) = \frac{A(\lambda_{\text{sample}}) - A(\lambda_{\text{blank}})}{L} \times 2.303 \quad (1)$$

This study focused on absorption at 350 nm (a_{350}) to quantify CDOM absorption in comparison with previous work (Uher et al., 2001; Hernes and Benner, 2003; Lønborg et al., 2010; Spencer et al., 2013).

Two different fluorometers were used: a Shimadzu RFPC-5301 (samples before 2009) and a Varian Eclipse (samples after 2009). The time lag between their usages precluded intercalibration of their results, though the similarity in response to analyzing the same standards or to Raman unit scaling has been reported (Cory et al., 2010). However, data treatment for each instrument was the same. Standard corrections for lamp excitation and detector emission were applied, and afterward, corrections for the inner filter effects were applied. Scanning was performed with an excitation ranging from 250 to 450 nm (by 5 nm) and emission ranging from 300 to 600 by at 1 nm resolution. Integration time on the RFPC-5301 instrument was 0.2 s (e.g., Boyd and Osburn, 2004). On the Varian instrument, scanning was performed with an excitation range from 240 to 450 nm in 5 nm increments and an emission range of 300 – 600 nm in 2 nm increments. Integration time on the Varian instrument was 0.125 s (Osburn et al., 2012). Shimadzu fluorescence results were resized in Matlab to match with Varian results over the excitation and emission wavelength ranges. Finally, the results were calibrated first to the water Raman signal of each instrument and then in quinine sulfate units (QSU). All fluorescence data were normalized to the total integrated fluorescence in each EEM prior to PARAFAC (Murphy et al., 2013).

DOC Analysis

Dissolved organic carbon (DOC) and $\delta^{13}\text{C}$ -DOC values were measured using wet chemical oxidation coupled with isotope ratio mass spectrometry (Osburn and St-Jean, 2007). Samples were acidified with 85% H_3PO_4 in the field (if not frozen) and stored in the dark until analysis. Samples were pre-sparged with ultrapure helium to remove inorganic carbon prior to analysis. WCO-IRMS system was calibrated daily with IAEA standards of glutamic acid, sucrose, oxalic acid, and caffeine. Routine analysis of the University of Miami Deep Sea Reference DOC (DSR) for this methodology produced DOC concentrations of $45 \pm 3 \mu\text{M}$ and $\delta^{13}\text{C}$ -DOC values of $-20.5 \pm 0.4\text{\textperthousand}$ ($N = 11$ for samples before 2008 and $N = 32$ for samples after 2008). Error on DOC concentrations by this method were <3% and reproducibility on $\delta^{13}\text{C}$ -DOC values was $\pm 0.4\text{\textperthousand}$.

Dissolved Lignin Analysis

Lignin was extracted from DOM via passage over C_{18} cartridges that were either assembled in the laboratory or purchased pre-assembled (Mega Bond Elut cartridges) (Loucheuarn et al., 2000; Kaiser and Benner, 2011). Samples were eluted from C_{18} cartridges with methanol, dried and oxidized to release lignin-derived phenols into solution. Microwave oxidation was used for all samples following Goñi and Montgomery (2000), except ARE samples from 2011, which used oven oxidation (Bianchi et al., 2013). Samples were then acidified, recovery standards added, then extracted into ethyl acetate and dried prior to

storage at 4°C . Prior to analysis, samples were re-dissolved into pyridine, derivatized with BSTFA+1% TMS, and then measured via gas chromatography-mass spectrometry. Calibration curves of 8 lignin derived phenols (vanillin, acetovanillone, vanillic acid, syringaldehyde, acetosyringone, syringic acid, p-coumaric acid, and ferulic acid) were used to quantify concentrations. Detailed methods for lignin analysis can be found in Osburn and Stedmon (2011), Bianchi et al. (2013), and Dixon (2014).

Statistical Analyses

Parallel factor analysis (PARAFAC) was conducted on EEMs from all estuaries in this study using the DOMFluor toolbox for Matlab (Mathworks, Natick MA) (Stedmon and Bro, 2008). Matlab statistical toolbox (releases spanning 2003 to present) was also used for other statistical tests. R^2 -values are adjusted values and significance of regression models was tested at $\alpha = 0.05$. Principle components analysis (PCA) was conducted using the PLS_Toolbox (Eigenvector, Inc., Seattle, WA) for Matlab. Autoscaling was used on variables measured prior to PCA.

RESULTS

Summary Statistics for Each System

CDOM, DOC, lignin, and (when available) $\delta^{13}\text{C}$ -DOC data for each system are summarized as boxplots (Figure 2) and presented in its entirety (Table S1). Note that $\delta^{13}\text{C}$ -DOC values were not available for ARE in summer 2011, and for some CHE

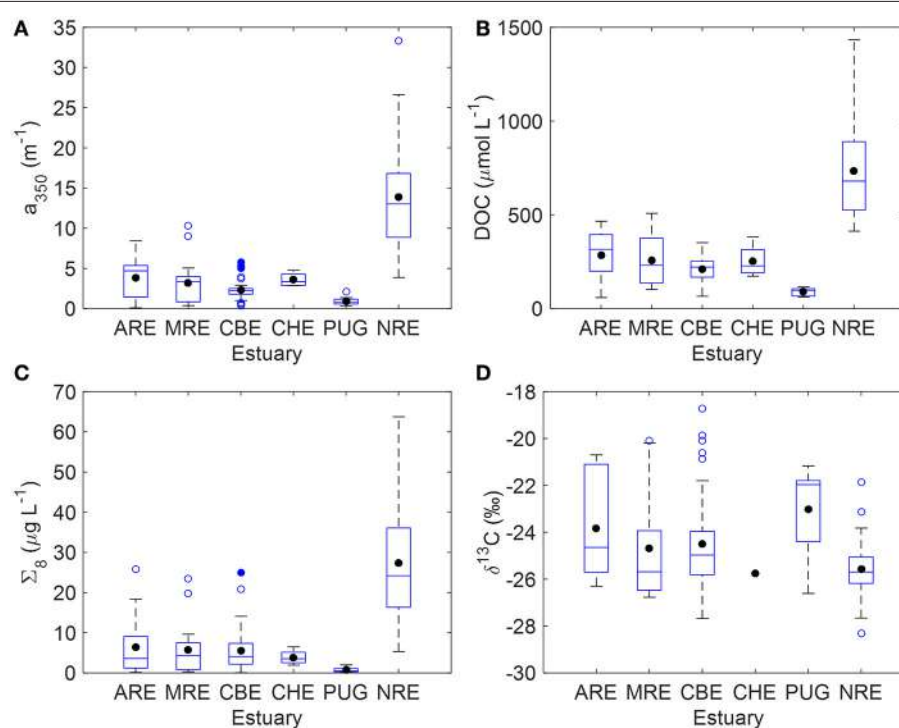


FIGURE 2 | Boxplots summarizing key variables measured for the six estuaries in this study. **(A)** CDOM absorption at 350 nm (a_{350}); **(B)** DOC concentration; **(C)** sum of 8 lignin phenols (Σ_8); **(D)** stable carbon isotope values of DOC ($\delta^{13}\text{C}$ -DOC). The blue solid line is the median and the black circle is the mean; the edges of the boxes denote the 25th and 75th percentiles, while the whiskers denote the 10th and 90th percentiles, and blue circles represent outliers.

and NRE samples. Mean CDOM absorption at 350 nm (a_{350}) was highest for NRE (13.03 m^{-1}) and lowest for Puget Sound (0.90 m^{-1}). The CBE and CHE estuaries had a_{350} values between 2 and 3 m^{-1} and the ARE and MRE estuaries had a_{350} values between 3 and 5 m^{-1} (Figure 2A). Mean DOC concentration for the NRE was $680 \mu\text{M}$ whereas for the other estuaries DOC averaged ca. $250 \mu\text{M}$ (Figure 2B). PUG DOC values were overall the lowest of the data set and averaged $90 \mu\text{M}$. The NRE also had the highest lignin concentration among the estuaries studied, with a mean Σ_8 of $24.2 \mu\text{g L}^{-1}$, while PUG again had the lowest amount of lignin (mean $\Sigma_8 = 0.8 \mu\text{g L}^{-1}$) (Figure 2C). The mean Σ_8 concentrations for CBE, CHE, ARE, and MRE ranged from 3.5 to $4.3 \mu\text{g L}^{-1}$. Both the CBE and NRE had more observations than other systems, especially CHE and PUG.

Stable carbon isotope values exhibited ranges common to estuarine environments and representing mixtures of terrestrial and planktonic organic matter (Figure 2D). Typically, riverine dissolved organic matter (DOM) values range from -26 to $-28\text{\textperthousand}$. By contrast, marine phytoplankton $\delta^{13}\text{C}$ values typically range from -22 to $-18\text{\textperthousand}$, reflecting different carbon fixation sources than land plants. Median $\delta^{13}\text{C}$ -DOC value was $-24.7 \pm 2.1\text{\textperthousand}$ which is typical of estuarine DOC (Bauer, 1997; Bianchi, 2007). Median $\delta^{13}\text{C}$ -DOC values for MRE and CBE were -24.7 and $-24.5\text{\textperthousand}$, respectively—close to median of the entire data set. Median $\delta^{13}\text{C}$ -DOC values for ARE and PUG were enriched at $-23.8\text{\textperthousand}$ and $-23.0\text{\textperthousand}$ respectively, suggesting more planktonic inputs. CHE only had one observation of $\delta^{13}\text{C}$ -DOM ($-25.8\text{\textperthousand}$). NRE had $\delta^{13}\text{C}$ -DOC values that were slightly depleted relative to the median at $-25.4\text{\textperthousand}$. Further, this system exhibited the largest range of $\delta^{13}\text{C}$ -DOC values (-22 to $-28\text{\textperthousand}$) with the most frequent value of $-26\text{\textperthousand}$.

Trends with Salinity

If coastal mixing between two end members (e.g., river and ocean) is conservative, chemical constituent concentrations plotted against salinity will exhibit a linear relationship. Deviations from conservative linear mixing are then interpreted to indicate biogeochemical cycling, for example, production or consumption of a chemical constituent or optical property. We examined trends in concentration of CDOM, DOC, and lignin against salinity for our entire dataset, considering this simple mixing scenario. For the most part, linear trends with salinity were found, even for multiple river inputs in systems such as CBE (Figure 3). NRE had the lowest salinity range (0–20) but also the largest seasonal variability probably due to the higher resolution of sampling.

Relationships Between CDOM Absorbance and Fluorescence

Many studies of CDOM and lignin have used a_{350} to quantify CDOM absorption, so this convention was used for the remainder of the study with the understanding that primary CDOM absorption is caused by conjugated systems such as aromatic rings which have peak absorption near 254 nm (Weishaar et al., 2003; Del Vecchio and Blough, 2004). We chose a_{350} following on the work of Ferrari (2000) and Hernes and Benner (2003)—some of the first reported CDOM-DOC and

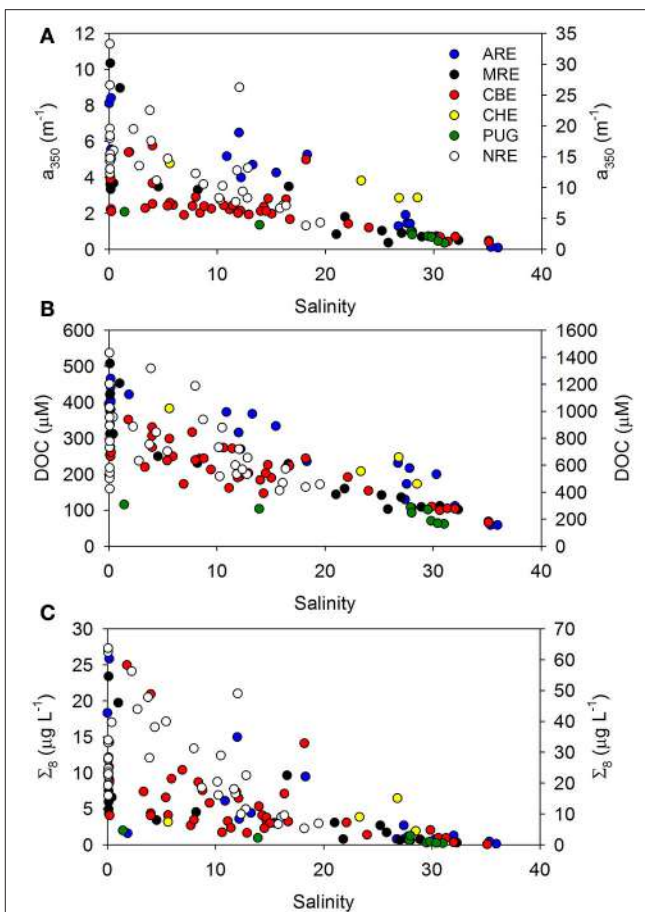


FIGURE 3 | Trends in (A) a_{350} , (B) DOC concentration, and (C) sum of 8 lignin-derived phenols (Σ_8) with salinity. Colors denote the individual points from the six estuaries studied. Neuse River estuary (NRE) samples are plotted on the right axis of each figure.

CDOM-lignin relationships for coastal waters (Baltic Sea and Mississippi River plume, respectively). CDOM concentrations at a_{254} and a_{350} were highly correlated ($R^2 = 0.96$; $P < 0.0001$; $N = 130$).

The PARAFAC model we fit to our entire dataset produced four validated components, three of which exhibited humic-like fluorescence (C1–C3) and one which was amino acid-like (C4) (Figures 4A–D). Spectra for these components are presented along with results of the split-half validation (Figure S1). These components were matched against the OpenFluor database for similarity with up to 75 PARAFAC models from a range of aquatic ecosystems including boreal lakes, small and large rivers, estuaries, coastal, and open ocean water. Component 1 (C1) had excitation (Ex) maxima of 260 and 345 nm and emission (Em) maximum of 476 nm (Figure 4A). This component closely resembles soil-derived fulvic acids (Senesi, 1990). C2 had Ex/Em maxima of 310/394 nm and this component has been surmised as originating from microbial humic substances (Coble, 1996) (Figure 4B). C3 had Ex/Em of 250/436 nm and resembles humic substances (Figure 4C). C4 had Ex/Em of 275/312 nm which is situated between the fluorescence maxima of tyrosine and

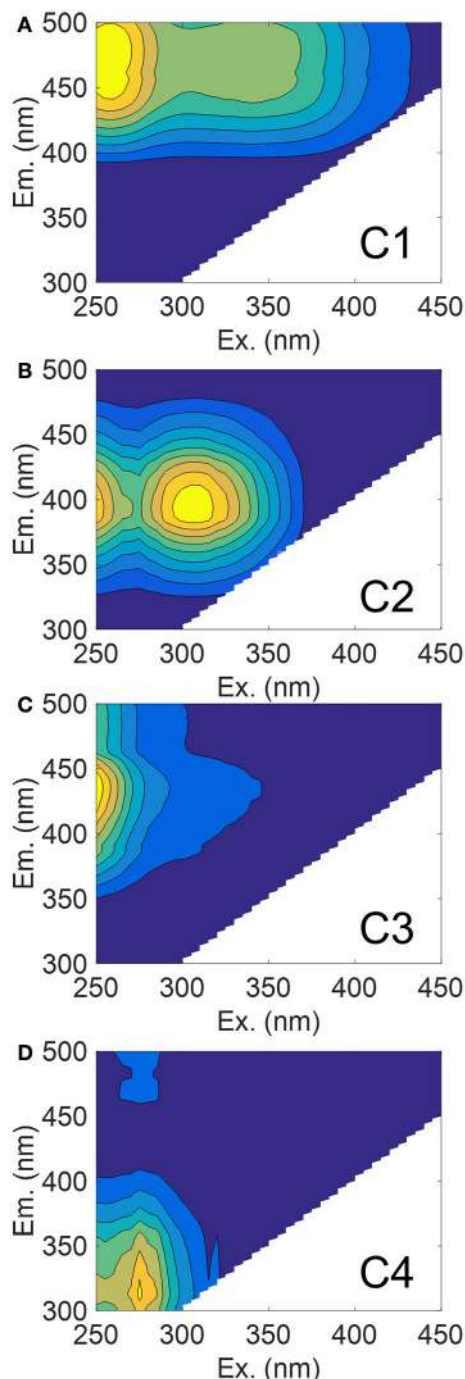


FIGURE 4 | EEM contour plots of the four PARAFAC components matched against the OpenFluor database. **(A)** C1 (soil fulvic acid); **(B)** C2 (microbial humic); **(C)** C3 (terrestrial humic); and **(D)** C4 (protein-like).

tryptophan, both of which are prevalent in natural waters (Wolfbeis, 1985; Figure 4D).

Of interest in this study were matches to our model components of those in river, estuaries, and coastal waters. Criteria for matching components were set at 95% similarity and assessed through Tucker's Congruence Coefficient via

TABLE 2 | Linear regression results between lignin concentration (Σ_8) and DOC concentration for four estuaries in this study.

Estuary	Slope	Intercept	R ²	P-value	N	Notes
ARE	17.4	69	0.99	< 0.001	7	Spring
MRE	18.2	81	0.98	0.005	4	Spring
CBE	46.6	101	0.71	< 0.001	17	2004 data
CBE	13.5	114	0.57	< 0.001	15	2005 data
CBE	8.8	143	0.84	< 0.001	8	2006 data
NRE	9.2	413	0.61	< 0.001	31	Outliers from winter and spring excluded (see text)

The linear regression equation was $DOC = \Sigma_8 \times Slope + Intercept$.

the OpenFluor database. Matches of each component with components from models in the database are also provided (Table S2). The maximum fluorescence intensity (FMax) values for C1 were most strongly corrected to a_{350} values over the entire dataset ($R^2 = 0.89$; $P < 0.001$). A stepwise multiple linear regression (MLR) was used to explore the importance of other components in explaining variation of a_{350} (data not shown). C2 was highly correlated to C1, while C3 only improved the model by <1%, which suggested their removal from the regression equation. C4 was not significant ($P = 0.126$).

Relationships Between DOC and Lignin

DOC and lignin concentrations for the six estuaries showed a positive correlation ($DOC = 17.05 \pm 1.04 \times \Sigma_8 + 175 \pm 18$; $R^2 = 0.68$; $P < 0.001$; $N = 130$) (Figure 5). Although linear, the R^2 -value of this relationship suggests that roughly 30% of DOC was not explained by lignin concentration. Seasonal variability in these estuaries, observed in plots of DOC or lignin vs. salinity (Figures 3A–C), was evident in relationships between DOC and lignin for four estuaries where there were observations during more than one season (Table 2). Linear regressions for spring samplings in ARE and MRE produced correlation coefficients, R^2 , >0.9. By contrast, CBE and NRE had much weaker correlations: $R^2 = 0.57$ –0.84 for CBE and $R^2 = 0.61$ for NRE. CBE in particular showed seasonal variability represented as three regression lines for each of 2004, 2005, and 2006 were fit to the data and had much higher correlation coefficients than did the fit to all 3 years ($R^2 = 0.35$). For NRE, a linear fit to all values produced a correlation coefficient similar to CBE ($R^2 = 0.29$). DOC values >900 μM were excluded from NRE and the regression analysis re-ran, producing a much better fit ($R^2 = 0.61$; Table 2).

DISCUSSION

Predicting DOC and Lignin Concentrations in Estuaries and Coastal Waters Using CDOM

The major aim of this study was to determine the extent to which a cross-system optical-biogeochemical model for DOM could be developed for hydrologically-variable estuaries. We

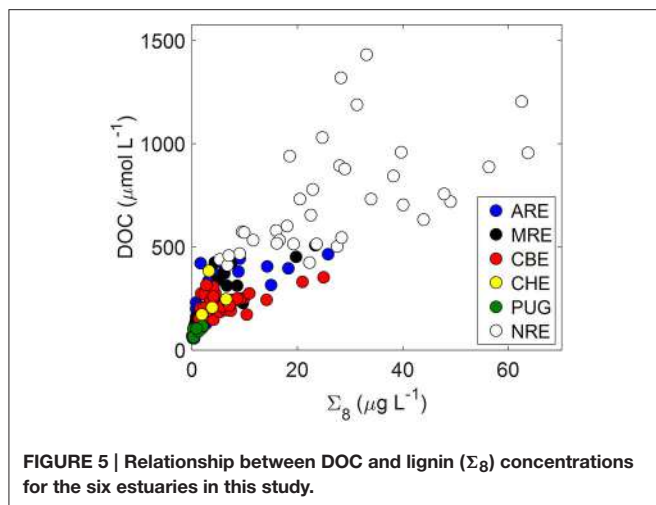


FIGURE 5 | Relationship between DOC and lignin (Σ_8) concentrations for the six estuaries in this study.

anticipated that the variability of estuarine ecosystems would complicate the robustness of one simple model to describe DOC or lignin concentrations across a gradient of estuaries and adjacent coastal waters. Using simple linear regression, we found that CDOM concentration measured at 350 nm explained greater than 70% of the variance both in DOC and dissolved lignin concentrations (Figures 6A,B). The higher correlation coefficient for the CDOM-lignin model than the CDOM-DOC model suggested that CDOM is generally terrestrial in many different estuaries. Results from the Mississippi River plume and boreal estuaries support this suggestion (e.g., Hernes and Benner, 2003; Asmala et al., 2012).

In fact, a_{350} serves as an excellent optical proxy for DOC for many estuaries as seen for North American rivers (Spencer et al., 2012). In that study, the authors showed consistent patterns of strong linear trends between a_{254} and DOC and a_{350} and DOC (see their Figure 5). That result was consistent with the linear relationship between a_{350} and DOC found for the estuaries in this study ($R^2 = 0.77$; $P < 0.001$; $N = 130$). Regression of DOC on a_{254} values produced similar results ($R^2 = 0.76$; $P < 0.001$; $N = 130$). Thus, it appears that general trends between optics and chemistry can be modeled with some certainty.

CDOM absorption at a_{350} also was an excellent proxy for lignin for the six estuaries we studied ($R^2 = 0.87$; Figure 6B). Using a_{350} , Hernes and Benner (2003) found higher R^2 -values (0.98) for the Mississippi River plume, but their model was only for one sampling in May 2000. Fichot and Benner (2012) found positive linear relationships for lignin vs. a_{350} for the Mississippi River Plume in all seasons over 2009–2010 (R^2 -values ranged from 0.89 to 0.99) and noted a seasonality in the slope coefficients for these relationships.

Intercepts of these types of regressions should be interpreted with some caution (Stedmon and Nelson, 2014). For the CDOM-DOC relationship, the y -intercept value (139 μM DOC) was significantly different from zero ($P < 0.001$). This would suggest that non-CDOM DOC in these estuaries approximates 140 μM but one must be careful in that these regressions are sensitive to seasonality and hydrology (see below discussion on seasonal and episodic variability). While Fichot and Benner found robust

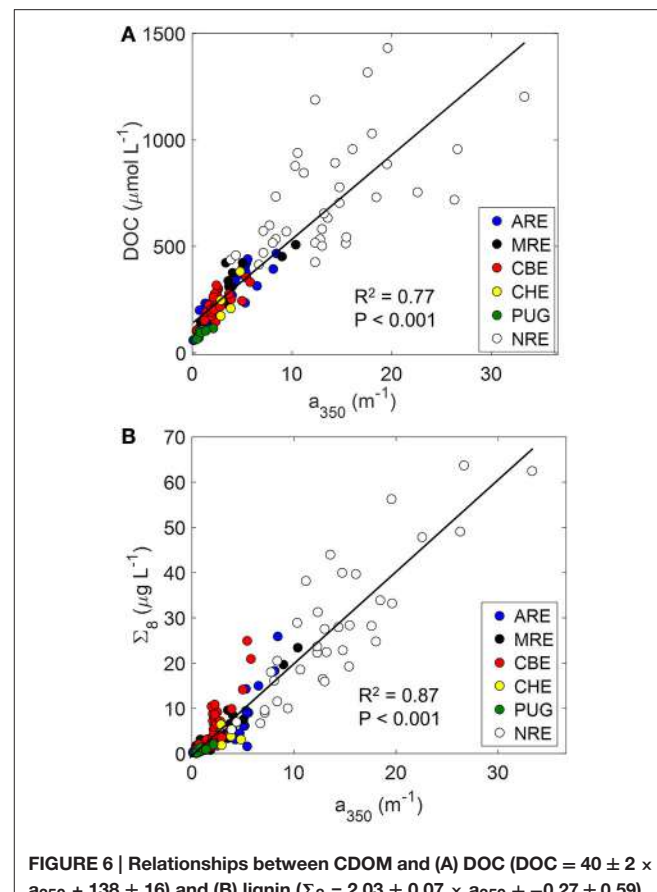


FIGURE 6 | Relationships between CDOM and (A) DOC ($\text{DOC} = 40 \pm 2 \times a_{350} + 138 \pm 16$) and (B) lignin ($\Sigma_8 = 2.03 \pm 0.07 \times a_{350} - 0.27 \pm 0.59$), linking the optics and chemistry of DOM. Regression lines are shown along with correlation coefficients for the regression.

CDOM-DOC and CDOM-lignin models for the Mississippi River plume, variability in regression statistics for CDOM-DOC models in Finnish boreal estuaries led to the suggestion that regional or sub-system models might be necessary (Asmala et al., 2012). The latter study's results were consistent with the findings for the North American estuaries in this study.

Fluorescence Indicated Dominant Influence of Terrestrial Sources of CDOM in Estuaries and Coastal Waters

Although CDOM absorption was a strong predictor for DOC and lignin, PARAFAC of EEM fluorescence provides a powerful means of characterizing DOC sources and prior work has shown good correspondence between fluorescence and lignin (Amon et al., 2003; Walker et al., 2009; Osburn and Stedmon, 2011) but also has identified planktonic fractions (Zhang et al., 2009; Romera-Castillo et al., 2011; Osburn et al., 2012). For example, a fluorescence component similar to our C3 was found to be important for predicting terrestrial DOM flux from the Baltic Sea though (Osburn and Stedmon, 2011). Combining that component with a protein-like component similar to our C4, those authors estimated terrestrial DOC flux from the Baltic Sea using multiple linear regression (MLR). Recently, Osburn

et al. (2015) applied the same fluorescence-based approach to modeling DOM dynamics in a small tidal creek system and found very strong relationships between fluorescence and DOM ($R^2 > 0.9$). Thus, we were interested in determining how this PARAFAC model, based on six estuaries (but weighted toward the CBE and NRE in terms of the numbers of samples), would perform with respect to identifying markers for terrestrial DOC (as lignin) and for planktonic DOC (as amino-acid like fluorescence, Osburn and Stedmon, 2011).

For this determination, stepwise MLR was run in a forward mode in which only positive coefficients with $P < 0.05$ were allowed to enter the model. The rationale was that to be predictive, fluorescence signals should have a positive relationships with lignin or with DOC. For lignin, we found that FMax values for C1 predicted about 82% of variability in Σ_8 values ($\Sigma_8 = -1.18 + 2.048 \times \text{FMaxC1}; P < 0.001; n = 130$). The intercept was not significant. C2 had a negative coefficient and was excluded which is sensible because this component matched with microbial humic substances. C3 was not significant in the model and C4 only increased the variance explained by about 1%. Therefore, C1 served as our terrestrial DOM marker.

C1 matched with 7 models on the OpenFluor database—all suggestive of terrestrial humic substances. This component's longwave emission properties (e.g., >450 nm) likely result from highly conjugated aromatic material and resemble isolated fulvic acids from soils and sediments (Senesi, 1990). C4 shared spectral features with 8 models on the OpenFluor database from estuarine and marine environments and, in each case, this component was attributed to protein-like or amino acid-like fluorescence. However, using partial least squares regression, Hernes et al. (2009) was able to demonstrate that fluorescence centered as Ex/Em wavelengths near our C4 was best predictive of lignin concentration. That result was not surprising given that lignin phenols originate as the fluorescent aromatic amino acid phenylalanine (Goodwin and Mercer, 1972), but does indicate the care that must be taken in calibrating fluorescence signals for prediction of chemical quantities. With this consideration in mind, we next attempted stepwise MLR to use FMax values from the PARAFAC model to predict DOC concentrations in these estuaries.

MLR produced the following model:

$$\begin{aligned} \text{DOC} = & 82.05 \times \text{FMaxC1} - 112.53 \times \text{FMaxC2} + 11.99 \times \\ & \text{FMaxC3} + 38.88 \times \text{FMaxC4} + 163.70 \end{aligned} \quad (2)$$

FMax values for all components were significant in the model ($P < 0.001$). C1 explained the most variance. The coefficient for C2 was negative, which meant that as C2 fluorescence increased, DOC concentration decreased. This result suggested consumption of DOC by bacteria, and is consistent with the removal of terrestrial DOC in estuaries by bacteria (Moran et al., 2000; Raymond and Bauer, 2000; McCallister et al., 2004). C3 and C4, while significant, were less important in terms of their explanatory power in the model. Thus, as expected, the strongest linkage between optics and chemistry in the DOM of these six estuaries of this study was due to terrestrial organic matter. Overall, the MLR model demonstrated the importance of

terrestrial organic matter as a dominant component of the DOC in these estuaries.

However, none of our four PARAFAC components matched to the Osburn and Stedmon (2011) model components which underscores the uncertainty in using fluorescence and provides a clear example of the considerations needed when using this approach. Universal models of fluorescence as a means to quantify DOC sources are likely unattainable because fluorescence properties are sensitive to biogeochemistry. For example, photodegradation is well known to cause proportionally more loss of fluorescence at longer excitation and emission wavelengths that arise from the conjugation and aromaticity that typify terrestrial CDOM sources (Boyle et al., 2009; Gonsior et al., 2009). Biodegradation, independently and in conjunction with photodegradation, can also cause a variety of spectral changes to fluorescence (Miller and Moran, 1997; Boyd and Osburn, 2004; Stedmon and Markager, 2005). Given the dynamics within and among estuaries, it is not surprising that our fluorescence results performed less well on hydrologically-variable estuaries than did those of Osburn and Stedmon (2011) which focused on one estuarine system. It is thus recommended that PARAFAC be limited to local or perhaps regional modeling of estuarine DOM.

Geographic Variability in CDOM-Lignin Relationships for Estuaries and Coastal Waters

The above discussion suggested ways in which both CDOM absorption and fluorescence could be utilized to link optical and chemical properties of estuaries and coastal waters both in terms of quantification (absorption) and estimates of DOM sources (fluorescence). PCA was then utilized to explore the optical and chemical data of these six estuaries with respect to each other (Figure 7). Ratios of syringyl lignin to vanillyl phenols (S:V) and ratio of cinnamyl to vanillyl phenols (C:V) were included in this analysis to identify plant tissue sources. FMax values for C2 were removed from the analysis because of the high correlation with C1. A 2-component PCA model explained 70% of the variance in these data.

Loadings for optical and chemical variables measured for these six estuaries showed interesting separation that supports the strong connection between CDOM and lignin in them (Figure 7A). Loadings for C1, a_{350} , DOC, and Σ_8 all clustered tightly in the lower right quadrant of the plot, closer to the PC1 axis than the PC2 axis and opposite of the loading for salinity. This result supports the concept that control of DOC and CDOM in these six estuaries was due to freshwater sources of terrestrial organic matter in rivers flowing into them. PC1 thus may be strongly tied to river flow; all CDOM, but especially C3, align with this axis.

Loadings for latitude and C:V and S:V ratios align most closely with PC2 and suggested some geographic influence on the DOM quality across these estuaries. Loadings for latitude were strongly negative on PC2 while loadings for S:V and C:V were strongly positive on PC2. This result was sensible because vegetation in lower latitudes typically has much more angiosperms than the gymnosperms that dominate boreal and Arctic environments.

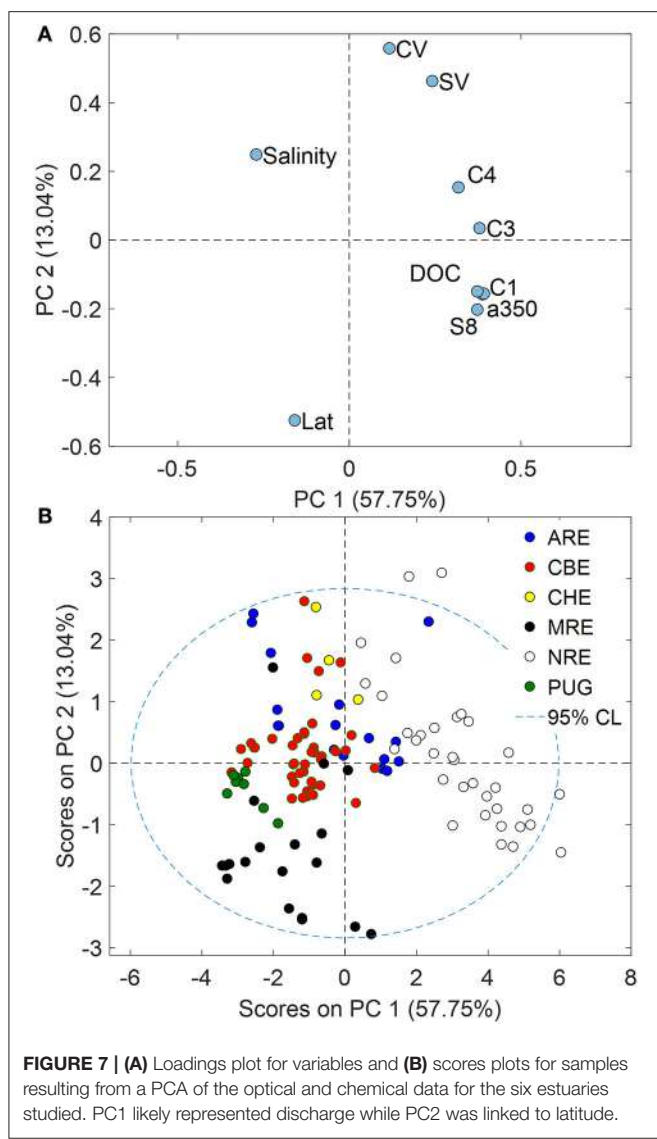


FIGURE 7 | (A) Loadings plot for variables and **(B)** scores plots for samples resulting from a PCA of the optical and chemical data for the six estuaries studied. PC1 likely represented discharge while PC2 was linked to latitude.

Lignin quality across broad geographic gradients typically is reflected in these ratios (Onstad et al., 2000; Amon et al., 2012).

Scores for our samples clearly support the trends with freshwater (PC1) and with latitude (PC2) (Figure 7B). Scores for NRE were most positive on PC1 and NRE was the most freshwater dominated estuary of those in this study, with the highest CDOM, DOC, and lignin concentrations. By contrast, MRE had the most negative scores on PC2, reflecting the dominance of lignin in NRE by conifers which are depleted in cinnamyl phenols and thus C:V ratios were near zero. Similarly, PUG scores were negative on PC2 representing the influence of mainly coniferous vegetation around the PUG and Snohomish River watersheds. However, CBE fell near the mean of the data set likely reflecting large vegetative and land use gradients in its watershed of this temperate estuary.

The PCA suggested PARAFAC provided little distinction between these estuaries, which was consistent with a recent

study of Arctic rivers (Walker et al., 2013). However, C4 fluorescence was more closely related to plant tissue type as indicated by loadings FMax values for C4, S:V, and C:V ratios that were positive both on PC1 and PC2. This could indicate that these lower latitude estuaries have more angiosperm and non-woody tissue producing this signal (Hernes et al., 2007). For example, tidal pulsing exported higher molecular weight, more aromatic and CDOM-rich marsh-derived DOC to the Rhode River sub-estuary of CBE (Tzortziou et al., 2008). Therefore, we may expect that more lignin also was exported from the marshes adjacent to the estuaries we studied. Most of our study sites were in temperate climates dominated by *Spartina* marsh plants—angiosperm grasses which would be enriched both in syringyl (S) and cinnamyl (C) phenols relative to vanillyl (V) phenols. Alternatively, these lower-latitude systems might coincidentally be more productive than the higher latitude systems. For example, one caveat to our results suggesting C4 is correlated to plant tissue type is that an unequal number of observations were made across six different systems and data for these cross-system regressions were dominated by CBE and NRE—both meso- to eutrophic estuaries (Paerl et al., 2006).

Seasonal and Episodic Variability in Optical Proxies for DOM within Specific Estuary Types

Fichot and Benner (2012) have developed remarkably consistent models relating CDOM absorption to lignin phenol concentration in surface waters from a large delta front estuary system, the Mississippi-Atchafalaya River System (MARS), of which ARE is a component. They noted seasonal variability of DOM in freshwater end members of these large river systems, and attributed most of that to seasonal variability in discharge. Asmala et al. (2012) also found substantial variability in CDOM-DOC relationships for boreal estuaries. The MARS was similar to the MRE whereas the boreal estuaries were similar to the coastal plain-type estuaries, NRE and CBE.

The strongest control on CDOM and DOC in the estuaries we studied was river flow, which contributed CDOM-rich terrestrial DOM to these estuaries and their coastal waters. This was evident because of the linear relationship between CDOM and DOC and CDOM and lignin that we found across multiple estuary types (Figures 6A,B). For the CDOM-lignin relationship, the y-intercept value ($-0.50 \mu\text{g L}^{-1}$) was not significantly different from zero ($P = 0.503$). This result suggested that the vast majority of CDOM in these estuaries originated from terrestrial sources. CDOM absorption at wavelengths $>300 \text{ nm}$ is primarily due to conjugated molecules such as lignin (Del Vecchio and Blough, 2004). Therefore, it makes sense that in estuaries and coastal waters where rivers and coastal wetlands contribute DOM, this material will be highly conjugated and chromophoric (Raymond and Spencer, 2014).

Variable hydrologic regimes are well known to influence concentrations and relationships of CDOM, DOC and lignin in rivers and this certainly appears the case in many estuaries (Hernes et al., 2008; Saraceno et al., 2009; Spencer et al., 2010).

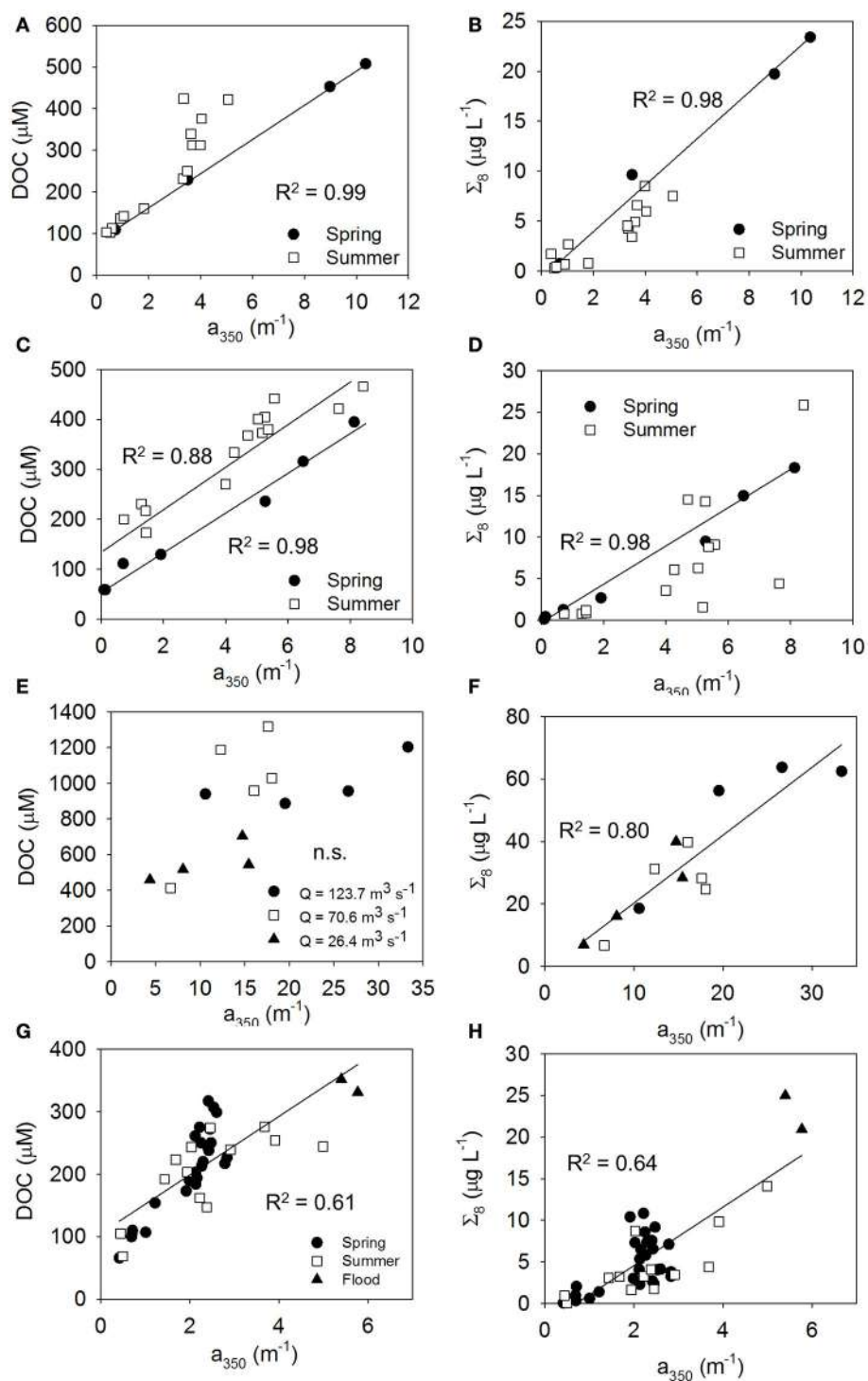


FIGURE 8 | Relationships between CDOM and DOC (left column of panels A, C, E, and G) and lignin (right column of panels B, D, F, and H) linking the optics and chemistry of DOM, influenced by hydrologic variability. (A,B) MRE showing influence of spring freshet, (C,D) ARE showing influence of 2011 Mississippi River flood, (E,F) NRE showing seasonal influence of river discharge, and (G,H) CBE showing the influence of heavy rains in summer 2006. Significant linear regressions are shown while slope and intercept values and regression statistics are in Table 3. For (F–H), the regressions were fit to all of the data.

For example, both CDOM and DOC doubled in concentration during the flushing hydroperiod of the tropical Epulu River (NE Congo) compared to the post-flush period, while Σ_8 values

tripled (Spencer et al., 2010). Discharge values for the major rivers flowing into the MRE, ARE, NRE, and CBE are listed in Table S3.

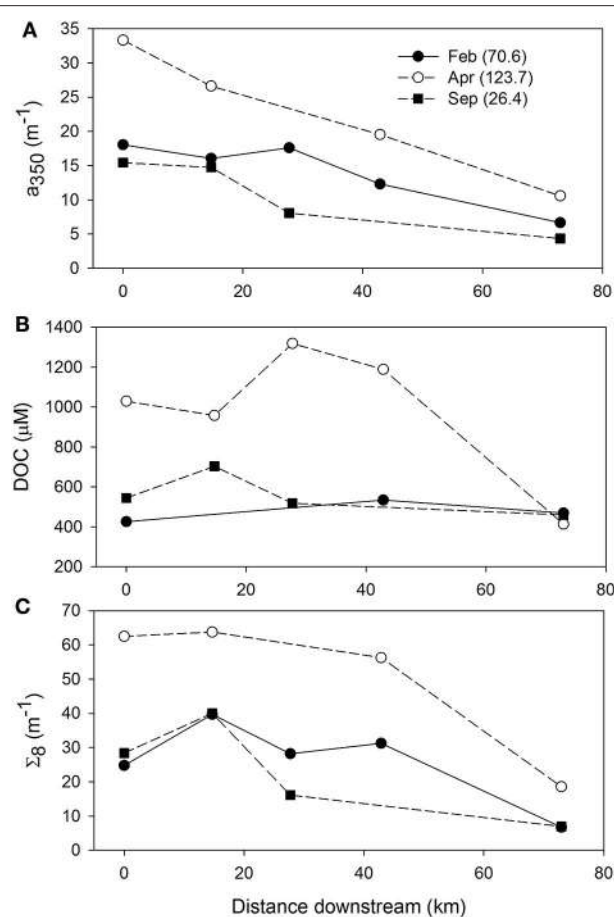


FIGURE 9 | Within system variability of (A) CDOM absorption at a_{350} , (B) DOC concentration, and (C) lignin concentration for the meso-eutrophic Neuse River Estuary. Values in parentheses for each month are the mean discharge at Ft. Barnwell, NC (USGS Station 02091814) for the 7 days preceding the date of sampling.

We found corroborating evidence of hydrologic variability in optical-biogeochemical models within estuaries for ARE, MRE, CBE, and NRE that was seasonal and episodic (Figures 8A–H). We do not extend our analysis of relationships beyond linear regression models as Fichot and Benner (2012) have done for DOC-normalized results; rather, we focus on the basic CDOM, DOC, and lignin measurements that can be used in a first order optical algorithm for satellite retrievals of properties related to ocean color (Mannino et al., 2008; Tehrani et al., 2013). These are expressed as either DOC or Σ_8 as a function of a_{350} . Further, some concern about collinearity of the Fichot and Benner models has been raised (Asmala et al., 2012). Our subsequent analysis of seasonal trends exclude CHE and PUG for which we have too few observations.

For MRE, spring and summer distinctions were clear in the relationships between CDOM and DOC or CDOM and lignin that coincided with the spring flush of freshwater from Arctic rivers (Table 3 and Table S3). For example, in MRE, far more CDOM, DOC, and lignin were found in June just after the freshet as opposed to late August when the river had returned to base flow (Figures 8A,B). This pattern is common of Arctic rivers

which deliver the majority of DOM during the freshet (Amon et al., 2012). Larger concentrations of Σ_8 during spring indicates that this also is the case for ARE. Spring meltwaters in the upper Midwest US might similarly create a freshwater pulse leading to high discharge of the entire Mississippi-Atchafalaya system as suggested by the results of Fichot and Benner (2012). Therefore, in LDEs the large river flow forcing in these systems could exhibit seasonally predictable patterns.

In contrast to ARE and MRE, which are both large delta front estuaries that extend well into coastal waters, NRE is a smaller, microtidal system with a long residence time between 20 and 120 days (Pinckney et al., 1998). However, like ARE and MRE, NRE is heavily riverine influenced, though this estuary exhibited a 3-fold range in CDOM, DOC, and lignin concentrations at the freshwater end member (Figure 3; Table S1). Variability of the NRE data around the regression line describing the general CDOM-DOC relationship we found for the estuaries in this study was the greatest and suggested some change in either the source or quality of DOM entering the NRE annually (Figure 6A).

The influence of discharge on CDOM, DOC, and lignin patterns across the NRE was further investigated (Figures 9A–C). River discharge (Q) to the NRE at Ft. Barnwell, NC, (USGS Gauging Station 02091814) was averaged for the 7 days prior to the sampling date on which the observations were made (Table S3). It was clear that high river flow contributed more CDOM, DOC, and lignin into the NRE than at lower flow. At lower flows ($Q = 26\text{--}70 \text{ m}^3 \text{ s}^{-1}$) CDOM decreased downstream but DOC and lignin were rather constant. This pattern changed substantially when $Q = 123.7 \text{ m}^3 \text{ s}^{-1}$ at Ft. Barnwell and concentrations of CDOM in the NRE doubled whereas concentrations of DOC and lignin nearly tripled. Thus, it is not surprising that the NRE data, which were collected roughly monthly over a 12-month period, captured the variability in high and low flow regimes. The change in DOM quality was somewhat larger than the load of terrestrial DOM as evidenced by the higher R^2 -value of the CDOM-lignin relationship as opposed to the CDOM-DOC relationship (Figures 6A,B).

In addition to seasonal variability, we had two examples of episodic loadings of terrestrial DOM into estuaries from high periods of rainfall that also contributed to deviations from general trends found in this study. In summer 2011, a flood in the Mississippi River basin delivered historically higher amounts of DOC to the coastal Gulf of Mexico (Bianchi et al., 2013). This resulted in large amounts of CDOM and lignin, as well (Figures 8C,D). Overall DOC concentrations were higher, illustrating how climatic events can perhaps increase the transfer of terrestrial DOC to coastal waters (Table 3). Other work in the northern Gulf of Mexico has shown that coastal marshes are a significant source of dissolved lignin to the estuaries and very shallow inner shelf regions (Bianchi et al., 2009), but not likely to the broader shelf areas (Fichot et al., 2014). Coastal marsh DOM could be mobilized as well during storm events. Large loads of terrestrial DOM have been shown to be delivered to the NRE by its watershed during tropical storms (Pael et al., 1998; Osburn et al., 2012).

In June 2006, summer squalls produced heavy rainfall in the mid-Atlantic United States, leading to 6- to 10-fold higher river discharges to the CBE (Table S3). We had two observations each

TABLE 3 | Parameter estimates (Est.) for linear regression models (DOC or $\Sigma_8 = m \times a_{350} + b$).

Estuary	Season	DOC	Est.	SE	adj R ²	P-value	Σ_8	Est.	SE	adj R ²	P-value
MRE	Spring	b	82	2	0.99	<0.001	b	0.22	1.27	0.98	0.881
MRE	Spring	m	41	1		<0.001	m	2.24	0.18		0.006
MRE	Summer	b	68	25	0.84	0.017	b	-0.21	0.65	0.79	0.751
MRE	Summer	m	69	8		<0.001	m	1.55	0.22		<0.001
ARE	Spring	b	59	11	0.98	<0.001	b	-0.52	0.62	0.98	0.442
ARE	Spring	m	39	2		<0.001	m	2.24	0.14		<0.001
ARE	Summer	b	181	35	0.87	<0.001	b	-0.74	3.04	0.37	0.813
ARE	Summer	m	29	3		<0.001	m	1.49	0.63		0.013
NRE	Spring, Summer, Autumn	b	477	153	0.35	0.010	b	-1.46	5.48	0.80	0.795
NRE	Spring, Summer, Autumn	m	24	9		0.019	m	2.17	0.31		<0.001
NRE	All	b	403	88	0.32	<0.001	b	-1.79	3.15	0.74	<0.001
NRE	All	m	24	6		<0.001	m	2.10	0.21		<0.001
CBE	Spring	b	44	20	0.74	0.034	b	-0.19	1.53	0.29	0.900
CBE	Spring	m	81	9		<0.001	m	2.47	0.72		0.002
CBE	Summer	b	117	27	0.49	0.001	b	-1.29	1.49	0.61	0.406
CBE	Summer	m	36	10		0.005	m	2.47	0.56		0.001
CBE	All	b	105	15	0.61	<0.001	b	-2.47	1.04	0.64	0.02
CBE	All	m	46	6		<0.001	m	3.51	0.41		<0.001

"SE" is the standard error of the regression parameter, "adj R²" is the adjusted correlation coefficient for the regression. "All" means the regression was carried out for all season (NRE and CBE only).

of CDOM, DOC, and lignin in the Potomac River, a sub-estuary of CBE, to provide a contrast of terrestrial DOM inputs between spring and summer (**Figures 8G,H**). These observations are titled "Flood" **Figures 8G,H** and demonstrate proportionally higher amounts of CDOM per unit DOC and lignin, respectively. These observations underscore the higher CDOM, DOC, and lignin values observed in the freshwater inputs to CBE (**Figures 3A–C**).

Finally, episodic variability in CDOM-DOC relationships for some estuaries could be linked to autotrophic sources of DOM within estuaries. NRE and CBE experience periodic, yet chronic, eutrophication caused by excessive nitrogen loading from their watersheds (Paerl et al., 2006; Paerl, 2009). Primary production from algae can add DOC to the estuary but not lignin. Phytoplankton-derived, and microbially-transformed, sources of CDOM have been documented for many estuaries and coastal waters though uncertainty in the magnitude of this source exists (Stedmon and Markager, 2005; Romera-Castillo et al., 2011; Osburn et al., 2012; Stedmon and Nelson, 2014). Spring and autumn blooms in NRE could explain why intercepts of seasonal regression models for DOC vs. a_{350} were often larger than in summer and winter (**Table 3**; Pinckney et al., 1998). Estuarine systems in which long residence time allows for substantial primary production can add a planktonic component to the overall estuarine CDOM signal (Fellman et al., 2011; Osburn et al., 2012). Evidence of this phenomenon likely explains the NRE results which were the most variable of estuaries studied here. Intertidal production of DOC is probably low in this microtidal estuary, but was observed in the Gironde estuary, which also has internal production of CDOM, further complicating optical-biogeochemical models (Abril et al., 2002; Huguet et al., 2009). Together, for NRE, these effects caused a disruption of classic binary mixing between river and seawater

that underlay the robust CDOM-DOC and CDOM-lignin relationships found by Fichot and Benner (2012) for the MARS.

Similar to NRE, the CBE exhibited large seasonal variability in CDOM-DOC and CDOM-lignin relationships. Direct evidence of phytoplankton production of CDOM in the Chesapeake Bay has been less well documented (Rochelle-Newall and Fisher, 2002). CBE also has multiple sub-estuaries flowing into it and rivers of these sub-estuaries have 50–80% more DOC than the Susquehanna River, which is the main tributary to CBE (Raymond and Bauer, 2000). Thus, it was not surprising that seasonal and interannual variability were also important to this estuary. We lacked sufficient observations from the Potomac River and York River estuaries, which comprise large amounts of flow to the lower CBE. A focus on these systems might improve the overall picture with respect to CDOM, DOC, and lignin dynamics in the CBE as well as parse out commonalities among eutrophic estuaries in contrast to LDEs.

CONCLUSIONS

This work has narrowed the knowledge gap between CDOM-DOC and CDOM-lignin relationships that have been developed for large rivers and coastal waters by focusing specifically on estuaries, which are notoriously heterogeneous. We found that both DOC and lignin can be quantified with CDOM absorption with roughly 75% certainty across several estuary types. CDOM fluorescence suggested that the dominant source of CDOM in the estuaries and coastal waters we studied was terrestrial inputs. Hydrologic variability in river flow appeared to be the dominant control on the linkage of CDOM and DOC we observed in these estuaries—and showed the major influence of terrestrial DOM. High river flow contributed more CDOM and lignin. Low river

flow and longer residence time within the estuary allowed for planktonic contributions to DOM. Much of the variability in DOM quality likely is explained by the history of this material in the soil organic matter pool and any subsequent biogeochemical processing across the terrestrial-marine continuum (Marín-Spiotta et al., 2014).

It was beyond the scope of this study to compute yields of terrestrial (or planktonic) DOC from these estuaries, but the models developed may be scaled to remote sensing platforms in space and *in situ* observatories (e.g., Mannino et al., 2008; Etheridge et al., 2014; Osburn et al., 2015). Wide variability in the models among these estuaries thus suggested that local or regional models should be developed for prediction of terrestrial DOM fluxes into the coastal ocean using optical properties. A one size fits all approach is not appropriate for estuaries collectively, but possible for classes of estuaries (e.g., large delta front vs. coastal plain) (Asmala et al., 2012). Upscaling to remotely sensed observations are entirely possible yet must require optimization of basic equations based on calibration and validation data sets. Results from such work will continue to spur new questions, hopefully integrating other disciplines, such as meteorology and climatology, and ultimately leading to a greater understanding of organic matter sources and cycling in coastal waters.

AUTHOR CONTRIBUTIONS

CO conceived of this manuscript, analyzed data, and lead the writing. TB provided data analysis, co-wrote, and assisted in data collection. MM and RC co-wrote and assisted in data collection. TB and HP contributed data and co-wrote.

REFERENCES

- Abrial, G., Nogueira, M., Etcheber, H., Cabeçadas, G., Lemaire, E., and Brogueira, M. J. (2002). Behaviour of organic carbon in nine contrasting European estuaries. *Estuar. Coast. Shelf Sci.* 54, 241–262. doi: 10.1006/ecss.2001.0844
- Amon, R. M. W., Budéus, G., and Meon, B. (2003). Dissolved organic carbon distribution and origin in the Nordic Seas: exchanges with the Arctic Ocean and the North Atlantic. *J. Geophys. Res.* 108, 3221. doi: 10.1029/2002jc001594
- Amon, R. M. W., Rinehart, A. J., Duan, S., Louchouarn, P., Prokushkin, A., Guggenberger, G., et al. (2012). Dissolved organic matter sources in large Arctic rivers. *Geochim. Cosmochim. Acta* 94, 217–237. doi: 10.1016/j.gca.2012.07.015
- Asmala, E., Stedmon, C. A., and Thomas, D. N. (2012). Linking CDOM spectral absorption to dissolved organic carbon concentrations and loadings in boreal estuaries. *Estuar. Coast. Shelf Sci.* 111, 107–117. doi: 10.1016/j.ecss.2012.06.015
- Bauer, J. E. (1997). “Carbon isotopic composition of DOM,” in *Biogeochemistry of Marine Dissolved Organic Matter, 1st Edn.*, eds D. A. Hansell and C. A. Carlson (Cambridge: Academic Press), 405–453.
- Bianchi, T. S. (2007). *Biogeochemistry of Estuaries*. New York, NY: Oxford University Press.
- Bianchi, T. S., DiMarco, S. F., Smith, R. W., and Schreiner, K. M. (2009). A gradient of dissolved organic carbon and lignin from Terrebonne-Timbalier Bay Estuary to the Louisiana Shelf (USA). *Mar. Chem.* 117, 32–41. doi: 10.1016/j.marchem.2009.07.010
- Bianchi, T. S., Garcia-Tigreros, F., Yvon-Lewis, S. A., Shields, M., Mills, H. J., Butman, D., et al. (2013). Enhanced transfer of terrestrially derived carbon to the atmosphere in a flooding event. *Geophys. Res. Lett.* 40, 116–122. doi: 10.1029/2012GL054145
- Boyd, T. J., and Osburn, C. L. (2004). Changes in CDOM fluorescence from allochthonous and autochthonous sources during tidal mixing and bacterial degradation in two coastal estuaries. *Mar. Chem.* 89, 189–210. doi: 10.1016/j.marchem.2004.02.012
- Boyle, E. S., Guerriero, N., Thiallet, A., Del Vecchio, R., and Blough, N. V. (2009). Optical properties of humic substances and CDOM: relation to structure. *Environ. Sci. Technol.* 43, 2262–2268. doi: 10.1021/es803264g
- Coble, P. G. (1996). Characterization of marine and terrestrial DOM in seawater using excitation emission matrix spectroscopy. *Mar. Chem.* 51, 325–346. doi: 10.1016/0304-4203(95)00062-3
- Coble, P. G. (2007). Marine optical biogeochemistry: the chemistry of ocean color. *Chem. Rev.* 107, 402–418. doi: 10.1021/cr050350+
- Cory, R. M., Miller, M. P., McKnight, D. M., Guerard, J. J., and Miller, P. L. (2010). Effect of instrument-specific response on the analysis of fulvic acid fluorescence spectra. *Limnol. Oceanogr. Methods* 8, 67–78. doi: 10.4319/lom.2010.8.00067
- Del Vecchio, R., and Blough, N. V. (2004). On the origin of the optical properties of humic substances. *Environ. Sci. Technol.* 38, 3885–3891. doi: 10.1021/es049912h
- Dixon, J. L. (2014). *Seasonal Changes in Estuarine Dissolved Organic Matter Due to Variations in Discharge, Flushing Times and Wind-driven Mixing Events*. Ph.D. thesis, North Carolina State University.
- Etheridge, J. R., Birgand, F., Osborne, J. A., Osburn, C. L., Burchell, M. R., and Irving, J. (2014). Using *in situ* ultraviolet–visual spectroscopy to measure nitrogen, carbon, phosphorus, and suspended solids concentrations at a high frequency in a brackish tidal marsh. *Limnol. Oceanogr. Methods* 12, 10–22. doi: 10.4319/lom.2014.12.10

FUNDING

The following agencies are thanked for their financial support: Strategic Environmental Research and Development Program, ER-1431 and ER-2124 (MM, CO); North Carolina Department of Environment and Natural Resources, Contracts #4443 and #5371 (HP, CO); and the Lower Neuse Basin Association (HP).

ACKNOWLEDGMENTS

We thank the following people for technical support during the field and laboratory work done for this study: Tiffanie Donowick, Erin Kelley, Jeff Denzel, Mike Shields, Lauren Handsel, and Jennifer Dixon. Special thanks to Warwick Vincent for logistical support for the Mackenzie River Estuary sampling. We also thank the captains and crews of the following vessels that were used to assemble this data set: RV *Cape Henlopen*, RV *John Sharp*, RV *Cape Hatteras*, RV *Barnes*, CCGS *Nahidik*, and RV *Pelican*. The following agencies are thanked for their financial support: Office of Naval Research (CO, TB, RC), Strategic Environmental Research and Development Program (MM, CO), NASA (CO, TB), and National Science Foundation Ecosystems Studies Program project 1119704 (HP), and the NC Dept. of Environment and Natural Resources-Lower Neuse Basin Association (HP, CO).

SUPPLEMENTARY MATERIAL

The Supplementary Material for this article can be found online at: <http://journal.frontiersin.org/article/10.3389/fmars.2015.00127>

- Fellman, J. B., Petrone, K. C., and Grierson, P. F. (2011). Source, biogeochemical cycling, and fluorescence characteristics of dissolved organic matter in an agro-urban estuary. *Limnol. Oceanogr.* 56, 243–256. doi: 10.4319/lo.2011.56.1.0243
- Ferrari, G. M. (2000). The relationship between chromophoric dissolved organic matter and dissolved organic carbon in the European Atlantic coastal area and in the West Mediterranean Sea (Gulf of Lions). *Mar. Chem.* 70, 339–357. doi: 10.1016/S0304-4203(00)00036-0
- Fichot, C. G., and Benner, R. (2011). A novel method to estimate DOC concentrations from CDOM absorption coefficients in coastal waters. *Geophys. Res. Lett.* 38:L03610. doi: 10.1029/2010GL046152
- Fichot, C. G., and Benner, R. (2012). The spectral slope coefficient of chromophoric dissolved organic matter (S275–295) as a tracer of terrigenous dissolved organic carbon in river-influenced ocean margins. *Limnol. Oceanogr.* 57, 1453–1466. doi: 10.4319/lo.2012.57.5.1453
- Fichot, C. G., Lohrenz, S. E., and Benner, R. (2014). Pulsed, cross-shelf export of terrigenous dissolved organic carbon to the Gulf of Mexico. *J. Geophys. Res. Oceans* 119, 1176–1194. doi: 10.1002/2013jc009424
- Góñi, M. A., and Montgomery, S. (2000). Alkaline CuO oxidation with a microwave digestion system: lignin analyses of geochemical samples. *Anal. Chem.* 72, 3116–3121. doi: 10.1021/ac991316w
- Gonsior, M., Peake, B. M., Cooper, W. T., Podgorski, D., D'Andrilli, J., and Cooper, W. J. (2009). Photochemically induced changes in dissolved organic matter identified by ultrahigh resolution Fourier transform ion cyclotron resonance mass spectrometry. *Environ. Sci. Technol.* 43, 698–703. doi: 10.1021/es8022804
- Goodwin, T. W., and Mercer, E. I. (1972). *Introduction to Plant Biochemistry*. New York, NY: Pergamon Press.
- Helms, J. R., Stubbins, A., Ritchie, J. D., Minor, E. C., Kieber, D. J., and Mopper, K. (2008). Absorption spectral slopes and slope ratios as indicators of molecular weight, source, and photobleaching of chromophoric dissolved organic matter. *Limnol. Oceanogr.* 53:955. doi: 10.4319/lo.2008.53.3.0955
- Hernes, P. J., and Benner, R. (2003). Photochemical and microbial degradation of dissolved lignin phenols: implications for the fate of terrigenous dissolved organic matter in marine environments. *J. Geophys. Res.* 108. doi: 10.1029/2002JC001421
- Hernes, P. J., Bergamaschi, B. A., Eckard, R. S., and Spencer, R. G. M. (2009). Fluorescence-based proxies for lignin in freshwater dissolved organic matter. *J. Geophys. Res.* 114, G00F03. doi: 10.1029/2009JG000938
- Hernes, P. J., Robinson, A. C., and Aufdenkampe, A. K. (2007). Fractionation of lignin during leaching and sorption and implications for organic matter "freshness." *Geophys. Res. Lett.* 34, L17401. doi: 10.1029/2007GL031017
- Hernes, P. J., Spencer, R. G., Dyda, R. Y., Pellerin, B. A., Bachand, P. A., and Bergamaschi, B. A. (2008). The role of hydrologic regimes on dissolved organic carbon composition in an agricultural watershed. *Geochim. Cosmochim. Acta* 72, 5266–5277. doi: 10.1016/j.gca.2008.07.031
- Huguet, A., Vacher, L., Relexans, S., Saubusse, S., Froidefond, J. M., and Parlanti, E. (2009). Properties of fluorescent dissolved organic matter in the Gironde Estuary. *Org. Geochem.* 40, 706–719. doi: 10.1016/j.orggeochem.2009.03.002
- Kaiser, K., and Benner, R. (2011). Characterization of lignin by gas chromatography and mass spectrometry using a simplified CuO oxidation method. *Anal. Chem.* 84, 459–464. doi: 10.1021/ac202004r
- Lønborg, C., Álvarez-Salgado, X. A., Davidson, K., Martínez-García, S., and Teira, E. (2010). Assessing the microbial bioavailability and degradation rate constants of dissolved organic matter by fluorescence spectroscopy in the coastal upwelling system of the Ría de Vigo. *Mar. Chem.* 119, 121–129. doi: 10.1016/j.marchem.2010.02.001
- Louchouarn, P., Opsahl, S., and Benner, R. (2000). Isolation and quantification of dissolved lignin from natural waters using solid-phase extraction and GC/MS. *Anal. Chem.* 72, 2780–2787. doi: 10.1021/ac9912552
- Mannino, A., Russ, M. E., and Hooker, S. B. (2008). Algorithm development and validation for satellite-derived distributions of DOC and CDOM in the US Middle Atlantic Bight. *J. Geophys. Res. Oceans* (1978–2012) 113, C07051. doi: 10.1029/2007JC004493
- Marín-Spiotta, E., Gruley, K. E., Crawford, J., Atkinson, E. E., Miesel, J. R., Greene, S., et al. (2014). Paradigm shifts in soil organic matter research affect interpretations of aquatic carbon cycling: transcending disciplinary and ecosystem boundaries. *Biogeochemistry* 117, 279–297. doi: 10.1007/s10533-013-9949-7
- McCallister, S. L., Bauer, J. E., Cherrier, J. E., and Ducklow, H. W. (2004). Assessing sources and ages of organic matter supporting river and estuarine bacterial production: a multiple-isotope ($\Delta^{14}\text{C}$, $\delta^{13}\text{C}$, and $\delta^{15}\text{N}$) approach. *Limnol. Oceanogr.* 49, 1687–1702. doi: 10.4319/lo.2004.49.5.1687
- Miller, W. L., and Moran, M. A. (1997). Interaction of photochemical and microbial processes in the degradation of refractory dissolved organic matter from a coastal marine environment. *Limnol. Oceanogr.* 42, 1317–1324. doi: 10.4319/lo.1997.42.6.1317
- Moran, M. A., Sheldon, W. M., and Zepp, R. G. (2000). Carbon loss and optical property changes during long-term photochemical and biological degradation of estuarine dissolved organic matter. *Limnol. Oceanogr.* 45, 1254–1264. doi: 10.4319/lo.2000.45.6.1254
- Murphy, K. R., Stedmon, C. A., Graeber, D., and Bro, R. (2013). Fluorescence spectroscopy and multi-way techniques. *PARAFAC. Anal. Methods* 5, 6557–6566. doi: 10.1039/c3ay41160e
- Onstad, G. D., Canfield, D. E., Quay, P. D., and Hedges, J. I. (2000). Sources of particulate organic matter in rivers from the continental USA: lignin phenol and stable carbon isotope compositions. *Geochim. Cosmochim. Acta* 64, 3539–3546. doi: 10.1016/S0016-7037(00)00451-8
- Osburn, C. L., Handsel, L. T., Mikan, M. P., Paerl, H. W., and Montgomery, M. T. (2012). Fluorescence tracking of dissolved and particulate organic matter quality in a river-dominated estuary. *Environ. Sci. Technol.* 46, 8628–8636. doi: 10.1021/es3007723
- Osburn, C. L., Mikan, M. P., Etheridge, J. R., Burchell, M. R., and Birgand, F. (2015). Seasonal variation in the quality of dissolved and particulate organic matter exchanged between a salt marsh and its adjacent estuary. *J. Geophys. Res. Biogeosci.* 120, 1430–1449. doi: 10.1002/2014jg002897
- Osburn, C. L., Retamal, L., and Vincent, W. F. (2009). Photoreactivity of chromophoric dissolved organic matter transported by the Mackenzie River to the Beaufort Sea. *Mar. Chem.* 115, 10–20. doi: 10.1016/j.marchem.2009.05.003
- Osburn, C. L., and Stedmon, C. A. (2011). Linking the chemical and optical properties of dissolved organic matter in the Baltic–North Sea transition zone to differentiate three allochthonous inputs. *Mar. Chem.* 126, 281–294. doi: 10.1016/j.marchem.2011.06.007
- Osburn, C. L., and St-Jean, G. (2007). The use of wet chemical oxidation with high-amplification isotope ratio mass spectrometry (WCO–IRMS) to measure stable isotope values of dissolved organic carbon in seawater. *Limnol. Oceanogr. Methods* 5, 296–308. doi: 10.4319/lom.2007.5.296
- Paerl, H. W. (2009). Controlling eutrophication along the freshwater-marine continuum: dual nutrient (N and P) reductions are essential. *Estuar. Coast.* 32, 593–601. doi: 10.1007/s12237-009-9158-8
- Paerl, H. W., Pinckney, J. L., Fear, J. M., and Peierls, B. L. (1998). Ecosystem responses to internal and watershed organic matter loading: consequences for hypoxia in the eutrophying Neuse River Estuary, North Carolina, USA. *Mar. Ecol. Prog. Ser.* 166:17. doi: 10.3354/meps166017
- Paerl, H. W., Valdes, L. M., Peierls, B. L., Adolf, J. E., and Harding, L. Jr. (2006). Anthropogenic and climatic influences on the eutrophication of large estuarine ecosystems. *Limnol. Oceanogr.* 51, 448–462. doi: 10.4319/lo.2006.51.1_part_2.0448
- Pinckney, J. L., Paerl, H. W., Harrington, M. B., and Howe, K. E. (1998). Annual cycles of phytoplankton community-structure and bloom dynamics in the Neuse River Estuary, North Carolina. *Mar. Biol.* 131, 371–381. doi: 10.1007/s002270050330
- Raymond, P. A., and Bauer, J. E. (2000). Bacterial consumption of DOC during transport through a temperate estuary. *Aquat. Microb. Ecol.* 22, 1–12. doi: 10.3354/ame022001
- Raymond, P. A., and Spencer, R. G. M. (2014). "Riverine DOM," in *Biogeochemistry of Marine Dissolved Organic Matter*, 2nd Edn., eds D. A. Hansell and C. A. Carlson (Cambridge, MA: Academic Press), 509–535.
- Rochelle-Newall, E. J., and Fisher, T. R. (2002). Chromophoric dissolved organic matter and dissolved organic carbon in Chesapeake Bay. *Mar. Chem.* 77, 23–41. doi: 10.1016/S0304-4203(01)00073-1
- Romera-Castillo, C., Sarmento, H., Álvarez-Salgado, X. A., Gasol, J. M., and Marrasé, C. (2011). Net production and consumption of fluorescent colored dissolved organic matter by natural bacterial assemblages growing on marine phytoplankton exudates. *Appl. Environ. Microbiol.* 77, 7490–7498. doi: 10.1128/AEM.00200-11

- Saraceno, J. F., Pellerin, B. A., Downing, B. D., Boss, E., Bachand, P. A. M., and Bergamaschi, B. A. (2009). High-frequency *in situ* optical measurements during a storm event: assessing relationships between dissolved organic matter, sediment concentrations, and hydrologic processes. *J. Geophys. Res.* 114:G00F09. doi: 10.1029/2009JG000989
- Senesi, N. (1990). Molecular and quantitative aspects of the chemistry of fulvic acid and its interactions with metal ions and organic chemicals. 2. The fluorescence spectroscopy approach. *Anal. Chim. Acta* 232, 77–106. doi: 10.1016/S0003-2670(00)81226-X
- Spencer, R. G., Aiken, G. R., Dornblaser, M. M., Butler, K. D., Holmes, R. M., Fiske, G., et al. (2013). Chromophoric dissolved organic matter export from US rivers. *Geophys. Res. Lett.* 40, 1575–1579. doi: 10.1002/grl.50357
- Spencer, R. G. M., Aiken, G. R., Wickland, K. P., Striegl, R. G. and Hernes, P. J. (2008). Seasonal and spatial variability in dissolved organic matter quantity and composition from the Yukon River basin, Alaska. *Glob. Biogeochem. Cycles* 22, doi: 10.1029/2008GB003231
- Spencer, R. G., Butler, K. D., and Aiken, G. R. (2012). Dissolved organic carbon and chromophoric dissolved organic matter properties of rivers in the USA. *J. Geophys. Res. Biogeosci.* (2005–2012) 117. doi: 10.1029/2011jg001928
- Spencer, R. G., Hernes, P. J., Ruf, R., Baker, A., Dyda, R. Y., Stubbins, A., et al. (2010). Temporal controls on dissolved organic matter and lignin biogeochemistry in a pristine tropical river, Democratic Republic of Congo. *J. Geophys. Res. Biogeosci.* (2005–2012) 115, G03013. doi: 10.1029/2009JG001180
- Stedmon, C. A., and Bro, R. (2008). Characterizing dissolved organic matter fluorescence with parallel factor analysis: a tutorial. *Limnol. Oceanogr. Methods* 6, 572–579. doi: 10.4319/lom.2008.6.572
- Stedmon, C. A., and Markager, S. (2005). Tracing the production and degradation of autochthonous fractions of dissolved organic matter by fluorescence analysis. *Limnol. Oceanogr.* 50, 1415–1426. doi: 10.4319/lo.2005.50.5.1415
- Stedmon, C. A., Markager, S., and Kaas, H. (2000). Optical properties and signatures of chromophoric dissolved organic matter (CDOM) in Danish coastal waters. *Estuar. Coast. Shelf Sci.* 51, 267–278. doi: 10.1006/ecss.2000.0645
- Stedmon, C. A., and Nelson, N. B. (2014). “The optical properties of DOM in the ocean,” in *Biogeochemistry of Marine Dissolved Organic Matter*, 2nd Edn., eds D. A. Hansell and C. A. Carlson (Cambridge, MA: Academic Press), 509–535.
- Tehrani, N. C., D'Sa, E. J., Osburn, C. L., Bianchi, T. S., and Schaeffer, B. A. (2013). Chromophoric dissolved organic matter and dissolved organic carbon from sea-viewing wide field-of-view sensor (SeaWiFS), Moderate Resolution Imaging Spectroradiometer (MODIS) and MERIS Sensors: case study for the Northern Gulf of Mexico. *Remote Sens.* 5, 1439–1464. doi: 10.3390/rs5031439
- Tzortziou, M., Neale, P. J., Osburn, C. L., Megonigal, J. P., Mate, N., and Jaffé, R. (2008). Tidal marshes as a source of optically and chemically distinctive colored dissolved organic matter in the Chesapeake Bay. *Limnol. Oceanogr.* 53, 148–159. doi: 10.4319/lo.2008.53.1.0148
- Uher, G., Hughes, C., Henry, G., and Upstill-Goddard, R. C. (2001). Non-conservative mixing behavior of colored dissolved organic matter in a humic-rich, turbid estuary. *Geophys. Res. Lett.* 28, 3309–3312. doi: 10.1029/2000GL012509
- Walker, S. A., Amon, R. M. W., Stedmon, C., Duan, S., and Louchouarn, P. (2009). The use of PARAFAC modeling to trace terrestrial dissolved organic matter and fingerprint water masses in coastal Canadian Arctic surface waters. *J. Geophys. Res.* 114:G00F06. doi: 10.1029/2009JG000990
- Walker, S. A., Amon, R. M., and Stedmon, C. A. (2013). Variations in high-latitude riverine fluorescent dissolved organic matter: a comparison of large Arctic rivers. *J. Geophys. Res. Biogeosci.* 118, 1689–1702. doi: 10.1002/2013JG002320
- Weishaar, J. L., Aiken, G. R., Bergamaschi, B. A., Fram, M. S., Fujii, R., and Mopper, K. (2003). Evaluation of specific ultraviolet absorbance as an indicator of the chemical composition and reactivity of dissolved organic carbon. *Environ. Sci. Technol.* 37, 4702–4708. doi: 10.1021/es030360x
- Wolfbeis, O. S. (1985). “The fluorescence of organic natural products,” in *Molecular Luminescence Spectroscopy: Part I: Methods and Applications*, ed S. G. Schulman (New York, NY: Wiley), 167–370.
- Zhang, Y., van Dijk, M. A., Liu, M., Zhu, G., and Qin, B. (2009). The contribution of phytoplankton degradation to chromophoric dissolved organic matter (CDOM) in eutrophic shallow lakes: field and experimental evidence. *Water Res.* 43, 4685–4697. doi: 10.1016/j.watres.2009.07.024

Conflict of Interest Statement: The authors declare that the research was conducted in the absence of any commercial or financial relationships that could be construed as a potential conflict of interest.

Copyright © 2016 Osburn, Boyd, Montgomery, Bianchi, Coffin and Paerl. This is an open-access article distributed under the terms of the Creative Commons Attribution License (CC BY). The use, distribution or reproduction in other forums is permitted, provided the original author(s) or licensor are credited and that the original publication in this journal is cited, in accordance with accepted academic practice. No use, distribution or reproduction is permitted which does not comply with these terms.



Linkages among fluorescent dissolved organic matter, dissolved amino acids and lignin-derived phenols in a river-influenced ocean margin

Youhei Yamashita^{1*}, Cédric G. Fichot^{2†}, Yuan Shen², Rudolf Jaffé³ and Ronald Benner^{2,4}

¹ Faculty of Environmental and Earth Science, Hokkaido University, Sapporo, Japan, ² Marine Science Program, University of South Carolina, Columbia, SC, USA, ³ Southeast Environmental Research Center, Department of Chemistry and Biochemistry, Florida International University, Miami, FL, USA, ⁴ Department of Biological Sciences, University of South Carolina, Columbia, SC, USA

OPEN ACCESS

Edited by:

Christopher Osburn,
North Carolina State University, USA

Reviewed by:

Christian Lønborg,
Australian Institute of Marine Science,
Australia
Robert Spencer,
Woods Hole Research Center, USA

*Correspondence:

Youhei Yamashita
yamashiy@ees.hokudai.ac.jp

†Present Address:

Cédric G. Fichot,
Jet Propulsion Laboratory, California
Institute of Technology, Pasadena,
USA

Specialty section:

This article was submitted to
Marine Biogeochemistry,
a section of the journal
Frontiers in Marine Science

Received: 05 August 2015

Accepted: 19 October 2015

Published: 05 November 2015

Citation:

Yamashita Y, Fichot CG, Shen Y, Jaffé R and Benner R (2015) Linkages among fluorescent dissolved organic matter, dissolved amino acids and lignin-derived phenols in a river-influenced ocean margin. *Front. Mar. Sci.* 2:92.
doi: 10.3389/fmars.2015.00092

Excitation emission matrix (EEM) fluorescence spectroscopy coupled with parallel factor analysis (PARAFAC) is commonly used to investigate the dynamics of dissolved organic matter (DOM). However, a lack of direct comparisons with known biomolecules makes it difficult to substantiate the molecular composition of specific fluorescent components. Here, coincident surface-water measurements of EEMs, dissolved lignin, and total dissolved amino acids (TDAA) acquired in the northern Gulf of Mexico were used to investigate the relationships between specific fluorescent components and DOM biomolecules. Two terrestrial humic-like components identified by EEM-PARAFAC using samples obtained from river to offshore waters were strongly linearly correlated with dissolved lignin concentrations. In addition, changes in terrestrial humic-like abundance were correlated with those in lignin phenol composition, suggesting such components are largely derived from lignin and its alteration products. By applying EEM-PARAFAC to offshore samples, two protein-like components were obtained. The tryptophan-like component was strongly correlated with TDAA concentrations, corroborating the suggested protein/peptide origin of this component. The ratios of tryptophan-like component to tyrosine-like component or dissolved organic carbon (DOC) concentrations were also correlated with DOC-normalized yields of TDAA, suggesting these proxies are useful indicators of the bioavailability of DOM in marine waters of the studied ecosystem.

Keywords: fluorescent dissolved organic matter, excitation-emission matrix, parallel factor analysis, lignin phenols, amino acids, northern Gulf of Mexico

INTRODUCTION

In natural waters, a fraction of dissolved organic matter (DOM, <0.2–0.7 μm pore-size filter) absorbs light (chromophoric DOM, CDOM), and a component of this light-absorbing fraction fluoresces (fluorescent DOM, FDOM) (Stedmon and Nelson, 2015). In the 1990s, Coble et al. (1990) introduced excitation emission matrix (EEM) spectroscopy as a means to characterize

the fluorescence features of FDOM. The fluorescence properties of FDOM were categorized into three humic-like and two protein-like fluorophores (Coble, 1996). Although Coble's categorization has been well accepted and widely used in qualitative studies of FDOM composition, recent chemometric techniques for characterizing EEMs have enabled more quantitative evaluations of FDOM composition (Stedmon et al., 2003; Boehme et al., 2004; Murphy et al., 2014). Parallel factor analysis (PARAFAC) enables to decompose an EEM into statistically independent fluorescent components (Stedmon et al., 2003). This technique is often applied to gain insights about the environmental dynamics of these different fluorescent components (e.g., Cory and McKnight, 2005; Yamashita and Jaffé, 2008; Yamashita et al., 2008; Jaffé et al., 2014).

Despite the popularity of PARAFAC, there is still a severe lack of direct evidence linking PARAFAC fluorescent components to molecularly characterized organic molecules in DOM. Lignins (Hernes et al., 2009) and tannins (Maie et al., 2007) are measurable components in DOM that are thought to be important contributors to the humic-like fluorescence. Aromatic amino acids (Yamashita and Tanoue, 2003a) and phenolic structures (Maie et al., 2007; Stedmon and Nelson, 2015) within macromolecules such as lignins and tannins are potential contributors to the protein-like fluorescence. Tannins are highly reactive (Maie et al., 2006, 2008), thereby suggesting that lignins and aromatic amino acids are the major contributors to the humic-like and protein-like fluorescence, respectively.

Previous investigations relating PARAFAC components and major organic compounds have yielded inconsistent results. Walker et al. (2009) found linear relationships between terrestrial humic-like PARAFAC components and lignin phenol concentrations in the Canadian Archipelago and Beaufort Sea surface waters. Similar observations were made in the Baltic–North Sea transition zone (Osburn and Stedmon, 2011). In contrast, no significant correlation was found between any of the PARAFAC components and lignin concentrations within the Sacramento River/San Joaquin River Delta (Hernes et al., 2009). More recently, Walker et al. (2013) noted that there is no universal linear relationship between terrestrial humic-like PARAFAC components and lignin phenol concentrations among large Arctic rivers, and attributed it to microbial processing. Thus, it appears that both source and biogeochemical processing are important factors affecting the relationship between humic-like fluorophores and lignin concentrations.

A strong correlation between tyrosine-like and tryptophan-like fluorescence intensity in EEMs, and tyrosine and tryptophan concentration was found in samples from Ise Bay to offshore waters of the Kuroshio current (Yamashita and Tanoue, 2003a). Similar correlations were found in a vertical profile from Sagami Bay (Yamashita and Tanoue, 2004). These results indicated that protein-like fluorescence was derived from aromatic amino acids (e.g., tyrosine and tryptophan) in marine environments. Yamashita and Tanoue (2003a) also found that protein-like fluorescence intensities were linearly correlated with concentrations of total dissolved amino acids (TDAA), suggesting that protein-like fluorescence can be a useful indicator of TDAA concentration. In addition, relationships between the

relative contribution (%) of protein-like PARAFAC components in total PARAFAC components and the biodegradable fraction (%) of dissolved organic carbon (DOC) were found in freshwater environments (Balcarczyk et al., 2009; Fellman et al., 2009; Hood et al., 2009). A correlation between degradation rates of protein-like fluorescence intensity and DOC was also observed in coastal environments (Lønborg et al., 2010). Since carbon-normalized yields of amino acids are known to be useful molecular indicators of biodegradable DOM (Davis and Benner, 2007; Benner and Kaiser, 2011), the linkage between bioavailable protein-like components and amino acids in DOM has been assumed based on empirical evidence.

Although the number of studies directly comparing DOM fluorescence and chemical composition remains limited, FDOM research performed over the past 15 years suggests that humic-like and protein-like fluorescence can be used as proxies for lignin and amino acids concentrations in DOM, respectively. If this is correct, FDOM and its corresponding organic molecules should change not only quantitatively but also qualitatively with biogeochemical processing. For example, the compositions of humic-like FDOM and lignin phenols are known to change with sunlight irradiation (e.g., Opsahl and Benner, 1998; Stedmon and Markager, 2005), and composition of protein-like FDOM and amino acid parameters (carbon-normalized yields of amino acids) co-vary with microbial processing (e.g., Davis and Benner, 2005; Cory and Kaplan, 2012). However, direct compositional comparisons between FDOM and its molecular constituents have scarcely been evaluated (Hernes et al., 2009). Thus, establishing compositional as well as quantitative relationships between FDOM and corresponding biomolecules is needed for the application of FDOM as proxies of lignin and amino acid concentrations and as indicators of bioavailability and photodegradability of DOM.

Here, we investigated how fluorescent components determined by PARAFAC were related to the concentrations and compositions of lignin phenols and amino acids in surface waters of the northern Gulf of Mexico (NGoM), the largest river-influenced ocean margin in North America. We assessed whether terrestrial humic-like and protein-like fluorescence can be used as valid proxies for the concentrations of total dissolved lignin phenols and amino acids, respectively. In addition, compositional comparisons between FDOM components and molecular parameters derived from lignin phenols and amino acids were investigated.

MATERIALS AND METHODS

Study Area and Sampling

Field samples and measurements were collected during four research cruises conducted in the northern Gulf of Mexico (NGoM) in April, July, and October–November 2009 and March 2010 (Fichot and Benner, 2012, 2014; Fichot et al., 2014). The NGoM is among the world's largest river-influenced ocean margins, where the Mississippi and Atchafalaya Rivers discharge about $6.6 \times 10^{11} \text{ m}^3 \text{ yr}^{-1}$ of freshwater and 2.70 Tg yr^{-1} of DOC into the margin (Shen et al., 2012).

Surface-water samples for DOC, CDOM, EEM-PARAFAC, and TDAA analyses were collected at about 50 stations during each cruise (**Figure 1** and **Table 1**). Samples for DOC and TDAA analysis were gravity filtered from Niskin bottles using precombusted GF/F filters (0.7- μm pore size) and stored frozen (-20°C) immediately after collection in precombusted borosilicate glass vials. Samples for CDOM and EEMs analysis were gravity filtered from Niskin bottles using Whatman Polycap Aqueous Solution (AS) cartridges (0.2- μm pore size), collected in precombusted borosilicate glass vials, and stored immediately at 4°C until analysis in the laboratory. Samples for dissolved lignin analysis were collected at 20–23 of the ~50 stations during each cruise (**Table 1**).

Most samples were collected under well-mixed conditions from Niskin bottles mounted on a rosette with a conductivity-temperature-depth sensor. Samples were collected with a

polypropylene bucket from the bow of the ship wherever a strong vertical salinity gradient was observed (e.g., river plume). Steep vertical salinity gradients like the ones often observed in the Mississippi River plume can be retained inside a Niskin bottle. The bucket sampling was therefore used to avoid any inconsistency that would result when collecting multiple samples from the same Niskin bottle. A total set of 198 samples for DOC/EEMs/CDOM/TDAA was collected along with a set of 86 dissolved lignin samples. The samples spanned a salinity range of 0–37, from nutrient-rich riverine waters to oligotrophic marine waters, and were collected during contrasting seasons and environmental conditions in terms of salinity, water temperature, and river discharge (**Table 1**). This data set is representative of the majority of water types and environmental conditions typically encountered in this river-influenced ocean margin.

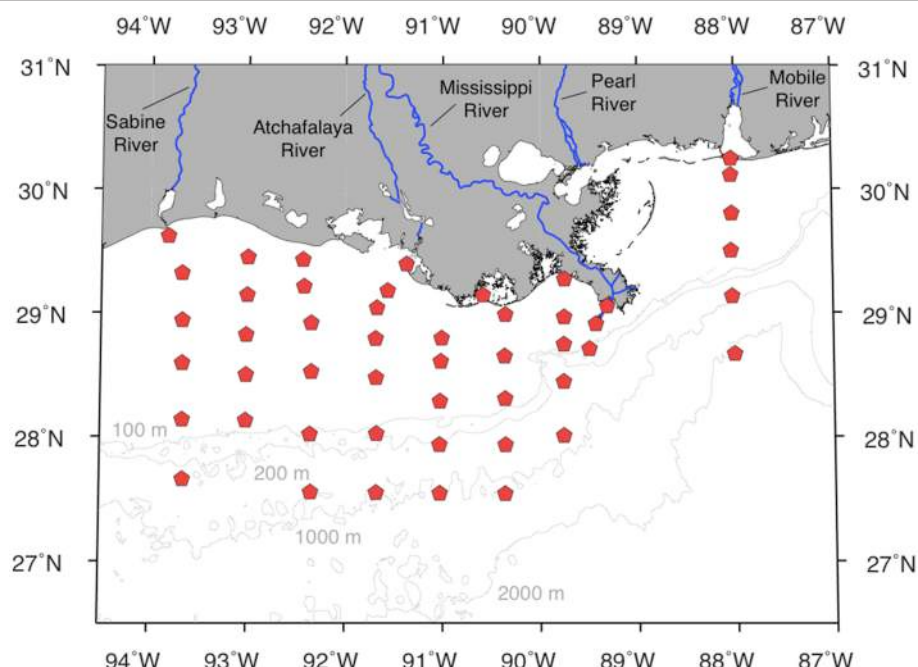


FIGURE 1 | Study region and sampling locations in the northern Gulf of Mexico (NGoM).

TABLE 1 | Sampling information and environmental conditions during the four GulfCarbon cruises to the northern Gulf of Mexico.

Season	Sampling periods	Number of measurements		Salinity*	Water temperature* (°C)	Mean M-ARS† discharge (km ³ d ⁻¹)
		DOC, EEMs, CDOM, TDAA	Lignin (TDLP ₉)			
Spring 2009	20 Apr.–30 Apr. 2009	50	23	0–36.95/34.20	15.1–24.6/22.7	2.78
Summer 2009	19 Jul.–29 Jul. 2009	50	21	0–36.77/32.01	27.5–30.8/29.7	1.41
Fall 2009	29 Oct.–07 Nov. 2009	48	22	0–36.63/33.13	16.7–27.4/24.1	2.82
Winter/spring 2010	11 Mar.–20 Mar. 2010	50	20	0–36.48/28.32	10.6–20.3/17.0	2.08
Total		198	86	0–36.95/32.00	10.6–30.8/23.1	

*Range/Median correspond to the DOC, EEMs, CDOM, TDAA samples.

†M-ARS, Mississippi-Atchafalaya River System.

DOC analysis

DOC analysis was conducted within a month of collection by high temperature combustion using a Shimadzu total organic carbon (TOC) TOC-V analyzer equipped with an autosampler (Benner and Strom, 1993). Blanks (Milli-Q UV-Plus water) were negligible and the coefficient of variation between injections of a given sample was typically $\pm 0.6\%$. Accuracy and consistency of measured DOC concentrations were checked by analyzing a deep seawater reference standard (University of Miami) every sixth sample.

CDOM Analysis and Calculation of $S_{275-295}$

Samples were analyzed for CDOM absorbance within a week after the cruise. After the water samples reached room temperature, absorbance of the samples was measured from $\lambda = 250$ – 800 nm using a Shimadzu ultraviolet (UV)-visible UV-1601 dual-beam spectrophotometer and 10-cm cylindrical quartz cells. For highly absorbing samples, 5-cm cylindrical quartz cells, or 1-cm quartz cuvettes were used. An exponential fit of the absorbance spectrum over an optimal spectral range was used to derive an offset value that was subtracted from the absorbance spectrum (Johannessen and Miller, 2001; Fichot and Benner, 2011). Absorbance corrected for offset was then converted to Napierian absorption coefficient, $a_g(\lambda)$ (m^{-1}). The dependence of $a_g(\lambda)$ on λ is described using Equation (1):

$$a_g(\lambda) = a_g(\lambda_0) \times \exp(-S(\lambda - \lambda_0)) \quad (1)$$

where $\lambda_0 < \lambda$ and S is the spectral slope coefficient in the λ_0 - λ nm spectral range. The spectral slope coefficient between 275 and 295 nm, $S_{275-295}$, was calculated as the slope of the linear regression of $\ln(a_g(\lambda))$ on λ , between $\lambda = 275$ and 295 nm (Helms et al., 2008; Fichot and Benner, 2011). Here, $S_{275-295}$ is reported with units of nm^{-1} .

EEM-PARAFAC Analysis

Samples were analyzed for EEM fluorescence within 10 days after the cruise. After the water samples reached room temperature, EEM fluorescence was measured according to Yamashita et al. (2011). Briefly, emission scans from 290 to 600 nm at 2-nm intervals were acquired at excitation wavelengths between 250 and 450 nm at 5-nm intervals. Bandpass was set at 5 nm for excitation and emission. Fluorescence spectra were scanned with 0.25 s of integration time and acquired in S/R ratio mode. Inner filter effects were corrected using the absorbance spectrum according to McKnight et al. (2001), and the EEM of Milli-Q water was subtracted from sample EEMs. The excitation and emission correction files obtained every month using rhodamine b and supplied by the manufacturers, respectively, were applied for the correction of the specific instrument's components (Cory et al., 2010). Fluorescence intensities were corrected to the area under the water Raman peak (excitation = 350 nm) analyzed daily (Lawaetz and Stedmon, 2009), and were converted to quinine sulfate units.

Two PARAFAC modeling exercises were conducted using complete data set ($n = 331$) and samples with salinities above 30 ($n = 145$), respectively. Each EEM was not normalized

to its total signal for both PARAFAC modeling. Thus, riverine samples with high fluorescence exert higher leverage in the first PARAFAC model. This procedure should be suitable to trace low abundance of terrigenous component in high salinity waters, but may fail to reveal minor marine-derived components. On the other hand, the gradients of fluorescence intensity is narrow in the second PARAFAC model, implying that while this model may not be best suited to capture terrigenous signals, it increases the chance for minor marine-derived components to be revealed. The modeling was carried out in MATLAB (Mathworks, Natick, MA) with the DOMFluor toolbox (Stedmon and Bro, 2008). The EEM of excitation wavelengths from 250 to 450 nm and emission wavelengths from 290 to 520 nm were used for PARAFAC modeling, and validation of the model was conducted by the split half validation and the random initialization according to Stedmon and Bro (2008).

Lignin Sampling, Extraction, and Analysis

Samples for lignin analysis (10-L) were gravity filtered from Niskin bottles using Whatman Polycap AS cartridges (0.2- μm pore size), acidified to $\text{pH} \simeq 2.5$ – 3 with sulfuric acid, and extracted onboard using C-18 cartridges (Louchouarn et al., 2000). Cartridges were stored at 4°C until elution in 30 mL of HPLC-grade methanol, and then stored at -20°C until analysis. Lignin was analyzed using the CuO oxidation method of Kaiser and Benner (2012). Concentrations of lignin phenols were measured as trimethylsilyl derivatives using an Agilent 7890 gas chromatograph equipped with a Varian DB5-MS capillary column and an Agilent 5975 mass selective detector. The concentrations of nine lignin phenols were measured in this study: *p*-hydroxybenzaldehyde (PAL), *p*-hydroxyacetophenone (PON), *p*-hydroxybenzoic acid (PAD), vanillin (VAL), acetovanillone (VON), vanillic acid (VAD), syringaldehyde (SAL), acetosyringone (SON), syringic acid (SAD). The sum of nine *p*-hydroxyl, vanillyl and syringyl lignin phenols (TDLP₉) are reported in units of nmol L^{-1} .

Amino Acid Hydrolysis and Analysis

The amino acids were analyzed using an Agilent 1100 high performance liquid chromatography system equipped with a fluorescence detector (Excitation: 330 nm; Emission: 450 nm). Hydrolysis and derivatization followed the approach of Kaiser and Benner (2005). In brief, water samples (100 μl) were dried with pure nitrogen gas and hydrolyzed using a vapor-phase technique with 6 mol L^{-1} hydrochloric acid at 150°C for 32.5 min in a CEM Mars 5000 microwave. After hydrolysis samples were neutralized and then separated as *o*-phthaldialdehyde (OPA) derivatives on a LiChrosphere RP18 column (4.6 \times 150 mm, 5 μm). Sixteen amino acids were included in the analysis: aspartic acid + asparagine (Asx), glutamic acid + glutamine (Glx), serine (Ser), glycine (Gly), threonine (Thr), β -alanine (β -Ala), arginine (Arg), alanine (Ala), γ -aminobutyric acid (γ -Aba), tyrosine (Tyr), valine (Val), phenylalanine (Phe), isoleucine (Ile), and lysine (Lys).

Concentrations of total dissolved amino acids (TDAA) were the sum of the sixteen amino acids. DOC-normalized yields of

TDAA were calculated as the percentage of DOC measured as amino acids using Equation (2):

$$\text{TDAA}(\% \text{DOC}) = [\text{TDAA} - C]/[\text{DOC}] \times 100 \quad (2)$$

where [DOC] and [TDAA-C] are concentrations of bulk DOC and carbon measured in total dissolved amino acids, respectively. β -Ala and γ -Aba are two non-protein amino acids thought to be products of diagenesis (Cowie and Hedges, 1994) and therefore they were not included in the calculation of TDAA yields.

RESULTS AND DISCUSSION

Riverine inputs exert a strong influence on the surface distribution of DOM in the NGOM (**Figure 2**). The concentrations of DOC, TDLP₉, and TDAA were much higher in the rivers than in ocean waters (salinity > 36.5), and displayed linear relationships with salinity ($r^2 = 0.82, 0.64$, and 0.64 , respectively). The strong influence of riverine inputs was also evident from the seasonal variability of DOC, TDLP₉, and TDAA concentrations in the riverine end-members. Furthermore, the Atchafalaya River is also enriched in bioavailable DOM relative to the Mississippi River (Chen and Gardner, 2004; Conmy et al., 2004; Shen et al., 2012; Fichot and Benner, 2014), and this important difference between riverine end-members was also evident from the variability of DOC, TDLP₉, and TDAA

(**Figure 2**). This DOM enrichment has been shown to result from the interaction of the Atchafalaya River with its productive, cypress-dominated floodplain (Shen et al., 2012).

PARAFAC Components

The significant contribution of terrigenous DOM was evident in the 0–30 salinity range of the NGOM. S_{275–295}, a tracer of terrigenous DOM, exhibited a non-linear dependence on salinity, indicating DOC was dominated by marine DOC at salinities > 30 (Fichot and Benner, 2012). Marine DOC concentrations were found to be highest at mid salinities (28–30) throughout the study period (Shen et al., pers. comm.). Two PARAFAC models were developed in the present study because optical parameters (e.g., fluorescence intensities and spectra) can be influenced by the physicochemical environment (Osburn et al., 2014), as well as biochemical components (e.g., lignin phenols and amino acids). The Gulf of Mexico (GoM) model was developed using all the data, and was used to evaluate the mixing of terrigenous and marine FDOM, and the photochemical and microbial processing of FDOM. The open ocean (OP) model was developed using high salinity (>30) samples to provide a more suitable evaluation of the dynamics of autochthonous (marine) FDOM.

A total of five and six PARAFAC components were obtained for the GoM and OP models, respectively (**Figure 3**; Supplemental Figure 1; **Table 2**). Two components from each model were similar (i.e., GoM3 and OP5; GoM4 and OP3;

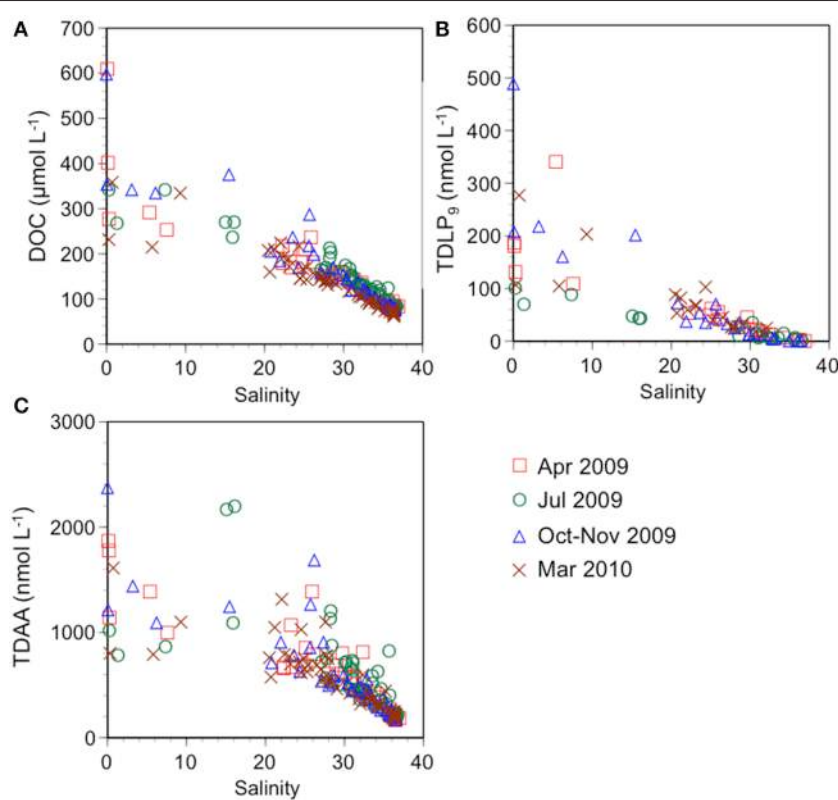


FIGURE 2 | Relationships between (A) dissolved organic carbon (DOC), (B) total dissolved lignin phenols (TDLP₉), (C) total dissolved amino acids (TDAA) and salinity.

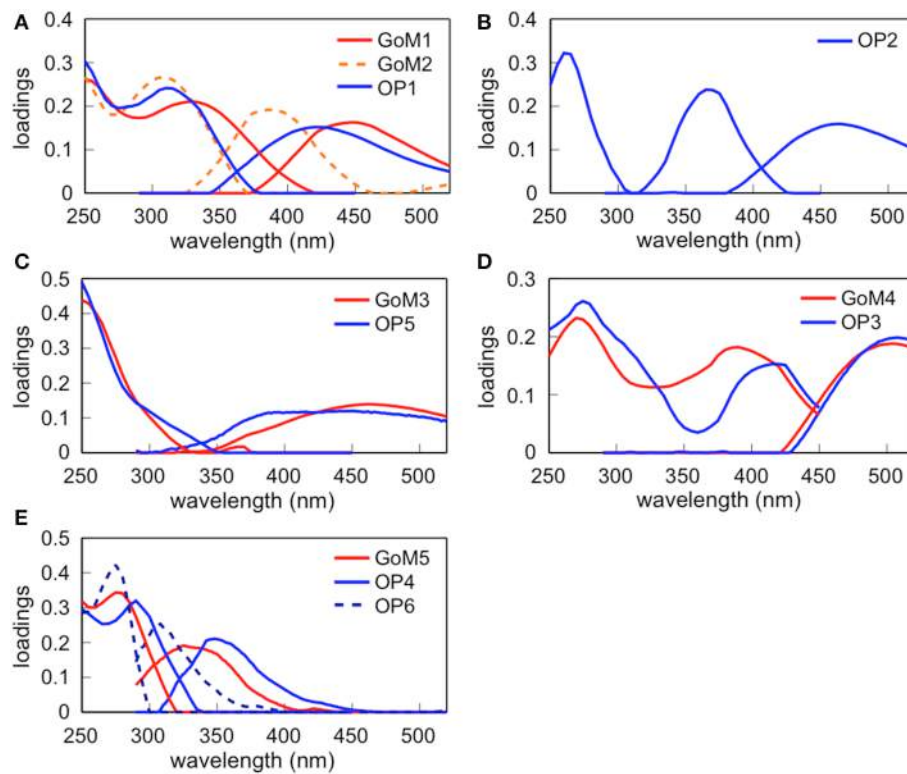


FIGURE 3 | Excitation and emission spectra of 5 and 6 fluorescent components obtained from GoM and OP PARAFAC, respectively. **(A)** GoM1, GoM2, and OP1, **(B)** OP2, **(C)** GoM3 and OP5, **(D)** GoM4 and OP3, and **(E)** GoM5, OP4, and OP6.

TABLE 2 | Fluorescence characteristics of PARAFAC components identified in both GoM and OP models.

GoM model (Ex/Em)	OP model (Ex/Em)	Coble's definition*	Description
GoM1 (<250, 330/446)		C	Terrestrial humic-like
GoM2 (<250, 310/386)	OP1 (<250, 310/420)	M	Marine (microbial) humic-like
	OP2 (260, 365/464)	-	Possibly microbial humic-like
GoM3 (<250/462)	OP5 (<250/450)	A	Terrestrial humic-like, photo-resistant/product
GoM4 (270, 390/504)	OP3 (275, 415/508)	-	Terrestrial humic-like, fulvic acid-type
GoM5 (275/326)	OP4 (290/348)	T	Protein (tryptophan)-like
	OP6 (275/308)	B	Protein (tyrosine)-like

*Coble (1996).

Figures 3C,D). GoM4 and OP3 had fluorescence maxima at longest emission wavelength among PARAFAC components. Similar components were previously found in riverine and coastal environments, and were categorized as terrigenous (Cory and McKnight, 2005; Yamashita et al., 2008, 2010; Kowalcuk et al., 2009). They were also found to be rich in fulvic acid fractions extracted from soils and estuarine sediments (Santini et al., 2009). GoM3 and OP5 corresponded to terrestrial humic-like peak A according to Coble (1996). Similar components have also been shown to be photo-resistant or products of photochemical processing (Stedmon et al., 2007; Chen et al., 2010; Cawley et al., 2012). Thus, GoM3 and OP5 are potential qualitative indicators of photooxidation of FDOM in the NGOM.

OP2 was unlike other components derived in the GoM model, and was characterized as a humic-like PARAFAC component of microbial origin (Cory and McKnight, 2005; Stedmon and Markager, 2005; Yamashita et al., 2010).

Interestingly, GoM5 and OP1 seemed to be separated into independent components in the models. GoM5 resembles a combination of OP4 and OP6, and OP1 is likely mixture of GoM1 and GoM2. Spectral features suggest OP1 (GoM1 and GoM2) belong to the traditionally defined terrestrial humic-like peak C and/or marine (microbial) humic-like peak M (Coble, 1996). Considering the GoM model was developed using the complete data set (river, coastal, and offshore waters), the terrestrial humic-like component (GoM1) might have separated from the

marine humic-like component (GoM2). The GoM5 component (OP4 and OP6) was found in the EEM region corresponding to protein-like fluorophores (Coble, 1996), and OP4 and OP6 can be categorized as tryptophan-like peak T and tyrosine-like peak B, respectively (Coble, 1996; Yamashita and Tanoue, 2003a). The OP model separated the protein-like fluorophores into tryptophan-like and tyrosine-like components, implying that spectral variability in protein-like fluorophores in offshore waters is larger than that of riverine and coastal waters.

Relationships between the Fluorescence Intensity of PARAFAC Components and the Concentrations of Lignin Phenols and Amino Acids

Fluorescence intensity of all PARAFAC components in the GoM model were positively correlated ($r = 0.79\text{--}0.91, p < 0.001$) with TDLP₉ concentrations (Figure 4), implying the distributions of all PARAFAC components in the NGoM were mainly controlled by riverine inputs, especially on the shelf where concentrations of terrigenous DOC were high (Fichot et al., 2014). $S_{275\text{--}295}$, an indicator of terrigenous DOM, decreased exponentially with increases in all PARAFAC components. The relationships between $S_{275\text{--}295}$ and GoM2, GoM3, and GoM5 were variable between summer (Jul 2009) and winter/spring (Mar 2010) (Supplemental Figure 2).

The correlation coefficients (r) between PARAFAC components and TDLP₉ were different among PARAFAC

components. The strongest correlations with TDLP₉ were found for GoM1 ($r = 0.91, p < 0.001$, Figure 4A) and GoM4 ($r = 0.91, p < 0.001$, Figure 4D), which were categorized to be terrestrial humic-like components based on spectral features (Table 2). These spectral features with strongest correlation with TDLP₉ suggest these components are mostly related to lignin among PARAFAC components obtained from GoM model. In addition, the strongest correlations imply that relationships between TDLP₉ and GoM1 or GoM4 are less variable among seasons. Strongest correlations between terrestrial humic-like GoM1 and GoM4 agreed with previous findings in coastal Canadian Arctic surface waters (Walker et al., 2009), implying that GoM1 and GoM4 can be robust proxies for terrestrial humic-like DOM. The lowest correlation coefficient was found between GoM5 and TDLP₉ ($r = 0.79, p < 0.001$, Figure 4E). GoM5 was categorized as a protein-like component from fluorescence characteristics (Table 2).

The correlation coefficients were of moderate strength for GoM2 vs. TDLP₉ ($r = 0.84, p < 0.001$, Figure 4B) and GoM3 vs. TDLP₉ ($r = 0.83, p < 0.001$, Figure 4C), suggesting that biogeochemical processing might affect the relationships. GoM2 was categorized as a marine (microbial) humic-like component based on spectral characteristics (Table 2). Likewise, addition of marine-derived components in shelf waters could affect the relationship between GoM2 vs. TDLP₉. Non-conservative mixing of a marine (microbial) humic-like component was also observed in low- to mid-salinity waters in the estuaries of central Japan and southeastern Alaska (Yamashita et al., 2008; Fellman

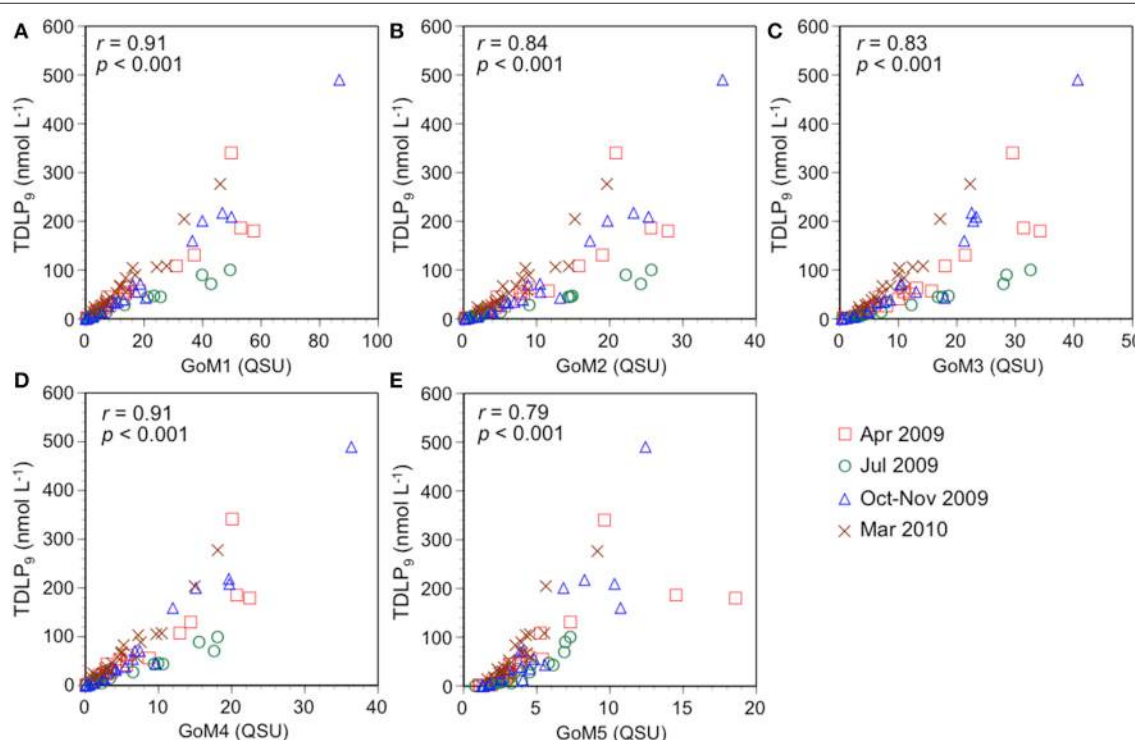


FIGURE 4 | Relationships between lignin phenol concentrations (TDLP₉) and fluorescence intensity of (A) terrestrial humic-like GoM1, (B) microbial humic-like GoM2, (C) terrestrial humic-like GoM3, (D) terrestrial humic-like GoM4, and (E) protein-like GoM5.

et al., 2010), suggesting that fluorescence of GoM2 in this study could originate from microbial products rather than lignin.

GoM3 was characterized as a terrestrial humic-like component (**Table 2**) but was weakly correlated with TDLP₉, unlike GoM1 and GoM4. The relationship between GoM3 and TDLP₉ in July 2009 was different from that in other seasons (**Figure 4C**). The ratio of GoM3 to TDLP₉ (GoM3/TDLP₉) in the river samples was higher during summer (0.32–0.39) than during other seasons (0.08–0.17) (**Table 3**), and likely affected the relationship between GoM3 and TDLP₉ in the shelf waters. However, the GoM3/TDLP₉ ratio increased from river to offshore waters (salinity > 30), irrespective of differences among seasons (**Table 3**). Photochemical alterations of lignin were enhanced during summer (Fichot and Benner, 2012), and the seasonal and spatial patterns of the GoM3/TDLP₉ ratio indicate GoM3 could be more resistant to photodegradation compared with river and offshore TDLP₉. The photo-resistant nature of GoM3 is consistent with previous observations for similar PARAFAC components (**Table 2**; Stedmon et al., 2007; Chen et al., 2010; Cawley et al., 2012). GoM3 values corresponding to S_{275–295} values in the 0.02–0.03 range were slightly higher in summer compared to winter/spring (Supplemental Figure 2), suggesting a photo-resistant characteristic of GoM3 compared with S_{275–295}. Some DOM occurs as supramolecular assemblies of small molecules (Peuravuori and Pihlaja, 2004; Romera-Castillo et al., 2014), and the increase in S_{275–295} could be related to disruption of the DOM macrostructure during photooxidation. The molecular weight of lignin has been shown to decrease during photooxidation (Opshal and Benner, 1998). It is possible that the destruction of supramolecular assemblies reduces fluorescence self-quenching of fluorescent molecules with other molecules, without changing lignin phenol concentrations.

The relationships of GoM1 and GoM4 with TDLP₉ were also slightly different in summer than during other seasons

TABLE 3 | Ratio of terrestrial humic-like components to TDLP₉(GoMX / TDLP₉) for Mississippi River, Atchafalaya River and offshore (Sal > 30) samples.

Component	Season	Mississippi R	Atchafalaya R	Sal > 30*
GoM1	Spring 2009	0.28	0.28	0.27 ± 0.03
	Summer 2009	0.60	0.49	0.36 ± 0.10
	Fall 2009	0.24	0.18	0.32 ± 0.09
	Winter/spring 2010	0.26	0.17	0.18 ± 0.04
GoM3	Spring 2009	0.16	0.17	0.33 ± 0.10
	Summer 2009	0.39	0.32	0.45 ± 0.11
	Fall 2009	0.11	0.08	0.33 ± 0.09
	Winter/spring 2010	0.13	0.08	0.18 ± 0.04
GoM4	Spring 2009	0.11	0.11	0.11 ± 0.03
	Summer 2009	0.25	0.18	0.17 ± 0.08
	Fall 2009	0.09	0.07	0.14 ± 0.05
	Winter/spring 2010	0.10	0.07	0.07 ± 0.02

*Sample number of Sal > 30 is 10, 13, 7, and 3 for Spring 2009, Summer 2009, Fall 2009, and Winter/spring 2010, respectively.

(**Figures 4A,D**). The GoM1/TDLP₉ and GoM4/TDLP₉ ratios in river waters were higher during summer (**Table 3**). However, these ratios did not increase consistently from river to offshore waters (**Table 3**), suggesting that seasonal differences in relationships among TDLP₉ and GoM4 as well as GoM1 were due to variability among fluorophores rather than photooxidation. Interestingly, relationships between S_{275–295} and GoM4 as well as GoM1 were similar between summer and winter/spring (Supplemental Figure 2), implying that physical mixing and photooxidation were largely responsible for maintaining these relationships.

All PARAFAC components derived from the GoM model were positively correlated with TDAA ($r = 0.81, p < 0.001$ for GoM1; $r = 0.84, p < 0.001$ for GoM2; $r = 0.85, p < 0.001$ for GoM3; $r = 0.82, p < 0.001$ for GoM4; $r = 0.83, p < 0.001$ for GoM5, respectively). The correlation coefficient between TDAA and the corresponding fluorescent component, i.e., tryptophan-like GoM5, was similar to those between TDAA and the humic-like components GoM1–4. The relationship between TDAA and the tryptophan-like GoM5 component varied with salinity, with a stronger correlation ($r = 0.80, p < 0.001$) occurring in high salinity (>30) waters (**Figure 5**). This suggests that the physicochemical environment of the DOM (e.g., ionic strength, pH) could affect the TDAA-GoM5 relationship. Given the large inputs of terrigenous DOM in low-salinity regions, these variable relationships with salinity indicate that terrigenous DOM might obscure the autochthonous GoM5-TDAA relationship. Differences in the biochemical compositions of land plants and phytoplankton could also affect the GoM5-TDAA relationship across the salinity gradient. For example, land plants have a group of structural glycoproteins containing certain amino acids (e.g., hydroxyproline) that are largely absent from plankton (Kieliszewski and Lampert, 1994). Tyrosine is typically 4–10 mol%, whereas tryptophan is typically absent in glycoproteins (Roberts et al., 1985). In addition, terrestrial phenolic compounds such as tannins (Maie et al., 2007, 2008) might contribute to GoM5 in low salinity waters.

The PARAFAC OP model used offshore samples (salinity > 30; **Figure 3**, **Table 2**) and identified two protein-like components (tryptophan-like OP4 and tyrosine-like OP6). Tyrosine-like OP6 was weakly correlated with concentrations of tyrosine ($r = 0.46, p < 0.001$; **Figure 6A**) and TDAA ($r = 0.54, p < 0.001$; **Figure 6B**). Yamashita and Tanoue (2003a) also found that tyrosine-like fluorescence intensity was not well correlated with tyrosine concentrations for offshore samples (tyrosine concentration is <10 nmol L⁻¹). Two factors can contribute to a weak correlation between tyrosine-like OP6 and tyrosine concentrations: (1) OP6 corresponds to a mixture of tyrosine and phenylalanine, another aromatic amino acid, (2) the fluorescence quantum yield of tyrosine in DOM is variable. The fluorescence characteristics of phenylalanine are similar to those of tyrosine (Lakowicz, 2006) and can potentially affect OP6. However, the fluorescence quantum yield of free phenylalanine is approximately one fifth of that of free tyrosine (Lakowicz, 2006), and therefore the influence of phenylalanine on OP6 is probably limited. As for the second factor, tyrosine fluorescence in peptides and proteins is often quenched due to

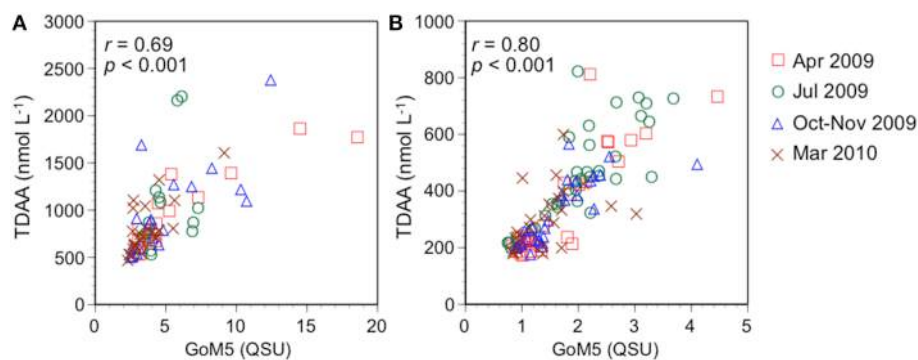


FIGURE 5 | Relationships between TDAA concentration and fluorescence intensity of protein-like GoM5 for (A) low salinity (<30) waters and (B) high salinity (>30) waters.

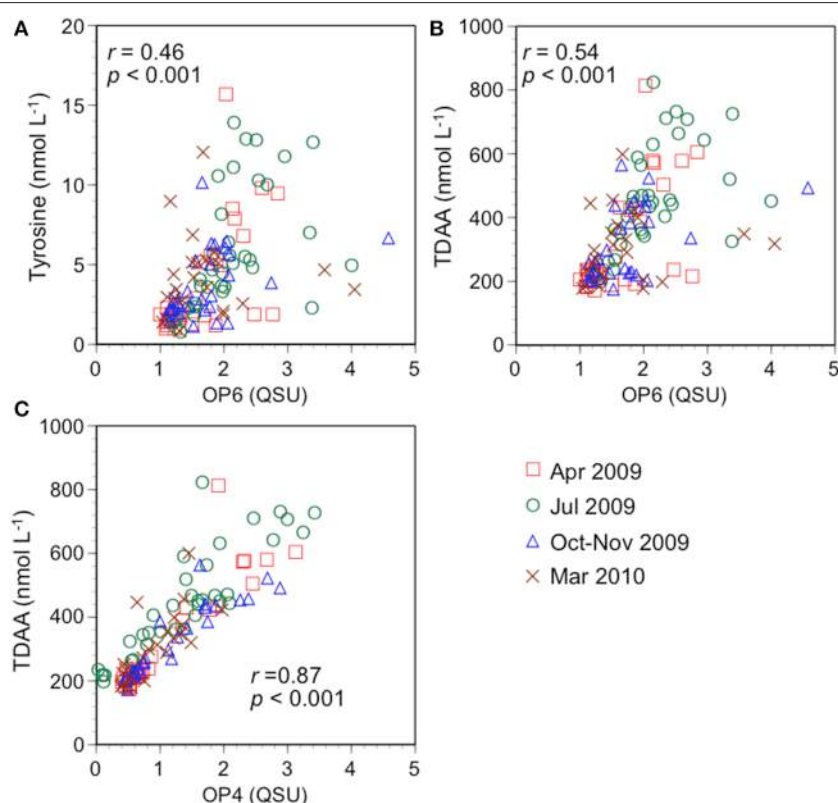


FIGURE 6 | Relationships between quantitative amino acid parameters and fluorescence intensity of protein-like components. (A) Tyrosine vs. tyrosine-like OP6, (B) TDAA vs. tyrosine-like OP6, and (C) TDAA vs. tryptophan-like OP4.

energy transfer to tryptophan molecules, or due to interactions with the peptide chain (Lakowicz, 2006). Thus, fluorescence quenching of tyrosine molecules seems a likely cause for the weak relationship between tyrosine-like OP6 and either TDAA or tyrosine concentrations.

A strong relationship was observed between tryptophan-like OP4 and concentrations of TDAA ($r = 0.87$, $p < 0.001$; Figure 6C), and bears similarities to the one observed between GoM5 and concentrations of TDAA at high salinity (Figure 5B).

Proteins/peptides containing both tyrosine and tryptophan molecules generally emit only tryptophan fluorescence due to energy transfer (Lakowicz, 2006). Thus, all tryptophan molecules in DOM potentially emit fluorescence. The strong correlation between TDAA concentrations and tryptophan-like OP4 implies that mol percentages of tryptophan in TDAA are not highly variable in the NGoM, which is consistent with previous tryptophan analysis for the bay and offshore waters (Yamashita and Tanoue, 2003b). While Yamashita and Tanoue (2003a) did

not use PARAFAC modeling, they found no correlation between tryptophan-like fluorescence intensity and concentrations of TDAA as well as tryptophan in offshore waters. The shoulder of the humic-like peak possibly overlaps with the peak position of tryptophan fluorescence. The PARAFAC analysis separates the tryptophan-like fluorescence from humic-like fluorescence, and the significant correlation between TDAA and OP4 found in this study appears to be due to the separation of OP4 from humic-like components by PARAFAC.

Compositional Relationships between Lignin and Humic-like Components

Lignin phenol concentrations have a major influence on the fluorescence intensity of the terrestrial humic-like components derived from PARAFAC modeling. Photochemical processes alter the composition and size of lignin and humic-like fluorophores, and these alterations are apparent in various chemical and optical parameters (e.g., Opshal and Benner, 1998; Stedmon and Markager, 2005). The ratios of GoM components to TDLP₉ (**Table 3**), and relationships between $S_{275-295}$ and the GoM components (Supplemental Figure 2) suggest that GoM3 is more resistant to photodegradation compared to GoM1. The ratio of two terrestrial humic-like components (GoM3/GoM1) was established as an indicator of the extent of photooxidation of terrestrial humic-like components. A high GoM3/GoM1 ratio indicates greater photochemical alteration of terrigenous

humic-like fluorophores. The acid-to-aldehyde ratios of vanillyl, syringyl, and *p*-hydroxyl phenols typically increase during photooxidation of lignin (Opshal and Benner, 1998; Spencer et al., 2009; Benner and Kaiser, 2011). The GoM3/GoM1 ratio was strongly correlated with the acid-to-aldehyde ratios of *p*-hydroxy and vanillyl phenol (**Figures 7B,C**), but was weakly correlated with that of syringyl phenols (**Figure 7A**). The *p*-hydroxy phenols are the least photoreactive components of lignin, whereas vanillyl and syringyl phenols have similar reactivities, with syringyl phenols tending to be slightly more photoreactive (Opshal and Benner, 1998; Benner and Kaiser, 2011). The GoM3/GoM1 ratio was strongly correlated with the ratio of *p*-hydroxy and vanillyl phenols (P/V), but not with the ratio of syringyl and vanillyl phenols (S/V) (**Figures 7D,E**).

Compositional variations among source vegetation and mixing processes on the Louisiana margin could have influenced the observed relationships between optical and chemical parameters. The Atchafalaya River has greater contributions of lignin from floodplain vegetation, such as cypress, than the Mississippi River (Shen et al., 2012). Cypress is a gymnosperm and its lignin is composed of *p*-hydroxy and vanillyl phenols and no syringyl phenols (Hedges and Mann, 1979; Opshal and Benner, 1995). Thus, the weak correlations between GoM3/GoM1 and S/V and acid-to-aldehyde ratio of syringyl phenols could be related to the varying compositions of lignin from the primary sources of terrestrial humic-like components.

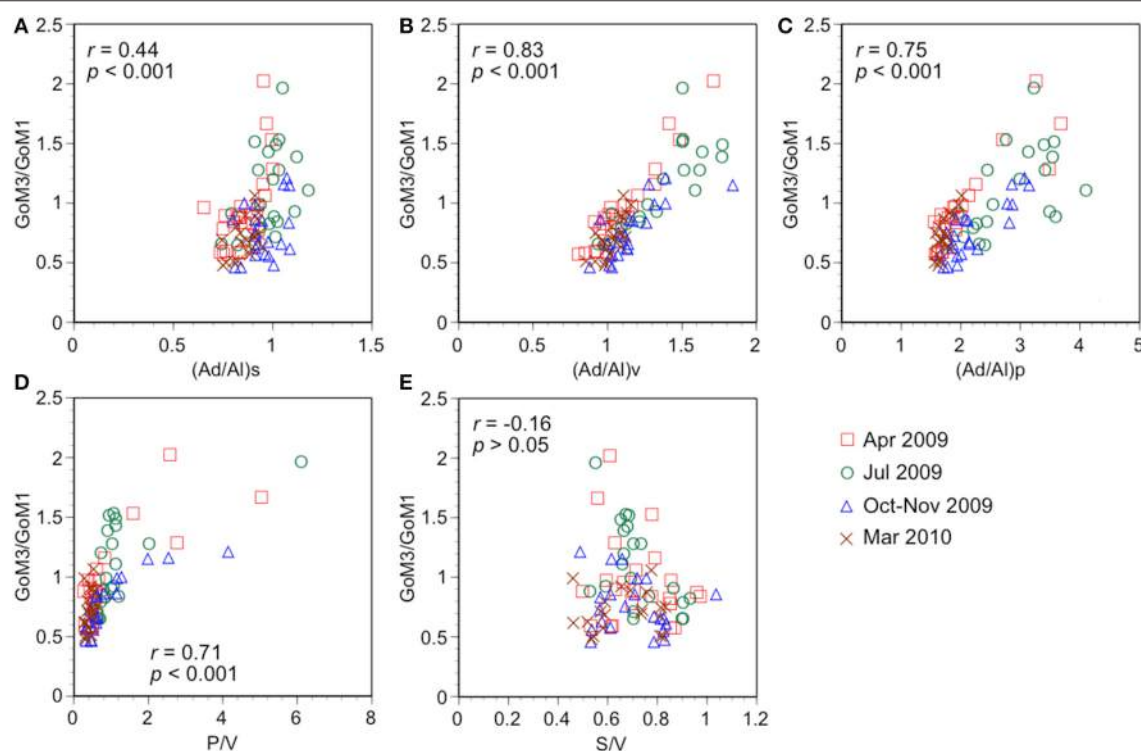


FIGURE 7 | Relationships between ratio of terrestrial humic-like components and lignin phenol parameters. GoM3/GoM1 vs. **(A)** ratio of acid to aldehyde in syringyl phenols, **(B)** ratio of acid to aldehyde in vanillyl phenols, **(C)** ratio of acid to aldehyde in *p*-hydroxy phenols, **(D)** ratio of *p*-hydroxy and vanillyl phenols (P/V), and **(E)** ratio of syringyl and vanillyl phenols (S/V).

In conclusion, photochemical alterations of terrestrial humic-like components are accompanied with changes of lignin phenols, even though variations in the source and composition of lignin phenols influence the observed relationships.

Compositional Relationships between Amino Acids and Protein-like Components

The DOC-normalized yields of amino acids (TDAA %DOC) have been demonstrated to be molecular indicators of DOM bioavailability in freshwater and marine environments (Davis and Benner, 2007; Benner and Kaiser, 2011; Shen et al., 2015). The use of this biochemical indicator in the NGoM was further validated by the shipboard bioassay experiments in spring 2010, which confirmed that amino acids were preferentially consumed and showed lower yield values in DOM of lower bioavailability (Shen et al. pers. comm.).

Amino acid yields (TDAA %DOC) were compared with protein-like components and related parameters obtained from the OP PARAFAC modeling using offshore samples (salinity > 30) on the Louisiana margin (**Figure 8**). Amino acid yields were mostly between 0.6 and 1.6% DOC, a range indicative of low concentrations of labile DOM (Davis and Benner, 2007). The relative contribution of protein-like PARAFAC components, which were found to be related to the bioavailable fraction of DOC in freshwater environments (Balcarczyk et al., 2009; Fellman et al., 2009; Hood et al., 2009), were negatively correlated with TDAA yields ($r = -0.68$, $p < 0.001$; **Figure 8A**).

A possible reason for the negative correlation is the complex nature of humic-like components. In addition to autochthonous production of protein-like components, the photodegradation and dilution of terrestrial humic-like components are possibly important factors controlling the relative abundance of protein-like components. Thus, the relative contribution of protein-like components does not appear to be a sensitive indicator of biodegradable DOM in high salinity waters of the NGoM.

The ratios of protein-like components to DOC, which is conceptually similar to the DOC-normalized yields of amino acids (i.e., ratio of amino acid-C to DOC), were compared with amino acid yields (**Figures 8B,C**). The ratio of tryptophan-like OP4 to DOC concentrations (OP4/DOC) was weakly but significantly correlated with TDAA yields ($r = 0.62$, $p < 0.001$; **Figure 8B**). However, OP6/DOC did not correlate significantly with TDAA yields ($p > 0.05$; **Figure 8C**), which was possibly due to fluorescence quenching of tyrosine molecules. Previous analysis of fluorescence properties of marine DOM in the surface Sagami Bay (Japan) showed that only tryptophan-like fluorescence was found in high molecular weight fractions, while tyrosine-like fluorescence was dominant in low molecular weight fraction (Yamashita and Tanoue, 2004). High molecular weight DOM is more easily degraded by microbes and has higher amino acid yields than low molecular weight DOM (Amon and Benner, 1994, 1996; Benner and Amon, 2015). Thus, tryptophan-like OP4 could be related to reactive high-molecular-weight DOM, while tyrosine-like OP6 might be quenching or

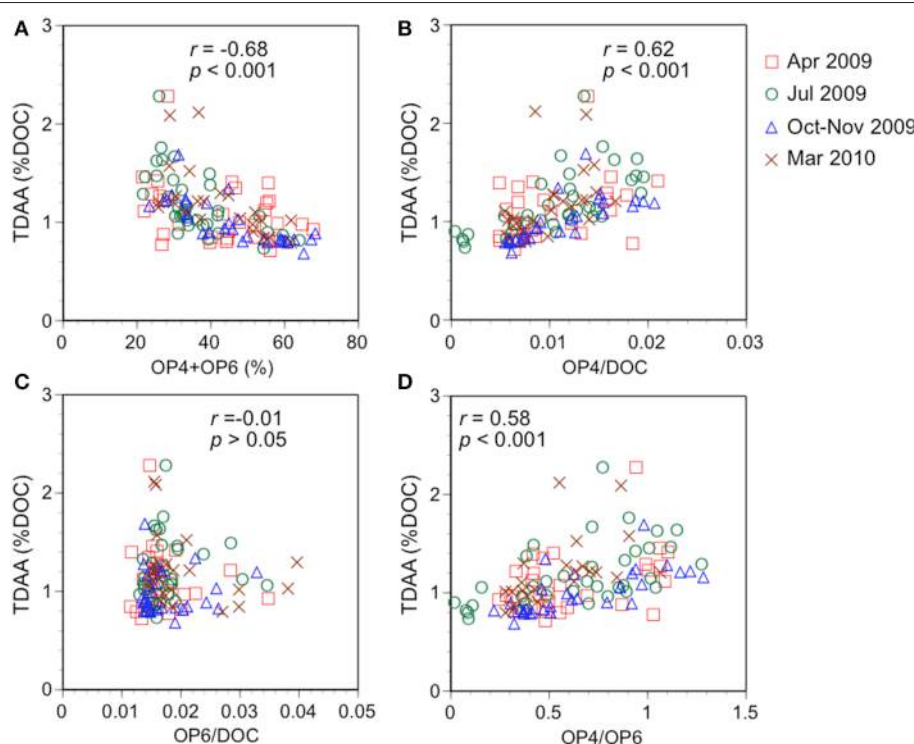


FIGURE 8 | Relationships between TDAA yields (%DOC) and (A) relative abundance of protein-like components, (B) OP4/DOC, (C) OP6/DOC, and (D) ratio of protein-like components (OP4/OP6).

derived from less reactive tyrosine-containing low-molecular-weight DOM. The ratio of tryptophan-like OP4 to tyrosine-like OP6 (OP4/OP6) was weakly correlated with TDAA yields ($r = 0.58$, $p < 0.001$; **Figure 8D**), confirming different reactivities between tryptophan-like and tyrosine-like components. Overall, the relationships obtained from the spatial distributions of TDAA yields and protein-like components in high salinity waters of the NGoM suggest that DOC-normalized yields of the tryptophan-like component (i.e., OP4/DOC in this study) and the ratio of tryptophan-like to tyrosine-like component (i.e., OP4/OP6 in this study) are useful optical indicators of the bioavailability of marine DOM.

CONCLUSIONS AND IMPLICATIONS

The transition from river water to seawater includes large changes in the physicochemical properties that can affect optical parameters without affecting biochemical parameters (Osburn et al., 2014). This study provides important insights about the fidelity of EEM-PARAFAC components as tracers of biochemical components of DOM in a river-influenced ocean margin.

- Terrestrial humic-like components, characterized as peak C type (GoM1) and fulvic acid type (GoM4), were useful tracers of lignin phenol concentrations.
- The ratio of terrestrial humic-like components, i.e., the ratio of peak A type (GoM3) to peak C type (GoM1), appeared to be indicative of the degree of photooxidation.
- Terrigenous DOM likely affected the relationship between the protein-like component (GoM5) and aromatic amino acids and total dissolved amino acid concentrations in riverine and coastal environments.
- The tryptophan-like component (OP4) was found to be a useful indicator of total dissolved amino acid concentrations in offshore environments.
- The ratios of tryptophan-like component to DOC (OP4/DOC) and tryptophan-like component to tyrosine-like component (OP4/OP6) are potentially useful indicators of DOM bioavailability in this system.

This study indicated that certain EEM-PARAFAC components are tightly linked with corresponding compounds, and suggested that other components are affected by variable sources

and biogeochemical processing. Such influences need to be considered when evaluating the fidelity of EEM-PARAFAC for tracing fluorescent DOM in the coastal ocean. Further studies are needed to develop general optical parameters that represent the quantity and quality of lignin using variable samples that cover a wide range of aquatic environments. In particular, linkages between optical properties and lignins should be explored in the open ocean where lignin phenol concentrations are quite low (Opshal and Benner, 1997). In addition, most DOC-normalized yields of amino acids observed in offshore waters of the NGoM were <1.6% DOC, indicating the concentrations of labile DOM were generally low. Further comparisons of fluorescence based indicators with amino acids yields in highly bioavailable DOM are necessary for expanding the application of optical parameters in a wide range of environments.

AUTHOR CONTRIBUTIONS

RB, RJ, CF, and YY contributed to the design of the study. CF collected the water samples. YY conducted the EEM-PARAFAC analyses, CF analyzed samples for TDLP₉ and DOC, and YS analyzed the TDAA. YY and CF performed data analyses with comments from other authors. YY wrote the initial draft of the manuscript and all authors contributed to its revision.

ACKNOWLEDGMENTS

We thank Steven E. Lohrenz and Wei-Jun Cai for providing berths on the GulfCarbon cruises, and Leanne Powers, Kevin Martin, and the crews of the R/V Cape Hatteras and the R/V Hugh Sharp for their assistance with sample collection onboard. Funding for this work was provided by National Science Foundation grant 0850653 to RB. Additional funding was provided through the George Barley endowment to RJ. This is contribution #764 from the Southeast Environmental Research Center.

SUPPLEMENTARY MATERIAL

The Supplementary Material for this article can be found online at: <http://journal.frontiersin.org/article/10.3389/fmars.2015.00092>

REFERENCES

- Amon, R. M. W., and Benner, R. (1994). Rapid cycling of high-molecular-weight dissolved organic matter in the ocean. *Nature* 369, 549–552. doi: 10.1038/369549a0
- Amon, R. M. W., and Benner, R. (1996). Bacterial utilization of different size classes of dissolved organic matter. *Limnol. Oceanogr.* 41, 41–51. doi: 10.4319/lo.1996.41.1.0041
- Balcarczyk, K. L., Jones, J. B. Jr., Jaffe, R., and Maie, N. (2009). Stream dissolved organic matter bioavailability and composition in watersheds underlain with discontinuous permafrost. *Biogeochemistry* 94, 255–270. doi: 10.1007/s10533-009-9324-x
- Benner, R., and Amon, R. M. W. (2015). The size-reactivity continuum of major bioelements in the ocean. *Annu. Rev. Mar. Sci.* 7, 185–205. doi: 10.1146/annurev-marine-010213-135126
- Benner, R., and Kaiser, K. (2011). Biological and photochemical transformations of amino acids and lignin phenols in riverine dissolved organic matter. *Biogeochemistry* 102, 209–222. doi: 10.1007/s10533-010-9435-4
- Benner, R., and Strom, M. (1993). A critical evaluation of the analytical blank associated with DOC measurements by high-temperature catalytic oxidation. *Mar. Chem.* 41, 153–160. doi: 10.1016/0304-4203(93)90113-3
- Boehme, J., Coble, P., Conmy, R., and Stovall-Leonard, A. (2004). Examining CDOM fluorescence variability using principal component analysis: seasonal

- and regional modeling of three-dimensional fluorescence in the Gulf of Mexico. *Mar. Chem.* 89, 3–14. doi: 10.1016/j.marchem.2004.03.019
- Cawley, K. M., Wolski, P., Mladenov, N., and Jaffé, R. (2012). Dissolved organic matter biogeochemistry along a transect of the Okavango delta, Botswana. *Wetlands* 32, 475–486. doi: 10.1007/s13157-012-0281-0
- Chen, M., Price, R. M., Yamashita, Y., and Jaffé, R. (2010). Comparative study of dissolved organic matter from groundwater and surface water in the Florida coastal Everglades using multi-dimensional spectrofluorometry combined with multivariate statistics. *Appl. Geochem.* 25, 872–880. doi: 10.1016/j.apgeochem.2010.03.005
- Chen, R. F., and Gardner, G. B. (2004). High-resolution measurements of chromophoric dissolved organic matter in the Mississippi and Atchafalaya River plume regions. *Mar. Chem.* 89, 103–125. doi: 10.1016/j.marchem.2004.02.026
- Coble, P. G. (1996). Characterization of marine and terrestrial DOM in seawater using excitation-emission matrix spectroscopy. *Mar. Chem.* 51, 325–346. doi: 10.1016/0304-4203(95)00062-3
- Coble, P. G., Green, S., Blough, N. V., and Gagosian, R. B. (1990). Characterization of dissolved organic matter in the Black Sea by fluorescence spectroscopy. *Nature* 348, 432–435. doi: 10.1038/348432a0
- Conney, R. N., Coble, P. G., Chen, R. F., and Gardner, G. B. (2004). Optical properties of colored dissolved organic matter in the Northern Gulf of Mexico. *Mar. Chem.* 89, 127–144. doi: 10.1016/j.marchem.2004.02.010
- Cory, R. M., and Kaplan, L. A. (2012). Biological lability of streamwater fluorescent dissolved organic matter. *Limnol. Oceanogr.* 57, 1347–1360. doi: 10.4319/lo.2012.57.5.1347
- Cory, R. M., and McKnight, D. M. (2005). Fluorescence spectroscopy reveals ubiquitous presence of oxidized and reduced quinones in dissolved organic matter. *Environ. Sci. Technol.* 39, 8142–8149. doi: 10.1021/es0506962
- Cory, R. M., Miller, M. P., McKnight, D. M., Guerard, J. J., and Miller, P. L. (2010). Effect of instrument-specific response on the analysis of fulvic acid fluorescence spectra. *Limnol. Oceanogr. Meth.* 8, 67–78. doi: 10.4319/lom.2010.8.0067
- Cowie, G. L., and Hedges, J. I. (1994). Biogeochemical indicators of diagenetic alteration in natural organic matter mixtures. *Nature* 369, 304–307. doi: 10.1038/369304a0
- Davis, J., and Benner, R. (2005). Seasonal trends in the abundance, composition and bioavailability of particulate and dissolved organic matter in the Chukchi/Beaufort Seas and western Canada Basin. *Deep-Sea Res. Part II* 52, 3396–3410. doi: 10.1016/j.dsr2.2005.09.006
- Davis, J., and Benner, R. (2007). Quantitative estimates of labile and semi-labile dissolved organic carbon in the western Arctic Ocean: a molecular approach. *Limnol. Oceanogr.* 52, 2434–2444. doi: 10.4319/lo.2007.52.6.2434
- Fellman, J. B., Hood, E., D'Amore, D. V., Edwards, R. T., and White, D. (2009). Seasonal changes in the chemical quality and biodegradability of dissolved organic matter exported from soils to streams in coastal temperate rainforest watersheds. *Biogeochemistry* 95, 277–293. doi: 10.1007/s10533-009-9336-6
- Fellman, J. B., Spencer, R. G. M., Hernes, P. J., Edwards, R. T., D'Amore, D. V., and Hood, E. (2010). The impact of glacier runoff on the biodegradability and biochemical composition of terrigenous dissolved organic matter in near-shore marine ecosystems. *Mar. Chem.* 121, 112–122. doi: 10.1016/j.marchem.2010.03.009
- Fichot, C. G., and Benner, R. (2011). A novel method to estimate DOC concentrations from CDOM absorption coefficients in coastal waters. *Geophys. Res. Lett.* 38, L03610. doi: 10.1029/2010GL046152
- Fichot, C. G., and Benner, R. (2012). The spectral slope coefficient of chromophoric dissolved organic matter ($S_{275-295}$) as a tracer of terrigenous dissolved organic carbon in river-influenced ocean margins. *Limnol. Oceanogr.* 57, 1453–1466. doi: 10.4319/lo.2012.57.5.1453
- Fichot, C. G., and Benner, R. (2014). The fate of terrigenous dissolved organic carbon in a river-influenced ocean margin. *Global Biogeochem. Cycles* 28, 300–318. doi: 10.1002/2013GB004670
- Fichot, C. G., Lohrenz, S. E., and Benner, R. (2014). Pulsed, cross-shelf export of terrigenous dissolved organic carbon to the Gulf of Mexico. *J. Geophys. Res.* 119, 1176–1194. doi: 10.1002/2013JC009424
- Hedges, J. I., and Mann, D. C. (1979). The characterization of plant issues by their lignin oxidation products. *Geochim. Cosmochim. Acta* 43, 1803–1807. doi: 10.1016/0016-7037(79)90028-0
- Helms, J. R., Stubbins, A., Ritchie, J. D., Minor, E. C., Kieber, D. J., and Mopper, K. (2008). Absorption spectral slopes and slope ratios as indicators of molecular weight, source, and photobleaching of chromophoric dissolved organic matter. *Limnol. Oceanogr.* 53, 955–969. doi: 10.4319/lo.2008.53.3.0955
- Hernes, P. J., Bergamaschi, B. A., Eckard, R. S., and Spencer, R. G. M. (2009). Fluorescence-based proxies for lignin in freshwater dissolved organic matter. *J. Geophys. Res.* 114, G00F03. doi: 10.1029/2009JG000938
- Hood, E., Fellman, J., Spencer, R. G. M., Hernes, P. J., Edwards, R., D'Amore, D., et al. (2009). Glaciers as a source of ancient and labile organic matter to the marine environment. *Nature* 462, 1044–1047. doi: 10.1038/nature08580
- Jaffé, R., Cawley, K. M., and Yamashita, Y. (2014). “Applications of excitation emission matrix fluorescence with parallel factor analysis (EEM-PARAFAC) in assessing environmental dynamics of natural dissolved organic matter (DOM) in aquatic environments: a review,” in *Physicochemical Characterization of Dissolved Organic Matter: Impact on Natural and Engineered Systems*, ed F. Rosario-Ortiz (Washington, DC: ACS Publications), 27–73.
- Johannessen, S. C., and Miller, W. L. (2001). Quantum yield for the photochemical production of dissolved inorganic carbon in seawater. *Mar. Chem.* 76, 271–283. doi: 10.1016/S0304-4203(01)00067-6
- Kaiser, K., and Benner, R. (2005). Hydrolysis-induced racemization of amino acids. *Limnol. Oceanogr.-Methods* 3, 318–325. doi: 10.4319/lom.2005.3.318
- Kaiser, K., and Benner, R. (2012). Characterization of lignin by gas chromatography and mass spectrometry using a simplified CuO oxidation method. *Anal. Chem.* 84, 459–464. doi: 10.1021/ac202004r
- Kieliszewski, M. J., and Lampert, D. T. (1994). Extensin: repetitive motifs, functional sites, post-translational codes, and phylogeny. *Plant J.* 5, 157–172. doi: 10.1046/j.1365-313X.1994.05020157.x
- Kowalczyk, P., Durako, M. J., Young, H., Kahn, A. E., Cooper, W. J., and Gonsior, M. (2009). Characterization of dissolved organic matter fluorescence in the South Atlantic Bight with use of PARAFAC model: interannual variability. *Mar. Chem.* 113, 182–196. doi: 10.1016/j.marchem.2009.01.015
- Lakowicz, J. R. (2006). *Principles of Fluorescence Spectroscopy*, 3rd Edn. New York, NY: Springer.
- Lawaetz, A. J., and Stedmon, C. A. (2009). Fluorescence intensity calibration using the Raman scatter peak of water. *Appl. Spectrosc.* 63, 936–940. doi: 10.1366/000370209788964548
- Lønborg, C., Álvarez-Salgad, X. A., Davidson, K., Martínez-García, S., and Teira, E. (2010). Assessing the microbial bioavailability and degradation rate constants of dissolved organic matter by fluorescence spectroscopy in the coastal upwelling system of the Ría de Vigo. *Mar. Chem.* 119, 121–129. doi: 10.1016/j.marchem.2010.02.001
- Louchouarn, P., Opsahl, S., and Benner, R. (2000). Isolation and quantification of dissolved lignin from natural waters using solid-phase extraction and GC/MS. *Anal. Chem.* 72, 2780–2787. doi: 10.1021/ac9912552
- Maie, N., Jaffé, R., Miyoshi, T., and Childers, D. L. (2006). Quantitative and qualitative aspects of dissolved organic carbon leached from senescent plants in an oligotrophic wetland. *Biogeochemistry* 78, 285–314. doi: 10.1007/s10533-005-4329-6
- Maie, N., Pisani, O., and Jaffé, R. (2008). Mangrove tannins in aquatic ecosystems: their fate and possible influence on dissolved organic carbon and nitrogen cycling. *Limnol. Oceanogr.* 53, 160–171. doi: 10.4319/lo.2008.53.1.0160
- Maie, N., Scully, N. M., Pisani, O., and Jaffé, R. (2007). Composition of a protein-like fluorophore of dissolved organic matter in coastal wetland and estuarine ecosystems. *Water Res.* 41, 563–570. doi: 10.1016/j.watres.2006.11.006
- McKnight, D. M., Boyer, E. W., Westerhoff, P. K., Doran, P. T., Kulbe, T., and Andersen, D. T. (2001). Spectrofluorometric characterization of aquatic fulvic acids for determination of precursor organic material and general structural properties. *Limnol. Oceanogr.* 46, 38–48. doi: 10.4319/lo.2001.46.1.00038
- Murphy, K. R., Bro, R., and Stedmon, C. A. (2014). “Chemometric analysis of organic matter fluorescence,” in *Aquatic Organic Matter Fluorescence*, eds P. G. Coble, J. Lead, A. Baker, D. M. Reynolds, and R. G. M. Spencer (New York, NY: Cambridge University Press), 339–375.
- Opshal, S., and Benner, R. (1995). Early diagenesis of vascular plant-tissues—lignin and cutin decomposition and biogeochemical implications. *Geochim. Cosmochim. Acta* 59, 4889–4904. doi: 10.1016/0016-7037(95)00348-7
- Opshal, S., and Benner, R. (1997). Distribution and cycling of terrigenous dissolved organic matter in the ocean. *Nature* 386, 480–482. doi: 10.1038/386480a0

- Opshal, S., and Benner, R. (1998). Photochemical reactivity of dissolved lignin in river and ocean waters. *Limnol. Oceanogr.* 43, 1297–1304. doi: 10.4319/lo.1998.43.6.1297
- Osburn, C. L., Del Vecchio, R., and Boyd, T. J. (2014). “Physicochemical effects on dissolved organic matter fluorescence in natural waters,” in *Aquatic Organic Matter Fluorescence*, eds P. G. Coble, J. Lead, A. Baker, D. M. Reynolds, R. G. M., and Spencer (New York, NY: Cambridge University Press), 233–277.
- Osburn, C. L., and Stedmon, C. A. (2011). Linking the chemical and optical properties of dissolved organic matter in the Baltic–North Sea transition zone to differentiate three allochthonous inputs. *Mar. Chem.* 126, 281–294. doi: 10.1016/j.marchem.2011.06.007
- Peuravuori, J., and Pihlaja, K. (2004). Preliminary study of Lake dissolved organic matter in light of nanoscale supramolecular assembly. *Environ. Sci. Technol.* 38, 5958–5967. doi: 10.1021/es0400411
- Roberts, K., Grief, C., Hills, G. J., and Shaw, P. (1985). Cell wall glycoproteins: structure and function. *J. Cell Sci.* 2, 105–127. doi: 10.1242/jcs.1985.Supplement_2.6
- Romera-Castillo, C., Chen, M., Yamashita, Y., and Jaffé, R. (2014). Fluorescence characteristics of size-fractionate dissolved organic matter: implications for a molecular assembly based structure? *Water Res.* 55, 40–51. doi: 10.1016/j.watres.2014.02.017
- Santín, C., Yamashita, Y., Otero, X. L., Álvarez, M. Á., and Jaffé, R. (2009). Characterizing humic substances from estuarine soils and sediments by excitation-emission matrix spectroscopy and parallel factor analysis. *Biogeochemistry* 96, 131–147. doi: 10.1007/s10533-009-9349-1
- Shen, Y., Chapelle, F. H., Strom, E. W., and Benner, R. (2015). Origins and bioavailability of dissolved organic matter in groundwater. *Biogeochemistry* 122, 61–78. doi: 10.1007/s10533-014-0029-4
- Shen, Y., Fichot, C. G., and Benner, R. (2012). Floodplain influence on dissolved organic matter composition and export from the Mississippi–Atchafalaya River system to the Gulf of Mexico. *Limnol. Oceanogr.* 57, 1149–1160. doi: 10.4319/lo.2012.57.4.1149
- Spencer, R. G. M., Stubbins, A., Hernes, P. J., Baker, A., Mopper, K., Aufdenkampe, A. K., et al. (2009). Photochemical degradation of dissolved organic matter and dissolved lignin phenols from the Congo River. *J. Geophys. Res.* 114, G03010. doi: 10.1029/2009jg000968
- Stedmon, C. A., and Bro, R. (2008). Characterizing dissolved organic matter fluorescence with parallel factor analysis: a tutorial. *Limnol. Oceanogr. Meth.* 6, 572–579. doi: 10.4319/lom.2008.6.5.572
- Stedmon, C. A., and Markager, S. (2005). Tracing the production and degradation of autochthonous fractions of dissolved organic matter by fluorescence analysis. *Limnol. Oceanogr.* 50, 1415–1426. doi: 10.4319/lo.2005.50.5.1415
- Stedmon, C. A., Markager, S., and Bro, R. (2003). Tracing dissolved organic matter in aquatic environments using a new approach to fluorescence spectroscopy. *Mar. Chem.* 82, 239–254. doi: 10.1016/S0304-4203(03)00072-0
- Stedmon, C. A., Markager, S., Tranvik, L., Kronberg, L., Slätis, T., and Martinsen, W. (2007). Photochemical production of ammonium and transformation of dissolved organic matter in the Baltic Sea. *Mar. Chem.* 104, 227–240. doi: 10.1016/j.marchem.2006.11.005
- Stedmon, C. A., and Nelson, N. B. (2015). “The optical properties of DOM in the ocean,” in *Biogeochemistry of Marine Dissolved Organic Matter*, 2nd Edn., eds D. A. Hansell and C. A. Carlson (London: Academic Press), 481–508.
- Walker, S. A., Amon, R. M. W., and Stedmon, C. A. (2013). Variations in high-latitude riverine fluorescent dissolved organic matter: a comparison of large Arctic rivers. *J. Geophys. Res.* 118, 1689–1702. doi: 10.1002/2013JG002320
- Walker, S. A., Amon, R. M. W., Stedmon, C., Duan, S., and Louchouarn, P. (2009). The use of PARAFAC modeling to trace terrestrial dissolved organic matter and fingerprint water masses in coastal Canadian Arctic surface waters. *J. Geophys. Res.* 114, G00F06. doi: 10.1029/2009jg000990
- Yamashita, Y., and Jaffé, R. (2008). Characterizing the interactions between trace metals and dissolved organic matter using excitation-emission matrix and parallel factor analysis. *Environ. Sci. Technol.* 42, 7374–7379. doi: 10.1021/es801357h
- Yamashita, Y., Jaffé, R., Maie, N., and Tanoue, E. (2008). Assessing the dynamics of dissolved organic matter (DOM) in coastal environments by excitation emission matrix fluorescence and parallel factor analysis (EEM-PARAFAC). *Limnol. Oceanogr.* 53, 1900–1908. doi: 10.4319/lo.2008.53.5.1900
- Yamashita, Y., Maie, N., Briceño, H., and Jaffé, R. (2010). Optical characterization of dissolved organic matter in tropical rivers of the Guayana Shield, Venezuela. *J. Geophys. Res.* 115, G00F10. doi: 10.1029/2009jg000987
- Yamashita, Y., Panton, A., Mahaffey, C., and Jaffé, R. (2011). Assessing the spatial and temporal variability of dissolved organic matter in Liverpool Bay using excitation–emission matrix fluorescence and parallel factor analysis. *Ocean Dyn.* 61, 569–579. doi: 10.1007/s10236-010-0365-4
- Yamashita, Y., and Tanoue, E. (2003a). Chemical characterization of protein-like fluorophores in DOM in relation to aromatic amino acids. *Mar. Chem.* 82, 255–271. doi: 10.1016/S0304-4203(03)00073-2
- Yamashita, Y., and Tanoue, E. (2003b). Distribution and alteration of amino acids in bulk DOM along a transect from bay to oceanic waters. *Mar. Chem.* 82, 145–160. doi: 10.1016/S0304-4203(03)00049-5
- Yamashita, Y., and Tanoue, E. (2004). Chemical characteristics of amino acid-containing dissolved organic matter in seawater. *Org. Geochem.* 35, 679–692. doi: 10.1016/j.orggeochem.2004.02.007

Conflict of Interest Statement: The authors declare that the research was conducted in the absence of any commercial or financial relationships that could be construed as a potential conflict of interest.

Copyright © 2015 Yamashita, Fichot, Shen, Jaffé and Benner. This is an open-access article distributed under the terms of the Creative Commons Attribution License (CC BY). The use, distribution or reproduction in other forums is permitted, provided the original author(s) or licensor are credited and that the original publication in this journal is cited, in accordance with accepted academic practice. No use, distribution or reproduction is permitted which does not comply with these terms.



Utilizing colored dissolved organic matter to derive dissolved black carbon export by arctic rivers

Aron Stubbins^{1*}, Robert G. M. Spencer², Paul J. Mann³, R. Max Holmes⁴, James W. McClelland⁵, Jutta Niggemann⁶ and Thorsten Dittmar⁶

¹ Department of Marine Sciences, Skidaway Institute of Oceanography, University of Georgia, Savannah, GA, USA

² Department of Earth, Ocean and Atmospheric Science, Florida State University, Tallahassee, FL, USA, ³ Department of Geography, Northumbria University, Newcastle-upon-Tyne, UK, ⁴ Woods Hole Research Center, Falmouth, MA, USA,

⁵ University of Texas Marine Science Institute, Port Aransas, TX, USA, ⁶ Research Group for Marine Geochemistry, Institute for Chemistry and Biology of the Marine Environment, University of Oldenburg, Oldenburg, Germany

OPEN ACCESS

Edited by:

Christopher Osburn,
North Carolina State University, USA

Reviewed by:

Mukesh Gupta,
Environment Canada, Canada
X. Antón Álvarez-Salgado,
Consejo Superior de Investigaciones
Científicas, Spain

*Correspondence:

Aron Stubbins
aron.stubbins@skio.uga.edu

Specialty section:

This article was submitted to
Marine Biogeochemistry,
a section of the journal
Frontiers in Earth Science

Received: 02 September 2015

Accepted: 06 October 2015

Published: 26 October 2015

Citation:

Stubbins A, Spencer RGM, Mann PJ, Holmes RM, McClelland JW, Niggemann J and Dittmar T (2015) Utilizing colored dissolved organic matter to derive dissolved black carbon export by arctic rivers. *Front. Earth Sci.* 3:63.
[doi: 10.3389/feart.2015.00063](https://doi.org/10.3389/feart.2015.00063)

Wildfires have produced black carbon (BC) since land plants emerged. Condensed aromatic compounds, a form of BC, have accumulated to become a major component of the soil carbon pool. Condensed aromatics leach from soils into rivers, where they are termed dissolved black carbon (DBC). The transport of DBC by rivers to the sea is a major term in the global carbon and BC cycles. To estimate Arctic river DBC export, 25 samples collected from the six largest Arctic rivers (Kolyma, Lena, Mackenzie, Ob', Yenisey, and Yukon) were analyzed for dissolved organic carbon (DOC), colored dissolved organic matter (CDOM), and DBC. A simple, linear regression between DOC and DBC indicated that DBC accounted for $8.9 \pm 0.3\%$ of DOC exported by Arctic rivers. To improve upon this estimate, an optical proxy for DBC was developed based upon the linear correlation between DBC concentrations and CDOM light absorption coefficients at 254 nm (a_{254}). Relatively easy to measure a_{254} values were determined for 410 Arctic river samples between 2004 and 2010. Each of these a_{254} values was converted to a DBC concentration based upon the linear correlation, providing an extended record of DBC concentration. The extended DBC record was coupled with daily discharge data from the six rivers to estimate riverine DBC loads using the LOADEST modeling program. The six rivers studied cover 53% of the pan-Arctic watershed and exported 1.5 ± 0.1 million tons of DBC per year. Scaling up to the full area of the pan-Arctic watershed, we estimate that Arctic rivers carry 2.8 ± 0.3 million tons of DBC from land to the Arctic Ocean each year. This equates to $\sim 8\%$ of Arctic river DOC export, slightly less than indicated by the simpler DBC vs. DOC correlation-based estimate. Riverine discharge is predicted to increase in a warmer Arctic. DBC export was positively correlated with river runoff, suggesting that the export of soil BC to the Arctic Ocean is likely to increase as the Arctic warms.

Keywords: carbon cycle, arctic, black carbon, colored dissolved organic matter (CDOM), climate change, rivers, hydrology

INTRODUCTION

Fire occurs in nearly all terrestrial ecosystems (Bowman et al., 2009) and is on the increase in the Arctic (Higuera et al., 2008; Hu et al., 2010). Black carbon (BC) refers to thermally altered organic material and it comes in many forms (Forbes et al., 2006), ranging in chemistry from minimally charred biomolecules (Myers-Pigg et al., 2015) to condensed aromatics formed at high temperatures (Dittmar, 2008). Once formed, condensed aromatics are ultra-refractory within soils, being preferentially preserved for hundreds to thousands of years (Schmidt et al., 2011). This stability, together with the ubiquity of fire, has resulted in condensed aromatics being distributed throughout the world's soils (Forbes et al., 2006; Guggenberger et al., 2008), where they have accumulated to represent approximately 10% of the global soil carbon store (Mitra et al., 2013). Wildfires have burned since the emergence of land plants 420 million years ago (Bowman et al., 2009). Without a significant loss term, condensed aromatics should have accumulated to represent an even greater pool of soil carbon than currently observed. The mobilization of soil condensed aromatics into solution and subsequent export by rivers to the oceans is the main loss term identified to date (Guggenberger et al., 2008; Dittmar et al., 2012a; Jaffé et al., 2013).

Once in solution, condensed aromatics are termed dissolved black carbon (DBC; Dittmar, 2008) and their export through rivers links the soil BC store to another major global carbon store, that of dissolved organic carbon (DOC) in the oceans (Hansell, 2013). As in soils, DBC in the oceans appears to be highly bio-refractory, based upon its ancient apparent radiocarbon age (Ziolkowski and Druffel, 2010), and has accumulated to become a major pool of global carbon ($>12,000$ Tg-C; Tg-C = 10^{12} grams of carbon; Dittmar and Paeng, 2009). Deep sea hydrothermal systems (Dittmar and Paeng, 2009) and atmospheric deposition (Jurado et al., 2008) have been proposed as sources of oceanic DBC. However, rivers are currently the major identified source of DBC to the ocean, delivering an estimated 26.5 Tg of DBC per year (Jaffé et al., 2013). Photo-degradation by sunlight is the major identified sink for DBC (Stubbins et al., 2010, 2012). However, at depth in the ocean, DBC behaves almost conservatively, suggesting minimal loss when light is not present (Dittmar and Paeng, 2009). Therefore, if DBC can reach areas of deep water formation before being photo-degraded, it may be in essence reburied in the deep ocean.

In this manuscript we present data for DBC concentrations in major Arctic rivers and estimate annual export of DBC from Arctic soils to the Arctic Ocean. While riverine inputs of DOC to the Arctic Ocean are well-constrained (Raymond et al., 2007; Spencer et al., 2009; Holmes et al., 2012), this is the first estimate of DBC export to the Arctic Ocean. To make this estimate, we quantified DBC in depth and flow integrated samples collected near the mouths of the six largest Arctic rivers under variable hydrological conditions (Figure 1; Kolyma, Lena, Mackenzie, Ob', Yenisey, and Yukon). Together, these six river watersheds cover 53% of the pan-Arctic watershed (Holmes et al., 2012). Discharge varies markedly with season in Arctic rivers. In winter, November to April, the watersheds and river surfaces are frozen such that groundwater derived discharge dominates, and only 10–15% of

the annual Arctic river DOC load is exported during this 6 month period (Holmes et al., 2012). With the warmth of spring, thawing winter snow and ice drive a massive discharge peak that is accompanied by highest annual DOC concentrations. As a consequence, typically 45–65% of the annual Arctic DOC load is exported during May and June, the 2 months of the spring freshet (Raymond et al., 2007; Spencer et al., 2009; Holmes et al., 2012). After the intense spring freshet, the months from July through October account for the remainder of the annual DOC export.

In the current study, DBC was quantified in 25 samples, collected over a broad range of runoff values in 2009. We also determined the Naperian light absorption coefficient of colored DOM (a CDOM; m^{-1}), an optical property of DOM that is a good proxy for the aromatic components of the DOM pool (Weishaar et al., 2003; Stubbins et al., 2008; Spencer et al., 2009), including DBC (Stubbins et al., 2012). a CDOM was determined for 410 samples spanning the seasonal hydrographs of each river and 7 years (2004–2010). The utility of a CDOM as a proxy for DBC within Arctic rivers was confirmed and used within a LOADEST modeling exercise to develop a robust estimate for DBC export to the Arctic Ocean.

METHODS

Sample Collection and Processing

Sample sites for each river were as follows, Salekhard (Ob'), Dudinka (Yenisey), Zhigansk (Lena), Cherskiy (Kolyma), Pilot Station (Yukon), and Tsigehtchic (Mackenzie). Discharge data ($m^3 s^{-1}$) was taken from the ArcticRIMS website (<http://rims.unh.edu/data.shtml>) for nearby gauging stations and converted to surface area normalized runoff ($m^3 km^{-2} s^{-1}$; Table S1). The gauging stations and sampling locations are near the mouths of the rivers, capturing 96% of the six rivers' combined watershed area (Figure 1; Table 1). Depth integrated, flow weighted samples were collected following US Geological Survey protocols, filtered through pre-cleaned capsules (0.45 μm ; Geotech), placed in acid-soaked Nalgene polycarbonate bottles and frozen until further processing (Holmes et al., 2012).

Dissolved Organic Carbon Concentrations

Aliquots of sample were transferred to pre-combusted 40 mL glass vials, acidified to pH 2 (hydrochloric acid), and analyzed for non-purgeable organic carbon using a Shimadzu TOC-VCPh analyzer fitted with a Shimadzu ASI-V autosampler. In addition to potassium hydrogen phthalate standards, aliquots of deep seawater reference material, Batch 10, Lot# 05-10, from the Consensus Reference Material Project (CRM) were analyzed to check the precision and accuracy of the DOC analyses. Analyses of the CRM deviated by <5% from the reported value for these standards (41–44 μM -DOC; <http://yyy.rsmas.miami.edu/groups/biogeochem/Table1.htm>). Routine minimum detection limits in the investigator's laboratory using the above configuration are $2.8 \pm 0.3 \mu M$ -C and standard errors are typically $1.7 \pm 0.5\%$ of the DOC concentration (Stubbins and Dittmar, 2012).

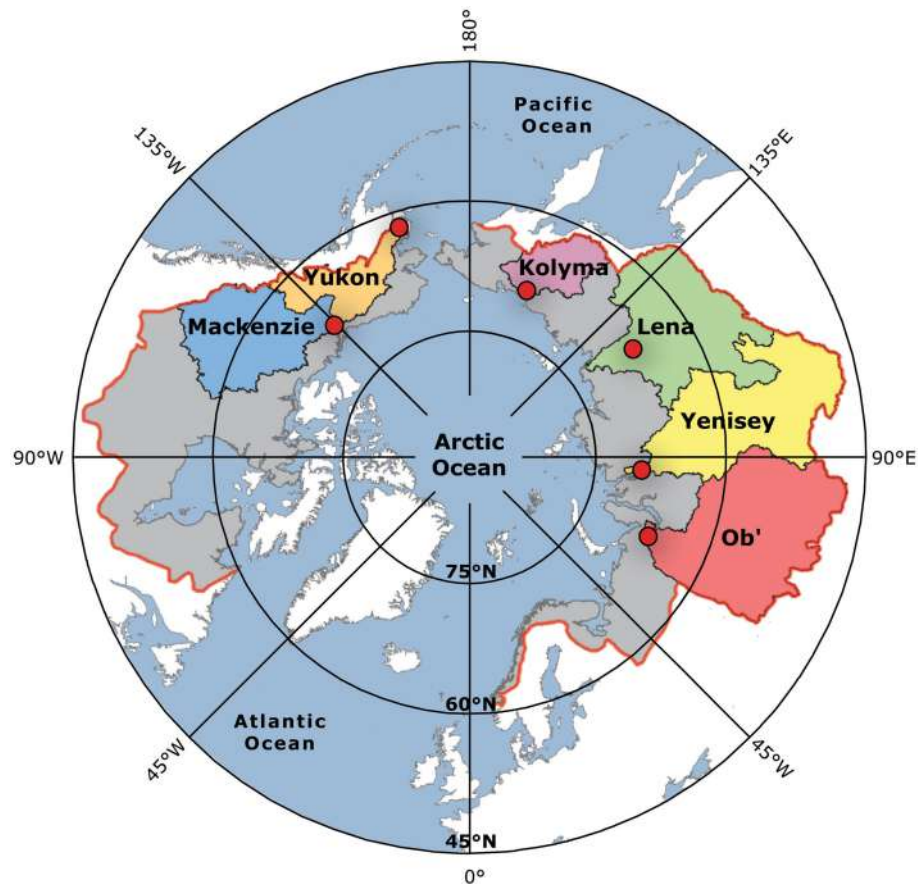


FIGURE 1 | Map showing the six Arctic river watersheds sampled. The red dots indicate the sampling locations. Red line indicates the boundary and the gray fill the area of the pan-Arctic Ocean watershed. Data points in all subsequent figures are colored to match the river watershed colors here.

TABLE 1 | Discharge gauging stations and watershed characteristics.

River/Watershed	Kolyma	Lena	Mackenzie	Ob'	Yenisey	Yukon
Discharge gauging station	Kolymskoye	Kyusyur	Tsiigehtchic	Salekhard	Igarka	Pilot station
Area (10^6 km^2) at gauged	0.53	2.43	1.68	2.99	2.4	0.83
Area (10^6 km^2) total	0.65	2.46	1.78	2.99	2.54	0.83
% Area captured	82%	99%	94%	100%	94%	100%
Discharge ($\text{km}^3 \text{ year}^{-1}$) gauged	111	581	298	427	636	208
Discharge ($\text{km}^3 \text{ year}^{-1}$) total	136	588	316	427	673	208
Interannual variation in discharge (St. Dev.)	20%	9%	10%	15%	4%	12%
Runoff (mm year^{-1})	166	240	177	143	259	248

Colored Dissolved Organic Matter Naperian Light Absorption

Sample was placed in a 1 cm quartz absorbance cell situated in the light path of an Agilent 8453 ultraviolet-visible spectrophotometer and sample CDOM absorbance spectra were recorded from 190 to 800 nm. Ultrapure water (Milli-Q) provided a blank. Blank corrected absorbance spectra were corrected for offsets due to scattering and instrument drift by subtraction of the average absorbance between 700 and 800 nm

(Stubbins et al., 2011). Data output from the spectrophotometer were in the form of dimensionless absorbance (i.e., optical density, OD) and were subsequently converted to the Napierian absorption coefficient, a (m^{-1}) (Hu et al., 2002).

Dissolved Black Carbon Concentration and Quality

Freeze dried river water samples were analyzed for DBC. DBC was determined at the molecular level via the

benzenopolycarboxylic acid (BPCA) method as described in Dittmar (2008) and with modifications following (Stubbins et al., 2012). In brief, $\sim 2 \mu\text{mol}$ of freeze dried DOC was transferred into pre-combusted (400°C , 4 h) 1 mL glass ampoules, and then redissolved in $500 \mu\text{L}$ of nitric acid (65%). The ampoules were sealed and heated to 170°C in a stainless steel pressure bomb inside a furnace for 9 h. After the ampoules cooled, $450 \mu\text{L}$ was transferred into 1 mL maximum recovery vials (Waters). The nitric acid was evaporated in a centrifugal evaporator (RVC 2-18, Christ, Germany) and the samples were redissolved in $100 \mu\text{L}$ of phosphate buffer solution (Na_2HPO_4 and NaH_2PO_4 each 5 mM in ultrapure water, buffered pH 7.2). BPCAs were determined on a Waters ACQUITY UPLC (Ultra Performance Liquid Chromatography) system composed of a binary solvent manager, a sample manager, a column manager and a photodiode array light absorbance detector (PDA e λ). BPCAs were separated on a Waters ACQUITY UPLC BEH C18 Column ($2.1 \times 150 \text{ mm}$, $1.7 \mu\text{m}$) with an aqueous phase / methanol gradient. The aqueous phase consisted of a tetrabutylammonium bromide solution (4 mM, ACS quality) in phosphate buffer (Na_2HPO_4 and NaH_2PO_4 each 5 mM in ultrapure water, pH 7.2). The injection volume was $10 \mu\text{L}$. BPCAs were identified according to retention time and absorbance spectra (220–380 nm). Quantification was performed using the absorption signal at 240 nm and external calibration.

DBC concentrations were calculated from the detected BPCA concentrations. The original equation to estimate DBC in nM of carbon (nM-C), from the molar BPCA concentrations of each BPCA (nM) (Dittmar, 2008) was:

$$[\text{DBC}] = 33.4([B6\text{CA}] + [B5\text{CA}] + 0.5[B4\text{CA}] + 0.5[B3\text{CA}]) \quad (1)$$

The factor of 33.4 is based upon a conservative estimate of the average number of C atoms within DBC molecules identified by FT-ICR MS in a variety of natural waters (Dittmar, 2008). Note that the [DBC] is in nM-C and the BPCA concentrations are reported in nM of each molecule. Each BPCA is constituted of several C atoms. For instance, B6CA includes the 6 Cs in the aromatic ring, plus 6 carboxyl group (COOH) Cs. Therefore, the conversion factor of 33.4 represents a factor of approximately 3 on a carbon basis. This compares with factors of 2.27 in an early study that assessed the yield of BPCAs from solid charcoals (Glaser et al., 1998) and a factor of four suggested for aquatic samples (Ziolkowski and Druffel, 2010; Ziolkowski et al., 2011). Under certain oxidation conditions the nitric acid oxidation of BC to BPCAs can yield nitrated analogs of the BPCAs that are not quantified here, but do constitute part of the DBC pool (Ziolkowski et al., 2011). Thus, the total DBC concentrations reported here represent a conservative estimate of total DBC in aquatic systems given that the conversion factor was lower than used elsewhere and nitrated-BPCAs were not included in the analysis.

The method used here as originally presented utilized each of the BPCAs to calculate [DBC] via equation 1 (Dittmar, 2008). Although, B3CAs were reported to be stable at 170°C (Dittmar, 2008), subsequent experience suggests that recoveries of B3CAs

are not always 100% (Stubbins et al., 2012). Furthermore, 1,2,4,5-B4CA is the only B4CA that is commercially available as a standard, prohibiting the confident conversion of the absorption signal at 240 nm for the other B4CAs to quantities. Therefore, as in a previous study (Stubbins et al., 2012), total DBC concentrations here were calculated directly from the robustly quantified B5CA and B6CA concentrations. An extensive BPCA data set collected for the Southern Ocean (Dittmar and Paeng, 2009), the Gulf of Mexico (Dittmar et al., 2012b) and other regions (unpublished) was used to develop a power-function relationship ($R = 0.998$, $n = 351$, $p < 0.0001$; Figure S1 on Data Sheet 1) to predict the concentration of DBC from the sum of the quantitatively dominant and robustly quantified B5CA and B6CA. This extrapolation reduced the analytical error range of replicate analysis for the calculation of total DBC within the model dataset to below 2% and provided a method to compare the data reported here with the total DBC concentrations reported elsewhere (Dittmar, 2008; Dittmar and Paeng, 2009; Dittmar et al., 2012a; Jaffé et al., 2013).

Given the differences in oxidation conditions and conversion factors applied in the literature, we also report the concentrations of the individual BPCAs to enable comparison with other datasets (Table S1).

RESULTS

The six rivers were sampled at variable discharge (Table S1). Concentrations of DOC ranged from 2.6 to 17.5 mg-C L^{-1} , and a_{254} from 12 to 148 m^{-1} . Concentrations of each BPCA quantified are listed in Table S1. B5CA was the most abundant BPCA and total DBC concentrations ranged from 0.14 to 1.51 mg-C L^{-1} . Changes in the quality of DBC being exported were also evident, with the B6CA:B5CA ratio ranging from 0.16 to 0.43 (Table S1). DBC loads on days when DBC concentrations were measured (i.e., DBC concentration \times daily discharge) varied from 0.26 to 194.5 kg s^{-1} (Table S1). Within each river, the concentrations and loads of DBC were highest during peak discharge.

DISCUSSION

Dissolved Black Carbon Concentrations

DBC concentrations varied by over an order of magnitude, from 0.14 to 1.51 mg-C L^{-1} (Table S1). For comparison, reported DBC concentrations ranged from 0.002 to 2.77 mg-C L^{-1} in global rivers (Jaffé et al., 2013) and from 0.02 to 0.88 mg-C L^{-1} in a small Arctic stream (Guggenberger et al., 2008). Upper limits to the concentrations of highly bio-labile forms of thermogenic DOC have been estimated in the Siberian rivers studied here based upon concentrations of levoglucosan (Myers-Pigg et al., 2015). These highly bio-labile forms of thermogenic DOC contribute up to $0.1\text{--}0.3 \text{ mg-C L}^{-1}$ to the DOC pool at the sites studied here (data from 2004 to 2006; Myers-Pigg et al., 2015).

Previous work in the Arctic has demonstrated a strong link between DOC concentration and river hydrology. Early in the year, under ice flow cannot access the organic-rich seasonally

thawed soil layer. Consequently, DOC concentrations in the river are low and sourced from groundwater (Table S1; Holmes et al., 2012). In the spring, soils and waterways thaw, and the spring freshet inundates the watershed. DOC concentrations reach maxima during this flushing event and subsequently decline as water levels fall (Holmes et al., 2012). For DBC, the same trend of high concentration at high flow, is apparent in the regression of DBC concentrations vs. runoff (watershed area normalized discharge; $\text{m}^3 \text{ km}^{-2} \text{ s}^{-1}$; Table S1), which reveals a significant linear correlation across the six rivers studied (**Figure 2A**; $R^2=0.63$; $n = 25$; $p < 0.0001$).

Plots of solute concentration vs. runoff are used in hydrological studies to learn more about potential solute sources and the mechanisms controlling their export (Evans and Davies, 1998). The simplest interpretation of the linear correlation between DBC and runoff requires the conservative mixing of only two sources. In the Paraíba do Sul River, Brazil, variations in DBC concentrations with hydrology were explained by a simple two endmember model, with low DBC concentrations in groundwater under base flow conditions mixing with inputs of higher, but constant DBC concentration waters from active soil layers as discharge increased (Dittmar et al., 2012a). In Arctic rivers, the relationship between hydrology and DBC concentration also indicates that in the winter, when the watersheds are frozen and discharge at a minimum, rivers are dominated by inputs from groundwater with low DBC. As runoff increases in the spring, the hydrological pathway incorporates soil active layers, which are rich in organics, including soluble BC (Guggenberger et al., 2008).

The lack of a plateau at high runoff in the current dataset (**Figure 2A**) suggests that if runoff were to increase, then DBC concentrations would also continue to increase, leading to greater DBC export. Eurasian Arctic river discharge has increased (Peterson et al., 2002). Modeling studies predict that runoff will increase further as the Arctic warms in the future, with the greatest increases occurring as an amplification of the spring freshet (Van Vliet et al., 2013). If these models are correct, **Figure 2A** suggests DBC exports will also increase, with the spring freshet contributing ever more to annual DBC loads. Thus, both the magnitude and the timing of DBC delivery to the Arctic Ocean are liable to change in the future.

Dissolved Black Carbon Quality

The molecular BPCA method as applied here quantifies broad classes of DBC oxidation products, each with a different number of carboxylic groups (Dittmar, 2008). These are the: benzeneTRIcarboxylic acids (B3); benzeneTETRAcarboxylic acids (B4); benzenePENTAcarboxylic acid (B5); and, benzeneHEXAcarboxylic acid (B6). Each of these PCAs provides structural information about DBC. B6 is indicative of highly condensed aromatics, whereas the benzene products with lower numbers of carboxylic substitutes are indicative of molecules with smaller numbers of condensed rings at their core (Schneider et al., 2010). As B6 and B5 were the most robustly quantified PCAs, only the ratios of these two PCAs are reported. The B6:B5 ratio provides an index, where higher values indicate greater levels of the most condensed forms of

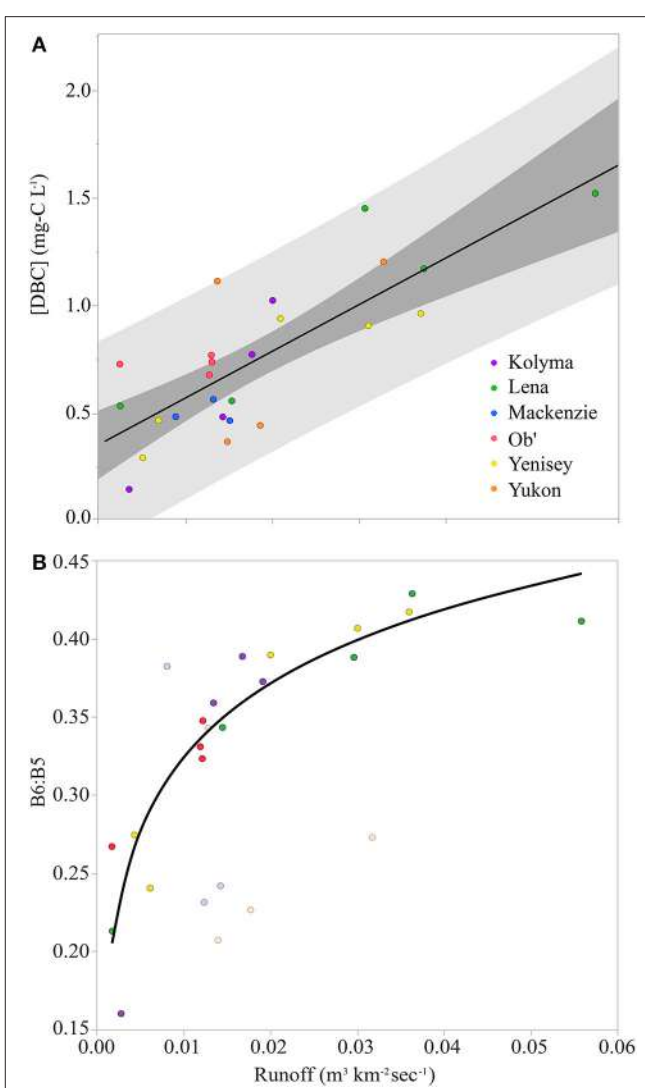


FIGURE 2 | (A) Dissolved black carbon concentrations ($[\text{DBC}]$) vs. runoff for samples from across the hydrographs of the six Arctic rivers. Black line represents the linear regression of the data ($[\text{DBC}] \text{ mg-C L}^{-1} = 0.359 + 21.94 \times \text{runoff}$; Standard error of the intercept = 0.075; Standard error of the slope = 3.48; $R^2 = 0.63$; $n = 25$; $p < 0.0001$). Dark gray represents extent of the confidence of fit (95% confidence limit). Light gray represents extent of confidence of prediction (95% confidence limit). **(B)** The ratio of benzeneHEXAcarboxylic acid to benzenePENTAcarboxylic acid ($\text{B}_6:\text{B}_5$) vs. runoff for samples from across the hydrographs of the six Arctic rivers. Data points from North American rivers are faded. Black line represents the logarithmic regression of the data from the Siberian rivers ($\text{B}_6:\text{B}_5 = 0.638 + 0.0683 \ln(\text{runoff})$; Standard error of the intercept = 0.033; Standard error of the slope = 0.007; $R^2 = 0.84$; $p < 0.0001$; $n = 18$).

DBC (Stubbins et al., 2012). B6:B5 ratios have been reported for Little Grawijka Creek, a small Arctic stream (watershed area 0.44 km^2 ; Guggenberger et al., 2008) within the watershed of the Yenisei River (watershed area $2.54 \times 10^6 \text{ km}^2$; **Table 1**). Comparison of B6:B5 values for the 6 large Arctic rivers (0.16 to 0.43; Table S1) to values in the Little Grawijka Creek (0.30 to 0.65; Guggenberger et al., 2008) suggests the DBC within the mainstems of the large Arctic rivers may be less condensed

than DBC in Little Grawjka Creek, and possibly other Arctic headwaters.

In the Siberian rivers (Kolyma, Lena, Ob', and Yenisey), there was a significant correlation between B6:B5 and runoff (**Figure 2B**). The logarithmic fit indicates that at low flow, these Siberian rivers are dominated by water from a source with low concentrations of DBC (**Figure 2A**) and that the DBC in this water is less condensed than the DBC exported at high runoff (**Figure 2B**). The B6:B5 ratio then approaches a plateau at high runoff, where the value reached at the plateau can be considered the B6:B5 ratio of a putative high runoff, high DBC concentration endmember derived from the soil active layer. The logarithmic fit to the data (**Figure 2B** caption) suggests this endmember would have a B6:B5 ratio of 0.63, α -value similar to the highest B6:B5 ratio observed at peak discharge during the spring freshet within Little Grawjka Creek (0.65; Guggenberger et al., 2008).

Although future work is required to determine the source of DBC to Arctic rivers, in the current study, both the concentrations (**Figure 2A**) and the degree of DBC condensation (**Figure 2B**) were elevated in the Siberian rivers during high flow, suggesting a soil source. It is unclear why this trend in B6:B5 was not apparent in the Yukon and Mackenzie Rivers of Northern America. The significantly higher sediment loads and associated sorption reactions in the North American rivers (Holmes et al., 2012) may differentiate their B6:B5 ratios from those observed in the sediment-poor Siberian rivers. Within the Mackenzie, B6:B5 ratios may also be influenced by inputs from petrogenic sources (Yunker et al., 2002). More data is required to verify these trends and, once verified, to seek mechanistic explanations.

Estimating Dissolved Black Carbon Export from Dissolved Organic Carbon

DBC and DOC concentrations were correlated ($R^2 = 0.96$; **Figure 3A**). Previous work has reported similar correlations between total DOC and DBC concentrations within rivers. For instance, Jaffé et al. (2013) conducted an assessment including 109 DBC concentrations for rivers diverse in stream order and latitude, including seasonally averaged values for the DBC values of the 6 Arctic rivers studied here (i.e., data for each of the 25 samples analyzed here were not presented in Jaffé et al. (2013), only their averages on a river-by-river basis). As in the current study, the intercept of the slope between DBC and DOC was statistically indistinguishable from zero (current study intercept = $-0.019 \pm 0.035 \text{ mg-CL}^{-1}$). Therefore, Jaffé et al. (2013) interpreted the slope of the linear regression to approximate the globally averaged contribution of DBC to riverine DOC concentrations. For their dataset, DBC was estimated to account for $10.5 \pm 0.7\%$ of global DOC exports. Following the same approach, reference to the slope in **Figure 3A** indicates that DBC constitutes $8.9 \pm 0.3\%$ of Arctic river DOC. This suggests Arctic river DOC is slightly depleted in DBC relative to rivers globally, though larger datasets for both global and Arctic rivers are required to strengthen this conclusion. Jaffé et al. (2013) used the percentage contribution of DBC to riverine DOC concentrations and a global DOC load of 250 Tg-C yr^{-1} (Hedges et al., 1997) to estimate that $26.5 \pm 0.8 \text{ Tg-C yr}^{-1}$ of DBC is exported to the oceans each year. An analogous calculation

based upon an Arctic DOC load of 34 Tg-C yr^{-1} (Holmes et al., 2012) and the DBC percentage for Arctic rivers, leads to an estimated DBC export by Arctic rivers of $3.0 \pm 0.1 \text{ Tg-C yr}^{-1}$.

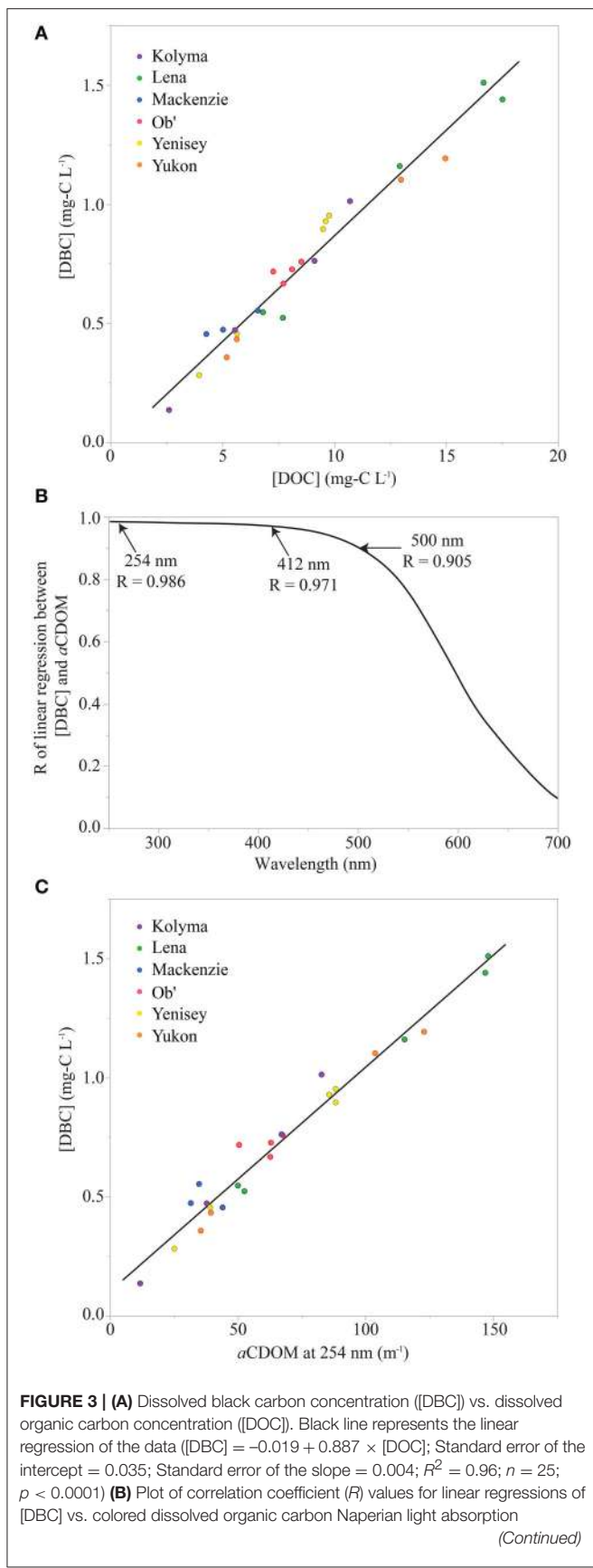
Refining Estimates of Dissolved Black Carbon Export Using CDOM

The above correlations between DOC and DBC provide a method of converting between relatively common DOC loads and rarer, more analytically challenging measurements of DBC. However, when looking for a proxy of aromatic carbon components, CDOM measurements offer even greater potential. First of all, light absorption by CDOM provides a robust empirical proxy for aromatic DOM components in Arctic rivers (Spencer et al., 2009) and model systems (Weishaar et al., 2003; Stubbins et al., 2008), including DBC concentrations in a photochemical degradation experiment (Stubbins et al., 2012). Second, measuring CDOM is simpler and cheaper than measuring DOC. Finally, estimates of CDOM can be made *in situ* with in water spectrophotometers (Spencer et al., 2007; Tait et al., 2015) and from space, using satellite remote sensing of water color (Griffin et al., 2011). To determine if CDOM could provide a robust proxy for DBC in Arctic rivers, a series of linear regressions were performed between DBC concentration and CDOM light absorption at wavelengths from 250 to 600 nm. Plotting the resultant correlation values (R) for the linear regressions against wavelength revealed which wavelengths provided the most robust proxies for DBC concentration (**Figure 3B**). Values for R peaked ($R = 0.986$) around 254 nm, a wavelength long used to estimate the relative aromatic content of DOM (Weishaar et al., 2003). At longer wavelengths, R declined gradually to 0.971 at 412 nm and 0.905 at 500 nm, before dropping more rapidly at increasing wavelengths (**Figure 3B**). The robust correlation at 412 nm is encouraging for those wishing to remote sense DBC from space, as estimates of CDOM at 412 nm can be retrieved from SeaWiFS (<http://oceancolor.gsfc.nasa.gov/SeaWiFS>) and MODIS (<http://modis.gsfc.nasa.gov>) satellites.

In the current study, the equation of the linear regression between DBC and CDOM light absorption at 254 nm (a_{254}) was used as a proxy to estimate DBC concentrations for each of the 410 samples analyzed for CDOM (**Figure 3C**). This increased the temporal extent and resolution of our DBC dataset from 25 samples over 1 year to 410 samples over 7 years. Under ice sampling for CDOM was limited as it is logistically challenging. Where data gaps exceeding 1 month occurred, the average under ice CDOM for each river was used to estimate winter concentrations of DBC for the modeling exercise below. This is unlikely to have significantly altered estimates of DBC export as under ice DOC concentration and water discharge are low and contribute minimally to annual Arctic river discharge and DOC loads (Holmes et al., 2012).

LOADEST Model Estimates of Daily Dissolved Black Carbon Loads

The goal of the current study was to develop a continuous record of DBC export for each river across 7 years. To achieve this, daily discharge values for each river, along with the 410 CDOM

**FIGURE 3 | Continued**

coefficients ($aCDOM$) vs. wavelength. **(C)** $[DBC]$ vs. $aCDOM$ at 254 nm ($a254$). Black line represents the linear regression of the data ($[DBC] = 0.104 + 0.00942 \times a254$; Standard error of the intercept = 0.028; Standard error of the slope = 0.00036; $R = 0.986$; $R^2 = 0.968$; $n = 25$; $p < 0.0001$).

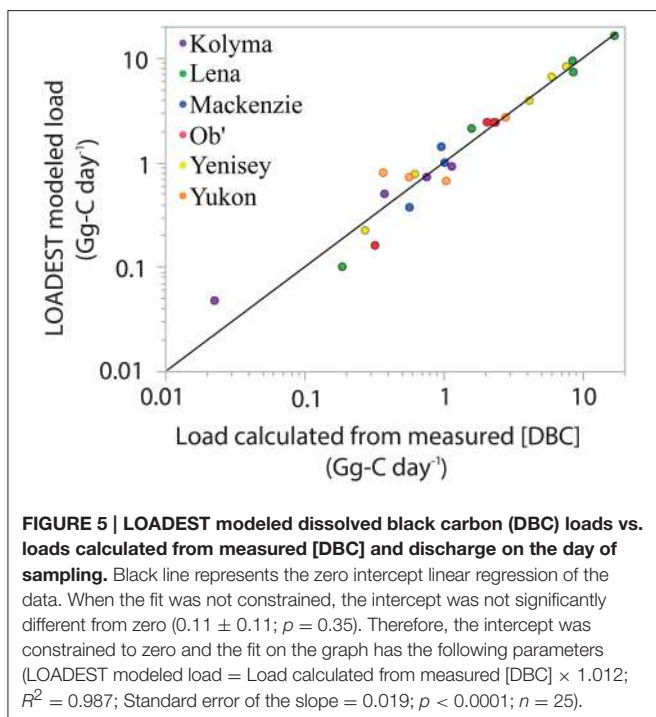
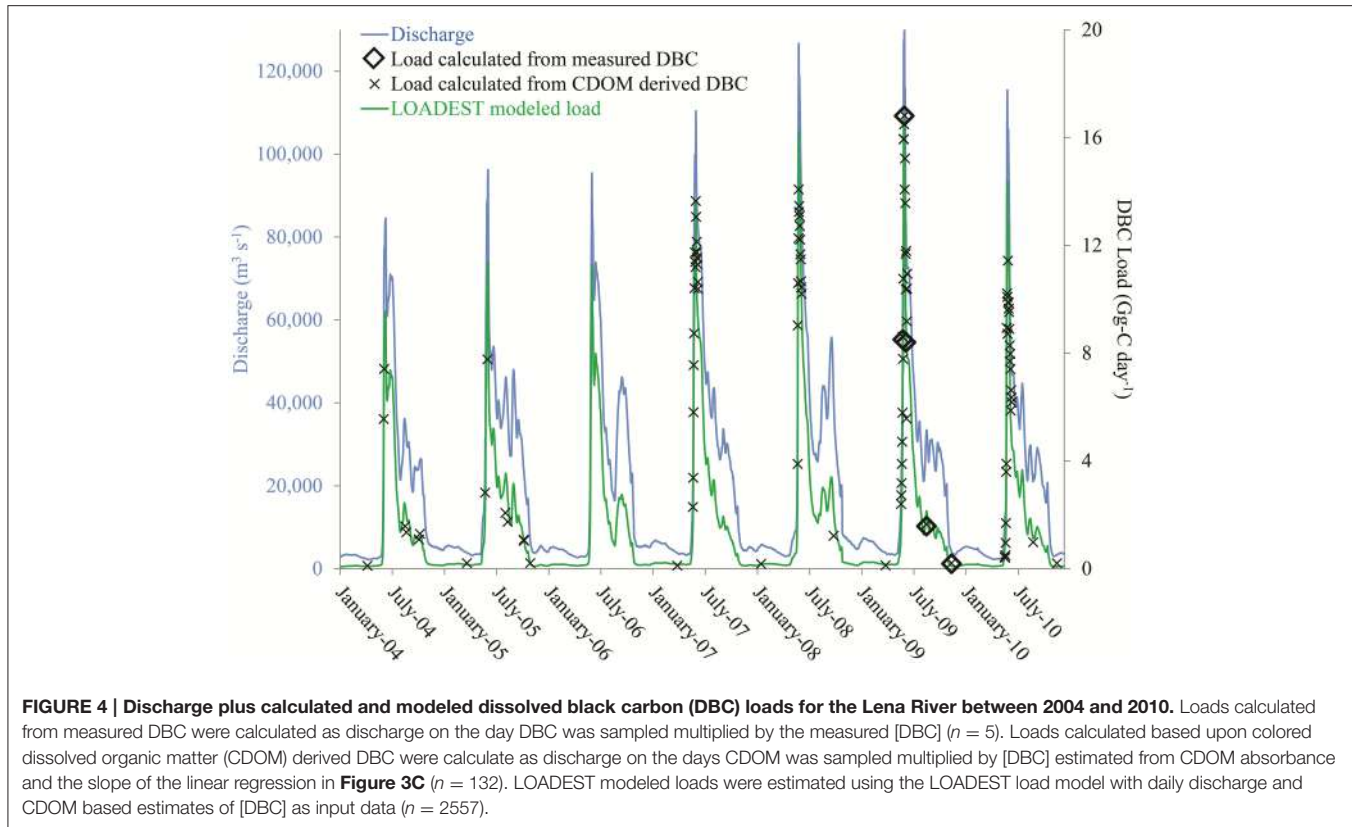
derived DBC concentrations, were entered into a hydrological load estimating model (LOADEST using predefined regression model 4; <http://water.usgs.gov/software/loadest>; Runkel et al., 2004) to determine daily and annual DBC loads. The predefined model 4 was chosen as it provides robust estimates of DOC export for Arctic rivers and to enable the resultant DBC loads to be compared directly to previous estimates of DOC loads made using the same model (Holmes et al., 2012). Output from the model provides estimated daily loads for DBC across the 7 years of hydrological data. To assess model performance, modeled daily loads were compared to daily loads calculated for the 25 days when DBC samples were collected. On these days, DBC loads were calculated as DBC concentration multiplied by measured discharge at the gauging station (Table S1). The hydrograph together with predicted and measured DBC loads for the Lena River are presented in Figure 4. Visual inspection indicates the model matches calculated data. Considering data for all rivers, the mean absolute error between modeled and calculated DBC loads was 11%. A two component linear regression ($R^2 = 0.987$; $p < 0.0001$) of modeled vs. calculated DBC loads yielded a slope of 0.999 ± 0.02 ($p < 0.0001$) and intercept of 0.11 ± 0.11 ($p = 0.3489$). The intercept was insignificantly different from zero. Forcing the slope through zero yielded a slope of 1.01 ± 0.02 ($R^2 = 0.987$; $p < 0.0001$; Figure 5). That the slope of the regression was insignificantly different from unity (i.e., 1) indicates that use of $a254$ as a proxy for DBC and the assumptions of the LOADEST model provided a quantitatively robust estimate of daily DBC loads.

Gauging stations were near the mouths of the rivers, capturing from 82 to 100 % of each individual river's discharge, and 96% of the six rivers' combined discharge (Table 1). To determine DBC loads (Gg-C yr^{-1}) for the entirety of the river watersheds, the DBC yields ($\text{Gg-C km}^{-2} \text{yr}^{-1}$) for the gauged river areas were extrapolated to the total river area (Table 1). The same modeling exercise was repeated for each BPCA quantified. Annual export of each BPCA to the Arctic Ocean is presented in the Supplementary Materials in (Tables S2A–D). Below we focus upon the total DBC flux estimates.

The annual DBC load for the six rivers ranged from 1.4 million tons per year in 2004 and 2010 to 1.7 million tons per year in 2007. Interannual variations in DBC loads were greater than interannual variation in discharge, highlighting how variations in discharge amplify variations in the export of dissolved organics (compare Table 1 and Table 2). The greatest year-to-year variation was observed in the Kolyma (33% st. dev.) and the Yukon (27% st. dev.) Rivers while the Yenisey River (5% st. dev.) showed the lowest interannual variation in loads (Table 2). The majority of the trend in interannual variability in DBC loads between rivers stems from their trends in interannual variability in discharge, which is also greatest

FIGURE 3 | (A) Dissolved black carbon concentration ($[DBC]$) vs. dissolved organic carbon concentration ($[DOC]$). Black line represents the linear regression of the data ($[DBC] = -0.019 + 0.887 \times [DOC]$; Standard error of the intercept = 0.035; Standard error of the slope = 0.004; $R^2 = 0.96$; $n = 25$; $p < 0.0001$) **(B)** Plot of correlation coefficient (R) values for linear regressions of $[DBC]$ vs. colored dissolved organic carbon Naperian light absorption coefficients ($aCDOM$) vs. wavelength. Black line represents the linear regression of the data ($[DBC] = 0.104 + 0.00942 \times a254$; Standard error of the intercept = 0.028; Standard error of the slope = 0.00036; $R = 0.986$; $R^2 = 0.968$; $n = 25$; $p < 0.0001$).

(Continued)



in the Kolyma (20%) and minimal in the Yenisey River (4%; **Table 1**). However, interannual variability in the Yukon River discharge was only 12%, suggesting that Yukon River DBC export

is particularly sensitive to discharge variation. The average annual DBC load for the six rivers was 1.5 ± 0.1 million tons per year (**Table 2**). This translates to an average areal yield of 138 ± 13 kg-C km^{-2} yr^{-1} , a DBC yield similar to that determined for a tundra forest watershed in Northern Siberia (100 kg-C km^{-2} yr^{-1} ; Guggenberger et al., 2008), but more than double that of the Parába do Sul which drains an area of intense slash-and-burn land clearing in Brazil (Dittmar et al., 2012a).

The gauged area of the six rivers studied covered $10.9 \times 10^6 \text{ km}^2$ or 53% of the pan-Arctic watershed (**Figure 1**). A pan-Arctic DBC load of 2.8 ± 0.25 million tons per year was estimated assuming DBC yields to be the same in the sampled and unsampled fractions of the pan-Arctic watershed. Riverine export of particulate BC has been presented for the six rivers studied here (Elmquist et al., 2008; **Table 2**). This estimate of particulate BC loads (Elmquist et al., 2008) was made using the chemothermic oxidation (CTO) method that over estimates BC in organic rich samples such as particulate organic matter samples (Hammes et al., 2007). Therefore, the particulate BC fluxes should be considered an upper limit or an over estimate of true loads. Despite the potential for the CTO particulate BC to be an overestimate, our calculated load based upon the BPCA method which yields conservative estimates of DBC from the six rivers is eight times that of particulate BC (**Table 2**). This makes riverine DBC export the largest quantified term for BC removal from the pan-Arctic watershed, suggesting that DBC export plays a major role in the Arctic storage of soil BC. This appears to be true elsewhere in the world. For instance, estimated DBC export

TABLE 2 | Average dissolved black carbon (DBC) loads, yields and interannual variation in both for the six rivers studied and for the pan-Arctic watershed, plus literature values for the rivers' dissolved organic carbon (DOC; Holmes et al., 2012), particulate organic carbon (POC; Stein and MacDonald, 2004) and particulate black carbon (PBC; Elmquist et al., 2008) loads.

River/ Watershed	DBC load (Gg-C yr ⁻¹)	DBC yield (kg-C km ⁻² yr ⁻¹)	Interannual variation (St. Dev.)	DOC load (Gg-C yr ⁻¹)	PBC load (Gg-C yr ⁻¹)	POC load (Gg-C yr ⁻¹)
Kolyma	62 ± 20	116 ± 38	33%	818	24	310
Lena	550 ± 68	226 ± 28	16%	5681	36	1200
Mackenzie	129 ± 20	77 ± 12	12%	1377	99	2100
Ob'	262 ± 44	87 ± 15	17%	4119	18	360
Yenisey	402 ± 19	167 ± 8	5%	4645	10	170
Yukon	102 ± 28	123 ± 34	27%	1472	1.1	12
Total for six rivers	1506 ± 133	138 ± 13	—	18,109	188	4152
Pan-Arctic	2842 ± 250	—	—	34,042	—	—

by a tropical river in Brazil is far greater than contemporary BC production in the watershed (Dittmar et al., 2012a).

Comparing DBC export to total organic carbon fluxes reveals that DBC contributes approximately 8% of DOC export (Holmes et al., 2012), which is slightly less than the 8.9% of DOC estimated using the linear correlation between DBC and DOC (**Figure 3A**). This flux equates to 36% of total particulate organic carbon (POC) export from the six rivers studied (Stein and MacDonald, 2004; **Table 2**). The export and burial of terrestrial POC in ocean margins is a significant long-term carbon sink (Blair and Aller, 2012). By analogy, if DBC is also locked away in the marine environment, riverine DBC export represents a translocation of refractory carbon from one store to another. If however, DBC is labile within the ocean, the once refractory carbon stored in the soil black carbon pool will re-enter the contemporary carbon cycle. As DBC is refractory in the deep ocean (Dittmar and Paeng, 2009; Ziolkowski and Druffel, 2010), yet highly labile when exposed to sunlight (Stubbins et al., 2010, 2012), the efficiency of carbon translocation from soil to ocean stores may be strongest in Arctic waters where it has been demonstrated that a significant fraction of other terrestrially derived, photo-labile aromatics survive transport to the major regions of North Atlantic Deep Water formation (Benner et al., 2005). Therefore, although Arctic rivers contribute 11% of the 26.5 million tons per year of DBC delivered to the oceans globally (Jaffé et al., 2013), their relative contribution to the global deep ocean store of DBC is potentially much higher. The Arctic rivers alone would replenish the global marine pool of DBC (>12 Pg-C; Dittmar and Paeng, 2009) in approximately 4300 years. This initial estimate is considerably shorter than the apparent age of DBC in the open ocean (Ziolkowski and Druffel, 2010) suggesting that Arctic river DBC export and subsequent entrainment into the abyssal ocean at points of deep water formation could provide the single most important pathway of DBC delivery to the deep ocean.

CONCLUSIONS

Today, the DBC mediated transfer of BC from the land to the oceans is a major term in the Arctic carbon cycle. In

terms of continued research, measurement of photo-labile, but bio-refractory thermogenic DOM, i.e., DBC quantified as BPCAs, and highly bio-labile thermogenic DOM quantified via levoglucosan offer an intriguing dual tracer approach to assess the dynamics of thermogenic DOM within aquatic systems (Myers-Pigg et al., 2015). Optical measurements of absorbance, including at 412 nm, a wavelength amenable to remote sensing, provide robust proxies for DBC concentrations in Arctic rivers that should enable us to resolve temporal and spatial patterns in DBC cycling. Looking to the future of the Arctic, Arctic warming is set to continue at rates exceeding global average temperature increases, leading to pronounced perturbations in the Arctic which are likely to increase the production and export of BC. Warming and associated changes to the water cycle appear to be increasing Arctic wildfire frequency (Higuera et al., 2008; Hu et al., 2010), potentially increasing BC production. Arctic soils store the largest pool of organic carbon on the planet (Gruber et al., 2004). Changing climate in the Arctic is increasing river water discharge (Peterson et al., 2002; Van Vliet et al., 2013). Increasing runoff will likely increase DBC export (**Figure 2**). Therefore, it is likely that the transfer of BC from Arctic soils to the ocean will accelerate. Measurements of CDOM light absorption for discrete water samples, using *in situ* spectrophotometers, or via remote sensing techniques could provide an effective way of monitoring future DBC fluxes to the Arctic Ocean so long as periodic checks are made to test the continuing veracity of the linear regression presented here (**Figure 3C**). The eventual fate of exported DBC in the Arctic and global ocean will influence the sign and degree of climate-carbon cycle feedbacks. If exported DBC is effectively photo-degraded in ocean surface waters, its carbon will likely enter the atmospheric CO₂ pool. However, if exported Arctic DBC reaches areas of deep water formation around Greenland, it will be reburied, not in the soils of the Arctic, but the deep waters of the global ocean.

AUTHOR CONTRIBUTIONS

All authors contributed to the design of the study. JN analyzed samples for dissolved black carbon. AS, RS, and PM conducted

modeling studies. All authors contributed to the writing of the manuscript.

ACKNOWLEDGMENTS

Ekaterina Bulygina is thanked for CDOM analyses, Ina Ulber for assistance with BPCA samples, Greg Fiske for assistance with GIS analysis and the preparation of **Figure 1**, and Anna Boyette for assistance with figures. This work was funded by the U.S. National Science Foundation (ANT-1203885, OPP-0732522, OPP-0732821, OPP-1107774, DEB-1146161, DEB-1145932, PLR-1500169) and a Fellowship from

the Hanse Institute for Advanced Studies (HWK, Delmenhorst, Germany) granted to AS. Data are archived at the Skidaway Institute of Oceanography and are attainable from AS or via the Arctic Great Rivers Observatory website (<http://arcticgreatrivers.org/>).

SUPPLEMENTARY MATERIAL

The Supplementary Material for this article can be found online at: <http://journal.frontiersin.org/article/10.3389/feart.2015.00063>

REFERENCES

- Benner, R., Louchouarn, P., and Amon, R. M. W. (2005). Terrigenous dissolved organic matter in the Arctic Ocean and its transport to surface and deep waters of the North Atlantic. *Global Biogeochem. Cycles* 19:GB2025. doi: 10.1029/2004GB002398
- Blair, N. E., and Aller, R. C. (2012). The fate of terrestrial organic carbon in the marine environment. *Ann. Rev. Mar. Sci.* 4, 401–423. doi: 10.1146/annurev-marine-120709-142717
- Bowman, D. M. J. S., Balch, J. K., Artaxo, P., Bond, W. J., Carlson, J. M., Cochrane, M. A., et al. (2009). Fire in the earth system. *Science* 324, 481–484. doi: 10.1126/science.1163886
- Dittmar, T. (2008). The molecular level determination of black carbon in marine dissolved organic matter. *Org. Geochem.* 39, 396–407. doi: 10.1016/j.orggeochem.2008.01.015
- Dittmar, T., De Rezende, C. E., Manecki, M., Niggemann, J., Coelho Ovalle, A. R., Stubbins, A., et al. (2012a). Continuous flux of dissolved black carbon from a vanished tropical forest biome. *Nat. Geosci.* 5, 618–622. doi: 10.1038/ngeo1541
- Dittmar, T., and Paeng, J. (2009). A heat-induced molecular signature in marine dissolved organic matter. *Nat. Geosci.* 2, 175–179. doi: 10.1038/ngeo440
- Dittmar, T., Paeng, J., Gihring, T. M., Suryaputra, I. G., and Huettel, M. (2012b). Discharge of dissolved black carbon from a fire-affected intertidal system. *Limnol. Oceanogr.* 57, 1171–1181. doi: 10.4319/lo.2012.57.4.1171
- Elmquist, M., Semiletov, I., Guo, L., and Gustafsson, Ö. (2008). Pan-Arctic patterns in black carbon sources and fluvial discharges deduced from radiocarbon and PAH source apportionment markers in estuarine surface sediments. *Global Biogeochem. Cycles* 22:GB2018. doi: 10.1029/2007GB002994
- Evans, C., and Davies, T. D. (1998). Causes of concentration/discharge hysteresis and its potential as a tool for analysis of episode hydrochemistry. *Water Resour. Res.* 34, 129–137. doi: 10.1029/97WR01881
- Forbes, M. S., Raison, R. J., and Skjemstad, J. O. (2006). Formation, transformation and transport of black carbon (charcoal) in terrestrial and aquatic ecosystems. *Sci. Total Environ.* 370, 190–206. doi: 10.1016/j.scitotenv.2006.06.007
- Glaser, B., Haumaier, L., Guggenberger, G., and Zech, W. (1998). Black carbon in soils: the use of benzenecarboxylic acids as specific markers. *Org. Geochem.* 29, 811–819. doi: 10.1016/S0146-6380(98)00194-6
- Griffin, C. G., Frey, K. E., Rogan, J., and Holmes, R. M. (2011). Spatial and interannual variability of dissolved organic matter in the Kolyma River, East Siberia, observed using satellite imagery. *J. Geophys. Res. Biogeosci.* 116:G03018. doi: 10.1029/2010JG001634
- Gruber, N., Friedlingstein, P., Field, C. B., Valentini, R., Heimann, M., Richey, J. E., et al. (2004). “The vulnerability of the carbon cycle in the 21st century: An assessment of carbon-climate-human interactions,” in *The Global Carbon Cycle: Integrating Humans, Climate, and the Natural World*, eds M. R. R. Christopher and B. Field (Washington, DC: Island Press), 45–76.
- Guggenberger, G., Rodionov, A., Shibistova, O., Grabe, M., Kasansky, O. A., Fuchs, H., et al. (2008). Storage and mobility of black carbon in permafrost soils of the forest tundra ecotone in Northern Siberia. *Glob. Change Biol.* 14, 1367–1381. doi: 10.1111/j.1365-2486.2008.01568.x
- Hammes, K., Schmidt, M. W. I., Smernik, R. J., Currie, L. A., Ball, W. P., Nguyen, T. H., et al. (2007). Comparison of quantification methods to measure fire-derived (black/elemental) carbon in soils and sediments using reference materials from soil, water, sediment and the atmosphere. *Glob. Biogeochem. Cycles* 21:GB3016. doi: 10.1029/2006GB002914
- Hansell, D. A. (2013). Recalcitrant dissolved organic carbon fractions. *Ann. Rev. Mar. Sci.* 5, 421–445. doi: 10.1146/annurev-marine-120710-100757
- Hedges, J., Keil, R., and Benner, R. (1997). What happens to terrestrial organic matter in the ocean? *Org. Geochem.* 27, 195–212. doi: 10.1016/S0146-6380(97)00066-1
- Higuera, P. E., Brubaker, L. B., Anderson, P. M., Brown, T. A., Kennedy, A. T., and Hu, F. S. (2008). Frequent fires in ancient shrub tundra: implications of paleorecords for arctic environmental change. *PLoS ONE* 3:e0001744. doi: 10.1371/journal.pone.0001744
- Holmes, R. M., McClelland, J. W., Peterson, B. J., Tank, S. E., Bulygina, E., Eglington, T. I., et al. (2012). Seasonal and annual fluxes of nutrients and organic matter from large rivers to the arctic ocean and surrounding seas. *Estuar. Coast.* 35, 369–382. doi: 10.1007/s12237-011-9386-6
- Hu, C., Muller-Karger, F. E., and Zepp, R. G. (2002). Absorbance, absorption coefficient, and apparent quantum yield: a comment on common ambiguity in the use of these optical concepts. *Limnol. Oceanogr.* 47, 1261–1267. doi: 10.4319/lo.2002.47.4.1261
- Hu, F. S., Higuera, P. E., Walsh, J. E., Chapman, W. L., Duffy, P. A., Brubaker, L. B., et al. (2010). Tundra burning in Alaska: linkages to climatic change and sea ice retreat. *J. Geophys. Res. Biogeosci.* 115:G04002. doi: 10.1029/2009JG001270
- Jaffé, R., Ding, Y., Niggemann, J., Vähälahti, A. V., Stubbins, A., Spencer, R. G. M., et al. (2013). Global charcoal mobilization from soils via dissolution and riverine transport to the oceans. *Science* 340, 345–347. doi: 10.1126/science.1231476
- Jurado, E., Dachs, J., Duarte, C. M., and Simo, R. (2008). Atmospheric deposition of organic and black carbon to the global oceans. *Atmos. Environ.* 42, 7931–7939. doi: 10.1016/j.atmosenv.2008.07.029
- Mitra, S., Zimmerman, A., Hunsinger, G., and Woerner, W. (2013). Black carbon in coastal and large river systems. *Biogeochem. Dyn. Major River Coast. Interfaces* 200, 200–236. doi: 10.1017/CBO9781139136853.012
- Myers-Pigg, A. N., Louchouarn, P., Amon, R. M., Prokushkin, A., Pierce, K., and Rubtsov, A. (2015). Labile pyrogenic dissolved organic carbon in major Siberian Arctic rivers: implications for wildfire-stream metabolic linkages. *Geophys. Res. Lett.* 42, 377–385. doi: 10.1002/2014GL062762
- Peterson, B. J., Holmes, R. M., McClelland, J. W., Vörösmarty, C. J., Lammers, R. B., Shiklomanov, A. I., et al. (2002). Increasing river discharge to the Arctic Ocean. *Science* 298, 2171–2173. doi: 10.1126/science.1077445
- Raymond, P. A., McClelland, J. W., Holmes, R. M., Zhulidov, A. V., Mull, K., Peterson, B. J., et al. (2007). Flux and age of dissolved organic carbon exported to the Arctic Ocean: a carbon isotopic study of the five largest arctic rivers. *Global Biogeochem. Cycles* 21:GB4011. doi: 10.1029/2007GB002934
- Runkel, R. L., Crawford, C. G., and Cohn, T. A. (2004). “Load Estimator (LOADEST): A FORTRAN program for estimating constituent loads in streams and rivers,” in *Techniques and Methods* (Colorado: United States Geological Survey).

- Schmidt, M. W. I., Torn, M. S., Abiven, S., Dittmar, T., Guggenberger, G., Janssens, I. A., et al. and Trumbore, S.E. (2011). Persistence of soil organic matter as an ecosystem property. *Nature* 478, 49–56. doi: 10.1038/nature10386
- Schneider, M. P. W., Hilf, M., Vogt, U. F., and Schmidt, M. W. I. (2010). The benzene polycarboxylic acid (BPCA) pattern of wood pyrolyzed between 200°C and 1000°C. *Org. Geochem.* 41, 1082–1088. doi: 10.1016/j.orggeochem.2010.07.001
- Spencer, R. G. M., Aiken, G. R., Butler, K. D., Dornblaser, M. M., Striegl, R. G., and Hernes, P. J. (2009). Utilizing chromophoric dissolved organic matter measurements to derive export and reactivity of dissolved organic carbon exported to the Arctic Ocean: a case study of the Yukon River, Alaska. *Geophys. Res. Lett.* 36:L06401. doi: 10.1029/2008GL036831
- Spencer, R. G. M., Pellerin, B. A., Bergamaschi, B. A., Downing, B. D., Kraus, T. E. C., Smart, D. R., et al. (2007). Diurnal variability in riverine dissolved organic matter composition determined by *in situ* optical measurement in the San Joaquin River (California, USA). *Hydrolog. Process.* 21, 3181–3189. doi: 10.1002/hyp.6887
- Stein, R., and MacDonald, R. W. (eds.). (2004). *The Organic Carbon Cycle in the Arctic Ocean*. Berlin; Heidelberg: Springer. doi: 10.1007/978-3-642-18912-8
- Stubbins, A., and Dittmar, T. (2012). Low volume quantification of dissolved organic carbon and dissolved nitrogen. *Limnol. Oceanogr. Methods* 10, 347–352. doi: 10.4319/lom.2012.10.347
- Stubbins, A., Hubbard, V., Uher, G., Law, C. S., Upstill-Goddard, R. C., Aiken, G. R., et al. (2008). Relating carbon monoxide photoproduction to dissolved organic matter functionality. *Environ. Sci. Technol.* 42, 3271–3276. doi: 10.1021/es703014q
- Stubbins, A., Law, C. S., Uher, G., and Upstill-Goddard, R. C. (2011). Carbon monoxide apparent quantum yields and photoproduction in the Tyne estuary. *Biogeosciences* 8, 703–713. doi: 10.5194/bg-8-703-2011
- Stubbins, A., Niggemann, J., and Dittmar, T. (2012). Photo-lability of deep ocean dissolved black carbon. *Biogeosciences* 9, 1661–1670. doi: 10.5194/bg-9-1661-2012
- Stubbins, A., Spencer, R. G. M., Chen, H., Hatcher, P. G., Mopper, K., Hernes, P. J., et al. (2010). Illuminated darkness: molecular signatures of Congo River dissolved organic matter and its photochemical alteration as revealed by ultrahigh precision mass spectrometry. *Limnol. Oceanogr.* 55, 1467–1477. doi: 10.4319/lo.2010.55.4.1467
- Tait, Z. S., Thompson, M., and Stubbins, A. (2015). Chemical fouling reduction of a submersible steel spectrophotometer in estuarine environments using a sacrificial zinc anode. *J. Environ. Qual.* 44, 1321–1325. doi: 10.2134/jeq2014.11.0484
- Van Vliet, M. T. H., Franssen, W. H. P., Yearsley, J. R., Ludwig, F., Haddeland, I., Lettenmaier, D. P., et al. (2013). Global river discharge and water temperature under climate change. *Glob. Environ. Change* 23, 450–464. doi: 10.1016/j.gloenvcha.2012.11.002
- Weishaar, J. L., Aiken, G. R., Bergamaschi, B. A., Fram, M. S., Fujii, R., and Mopper, K. (2003). Evaluation of specific ultraviolet absorbance as an indicator of the chemical composition and reactivity of dissolved organic carbon. *Environ. Sci. Technol.* 37, 4702–4708. doi: 10.1021/es030360x
- Yunker, M., Backus, S., Pannatier, E. G., Jeffries, D., and MacDonald, R. (2002). Sources and significance of alkane and PAH hydrocarbons in Canadian arctic rivers. *Estuar. Coast. Shelf Sci.* 55, 1–31. doi: 10.1006/ecss.2001.0880
- Ziolkowski, L. A., Chamberlin, A., Greaves, J., and Druffel, E. R. (2011). Quantification of black carbon in marine systems using the benzene polycarboxylic acid method: a mechanistic and yield study. *Limnol. Oceanogr. Methods* 9, 140–140. doi: 10.4319/lom.2011.9.140
- Ziolkowski, L. A., and Druffel, E. R. M. (2010). Aged black carbon identified in marine dissolved organic carbon. *Geophys. Res. Lett.* 37:L16601. doi: 10.1029/2010GL043963

Conflict of Interest Statement: The Guest Associate Editor Christopher Osburn declares that, despite having collaborated with authors Thorsten Dittmar and Jutta Niggemann, the review process was handled objectively. The authors declare that the research was conducted in the absence of any commercial or financial relationships that could be construed as a potential conflict of interest.

Copyright © 2015 Stubbins, Spencer, Mann, Holmes, McClelland, Niggemann and Dittmar. This is an open-access article distributed under the terms of the Creative Commons Attribution License (CC BY). The use, distribution or reproduction in other forums is permitted, provided the original author(s) or licensor are credited and that the original publication in this journal is cited, in accordance with accepted academic practice. No use, distribution or reproduction is permitted which does not comply with these terms.



Are Extracted Materials Truly Representative of Original Samples? Impact of C18 Extraction on CDOM Optical and Chemical Properties

Andrea A. Andrew¹, Rossana Del Vecchio^{2*}, Yi Zhang¹, Ajit Subramaniam³ and Neil V. Blough^{1*}

¹ Department of Chemistry and Biochemistry, University of Maryland, College Park, MD, USA, ² Earth System Science Interdisciplinary Center, University of Maryland, College Park, MD, USA, ³ Lamont Doherty Earth Observatory at Columbia University, Palisades, NY, USA

OPEN ACCESS

Edited by:

Christopher Osburn,
North Carolina State University, USA

Reviewed by:

Colin Andrew Stedmon,
Technical University of Denmark,
Denmark
Joanna D. Kinsey,
North Carolina State University, USA

*Correspondence:

Rossana Del Vecchio
rossdv@umd.edu;
Neil V. Blough
neilb@umd.edu

Specialty section:

This article was submitted to
Marine Biogeochemistry,
a section of the journal
Frontiers in Chemistry

Received: 30 September 2015

Accepted: 18 January 2016

Published: 05 February 2016

Citation:

Andrew AA, Del Vecchio R, Zhang Y, Subramaniam A and Blough NV (2016) Are Extracted Materials Truly Representative of Original Samples? Impact of C18 Extraction on CDOM Optical and Chemical Properties. *Front. Chem.* 4:4.
doi: 10.3389/fchem.2016.00004

Some properties of dissolved organic matter (DOM) and chromophoric dissolved organic matter (CDOM) can be easily measured directly on whole waters, while others require sample concentration and removal of natural salts. To increase CDOM content and eliminate salts, solid phase extraction (SPE) is often employed. Biases following extraction and elution are inevitable, thus raising the question of how truly representative the extracted material is of the original. In this context, we investigated the wavelength dependence of extraction efficiency for C18 cartridges with respect to CDOM optical properties using samples obtained from the Middle Atlantic Bight (MAB) and the Equatorial Atlantic Ocean (EOA). Further, we compared the optical changes of C18 extracts and the corresponding whole water following chemical reduction with sodium borohydride (NaBH_4). C18 cartridges preferentially extracted long-wavelength absorbing/emitting material for samples impacted by riverine input. Extraction efficiency overall decreased with offshore distance away from riverine input. Spectral slopes of C18-OM samples were also almost always lower than those of their corresponding CDOM samples supporting the preferential extraction of higher molecular weight absorbing material. The wavelength dependence of the optical properties (absorption, fluorescence emission, and quantum yield) of the original water samples and their corresponding extracted material were very similar. C18 extracts and corresponding water samples further exhibited comparable optical changes following NaBH_4 reduction, thus suggesting a similarity in nature (structure) of the optically active extracted material, independent of geographical locale. Altogether, these data suggested a strong similarity between C18 extracts and corresponding whole waters, thus indicating that extracts are representative of the CDOM content of original waters.

Keywords: CDOM absorbance, fluorescence, C18 extraction, extraction efficiency, NaBH_4 reduction

INTRODUCTION

The optical properties of chromophoric dissolved organic matter (CDOM; and humic substances, HS) have been intensively studied over the last several decades. However, inter-laboratory data comparison is often impossible due to various methods employed to collect, extract, and analyze DOM and CDOM. Despite a few very sensitive analytical techniques such as optical spectroscopy which allow direct measures of bulk CDOM in natural waters, the majority of the available techniques require prior extraction, concentration of DOM/CDOM, and salt removal.

Many solid phase extraction (SPE) techniques for DOM isolation from fresh to salt waters have thus been widely used including cartridges pre-packed with XAD resins (Daignault et al., 1988), C18-bonded silica sorbents (Benner, 2002 and references therein), and more recently, modified styrene-divinylbenzene copolymer type sorbents (PPL) (Dittmar et al., 2008). Reverse osmosis (RO) has also been used for retention and concentration of DOM from fresh waters (Serkiz and Perdue, 1990). Most recently, a new technique for more efficient isolation of DOM from seawater was developed by combining RO with electrodialysis (RO/ED; Vetter et al., 2007). However, extraction efficiencies vary among these techniques and are routinely expressed relative to dissolved organic carbon (DOC).

XAD resins have been widely used to remove hydrophobic compounds of various molecular sizes. International Humic Substances Society (IHSS) has used XAD-8 to extract standard reference materials (Suwannee River Fulvic and Humic Acids, SRFA, and SRHA) from natural waters. However, XAD-8 resins used for the extraction of DOM are either no longer available (Dittmar et al., 2008) or are difficult to obtain and require extensive purifications before use (IHSS). C18 sorbents have been more widely employed for reversed phase extraction of nonpolar to moderately polar compounds from water. Retention is based on the partitioning of the nonpolar organic analyte into the nonpolar sorbent. Thus, charged compounds are usually not retained and require ion exchange SPE for their extraction. Sequential SPE through two different XAD resins has been shown to recover comparable DOC as silica-C18, with percent DOC recovery ranging from 23 to 40% (Amador et al., 1990; Druffel et al., 1992). More recently, PPL sorbents have been employed for extracting DOM. As with XAD and silica-C18, PPL retains moderately polar to nonpolar substances from large volumes of water. Dittmar et al. (2008) showed that the use of PPL was more efficient in the extraction process, reporting that an average 62% of DOC was recovered as salt-free extracts. The most recent extraction methods using RO/ED has been shown to have DOC recoveries of 60% (Vetter et al. (2007)). Similarly, Helms et al. (2013) reported DOC recoveries of 78 ± 3% and fluorescence recoveries in the EEM Peak C and M regions roughly in proportion to DOC, for 674 m Pacific waters extracted by RO/ED.

These extraction processes facilitate the elimination of the high concentrations of inorganic salts occurring in marine waters. Thus, highly concentrated organic samples with relatively

low salt content can be generated and different analytical techniques can be performed on the extracts. However, most of the studies have mainly focused on recovery/extraction efficiency in terms of % DOC. Extraction efficiency of carbon (% DOC) would not necessarily match extraction efficiency of CDOM, the carbon pool that absorbs light, given the variable dependence of CDOM to DOC. Further, DOC may be contaminated with carbon from solvents employed for elution. On this basis, the question as to how representative the extracts reflect the properties of the original samples as a whole needs further consideration.

Some earlier studies have made attempts to better address this question by comparing the optical properties of whole natural water collected from different environments to their corresponding C18 extracts (C18-OM). Green and Blough (1994) employed water samples from southern and western coast of Florida to the eastern Gulf of Mexico, and compared spectral slopes, absorption coefficient at 355 nm and fluorescence quantum yields for CDOM and C18-OM. They also examined the efficiency of extraction of the various water types. Their results indicated that longer wavelength absorbing material was isolated with greater efficiency, which was reflected in lower S values for C18 extracts relative to CDOM. Similarly, fluorescence results also indicated greater retention of longer wavelength fluorescing components, 65% of that excited at 450 nm, compared to 35% at 325 nm. Boyle et al. (2009) investigated the optical properties of CDOM and C18-OM, using samples from the Middle Atlantic Bight (MAB), but only compared $\text{aCDOM}(355)$ and spectral slopes. Helms et al. (2013) reported minor effects of RO/ED on the optical properties of SUVA254, spectral slope, and fluorescence indices for extracts of Pacific waters. Their results showed a slight increase in S275-295 slope ratio and decrease in Peak A and M fluorescence. These studies (Green and Blough, 1994; Boyle et al., 2009; Helms et al., 2013) were limited in terms of (1) the number and types of samples studied; (2) limited number wavelengths examined; and (3) did not explore the effect, if any, of the preferential extraction of long wavelength absorbing and fluorescing components on the chemical properties and reactivity of C18 extracts relative to CDOM.

In this study, we present a more extensive comparison of the optical properties of original CDOM and C18-OM samples. This study further examined the changes in the optical properties of CDOM and C18-OM following chemical reduction with sodium borohydride (NaBH_4). Samples were collected from very different geographic locales spanning riverine, estuarine, and marine type environments: (a) along a transect from the Delaware River to the Sargasso Sea (Middle Atlantic Bight, MAB); and (b) across the Equatorial Atlantic Ocean (EAO) from the open ocean gyre to the Congo River Plume. To our knowledge no study has done such a detailed comparison from such a wide range of water types. Absorption and fluorescence were measured directly for natural waters (CDOM) and compared to those of C18 extracts (C18-OM); similarly, absorption and fluorescence were measured directly for NaBH_4 reduced CDOM and compared to NaBH_4 reduced C18-OM. The wavelength dependence of extraction efficiency of C18 cartridges was examined in relation to the optical properties (MAB and EAO).

MATERIALS AND PROCEDURES

Samples

Samples from the Mid Atlantic Bight (MAB) were collected onboard the R/V Cape Henlopen and R/V Cape Hugh Sharp from August to December during three cruises from 2005 to 2006: September 20–24, 2005; August 24–28, 2006; and November 30–December 4, 2006. A typical transect from the Delaware River (~40 N; ~75 W) to the western boundary of the Gulf Stream (~36 N; ~72 W) was visited during all cruises (**Figure 1A**). The water column was thermally- and density-stratified during the summertime, typical of coastal waters on the shelf of the MAB, while stratification was absent or not fully developed during the spring, fall, and winter surveys (Del Vecchio and Blough, 2004b). Ocean samples were collected onboard the R/V Endeavor in the EAO in May–June 2009 over a 5 week period, encompassing three zonal and meridional sections between 23 W and 5 E, and 3 N and 3 S, respectively (Andrew et al., 2013).

Water samples for the optical measurements of CDOM were collected as previously reported (Del Vecchio and Blough, 2004b). Briefly, samples were collected employing a CTD (conductivity–temperature–depth) rosette equipped with Niskin bottles and were immediately filtered using GF/F filters (0.7- μm pore size). Samples for optical measurements were stored in the dark at 4°C until measurement (about 2 weeks for coastal samples and 3 months for ocean samples). Before measurement, samples were re-filtered through 0.2- μm pore-size nylon syringe filters to ensure removal of all particles.

Water samples for optical measurements of C18 extracted material were collected from the vessel's surface water pumping system (2 and 5 m) and CTD rosette and were immediately filtered through an in-line Gelman fluted capsule filter (0.2 μm pore size). A clean Teflon line for the pumping system was supplied at the beginning of each cruise to prevent contamination by material accumulating in the line. Filtered water samples (20 L) were acidified to pH 2 (pre extraction) and then pumped through the SPE cartridge (C18 extraction column, UCT) at the flow rate of 50 mL min⁻¹ as described by Boyle et al. (2009). The cartridges were pretreated with 100 ml of high purity methanol followed by 50 mL of acidified (pH 2) Milli-Q water prior to extraction. After extraction each cartridge was rinsed with 1 L of acidified (pH 2) Milli-Q water to remove salts and stored in the refrigerator (4°C) until further processing. The post cartridge eluent was stored for further analysis (post extraction).

DOM was extracted from the C18 cartridges with 50 mL of high purity methanol: the first fraction (5 mL) that contained some aqueous residue was separated from the second fraction (45 mL). The second fraction was collected into a 100 mL round bottom flask and evaporated to dryness under vacuum using a rotary evaporator at 30–35°C. The dried material was re-dissolved with Milli-Q water (~2 mL), neutralized with diluted NaOH solution to pH 7 and stored frozen till further analysis. This material is here on referred to as C18-OM.

Optical Measurements

CDOM absorption spectra were acquired with a Shimadzu 2401-PC spectrophotometer employing a 10 cm optical cell (1 cm cell for C18-OM) using Milli-Q water as the blank, as

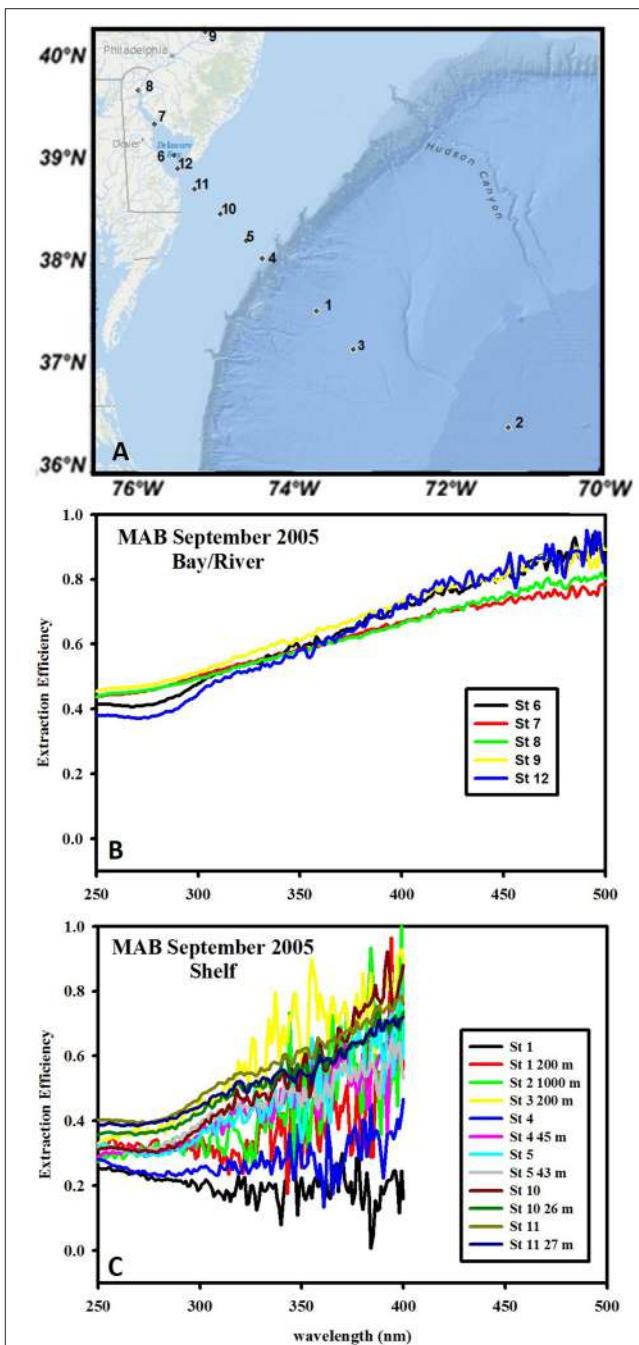


FIGURE 1 | Wavelength dependence of extraction efficiency of C18 cartridges for waters from the MAB during September 2005. **(A)** Typical transect for all cruises, extending from the Delaware River to shelf/offshore waters. **(B)** Extraction efficiency for river and bay samples. **(C)** Extraction efficiency for shelf and shelf break samples. The large noise at longer wavelengths is due to the small absorbance values. Values at >~400 nm are at or below the detection limit and were thus omitted.

reported previously (Vodacek et al., 1997; Del Vecchio and Blough, 2004b). Absorption spectra for offshore CDOM samples (including samples from the EAO as well as samples further offshore in the MAB region) were obtained on a liquid core capillary waveguide long path spectrometer (WPI) using the 10, 50, or 200 cm fiber optic cell. Salinity-matched solutions were used as reference to avoid absorbance baseline offsets caused by refractive index differences between reference and sample. Absorption spectra were recorded over the range 200–800 nm. Absorption coefficients $a(\lambda)$ were calculated using the following equation,

$$a(\lambda) = 2.303A(\lambda)/L \quad (1)$$

as in Blough and Del Vecchio (2002), where $A(\lambda)$ is the absorbance over pathlength, L . The spectra were then fit to an exponential function,

$$a(\lambda) = a(\lambda_0)e^{-S(\lambda-\lambda_0)} \quad (2)$$

using a nonlinear least squares fitting routine (NLF) over the range 300–700 nm (Blough and Del Vecchio, 2002). Here λ_0 is a reference wavelength and S is the spectral slope parameter.

Optical measurements for C18-OM samples were collected for all EAO samples, and for 23 of the 43 C18-OM samples for the MAB (as they were the only ones available in storage). However, these samples more than adequately represented all the various water types under study.

The wavelength dependence of C18 extraction efficiency was calculated using Equation (3) below, where pre extraction acidified waters refer to the pH 2 water before passage through the C18 column, while post extraction acidified waters refer to the pH 2 water collected after passage over the column.

Extraction efficiency

$$= 1 - \frac{\text{Abs (post extraction acidified waters, pH 2)}}{\text{Abs (pre extraction acidified waters, pH 2)}} \quad (3)$$

The wavelength dependence of extraction efficiency was only obtained for the MAB samples, because the post extraction waters for EAO samples were not collected at the time of extraction.

CDOM and C18-OM fluorescence measurements were acquired with an Aminco-Bowman AB2 luminescence spectrometer employing a 1-cm optical cell and Milli-Q water as blank. C18-OM samples were diluted prior to acquiring fluorescence measurements in order to avoid inner filter effects, while CDOM samples were measured as is. Both the excitation and emission monochromator bandpasses were set to 4 nm for extracts (C18-OM) and 8 nm for the natural waters (CDOM). The emission spectra were recorded from 10 nm greater than λ_{exc} to 700 nm, with λ_{exc} incremented every 10 nm over the range 290–600 nm. The spectra were corrected for the instrument response using factors supplied by the manufacturer. Fluorescence emission was normalized to the integrated emission of 1 ppb quinine sulfate with excitation at 350 nm and reported in quinine sulfate equivalents (QSE). The wavelength dependence

of fluorescence emission maxima (λ_{max}) and apparent quantum yields (ϕ) were measured as described in Del Vecchio and Blough (2004a) and (Green and Blough, 1994), respectively. Fluorescence quantum yields were calculated relative to quinine sulfate (QS) as a reference (λ_{exc} 350 nm) in 0.1 N H₂SO₄:

$$\phi(\lambda) = \frac{F'(\lambda).A(\lambda)_r}{F'(\lambda)_r.A(\lambda)} \cdot 0.54 \quad (4)$$

Subscript r refers to the reference (Quinine sulfate), $A(\lambda)$ is the absorbance at the excitation wavelength, and F' is the integrated corrected fluorescence emission produced by excitation at wavelength λ and 0.54 is the QS quantum yield (Green and Blough, 1994).

NaBH₄ Reduction

Selected CDOM and corresponding C18-OM samples were chosen for the NaBH₄ reduction analysis based on geographic locale. These samples consisted of waters from river (0 ppt), bay (17.6 ppt), shelf (32.5 ppt), and open ocean (35.4 ppt) regions.

Reduction with NaBH₄ (Fisher) was performed as described by Andrew et al. (2013). Briefly, natural waters (20.0–30.0 mL) were placed in a glass vial, capped, and sparged with ultrapure N₂ for 35 min. Solid NaBH₄ was added to the vial using a one-to-one ratio of NaBH₄ (mg) to sample volume (mL) (resulting in very large mass excess of NaBH₄ relative to CDOM to compensate for the large ratio of water to organic matter in these samples). NaBH₄ was added under continuous N₂ flow. C18-OM was reduced in a 1 cm quartz cuvette using 3.0 mL of sample and mass excess of NaBH₄ (~50 fold) based on approximate organic matter content (derived from matching absorbance spectra to that of known concentrations of SRFA). This was accomplished by adding ~85–95 µL of a concentrated NaBH₄ stock solution (~45.7 mg NaBH₄ in 3.0 mL of Milli-Q at pH 12) to the C18-OM sample. The reduction was considered to be complete when no further changes in absorption spectra were observed (~24 h). Sample pH increased from pH 7–8 to pH 10–11 due to the reaction of excess NaBH₄ with water (Tinnacher and Honeyman, 2007; Ma et al., 2010; Golanoski et al., 2012). Thus, sample pH was readjusted to the original pH to allow for comparison with the untreated natural water sample.

Optical properties were measured prior to and following reduction and reported relative to the untreated sample as A_f (fraction of absorbance remaining), ΔF (change in fluorescence emission), and F_f (fraction of fluorescence emission remaining), defined by the following equations:

$$A_f = \frac{A(t)}{A(0)} \quad (5)$$

$$\Delta F = F(t) - F(0) \quad (6)$$

$$F_f = \frac{F(t)}{F(0)} \quad (7)$$

where $A(t)$ is the absorbance of the treated sample and $A(0)$ is the absorbance of the original sample. Likewise, $F(t)$ and $F(0)$ are the fluorescence emission spectrum of the treated and untreated sample, respectively.

RESULTS AND DISCUSSION

Extraction Efficiency

The C18 extraction efficiency was calculated for MAB waters only (**Figure 1**) as post extraction waters for EAO samples were not stored at the time of collection. The C18 extraction efficiency for inshore MAB waters (river and bay) was approximately 0.4–0.45 at 250 nm and monotonically increased with increasing wavelengths to ~0.9–1.0 at 500 nm, thus clearly exhibiting a preferential retention of the long-wavelength absorbing material from the bulk CDOM (**Figure 1B**) consistent with previous work (Green and Blough, 1994). Offshore samples clearly exhibited lower extraction efficiency (~0.25–0.3) at short wavelength < 300 nm that sometimes, but not always, increased with increasing wavelengths ranging from 0.3 to 0.8. The varying wavelength dependence of the extraction efficiency for offshore samples at longer wavelengths was possibly impacted by the occasionally extremely low CDOM absorption values for these samples (at or below the detection limit) resulting in higher errors in the

calculated values for extraction efficiency (**Figure 1C**). Overall the extraction efficiency was higher for fresh (river) waters than for offshore waters at short wavelengths and increased with increasing wavelength for fresh (river, bay) waters while this trend was more variable for offshore waters.

Absorbance and Spectral Slope

The spectral slopes for C18-OM samples were lower relative to those for CDOM samples (**Table 1** and **Figure 2**) indicating enrichment of long wavelength absorbing components by the extraction process. It was also generally observed that spectral slope values for surface CDOM samples increased from river to open ocean, ranging from 0.015 to ~0.030 m⁻¹, respectively (**Figure 2A**). Contrarily, spectral slope values for CDOM samples below the surface remained within a much narrower range of 0.016–0.020 m⁻¹ (**Figure 2B**). A similar trend of increasing slopes from river to ocean surface samples was generally observed for C18-OM though the overall range was shifted toward slightly lower values. This observation supports the finding that lower

TABLE 1 | Spectral slope values (S, nm⁻¹) for MAB samples in August, December, and September 2006, and EAO samples in June 2009.

Sample	Geographic locale	Position		Salinity (ppt)	S (nm ⁻¹)		Sample	Position		Salinity	S (nm ⁻¹)	
		Lat.	Long.		CDOM	C18-OM		Lat.	Long.		CDOM	C18-OM
MAB August												
St 1 2 m	Bay mouth	38.9	-75.1	29.6	0.0184	0.0160	St 22	3.0	-23.0	34.6	NA	NA
St 1 17 m	Bay mouth	38.9	-75.1	31.5	0.0178	0.0152	St 26	3.50	-10.00	34.4	0.0217	0.0229
St 4 2 m	Shelf	38.0	-74.0	31.6	0.0219	0.0181	St 48	-5.00	-10.00	35.3	0.0227	0.0207
St 4 75 m	Shelf	38.0	-74.0	35.1	0.0168	0.0143	St 51	-5.00	0.00	35.2	0.0319	0.0221
St 7 1000m	Gulf stream	36.2	-71.8	35.1	0.0160	0.0133	St 61	-0.67	0.00	35.4	0.0314	0.0209
St 10 2 m	Mid shelf	38.2	-74.3	31.5	0.0240	0.0200	St 73	3.00	0.00	34.7	0.0288	0.0232
St 10 35 m	Mid shelf	38.2	-74.3	33.1	0.0168	0.0151	St 75	3.00	5.00	35.1	0.0220	0.0221
St 12 2 m	Lower bay	39.0	-75.1	28.4	0.0199	0.0160	St 89	-2.00	5.00	36.1	0.0207	0.0186
St 14 2 m	Mid bay	39.3	-75.4	17.6	0.0177	0.0161	St 96	-6.00	5.00	34.1	0.0168	0.0153
St 19 2 m	River	40.1	-74.8	0.1	0.0173	0.0149						
St 20 2 m	Mid bay	39.3	-75.4	12.5	0.0177	0.0166						
MAB December												
St 2 2 m	Offshore	38.00	-74.05	33.7	0.0192	0.0162	EAO (5 m)					
St 2 50 m	Offshore	38.00	-74.05	33.8	0.0192	0.0159	St 22	3.0	-23.0	34.6	0.0179	0.0160
St 3 30m	Shelf	38.18	-74.25	33.7	0.0192	0.0130	St 26	3.5	-10.0	34.7	0.0188	0.0158
St 4 20 m	Bay mouth	38.68	-74.89	31.8	0.0181	0.0104	St 48	-5.0	-10.0	34.6	0.0214	0.0164
St 6	Bay mouth	38.88	-75.09	26.44	0.0180	0.0126	St 51	-5.0	0.0	34.6	0.0175	0.0152
St 6 15m	Bay mouth	38.88	-75.09	28.3	0.0180	0.0102	St 61	-0.7	0.0	34.6	0.0206	0.0151
St 7	River	39.97	-75.13	0.08	0.0156	0.0107	St 73	3.0	0.0	34.6	0.0152	0.0153
St 8	Upper bay	39.58	-75.55	0.09	0.0162	0.0147	St 75	3.0	5.0	34.6	0.0180	0.0153
St 9	Shelf	38.44	-74.57	32.53	0.0185	0.0109	St 89	-2.0	5.0	34.6	0.0173	0.0163
St 9 20 m	Shelf	38.44	-74.57	32.5	0.0185	0.0122	St 96	-6.0	5.0	34.6	0.0154	0.0157
St 11	Lower bay	38.99	-75.14	23.28	0.0180	0.0128						
St 13	Upper bay	39.62	-75.58	0.12	0.0162	0.0118						
St 14	Bay mouth	38.88	-75.09	28.66	0.0185	0.0126						
MAB September												
St 2 1000m		36.5	-71.2	36.0	0.0198	0.0166	EAO (1000m)					
St 5		38.2	-74.3	32.5	0.0241	0.0208	St 22	3.0	-23.0	34.6	0.0179	0.0160
St 5 41m		38.2	-74.3	32.5	0.0182	0.0163	St 26	3.5	-10.0	34.7	0.0188	0.0158
St 7		39.3	-75.4	14.4	0.0178	0.0158	St 48	-5.0	-10.0	34.6	0.0214	0.0164

NA, data not available.

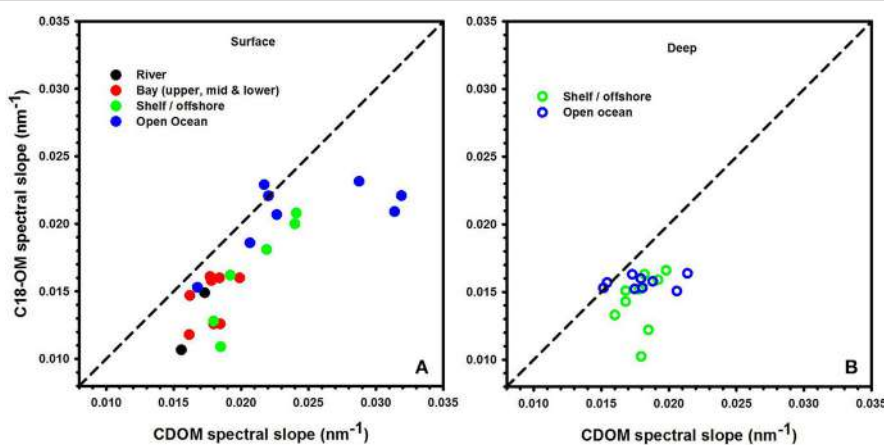


FIGURE 2 | Spectral slope values acquired for CDOM and C18-OM for river, bay, shelf, and open ocean waters from the MAB and EAO. Solid symbols represent surface samples (A). Open symbols represent depths below the surface (B). 1:1 line is also shown.

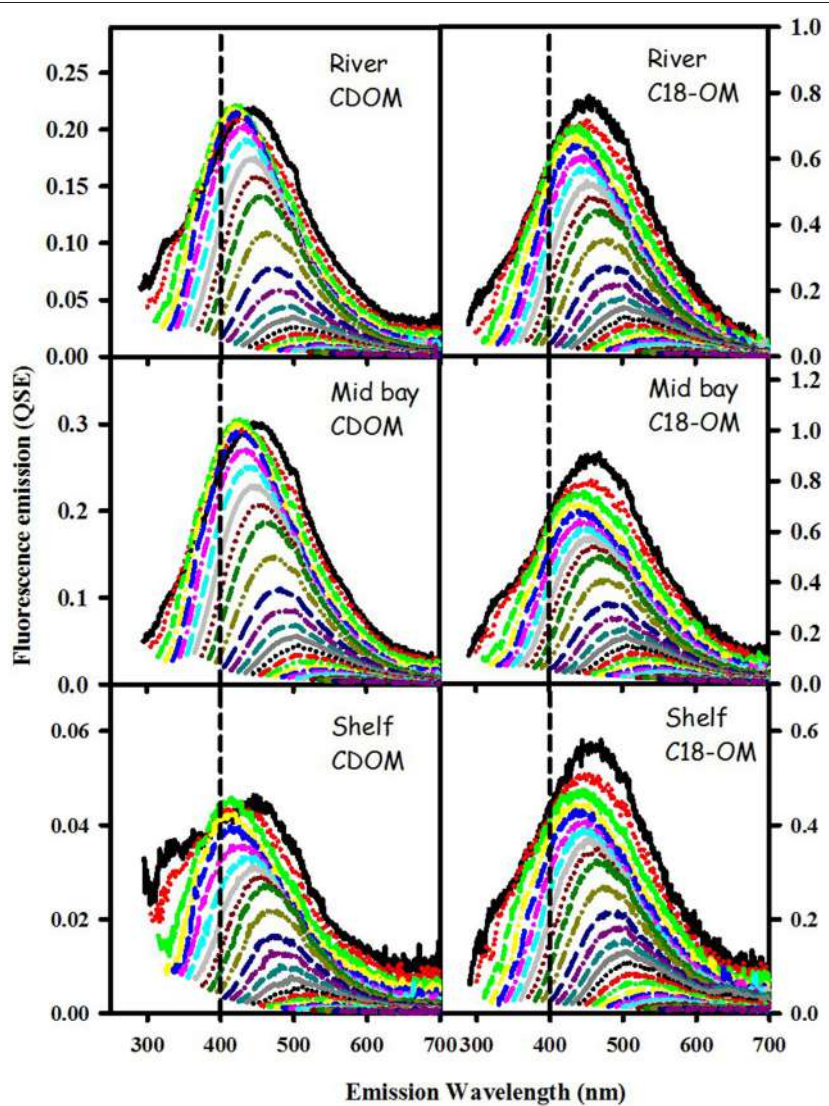


FIGURE 3 | Corrected fluorescence emission spectra for CDOM and corresponding C18-OM samples from the MAB river, bay, and shelf waters.

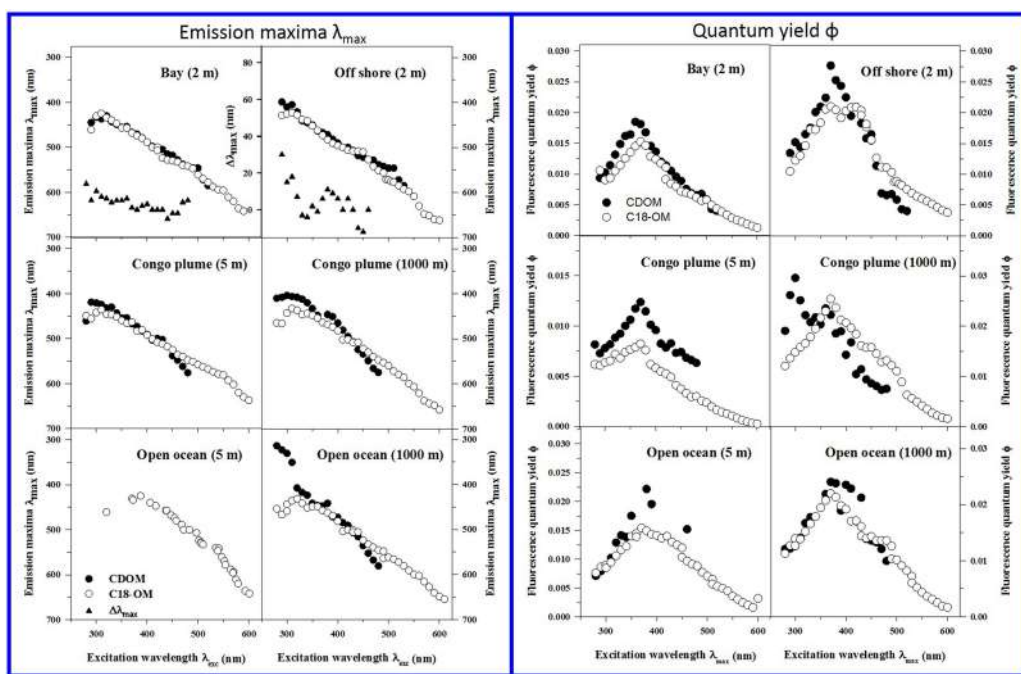


FIGURE 4 | Corrected fluorescence emission maxima (left panels) and quantum yields (right panels) for representative CDOM (solid symbols) and C18-OM (open symbols) samples from MAB bay and offshore, Congo plume, and open ocean waters. Emission maxima for CDOM open ocean (5 m) could not be determined due to high signal-to-noise in emission spectra. Emission maxima plots for Bay and Offshore samples also include $\Delta\lambda_{\max}$ plots; $\Delta\lambda_{\max} > 0$, indicates a red shift in λ_{\max} for C18-OM relative to CDOM.

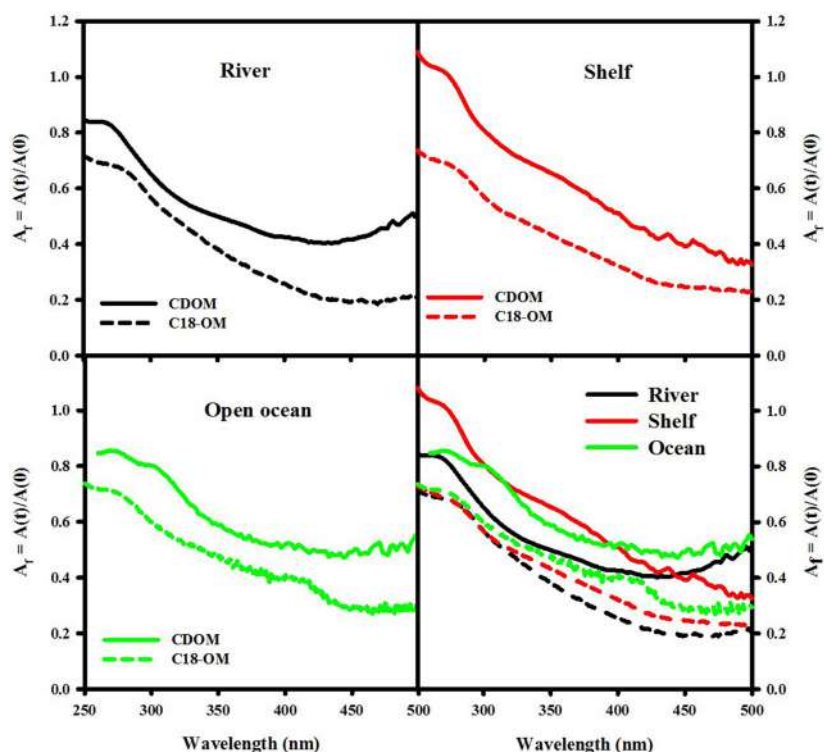


FIGURE 5 | Wavelength dependence of fractional absorption loss ($[A(t)]/[A(0)]$) following reduction of CDOM and C18-OM samples from MAB (river—August 2006 St 19, 2 m; shelf—December 2006 St. 9, 20 m) and EAO (June 2009 St 51, 1000 m).

molecular weight material appears to be less efficiently extracted by C18 cartridges. In addition, the C18-OM spectral slopes were closer to the CDOM spectral slope values for most of the surface ocean samples (**Figure 2A**, closer to the one-to-one line) relative to shelf and river waters, possibly indicative of a more uniform extraction in offshore waters. However, a few surface ocean samples did not follow this trend, which may have resulted from poorer non linear fits as a result of low absorbance in surface ocean waters.

Consistent with previous work, S has been shown to decrease with increasing molecular size (Green and Blough, 1994; Boyle et al., 2009; Yan et al., 2012; Sharpless and Blough, 2014). Thus, lower values of S for C18-OM is suggestive of the presence of higher molecular weight material, implying the preferential extraction/elution of larger size material. This is a reasonable expectation, as larger material is generally considered to be more nonpolar, more easily adsorbed and thus extracted.

Fluorescence Emission and Quantum Yield

CDOM and C18-OM samples from the MAB and EAO exhibited very similar spectral dependencies of fluorescence emission. Emission spectra were broad and unstructured (**Figure 3**) and their maxima (λ_{max}) continuously red-shifted with increasing excitation wavelength ($\lambda_{\text{exc}} \geq \sim 300 \text{ nm}$) (**Figure 4** left panels). Additionally, λ_{max} for C18-OM was

generally more red-shifted relative to that of CDOM samples at short wavelengths, suggestive of greater molecular size for C18-OM relative to CDOM, consistent with the absorption measurements.

CDOM and C18-OM exhibited a very similar wavelength dependence of apparent quantum yields (**Figure 4** right panels). Values for ϕ increased with increasing excitation wavelength up to $\sim 370 \text{ nm}$, and then decreased monotonically at longer excitation wavelengths. C18-OM samples from the Congo River plume exhibited lower ϕ values at shorter λ_{exc} ($< 380 \text{ nm}$) relative to CDOM. In contrast, CDOM and C18-OM from the MAB and EAO (open ocean) exhibited comparable ϕ values at $\lambda_{\text{exc}} \leq 370 \text{ nm}$, especially at depth. Effective comparison at longer wavelengths ($\geq 370 \text{ nm}$) could not be made due to very low absorption coefficients in some cases (close to detection limit) or very low fluorescence emission for the CDOM samples resulting in larger uncertainties.

Occasionally discrete peaks were observed in the UV region for samples from the Congo River Plume and from open oceans; these bands exhibited very high quantum efficiencies relative to the bulk CDOM (**Figure 4** right panel, Congo Plume 1000 m; Figures 6 and 9 in Andrew et al., 2013), and were not extracted by C18 cartridges indicating that these species are structurally different from the long-wavelength absorbing/emitting CDOM.

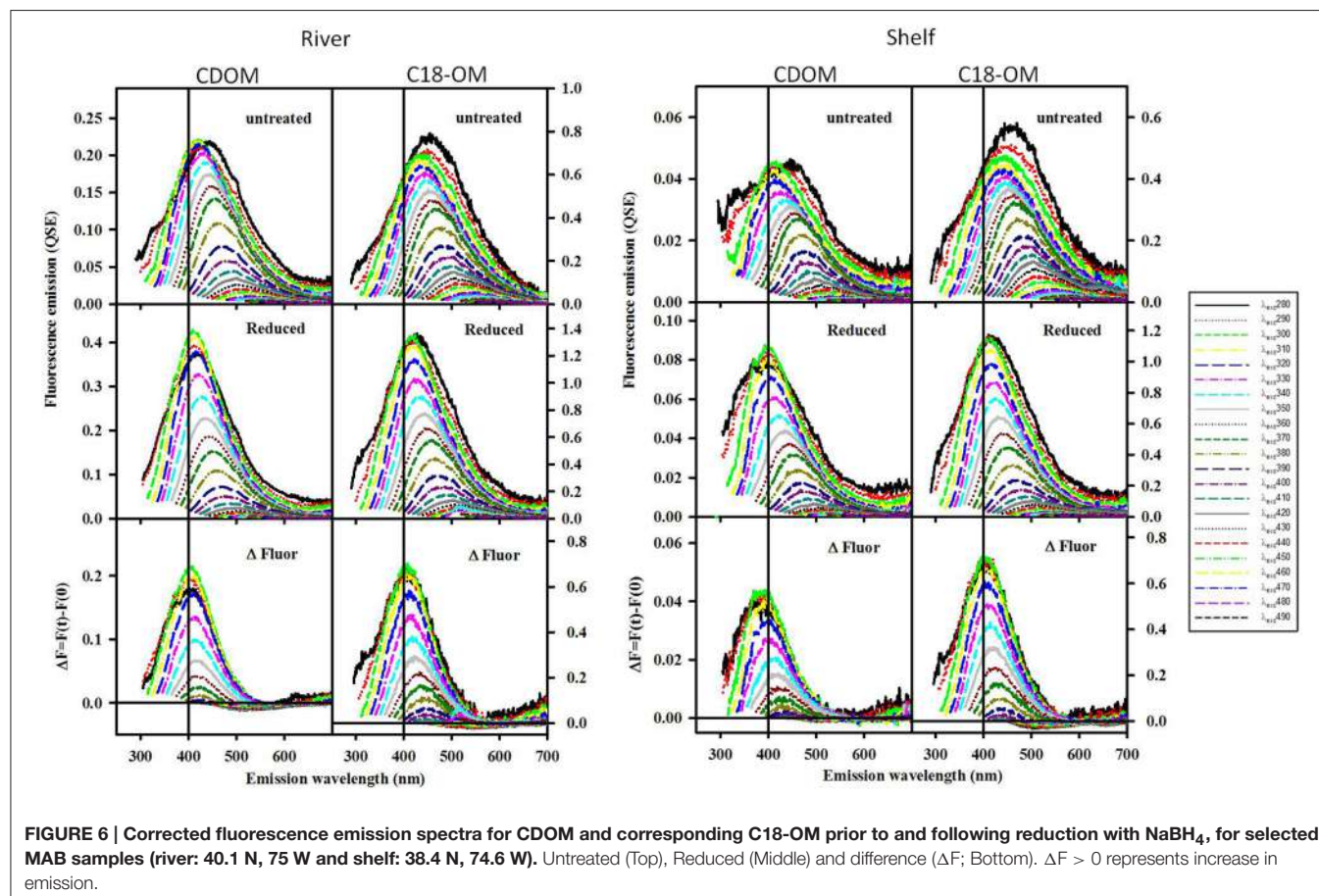


FIGURE 6 | Corrected fluorescence emission spectra for CDOM and corresponding C18-OM prior to and following reduction with NaBH_4 , for selected MAB samples (river: 40.1 N, 75 W and shelf: 38.4 N, 74.6 W). Untreated (Top), Reduced (Middle) and difference (ΔF ; Bottom). $\Delta F > 0$ represents increase in emission.

NaBH₄ Reduction

Reduction of both CDOM and C18-OM samples with NaBH₄ resulted in a significant loss in absorbance across the UV-visible wavelengths, with the largest fractional losses observed in the visible wavelength regime (**Figure 5**) consistent with past observations (Ma et al., 2010; Zhang et al., 2012; Golanski et al., 2012; Andrew et al., 2013; Baluha et al., 2013; Guo and Ma, 2014; Phillips and Smith, 2014, 2015; Sharpless and Blough, 2014). Absorption losses of ~50% were observed for CDOM from both MAB (river and shelf) and EAO (open ocean). However, much greater losses (as much as 80% over the longer

wavelength visible regime) were reported for C18-OM. Although the spectral dependence of fractional absorbance loss looks very similar, CDOM fractional absorbance values were always smaller than the corresponding C18-OM values. This difference may possibly be due to (a) the greater initial content of long-wavelength absorbing material in C18-OM relative to CDOM; or (b) in part be artifactual due to changes in the refractive index (and thus baseline) measured using the long path spectrometer resulting from the addition of borohydride. Thus, the magnitude of fractional loss for CDOM samples may actually be closer to the fractional losses observed for C18-OM.

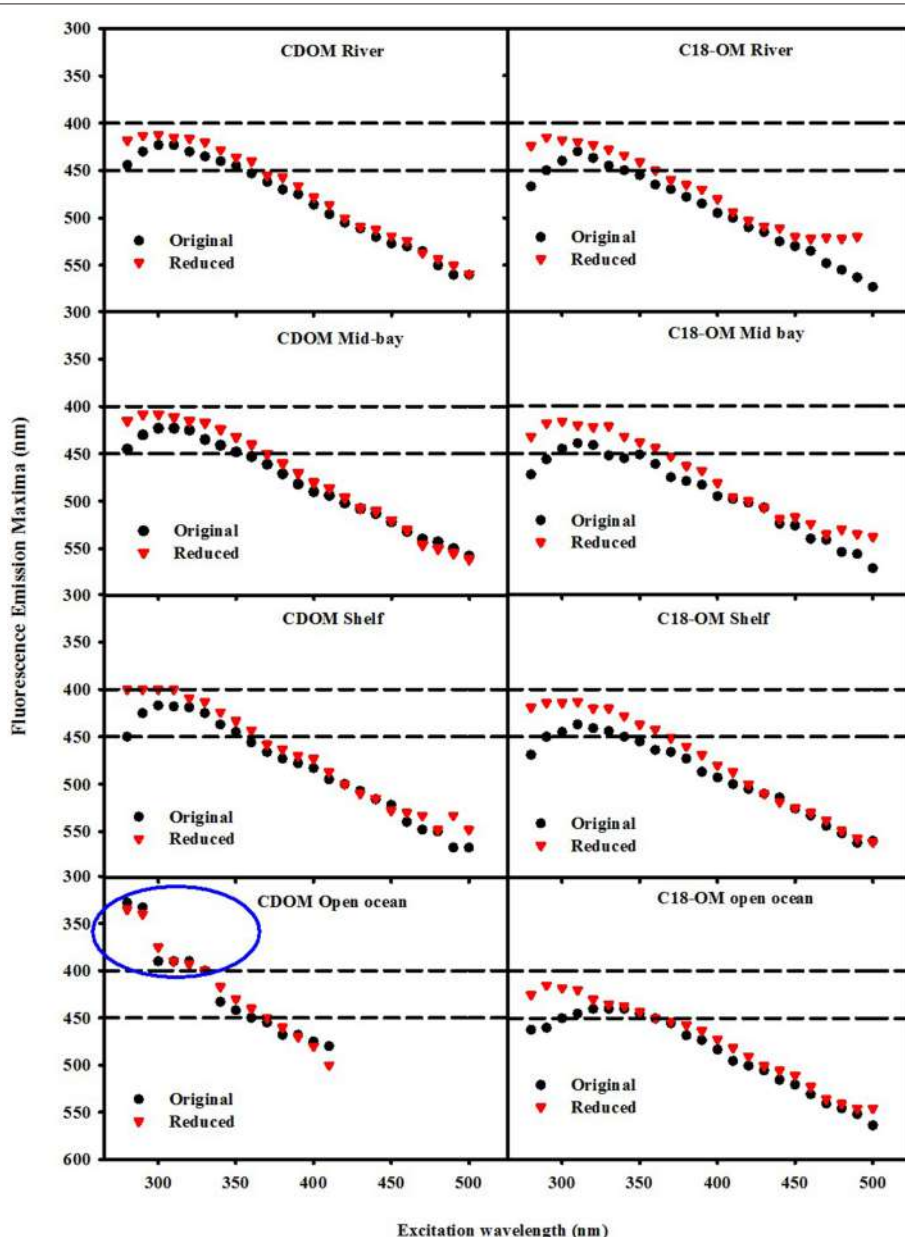


FIGURE 7 | Wavelength dependence of fluorescence emission maxima λ_{max} for CDOM and C18-OM samples prior to and following NaBH₄ reduction. Area in the blue circle represents the emission maxima of a UV emitting species observed in the EAO CDOM sample that failed to be extracted by the C18 cartridges.

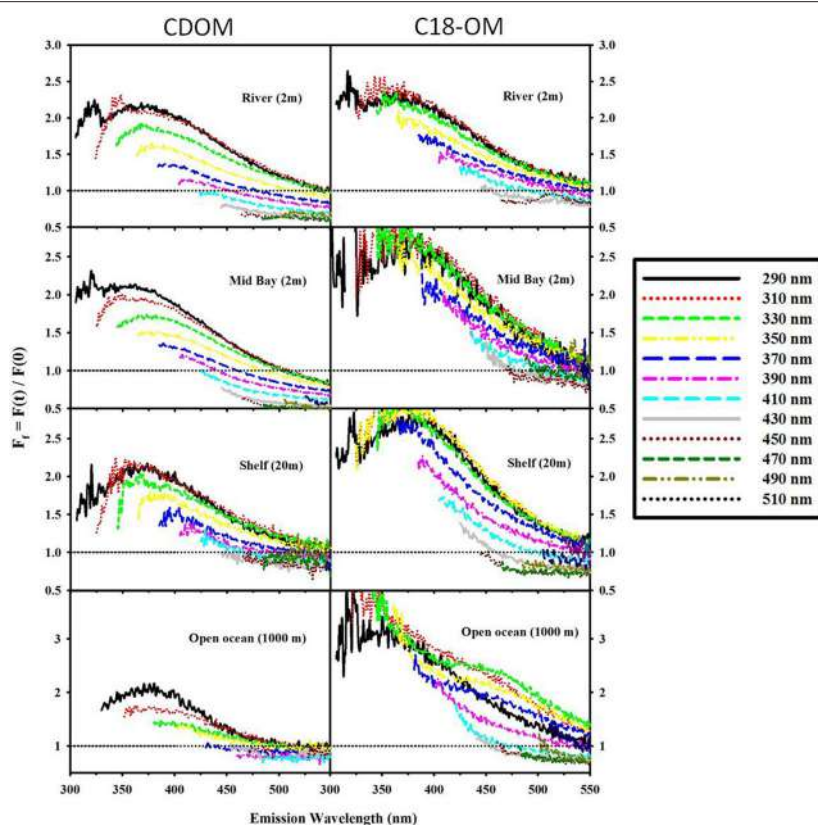


FIGURE 8 | Fractional fluorescence emission spectra for selected CDOM samples and their corresponding C18-OM: MAB (river: 40.1 N, 75 W; Mid bay: 39.3 N, 75.4 W and shelf: 38.4 N, 74.6 W) and EAO (open ocean: 4.98 S, 0.0 E). $F_f > 1$ (horizontal black dotted line) signifies an increase in fluorescence after reduction. Spectra are presented for excitation wavelengths every 20 nm starting with λ_{exc} 290 nm.

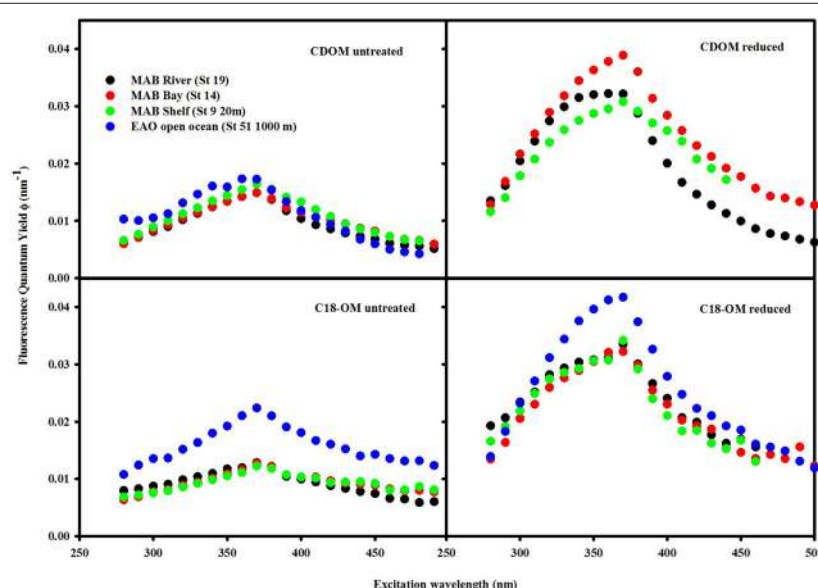


FIGURE 9 | Wavelength dependence of fluorescence quantum yields for CDOM and C18-OM samples prior to and following NaBH_4 reduction. QY values for the reduced CDOM sample EAO (St 51 1000 m) could not be calculated as a result of absorbance values being too low after reduction.

Following reduction, fluorescence emission intensities increased similarly at short excitation wavelength for both CDOM and C18-OM from the MAB and EAO [MAB Figure 6; EAO Figures 10, 11 in Andrew et al. (2013)] consistent with previous work (Tinnacher and Honeyman, 2007; Ma et al., 2010; Guo and Ma, 2014; Phillips and Smith, 2014, 2015; Sharpless and Blough, 2014). Additionally, the emission maxima shifted to the blue by approximately 10–15 nm relative to the untreated samples (**Figure 7**), with a larger shift observed for C18-OM due to the more red-shifted emission observed in the untreated C18-OM. Loss in emission intensity was observed for both CDOM and C18-OM at longer λ_{exc} (>410 and >430 nm, respectively) (**Figure 6** ΔF; **Figure 8** values below the horizontal black line). These results are consistent with results previously reported (Ma et al., 2010; Sharpless, 2012). Overall, the wavelength dependence of fractional changes (gains and losses) in emission intensity before and after reduction were similar for both CDOM and C18-OM samples (**Figure 8**) consistent with the absorption changes upon NaBH₄ reduction (**Figure 5**). The greater changes observed for C18-OM samples do not imply different samples' reactivity; instead they could be due to the following factors: (1) Solid NaBH₄ was added to 30 mL CDOM sample (at low concentration, and neutral pH), thus resulting in kinetic competition between the loss of borohydride through reaction with water and with reduction of carbonyl groups within the CDOM samples, (2) C18-OM is enriched in higher molecular weight material (lower S, more visible absorption at longer wavelengths, greater fluorescence emission for the untreated C18-OM samples) resulting in a greater blue-shift in emission maxima and emission intensity following reduction.

The fluorescence quantum yields for CDOM and C18-OM in the MAB and EAO were substantially enhanced following reduction, particularly at $\lambda_{\text{exc}} \sim 350$ –390 nm (**Figure 9**). In previous work by Ma et al. (2010), this enhancement in ϕ was attributed to two factors: (1) the increase in fluorescence emission at $\lambda_{\text{exc}} \leq 350$ nm, and (2) the significant decrease in absorption over these same wavelengths, which also holds true for this work as well.

Comparison of C18-OM to CDOM and Comparison among C18-OM

There is slight biasing with the C18 extraction, with some enhancement of absorption in the visible, and some distinct fluorescing components are not extracted. However, the wavelength dependence of absorbance and emission are very comparable, as is the wavelength dependence of the quantum yield. Moreover, C18-OM and CDOM show the similar spectral dependence upon NaBH₄ reduction, which suggests that these are very similar materials. This indicates that we are not dramatically altering the composition of the CDOM samples upon SPE extraction.

Not only are the C18-OM similar to the original waters, but surprisingly, the C18-OM gathered from very different geographic locales also look very similar, which suggests that there may be a common structural basis amongst all these samples. The wavelength dependence of absorbance, fluorescence

(**Figure 3**, right panel) and emission maxima (**Figure 7**, right panel) appear to be almost identical. This result suggests that the organic material being extracted is very similar, independent of sample location. The similarity in the changes in optical properties upon NaBH₄ reduction further highlights this observation. The fractional absorbance spectra (**Figure 5**), the changes in fluorescence emission maxima (**Figures 6, 7**) and fractional loss in fluorescence emission (**Figure 8**) upon reduction are also very similar, indicating a similarity not only in optical properties, but also in chemical behavior and structural origin of the extracted organic matter.

SUMMARY AND CONCLUSION

The extraction efficiency increased with wavelength in areas influenced by fresh water inputs indicative of preferential extraction of longer wavelength absorbing material. Such trend was less evident for offshore waters due to low absorbance values for these samples. Nevertheless, CDOM and C18-OM exhibited remarkably similar wavelength dependence of absorbance, fluorescence emission and fluorescence quantum yields, that appeared to be largely unaffected by the preferential extraction of longer wavelength absorbing material. Thus, these results provide strong evidence that the optical properties of C18-OM and the corresponding CDOM sample are very similar overall.

The results from the NaBH₄ reduction provide further evidence that the preferential enrichment of long wavelength absorbing material did not largely affect the chemical properties of CDOM and C18-OM. Following reduction, CDOM and C18-OM exhibited comparable changes in fractional absorbance and fluorescence, fluorescence emission maxima and quantum yields that did not vary largely with geographical area.

Remarkably, C18-OM extracts exhibited very similar optical properties and response to chemical reduction independent of location, suggesting a common structural basis for the extracted organic matter.

Overall, the results from this study indicate that enrichment of CDOM by SPE using C18 cartridges does not substantially alter the optical properties of CDOM. Altogether, these results suggest that not only is the structural basis of the optical properties of both the extracted material and original samples comparable, but that similar type of organic material is being extracted independent of sample location. We conclude that C18-OM extracts are representative of CDOM, at least in terms of their optical properties.

AUTHOR CONTRIBUTIONS

AA, YZ collected, analyzed, and interpreted data. RD, NB, AS contributed to the manuscript writing.

ACKNOWLEDGMENTS

The authors gratefully acknowledge the funding sources for this work: LDEO contribution number is 7970 for this article. NASA

Ocean Biology and Biogeochemistry (grant no. NNG05GR37G to AS); the National Science Foundation (OCE-0443217, OCE 0648414 RD, NB). We thank Tamami Pisano, Emily Vincent,

Jeanne Yang, Timothy Graham, Darya Melnyk, and Yadira Castillo for assistance in sample collection, processing and storage, and data analysis.

REFERENCES

- Amador, J. A., Milne, P. J., Moore, C. A., and Zika, R. G. (1990). Extraction of chromophoric humic substances from seawater. *Mar. Chem.* 29, 1–17. doi: 10.1016/0304-4203(90)90002-T
- Andrew, A. A., Del Vecchio, R., Subramaniam, A., and Blough, N. V. (2013). Chromophoric dissolved organic matter (CDOM) in the Equatorial Atlantic Ocean: optical properties and their relation to CDOM structure and source. *Mar. Chem.* 148, 33–43. doi: 10.1016/j.marchem.2012.11.001
- Baluha, D. R., Blough, N. V., and Del Vecchio, R. (2013). Selective mass labeling for linking the optical properties of chromophoric dissolved organic matter to structure and composition via ultrahigh resolution electrospray ionization mass spectrometry. *Environ. Sci. Technol.* 47, 9891–9897. doi: 10.1021/es402400j
- Benner, R. (2002). “Chemical composition and reactivity,” in *Biogeochemistry of Marine Dissolved Organic Matter*, eds D. Hansell and C. Carlson (San Diego, CA: Academic Press), 59–90. doi: 10.1016/b978-012323841-2/50005-1
- Blough, N. V., and Del Vecchio, R. (2002). “Chromophoric DOM in the coastal environment,” in *Biogeochemistry of Marine Dissolved Organic Matter*, eds D. A. Hansell and C. A. Carlson (San Diego, CA: Academic Press), 509–546. doi: 10.1016/b978-012323841-2/50012-9
- Boyle, E. S., Guerrero, N., Thiallet, A., Del Vecchio, R., and Blough, N. V. (2009). Optical properties of humic substances and CDOM: relation to structure. *Environ. Sci. Technol.* 43, 2262–2268. doi: 10.1021/es803264g
- Daignault, S. A., Noot, D. K., Williams, D. T., and Huck, P. M. (1988). A review of the use of XAD resins to concentrate organic compounds in water. *Water Res.* 22, 803–813. doi: 10.1016/0043-1354(88)90017-6
- Del Vecchio, R., and Blough, N. V. (2004a). On the origin of the optical properties of humic substances. *Environ. Sci. Technol.* 38, 3885–3891. doi: 10.1021/es049912h
- Del Vecchio, R., and Blough, N. V. (2004b). Spatial and seasonal distribution of chromophoric dissolved organic matter and dissolved organic carbon in the Middle Atlantic Bight. *Mar. Chem.* 89, 169–187. doi: 10.1016/j.marchem.2004.02.027
- Dittmar, T., Koch, B., Hertkorn, N., and Kattner, G. (2008). A simple and efficient method for the solid-phase extraction of dissolved organic matter (SPE-DOM) from seawater. *Limnol. Oceanogr. Methods* 6, 230–235. doi: 10.4319/lom.2008.6.230
- Druffel, E. R. M., Williams, P. M., Bauer, J. E., and Ertel, J. R. (1992). Cycling of dissolved and particulate organic matter in the open ocean. *J. Geophys. Res. Oceans* 97, 15639–15659. doi: 10.1029/92JC01511
- Golanoski, K. S., Fang, S., Del Vecchio, R., and Blough, N. V. (2012). Investigating the mechanism of phenol photooxidation by humic substances. *Environ. Sci. Technol.* 46, 3912–3920. doi: 10.1021/es300142y
- Green, S. A., and Blough, N. V. (1994). Optical absorption and fluorescence properties of chromophoric dissolved organic matter in natural waters. *Limnol. Oceanogr.* 39, 1903–1916. doi: 10.4319/lo.1994.39.8.1903
- Guo, R. R., and Ma, J. H. (2014). Reduction-induced molecular signature of humic substances: structural evidence for optical changes. *RSC Adv.* 4, 25880–25885. doi: 10.1039/c4ra03051f
- Helms, J. R., Stubbins, A., Perdue, E. M., Green, N. W., Chen, H., and Mopper, K. (2013). Photochemical bleaching of oceanic dissolved organic matter and its effect on absorption spectral slope and fluorescence. *Mar. Chem.* 155, 81–91. doi: 10.1016/j.marchem.2013.05.015
- Ma, J., Del Vecchio, R., Golanoski, K. S., Boyle, E. S., and Blough, N. V. (2010). Optical properties of humic substances and CDOM: effects of borohydride reduction. *Environ. Sci. Technol.* 44, 5395–5402. doi: 10.1021/es100880q
- Phillips, S. M., and Smith, G. D. (2014). Light absorption by charge transfer complexes in brown carbon aerosols. *Environ. Sci. Technol. Lett.* 1, 382–386. doi: 10.1021/ez500263j
- Phillips, S. M., and Smith, G. D. (2015). Further evidence for charge transfer complexes in brown carbon aerosols from excitation-emission matrix fluorescence spectroscopy. *J. Phys. Chem. A* 119, 4545–4551. doi: 10.1021/jp510709e
- Serkiz, S. M., and Perdue, E. M. (1990). Isolation of dissolved organic matter from the Suwannee river using reverse-osmosis. *Water Res.* 24, 911–916. doi: 10.1016/0043-1354(90)90142-S
- Sharpless, C. M. (2012). Lifetimes of Triplet Dissolved Natural Organic Matter (DOM) and the Effect of NaBH₄ reduction on singlet oxygen quantum yields: implications for DOM photophysics. *Environ. Sci. Technol.* 46, 4466–4473. doi: 10.1021/es300217h
- Sharpless, C. M., and Blough, N. V. (2014). The importance of charge-transfer interactions in determining chromophoric dissolved organic matter (CDOM) optical and photochemical properties. *Environ. Sci. Process. Impacts.* 16, 654–671. doi: 10.1039/c3em00573a
- Tinnacher, R. M., and Honeyman, B. D. (2007). A new method to radiolabel natural organic matter by chemical reduction with tritiated sodium borohydride. *Environ. Sci. Technol.* 41, 6776–6782. doi: 10.1021/es070563b
- Vetter, T. A., Perdue, E. M., Ingall, E., Koprivnjak, J. F., and Pfleiderer, P. H. (2007). Combining reverse osmosis and electrodialysis for more complete recovery of dissolved organic matter from seawater. *Sep. Purif. Technol.* 56, 383–387. doi: 10.1016/j.seppur.2007.04.012
- Vodacek, A., Blough, N. V., DeGrandpre, M. D., Peltzer, E. T., and Nelson, R. K. (1997). Seasonal variation of CDOM and DOC in the Middle Atlantic Bight: terrestrial inputs and photooxidation. *Limnol. Oceanogr.* 42, 674–686. doi: 10.4319/lo.1997.42.4.0674
- Yan, M., Korshin, G., Wang, D., and Cai, Z. (2012). Characterization of dissolved organic matter using high-performance liquid chromatography (HPLC)-size exclusion chromatography (SEC) with a multiple wavelength absorbance detector. *Chemosphere* 87, 879–885. doi: 10.1016/j.chemosphere.2012.01.029
- Zhang, Y., Del Vecchio, R., and Blough, N. V. (2012). Investigating the mechanism of hydrogen peroxide photoproduction by humic substances. *Environ. Sci. Technol.* 46, 11836–11843. doi: 10.1021/es302958z

Conflict of Interest Statement: The authors declare that the research was conducted in the absence of any commercial or financial relationships that could be construed as a potential conflict of interest.

Copyright © 2016 Andrew, Del Vecchio, Zhang, Subramaniam and Blough. This is an open-access article distributed under the terms of the Creative Commons Attribution License (CC BY). The use, distribution or reproduction in other forums is permitted, provided the original author(s) or licensor are credited and that the original publication in this journal is cited, in accordance with accepted academic practice. No use, distribution or reproduction is permitted which does not comply with these terms.



Mass and UV-visible spectral fingerprints of dissolved organic matter: sources and reactivity

Heather E. Reader^{1,2*}, Colin A. Stedmon², Nikoline J. Nielsen³ and Emma S. Kritzberg¹

¹ Department of Biology/Aquatic Ecology, Lund University, Lund, Sweden, ² Section for Marine Ecology and Oceanography, National Institute of Aquatic Resources, Technical University of Denmark, Charlottenlund, Denmark, ³ Department of Plant and Environmental Sciences, University of Copenhagen, Copenhagen, Denmark

OPEN ACCESS

Edited by:

Christopher Osburn,
North Carolina State University, USA

Reviewed by:

John Robert Helms,
Morningside College, USA
Marta Plavsic,
Rudjer Boskovic Institute, Croatia

***Correspondence:**

Heather E. Reader
hrea@aqua.dtu.dk

Specialty section:

This article was submitted to
Marine Biogeochemistry,
a section of the journal
Frontiers in Marine Science

Received: 14 August 2015

Accepted: 14 October 2015

Published: 29 October 2015

Citation:

Reader HE, Stedmon CA, Nielsen NJ and Kritzberg ES (2015) Mass and UV-visible spectral fingerprints of dissolved organic matter: sources and reactivity. *Front. Mar. Sci.* 2:88.
doi: 10.3389/fmars.2015.00088

Advanced analytical techniques have revealed a high degree of complexity in the chemical makeup of dissolved organic matter (DOM). This has opened the door for a deeper understanding of the role of DOM in the aquatic environment. However, the expense, analytical cost, and challenges related to interpretation of the large datasets generated by these methods limit their widespread application. Optical methods, such as absorption and fluorescence spectroscopy are relatively inexpensive and easy to implement, but lack the detailed information available in more advanced methods. We were able to directly link the analysis of absorption spectra to the mass spectra of DOM using an in-line detector system coupled to multivariate data analysis. Monthly samples were taken from three river mouths in Sweden for 1 year. One subset of samples was exposed to photochemical degradation and another subset was exposed to long-term (4 months) biological degradation. A principle component analysis was performed on the coupled absorption-mass spectra data. Loading spectra for each principle component show distinct fingerprints for both reactivity (i.e., photochemical, biological degradation) and source (i.e., catchment land cover, temperature, hydrology). The fingerprints reveal mass-to-charge values that contribute to optical signals and characteristics seen in past studies, and emphasize the difficulties in interpreting changes in bulk CDOM characteristics resulting from multiple catchment processes. The approach provides a potential simple method for using optical indicators as tracers for more complex chemical processes both with regards to source material for DOM and the past reactive processing of DOM.

Keywords: dissolved organic matter, optical properties, absorbance spectra, mass spectrometry, biogeochemistry

INTRODUCTION

Dissolved organic matter (DOM) is a large and dynamic pool of reduced carbon, and is an active component of aquatic systems. One of the characteristics of DOM is the ability of a fraction of DOM to absorb light (i.e., chromophoric or colored DOM, CDOM). Typically, the absorption spectrum of CDOM is characterized by a smooth decrease from the ultraviolet across the visible. The spectrum generally appears featureless, with a near exponential decline with increasing wavelength. Despite this, particular absorption properties are linked to the general characteristics of DOM as a whole.

The slope of the absorption spectrum has been shown to be inversely correlated to molecular size (Helms et al., 2008), and the specific ultraviolet absorbance (SUVA, ratio of absorbance at 254 nm to dissolved organic carbon concentration) is positively correlated to aromatic content (Weishaar et al., 2003). CDOM and its fluorescent fraction (FDOM) have been suggested as tracers of processes both biotic (i.e., plankton growth, microbial degradation) and abiotic (photochemistry, physical mixing) in aquatic environments (Coble et al., 1993; Helms et al., 2008; Walker et al., 2009). While the ease of measuring these optical characteristics lends themselves to use as tracers, studies show that they are not always conservative (Vodacek et al., 1997; Granskog et al., 2012).

Recent advances in analytical capabilities have allowed for a more detailed look at the molecular characteristics of DOM. In particular, ultra-high resolution mass spectrometry has revealed the presence of tens of thousands of distinct molecular formulae making up the whole of the DOM (Kujawinski et al., 2004; Koch et al., 2005; Mopper et al., 2007). Other molecular level analyses, such as nuclear magnetic resonance (NMR) techniques reveal similar complexity in the DOM pool (Hertkorn et al., 2013). The information inherent in these analyses is vast, but the difficulty of operating and expense of these analyses limit their application on a large scale, as well as do the challenges related to data interpretation.

There is a growing need to understand CDOM on a molecular level, in order to better understand what insight it can provide on both the fate of DOM and its effects on aquatic ecosystems (Stubbins et al., 2014). A molecular understanding of CDOM will facilitate the use of CDOM as a tracer of biogeochemical processes, and help to elucidate its function as an active component of the carbon cycle. Progress is impeded by the vast amounts of data generated by current analytical techniques and discrepancies between the analytical windows of different techniques. What is required to use these techniques to their full advantage is the development of suitable data analysis approaches that can link different analyses.

To achieve a better understanding of the molecular and optical characteristics of DOM and how they are linked, we sampled three contrasting boreal rivers in Sweden monthly over a period of 1 year. Seasonal sub-samples were exposed to both photochemical and biological degradation. Samples were further analyzed with coupled absorbance spectroscopy and mass spectrometry. The incorporation of geographic, seasonal, microbial, and photochemical variability in the DOM composition in the dataset made it ideal for developing a multivariate data analysis approach capable of fusing data from different detectors and ultimately linking the optical and mass spectrometric characteristics of DOM from these three catchments.

MATERIALS AND METHODS

Sampling and Reactivity Experiments

Three distinct river catchments were selected for the year-long study of DOM chemistry (March 2012–February 2013, **Figure 1**).

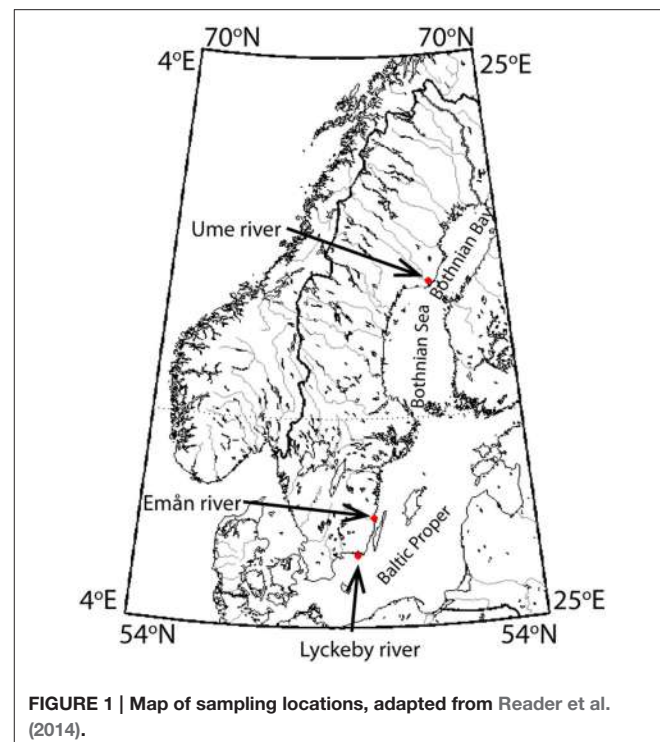


FIGURE 1 | Map of sampling locations, adapted from Reader et al. (2014).

Ume river, by far the largest catchment, is also the most northern catchment. Ume catchment covers a large range of altitudes, with its headwaters originating high in the Swedish alps, and has a large variety of catchment land cover types. The larger Ume catchment is divided into two large subcatchments, Ume river, which is high altitude and also highly regulated with several hydropower dams and Vindeln catchment, which is unregulated and largely forested. The forested parts of the catchment have been previously shown to drive seasonal DOM dynamics (Reader et al., 2014), thus characteristics such as flow and temperature have been calculated for the Krycklan subcatchment, which is a forested, low altitude subcatchment of Vindeln catchment (Laudon et al., 2013). The two smaller rivers, Emå river, and Lyckeby river, are located in southern Sweden. In contrast to Ume, Emå, and Lyckeby catchments are entirely low altitude, strongly forest dominated, and possess only one main catchment. Details of specific catchment characteristics can be found in **Table 1**.

Samples were collected in acid-cleaned polycarbonate bottles and stored on ice in the dark until return to the laboratory (<8 h). Samples for *in situ* extractions were filtered through GF/F filters (ashed, 4 h, 450°C, Whatman) and subsequently through 0.2 µm polycarbonate filters (Millipore). After filtration, samples were acidified to pH = 2 using 2 M HCl and stored at 4°C until extraction (<1 week). Samples for photochemistry were filtered in the same manner as the field samples, but they were left at their original pH until after irradiation. Samples for microbial degradation were filtered only through GF/F filters to remove large particles and plankton, whilst keeping the microbial community largely intact.

TABLE 1 | Catchment characteristics (adapted from Reader et al., 2014).

River	Latitude	Longitude	Area (km ²)	% Forest	% Pasture	% Crop	% Peat	% Water	% Other	Month of spring flood
Ume	63.82	20.26	26,815	62	<1	<1	7	8	22	May/June
Emån	57.14	16.47	4471	69	5	8	1	6	10	January
Lyckeby	56.08	15.59	810	72	5	3	2	4	9	January

Samples for microbial degradation were spiked with inorganic nutrients (NH_4^+ , NO_3^- , PO_4^{3-}) to a final ratio better than 45C:9N:1P, to ensure carbon limitation rather than any other nutrient (Goldman et al., 1987). Samples were then placed in the dark at ambient temperature (mean 20.6°C) for 4 months. The months for microbial incubations were chosen to cover a variety of catchment conditions, and were March, May, August, and January, representing early spring, late spring, summer and winter conditions, respectively. After incubation, samples were filtered through 0.2 µm, and acidified to pH = 2.

Samples for photochemical degradation were irradiated in 1 L beakers with depths of 11 cm sealed with quartz lids at 15°C under UV-A centered lamps for 6 days (intensity of 1.07 mW cm⁻², integrated from 250 to 700 nm). Months used for photochemical degradation were May, August, October, and January, representing spring, summer, fall, and winter, respectively. After irradiation, samples were acidified to pH = 2 prior to solid phase extraction.

Extraction and Preparation for Analysis

Total organic carbon content was measured using a Shimadzu TOC V-CPN in TC mode. In TC mode, dissolved organic carbon (DOC) is measured as the difference between the total carbon (TC) in the filtered sample and the inorganic carbon (IC), purged from the sample using hydrochloric acid (HCl) in the sampling syringe. The TOC was calibrated daily using sodium hydrogen phthalate standards for organic carbon and sodium carbonate for inorganic carbon. Total volume of sample extracted for analysis was calculated with the goal of loading 2.5 mg of organic matter on 1 g of PPL cartridge. For the microbial and photochemical treatments, the total volume extracted was the same as *in situ* sample. Two 1-g cartridges were used for each sample. Volumes of water extracted on each cartridge ranged from 100 mL to 2 L. Prior to extraction, cartridges were soaked in methanol overnight to remove any potential contaminants on the PPL, and then rinsed with 100 mL of Milli-Q water. After sample loading, cartridges were rinsed with 30 mL of pH = 2 Milli-Q water (adjusted with 2 M HCl). Cartridges were dried with air, and then subsequently extracted using 20 mL HPLC grade methanol (Merck) at 2 mL/min. Samples were evaporated to a total volume of 4 mL and stored at -18°C until analysis.

Details on MS Analysis

Aliquots of 400 µL were evaporated to dryness and reconstituted in an equivalent volume of mobile phase. Samples were analyzed on an Acuity UPLC (Waters, Milford, MA, USA) equipped with a binary solvent delivery system and operated in direct

injection mode. The UPLC is connected in series to a diode-array detector (DAD, 220–499 nm, 1 nm resolution, 20 scans s⁻¹) and to an electrospray ionization (ESI) Ultima Global quadrupole time-of-flight (QTOF) mass spectrometer (Waters Micromass). Ionization was performed in both positive and negative ion mode, and the MS operated in TOF scan mode (m/z = 100–2000), and the quadrupole served as an ion focusing devise (RF only). The ESI source operating conditions were: ion source temperature 120°C, desolvation gas temperature 250°C, cone gas flow 25 L h⁻¹ (ESI^+) and 50 L h⁻¹ (ESI^-), desolvation gas flow 700 L h⁻¹, capillary voltage 2.5 kV (ESI^+) and 2.0 kV (ESI^-), cone voltage 20 V, scan time 1 s and interscan delay 0.1 s. Results presented here are only from the negative ion mode. The mobile phase consisted of 10 mmol NH_4HCO_3 dissolved in 80:20 (v/v) glass distilled water:methanol and adjusted to pH 8.2 with drops of NH_4OH . The injection volume was 1 µL and the flow operated at 0.100 mL/min (DI). Samples were run in a randomized order, with repeated analysis of two randomly chosen samples, and a third sample that was extracted multiple times.

Transferring Data to Computing Environment

Data was retrieved using the Masslynx v4.2 (Waters Micromass), and exported as NetCDF-files with the DataBridge application. NetCDF-files were imported into MATLAB 7.9.0 (R2009b; The MathWorks) using in-house programmed routines (courtesy of G. Tomasi and J. Christensen, Copenhagen University) while binning the TOF m/z -axis to nominal m/z -values.

Data Analysis

To prepare the data for principle component analysis both the mass spectra and the absorbance spectra were subjected to pre-processing routines. The goal of the pre-processing was to ensure that neither the mass nor the absorbance spectra would dominate the analysis alone. The mass spectra were binned to integer m/z -values from 100 to 2000, and the ion count was summed for each m/z across the injection peak, summing a total of 156 scans for each sample. Prior to statistical analysis, each spectra were normalized to the total ion count, and then the columns (i.e., m/z -values) were mean centered. The normalization and mean centering of the data removes concentration effects and focuses the analysis on variability between samples (Christensen and Tomasi, 2007).

Absorbance spectra from 250 to 499 nm at the height of the injection peak were off scale due to the highly colored nature of the samples, and therefore discarded. Only spectra from the leading and tailing edge of the injection peak, where the measurement was within the linear range used in the subsequent

analysis. Each spectrum was normalized to its integral to remove intensity effects and the mean of these normalized spectra was taken for analysis. Samples were then mean centered.

After individual normalization routines, the corresponding mass spectra and absorbance spectra were concatenated into a single “spectrum.” The samples were then split into two data sets, one containing all of the *in situ* samples, the biological samples, the photochemical samples and several re-extracted samples for a total of 66 samples. The second data set (total of 28 samples) contained the repeated measurements of two randomly chosen samples (Ref1 and Ref2) to allow an assessment of the analytical reproducibility of the chemical analysis. It further contained an additional five samples that were separate extractions of the same sample, to allow for an assessment of the analytical reproducibility of the method including the laboratory extraction.

A matrix was created to classify each sample in the analysis by river, month of sampling, and treatment. Principle component analysis was run on the sample data set using PLS Toolbox (7.2 Eigenvector). The reference samples were projected onto the model identified and the standard deviation of each reference was calculated for each principle component. To ensure the validity of the results, and specifically to ensure that neither the mass spectra nor the UV-visible spectra were overwhelming the results, principle component analysis was also run on the two spectra separately. Both of the separate analyses returned the same components as the concatenated model, verifying the validity of the results.

Flow data for each site for the duration of the sampling period was obtained from the Swedish Meteorological and Hydrological Institute’s Vattenweb (SMHI, <http://vattenwebb.smhi.se/station/>). Temperature data was obtained from the SMHI’s Luftweb (<http://luftwebb.smhi.se/>). Catchment areas and land cover data were obtained from the Swedish Statistical Board (<http://www.scb.se>).

RESULTS

A five principle component model that explained 91.47% of the variance in the dataset was identified (PC1→59.38%, PC2→21.17%, PC3→7.81%, PC4→1.65%, PC5→1.45%). Each principle component was related to an identifiable environmental variable within the dataset. In all, the analytical and experimental variability was minor. The individual reference scores on each component clustered together, as indicated by small standard deviation for each component (Table 2). Furthermore, in all

PCs the range of scores is several times higher than the mean standard deviation of the references. The standard deviation for the experimental reference (*E-test*), was not larger than that of the two analytical references (Ref1 and Ref2), indicating that variations in the laboratory due to sample preparation and extraction were negligible compared to the analytical variability.

PC1

Principle component 1 represented the changes in the mass and absorbance spectra that were driven by photochemical degradation. Photodegraded samples scored higher (all positively) on PC1 compared to the original *in situ* non-degraded samples, for all seasons (Figure 2A). The relative analytical error for PC1 (i.e., mean error PC1/std.dev. of the change in scores for each river) was 8, 11, and 16% for Ume, Emån, and Lyckeby rivers, respectively. The mass spectrum loadings show that for the positively scoring photodegraded samples there is a loss of compounds with masses above 550 Da as well as below 200 Da (Figure 2C), while in the mid-range values there is an overall production, resulting from the breakdown of larger molecules.

The absorbance loadings (Figure 2B) show a broad decrease in loading across the visible and UV, with a maximum relative decrease between 300 and 350 nm. Below approximately 277 nm, there is an increase in loading. The combination of increase in the low UV wavelengths and decrease across the mid-range UVs and into the visible corresponds to a steepening of the absorption spectrum of the sample. This is further supported by the change in the UV spectral slope of the original pre-normalization absorption spectrum, which shows increases in spectral slope for all photodegraded samples (Figure 3). Furthermore, Figure 4 shows how the average mass of the samples decreases with increasing spectral slope, with the photochemically degraded samples clustering with high slope and low average mass.

PC2

The second principle component (PC2) is correlated to flow conditions in the catchments. When discharge is low relative to the annual mean discharge in the catchment, the score on PC2 is high. As the relative flow increases, the score on PC2 decreases (Figure 2D). The relationship is statistically significant for both Emån ($r = -0.77, p < 0.01$) and Lyckeby catchments, ($r = -0.73, p < 0.01$), the two smaller and largely forested catchments. In Ume catchment the correlation is not significant ($r = -0.3549, p = 0.2586$), however, when considering flow in just the forested parts of the catchment, the relationship becomes significant ($r = -0.58, p < 0.05$). The higher scores for low flow

TABLE 2 | Standard deviations of principle component scores for the three reference samples and the range of scores for each PC.

PC	Ref1	Ref2	E-test	Mean error	Range of scores
1	1.277×10^{-4}	1.677×10^{-4}	8.34×10^{-5}	1.263×10^{-4}	-3.843×10^{-3} to $+5.081 \times 10^{-3}$
2	1.502×10^{-4}	2.028×10^{-4}	2.002×10^{-4}	1.844×10^{-4}	-4.508×10^{-3} to $+2.431 \times 10^{-3}$
3	2.101×10^{-4}	1.414×10^{-4}	1.244×10^{-4}	1.586×10^{-4}	-2.338×10^{-3} to $+2.394 \times 10^{-3}$
4	5.60×10^{-5}	3.07×10^{-5}	5.98×10^{-5}	4.88×10^{-5}	-5.796×10^{-4} to $+1.281 \times 10^{-3}$
5	8.95×10^{-5}	1.043×10^{-4}	1.294×10^{-4}	1.077×10^{-4}	-7.376×10^{-4} to $+5.718 \times 10^{-4}$

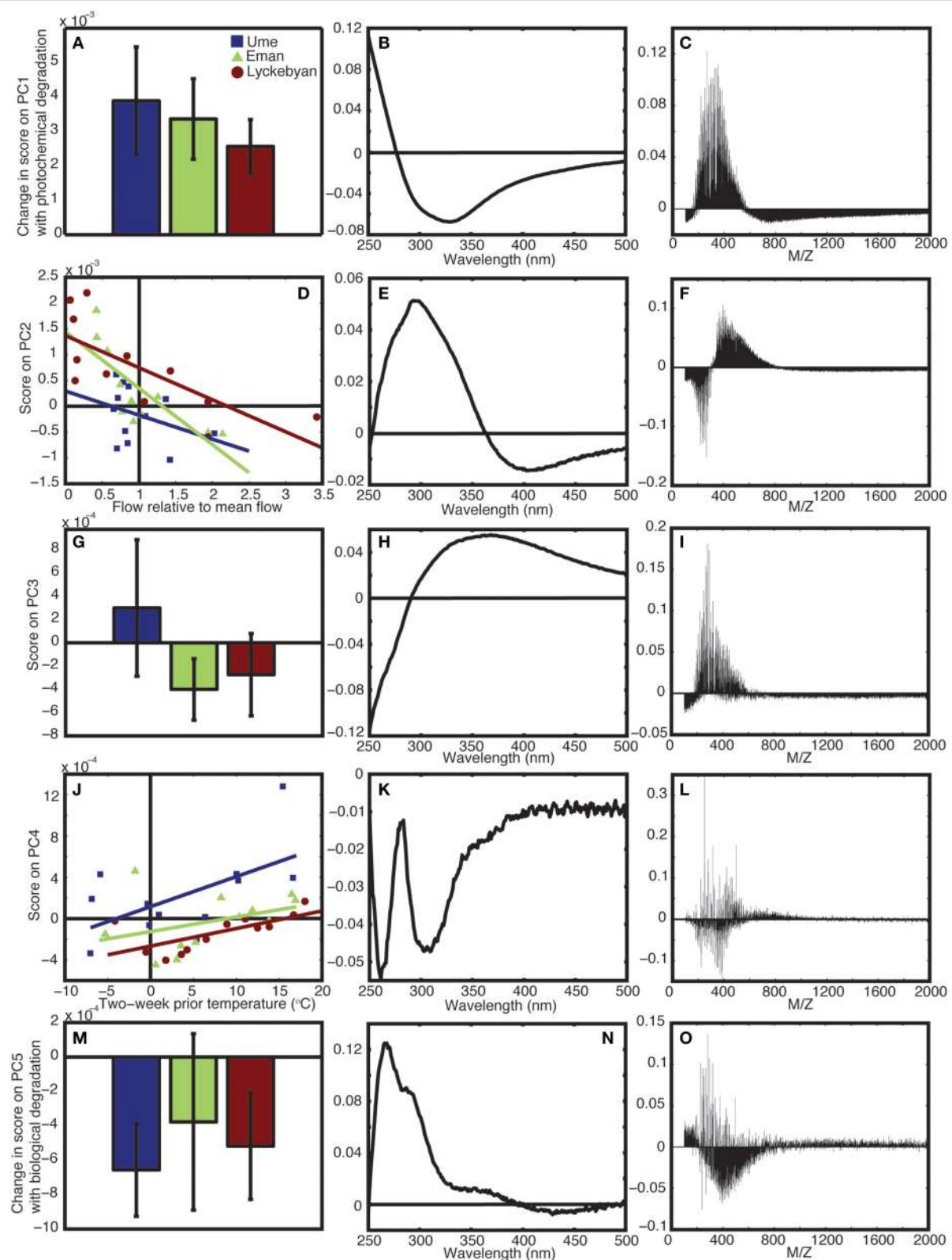


FIGURE 2 | Results from principle component analysis. **(A)** Shows the change in score on PC1 with photochemical degradation, **(B,C)** show the corresponding absorbance and mass loadings for PC4, respectively. **(D)** Shows the scores on PC2 relative to flow in the rivers, **(E,F)** show the corresponding absorbance and mass loadings for PC2, respectively. **(G)** Shows the mean and range of the PC3 scores for *in situ* samples for each river, **(H,I)** show the corresponding absorbance and mass loadings for PC3, respectively. **(J)** Shows the scores on PC4 versus two-week prior temperature (°C). **(K,L)** show the corresponding absorbance and mass loadings for PC4, respectively. **(M)** Shows the change in score on PC5 with biological degradation for each river, **(N,O)** show the corresponding absorbance and mass loadings for PC5, respectively. **(Continued)**

FIGURE 2 | Continued

mass loadings for PC4, respectively. (J) Shows the scores on PC4 relative to the temperature in the catchment, (K,L) show the corresponding absorbance and mass loadings for PC4, respectively. (M) Shows the change in score on PC5 for the long-term biological degradation samples, (N,O) show the corresponding absorbance and mass loadings for PC5, respectively. In all cases, blue is Ume river, green is Em  n river, and red is Lyckeby river.

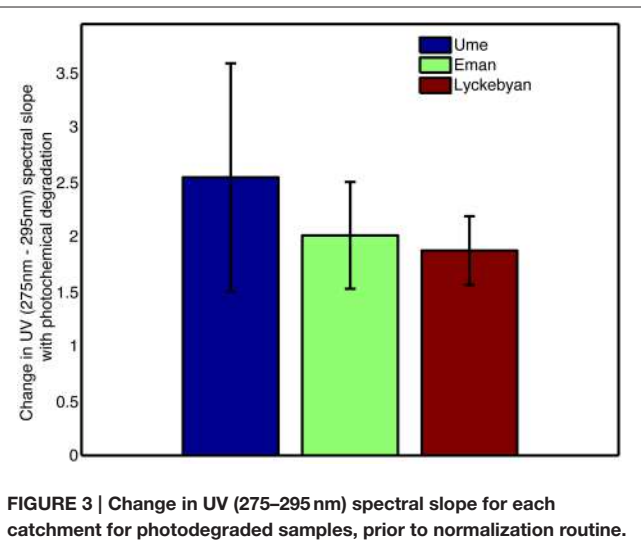


FIGURE 3 | Change in UV (275–295 nm) spectral slope for each catchment for photodegraded samples, prior to normalization routine.

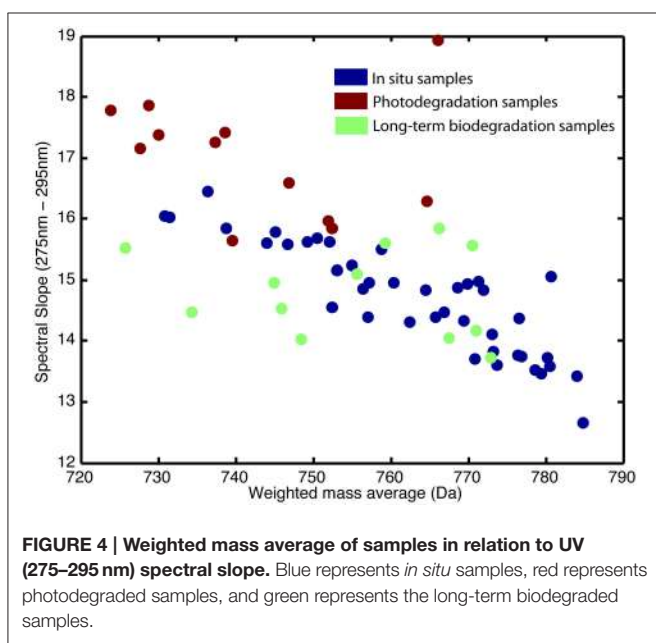


FIGURE 4 | Weighted mass average of samples in relation to UV (275–295 nm) spectral slope. Blue represents *in situ* samples, red represents photodegraded samples, and green represents the long-term biodegraded samples.

conditions corresponds to an increase in mid-range mass values, from 300 to 800 Da, along with a strong decrease in the relative contribution of masses below 300 Da (Figure 2F).

In the corresponding absorbance loading, the low flow conditions lead to an increase in UV absorbance, with the highest relative increase at 300 nm, and a decrease in relative absorbance in the visible wavelengths (Figure 2E). As the flow approaches the annual mean discharge value (1 on the x axis) and beyond,

into spring flood and high precipitation event type conditions, the score on PC2 approaches 0 and even extends slightly below 0. This means that the loading patterns indicated in the mass spectrum and the absorbance spectrum are no longer found in the total spectrum, or that their contribution is in fact very low during these conditions.

PC3

The third principle component (PC3) splits between the three different catchments. Em  n and Lyckeby catchments are similar in terms of forest cover and agricultural land-use (see Table 1), while Ume catchment covers a much larger variety of land covers. This can be seen in the PC3 scores (Figure 2G) where over the year Em  n and Lyckeby catchments score overall negatively (or very weakly positively), while Ume catchment scores positively or weakly negatively over the year. The analytical error on this component is between 27 and 60% of the total range of scores.

There is a greater proportion of masses within sizes 200–500 Da in Ume catchment compared to both Em  n and Lyckeby catchments (Figure 2I). Interestingly, the *m/z* loading spectrum for this component is more specific with selected *m/z* peaks in the 250–500 Da range also showing removal. The absorbance loadings (Figure 2H) show a broad increase in Ume at wavelengths above 300 nm with a decrease below 300 nm, while the opposite occurs in Em  n and Lyckeby catchments (i.e., these two catchments see a relative increase in the low UV and a relative decrease above 300 nm). This corresponds to more shallow spectral slopes for Ume catchment samples and steeper of spectral slopes in both Em  n and Lyckeby catchments.

PC4

Principle component 4 (PC4) is correlated to temperature within the catchment (2-week mean temperature prior to sampling date, Figure 2J). In both Ume and Lyckeby catchment the correlation is significant ($r = 0.58, p < 0.05$; $r = 0.67, p < 0.05$, respectively). In Em  n catchment, the relationship is not significant ($r = 0.37, p = 0.24$), however this is driven by an outlier value in February only. Removal of this month from the analysis renders the correlation significant ($r = 0.75, p < 0.001$). Scores on PC4 also increase with increasing lake area in the catchments (Table 1 and Figure 2J), with Ume having higher scores on average, decreasing with Em  n and again with Lyckeby.

In contrast to the first three principle components, the loadings for both the mass spectra and the absorbance spectrum are more variable. Within the same size class, mass values are both produced and removed from the mass spectrum (Figure 2L). In colder temperatures, the loadings show depletion of all mass values with positive loadings, and production of mass values with negative loadings. In the warmer summer months the opposite is true, with preferential removal of the

TABLE 3 | Mass spectrum peaks of note from PC4 (with loading intensities higher or lower than 0.05/–0.05).

Positive loading	Negative loading	Positive loading	Negative loading
221	179	390	329
239	197	392	331
248	207	404	341
249	209	406	343
262	223	418	355
267	225	420	357
275	237	422	359
277	251	434	368
289	265	436	370
303	269	448	382
312	282	450	384
316	292	466	396
351	294	482	398
363	306	504	400
376	319	520	412
378	327		

mass values with negative loadings and production of those with positive loadings. **Table 3** shows significantly high/low loaded *m/z*-values for PC4. There are indications of pairs or series of separated by unit spacing of 14 (i.e., CH₂) groups being removed, suggestive of degradation of hydrocarbon chains. Similarly, the absorbance loading spectrum (**Figure 2K**) is more complex, with all values loading negatively (i.e., removed from the spectrum in the positively scoring warm summer months, and added to the spectrum in the negatively or zero scoring cold winter months). Two peaks of interest occur, being much more strongly removed in the summer months, at 260 and ~305 nm.

PC5

Principle component 5 (PC5) shows a strong decrease in loadings for all three rivers, across the four seasons sampled as a result of biodegradation (**Figure 2M**). The *in situ* samples score positively or near to zero, while all samples subjected to long-term (4 months) biological degradation processes score negatively. Though the total amount of variance explained by this component is relatively small, the analytical error is smaller than the variance of the means and differences (Ume: 37%, Emåns: 20%, Lyckeby: 33%), indicating that this component is a valid explanatory variable in this model. Like PC4, the mass spectrum (**Figure 2O**) shows more selectivity than the first three components. There appears to be a broad production of organic matter metabolites between 250 and 700 Da with peak degradation 450 Da. However, this is not consistent and there are many *m/z*-values that are strongly degraded (positive loading) in this region as well. **Table 4** shows the values of strongly degraded and produced *m/z*-values (loading intensity larger than ±0.04) for PC5. This selectivity is an additional indicator of microbial processing.

TABLE 4 | Mass spectrum peaks of note from PC5 (with loading intensities higher or lower than 0.04/–0.04).

Positive loading	Negative loading	Positive loading
227		166
241	193	300
248	225	304
249	239	312
251	269	317
253		327
265		335
277		365
279		410
289		482

The absorbance loading (**Figure 2N**) shows a characteristic selective decrease with biological degradation (positive loading), with a peak decrease at 265–270 nm and a shoulder in the spectrum at 285–295 nm. There is again a slight shoulder around 370 nm and very little loading in the visible wavelengths, indicating that long-term biodegradation mostly affects the UV portion of the absorbance spectrum.

DISCUSSION

Recent advances in analytical methods to characterize DOM have led to widespread availability of both molecular and optical data sets (Coble, 2007; Mopper et al., 2007; Nelson and Siegel, 2013). The complexity of the DOM pool is clear from ultra-high resolution mass spectrometry studies, as they generally find that DOM occupies all of the compositional space (Mopper et al., 2007; Kujawinski et al., 2009). Data reduction is necessary to extract meaningful variability in the data. Here, the use of PCA focuses on the variability between samples. The analysis offers an advantage over bulk approaches as additional information is gained by linking the mass spectra and the absorbance spectra in the same analysis. The absorbance detector and the mass detector are in-line, meaning that the two sample properties are measured on the same sample that has experienced the same treatment (extraction, concentration, etc.). The advantage of linking the two together directly in the PCA is that the absorbance loadings and mass spectrum loadings are caused by the same features in the sample, i.e. the compounds that make up the mass spectrum in each loading are the ones that cause the features seen in the absorbance spectrum or are at least strongly correlated to them.

Reactivity Fingerprints—Photochemistry

The most dominant signal in the dataset is driven by photochemical degradation. A clear signal of photochemical fading is seen in the absorbance loadings for PC1; large scale removal of absorbance in the UV and visible, and a relative increase in absorbance at wavelengths between 250 and 290 nm. This relative shift in the spectrum corresponds to a steepening of the spectral slope of CDOM absorbance in the UV, which is a well-known photochemical phenomenon (Del Vecchio and Blough, 2002; Helms et al., 2008). This steepening of the spectral

slope is easily seen in the original absorbance spectra before the PCA normalization (**Figure 3**), lending further support to the identification of photochemical processes in these samples. This commonly observed steepening of the spectral slope of CDOM is due to a shift in overall average molecular size of the DOM (**Figure 4**; Helms et al., 2008; Dalzell et al., 2009), which is clearly seen in the mass spectrum loadings of PC1 (**Figure 2C**). The loadings are dominated by a marked shift in *m/z*-values, with preferential degradation of molecules with *m/z* over 550, which subsequently produces smaller molecules, with masses between 200 and 550 *m/z*. This shift in molecule size of the entire pool from large average molecular size to smaller average molecular size is consistent with what is known of photochemical mechanisms in natural waters; particularly the production of indiscriminate reactive oxygen species leads to the breakdown of large structures into smaller ones (Blough and Zepp, 1995; Andrews et al., 2000).

Reactivity Fingerprints—Microbial Activity

The fifth PC is driven by long-term microbial degradation processes. While there is a general trend of production at smaller *m/z* ranges (i.e., 250–800), there are striking patterns of selective degradation of certain *m/z*-values within this range (see **Table 4**). These select *m/z*-values have the potential to be used as biomarkers of microbial degradation due to their unique signature, and deserve further consideration in future studies. In general, microbial degradation is more selective than photochemical degradation. There is some selectivity also seen in the absorbance loading where there is a strong peak and shoulder being removed from the absorbance spectrum in the microbially degraded samples. Despite general production of relatively low mass values, this does not correspond to a concurrent increase in CDOM absorbance.

Catchment Fingerprints

The catchment related components show both differences between catchments, as well as more general environmental forcing. PC3 is catchment specific, showing a clear difference between Ume catchment and the relatively similar Emå and Lyckeby catchments. The increase in smaller compounds (*m/z* range 200–500) in Ume catchment suggests that these compounds come from grass and scrubland rather than the more diagenetically altered and potentially more condensed peat and forest sourced compounds (present in all three catchments). The absorbance loadings show a concurrent lessening of the influence of mid-UV absorbance for Ume as well, which further suggests a lower relative contribution from aromatic and conjugated compounds in that catchment.

PC2 and PC4 both show environmental forcing, namely, hydrology and temperature, respectively. In PC2, low flow conditions lead to an increase in the relative contribution of peat and wetlands, as well as drainage through deeper layers of forest soil. The importance of the boreal forest and associated peat and wetlands has been seen before in bulk DOC studies (Bishop et al., 1993; Cole et al., 2007; Asmala et al., 2013), and specifically in these catchments (Reader et al., 2014). Here we can see the expected shift in the absorbance spectra as these sources become

dominant under low flow conditions, with a strong increase in mid- to-low UV absorption and a smaller decrease from 350 nm into the visible, effectively an increase in the spectral slope ratio (S_R ; Helms et al., 2008). The mass spectrum loading shows that this effect is driven by ions with higher *m/z*-values. Correlation between increasing S_R and increased *m/z*-value as seen in the PC2 loadings during low flow has been previously reported in bulk DOM studies (Helms et al., 2008). The compounds in this type of DOM have typically undergone more diagenesis than fresher material delivered to aquatic systems during high flow conditions, and are made up of more aromatic and condensed structures, hence the higher mass and absorption signals.

PC4 reflects a different kind of microbial activity than PC5. The increase in loading of PC4 with increasing catchment temperatures is seen in all three catchments, with a maximum in the summer months when microbial activity is highest. Moreover, there is a concurrent increase in the loading of PC4 with the total lake area, further supporting the importance of microbial processing of the DOM within the catchment. The mass loadings here show more selectivity with respect to *m/z*-values, unlike the loadings driven by river flow in PC2, where the *m/z* loading shows a distinct shift between high and low values. The selective nature of this PC is reflected again in the absorbance loading which shows two distinct peaks of negative loadings in the UV (i.e., the two troughs seen in **Figure 2K**). Shifts in the absorbance spectrum of CDOM due to microbial activity are often subtle (Miller and Moran, 1997), however, given the selective nature of microbial activity, it is likely to cause this type of peak followed by trough character.

This method of analysis highlights the true effect of microbial activity on the absorbance spectra of natural waters, which cannot be seen with simplified methods such as spectral slope or wavelength ratios. At this point, it is not possible to determine whether this signal is driven by bacterial degradation or by phytoplankton growth, since both these processes tend to exhibit maxima under similar conditions (i.e., warm, high insolation summer months). However, given the ease with which this effect was detected in the analysis, it would be relatively straightforward to address this in future studies.

The results presented emphasize how difficult it can be to use bulk CDOM measures, such as spectral slope, to systematically indicate changes in CDOM character resulting from changes in the balance of catchment processes (e.g. microbial activity and hydrological residence time). This in part may explain contradictory seasonal trends from different catchments. It is clear that the analysis presented here is able to distinguish the different processes in such a way that much more information about the DOM character is revealed.

An Approach for Better Understanding the Biogeochemistry of DOM

Repeated analysis of three independent and randomly chosen samples allowed for an assessment of the ability of the method to successfully detect differences between samples. For all five PCs the spread of the repeated measures was small compared to the differences between treatments/sources etc. Low error combined

with the easily identifiable environmental variables for each PC, means the multivariate approach to fingerprinting DOM in aquatic environments offers novel and powerful insight into the cycling of DOM. The breakdown of an individual sample's mass and/or absorbance spectrum into individual components allows for these samples characteristics to be used as effective tracers of source and reactivity in the environment. The consistent and logical patterns that are seen in this dataset confirm the power of this approach.

Several series of mass peaks were found to be preferentially removed or produced by biological processes in the samples. While the resolution of the mass spectrometer employed in this study is not high enough to conclusively identify the individual molecular formulas producing these signals, this result offers a direction that ultra-high resolution studies could take by targeting specific mass values of interest. These potentially novel biomarkers could lend insight into the cycling of DOM through aquatic systems, as well as informing what compounds produce the unique absorbance signals seen in the couple absorbance loadings.

Furthermore, the uncoupled mass and absorbance spectra revealed that these components are easily identifiable without putting the two datasets together. This not only lends support to the integrity of the analysis, but also offers a simple and fast approach to optical DOM tracers, where one could envision using this approach on simple absorbance data, if the mass spectrometer were not available.

The approach presented in this study is the first of its kind to conclusively link the mass spectra and absorbance spectra of dissolved organic matter into one analysis. The technique provides insight into the cycling of organic matter, both source and reactivity in aquatic systems. Results confirm what earlier

bulk chemical studies suggested about the effect of broad abiotic processing of DOM and its effect on both the molecular content of DOM, as well as the optical properties DOM imparts on aquatic systems. Furthermore, this technique allows for the fingerprinting of more subtle biotic processes, which have long been known to be more selective than abiotic chemistry, and reveals their distinct signature on DOM's molecular composition and optical activity. The potential biomarkers, identified in both the mass spectra and the absorbance spectra offer directions for further study into the interactions of the microbial community and DOM cycling. The sources and reactivity of DOM in these rivers have been systematically identified, and these fingerprints have the potential to be used to trace these characteristics throughout the aquatic system, leading to a better understanding of the complex dynamics of DOM in the global carbon cycle.

AUTHOR CONTRIBUTIONS

HR, CS, EK designed the study, HR performed fieldwork, and prepared samples for analysis, NN ran samples on the UPLC system, transferred the data to the computing environment and contributed methods to the manuscript, HR analyzed the data and wrote the manuscript with significant input from CS and EK.

ACKNOWLEDGMENTS

This work was supported by the Swedish Research Council (VR, no. 2010-4081; granted to EK), the Managing Multiple Stressors in the Baltic Sea project, FORMAS grant no. 217-2010-1267, and Danish Research Council for Independent Research (DFF 1323-00336).

REFERENCES

- Andrews, S. S., Caron, S., and Zafiriou, O. C. (2000). Photochemical oxygen consumption in marine waters: a major sink for colored dissolved organic matter? *Limnol. Oceanogr.* 45, 267–277. doi: 10.4319/lo.2000.45.2.0267
- Asmala, E., Autio, R., Kaartokallio, H., Pitkänen, L., Stedmon, C. A., and Thomas, D. N. (2013). Bioavailability of riverine dissolved organic matter in three Baltic Sea estuaries and the effect of catchment land use. *Biogeosciences* 10, 6969–6986. doi: 10.5194/bg-10-6969-2013
- Bishop, K. H., Lundström, U. S., and Giesler, R. (1993). Transfer of organic C from forest soils to surface waters: example from northern Sweden. *Appl. Geochemistry* 8(Suppl.), 11–15. doi: 10.1016/S0883-2927(09)80003-6
- Blough, N. V. and Zepp, R. G. (1995). “Reactive oxygen species in natural waters,” in *Active Oxygen in Chemistry*, ed C. S. Foote (Dordrecht: Springer Netherlands), 280–333.
- Christensen, J. H., and Tomasi, G. (2007). Practical aspects of chemometrics for oil spill fingerprinting. *J. Chromatogr. A* 1169, 1–22. doi: 10.1016/j.chroma.2007.08.077
- Coble, P. G. (2007). Marine optical biogeochemistry: the chemistry of ocean color. *Chem. Rev.* 107, 402–418. doi: 10.1021/cr050350+
- Coble, P. G., Schultz, C. A., and Mopper, K. (1993). Fluorescence contouring analysis of doc intercalibration experiment samples -z a comparison of techniques. *Mar. Chem.* 41, 173–178. doi: 10.1016/0304-4203(93)90116-6
- Cole, J. J., Prairie, Y. T., Caraco, N. F., McDowell, W. H., Tranvik, L. J., Striegl, R. G., et al. (2007). Plumbing the global carbon cycle: integrating inland waters into the terrestrial carbon budget. *Ecosystems* 10, 171–184. doi: 10.1007/s10021-006-9013-8
- Dalzell, B. J., Minor, E. C., and Mopper, K. M. (2009). Photodegradation of estuarine dissolved organic matter: a multi-method assessment of DOM transformation. *Org. Geochem.* 40, 243–257. doi: 10.1016/j.orggeochem.2008.10.003
- Del Vecchio, R., and Blough, N. V. (2002). Photobleaching of chromophoric dissolved organic matter in natural waters: kinetics and modeling. *Mar. Chem.* 78, 231–253. doi: 10.1016/S0304-4203(02)00036-1
- Goldman, J. C., Caron, D. A., and Dennett, M. R. (1987). Regulation of gross growth efficiency and ammonium regeneration in bacteria by substrate C:N ratio. *Limnol. Oceanogr.* 32, 1239–1252. doi: 10.4319/lo.1987.32.6.1239
- Granskog, M. A., Stedmon, C. A., Dodd, P. A., Amon, R. M. W., Pavlov, A. K., de Steur, L., et al. (2012). Characteristics of colored dissolved organic matter (CDOM) in the Arctic outflow in the Fram Strait: assessing the changes and fate of terrigenous CDOM in the Arctic Ocean. *J. Geophys. Res.* 117:C12021. doi: 10.1029/2012jc008075
- Helms, J. R., Stubbins, A., Ritchie, J. D., Minor, E. C., Kieber, D. J., and Mopper, K. (2008). Absorption spectral slopes and slope ratios as indicators of molecular weight, source, and photobleaching of chromophoric dissolved organic matter. *Limnol. Oceanogr.* 53, 955–969. doi: 10.4319/lo.2008.53.3.0955
- Hertkorn, N., Harir, M., Koch, B. P., Michalke, B., and Schmitt-Kopplin, P. (2013). High-field NMR spectroscopy and FTICR mass spectrometry: powerful discovery tools for the molecular level characterization of marine dissolved organic matter. *Biogeosciences* 10, 1583–1624. doi: 10.5194/bg-10-1583-2013

- Koch, B. P., Witt, M. R., Engbrodt, R., Dittmar, T., and Kattner, G. (2005). Molecular formulae of marine and terrigenous dissolved organic matter detected by electrospray ionization Fourier transform ion cyclotron resonance mass spectrometry. *Geochim. Cosmochim. Acta* 69, 3299–3308. doi: 10.1016/j.gca.2005.02.027
- Kujawinski, E. B., Del Vecchio, R., Blough, N. V., Klein, G. C., and Marshall, A. G. (2004). Probing molecular-level transformations of dissolved organic matter: insights on photochemical degradation and protozoan modification of DOM from electrospray ionization Fourier transform ion cyclotron resonance mass spectrometry. *Mar. Chem.* 92, 23–37. doi: 10.1016/j.marchem.2004.06.038
- Kujawinski, E. B., Longnecker, K., Blough, N. V., Del Vecchio, R., Finlay, L., Kitner, J. B., et al. (2009). Identification of possible source markers in marine dissolved organic matter using ultrahigh resolution mass spectrometry. *Geochim. Cosmochim. Acta* 73, 4384–4399. doi: 10.1016/j.gca.2009.04.033
- Laudon, H., Taberman, I., Ågren, A., Futter, M., Ottosson-Löfvenius, M., and Bishop, K. (2013). The Krycklan Catchment Study—a flagship infrastructure for hydrology, biogeochemistry, and climate research in the boreal landscape. *Water Resour. Res.* 49, 7154–7158. doi: 10.1002/wrcr.20520
- Miller, W. L., and Moran, M. A. (1997). Interaction of photochemical and microbial processes in the degradation of refractory dissolved organic matter from a coastal marine environment. *Limnol. Oceanogr.* 42, 1317–1324. doi: 10.4319/lo.1997.42.6.1317
- Mopper, K., Stubbins, A., Ritchie, J. D., Bialk, H. M., and Hatcher, P. G. (2007). Advanced instrumental approaches for characterization of marine dissolved organic matter: extraction techniques, mass spectrometry, and nuclear magnetic resonance spectroscopy. *Chem. Rev.* 107, 419–442. doi: 10.1021/cr050359b
- Nelson, N. B., and Siegel, D. A. (2013). The global distribution and dynamics of chromophoric dissolved organic matter. *Ann. Rev. Mar. Sci.* 5, 447–476. doi: 10.1146/annurev-marine-120710-100751
- Reader, H. E., Stedmon, C. A., and Kritzberg, E. S. (2014). Seasonal contribution of terrestrial organic matter and biological oxygen demand to the Baltic Sea from three contrasting river catchments. *Biogeosciences* 11, 3409–3419. doi: 10.5194/bg-11-3409-2014
- Stubbins, A., Lapierre, J.-F., Berggren, M., Prairie, Y. T., Dittmar, T., and del Giorgio, P. A. (2014). What's in an EEM? Molecular signatures associated with dissolved organic fluorescence in boreal Canada. *Environ. Sci. Technol.* 48, 10598–10606. doi: 10.1021/es502086e
- Vodacek, A., Blough, N. V., DeGrandpre, M. D., Peltzer, E. T., and Nelson, R. K. (1997). Seasonal variation of CDOM and DOC in the Middle Atlantic Bight: terrestrial inputs and photooxidation. *Limnol. Oceanogr.* 42, 674–686. doi: 10.4319/lo.1997.42.4.0674
- Walker, S. A., Amon, R. M. W., Stedmon, C., Duan, S. W., and Loucheurn, P. (2009). The use of PARAFAC modeling to trace terrestrial dissolved organic matter and fingerprint water masses in coastal Canadian Arctic surface waters. *J. Geophys. Res.* 114:G00F06. doi: 10.1029/2009jg000990
- Weishaar, J. L., Aiken, G. R., Bergamaschi, B. A., Fram, M. S., Fujii, R., and Mopper, K. (2003). Evaluation of specific ultraviolet absorbance as an indicator of the chemical composition and reactivity of dissolved organic carbon. *Environ. Sci. Technol.* 37, 4702–4708. doi: 10.1021/es030360x

Conflict of Interest Statement: The authors declare that the research was conducted in the absence of any commercial or financial relationships that could be construed as a potential conflict of interest.

Copyright © 2015 Reader, Stedmon, Nielsen and Kritzberg. This is an open-access article distributed under the terms of the Creative Commons Attribution License (CC BY). The use, distribution or reproduction in other forums is permitted, provided the original author(s) or licensor are credited and that the original publication in this journal is cited, in accordance with accepted academic practice. No use, distribution or reproduction is permitted which does not comply with these terms.



Associations Between the Molecular and Optical Properties of Dissolved Organic Matter in the Florida Everglades, a Model Coastal Wetland System

Sasha Wagner^{1*}, Rudolf Jaffé², Kaelin Cawley³, Thorsten Dittmar⁴ and Aron Stubbins¹

¹ Marine Sciences Department, Skidaway Institute of Oceanography, The University of Georgia, Savannah, GA, USA

² Southeast Environmental Research Center, Department of Chemistry and Biochemistry, Florida International University, Miami, FL, USA

³ Department of Civil, Environmental and Architectural Engineering, Institute of Arctic and Alpine Research, University of Colorado at Boulder, Boulder, CO, USA

⁴ Research Group for Marine Geochemistry (ICBM-MPI Bridging Group), Institute for Chemistry and Biology of the Marine Environment, Carl von Ossietzky University of Oldenburg, Oldenburg, Germany

OPEN ACCESS

Edited by:

Thomas S. Bianchi,
University of Florida, USA

Reviewed by:

Mukesh Gupta,
Environment Canada, Canada
Ana Rosa Arellano,
University of Florida, USA

***Correspondence:**

Sasha Wagner
sasha.wagner@skio.uga.edu

Specialty section:

This article was submitted to
Marine Biogeochemistry,
a section of the journal
Frontiers in Chemistry

Received: 30 September 2015

Accepted: 12 November 2015

Published: 25 November 2015

Citation:

Wagner S, Jaffé R, Cawley K, Dittmar T and Stubbins A (2015) Associations Between the Molecular and Optical Properties of Dissolved Organic Matter in the Florida Everglades, a Model Coastal Wetland System. *Front. Chem.* 3:66.
doi: 10.3389/fchem.2015.00066

Optical properties are easy-to-measure proxies for dissolved organic matter (DOM) composition, source, and reactivity. However, the molecular signature of DOM associated with such optical parameters remains poorly defined. The Florida coastal Everglades is a subtropical wetland with diverse vegetation (e.g., sawgrass prairies, mangrove forests, seagrass meadows) and DOM sources (e.g., terrestrial, microbial, and marine). As such, the Everglades is an excellent model system from which to draw samples of diverse origin and composition to allow classically-defined optical properties to be linked to molecular properties of the DOM pool. We characterized a suite of seasonally- and spatially-collected DOM samples using optical measurements (EEM-PARAFAC, SUVA₂₅₄, S_{275–295}, S_{350–400}, SR, FI, freshness index, and HIX) and ultrahigh resolution mass spectrometry (FTICR-MS). Spearman's rank correlations between FTICR-MS signal intensities of individual molecular formulae and optical properties determined which molecular formulae were associated with each PARAFAC component and optical index. The molecular families that tracked with the optical indices were generally in agreement with conventional biogeochemical interpretations. Therefore, although they represent only a small portion of the bulk DOM pool, absorbance, and fluorescence measurements appear to be appropriate proxies for the aquatic cycling of both optically-active and associated optically-inactive DOM in coastal wetlands.

Keywords: dissolved organic matter, fluorescence, absorbance, EEM-PARAFAC, ultrahigh resolution mass spectrometry, Florida coastal Everglades, subtropical wetland

INTRODUCTION

Dissolved organic matter (DOM) is an integral component of aquatic systems. DOM is fundamentally involved in many environmental processes, such as the binding of metals (Haitzer et al., 2002), transport of pollutants (Schwarzenbach et al., 2003), attenuation of light (Morris et al., 1995), and cycling of nutrients (Opsahl and Benner, 1997). DOM can also be chemically-altered

via photoreactive (Spencer et al., 2009; Stubbins et al., 2010) and biodegradative (Spencer et al., 2015) processing. The composition of DOM is a reflection of both original source material and the degradative processing it undergoes once released in the aquatic environment. Elucidating the biogeochemical structure of DOM is key to understanding its dynamics and ultimate fate in aquatic ecosystems.

Optical spectroscopic techniques (e.g., absorbance and fluorescence) are a quick and relatively inexpensive means for assessing DOM quality (Fellman et al., 2010; Coble et al., 2014). Optical properties have been established as efficiently-measured proxies for DOM source and reactivity (Stedmon et al., 2003; Jaffé et al., 2008; Hernes et al., 2009). For example, bulk DOM aromaticity has been correlated with specific UV absorbance (SUVA₂₅₄; Weishaar et al., 2003) and the fluorescence index (FI) can reflect relative contributions of microbial- or terrestrially-derived DOM sources (McKnight et al., 2001; Cory and McKnight, 2005). Three-dimensional excitation emission matrices (EEMs) have been widely used for the fluorescence-based characterization of DOM (Coble et al., 1990; Coble, 1996; Fellman et al., 2010; Ishii and Boyer, 2012). Early studies employed a “peak-picking” method to track changes in the EEM topography and relate these changes to DOM biogeochemistry (Coble et al., 1990; Coble, 1996). Current studies commonly use EEMs combined with parallel factor analysis (PARAFAC) to assess the environmental dynamics of DOM in diverse aquatic ecosystems (Jaffé et al., 2014). PARAFAC is a multivariate modeling technique, which statistically breaks down the EEM topographic signal into individual fluorescent components and estimates the relative contribution of these extracted components to the total EEM fluorescence of each DOM sample (Stedmon et al., 2003; Cory and McKnight, 2005). Although generally informative of DOM source and reactivity, optical measurements can only provide information about the optically-active compounds (e.g., chromophores and fluorophores) which exist as part of the bulk DOM pool. As such, very little is known about the optically-inactive compounds that track with chromophores and fluorophores as they enter and are then processed within aquatic ecosystems.

Fourier transform ion cyclotron resonance mass spectrometry (FTICR-MS) offers detailed molecular-level information regarding the composition of DOM (Kujawinski, 2002; Dittmar and Koch, 2006; Sleighter and Hatcher, 2007; Dittmar and Paeng, 2009). Due to ultrahigh mass accuracy, FTICR-MS resolves complex DOM mixtures allowing elemental formulae to be assigned to individual mass spectral peaks. As such, FTICR mass spectra yield unique molecular “fingerprints” for DOM. Although formulae cannot inherently be linked with specific molecular structures, as each represents many possible isomeric arrangements, they can be categorized by compound class using elemental ratios to help summarize the mass spectral composition of DOM (Šantl-Temkiv et al., 2013). Recent studies have correlated FTICR-MS signal intensities of individual molecular formulae with optical properties to assess which molecular families track with different PARAFAC components and optical indices in a drinking water reservoir (Herzsprung et al., 2012), boreal lakes (Kellerman et al., 2015), and rivers

(Stubbins et al., 2014), and the open ocean (Timko et al., 2015). However, such comparisons have yet to be carried out in coastal or estuarine environments.

The Florida coastal Everglades is a subtropical wetland with diverse vegetation (sawgrass prairies, mangrove forests, seagrass meadows), salinity (ranging from fresh to hypersaline), and DOM sources (terrestrial, microbial and marine). Wetland DOM dynamics are complex due to variable OM inputs, geomorphology, hydrology, primary production, and degradation processes (Qualls and Richardson, 2003; Larsen et al., 2010; Yamashita et al., 2010; Chen et al., 2013; Chen and Jaffé, 2014). Since the Everglades is an oligotrophic wetland system, DOM also plays a key role with regards to nutrient cycling, as most nitrogen (N) exists in the organic form (Boyer et al., 1997; Boyer, 2006), a feature which is detectable by FTICR-MS (Hertkorn et al., 2015). Due to its heterogeneity, the Everglades is an excellent model system for assessing how classically-defined optical properties are linked to molecular properties of this highly diverse DOM pool. In this study, a suite of seasonally- and spatially-collected DOM samples were characterized using optical measurements (EEM-PARAFAC, SUVA₂₅₄, S_{275–295}, S_{350–400}, S_R, FI, freshness index and HIX), and FTICR-MS. Spearman’s rank correlations between molecular formulae assigned to mass spectral peak intensities and optical indices were obtained to determine which molecular families associated with different DOM optical properties. Molecular families which were found to be associated with multiple optical properties are also discussed.

MATERIALS AND METHODS

Sample Location and Collection

The Everglades is situated on the southern tip of the Florida peninsula where the regional climate is subtropical with distinct dry (November through April) and wet (May through October) seasons (Lodge, 2005). Vegetation cover is highly varied and its distribution is primarily driven by hydrology and salinity (Lodge, 2005). Sixty two surface water samples were collected monthly along two major flow paths between 2010 and 2011 at six sites (**Figure 1**) which are extensively monitored as part of the Florida Coastal Everglades long-term ecological research program (fce.fclternet.edu). The sampling sites are described in brief, however further details can be found in Lodge (2005). Water drains through the Shark River Slough (SRS) from the north to the southwest into the Gulf of Mexico and is underlain with peat-based soil. In contrast, Taylor Slough (TS) drains in a general southern direction into Florida Bay, and is underlain primarily by marl-based soils. Sites SRS2 and TS2 are located in areas of freshwater marsh where the dominant vegetation is composed of emergent plants such as sawgrass and spikerush, and abundant periphyton mats. SRS2 and TS2 have distinctively different hydrological characteristics, with SRS2 featuring long hydroperiods (water depth and inundation time) compared to TS2 which undergoes routine dry-out during the dry season. SRS4, SRS6, and TS7 are estuarine sampling locations where flow paths are lined with mangrove forests. TS7, located at the

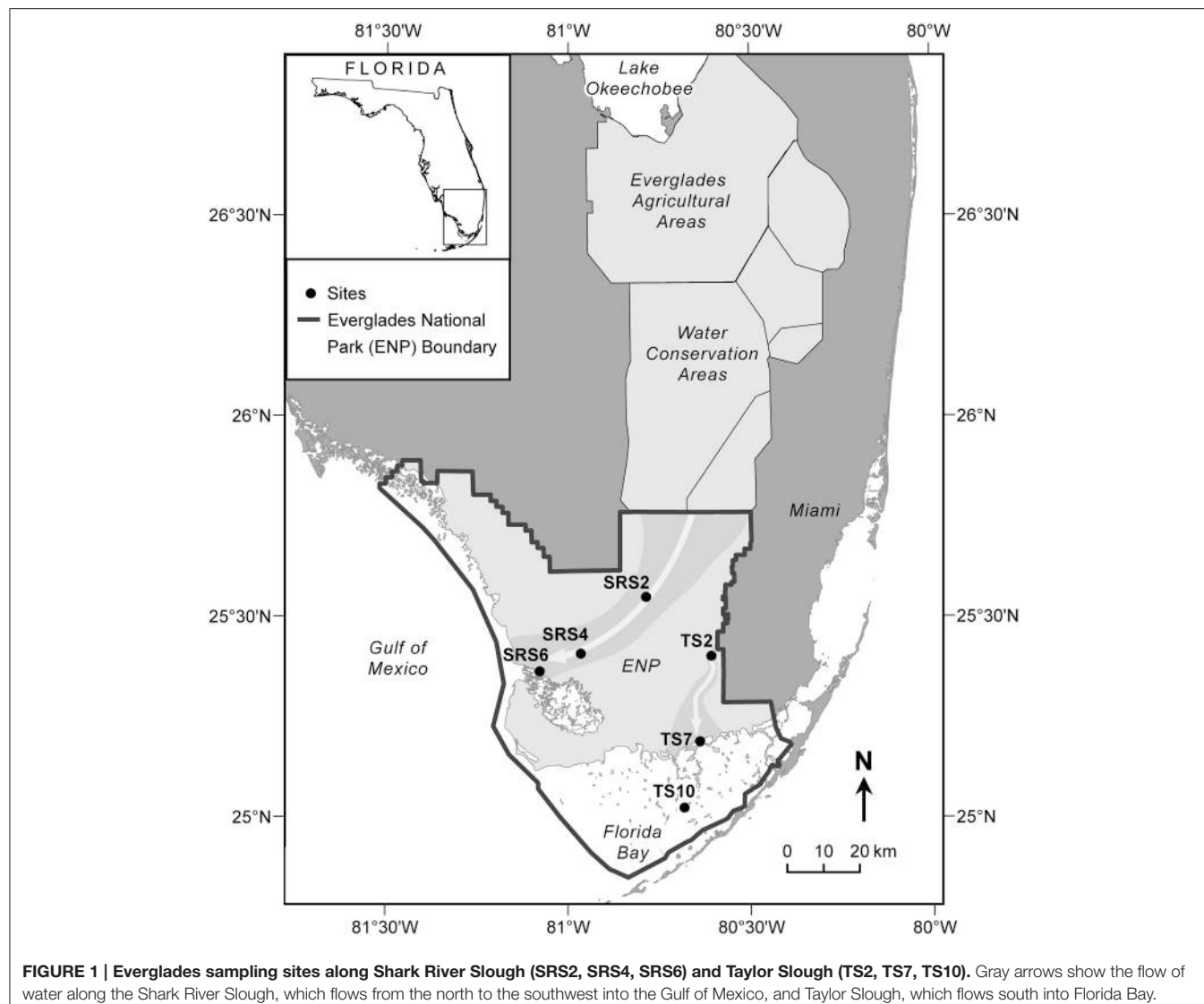


FIGURE 1 | Everglades sampling sites along Shark River Slough (SRS2, SRS4, SRS6) and Taylor Slough (TS2, TS7, TS10). Gray arrows show the flow of water along the Shark River Slough, which flows from the north to the southwest into the Gulf of Mexico, and Taylor Slough, which flows south into Florida Bay.

mouth of the Taylor River, is highly influenced by hydrological changes between the wet and dry seasons when water is sourced primarily from inland freshwaters and Florida Bay, respectively. TS10 is a high salinity sampling location within Florida Bay, where seagrass meadows are the dominant form of vegetation. The current sample set includes monthly samples collected for 1 year (2010 to 2011) from SRS2 ($n = 9$), SRS4 ($n = 12$), SRS6 ($n = 11$), TS2 ($n = 7$), TS7 ($n = 12$), and TS10 ($n = 10$). Sites SRS2, SRS6, TS2, TS10 do not have samples representing all months. In these cases, the missing samples were either unavailable for analysis or not collected due to lack of water during the dry season. A complete list of sampling dates and exact locations are listed in Supplementary Table 1. Surface water samples were collected in pre-cleaned amber Nalgene bottles and stored on ice during transport back to the laboratory at Florida International University. Samples were filtered through pre-combusted GF/F filters (0.7 μm) within 24 h of collection and stored in the dark at 4°C until further analysis.

Analysis of Dissolved Organic Carbon and Optical Measurements

DOC concentrations were measured for filtered samples using a Shimadzu TOC-V total organic carbon analyzer which employs the high-temperature catalytic combustion method (Stubbins and Dittmar, 2012). Absorbance spectra were collected (250–800 nm) using a Varian Cary 50 Bio UV-visible spectrophotometer and a quartz cuvette with a 1 cm path length. Absorbance at 254 nm was converted to Napierian absorbance coefficients (m^{-1} ; Hu et al., 2002) and used to measure chromophoric DOM content. Specific UV absorbance at 254 nm (SUVA₂₅₄) is an indicator of DOM aromaticity and was defined as the absorbance at 254 nm (m^{-1}) normalized to DOC (mg-C L⁻¹; Weishaar et al., 2003). While the presence of iron has been shown to influence SUVA₂₅₄ and other optical measurements (Poulin et al., 2014), the Everglades is underlain by limestone, severely limiting iron availability in this particular system. As such, SUVA₂₅₄ corrections for iron were not carried out. Spectral

slopes and the slope ratio (S_R) have been used as proxies for DOM molecular weight, photo-alteration, bio-alteration (Helms et al., 2008), and lignin-normalized carbon yields (Spencer et al., 2010). Spectral slopes $S_{275-295}$ and $S_{350-400}$ were calculated by fitting a linear regression to the natural log-transformed absorbance between 275–295 and 350–400 nm, respectively. S_R was then simply calculated as the ratio of these spectral slopes (Helms et al., 2008).

Excitation-emission matrices (EEMs) were obtained using a Horiba Jovin Yvon SPEX Fluoromax-3 spectrophotometer equipped with a 150 W continuous output Xe arc lamp in a 1 cm quartz cuvette (Maie et al., 2006; Chen et al., 2010). Excitation and emission slit widths were 5.7 and 2 nm, respectively. Forty emission scans were acquired at excitation wavelengths (λ_{ex}) 260–455 nm at 5 nm intervals. Emission wavelengths were scanned from $\lambda_{ex} + 10$ to $\lambda_{ex} + 250$ nm (i.e., between 250 and 705 nm) at 2 nm intervals. Individually-scanned spectra were then concatenated to generate EEMs. Post-acquisition data were blank-subtracted with Milli-Q water, absorbance data was used to correct for inner filter effects (McKnight et al., 2001) and fluorescence measurements were converted to quinine sulfate units. PARAFAC modeling was carried out using the Stedmon and Bro (2008) tutorial and accompanying Matlab code. EEMs from 57 of the 62 samples were used to develop the model and were normalized to a maximum intensity of 1 after being trimmed to remove the first and second order Rayleigh scatter. A four component model was validated using the split-half technique. EEM spectra were collected over a larger range than what is presented for the current PARAFAC model. Emission spectra collected at longer wavelengths tend to exhibit higher signal-to-noise ratios, thereby preventing model validation (Murphy et al., 2013). Therefore, EEMs for individual PARAFAC components shown in Figure 2 represent the validated spectral range. Upon validation, the model was applied to the original non-normalized EEMs in order to produce loadings that represented the original EEM intensities. In addition to PARAFAC, other fluorescence-derived indices were measured. The fluorescence index (FI) was measured as the ratio of emission intensity at 470 and 520 nm at excitation wavelength 370 nm (Cory and McKnight, 2005). The freshness index was calculated as the ratio of emission intensity at 380 nm to the maximum emission intensity between 420 and 435 nm at excitation wavelength 310 nm (Parlanti et al., 2000). The humification index (HIX) was calculated as the area under the emission spectra between 435 and 480 nm divided by the sum of peak areas 300 to 345 nm and 435 to 480 nm (Ohno, 2002).

Dissolved Organic Matter Extraction and Mass Spectrometry

Filtrates were acidified to pH 2 using concentrated HCl and the DOM was extracted following Dittmar et al. (2008). Briefly, DOM was isolated by solid phase extraction (SPE) by passing the acidified sample through a Varian Bond Elut PPL cartridge (5 g). SPE sorbent was first conditioned with MeOH and equilibrated with pH 2 Milli-Q water prior to DOM extraction. The filtrate passed through the cartridge via gravity and the sorbent was subsequently rinsed with pH 2 Milli-Q water for excess salt

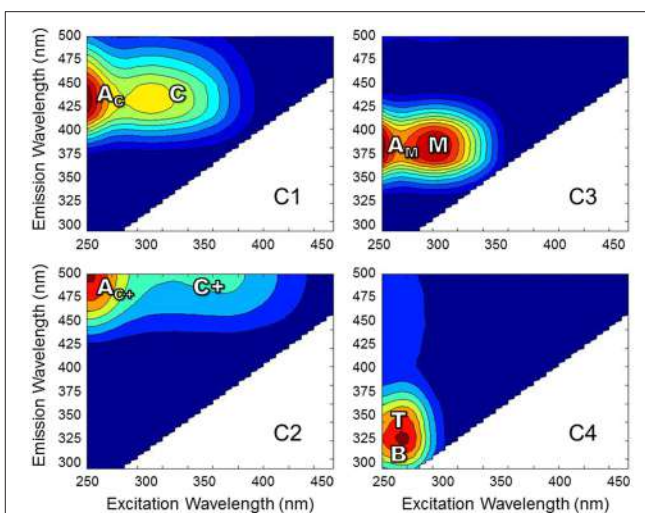


FIGURE 2 | EEMs of PARAFAC components for Everglades DOM.

Fluorescence spectra are labeled with conventional peaks A_C , C , A_{C+} , C_+ , A_M , M , B , and T (defined in the text).

removal prior to drying under N_2 . DOM was then eluted with MeOH and stored in the dark at -20°C until mass spectral analysis.

Methanol PPL extracts were mixed with Milli-Q water (1:1 v/v) and continuously infused into the electrospray ionization (ESI) source of a Bruker Solarix 15 T FTICR-MS instrument (University of Oldenburg, Germany) at a flow rate of $120 \mu\text{L h}^{-1}$ in negative ion mode (500 scans). Mass spectra were calibrated using a reference mass list to achieve mass accuracies with an error less than 0.2 ppm. Molecular formulae consisting of C, H, O, N, S, and/or P were assigned to peaks with signal-to-noise ratios >5 according to published rules (Koch et al., 2007; Stubbins et al., 2010; Singer et al., 2012). Peak detection limits were standardized among samples by adjusting the dynamic range (DR) of each sample to that with the lowest DR (Stubbins et al., 2014). The DR was calculated for each sample as the average peak intensity of the highest 500 peaks divided by the signal-to-noise threshold intensity (average intensity of 10 lowest peaks). The standardized detection limit (SDL) was then set for each sample by dividing the average peak intensity of the 500 highest peaks by the lowest DR within the sample set. For each sample, peaks falling below the SDL were filled in with the SDL to prevent false negatives for samples with a low DR. ESI-FTICR-MS in negative ion mode primarily ionizes polar, organic compounds, which makes it the analytical method of choice for assessing the complex molecular composition of DOM mixtures (Kujawinski, 2002; Kim et al., 2003). However, it is well understood that ionization efficiencies are not equal among different compound classes. Therefore, the relative intensities of FTICR-MS peaks may not accurately reflect actual concentrations or be truly representative of the entire DOM pool.

Assigned molecular formulae were categorized by compound class according to elemental stoichiometries (Šantl-Temkiv et al., 2013). The modified aromaticity index (AI-mod) (Koch and Dittmar, 2006) classifies formulae as aromatic (polyphenols; 0.5

= AI-mod < 0.67) and condensed aromatic (black carbon; AI-mod = 0.67) formulae. Compound classes were further defined as highly unsaturated (AI-mod < 0.5, H/C < 1.5, O/C < 0.9), unsaturated aliphatics (1.5 = H/C < 2, O/C < 0.9, N = 0), saturated fatty acids (H/C = 2, (O/C < 0.9), sugars (O/C = 0.9), and peptides (1.5 = H/C < 2, O/C < 0.9, N < 0). Since an individual formulae could occur in multiple isomeric structures, these classifications only serve as a guide to the structures present within DOM.

Spearman's Rank Correlations

Intensities for PARAFAC components were normalized to the sum of component fluorescence intensities within a sample. Mass spectral peak intensities were normalized to the sum intensity of all peaks within a sample. Pairwise Spearman's rank correlations (r) were then obtained between normalized PARAFAC components, optical indices (a_{254} , SUVA₂₅₄, S_{275–295}, S_{350–400}, S_R, FI, freshness index, HIX), and normalized mass peak intensities. Correlations between molecular formulae and optical parameters were considered significant at the 99% confidence level ($p < 0.01$; Stubbins et al., 2014). Multivariate statistical analyses were carried out using JMP Pro 11 (SAS Institute Inc.).

RESULTS

Dissolved Organic Carbon and Optical Measurements

DOC concentrations ranged from 3.3 to 20.4 mg-C L⁻¹. DOC concentrations and salinity values for each sample are listed in Supplementary Table 1. Chromophoric DOM a_{254} ranged from 10 to 204 m⁻¹ and SUVA₂₅₄ from 0.7 to 4.9 mg-C L⁻¹ m⁻¹. The S_{275–295}, S_{350–400}, and S_R spanned ranges of 0.016 to 0.034 nm⁻¹, 0.005 to 0.032 nm⁻¹, and 0.68 to 3.15, respectively. Everglades FI ranged from 1.29 to 1.53, the freshness index from 0.45 to 0.87, and HIX from 1.6 to 15.1. A complete list of optical index values for all samples is detailed in Supplementary Table 2. PARAFAC modeling yielded four fluorescent components (C1–C4; Figure 2). The loadings for each PARAFAC component are shown in Supplementary Figure 1. C1 is a "humic-like" component comprised of conventional peaks A_C and C (Figure 2). C2, another "humic-like" component, is shifted

to longer emission wavelengths relative to C1 corresponding to conventional peak A_{C+} and C₊ (Figure 2). C3 exhibits fluorescence within the region of conventional peaks A_M and M (Figure 2). C4 is a "protein-like" component, whose intensity maximum falls within the region of conventional peaks B and T (Figure 2). Prior EEM-PARAFAC studies on DOM in the greater Everglades (e.g., Chen et al., 2010; Yamashita et al., 2010) have employed an eight component PARAFAC model (from here on referred to as the FCE model where components are FCE1–FCE8; Chen et al., 2010). In the present study, EEMs were collected after sample dilution, resulting in a PARAFAC model that best fit only four components. Therefore, the eight component FCE model could not be directly applied to this particular data set. However, each of the 4 PARAFAC components employed in this study were statistically related to one or more components of the FCE model. At the 90% confidence level, C1 represented a mixture of model FCE1 + FCE3 (but not FCE1 alone), with likely contributions from FCE2 which exhibited similar emission patterns. However, the link between C1 and FCE2 could not be statistically validated. C2 represented FCE1 + FCE5, C3 represented FCE4 + FCE6 (but not FCE6 alone) and C4 represented FCE7. As such, the current 4 component model will be linked to the established FCE model in the discussion. Excitation and emission maxima for the current four component PARAFAC model are detailed in Table 1 where they are related to conventional peak assignments and FCE model components.

Ultrahigh Resolution Mass Spectra

FTICR-MS allowed for the assignment of 6716 molecular formulae to resolved peaks across all DOM samples (Table 2). The formulae spanned a molecular mass range from 150 to 750 Da and most contained one or more N, S, and/or P atoms ($n = 3756$, 44% of intensity; Table 2). Of N-, S-, or P-containing formulae, CHON ($n = 2494$; 36% of total intensity) were the most abundant, followed by CHOS ($n = 1531$; 23% of total intensity; Table 2). Formulae with P were much less abundant ($n = 251$; 3% of total intensity; Table 2). CHO-only formulae contributed to less than half of the molecular formulae for this particular dataset ($n = 2960$, 45% of intensity; Table 2). Highly unsaturated formulae were ubiquitous and the dominant class of compounds for Everglades DOM ($n = 3668$, 53% of intensity; Table 2). Unsaturated aliphatics were also well represented ($n =$

TABLE 1 | Excitation and emission maxima of PARAFAC components and their relation to conventional peaks as described by Coble et al. (2014).

PARAFAC Component	Excitation/Emission Maxima (nm/nm)	Corresponding Conventional Peak(s)	Corresponding Component(s) from the FCE Model	Description
C1	<260(ex)/425(em), 310(ex)/425(em)	A _C /C	FCE1, FCE3	Ubiquitous humic-like Terrestrial humic-like
C2	260(ex)/>500(em), 370(ex)/>500(em)	A _{C+} /C ₊	FCE1, FCE5	Ubiquitous humic-like Terrestrial humic-like
C3	<260(ex)/375(em), 300(ex)/375(em)	A _M /M	FCE4, FCE6	Microbial humic-like
C4	275(ex)/320(em)	B/T	FCE7	Protein-like

Components from the FCE PARAFAC model (Chen et al., 2010), which were statistically related to C1–C4 at the 90% confidence level, and their descriptions (from Yamashita et al., 2010) are also listed.

TABLE 2 | Mean molecular mass, elemental groupings, and formula categorization of molecular formulae which correlated positively ($r > 0, p < 0.01$) with PARAFAC components C1–C4.

Mean m/z (Da)	All Formulae		C1		C2		C3		C4	
	408	%	450	%	408	%	386	%	372	%
Total no. formulae	6716	100	1980	29	2146	33	1761	26	1892	28
CHO only	2960	100	1122	37	1465	50	375	13	460	16
CHON	2494	100	842	34	238	10	986	39	952	38
CHOS	1531	100	55	3	462	32	528	34	628	41
CHOP	251	100	36	14	22	9	55	24	58	25
Contains N,S and/or P	3756	100	858	28	681	24	1386	45	1432	48
Black carbon	587	100	166	28	371	64	8	1	16	3
Polyphenols	1140	100	543	47	651	58	49	4	60	5
Highly unsaturated	3668	100	1214	33	1089	31	1069	28	1037	28
Unsaturated aliphatics	909	100	14	1	9	1	473	52	587	65
Saturated fatty acids	100	100	10	9	4	3	24	24	24	25
Sugars	37	100	11	29	10	28	3	9	2	6
Peptides	275	100	22	8	12	4	135	50	166	62

Mean m/z is the intensity-weighted average mass (Da). Listed integers reflect the number of molecular formulae and percentages in parentheses represent the percent of peak intensity contributed by each classification of molecular formulae.

909, 14% of intensity; **Table 2**). Aromatic compounds, such as black carbon ($n = 587$, 9% of intensity) and polyphenols ($n = 1140$, 18% of intensity) also had considerable contributions to the overall molecular signature (**Table 2**). Peptides ($n = 275$, 4% of intensity), saturated fatty acids ($n = 100$, 1% of intensity) and sugars ($n = 37$, 1% of intensity) contributed less to the molecular composition compared to other compound classes (**Table 2**).

DISCUSSION

Dissolved Organic Carbon Concentrations and Optical Indices

The Everglades landscape has diverse vegetation and its waters, which range from fresh to hypersaline, receive DOM inputs from both allochthonous and autochthonous sources (Chen et al., 2013). DOC concentrations and DOM optical properties vary considerably on both spatial and temporal scales. Everglades DOC concentrations have been reported to range from 3.6 to 28.0 mg-C L⁻¹ (Yamashita et al., 2010; Chen et al., 2013; Ding et al., 2014) and SUVA₂₅₄ values from 1.1 to 4.8 mg-C L⁻¹ m⁻¹ (Jaffé et al., 2008; Chen et al., 2013). The current sample set captured much of this variability in both DOC concentration and SUVA₂₅₄ (Supplementary Tables 1, 2), the latter indicating that our Everglades DOM samples spanned a wide range in aromatic content (Weishaar et al., 2003; Stubbins et al., 2008). Spectral slopes and their ratio (S_R) vary with the source, molecular weight and the photochemical and biological processing of DOM (Helms et al., 2008). Spectral slopes $S_{275-295}$ and $S_{350-400}$ have not been reported previously for the Everglades, however S_R values generally range from 0.7 to 9.0 from aromatic-rich swamp waters to the open ocean (Helms et al., 2008; Yamashita et al., 2010; Chen et al., 2013) but can exceed 13.0 in the high salinity waters of Florida Bay (Timko et al., 2014). The slope values

reported here (Supplementary Table 2) cover a wide range of those reported for the Everglades and across gradients from highly terrigenous, black water swamp to open ocean DOM where $S_{275-295}$ ranges from 0.013 to 0.036 nm⁻¹, $S_{350-400}$ from 0.008 to 0.019 nm⁻¹, and S_R from 0.70 to 4.56 (Helms et al., 2008). Similarly, the measured FI for the current sample set (Supplementary Table 2) spans much of the variability reported for the Everglades which ranges from 1.28 to 1.47 (Yamashita et al., 2010). Across aquatic environments, FI values can range from 1.0 to 1.8 where low values indicate terrestrially-derived DOM and high values suggest DOM derived from microbial sources (Cory and McKnight, 2005; Jaffé et al., 2008). Although, HIX and freshness indices have not yet been reported for the Everglades, our dataset is representative of the possible range of HIX values from 4.5 to 16.0 (Singh et al., 2010) and freshness values from 0.4 to 0.9 (Huguet et al., 2010; Dixon et al., 2014) observed for other coastal systems which receive both terrestrial and marine DOM inputs. The diversity of DOM optical quality within the Everglades makes it an excellent model system from which to draw samples to allow classically defined optical properties to be linked to the molecular properties of the DOM pool. Based upon the above, the sample set analyzed here captured a wealth of this variability.

PARAFAC Components

Four PARAFAC components were assigned to the dataset (**Table 1**; **Figure 2**; Supplementary Figure 1). Their nomenclature is indicative of their proportional contribution to total fluorescence, which decreased from C1 to C4. C1 exhibited a primary peak at <260 nm(ex)/425 nm(em) and a secondary peak at 310 nm(ex)/425(em; **Table 1**; **Figure 2**). The primary peak falls in the region of the A_C peak and the secondary peak is within the region of the C peak as defined by the classical EEMs nomenclature (Stedmon et al., 2003; Fellman et al., 2010;

Coble et al., 2014). Peaks A_C and C are typically described as representing terrigenous, high molecular weight, and aromatic DOM as they are commonly identified in forested and wetland environments (Fellman et al., 2010). C1 likely represents a mixture of “humic-like” components FCE1, FCE2, and FCE3 for the eight component model established by Chen et al. (2010; **Table 1**), where FCE1 is typically the most abundant fluorescent contributor (Chen et al., 2013). FCE2 is mainly derived from soil OM oxidation in the northern Everglades (Yamashita et al., 2010). FCE2 also represents fluorophores which are resistant to photo-degradation, while FCE3 has been suggested to be a photo-intermediate (Chen and Jaffé, 2014). As such, C1 in the current study likely represents the primary “humic-like,” soil-derived components in Everglades DOM. C2 exhibited a peak at 260 nm(ex)/>500 nm(em) with a shoulder peak at 370 nm(em) (**Table 1**; **Figure 2**) which has been observed in other terrestrially-dominated systems (e.g., Stedmon et al., 2003; Santín et al., 2009; Chen et al., 2010; Stubbins et al., 2014). This long wavelength peak has been referred to as the A_{C+}/C+ peak and as being associated with older, terrestrial, or soil-derived organic material (Coble et al., 2014). C2 is similar to FCE1 + FCE5, both of which are terrestrially-derived, humic-like components and usually exhibit very similar environmental trends in the Everglades (Yamashita et al., 2010; Chen et al., 2013). C3 consisted of a primary peak at <260 nm(ex)/375 nm(em) and a secondary peak at 300 nm(em)/375 nm(em; **Table 1**; **Figure 2**). The peaks associated with C3 fall within the region of classical peaks A_M and M, which have been commonly found in marine surface waters and associated with microbial, freshly-produced and/or biolabile DOM (Coble et al., 1998, 2014; Fellman et al., 2010). C3 is also closely associated with FCE4 + FCE6, which have both been characterized as microbial humic-like components (Chen et al., 2010; Yamashita et al., 2010). FCE6 has also been shown to be highly photo-reactive (Chen and Jaffé, 2014). The C4 peak exhibited an intensity maximum at 275 nm(ex)/320 nm(em; **Table 1**; **Figure 2**). C4 is commonly referred to as a “protein-like” component (Fellman et al., 2010), and has been correlated with total hydrolysable amino acids (Yamashita and Tanoue, 2003). However, small nitrogen-free aromatic monomers have also been shown to fluoresce within the same region (Maie et al., 2007; Hernes et al., 2009). C4 is also well correlated with FCE7, which exhibits tyrosine-like fluorescence and has higher contributions to the fluorescence signature in areas of the Everglades where periphyton mats or seagrasses are abundant (Maie et al., 2012; Chen et al., 2013).

Associations Between PARAFAC Components and Molecular Families

Spearman’s rank correlations between normalized mass spectral peak intensities and normalized fluorescence intensities were carried out in order to elucidate groups of compounds associated with each PARAFAC component. The majority of assigned formulae tracked positively with one or more PARAFAC component ($n = 5497$, 82% of intensity), which suggests that C1 through C4 represented >80% of the molecular composition under the specific preparative and analytical conditions described

for this study (i.e., PPL extraction followed by ESI-FTICR-MS analysis). Where EEM spectra are used to display the topographical distributions of fluorescence data, the molecular character of DOM revealed by FTICR-MS is facilitated by van Krevelen diagrams, where individual formulas are graphed according to their H/C and O/C ratios (Kim et al., 2003). Van Krevelen plots of molecular formulae associated with each PARAFAC component are shown in **Figure 3**. Additional van Krevelen distributions of each molecular grouping separated by N and S content are shown in Supplementary Figures 2–5.

As noted above, C1 (conventional peaks A_C and C; FCE1 + FCE3) and C2 (conventional peak A_{C+}/C+; FCE1 + FCE5) represent “humic-like” components, which within the Everglades system are most likely terrestrially-sourced. Although C1 and C2 were both associated with high molecular weight, aromatic carbon-rich DOM (**Table 2**), individual formulae associated with these components spanned a wide range of masses, with small numbers of low molecular weight, aliphatic compounds also tracking with the “humic-like” fluorophores. Humic substances have been described to consist of supramolecular assemblies of smaller, heterogeneous molecules held together by weak dispersive forces or cation bridging (Piccolo, 2001; Simpson et al., 2002; Romera-Castillo et al., 2014). As such, the covariation of optically active (e.g., aromatic) and inactive (e.g., aliphatic) formulae may result from physical or chemical associations between these DOM components in natural waters. Optical measurements are a reflection of both the inherent optical properties of DOM compounds and how they functionally interact with one another. For example, DOM can participate in charge transfer (Sharpless and Blough, 2014) and interact with iron (Poulin et al., 2014), thereby altering the cumulative absorbent and/or fluorescent behavior of DOM. As such, DOM optical measurements may be better described as emergent properties of the total functionality and molecular interactions

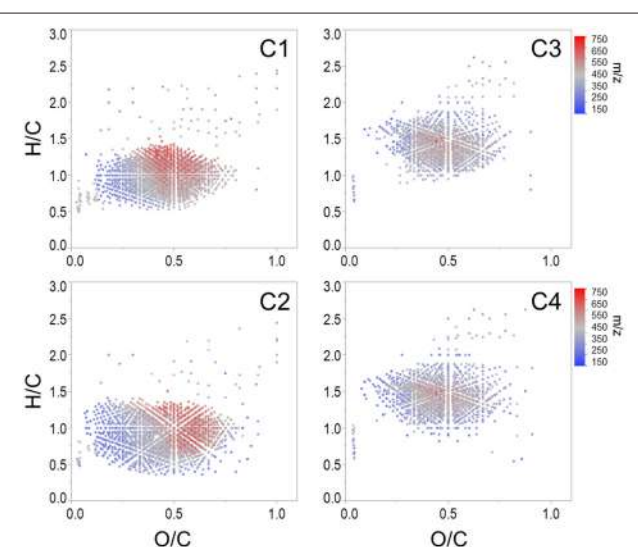


FIGURE 3 | Van Krevelen distributions of molecular formulae positively correlated with each Everglades PARAFAC component (corresponding EEMs are shown in **Figure 2**).

among all organic and inorganic constituents within a natural water sample (Stubbins et al., 2014).

C1 and C2 were broadly correlated with similar molecular families (**Figure 3**), however several notable distinctions exist. C1 was enriched in both CHO ($n = 1122$, 37% of intensity) and CHON ($n = 842$, 34% of intensity) formulae with considerable contributions from aromatic compounds, including black carbon and polyphenols ($n = 166$, 28% of intensity and $n = 543$, 47% of intensity, respectively; **Table 2**). C1 is a ubiquitous “humic-like” fluorophore which has been associated with terrestrial OM sources (Yamashita et al., 2010). In the Everglades, significant contributions of such “humic-like” components originate from soil OM oxidation throughout the system, primarily from the northern-most region of the Everglades Agricultural Area (EAA; **Figure 1**; Yamashita et al., 2010). Wildfires are common in the Everglades, and dissolved black carbon has been reported at relatively elevated levels compared to other locations globally (Jaffé et al., 2013; Ding et al., 2014), the routine burning of massive amounts of sugarcane in the EAA can serve as an additional source of highly aromatic pyrogenic DOM to the region. The CHON formulae associated with C1 are mainly aromatic, which may include dissolved black nitrogen (Wagner et al., 2015a) or other heterocyclic nitrogen compounds (Hertkorn et al., 2015). Enrichments in CHON formulae have been previously linked to anthropogenic land use (Wagner et al., 2015b). Therefore, C1 could indicate some degree of DOM input from the upstream EAA. Molecular formulae associated with C2 exhibited greater degrees of aromaticity compared to C1, with increased contributions from black carbon ($n = 371$, 64% of intensity) and polyphenols ($n = 651$, 58% of intensity; **Table 2**). In contrast to C1, formulae associated with C2 were relatively depleted in N, but enriched in CHOS formulae ($n = 462$, 32% of intensity; **Table 2**; Supplementary Figure 3). Although the aquatic cycling of dissolved organic sulfur in the Everglades is not well understood, subsurface peat soils can become enriched in sulfur-containing organic matter (Bates et al., 1998). Enrichments in CHOS formulae, likely resulting from the early diagenetic sulfurization of DOM, have been observed in soil and sediment pore waters of other marine-influenced systems (Schmidt et al., 2009). Such S-containing formulae have been previously reported for Everglades DOM (Hertkorn et al., 2015). Therefore, C2 may represent soil-derived or highly degraded DOM due to high S content and high relative contributions from biorefractory compound classes such as black carbon and other aromatics (**Table 2**).

Formulae associated with C3 and C4 shared very similar molecular compositions characterized by relatively low average molecular masses (386 Da and 372 Da, respectively) with increased contributions from N-, P-, or S-containing formulae, unsaturated aliphatics and peptides (**Table 2**, Supplementary Figures 4, 5). These components exhibited fluorescence at shorter wavelengths compared to C1 and C2, which may reflect an enrichment in aliphatics and lower molecular weight compounds from microbially-sourced DOM (Fellman et al., 2010). It was initially surprising to observe such a significant overlap between the molecular families associated with both C3 and C4 (**Table 2**; **Figure 3**). However, C3 and C4 were strongly correlated to one another for this dataset ($r = 0.66$, $p < 0.001$), and similar

PARAFAC components for the FCE model (FCE4, FCE6, FCE7; Chen et al., 2010) have been observed to share similar spatial distributions throughout the Everglades landscape (Yamashita et al., 2010; Maie et al., 2012). Such similarities between C3 and C4 suggest common DOM sources (e.g., seagrasses, periphyton mats, primary productivity, or aquatic plants) and/or processing (e.g., bioavailability). Similar associations between conventional peaks M, B, and T and molecular formulae that are enriched in N, S, or P and aliphatic carbon have been observed previously across boreal river systems (Stubbins et al., 2014). In all cases, the PARAFAC components were associated with molecular formulas and characteristics are representative of their presumed origins and adequately describe their utility as proxies for bulk DOM characteristics.

Associations Between Non-PARAFAC Optical indices and Molecular Families

To expand on recent literature which primarily focused on how molecular formulae covaried with PARAFAC components alone (Stubbins et al., 2014), we also present formula groups associated with other commonly-employed optical indices. Measured values for all optical indices ($SUVA_{254}$, $S_{275-295}$, $S_{350-400}$, S_R , FI, freshness index, HIX) are listed in Supplementary Table 2. Spearman’s correlations between ranked optical indices and normalized mass spectral peak intensities were obtained to identify molecular formulae associated with each index ($r > 0$, $p < 0.01$). The molecular composition of formulae positively correlated with each index is summarized in **Table 3** and van Krevelen distributions are shown in **Figures 4, 5**. Detailed van Krevelen distributions of molecular formulae, separated by N and S content, associated with individual optical indices can be found in Supplementary Figures 6–12.

$SUVA_{254}$ increases with the chromophoric nature and degree of aromaticity of DOM (Weishaar et al., 2003). HIX has been shown to increase with the microbial processing of DOM (Wickland et al., 2007) and has been used to describe the degree of DOM humification (Zsolnay et al., 1999; Ohno, 2002). Optical indices $SUVA_{254}$ and HIX were similarly effective in tracking a terrestrially-derived group of compounds enriched in aromatic formulae and depleted N, P, and S content (**Table 3**, **Figures 4A,B**). Black carbon compounds tracked most closely with $SUVA_{254}$, whereas less condensed aromatic structures, such as polyphenols were more broadly associated with both HIX and $SUVA_{254}$ (**Table 3**). Highly aromatic groups of DOM, as indicated by high a_{254} and $SUVA_{254}$, can be photoreactive and degrade quickly when exposed to sunlight (Stubbins et al., 2008, 2010; Spencer et al., 2009; Stubbins and Dittmar, 2015). In addition, dissolved black carbon, as measured by chemo-oxidation methods, has been shown to be preferentially photodegraded relative to bulk DOM (Stubbins et al., 2012; Wagner and Jaffé, 2015). In this respect, the group of molecular formulae which tracked with $SUVA_{254}$ and HIX in the Everglades (**Figures 4A,B**) overlap with those identified as photolabile in other studies (Kujawinski et al., 2004; Gonsior et al., 2009; Stubbins et al., 2010). As such, the covariation of formulae between these optical indices

TABLE 3 | Mean molecular mass, elemental groupings, and formula categorization of molecular formulae which correlated positively ($r > 0, p < 0.01$) with optical indices FI, freshness index, HIX, SUVA₂₅₄, S_{275–295}, S_{350–400}, and S_R.

Mean m/z (Da)	All Formulae		FI		Freshness		HIX		SUVA ₂₅₄		S _{275–295}		S _{350–400}		S _R	
	408	%	383	%	385	%	450	%	413	%	382	%	407	%	379	%
Total no. formulae	6716	100	1447	21	1869	27	2170	32	2162	33	1711	25	360	5	1635	24
CHO only	2960	100	125	4	362	12	1341	45	1429	49	320	11	35	1	372	13
CHON	2494	100	925	37	1016	40	683	28	388	16	912	36	312	12	734	29
CHOS	1531	100	530	34	641	42	195	13	359	25	599	39	9	1	634	41
CHOP	251	100	31	14	55	24	43	17	16	7	42	18	8	3	42	18
Contains N,S and/or P	3756	100	1322	44	1507	50	829	28	733	26	1391	46	325	10	1263	42
Black carbon	587	100	6	1	8	1	181	30	324	56	8	1	8	1	10	2
Polyphenols	1140	100	42	4	50	4	575	50	675	60	49	4	56	5	52	5
Highly unsaturated	3668	100	942	25	1129	30	1355	37	1135	32	1078	29	274	7	954	26
Unsaturated aliphatics	909	100	301	34	503	56	10	1	7	1	447	50	17	2	487	54
Saturated fatty acids	100	100	3	3	23	23	9	8	2	2	17	17	2	2	16	16
Sugars	37	100	3	9	4	12	13	36	8	22	2	6	3	8	1	3
Peptides	275	100	150	56	152	57	27	9	11	4	110	41	0	0	115	43

Mean m/z is the intensity-weighted average mass (Da). Listed integers reflect the number of molecular formulae and percentages in parentheses represent the percent of peak intensity contributed by each classification of molecular formulae.

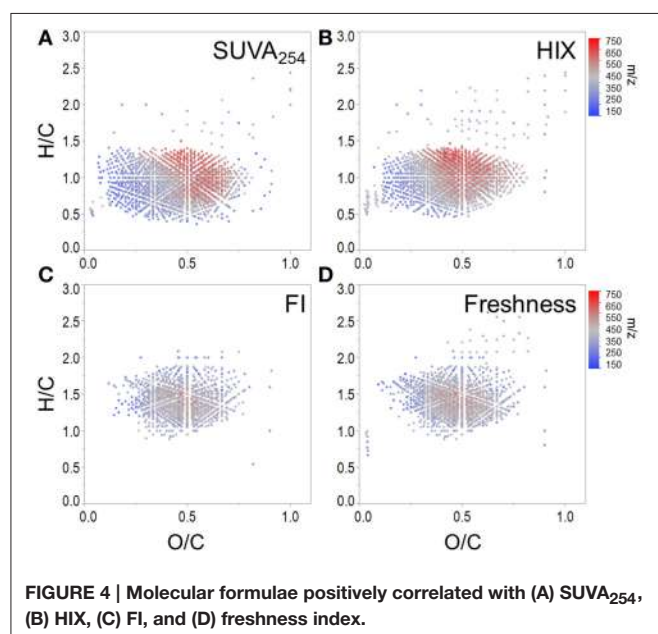
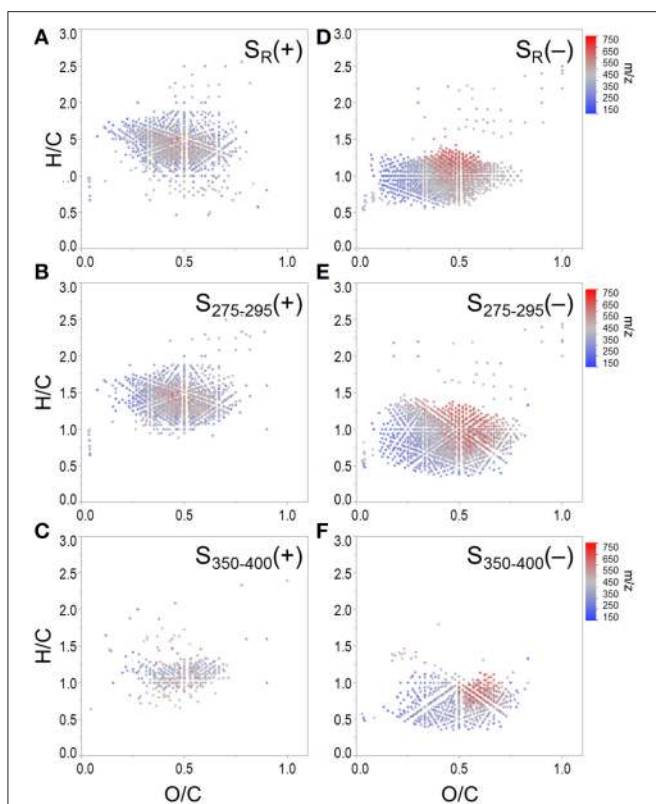


FIGURE 4 | Molecular formulae positively correlated with (A) SUVA₂₅₄, (B) HIX, (C) FI, and (D) freshness index.

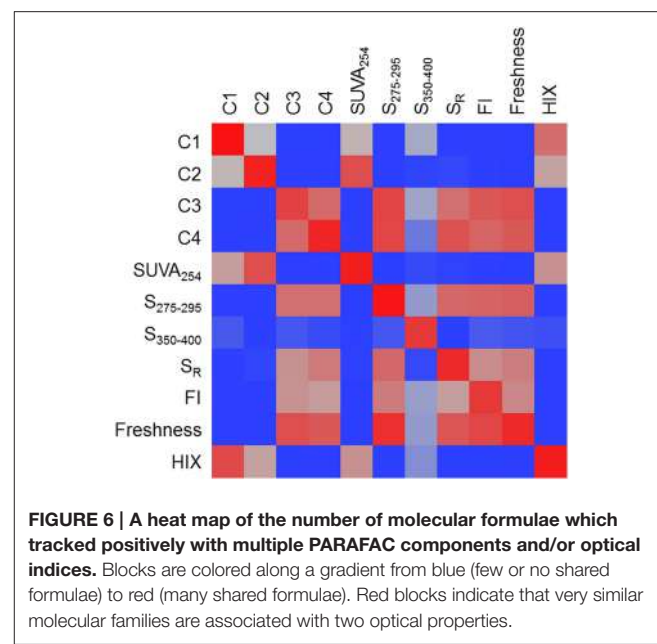
could be driven by both DOM source (e.g., soils or microbially degraded organic matter) and degradative processing (e.g., photodegradation). FI, initially put forth by McKnight et al. (2001), has been used to assess relative inputs from microbial vs. terrestrial precursor OM, and the freshness index estimates the relative proportion of recently-produced DOM (Parlanti et al., 2000; Wilson and Xenopoulos, 2009; Huguet et al., 2010). Both FI and the freshness index broadly represent autochthonous pools of DOM associated with microbial activity or exhibiting high degrees of biolability and were found to significantly correlate with one another for this particular dataset ($r = 0.79, p < 0.001$). As such, similar molecular families, enriched

in biolabile aliphatic formulae (Spencer et al., 2015), were commonly associated with these indices (Table 3, Figure 4B). Previous work suggests that, in the Everglades, high FI/low SUVA₂₅₄ values are indicative of tidal/marine or microbial DOM inputs and low FI/high SUVA₂₅₄ values are indicative of freshwater marsh or mangrove-derived DOM inputs (Chen et al., 2013), which is consistent with the molecular trends observed here.

Spectral slopes and slope ratios derived from absorbance data have been related to DOM molecular weight, and the degree of CDOM photo- and bio-alteration (Helms et al., 2008). Van Krevelen distributions of molecular formulae positively and negatively correlated with S_R, S_{275–295}, and S_{350–400} are shown in Figure 5. S_R has been used as a proxy for DOM molecular weight, with higher S_R being indicative of lower molecular weight (Helms et al., 2008). Therefore, it is of interest that the group of formulae positively associated with S_R had, on average, relatively low masses (379 Da, Table 3; Figure 5A). Conversely, the group of formulae found to negatively associate with S_R had, on average, relatively high molecular masses (430 Da, Figure 5D). A considerable number of aliphatic molecular formulae ($n = 1375$) were positively correlated with both S_{275–295} and S_R (Table 3; Figures 5A,B), however a relatively unique molecular family was positively correlated with S_{350–400} (Figure 5C). Shallower spectral slopes across both wavelength ranges were generally associated with aromatic-rich, terrigenous DOM (e.g., low H/C, high molecular weight, more aromatic), but the molecular associations of S_{275–295} and S_{350–400} indicate that they may track with different pools of photolabile, terrestrially-derived material (Figures 5E,F). Formulae associated with shallower S_{275–295} (Figure 5E) fall within the same van Krevelen regions as those which were positively correlated with SUVA₂₅₄, HIX and C2, indicating that S_{275–295} provides similar information to these other indices. However,



formulae which were negatively correlated with $S_{350-400}$ occupy a unique region of van Krevelen space (Figure 5F) and were more oxidized (weighted average O/C = 0.50) and more aromatic (weighted average AI-mod = 0.56) than formulae negatively correlated with $S_{275-295}$ (O/C = 0.45, AI-mod = 0.50; Figure 5E). Such highly oxidized, aromatic pools of DOM associated with $S_{350-400}$ could be indicative of quinone-type moieties derived from terrestrial sources. A shallow spectral slope in the 350 to 400 nm range is indicative of high absorbance at long wavelengths (i.e., approaching 400 nm), which in turn indicates low energy transitions (Planck, 1901). The lower energy, longer wavelength absorbance of CDOM has been posited to arise from intra-molecular charge transfer facilitated by the presence of electron donor and acceptor groups within DOM molecules (Del Vecchio and Blough, 2004). The aromatic moieties that act as donors (e.g., polyhydroxylated aromatics, phenols, or indoles) and acceptors (e.g., quinones) all have oxygen containing substituent groups and are proposed to derive from the partial oxygenation of common terrigenous precursors such as lignin, tannins, and melanins. Therefore, perhaps the oxygen-enriched DOM compounds associated with shallow $S_{350-400}$ (Figure 5F) are indicative of moieties which facilitate charge transfer.



Assessing Molecular Covariance Among PARAFAC Components and Optical Indices

A heat map was constructed to visually describe the number of molecular formulae shared among PARAFAC components and/or optical indices (Figure 6). Blocks are colored along a gradient from blue (few or no shared formulae) to red (many shared formulae; Figure 6). Line plots showing the mass, H/C and AI-mod distribution of molecular formulae associated with PARAFAC components and the other optical indices are shown in Figure 7. The distinct difference in molecular compositions associated with C1 and C2 vs. C3 and C4 is clearly apparent (Figures 7A–C). All non-PARAFAC optical indices were categorized into one of two groups: those which generally tracked with aromatic-rich, allochthonous/terrestrial DOM (Figures 7D–F) and those which generally tracked with autochthonous/microbial DOM (Figures 7G–I). The line distribution plots allow for a more detailed comparison among molecular families associated with optical properties. For example, a group of high molecular weight, terrestrially-derived formulae found to be associated with C1 also tracked similarly with HIX (Figure 7). C2 and SUVA₂₅₄ were both correlated with the most aromatic-enriched pools of molecular formulae (Figure 7). Similarities in molecular character between C3 and C4 have been described above, however FI, freshness index, $S_{295-275}(+)$ and $S_R(+)$ seem to be equally as effective in tracking the same pool of aliphatic-enriched compounds as the two PARAFAC components (Figures 6, 7). $S_{350-400}$ resolved a distinct group of molecular formulae (described above) which was not associated with any PARAFAC component (Figures 6, 7D–F). This suggests that, for the current dataset, absorbance data (e.g., SUVA₂₅₄, $S_{295-275}$, and S_R) can provide nearly equivalent information regarding the molecular composition of DOM as PARAFAC modeling. However, it is important to note that such an observation can only be made for this particular

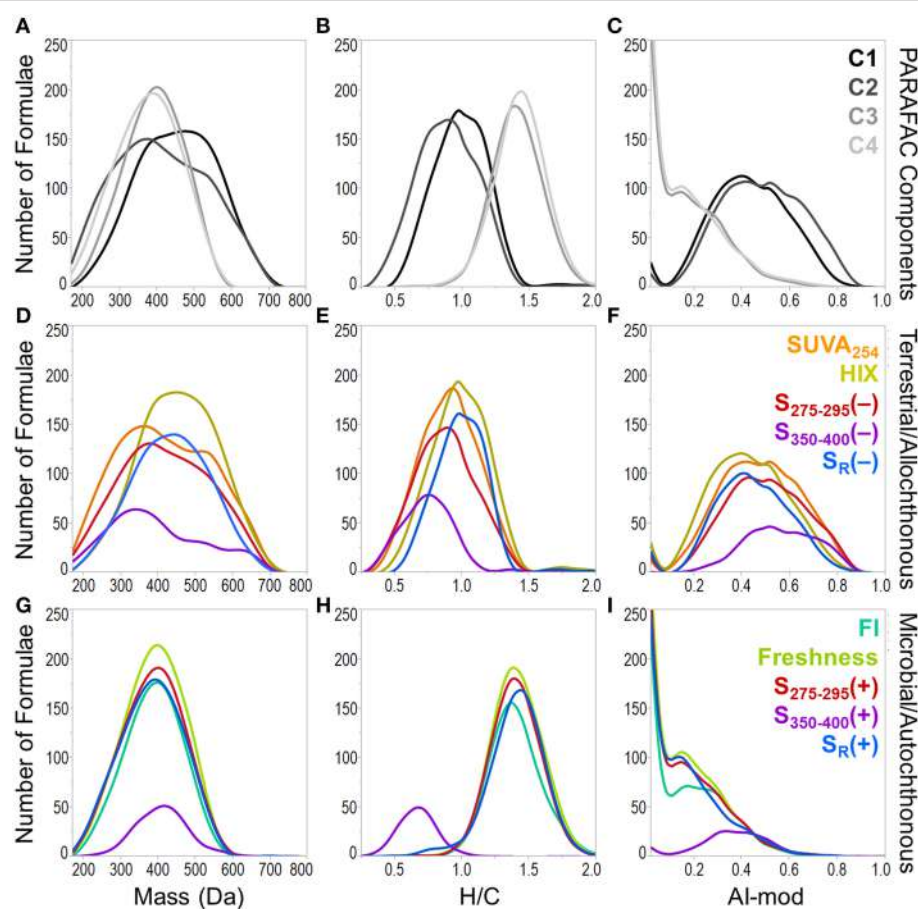


FIGURE 7 | Molecular mass (first column), H/C ratio (second column) and modified aromaticity index (Al-mod; third column) distributions of formulae associated with optical properties. Plots (A–C) show the distributions of formulae which positively correlated with PARAFAC components. Plots (D–F) show the distributions for optical properties which track with allochthonous or terrestrial-type DOM (formulae positively correlated with SUVA₂₅₄, HIX and formulae negatively correlated with S_{275–295}, S_{350–400}, and S_R). Plots (G–I) show the distributions for optical properties which track with autochthonous or microbial-type DOM (formulae positively correlated with FI, freshness index, S_{275–295}, S_{350–400}, and S_R).

suite of DOM samples using a four component PARAFAC model, which only offers coarse resolution of the EEM topography. The extraction of additional components may reveal more refined associations between molecular formulae and identified fluorophores for specific aquatic systems (e.g., see Stubbins et al., 2014; Kellerman et al., 2015).

CONCLUSIONS

Conventional biogeochemical interpretations of PARAFAC components and other optical indices were generally in agreement with the bulk DOM molecular composition of formulae with which they were associated for the Everglades system. These patterns were also fairly consistent with previous research assessing optical and molecular linkages in other terrestrial aquatic systems (Stubbins et al., 2014; Kellerman et al., 2015). Allochthonous and autochthonous molecular families, which tracked with SUVA₂₅₄/HIX and FI/freshness index, respectively (Figure 4), were in agreement with molecular

associations put forth by Kellerman et al. (2015). Regarding PARAFAC components, a significant overlap in formulae associated with both conventional A_M/M and B/T peaks (i.e., characterized by low molecular weight, aliphatic, high N content) was also observed in high latitude lakes (Kellerman et al., 2015) and boreal rivers (Stubbins et al., 2014), which suggests that “microbial humic-like” and “protein-like” fluorescence may serve as equally reliable trackers of autochthonous DOM across diverse aquatic environments. Although, “humic-like” components were generally associated with terrestrially-sourced, aromatic and high molecular weight formulae in lakes (Kellerman et al., 2015), rivers (Stubbins et al., 2014) and wetlands (this study), notable differences were evident with regards to N content. For example, formulae associated with conventional A_C/C peaks in lacustrine (Kellerman et al., 2015) and wetland (this study) environments had considerable contributions from CHON formulae, whereas molecular signatures associated with similar fluorescence peaks identified in boreal rivers were much more depleted in N (Stubbins et al., 2014). Such molecular discrepancies may be

driven by fundamental differences in source OM (e.g., primary productivity in lakes and wetlands vs. higher plants and soils in terrestrial river systems) or DOM processing. Stubbins et al. (2014) have suggested that the conventional Ac peak may serve as a proxy for black carbon due to the enrichment in condensed aromatic formulae which tracked with that particular component in boreal rivers. However, black carbon formulae tracked more closely with PARAFAC components exhibiting the Ac_+ peak in both the Everglades and lake environments (Kellerman et al., 2015). Aquatic systems can vary significantly with regards to DOM source, functionality and reactivity. As such, researchers interested in correlating molecular composition with chromophores and fluorophores are encouraged to establish such relationships for their own systems and assess how formulae associated with such optical parameters compare across different environments.

Optical measurements, which reflect both the light-absorbing and light-emitting molecular components of DOM, are indicative of both the inherent optical properties of DOM compounds and how they interact with one another under specific environmental conditions. As such, DOM absorbance and fluorescence measurements are better described as emergent properties of the physico-chemical interactions among all organic and inorganic constituents which exist in the dissolved phase of a natural water sample. In the current study, the molecular families which tracked with optical indices were generally in agreement with conventional biogeochemical interpretations. In most cases, the optical indices broadly represented either terrestrial/alochthonous or microbial/autochthonous groups of DOM formulae. Although absorbance and fluorescence measurements represent a relatively small portion of bulk DOM pools, they have been validated here as informative proxies

for the aquatic cycling of both optically-active and associated optically-inactive DOM in coastal wetlands and other aquatic environments.

AUTHOR CONTRIBUTIONS

KC collected optical data and built the PARAFAC model and TD collected FTICR-MS data. SW interpreted the data and conducted statistical analyses with comments and suggestions from AS, RJ, and KC. SW wrote the manuscript with critical reviews and input from AS, RJ, KC, and TD.

ACKNOWLEDGMENTS

This material is based upon work supported by the National Science Foundation (NSF) Florida Coastal Everglades Long-Term Ecological Research program under Grant No. DEB-1237517 (to RJ), the NSF MacroSystems Biology program under Grant No. 1340764 (to AS) and the George Barley Endowment (to RJ). We thank Dr. Yan Ding for preparing the PPL extracts, Mike Rugge for providing the site map and the FCE-LTER field crew for their assistance in sample collection. We also thank Katrin Klaproth for assistance with FTICR-MS analyses. This is contribution number 767 from the Southeast Environmental Research Center.

SUPPLEMENTARY MATERIAL

The Supplementary Material for this article can be found online at: <http://journal.frontiersin.org/article/10.3389/fchem.2015.00066>

REFERENCES

- Bates, A. L., Spiker, E. C., and Homes, C. W. (1998). Speciation and isotopic composition of sedimentary sulfur in the Everglades, Florida, USA. *Chem. Geol.* 146, 155–170. doi: 10.1016/S0009-2541(98)00008-4
- Boyer, J. N. (2006). Shifting N and P limitation along a north-south gradient of mangrove estuaries in South Florida. *Hydrobiologia* 269, 167–177. doi: 10.1007/s10750-006-0130-3
- Boyer, J. N., Fourqurean, J. W., and Jones, R. D. (1997). Spatial characterization of water quality in Florida Bay and Whitewater Bay by multivariate analyses: zones of similar influence. *Estuaries* 20, 743–758. doi: 10.2307/1352248
- Chen, M., and Jaffé R. (2014). Photo- and bio-reactivity patterns of dissolved organic matter from biomass and soil leachates and surface waters in a subtropical wetland. *Water Res.* 61, 181–190. doi: 10.1016/j.watres.2014.03.075
- Chen, M., Maie, N., Parish, R., and Jaffé, R. (2013). Spatial and temporal variability of dissolved organic matter quantity and composition in an oligotrophic subtropical coastal wetland. *Biogeochemistry* 115, 167–183. doi: 10.1007/s10533-013-9826-4
- Chen, M., Price, R. M., Yamashita, Y., and Jaffé, R. (2010). Comparative study of dissolved organic matter from groundwater and surface water in the Florida coastal Everglades using multi-dimensional spectrofluorometry combined with multivariate statistics. *Appl. Geochem.* 25, 872–880. doi: 10.1016/j.apgeochem.2010.03.005
- Coble, P. G. (1996). Characterization of marine and terrestrial DOM in seawater using excitation-emission matrix spectroscopy. *Mar. Chem.* 51, 325–346. doi: 10.1016/0304-4203(95)00062-3
- Coble, P. G., Del Castillo, C. E., and Avril, B. (1998). Distribution and optical properties of CDOM in the Arabian Sea during the 1995 SW monsoon. *Deep Sea Res. II* 45, 2195–2223. doi: 10.1016/S0967-0645(98)00068-X
- Coble, P. G., Green, S. A., Blough, N. V., and Gagosian, R. B. (1990). Characterization of dissolved organic matter in the Black Sea by fluorescence spectroscopy. *Nature* 348, 432–435. doi: 10.1038/348432a0
- Coble, P. G., Lead, J., Baker, A., Reynolds, D. M., and Spencer, R. G. M. (2014). *Aquatic Organic Matter Fluorescence*. New York, NY: Cambridge University Press.
- Cory, R. M., and McKnight, D. M. (2005). Fluorescence spectroscopy reveals ubiquitous presence of oxidized and reduced quinones in dissolved organic matter. *Environ. Sci. Technol.* 39, 8142–8149. doi: 10.1021/es0506962
- Del Vecchio, R., and Blough, N. V. (2004). On the origin of the optical properties of humic substances. *Environ. Sci. Technol.* 38, 3885–3891. doi: 10.1021/es049912h
- Ding, Y., Cawley, K. M., da Cunha, C. N., and Jaffé, R. (2014). Environmental dynamics of dissolved black carbon in wetlands. *Biogeochemistry* 119, 259–273. doi: 10.1007/s10533-014-9964-3
- Dittmar, T., Koch, B., Hertkorn, N., and Kattner, G. (2008). A simple and efficient method for the solid-phase extraction of dissolved organic matter (SPE-DOM) from seawater. *Limnol. Oceanogr. Methods* 6, 230–235. doi: 10.4319/lom.2008.6.230
- Dittmar, T., and Koch, B. P. (2006). Thermogenic organic matter dissolved in the abyssal ocean. *Mar. Chem.* 102, 208–217. doi: 10.1016/j.marchem.2006.04.003
- Dittmar, T., and Paeng, J. (2009). A heat-induced molecular signature in marine dissolved organic matter. *Nat. Geosci.* 2, 175–179. doi: 10.1038/ngeo440

- Dixon, J. L., Osburn, C. L., Paerl, H. W., and Peierls, B. L. (2014). Seasonal changes in estuarine dissolved organic matter due to variable flushing time and wind-driven mixing events. *Estuar. Coast. Shelf Sci.* 151, 210–220. doi: 10.1016/j.ecss.2014.10.013
- Fellman, J. B., Hood, E., and Spencer, R. G. M. (2010). Fluorescence spectroscopy opens new windows into dissolved organic matter dynamics in freshwater ecosystems: a review. *Limnol. Oceanogr.* 55, 2452–2462. doi: 10.4319/lo.2010.55.6.2452
- Gonsior, M., Peake, B. M., Cooper, W. T., Podgorski, D., DAndrilli, J., and Cooper, W. J. (2009). Photochemically induced changes in dissolved organic matter identified by ultrahigh resolution Fourier transform ion cyclotron resonance mass spectrometry. *Environ. Sci. Technol.* 43, 698–703. doi: 10.1021/es8022804
- Haitzer, M., Aiken, G. R., and Ryan, J. N. (2002). Binding of mercury(II) to dissolved organic matter—the role of the mercury-to-DOM concentration ratio. *Environ. Sci. Technol.* 36, 3564–3570. doi: 10.1021/es0256991
- Helms, J. R., Stubbins, A., Ritchie, J. D., Minor, E. C., Kieber, D. J., and Mopper, K. (2008). Absorption spectral slopes and slope ratios as indicators of molecular weight, source, and photobleaching of chromophoric dissolved organic matter. *Limnol. Oceanogr.* 53, 955–969. doi: 10.4319/lo.2008.53.3.0955
- Hernes, P. J., Bergamaschi, B. A., Eckard, R. S., and Spencer, R. G. M. (2009). Fluorescence-based proxies for lignin in freshwater dissolved organic matter. *J. Geophys. Res.* 114, G00F03. doi: 10.1029/2009JG000938
- Hertkorn, N., Harir, M., Cawley, K. M., Schmitt-Kopplin, P., and Jaffé, R. (2015). Molecular characterization of dissolved organic matter from subtropical wetlands: a comparative study through the analysis of optical properties, NMR and FTICR/MS. *Biogeoosci. Discuss.* 12, 13711–13765. doi: 10.5194/bgd-12-13711-2015
- Herzsprung, P., von Tümpeling, W., Hertkorn, N., Harir, M., Büttner, O., Bravidor, J., et al. (2012). Variations of DOM quality in inflows of a drinking water reservoir: linking of van Krevelen diagrams with EEM spectra by rank correlation. *Environ. Sci. Technol.* 46, 5511–5518. doi: 10.1021/es300345c
- Hu, C. M., Muller-Karger, F. E., and Zepp, R. G. (2002). Absorbance, absorption coefficient, and apparent quantum yield: a comment on common ambiguity in the use of these optical concepts. *Limnol. Oceanogr.* 47, 1261–1267. doi: 10.2307/3069048
- Huguet, A., Vacher, L., Saubusse, S., Etcheber, H., Abril, G., Relexans, et al. (2010). New insights into the size distribution of fluorescent dissolved organic matter in estuarine waters. *Org. Geochem.* 41, 595–610. doi: 10.1016/j.orggeochem.2010.02.006
- Ishii, S. K. L., and Boyer, T. H. (2012). Behavior of reoccurring PARAFAC components in fluorescent dissolved organic matter in natural and engineered systems: a critical review. *Environ. Sci. Technol.* 46, 2006–2017. doi: 10.1021/es2043504
- Jaffé, R., Cawley, K., and Yamashita, Y. (2014). “Applications of excitation emission matrix fluorescence with parallel factor analysis (EEM-PARAFAC) in assessing environmental dynamics of natural dissolved organic matter (DOM) in aquatic environments: a review,” in *Advances in the Physicochemical Characterization of Organic Matter: Impact on Natural and Engineered Systems*, ed F. Rosario-Ortiz (Washington, DC: Oxford University Press), 27–73. doi: 10.1021/bk-2014-1160.ch003
- Jaffé, R., Ding, Y., Niggemann, J., Vähäalto, A. V., Stubbins, A., Spencer, R. G. M., et al. (2013). Global charcoal mobilization from soils via dissolution and riverine transport to the oceans. *Science* 340, 345–347. doi: 10.1126/science.1231476
- Jaffé, R., McKnight, D., Maie, N., Cory, R., McDowell, W. H., and Campbell, J. L. (2008). Spatial and temporal variations in DOM composition in ecosystems: the importance of long-term monitoring of optical properties. *J. Geophys. Res.* 113, G04032. doi: 10.1029/2008JG000683
- Kellerman, A. M., Kothawala, D. N., Dittmar, T., and Tranvik, L. J. (2015). Persistence of dissolved organic matter in lakes related to its molecular characteristics. *Nat. Geosci. Lett.* 8, 454–457. doi: 10.1038/ngeo2440
- Kim, S., Kramer, R. W., and Hatcher, P. G. (2003). Graphical method for analysis of ultrahigh-resolution broadband mass spectra of natural organic matter, the van Krevelen diagram. *Anal. Chem.* 75, 5336–5344. doi: 10.1021/ac034415p
- Koch, B. P., and Dittmar, T. (2006). From mass to structure: an aromaticity index for high-resolution mass data of natural organic matter. *Rapid Commun. Mass Spectrom.* 20, 926–932. doi: 10.1002/rcm.2386
- Koch, B. P., Dittmar, T., Witt, M., and Kattner, G. (2007). Fundamentals of molecular formula assignment to ultrahigh resolution mass data of natural organic matter. *Anal. Chem.* 79, 1758–1763. doi: 10.1021/ac061949s
- Kujawinski, E. B. (2002). Electrospray ionization Fourier transform ion cyclotron resonance mass spectrometry (ESI FT-ICR MS): characterization of complex environmental mixtures. *Environ. Forensics* 3, 207–216. doi: 10.1080/713848382
- Kujawinski, E. B., Del Vecchio, R., Blough, N. V., Klein, G. C., and Marshall, A. G. (2004). Probing molecular-level transformations of dissolved organic matter: insights on photochemical degradation and protozoan modification of DOM from electrospray ionization Fourier transform ion cyclotron resonance mass spectrometry. *Mar. Chem.* 92, 23–37. doi: 10.1016/j.marchem.2004.06.038
- Larsen, L. G., Aiken, G. R., Harvey, J. W., Noe, G. B., and Crimaldi, J. P. (2010). Using fluorescence spectroscopy to trace seasonal DOM dynamics, disturbance effects, and hydrologic transport in the Florida Everglades. *J. Geophys. Res.* 115, G03001. doi: 10.1029/2009JG001140
- Lodge, T. E. (2005). *The Everglades Handbook: Understanding the Ecosystem*, 2nd Edn. Florida, FL: CRC Press.
- Maie, N., Parish, K. J., Watanabe, A., Knicker, H., Benner, R., Abe, T., et al. (2006). Chemical characteristics of dissolved organic nitrogen in an oligotrophic subtropical coastal wetland. *Geochim. Cosmochim. Acta* 70, 4491–4506. doi: 10.1016/j.gca.2006.06.1554
- Maie, N., Scully, N. M., Pisani, O., and Jaffé, R. (2007). Composition of a protein-like fluorophore of DOM in coastal wetland and estuarine systems. *Water Res.* 41, 563–570. doi: 10.1016/j.watres.2006.11.006
- Maie, N., Yamashita, Y., Cory, R. M., Boyer, J., and Jaffé, R. (2012). Characterizing the environmental dynamics of dissolved organic matter (DOM) in a subtropical estuary: source composition and physical disturbance control on spatial and seasonal variability. *Appl. Geochem.* 27, 917–929. doi: 10.1016/j.apgeochem.2011.12.021
- McKnight, D. M., Boyer, E. W., Westerhoff, P. K., Doran, P. T., Kulbe, T., and Andersen, D. T. (2001). Spectrofluorometric characterization of dissolved organic matter for indication of precursor organic material and aromaticity. *Limnol. Oceanogr.* 46, 38–48. doi: 10.4319/lo.2001.46.1.00038
- Morris, D. P., Zagarese, H., Williamson, C. E., Balseiro, E. G., Hargreaves, B. R., Modenutti, B., et al. (1995). The attenuation of solar UV radiation in lakes and the role of dissolved organic carbon. *Limnol. Oceanogr.* 40, 1381–1391. doi: 10.4319/lo.1995.40.8.1381
- Murphy, K. R., Stedmon, C. A., Graeber, D., and Bro, R. (2013). Fluorescence spectroscopy and multi-way techniques. *PARAFAC. Anal. Methods* 5, 6557–6566. doi: 10.1039/c3ay41160e
- Ohno, T. (2002). Fluorescence inner-filtering correction for determining the humification index of dissolved organic matter. *Environ. Sci. Technol.* 36, 742–746. doi: 10.1021/es0155276
- Opsahl, S., and Benner, R. (1997). Distribution and cycling of terrigenous dissolved organic matter in the ocean. *Nature* 386, 480–482. doi: 10.1038/386480a0
- Parlanti, E., Wörz, K., Geoffroy, L., and Lamotte, M. (2000). Dissolved organic matter fluorescence spectroscopy as a tool to estimate biological activity in a coastal zone submitted to anthropogenic inputs. *Org. Geochem.* 31, 1765–1781. doi: 10.1016/S0146-6380(00)00124-8
- Piccolo, A. (2001). The supramolecular structure of humic substances: a novel understanding of humus chemistry and implications in soil science. *Adv. Agron.* 75, 57–134. doi: 10.1016/S0065-2113(02)75003-7
- Planck, M. (1901). Ueber das Gesetz der Energieverteilung im Normalspectrum. *Ann. Phys.* 309, 553–563. doi: 10.1002/andp.19013090310
- Poulin, B. A., Ryan, J. N., and Aiken, G. R. (2014). Effects of iron on optical properties of dissolved organic matter. *Environ. Sci. Technol.* 48, 10098–10106. doi: 10.1021/es502670r
- Qualls, R. G., and Richardson, C. J. (2003). Factors controlling concentration, export, and decomposition of dissolved organic nutrients in the Everglades of Florida. *Biogeochemistry* 62, 197–229. doi: 10.1023/A:1021150503664
- Romera-Castillo, C., Chen, M., Yamashita, Y., and Jaffé, R. (2014). Fluorescence characteristics of size-fractionated dissolved organic matter: implications for a molecular assembly based structure? *Water Res.* 55, 40–51. doi: 10.1016/j.watres.2014.02.017
- Santín, C., Yamashita, Y., Otero, X. L., Álvarez, M. Á., and Jaffé, R. (2009). Characterizing humic substances from estuarine soils and sediments

- by excitation-emission matrix spectroscopy and parallel factor analysis. *Biogeochemistry* 96, 131–147. doi: 10.1007/s10533-009-9349-1
- Šantl-Temkiv, T., Finster, K., Dittmar, T., Hansen, B. M., Thyrhaug, R., Nielsen, N. W., et al. (2013). Hailstones: a window into the microbial and chemical inventory of a storm cloud. *PLoS ONE* 8:e53550. doi: 10.1371/journal.pone.0053550
- Schmidt, F., Elvert, M., Koch, B. P., Witt, M., and Hinrichs, K.-U. (2009). Molecular characterization of dissolved organic matter in pore water of continental shelf sediments. *Geochim. Cosmochim. Acta* 73, 3337–3358. doi: 10.1016/j.gca.2009.03.008
- Schwarzenbach, R. P., Gschwend, P. M., and Imboden, D. M. (2003). *Environmental Organic Chemistry, 2nd Edn.* New Jersey, NJ: John Wiley & Sons, Inc.
- Sharpless, C. M., and Blough, N. V. (2014). The importance of charge-transfer interactions in determining chromophoric dissolved organic matter (CDOM) optical and photochemical properties. *Environ. Sci. Process Impacts* 16, 654–671. doi: 10.1039/c3em00573a
- Simpson, A. J., Kingery, W. L., Hayes, M. H. B., Spraul, M., Humpfer, E., Dvortsak, P., et al. (2002). Molecular structures and associations of humic substances in the terrestrial environment. *Naturwissenschaften* 89, 84–88. doi: 10.1007/s00114-001-0293-8
- Singer, G. A., Fasching, C., Wilhelm, L., Niggemann, J., Steier, P., Dittmar, T., et al. (2012). Biogeochemically diverse organic matter in Alpine glaciers and its downstream fate. *Nat. Geosci.* 5, 710–714. doi: 10.1038/ngeo1581
- Singh, S., D'Sa, E. J., and Swenson, E. M. (2010). Chromophoric dissolved organic matter (CDOM) variability in Barataria Basin using excitation-emission matrix (EEM) fluorescence and parallel factor analysis (PARAFAC). *Sci. Total Environ.* 408, 3211–3222. doi: 10.1016/j.scitotenv.2010.03.044
- Sleighter, R. L., and Hatcher, P. G. (2007). The application of electrospray ionization coupled to ultrahigh resolution mass spectrometry for the molecular characterization of natural organic matter. *J. Mass Spectrom.* 42, 559–574. doi: 10.1002/jms.1221
- Spencer, R. G. M., Hernes, P. J., Ruf, R., Baker, A., Dyda, R. Y., Stubbins, A., et al. (2010). Temporal controls on dissolved organic matter and lignin biogeochemistry in a pristine tropical river. *J. Geophys. Res.* 115, G03013. doi: 10.1029/2009JG001180
- Spencer, R. G. M., Mann, P. J., Dittmar, T., Eglington, T. I., McIntyre, C., Holmes, R. M., et al. (2015). Detecting the signature of permafrost thaw in Arctic rivers. *Geophys. Res. Lett.* 42, 2830–2835. doi: 10.1002/2015GL063498
- Spencer, R. G. M., Stubbins, A., Hernes, P. J., Baker, A., Mopper, K., Aufdenkampe, A. K., et al. (2009). Photochemical degradation of dissolved organic matter and dissolved lignin phenols from the Congo River. *J. Geophys. Res.* 114, G03010. doi: 10.1029/2009JG000968
- Stedmon, C. A., and Bro, R. (2008). Characterizing dissolved organic matter fluorescence with parallel factor analysis: a tutorial. *Limnol. Oceanogr. Methods* 6, 572–579. doi: 10.4319/lom.2008.6.572
- Stedmon, C. A., Markager, S., and Bro, R. (2003). Tracing dissolved organic matter in aquatic environments using a new approach to fluorescence spectroscopy. *Mar. Chem.* 82, 239–254. doi: 10.1016/S0304-4203(03)00072-0
- Stubbins, A., and Dittmar, T. (2012). Low volume quantification of dissolved organic carbon and dissolved nitrogen. *Limnol. Oceanogr. Methods* 10, 347–352. doi: 10.4319/lom.2012.10.347
- Stubbins, A., and Dittmar, T. (2015). Illuminating the deep: molecular signatures of photochemical alteration of dissolved organic matter from the North Atlantic Deep Water. *Mar. Chem.* 177, 318–324. doi: 10.1016/j.marchem.2015.06.020
- Stubbins, A., Hubbard, V., Uher, G., Law, C. S., Upstill-Goddard, R. C., Aiken, G. R., et al. (2008). Relating carbon monoxide photoproduction to dissolved organic matter functionality. *Environ. Sci. Technol.* 42, 3271–3276. doi: 10.1021/es703014q
- Stubbins, A., Lapierre, J.-F., Berggren, M., Prairie, Y. T., Dittmar, T., and del Giorgio, P. A. (2014). What's in an EEM? Molecular signatures associated with dissolved organic fluorescence in boreal Canada. *Environ. Sci. Technol.* 48, 10598–10606. doi: 10.1021/es502086e
- Stubbins, A., Niggemann, J., and Dittmar, T. (2012). Photo-lability of deep ocean dissolved black carbon. *Biogeosciences* 9, 1661–1670. doi: 10.5194/bg-9-1661-2012
- Stubbins, A., Spencer, R. G. M., Chen, H. M., Hatcher, P. G., Mopper, K., Hernes, P. J., et al. (2010). Illuminated darkness: molecular signatures of Congo River dissolved organic matter and its photochemical alteration as revealed by ultrahigh precision mass spectrometry. *Limnol. Oceanogr.* 55, 1467–1477. doi: 10.4319/lo.2010.55.4.1467
- Timko, S. A., Maydanov, A., Pittelli, S. L., Conte, M. H., Cooper, W. J., Koch, B. P., et al. (2015). Depth-dependent photodegradation of marine dissolved organic matter. *Front. Mar. Sci.* 2:66. doi: 10.3389/fmars.2015.00066
- Timko, S. A., Romera-Castillo, C., Jaffé, R., and Cooper, W. J. (2014). Photo-reactivity of natural dissolved organic matter from fresh to marine waters in the Florida Everglades, USA. *Environ. Sci. Process. Impacts* 16, 866–878. doi: 10.1039/C3EM00591G
- Wagner, S., Dittmar, T., and Jaffé, R. (2015a). Molecular characterization of dissolved black nitrogen via electrospray ionization Fourier transform ion cyclotron mass spectrometry. *Org. Geochem.* 79, 21–30. doi: 10.1016/j.orggeochem.2014.12.002
- Wagner, S., and Jaffé, R. (2015). Effect of photodegradation on molecular size distribution and quality of dissolved black carbon. *Org. Geochem.* 86, 1–4. doi: 10.1016/j.orggeochem.2015.05.005
- Wagner, S., Riedel, T., Niggemann, J., Vähäntalo, A. V., Dittmar, T., and Jaffé, R. (2015b). Linking the molecular signature of heteroatomic dissolved organic matter to watershed characteristics in world rivers. *Environ. Sci. Technol.* doi: 10.1021/acs.est.5b00525. [Epub ahead of print].
- Weishaar, J. L., Aiken, G. R., Bergamaschi, B. A., Fram, M. S., Fujii, R., and Mopper, K. (2003). Evaluation of specific ultraviolet absorbance as an indicator of the chemical composition and reactivity of dissolved organic carbon. *Environ. Sci. Technol.* 37, 4702–4708. doi: 10.1021/es030360x
- Wickland, K. P., Neff, J. C., and Aiken, G. R. (2007). Dissolved organic carbon in Alaskan boreal forest: sources, chemical characteristics, and biodegradability. *Ecosystems* 10, 1323–1340. doi: 10.1007/s10021-007-9101-4
- Wilson, H. F., and Xenopoulos, M. A. (2009). Effects of agricultural land use on the composition of fluvial dissolved organic matter. *Nat. Geosci.* 2, 37–41. doi: 10.1038/ngeo391
- Yamashita, Y., Scinto, L. J., Maie, N., and Jaffé, R. (2010). Dissolved organic matter characteristics across a subtropical wetland's landscape: application of optical properties in the assessment of environmental dynamics. *Ecosystems* 13, 1006–1019. doi: 10.1007/s10021-010-9370-1
- Yamashita, Y., and Tanoue, E. (2003). Chemical characterization of proteinlike fluorophores in DOM in relation to aromatic amino acids. *Mar. Chem.* 82, 255–271. doi: 10.1016/S0304-4203(03)00073-2
- Zsolnay, A., Baigar, E., Jimenez, M., Steinweg, B., and Saccomandi, F. (1999). Differentiating with fluorescence spectroscopy the sources of dissolved organic matter in soils subjected to drying. *Chemosphere* 38, 45–50. doi: 10.1016/S0045-6535(98)00166-0

Conflict of Interest Statement: The authors declare that the research was conducted in the absence of any commercial or financial relationships that could be construed as a potential conflict of interest.

Copyright © 2015 Wagner, Jaffé, Cawley, Dittmar and Stubbins. This is an open-access article distributed under the terms of the Creative Commons Attribution License (CC BY). The use, distribution or reproduction in other forums is permitted, provided the original author(s) or licensor are credited and that the original publication in this journal is cited, in accordance with accepted academic practice. No use, distribution or reproduction is permitted which does not comply with these terms.



Fluorescence Quantum Yields of Natural Organic Matter and Organic Compounds: Implications for the Fluorescence-based Interpretation of Organic Matter Composition

Urban J. Wünsch^{1*}, Kathleen R. Murphy² and Colin A. Stedmon¹

¹ Section for Marine Ecology and Oceanography, National Institute of Aquatic Resources, Technical University of Denmark, Charlottenlund, Denmark, ² Water Environment Technology, Chalmers University of Technology, Gothenburg, Sweden

OPEN ACCESS

Edited by:

Christopher Osburn,
North Carolina State University, USA

Reviewed by:

Mukesh Gupta,
Environment Canada, Canada
Kenneth Mopper,
Old Dominion University, USA

*Correspondence:

Urban J. Wünsch
urbw@aqua.dtu.dk

Specialty section:

This article was submitted to
Marine Biogeochemistry,
a section of the journal
Frontiers in Marine Science

Received: 21 August 2015

Accepted: 02 November 2015

Published: 13 November 2015

Citation:

Wünsch UJ, Murphy KR and Stedmon CA (2015) Fluorescence Quantum Yields of Natural Organic Matter and Organic Compounds: Implications for the Fluorescence-based Interpretation of Organic Matter Composition. *Front. Mar. Sci.* 2:98.
doi: 10.3389/fmars.2015.00098

Absorbance and fluorescence spectroscopy are economical tools for tracing the supply, turnover and fate of dissolved organic matter (DOM). The colored and fluorescent fractions of DOM (CDOM and FDOM, respectively) are linked by the apparent fluorescence quantum yield (AQY) of DOM, which reflects the likelihood that chromophores emit fluorescence after absorbing light. Compared to the number of studies investigating CDOM and FDOM, few studies have systematically investigated AQY spectra for DOM, and linked them to fluorescence quantum yields (Φ) of organic compounds. To offer a standardized approach, a MATLAB toolbox for the determination of apparent quantum yields of DOM (*aquaDOM*), featuring two calculation approaches, was developed and used to derive AQYs for samples from the Norwegian Sea. Φ of the organic compounds varied between 0.00079 and 0.35, whereas the average AQY for DOM samples at 350 nm was 0.011 ± 0.003 . The AQY at 350 nm increased with depth, while the AQY at 250 nm showed no trend. Laboratory tests indicated that Φ of compound mixtures are additive and represent an intermediate of the constituents. Additionally, the presence of non-fluorescent chromophores greatly suppressed calculated AQYs. Similar trends in the DOM AQY at 350 nm were observed in natural samples. We therefore hypothesize that fluorescence AQYs can indicate changes in the relative abundances of CDOM and FDOM. Additionally, the optical properties of 15 potential DOM constituents were determined and compared to more than 200 modeled spectra (PARAFAC components) in the OpenFluor database. Apparent matches, based on spectral similarity, were subsequently evaluated using molar fluorescence and absorbance. Five organic compounds were potential matches with PARAFAC components from 16 studies; however, the ability to confirm matches was limited due to multiple compounds exhibiting very similar spectra. This reiterates the fact that spectral similarity alone is insufficient evidence of the presence of particular compounds, and additional evidence is required.

Keywords: *aquaDOM*, *OpenFluor*, *PARAFAC*, *spectral matching*, *EEM*, *FDOM*, *CDOM*

INTRODUCTION

As the largest pool of reduced carbon, dissolved organic matter (DOM) plays an important role in the biogeochemical processes of aquatic environments (Prairie, 2008). Furthermore, it links soil and aquatic ecosystems (Jansen et al., 2014), is a key factor for the attenuation of light in the water column (Morris et al., 1995; Williamson et al., 1999), and affects the solubility and transport of metals (Ravichandran, 2004).

DOM can be analyzed via ultraviolet and visible spectroscopy. A fraction of DOM absorbs light, and its optical properties can be characterized by absorbance and fluorescence spectroscopy. The measurement of the colored fraction of DOM (CDOM) can be considerably faster than the detailed compound-specific chemical analysis of DOM. Moreover, CDOM dynamics can be monitored across large scales using satellite remote sensing (Siegel et al., 2005). However, the link between chemical and optical properties of DOM remains poorly understood despite recent efforts to link molecular signatures with optical properties (Stubbins et al., 2014; Kellerman et al., 2015). Moreover, the relative contribution of fluorescent DOM (FDOM) to CDOM, as well as CDOM to DOM, is largely unknown (Stedmon and Nelson, 2015).

For pure fluorophores, the fluorescence quantum yield (Φ) represents the probability of a fluorophore to emit light while returning to its ground state after being excited by light of higher energy (Lakowicz, 2006). Given this definition, the absorbance and fluorescence properties of DOM are linked by Φ of FDOM (Green and Blough, 1994). However, since CDOM is a complex mixture of organic molecules, not all of which fluoresce, its fluorescence efficiency represents a combined signal. The quantum yield of CDOM is therefore referred to as the apparent fluorescence quantum yield (AQY) to emphasize the contrast to Φ , which can only be determined for pure fluorophores or mixtures of fluorophores.

Compared to the number of studies focusing on optical properties of DOM, its AQY has not been studied extensively in the past. However, studies have shown that the apparent quantum yield of DOM changes as a function of the excitation wavelength, with values generally ranging from 0.1 to 2.8%, while distinct emission bands in the ultraviolet can cause significantly higher DOM AQYs of 5–7% (Green and Blough, 1994; Del Vecchio and Blough, 2004; Andrew et al., 2013; Cawley et al., 2015). All previous studies show that the AQY is highest around 370 nm, while subsequently decreasing steadily with wavelength (Sharpless and Blough, 2014).

Several studies have revealed links between DOM AQYs and biogeochemical parameters. Ferrari et al. (1996) showed that increased algal abundance can increase DOM AQYs, presumably due to the production of highly fluorescent polyphenols. AQYs are also generally higher in deep than in shallow waters (Ferrari, 2000; Cawley et al., 2015) and increase with salinity in estuaries (Zepp et al., 2004). Moreover, an early study by Stewart and Wetzel (1980) highlighted the observation that the ratio between fluorescence and absorbance differs between molecular weight fractions of DOM by a factor of four, with the low molecular weight fraction exhibiting greater fluorescence per unit of absorbance. A recent study by Catalá et al. (2015) reported

increasing AQYs for aging water masses. Together, these studies highlight the potential for DOM apparent quantum yields to indicate changing DOM characteristics as a result of microbial turnover of DOM (i.e., “humification”).

Recent efforts to link optical and chemical properties of DOM include the comparison of fluorescence excitation-emission matrices (EEMs) with ultrahigh resolution mass spectrometry using correlation analysis (Stubbins et al., 2014). However, due to analytical limitations during sample preparation and analysis (Dittmar et al., 2008; Hertkorn et al., 2008), the comparison of data originating from mass-spectrometry and fluorescence spectroscopy remains a challenge. To assess the plausibility of chemical formulae and/or structure assignments to FDOM components in this context, knowledge of fluorescence quantum yields is essential, since it reflects the likelihood of molecules to fluoresce. Nonetheless, with the exception of functional fluorophores used as probes, sensors and reporters (Würth et al., 2013), the quantum yield of many organic compounds is unknown or not available in an accessible database.

The purpose of this study is to provide an indication of the chemical structures contributing to DOM fluorescence by comparing the fluorescence characteristics of organic compounds with those of natural samples. Moreover, the aim was to introduce an open-source MATLAB toolbox to allow the comparable determination of apparent quantum yields of DOM and Φ of organic compounds. The objective was to first compare approaches for determining quantum yields, and afterwards assess the informative value of spectral data for AQYs of natural samples and Φ of pure compounds.

MATERIALS AND METHODS

Samples

Natural DOM samples were collected from 25 to 28 May 2015 along a transect from Tromsø (Norway) to Hirtshals (Denmark) on the research vessel Dana. The transect consisted of 11 stations along the Norwegian coast (Figure 1A). Samples were gravity-filtered directly from Niskin bottles using a 0.2 μm flow-through filter (PALL Life Sciences). The filter was rinsed with 400 mL seawater between usages. Samples were stored at 4°C in 40 mL combusted amber glass vials (VWR International). Fluorescence and absorbance spectra were collected within 30 days of sampling. Subsamples for the determination of dissolved organic carbon (DOC) were stored at -20°C in acid-cleaned HDPE bottles (10% w/v hydrochloric acid, VWR International). A suite of 15 organic compounds was also purchased and characterized (Supplementary Table 1). All compounds were dissolved in 1 mmol L⁻¹ phosphate buffer (Fluka Analytical) adjusted to pH 7.5. The compounds were selected as they have previously been suggested to be structures in DOM or to represent similar fluorophores (Yamashita and Tanoue, 2003; Aiken, 2014; Stedmon and Nelson, 2015).

Measurements

Absorbance measurements were carried out using a Shimadzu UV2401PC spectrophotometer in combination with a 10 cm

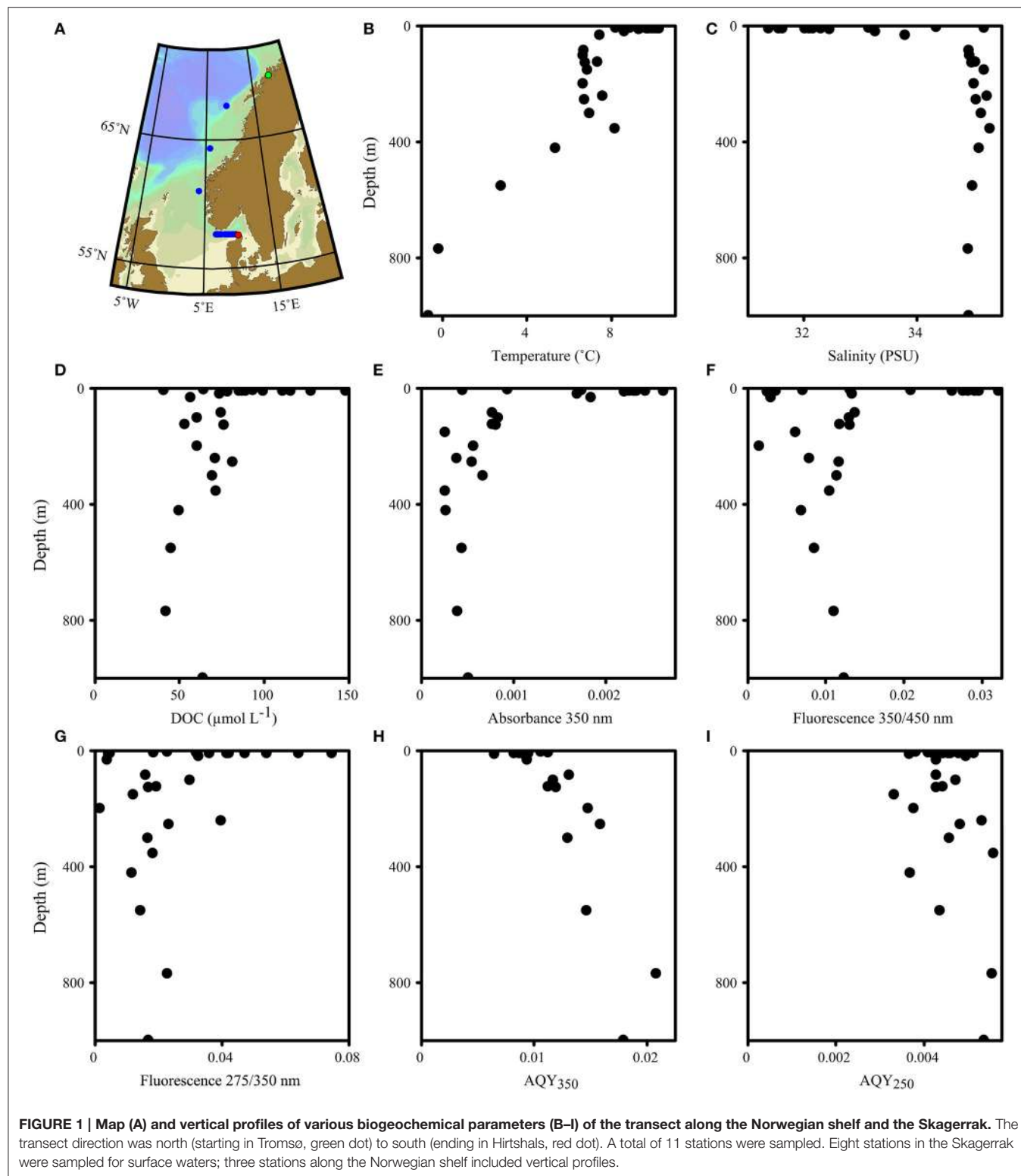


FIGURE 1 | Map (A) and vertical profiles of various biogeochemical parameters (B–I) of the transect along the Norwegian shelf and the Skagerrak. The transect direction was north (starting in Tromsø, green dot) to south (ending in Hirtshals, red dot). A total of 11 stations were sampled. Eight stations in the Skagerrak were sampled for surface waters; three stations along the Norwegian shelf included vertical profiles.

quartz cell. The absorbance signal of ultrapure water, 1 mmol L^{-1} phosphate buffer (pH 7.5), and 0.1 N H_2SO_4 was subtracted from samples, organic compounds and quinine sulfate, respectively. Small residual baseline offsets were corrected by subtracting the

average absorbance signal between 700 and 800 nm. The noise level of absorbance measurements was estimated from the range of absorbance values in the 2nd derivative spectrum between 550 and 600 nm.

Fluorescence measurements were obtained using a HORIBA Jobin Yvon AquaLog fluorometer. Calibrations for excitation monochromators and the emission detector, as well as optical immaculacy of cuvettes, were validated daily using a fixed routine (Supplementary Material). Fluorescence emission wavelengths were 240–600 nm (increment 2 nm) and excitation wavelengths 240–600 nm (increment 5 nm). The emission integration time was adjusted to account for varying FDOM concentrations between samples. The obtained fluorescence data was processed in MATLAB using the *drEEM* toolbox (version 0.2.0, Murphy et al., 2013). For quantum yield standards, the respective solvents (ultrapure water for salicylic acid, 0.1 N H₂SO₄ for quinine sulfate) were used as blanks, while ultrapure water was used as blanks for CDOM samples. Since a quantum yield standard calibration was carried out daily, no Raman normalization was performed. Instead, the EEMs were normalized to a 1 s integration time, and raw fluorescence counts were used as basis for quantum yield calculations. For organic compounds, a one-component parallel factor analysis (PARAFAC, e.g., Murphy et al., 2013) model was fitted to reduce noise and allow extrapolation of signals to scatter-affected regions of the EEM (Murphy et al., 2014b).

DOC was measured using high-temperature catalytic oxidation, whereby organic carbon was oxidized to carbon dioxide, then measured with a non-dispersive infrared detector (TOC/V_{CPH}, Shimadzu). A 15 mL sample was poured into a combusted glass vial and acidified to pH 2 using hydrochloric acid. Samples were subsequently sparged with CO₂-free air to remove inorganic carbon. Acidified samples were injected onto the catalyst (heated to 680°C) and DOC concentrations were averaged over the best three of up to seven repeated injections. The instrument was calibrated using acetanilide (Cauwet, 1999). For quality control of measured DOC concentrations, a deep-sea reference (Hansell laboratory, Miami) was used.

(Apparent) Quantum Yield Calculation

A MATLAB® toolbox for the calculation of apparent quantum yields of DOM (*aquaDOM*) was developed and utilized in this study (available in the Supplementary Material). Since the calculation of Φ of pure compounds and DOM AQYs do not differ, this section explains the calculations exemplarily for DOM AQYs. The determination of the DOM AQYs of a sample, *X*, was based the relative approach using a quantum yield standard, *St*, as follows (Parker and Rees, 1960):

$$AQY_X(\lambda) = \Phi_{St} * \frac{\int_{240nm}^{600nm} F_X(\lambda) * A_{St}(\lambda_{max})}{A_X(\lambda) * \int_{240nm}^{600nm} F_{St}(\lambda_{max})} * \frac{\eta^2_X}{\eta^2_{St}}, \quad (1)$$

where AQY is the apparent fluorescence quantum yield, $\int F(\lambda)/A(\lambda)$ represents the ratio of the integral of the fluorescence emission *F* and the absorbance *A* at excitation wavelength λ , and η is the refractive index. Since the refractive index of water across the salinity range of seawater varies by only 0.5% at 404 nm (Austin and Halikas, 1976), the last term of Equation (1) can be omitted and Equation (1) simplifies to:

$$AQY_X(\lambda) = \Phi_{St} * \frac{\int_{240nm}^{600nm} F_X(\lambda) * A_{St}(\lambda_{max})}{A_X(\lambda) * \int_{240nm}^{600nm} F_{St}(\lambda_{max})}. \quad (2)$$

To determine AQYs, two variations of the relative approach were tested. In the first approach, a single absorbance and fluorescence measurement was carried out to determine $\int F_X(\lambda)/A_X(\lambda)$ experimentally. This approach forces the intercept of the single point regression through zero (hereafter called “zero-intercept approach”). The precision of determined AQYs was estimated (only for selected samples) for every excitation wavelength using the standard error propagation approach as follows:

$$\frac{\sigma_{AQY}}{AQY_X} = \Phi_{St} \sqrt{\frac{\sigma \int F_X^2}{\bar{F}_X} + \frac{\sigma A_X^2}{\bar{A}_X} + \frac{\sigma \int F_{St}^2}{\bar{F}_{St}} + \frac{\sigma A_{St}^2}{\bar{A}_{St}}}, \quad (3)$$

where σ_{AQY} is the precision estimate, $\sigma \int F$ and σA represent the range of absorbance and fluorescence observations in five repeated measurements, and \bar{F} and \bar{A} represent the average fluorescence integral and average absorbance level of five repeated measurements. In the second approach, a five-point dilution series of standards and samples was measured to determine $\int F_X(\lambda)/A_X(\lambda)$ by robust linear regression, allowing non-zero intercepts to account for instrument-specific differences in fluorescence and absorbance detection limits (hereafter called “variable-intercept approach”). The precision of AQYs in this approach were determined using the 95% confidence interval of the slope estimate. AQYs were only reported if the signal-to-noise ratio (S/N) for absorbance measurements exceeded 25 for both approaches (if not otherwise stated), since this ratio-filter excluded visibly erroneous AQYs. Additionally, in the variable-intercept approach, linear fits with $R^2 < 0.95$ were discarded (if not otherwise stated).

To confirm the accuracy of the obtained AQYs, cross-calibrations with reference materials were performed daily. Five-point dilution series (in the case of the variable-intercept approach), or five replicate measurements (in the case of the zero-intercept approach) of quinine sulfate (NIST standard reference material 936a dissolved in 0.05 M H₂SO₄, $\Phi = 0.51$ at 350 nm, Melhuish, 1961; Velapoldi and Tønnesen, 2004), and salicylic acid (dissolved in ultrapure water, $\Phi = 0.36$ at 296 nm, Pozdnyakov et al., 2009) were measured. Cross-calibrations were performed by treating one reference material as a sample while the second reference material was used to estimate Φ (and vice versa). Further sample measurements were conducted only if the cross calibration resulted in deviations of <10% from the literature values. Since quinine sulfate is a widely recognized standard in luminescence spectroscopy (Brouwer, 2011), its properties were always used as the basis for the AQY determination of CDOM samples, while salicylic acid was used to confirm its validity.

To calculate the Stokes shift of organic compounds, wavelength dependent intensities I_λ in the EEMs were converted to wavenumber intensities ($I_{\bar{v}}$) as follows (Lakowicz, 2006):

$$I_{\bar{v}} = \lambda^2 I_\lambda. \quad (4)$$

$I_{\overline{\nu}}$ was used to calculate the Stokes shift as the difference between the position of the fluorescence emission peak and the highest excitation peak. This result was converted from cm^{-1} to eV to express the Stokes shift as an energy difference.

Spectral Matching

Purchased organic compounds were compared to more than 200 modeled spectra available in the OpenFluor database¹ (Murphy et al., 2014c). The database assesses spectral similarity using the Tucker congruence coefficient (Tucker, 1951). Spectral matches were restricted to Tucker congruence coefficients of >0.9 in emission and excitation, while the combined Tucker congruence coefficient was restricted to >0.81 .

RESULTS

Optical Properties of Samples and Organic Compounds

The waters sampled along the Norwegian shelf reflected three groups: comparatively warm and less-saline surface water with high DOC ($>80 \mu\text{M}$) influenced by continental run off; intermediate waters with depths of 100–400 m, essentially representing Atlantic water; and Norwegian Sea bottom water with sub-zero temperatures (Figure 1). The fluorescence characteristics resembled those expected for shelf waters (Blough and Del Vecchio, 2002; Stedmon and Nelson, 2015) with a broad fluorescence peak at visible wavelengths, and a pronounced UVA peak (Figure 2).

¹<http://openfluor.org>

The fluorescence properties of the purchased organic compounds are shown in Figure 3, and described in Table 1. The molar absorptivity ranged from 153 (phenylalanine) to $15,791 \text{ L mol}^{-1} \text{ cm}^{-1}$ (caffeine). Peaks in absorbance spectra extended from 256 (phenylalanine) to 295 nm (salicylic acid), while absorbance was measurable up to a maximum of 550 nm (ferulic acid). The molar fluorescence varied between 0.03 (benzoic acid) and 38.50 Raman units $\text{L} \mu\text{mol}^{-1}$ (indole). Stokes shifts extended from 0.32 (benzoic acid) to 1.38 eV (ferulic acid). Organic compounds seemingly fell into two groups; the first group with Stokes shifts ranging from 0.32 to 0.57 eV and emission maxima from 281 to 339 nm, and the second group with Stokes shifts of 0.97–1.38 eV with emission maxima from 333 to 413 nm. In some cases (e.g., coumarin or coniferyl alcohol), absorbance spectra did not match the fluorescence excitation loadings (Figure 3), although these should theoretically be identical for pure compounds. However, for other compounds (e.g., phenylalanine, tyrosine, and tryptophan), absorbance and fluorescence excitation spectra were a close match. Compounds with identical fluorophore groups had similar optical properties. For example, the two phenols p-Cresol and Tyrosine were characterized by relatively similar molar absorptivity maxima (1928 and 1206, respectively), similar quantum yields (0.11 and 0.13, respectively) and similar stokes shifts (0.45 and 0.49 eV, respectively). However, other structurally related compounds such as tryptophan and indole showed noticeably differing Φ (0.15 and 0.28, respectively), although other optical properties were highly similar (Table 1). The excitation and emission spectra of all purchased organic compounds have been uploaded to the OpenFluor database (Murphy et al., 2014c).

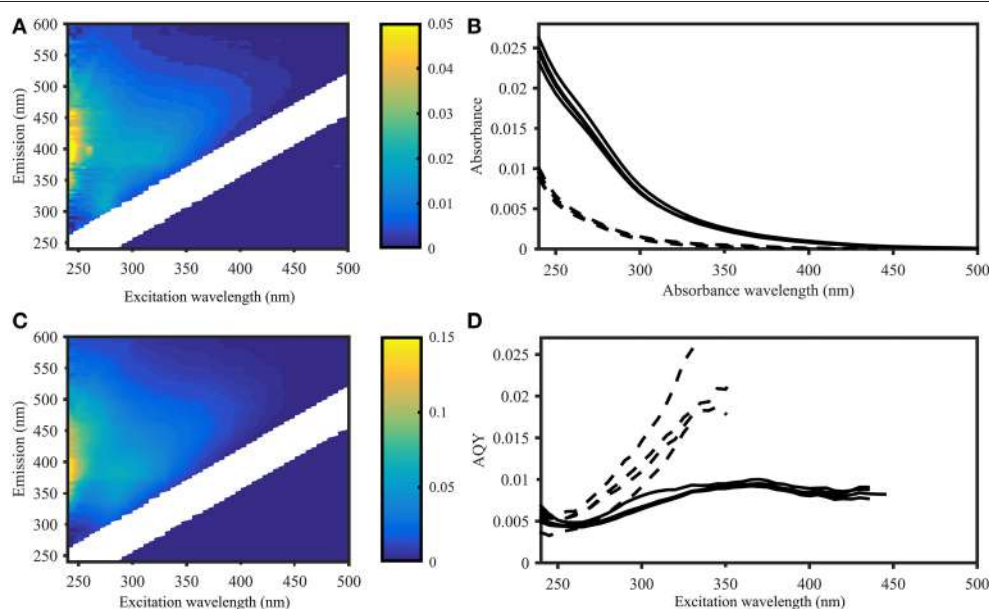


FIGURE 2 | Apparent quantum yield and fluorescence in samples from the Norwegian Sea (Station 2, deep sea) and Skagerrak (Station 14, surface water). Left panel: EEMs of deep (A) and surface (C) samples in Raman units (different scales as indicated by colorbar). Right panel: CDOM absorbance (B) and CDOM apparent fluorescence quantum yields (D) of four deep sea samples (dashed lines) and four surface water samples (solid lines), showing deep sea AQYs consistently higher than in surface waters. AQYs at wavelengths where signal to noise ratios were below 25 are missing values.

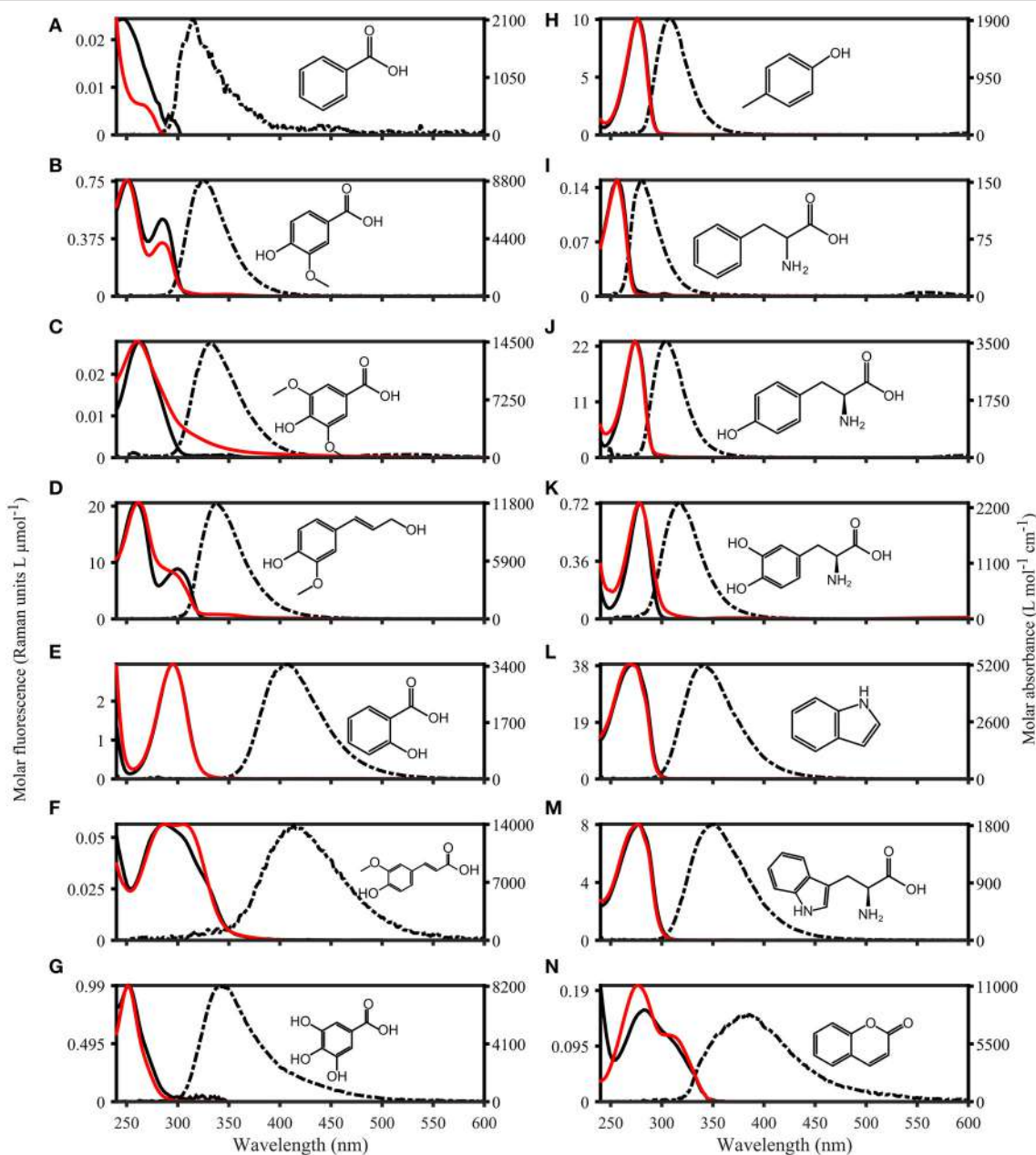


FIGURE 3 | Absorbance and Fluorescence spectra of organic compounds dissolved in water with 1 mmol L^{-1} PO_4 buffer (pH 7.5). The molar absorptivity is shown as a solid red line, excitation loadings are solid black lines, and emission loadings are dashed black lines. **(A–G)** Benzoic acid, vanillic acid, syringic acid, coniferyl alcohol, salicylic acid, ferulic acid, gallic acid. **(H–N)** p-Cresol, phenylalanine, tyrosine, dihydroxyphenylalanine, indole, tryptophan, coumarin.

Organic compounds with identical fluorophores were characterized by highly similar fluorescence emission peaks, while absorbance spectra differed in peak positions and shapes (e.g., benzoic acid derivatives, Figures 3A–C). Furthermore, the two phenols (p-cresol and tyrosine, Figures 3H,J), as well as the two indols (Figures 3L,M), had highly similar peak positions and shapes for both absorbance and fluorescence emission peaks. Organic compounds with the highest degree of conjugation (coumarin, ferulic acid, salicylic acid, Figures 3E,F,N) exhibited

the broadest emission peaks, compared to narrow emission peaks of organic compounds with a lower degree of conjugation (e.g., p-cresol, and phenylalanine, Figures 3H,I).

Method Comparison: Apparent Quantum Yield Calculations

To compare the two AQY calculation approaches (variable-intercept vs. zero-intercept approach), results were compared for three Norwegian Sea samples and a Suwannee River XAD-8

TABLE 1 | Optical properties of organic compounds dissolved in 1 mmol L⁻¹ phosphate buffer (pH 7.5).

Name	Molecular formula	Molecular weight (g mol ⁻¹)	λ_{max} (nm)	Δ_{em} (nm)	Molar fluorescence (R.U. μmol^{-1} L)	Molar absorbance (L mol^{-1} cm ⁻¹)	Stokes shift (eV)	Φ (\pm %)
Caffeine	C ₈ H ₁₀ N ₄ O ₂	194.19	258	—	—	15,791	—	
Coniferyl alcohol	C ₁₀ H ₁₂ O ₃	180.2	262			11,854		
			295	338	20.59	7210	0.49	0.10 (9)
Coumarin	C ₉ H ₆ O ₂	146.14	276			9228		
			306	385	0.20	5357	1.19	<0.001 (2)
p-Cresol	C ₇ H ₈ O	108.14	276	307	10.06	1930	0.49	0.11 (27)
Ferulic acid	C ₁₀ H ₁₀ O ₄	194.18	287	413	0.06	14,147	1.38	0.002 (30)
Gallic acid	C ₇ H ₆ O ₅	170.12	258	341	0.99	8283	1.37	0.006 (4)
Indole	C ₈ H ₇ N	117.15	269	340	38.50	5235	0.93	0.28 (10)
Benzoic acid	C ₇ H ₆ O ₂	122.12	223			7772	0.32	
			266	315	0.02	553.9		<0.001
L-Phenylalanine	C ₉ H ₁₁ NO ₂	165.19	256	281	0.15	153	0.43	0.018 (6)
L-dihydroxy-phenylalanine	C ₉ H ₁₁ NO ₄	197.19	278	318	0.724	2296	0.57	0.075 (25)
Salicylic acid	C ₇ H ₆ O ₃	138.12	295	407	2.95	3464	1.16	0.35 (3)
Syringic acid	C ₉ H ₁₀ O ₅	198.17	260	333	0.03	14577	1.02	0.009 (34)
DL-Tryptophan	C ₁₁ H ₁₂ N ₂ O ₂	204.23	277	350	8.03	5358	0.94	0.15 (7)
L-Tyrosine	C ₉ H ₁₁ NO ₃	181.19	274	304	22.93	1207	0.45	0.13 (31)
Vanillic acid	C ₈ H ₈ O ₄	168.14	250			8816	0.57	0.03 (17)
			285	325	0.75	4043		

The molar absorbance is reported for the absorbance maximum and the secondary absorbance peak if present, while the molar fluorescence is only provided for the absorbance maximum. The quantum yield precision was estimated using the 95% confidence interval [see Section (Apparent) Quantum Yield Calculation] and is stated as the percentage of the estimated quantum yield.

fulvic acid extract (Figure 4). For both approaches, the AQY accuracy typically varied between 0.1 and 6% (all data not shown). Calculated AQYs, as well as the overall spectral shape were highly similar between approaches. However, the spectral range of viable AQYs differed; for the majority of samples, the variable-intercept method consistently yielded a narrower wavelength range of viable AQYs (i.e., exceeding the signal to noise threshold of 25). For example, for Suwannee River fulvic acid, the zero-intercept approach yielded AQYs up to an excitation wavelength of 565 nm, while the variable intercept approach yielded AQYs only up to 515 nm (Figure 4D). In addition, the two approaches provided different precision estimates. Across the whole AQY spectrum, the zero-intercept approach resulted in higher precision (e.g., for the AQY at 350 nm, precision estimates were $\pm 2.4\%$ and $\pm 1.3\%$ using the variable- and zero-intercept approach, respectively).

Apparent Quantum Yields of CDOM and Φ of Organic Compounds

The AQY spectra of the 28 samples from the Norwegian shelf transect were very similar (Figures 2D, 4), with minima around 250 nm increasing to maxima between 340 and 380 nm. For samples with low organic matter concentrations (predominantly deep sea samples, DOC < 60 μM), the AQYs could not be determined for wavelengths $>\sim 350$ nm due to low signal-to-noise ratios in both absorbance and fluorescence measurements at longer wavelengths.

AQYs at 350 nm (AQY₃₅₀) ranged from 0.006 to 0.021, with AQYs in surface waters (< 10 m, $n = 12$, average 0.009 ± 0.001) significantly lower than in deep-sea waters (>100 m, $n = 8$, average 0.014 ± 0.003 , one-tailed student t -test $p < 0.001$, Figures 1H, 2D). In contrast, AQYs at 250 nm (AQY₂₅₀) were less variable (average 0.004 ± 0.0006) and exhibited no observable trends with depth or latitude (Figure 1I).

To identify the key parameter responsible for the vertical AQY₃₅₀ variability, absorbance at 350 nm (A₃₅₀) and fluorescence at 350/450 nm (F_{350/450}) were normalized to the maximum for each station. The ratio of the normalized F_{350/450} and A₃₅₀ was then used to investigate the vertical change in absorbance and fluorescence (Figure 5A). Surface waters were dominated by ratios <1, indicating a relative lack of DOM fluorescence or an excess of CDOM absorbance. In contrast, [with the exception of two samples that showed unusually low fluorescence and high absorbance (samples at 197 m and 548 m, respectively)] subsurface waters showed ratios >1, indicating excess DOM fluorescence or a lack of CDOM absorbance. Moreover, AQY₃₅₀ was significantly correlated to absorbance levels at 350 nm (Figure 5B).

Φ of organic compounds at their respective absorbance peak varied from 0.00079 for benzoic acid to 0.35 for salicylic acid (Table 1), and were spectrally featureless for many compounds (e.g., phenylalanine, vanillic acid, gallic acid, Figure 6A). However, for other compounds (e.g., salicylic acid, coniferyl alcohol, and indole) Φ did vary with wavelength. Spectral structure was observed in various scenarios. Firstly, Φ was

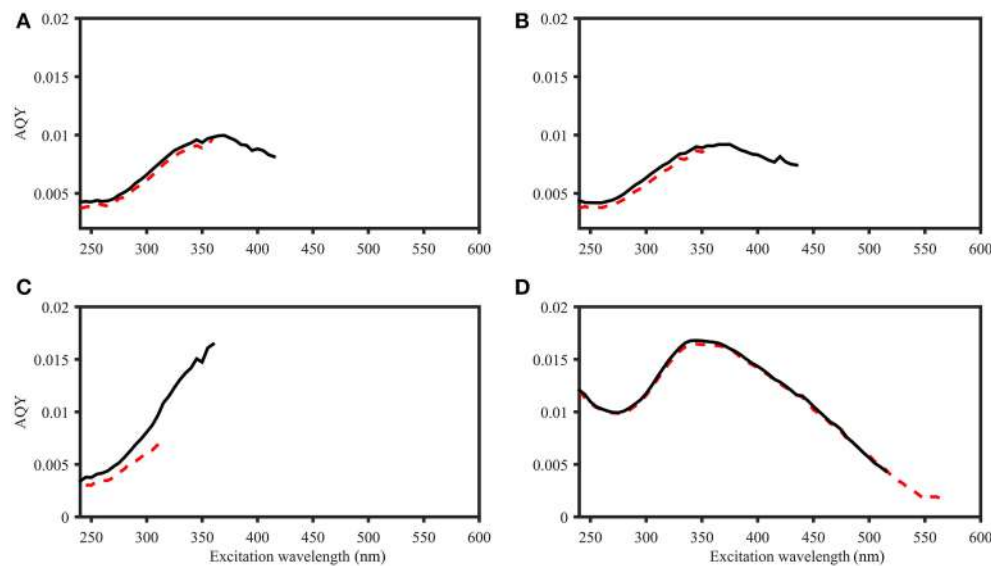


FIGURE 4 | Comparison of AQY calculations for four samples. Black line: Zero-intercept approach. Red dashed line: Variable-intercept approach. **(A–C)** Norwegian shelf DOM, water depth: 30, 10, and 200 m (**A–C**, respectively). **(D)** 2.5 mg L⁻¹ Suwannee River XAD-8 fulvic acid extract. Figures do not include error bars for ease of viewing, but in all cases, AQY values of the two calculation approaches were within the precision estimates (e.g., $\pm 0.22 \times 10^{-4}$ and 0.61×10^{-4} for zero- and variable-intercept approach in **(D)**, respectively).

often unstable at wavelengths where the molar absorptivity was low, whereby the direction of the variability for a given compound varied on a daily basis. Particularly for salicylic acid, Φ increased in some measurement runs and decreased in others (Supplementary Figure 1). Secondly, spectral structure in Φ for organic compounds was found in regions with high molar absorptivity. For example, Φ of salicylic acid consistently dropped from 0.35 at 295 nm to 0.15 at 250 nm. Another example of spectral dependence of Φ was coniferyl alcohol, which showed a distinct minimum of 0.06 at 300 nm, and two maxima at 250 nm and 315 nm (0.11 and 0.16, respectively). The comparison of absorbance and fluorescence excitation spectra for these organic compounds revealed distinct differences. Therefore, spectral dependence of Φ might originate from the presents of impurities.

To investigate the behavior of Φ for mixtures of organic compounds, Φ was determined for an equimolar mixture of tyrosine, tryptophan and salicylic acid. Φ of the mixture (Figure 6B) exhibited optical properties that were intermediate to the isolated constituents. However, at wavelengths where there was no overlapping absorbance, Φ of the mixture resembled that of the specific compound. This is particularly clear at wavelengths above 310 nm, where only salicylic acid absorbed (Figure 3). Therefore, Φ of a mixture of i fluorescing organic compounds is determined as follows:

$$\Phi_X(\lambda) = \Phi_{St} * \sum_i \frac{\int F_i(\lambda)}{A_i}(\lambda) * \frac{A_{St}(\lambda_{max})}{\int F_{St}(\lambda_{max})}. \quad (5)$$

Spectral Matching of Organic Compounds with PARAFAC Spectra

The OpenFluor fluorescence database contains excitation and emission spectra for more than 200 PARAFAC components,

mathematically extracted from fluorescence EEMs of NOM mixtures. The database was searched for matches with the 14 fluorescing organic compounds in this study. Potential spectral matches were found for p-cresol, tryptophan, indole, L-dihydroxyphenylalanine, tyrosine, coumarin, salicylic acid, ferulic acid, and benzoic acid (in order of frequency, see Table 2 for complete list, and Figure 7 for examples). Numerous matches for the emission spectrum of ferulic acid were found; however, the excitation spectrum of ferulic acid was often blue-shifted compared to the PARAFAC spectra. The spectra of p-cresol and tryptophan, as well as indole and tyrosine, were very similar and each pair yielded hits for the same PARAFAC components (Figure 8). Therefore, unambiguous matching of PARAFAC component with organic compounds was impossible for these fluorophores.

DISCUSSION

DOM Apparent Fluorescence Quantum Yields

With typical values ranging from 0.001 to 0.02, the apparent fluorescence quantum yields of FDOM are regarded as very low (Sharpless and Blough, 2014). This is particularly evident in comparison to Φ of organic compounds (up to 0.35, Figure 6A). However, Φ of mixtures of fluorescing organic compounds is dependent on the relative contribution of each fluorophore (Figure 6B, Equation 5). Moreover, DOM consists of FDOM, as well as non-fluorescent CDOM, which is the reason why DOM quantum yields can only be reported as “apparent” quantum yields. The implications of this fact can be demonstrated with simple mixtures of organic compounds using Equation (5): Φ of salicylic acid in 1 mmol L⁻¹ phosphate buffer at 258 nm

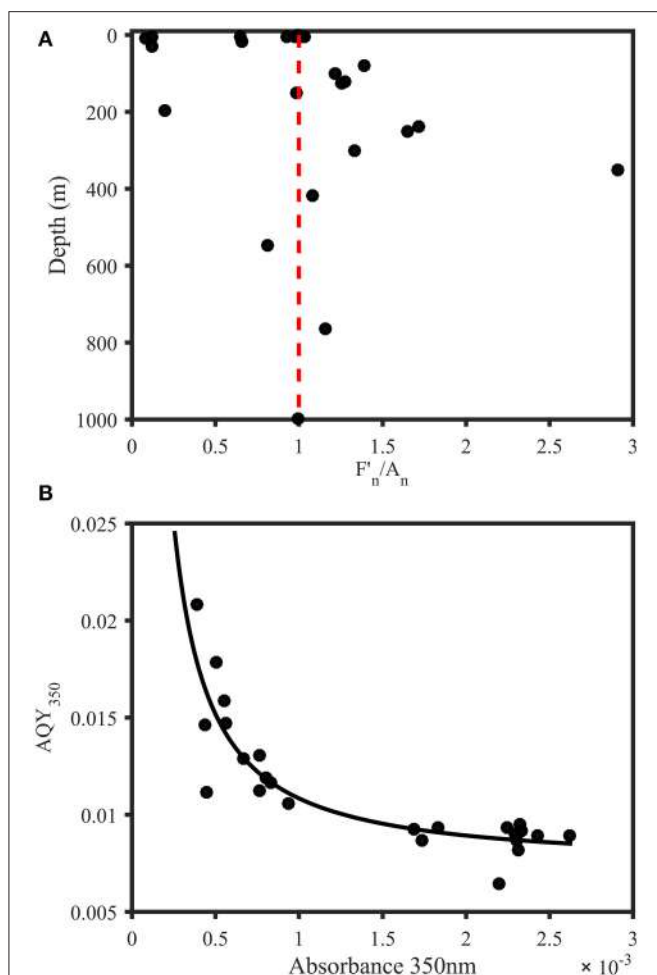


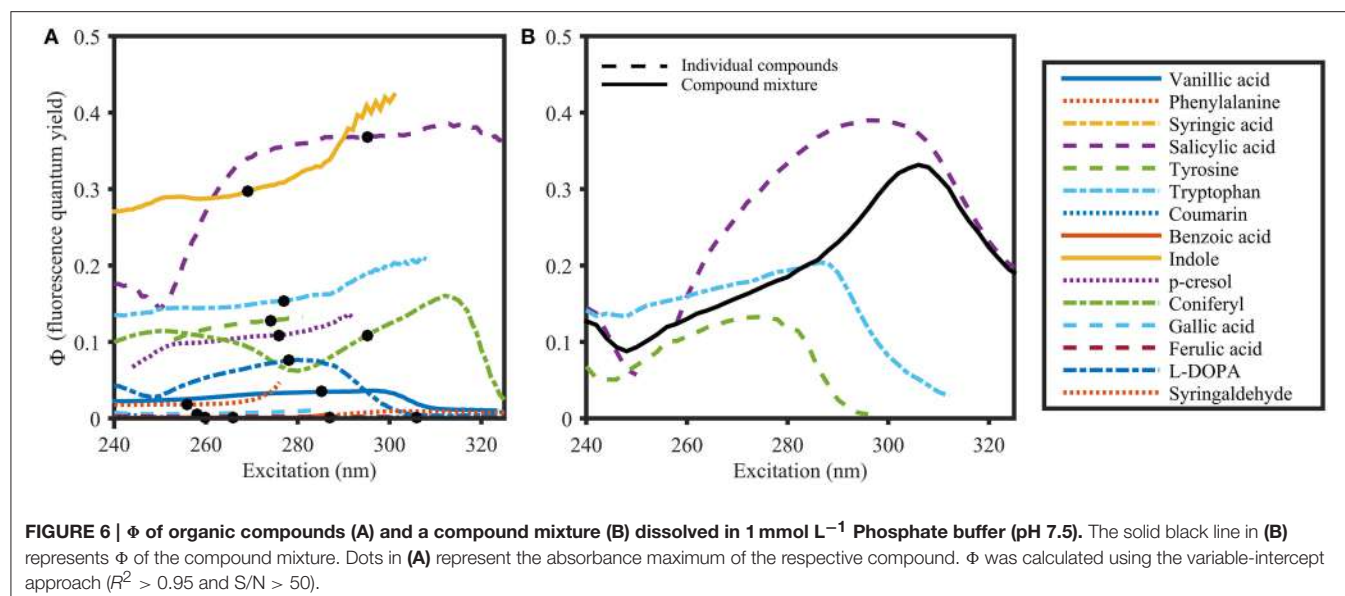
FIGURE 5 | Trends in AQYs of natural samples from the Norwegian shelf and Skagerrak. (A) Depth profile of $F'_{350}/450$ divided by A_{350} (both normalized to station maximum) for samples from 11 stations in the Norwegian Sea and Skagerrak ($n = 28$). Red line indicates a ratio of 1 and represents equal relative contribution of fluorescence and absorbance. Subsurface waters were characterized by a strong fluorescence contribution, with the exception of two samples with abnormally low fluorescence (197 m) and abnormally high absorbance (548 m). Surface waters either showed equal FDOM and CDOM levels or dominant CDOM absorbance contribution. **(B)** AQY vs. absorbance at 350 nm. The black line represents a power fit ($a \times a_{350\text{nm}}^b + c$, $a = 9.821 \times 10^{-6}$, $b = -1.181$, $c = 0.0074$, $R^2 = 0.75$).

was determined to be 0.24 in this study (Figure 6). At the same wavelength, the apparent quantum yield of an equimolar mixture of salicylic acid and the non-fluorescent compound caffeine would drop to 0.0046 since (apparent) quantum yields assume intermediate values of the individual components as demonstrated above (Figure 6). Similarly, the AQYs of a mixture of 1 mol L⁻¹ salicylic acid and 0.01–1 mol L⁻¹ caffeine drop from 0.15 to 0.0046 (Figure 9, see Supplementary Material for detailed calculation). However, since caffeine does not absorb above 310 nm, the AQY resumes a value of 0.35 at wavelengths exceeding 310 nm, and becomes a true quantum yield again. Similarly, in relative terms, the gradual increase of FDOM AQYs from 240 to 350 nm suggests that CDOM absorbance dominates

between 240 and 300 nm while DOM fluorescence prevails over DOM absorbance from 300 to 380 nm. Moreover, all studies thus far report similar spectral shapes for AQY, indicating a stable spectral CDOM to FDOM relationship (Green and Blough, 1994; Del Vecchio and Blough, 2004; Andrew et al., 2013; Cawley et al., 2015). The fact that the effect of the addition of non-fluorescent material (Figure 9) closely resembles the observations made in natural samples (Figure 5B) suggests that AQYs can be used to systematically observe changes in the ratio of FDOM to CDOM. However, to further investigate this hypothesis, knowledge about a greater number of the optically active DOM constituents, as well as the behavior of DOM AQYs of a larger number of aquatic systems, is needed.

The range, as well as the spectral distribution of AQYs for FDOM samples from the Norwegian Sea and the Skagerrak (0.011 ± 0.003 at 350 nm) was similar to previous studies (e.g., Green and Blough, 1994; Andrew et al., 2013). Romera-Castillo et al. (2011) also reported similar trends in the vertical distribution of AQY₃₅₀ for the Ria de Vigo (Spain) as those reported here for the Norwegian shelf, with high AQY₃₅₀ in deep waters and low AQY in surface waters. With our data, F_n/A_n was derived to distinguish between CDOM and FDOM to elucidate this significant vertical variability. Our observation of $F_n/A_n > 1$ for subsurface waters suggests a proportionally greater production of FDOM relative to CDOM at depth in association with the remineralization of organic matter. At UVA wavelengths, both CDOM and FDOM are known to increase with depth in the global ocean (Stedmon and Nelson, 2015), which might suggest a constant AQY. In the waters sampled in this study, the trend of low AQY at the surface appears to be driven by the presence of high-CDOM waters (Figure 1), which represent terrestrial DOM from the Baltic and German Bight (Osburn and Stedmon, 2011). The fact that the ratio increases in association with the organic matter remineralization horizon indicates that there is a proportionally greater increase in FDOM relative to CDOM in association with microbial turnover of detrital organic matter (although no clear trend was apparent with oxygen utilization for this relatively limited dataset).

For wavelengths > 380 nm, AQYs have previously been described as monotonously decreasing (Sharpless and Blough, 2014 and references therein). However, one should bear in mind that fluorescence EEMs are affected by a diagonal region of Rayleigh and Raman scatter. This diagonal scatter also represents the physical limit of the fluorescence phenomenon, since emission of fluorescence always occurs at wavelengths greater than the applied excitation wavelength. Since EEMs are generally recorded over a fixed emission range (e.g., 240 to 600 nm), the number of data points capturing relevant fluorescence emission therefore decreases linearly with increasing excitation wavelength due to the incision made by the scatter region. In a theoretical scenario, the fluorescence intensity of a mixture of organic compounds affected by these limitations would therefore have to increase in order to exhibit spectrally flat AQYs (assuming a constant absorbance of the mixture). For DOM however, due to the near-exponential decrease of absorbance with wavelength, such an increase in fluorescence intensity is not plausible. It is therefore likely that the gradual decrease in AQYs at



wavelengths >400 nm (Figure 4D) can in part be attributed to the methodological and physical constraints of fluorescence spectroscopy, rather than specific electronic phenomena.

Method Comparison: Quantum Yield Calculations

Both approaches for the calculation of AQYs of DOM samples yielded comparable results with regards to accuracy of AQY estimates. However, the variable-intercept approach yielded less precise estimates compared to the zero-intercept approach. The variable intercept approach also generally provided AQYs for a smaller spectral range since a multiple-point dilution is required to obtain AQYs with confidence. This results in absorption measurements in particular falling below the detection limit, and therefore hinders the determination of sensible AQYs. Since the zero-intercept approach only requires a sample to be measured once, it is the less time-consuming approach. We therefore conclude that, since both approaches provide comparable estimates (Figure 4), the zero-intercept approach is most suitable for the routine determination of AQYs of DOM samples.

Conversely, for the complete spectral characterization of specific organic compounds, the variable-intercept approach offers advantages. Especially at low S/N levels, instrumental noise and baseline offsets can cause the absorbance and fluorescence of organic compounds to vary independently. The variable-intercept approach provides quantum yields via the slope of linear fits, whereby the intercept is allowed to vary, thus accounting for wavelength-dependent instrument noise. Unlike for CDOM samples, the signal intensity for organic compounds is generally high, and the variable-intercept approach can produce stable quantum yields over a wide spectral range. In addition, the approach provides more appropriate means (compared to a single measurement method) to estimate the molar fluorescence and absorptivity of organic compounds due

to increased confidence of measurements obtained in a dilution series.

Since Φ represents a physical property of an individual chemical compound, it should be spectrally constant, and thus is typically reported at a single wavelength (the absorbance maximum, e.g., Pozdnyakov et al., 2009). However, Φ of the organic compounds in our study did not appear spectrally flat. Unstable Φ in areas with low molar absorptivity represent an analytical challenge that can be addressed to some extent with an adequate pathlength for absorbance measurements, and appropriate data processing. For example, baseline offset correction is a crucial step during data processing; it mitigates monotonic Φ trends in areas with low fluorescence or absorbance, as well as spurious Φ offsets. Moreover, for the determination of Φ , the chemical purity of compounds is important for the spectral stability and overall accuracy. For example, spectral instability of Φ (along with mismatching absorbance and excitation spectra) was repeatedly seen in salicylic acid at short wavelengths, and across the spectrum of coniferyl alcohol (Figure 6A). These observations are consistent with the presence of impurities affecting a small part of the spectrum in the case of salicylic acid, and large portions of the spectrum for coniferyl alcohol, benzoic acid, and coumarin. Moreover, impurities probably lowered Φ of chemicals with mismatching absorbance and fluorescence excitation spectra, and also affected the reported molar absorptivity and fluorescence. Therefore, some compounds should be purified prior to determining Φ .

The optical properties of organic compounds generally matched those of previous studies. For example, in the case of salicylic acid, the excitation and emission peak position was within 1 nm of values reported in Pozdnyakov et al. (2009), while molar absorbance, Φ , and Stokes shift differed by 1.3, 2.9, and 0.4%, respectively. Similarly, for ferulic acid, fluorescence spectra shown in Meyer et al. (2003) indicate a close match in peak positions. Moreover, Φ of tyrosine

TABLE 2 | Similarities between fluorescence spectra of PARAFAC components in the OpenFluor database and the spectra of organic compounds.

Name	Study	Component	TCC excitation	TCC emission	TCC excitation x emission
Coniferyl alcohol	–				
Coumarin	CS-Flocc ^a	2	1	0.96	0.96
	Swimpool ^b	1	0.94	0.94	0.89
p-Cresol	Florida Keys ^c	3	0.98	0.97	0.95
	CWT ^d	4	0.97	0.98	0.95
	LiverpoolBay ^e	6	0.94	0.94	0.88
	Atlantic6AMT20 ^f	4	0.97	0.99	0.95
	BWE7 ^g	1	0.97	0.96	0.93
	Recycle_WRAMS ^h	3	0.96	0.96	0.92
	Beringa2005 ⁱ	5	0.91	0.91	0.83
	HF2005 ^j	8	0.97	0.96	0.93
	ONR ^k	6	0.92	0.90	0.84
			0.92	0.91	0.83
Ferulic acid	CS-Flocc ^a	2	0.92	0.91	0.84
Gallic acid	–				
Indole	LiverpoolBay ^d	5	0.93	0.97	0.90
	Atlantic6AMT20 ^e	3	0.99	0.93	0.92
	BWE7 ^e	6	0.98	0.94	0.92
	Antarctic ^l	3	0.95	0.98	0.93
	CS-Galathea ^m	2	0.93	0.98	0.91
Benzoic acid	Recycle_StMary ^g	4	0.96	0.95	0.92
L-Phenylalanine	–				
L-dihydroxy-phenylalanine	FloridaKeys ^b	3	0.96	0.95	0.91
	CWT ^c	4	0.96	0.96	0.92
	Kauai ⁿ	6	0.96	0.96	0.92
	Recycle_WRAMS ^g	3	0.95	0.98	0.93
	ONR	6	0.96	0.98	0.94
Salicylic acid	Atlantic6AMT20 ^e	5	0.99	0.98	0.97
	Beringia2005 ^h	6	0.99	0.99	0.98
Syringic acid	–				
L-Tyrosine	FloridaKeys ^b	3	0.97	0.96	0.93
	CWT ^c	4	0.96	0.95	0.91
	LiverpoolBay ^d	6	0.96	0.97	0.93
	Atlantic6AMT20 ^e	4	0.99	1	0.99
	BWE7 ^e	1	1	0.98	0.98
	Kauai ^c	5	0.94	0.97	0.91
	Recycle_WRAMS ^g	3	0.96	0.93	0.89
	HF2005 ^j	8	0.95	0.97	0.92
DL-Tryptophane	Atlantic6AMT20 ^e	3	0.98	0.92	0.90
	Horsens ^o	5	0.94	0.93	0.87
	HF2005 ^j	7	0.94	0.99	0.93
Vanillic acid	–				

Matches were restricted to Tucker congruence coefficients (TCC) of >0.9 and peak deviations <15 nm. ^aSøndergaard et al. (2003); ^bSeredyńska-Sobecka et al. (2011); ^cYamashita et al. (2013); ^dYamashita et al. (2011a); ^eYamashita et al. (2011b); ^fKowalcuk et al. (2013); ^gMurphy et al. (2006); ^hMurphy et al. (2011); ⁱWalker et al. (2009); ^jStedmon and Markager (2005); ^kOsburn and Stedmon (2011); ^lStedmon et al. (2011); ^mJørgensen et al. (2011); ⁿMurphy et al. (2008); ^oMurphy et al. (2014a).

and tryptophan was similar to previously published values (Chen, 1967). However, Φ of phenylalanine was 25% lower compared to values reported in Chen (1967). One explanation of this discrepancy is the presence of impurities, as those would likely lower Φ . This supports the conclusion that some

compounds should be purified before measurements, as stated above.

As previously observed (Cawley et al., 2015), the determination of sensible AQYs for wavelengths > 450 nm is analytically challenging due to overall low signal intensities in

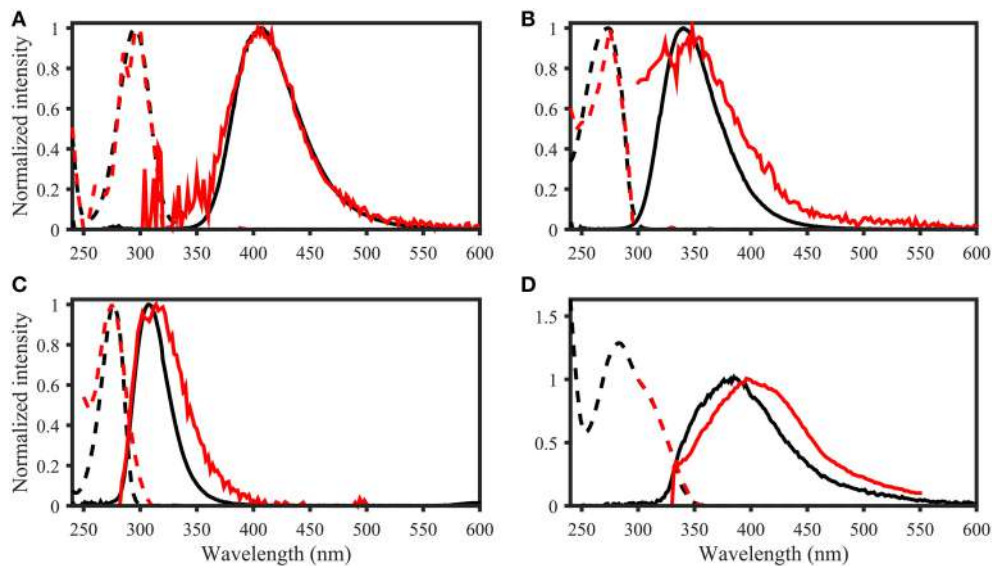


FIGURE 7 | Examples of spectral matching between PARAFAC components in the OpenFluor database with organic compounds. Dashed lines represent excitation loadings, solid lines show emission loadings. Organic compounds are shown in black, PARAFAC components in red. **(A)** Salicylic acid against component 5 from Kowalcuk et al. (2013), **(B)** Indole against component 3 from Kowalcuk et al. (2013), **(C)** p-cresol against component 3 from Murphy et al. (2011), **(D)** Coumarin against component 2 from Søndergaard et al. (2003).

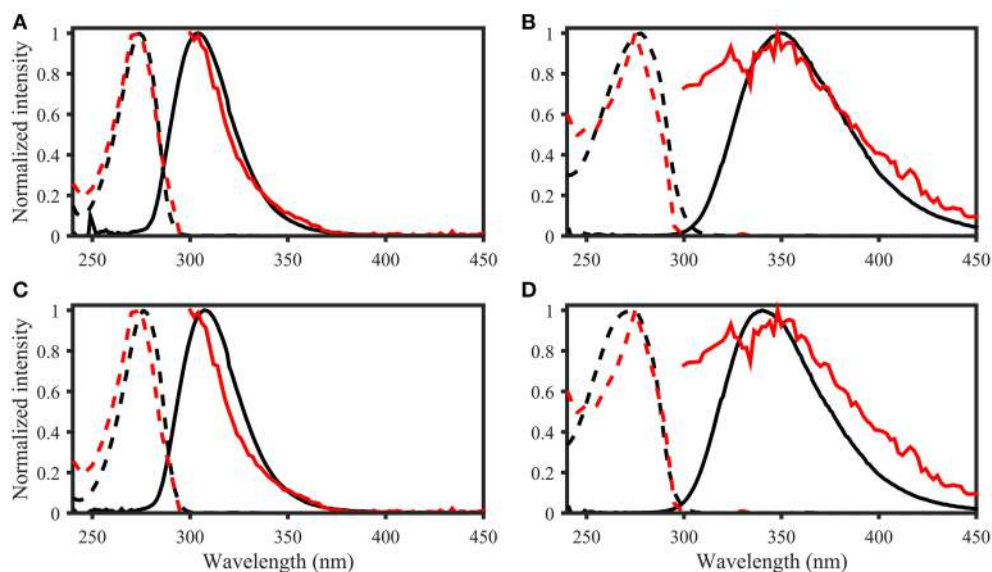


FIGURE 8 | OpenFluor matches of (A) tyrosine, (B) tryptophan, (C) p-cresol, and (D) indole (all in black) with PARAFAC components (all in red) from Kowalcuk et al. (2013). Dashed lines represent excitation loadings, solid lines show emission loadings. Tryptophan and indole, as well as tyrosine and p-cresol yield matches with the same PARAFAC component.

this spectral region, particularly for oceanic samples (as observed in this study). Since absorbance is the less sensitive measurement, it represents the limiting factor in AQY determinations; even when using a pathlength of 10 cm. We therefore recommend reporting either AQY values for specific wavelengths (e.g., 350 nm), or the spectral maximum AQY, since such values can usually be obtained with confidence.

Linking Optical and Chemical Properties

Current efforts to link optical and chemical properties of DOM include the combined characterization of DOM by means of ultrahigh-resolution mass spectrometry, PARAFAC of EEMs, as well as absorbance spectroscopy and subsequent comparison using correlation analysis (Stubbins et al., 2014; Kellerman et al., 2015). An additional approach is to compare

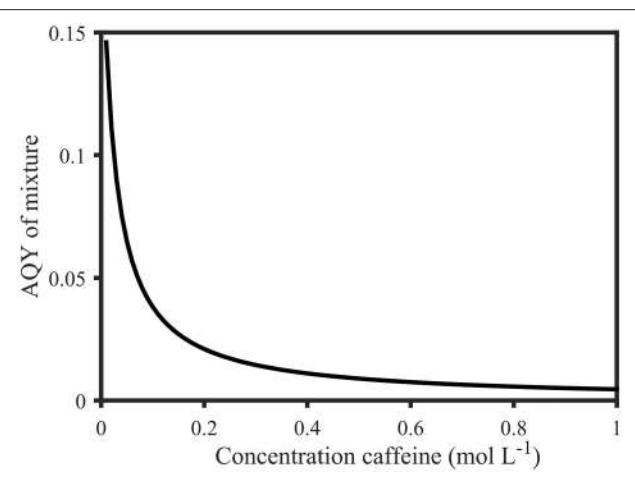


FIGURE 9 | Calculated apparent quantum yields of a mixture of 1 mol L⁻¹ salicylic acid solution with variable molar parts of caffeine (0.01–1 mol L⁻¹) at 258 nm. The apparent quantum yield decreases from 0.15 (0.01 mol L⁻¹ caffeine) to 0.0046 (1 mol L⁻¹ caffeine). Calculations were based on Equation (5) and are explained in the Supplementary Material.

the growing database of natural DOM fluorescence spectra obtained by PARAFAC analysis (Murphy et al., 2014c) to the spectra of organic compounds. Besides comparing excitation and emission spectra, additional optical information, such as molar absorptivity and fluorescence, represent valuable Supplementary Data since they can be used to dismiss otherwise reasonable spectral matches between organic compounds and modeled FDOM spectra. Specific organic compounds in marine waters can reach concentration on the order nanomoles per liter (e.g., amino acids, Yamashita and Tanoue, 2003). The plausibility of the presence of the organic compounds investigated in this study can be assessed by comparing the information on molar absorptivity and fluorescence (Table 2) with absorbance and fluorescence levels observed in natural samples. Absorption coefficients of CDOM in the ocean typically range between 0 and 0.1 m⁻¹, depending on wavelength, geographical location, and season, while fluorescence typically ranges from 0 to 0.02 Raman units (Stedmon and Nelson, 2015). The molar absorptivity and fluorescence of an equivalent of 1 nmol L⁻¹ yields 35×10^{-5} to 0.0036 m⁻¹ for absorbance, and 25×10^{-5} to 0.038 Raman units for fluorescence for the organic compounds investigated in this study. Since these values are within the range of observed signals in natural samples, it is plausible to assume that they can be constituents of CDOM/FDOM.

On the basis of molar absorptivity and fluorescence, spectral matches with the OpenFluor database for indole, tyrosine, p-cresol, salicylic acid, and L-dihydroxyphenylalanine are reasonable. However, the ability to match chemical compounds with PARAFAC components is limited by the resolving power of fluorescence spectroscopy, which is defined by the instrument or chosen by the user in form of excitation increments. As is clear from Figure 3, subtle changes in chemical structure influence the absorption properties to a large extent. However, the fluorescence emission spectra are

less variable, and the position and peak width is particularly influenced by double-bond conjugation. These observations are especially apparent for indole and tryptophan, as well as p-cresol and tyrosine, as they could not be unambiguously distinguished using spectral matching. Therefore, rather than representing chemical compounds, it is more likely that PARAFAC components resemble fluorophores (i.e., for example benzoic acid, phenol, or indole), and are comprised of a number of organic compounds [as proposed earlier in Stedmon and Bro (2008)]. The individual compounds within these fluorophore groups are possibly characterized by drastically different molar fluorescence and absorbance levels. Therefore, PARAFAC components should only be assigned to specific organic compounds if spectral matches with very high Tucker congruence coefficients (>0.99) are obtained in both excitation and emission spectra, and measured concentrations appear plausible on the basis of the molar fluorescence for the assigned organic compound.

The organic compounds investigated in this study only exhibited significant quantum yields from 240 to 325 nm. However, a considerable amount of fluorescence in EEMs occurs at excitation wavelengths above 325 nm. It is therefore necessary to characterize additional organic compounds, and obtain further spectral matches between organic compounds and PARAFAC components in order to proceed in linking optical and chemical properties of DOM. The results shown here indicate that compounds with extended conjugation will likely result in visible humic-like fluorescence. However, the ability to match spectra of organic compounds with humic-like fluorescence is challenging, since such molecules likely contain multiple fluorophores that are profoundly affected in their fluorescence emission maximum and efficiency by neighboring moieties. For example, this is a known factor in tryptophan fluorescence of proteins (Vivian and Callis, 2001). An exact match would likely only be found if such a molecule could be obtained and characterized in its pure form. Moreover, some factors influencing spectral matching might also be particularly challenging to recreate *in vitro*, considering the large number of possible individual molecules in DOM (as evident by ultrahigh-resolution mass spectrometry, e.g., Hertkorn et al., 2013). For example, large, humic-like molecules with multiple fluorophores are likely to be particularly influenced by changes in their matrix with regards to e.g., pH, and ionic strength (Gao et al., 2015). Moreover, recent studies suggest that humic-like fluorophores are significantly influenced by charge-transfer interactions (Sharpless and Blough, 2014). Therefore, the investigation of the importance of these factors for the fluorescence of individual organic compounds needs to be subject of further studies.

CONCLUSIONS

In an effort to link optical and chemical properties of DOM, matching of fluorescence spectra of organic compounds with modeled spectra of natural samples provided valuable insights. In addition, the comprehensive characterization of potential DOM constituents is vital to assessing their plausibility. However,

the capability to distinguish between organic compounds using spectral matching is limited, as many organic compounds show highly similar spectral properties. This reinforces the fact that spectral similarity alone is insufficient evidence for the presence of a particular compound, and PARAFAC components represent fluorophores, rather than specific compounds. The presented open-source MATLAB toolbox is a reliable tool for the systematic investigation of DOM AQYs, as well as Φ of organic compounds and paves the way for a more systematic cross-system analysis of apparent quantum yields. By investigating simple mixtures of organic compounds, the additive behavior of Φ was demonstrated, and the influence of non-fluorescent compounds on suppressing AQYs was illustrated. In connection with these findings, the vertical trends in AQYs of marine DOM were driven by changes in absorbance levels. Therefore, DOM AQYs mainly represent an interference of CDOM absorbance, and indicate changes in the ratio of CDOM to FDOM.

ACKNOWLEDGMENTS

This work is supported by Technical University of Denmark and Chalmers Technical University Nordic5Tech collaboration. CS would like to acknowledge the Danish Research Council for Independent Research (DFF 1323- 00336), and KM acknowledges funding by the Swedish Research Council for Environment, Agricultural Sciences and Spatial Planning (FORMAS grant 2013-1214). UW would like to acknowledge the assistance of Joseph Needoba during the setup of the daily startup routine for the spectrofluorometer. We thank Stephen Fortuna for the proofreading of this manuscript.

SUPPLEMENTARY MATERIAL

The Supplementary Material for this article can be found online at: <http://journal.frontiersin.org/article/10.3389/fmars.2015.00098>

REFERENCES

- Aiken, G. (2014). "Fluorescence and dissolved organic matter: a chemist's perspective," in *Aquatic Organic Matter Fluorescence*, eds P. Coble, J. Lead, A. Baker, D. Reynolds, and R. G. M. Spencer (New York, NY: Cambridge University Press), 35–74. doi: 10.1017/cbo9781139045452.005
- Andrew, A. A., Del Vecchio, R., Subramaniam, A., and Blough, N. V. (2013). Chromophoric dissolved organic matter (CDOM) in the equatorial atlantic ocean: optical properties and their relation to CDOM structure and source. *Mar. Chem.* 148, 33–43. doi: 10.1016/j.marchem.2012.11.001
- Austin, R. W., and Halikas, G. (1976). *The Index of Refraction of Seawater*. La Jolla, CA: University of California.
- Blough, N. V., and Del Vecchio, R. (2002). "Chromophoric DOM in the coastal environment," in *Biogeochemistry of Marine Dissolved Organic Matter*, eds D. A. Hansell and C. A. Carlson (San Diego, CA: Elsevier Inc.), 502–546.
- Brouwer, A. M. (2011). Standards for photoluminescence quantum yield measurements in solution (IUPAC Technical Report). *Pure Appl. Chem.* 83, 2213–2228. doi: 10.1351/PAC-REP-10-09-31
- Catalá, T. S., Reche, I., Álvarez, M., Khatiwala, S., Guallart, E. F., Benítez-Barrios, V. M., et al. (2015). Water mass age and aging driving chromophoric dissolved organic matter in the dark global ocean. *Global Biogeochem. Cycles* 29, 917–934. doi: 10.1002/2014GB005048
- Cauwet, G. (1999). "Determination of dissolved organic carbon and nitrogen by high temperature combustion," in *Methods of Seawater Analysis*, eds K. Grasshoff, K. Kremling, and M. Ehrhardt (Weinheim: Wiley-VCH), 407–420.
- Cawley, K. M., Korak, J. A., and Rosario-Ortiz, F. L. (2015). Quantum yields for the formation of reactive intermediates from dissolved organic matter samples from the Suwannee River. *Environ. Eng. Sci.* 32, 31–37. doi: 10.1089/ees.2014.0280
- Chen, R. F. (1967). Fluorescence quantum yields of tryptophan and tyrosine. *Anal. Lett.* 1, 35–42. doi: 10.1080/00032716708051097
- Del Vecchio, R., and Blough, N. V. (2004). On the origin of the optical properties of humic substances. *Environ. Sci. Technol.* 38, 3885–3891. doi: 10.1021/es049912h
- Dittmar, T., Koch, B., Hertkorn, N., and Kattner, G. (2008). A simple and efficient method for the solid-phase extraction of dissolved organic matter (SPE-DOM) from seawater. *Limnol. Ocean. Methods* 6, 230–235. doi: 10.4319/lom.2008.6.230
- Ferrari, G. M. (2000). The relationship between chromophoric dissolved organic matter and dissolved organic carbon in the European atlantic coastal area and in the West Mediterranean Sea (Gulf of Lions). *Mar. Chem.* 70, 339–357. doi: 10.1016/S0304-4203(00)00036-0
- Ferrari, G. M., Dowell, M. D., Grossi, S., and Targa, C. (1996). Relationship between the optical properties of chromophoric dissolved organic matter and total concentration of dissolved organic carbon in the southern Baltic Sea region. *Mar. Chem.* 55, 299–316. doi: 10.1016/S0304-4203(96)00061-8
- Gao, Y., Yan, M., and Korshin, G. V. (2015). Effects of ionic strength on the chromophores of dissolved organic matter. *Environ. Sci. Technol.* 49, 5905–5912. doi: 10.1021/acs.est.5b00601
- Green, S. A., and Blough, N. V. (1994). Optical absorption and fluorescence properties of chromophoric dissolved organic-matter in natural-waters. *Limnol. Oceanogr.* 39, 1903–1916. doi: 10.4319/lo.1994.39.8.1903
- Hertkorn, N., Fromberger, M., Witt, M., Koch, B. P., Schmitt-Kopplin, P., and Perdue, E. M. (2008). Natural organic matter and the event horizon of mass spectrometry. *Ger. Res.* 80, 8908–8919. doi: 10.1021/ac800464g
- Hertkorn, N., Harir, M., Koch, B. P., Michalke, B., and Schmitt-Kopplin, P. (2013). High-field NMR spectroscopy and FTICR mass spectrometry: powerful discovery tools for the molecular level characterization of marine dissolved organic matter. *Biogeosciences* 10, 1583–1624. doi: 10.5194/bg-10-1583-2013
- Jansen, B., Kalbitz, K., and McDowell, W. H. (2014). Dissolved organic matter: linking soils and aquatic systems. *Vadose Zone J.* 13, 1–4. doi: 10.2136/vzj2014.05.0051
- Jørgensen, L., Stedmon, C. A., Kragh, T., Markager, S., Middelboe, M., and Søndergaard, M. (2011). Global trends in the fluorescence characteristics and distribution of marine dissolved organic matter. *Mar. Chem.* 126, 139–148. doi: 10.1016/j.marchem.2011.05.002
- Kellerman, A. M., Kothawala, D. N., Dittmar, T., and Tranvik, L. J. (2015). Persistence of dissolved organic matter in lakes related to its molecular characteristics. *Nat. Geosci.* 8, 454–457. doi: 10.1038/ngeo2440
- Kowalcuk, P., Tilstone, G. H., Zablocka, M., Röttgers, R., and Thomas, R. (2013). Composition of dissolved organic matter along an Atlantic Meridional Transect from fluorescence spectroscopy and Parallel Factor Analysis. *Mar. Chem.* 157, 170–184. doi: 10.1016/j.marchem.2013.10.004
- Lakowicz, J. R. (2006). *Principles of Fluorescence Spectroscopy*, 3rd Edn. New York, NY: Springer US. doi: 10.1007/978-0-387-46312-4
- Melhuish, W. H. (1961). Quantum efficiencies of fluorescence of organic substances: effect of solvent and concentration of the fluorescent solute. *J. Phys. Chem.* 65, 229–235. doi: 10.1021/j100820a009
- Meyer, S., Cartelat, A., Moya, I., and Cerovic, Z. G. (2003). UV-induced blue-green and far-red fluorescence along wheat leaves: a potential signature of leaf ageing. *J. Exp. Bot.* 54, 757–769. doi: 10.1093/jxb/erg063
- Morris, D. P., Zagarese, H., Williamson, C. E., Balseiro, E. G., Hargreaves, B. R., Modenutti, B., et al. (1995). The attenuation of solar UV radiation in lakes

- and the role of dissolved organic carbon. *Limnol. Oceanogr.* 40, 1381–1391. doi: 10.4319/lo.1995.40.8.1381
- Murphy, K. R., Bro, R., and Stedmon, C. A. (2014a). “Chemometric analysis of organic matter fluorescence,” in *Aquatic Organic Matter Fluorescence*, eds P. Coble, A. Baker, J. Lead, D. Reynolds, and R. Spencer (New York, NY: Cambridge University Press), 339–375.
- Murphy, K. R., Hamblly, A., Singh, S., Henderson, R. K., Baker, A., Stuetz, R., et al. (2011). Organic matter fluorescence in municipal water recycling schemes: toward a unified PARAFAC model. *Environ. Sci. Technol.* 45, 2909–2916. doi: 10.1021/es103015e
- Murphy, K. R., Parcisi, G., and Stuetz, R. M. (2014b). Non-methane volatile organic compounds predict odor emitted from five tunnel ventilated broiler sheds. *Chemosphere* 95, 423–432. doi: 10.1016/j.chemosphere.2013.09.076
- Murphy, K. R., Ruiz, G. M., Dunsmuir, W. T. M., and Waite, T. D. (2006). Optimized parameters for fluorescence-based verification of ballast water exchange by ships. *Environ. Sci. Technol.* 40, 2357–2362. doi: 10.1021/es0519381
- Murphy, K. R., Stedmon, C. A., Graeber, D., and Bro, R. (2013). Fluorescence spectroscopy and multi-way techniques. *PARAFAC Anal. Methods* 5, 6557. doi: 10.1039/c3ay41160e
- Murphy, K. R., Stedmon, C. A., Waite, T. D., and Ruiz, G. M. (2008). Distinguishing between terrestrial and autochthonous organic matter sources in marine environments using fluorescence spectroscopy. *Mar. Chem.* 108, 40–58. doi: 10.1016/j.marchem.2007.10.003
- Murphy, K. R., Stedmon, C. A., Wenig, P., and Bro, R. (2014c). OpenFluor—an online spectral library of auto-fluorescence by organic compounds in the environment. *Anal. Methods* 6, 658–661. doi: 10.1039/C3AY41935E
- Osburn, C. L., and Stedmon, C. A. (2011). Linking the chemical and optical properties of dissolved organic matter in the Baltic-North Sea transition zone to differentiate three allochthonous inputs. *Mar. Chem.* 126, 281–294. doi: 10.1016/j.marchem.2011.06.007
- Parker, C. A., and Rees, W. T. (1960). Correction of fluorescence spectra and measurement of fluorescence quantum efficiency. *Analyst* 85:587. doi: 10.1039/an9608500587
- Pozdnyakov, I. P., Pigliucci, A., Tkachenko, N., Plyusnin, V. F., Vauthheyb, E., and Lemmettyinen, H. (2009). The photophysics of salicylic acid derivatives in aqueous solution. *J. Phys. Org. Chem.* 22, 449–454. doi: 10.1002/poc.1489
- Prairie, Y. T. (2008). Carbocentric limnology: looking back, looking forward. *Can. J. Fish. Aquat. Sci.* 65, 543–548. doi: 10.1139/f08-011
- Ravichandran, M. (2004). Interactions between mercury and dissolved organic matter - A review. *Chemosphere* 55, 319–331. doi: 10.1016/j.chemosphere.2003.11.011
- Romera-Castillo, C., Nieto-Cid, M., Castro, C. G., Marrasé, C., Largier, J., Barton, E. D., et al. (2011). Fluorescence: absorption coefficient ratio - Tracing photochemical and microbial degradation processes affecting coloured dissolved organic matter in a coastal system. *Mar. Chem.* 125, 26–38. doi: 10.1016/j.marchem.2011.02.001
- Seredyńska-Sobecka, B., Stedmon, C. A., Boe-Hansen, R., Waul, C. K., and Arvin, E. (2011). Monitoring organic loading to swimming pools by fluorescence excitation-emission matrix with parallel factor analysis (PARAFAC). *Water Res.* 45, 2306–2314. doi: 10.1016/j.watres.2011.01.010
- Sharpless, C. M., and Blough, N. V. (2014). The importance of charge-transfer interactions in determining chromophoric dissolved organic matter (CDOM) optical and photochemical properties. *Environ. Sci. Process. Impacts* 16, 654–671. doi: 10.1039/c3em00573a
- Siegel, D. A., Maritorena, S., Nelson, N. B., Behrenfeld, M. J., and McClain, C. R. (2005). Colored dissolved organic matter and its influence on the satellite-based characterization of the ocean biosphere. *Geophys. Res. Lett.* 32, 1–4. doi: 10.1029/2005GL024310
- Søndergaard, M., Stedmon, C. A., and Borch, N. H. (2003). Fate of terrigenous dissolved organic matter (DOM) in estuaries: aggregation and bioavailability. *Ophelia* 57, 161–176. doi: 10.1080/00785236.2003.10409512
- Stedmon, C. A., and Bro, R. (2008). Characterizing dissolved organic matter fluorescence with parallel factor analysis: a tutorial. *Limnol. Oceanogr. Methods* 6, 572–579. doi: 10.4319/lom.2008.6.572
- Stedmon, C. A., and Markager, S. (2005). Resolving the variability of dissolved organic matter fluorescence in a temperate estuary and its catchment using PARAFAC analysis. *Limnol. Oceanogr.* 50, 686–697. doi: 10.4319/lo.2005.50.2.00686
- Stedmon, C. A., and Nelson, N. B. (2015). “The optical properties of DOM in the ocean,” in *Biogeochemistry of Marine Dissolved Organic Matter*, eds D. A. Hansell and C. A. Carlson (San Diego, CA: Elsevier Inc.), 481–508.
- Stedmon, C. A., Thomas, D. N., Papadimitriou, S., Granskog, M. A., and Dieckmann, G. S. (2011). Using fluorescence to characterize dissolved organic matter in Antarctic sea ice brines. *J. Geophys. Res. Biogeosci.* 116, 1–9. doi: 10.1029/2011jg001716
- Stewart, A. J., and Wetzel, R. G. (1980). Fluorescence: absorbance ratios—a molecular-weight tracer of dissolved organic matter. *Limnol. Oceanogr.* 25, 559–564. doi: 10.4319/lo.1980.25.3.0559
- Stubbins, A., Lapierre, J.-F., Berggren, M., Prairie, Y. T., Dittmar, T., and Del Giorgio, P. A. (2014). What’s in an EEM? Molecular signatures associated with dissolved organic fluorescence in Boreal Canada. *Environ. Sci. Technol.* 48, 10598–10606. doi: 10.1021/es502086e
- Tucker, L. R. (1951). *A Method for Synthesis of Factor Analysis Studies*. Personnel Research Section Report No. 984, Department of the Army, Washington, DC.
- Velapoldi, R. A., and Tønnesen, H. H. (2004). Corrected emission spectra and quantum yields for a series of fluorescent compounds in the visible spectral region. *J. Fluoresc.* 14, 465–472. doi: 10.1023/B:JOFL.0000031828.96368.c1
- Vivian, J. T., and Callis, P. R. (2001). Mechanisms of tryptophan fluorescence shifts in proteins. *Biophys. J.* 80, 2093–2109. doi: 10.1016/S0006-3495(01)76183-8
- Walker, S. A., Amon, R. M. W., Stedmon, C. A., Duan, S., and Louchouarn, P. (2009). The use of PARAFAC modeling to trace terrestrial dissolved organic matter and fingerprint water masses in coastal Canadian Arctic surface waters. *J. Geophys. Res. Biogeosci.* 114, 1–12. doi: 10.1029/2009jg000990
- Williamson, C. E., Morris, D. P., Pace, M. L., and Olson, O. G. (1999). Dissolved organic carbon and nutrients as regulators of lake ecosystems: resurrection of a more integrated paradigm. *Limnol. Oceanogr.* 44, 795–803. doi: 10.4319/lo.1999.44.3_part_2.0795
- Würth, C., Grabolle, M., Pauli, J., Spieles, M., and Resch-Genger, U. (2013). Relative and absolute determination of fluorescence quantum yields of transparent samples. *Nat. Protoc.* 8, 1535–1550. doi: 10.1038/nprot.2013.087
- Yamashita, Y., Boyer, J. N., and Jaffé, R. (2013). Evaluating the distribution of terrestrial dissolved organic matter in a complex coastal ecosystem using fluorescence spectroscopy. *Cont. Shelf Res.* 66, 136–144. doi: 10.1016/j.csr.2013.06.010
- Yamashita, Y., Kloepel, B. D., Knoepp, J., Zausen, G. L., and Jaffé, R. (2011a). Effects of watershed history on dissolved organic matter characteristics in headwater streams. *Ecosystems* 14, 1110–1122. doi: 10.1007/s10021-011-9469-z
- Yamashita, Y., Panton, A., Mahaffey, C., and Jaffé, R. (2011b). Assessing the spatial and temporal variability of dissolved organic matter in Liverpool Bay using excitation-emission matrix fluorescence and parallel factor analysis. *Ocean Dyn.* 61, 569–579. doi: 10.1007/s10236-010-0365-4
- Yamashita, Y., and Tanoue, E. (2003). Chemical characterization of protein-like fluorophores in DOM in relation to aromatic amino acids. *Mar. Chem.* 82, 255–271. doi: 10.1016/S0304-4203(03)00073-2
- Zepp, R. G., Sheldon, W. M., and Moran, M. A. (2004). Dissolved organic fluorophores in southeastern US coastal waters: correction method for eliminating Rayleigh and Raman scattering peaks in excitation-emission matrices. *Mar. Chem.* 89, 15–36. doi: 10.1016/j.marchem.2004.02.006

Conflict of Interest Statement: The Guest Associate Editor Dr. Christopher Osburn declares that, despite co-authoring a paper with author Dr. Colin A. Stedmon, the review process was handled objectively and no conflict of interest exists. The authors declare that the research was conducted in the absence of any commercial or financial relationships that could be construed as a potential conflict of interest.

Copyright © 2015 Wünsch, Murphy and Stedmon. This is an open-access article distributed under the terms of the Creative Commons Attribution License (CC BY). The use, distribution or reproduction in other forums is permitted, provided the original author(s) or licensor are credited and that the original publication in this journal is cited, in accordance with accepted academic practice. No use, distribution or reproduction is permitted which does not comply with these terms.



Corrigendum: Fluorescence Quantum Yields of Natural Organic Matter and Organic Compounds: Implications for the Fluorescence-based Interpretation of Organic Matter Composition

Urban J. Wünsch^{1*}, Kathleen R. Murphy² and Colin A. Stedmon¹

¹ Section for Marine Ecology and Oceanography, National Institute of Aquatic Resources, Technical University of Denmark, Charlottenlund, Denmark, ² Water Environment Technology, Chalmers University of Technology, Gothenburg, Sweden

Keywords: aquaDOM, OpenFluor, PARAFAC, spectral matching, EEM, FDOM, CDOM

A Corrigendum on

Fluorescence Quantum Yields of Natural Organic Matter and Organic Compounds: Implications for the Fluorescence-based Interpretation of Organic Matter Composition.
by Wiinsch, U. J., Murphy, K. R., and Stedmon, C. A. (2015) *Front. Mar. Sci.* 2:98. doi: 10.3389/fmars.2015.00098

OPEN ACCESS

Edited and reviewed by:

Christopher Osburn,
North Carolina State University, USA

***Correspondence:**
Urban J. Wünsch
urbw@aqua.dtu.dk

Specialty section:

This article was submitted to
Marine Biogeochemistry,
a section of the journal
Frontiers in Marine Science

Received: 13 January 2016

Accepted: 22 January 2016

Published: 10 February 2016

Citation:

Wünsch UJ, Murphy KR and
Stedmon CA (2016) Corrigendum:
Fluorescence Quantum Yields of
Natural Organic Matter and Organic
Compounds: Implications for the
Fluorescence-based Interpretation of
Organic Matter Composition.
Front. Mar. Sci. 3:9.
doi: 10.3389/fmars.2016.00009

The authors wish to include the following corrections to the original article. Some data presented in the published article were inaccurate due to improper instrumental correction factors resulting in incorrect fluorescence intensities. Moreover, we have corrected an error in the aquaDOM toolbox that affected the molar fluorescence and absorbance of organic compounds reported in the original article. Since these issues influenced data reported in **Tables 1, 2** and figures (**Figures 1–9**), there is a need for this corrigendum. The findings of the original manuscript were unaffected by these issues and remain the same.

Corrections are listed below in bold and underlined font. For page numbers, section heading, and paragraph numbers please refer to <http://dx.doi.org/10.3389/fmars.2015.00098>.

PAGE 1. ABSTRACT

- Range of Φ of organic compounds changed from 0.00079–0.35 to **0.001–0.37**
- Range of DOM AQY changed from 0.011 ± 0.003 to **0.012 ± 0.004**
- Number of studies that contained matches with this study changed from 16 to **21**

PAGE 4. MATERIALS AND METHODS. (APPARENT) QUANTUM YIELD CALCULATION.

- Paragraph 1: The MATLAB toolbox is now available at <https://github.com/urbanwuensch/aquaDOM/releases>. The toolbox published with the original article is available as v1.0.0. For the corrigendum, v1.0.1 was used. Further updates will be published on this website if necessary.
- Paragraph 3: The molar fluorescence of the cross-reference salicylic acid was previously underestimated and led to the conclusion that 0.54 is the true reference quantum yield for

TABLE 1 | Optical properties of organic compounds dissolved in 1 mmol L⁻¹ phosphate buffer (pH 7.5).

Name	Molecular formula	Molecular weight (g mol ⁻¹)	$\lambda_{\text{max}}(\text{nm})$	$\lambda_{\text{em}}(\text{nm})$	Molar fluorescence (R.U. μmol^{-1} L)	Molar absorbance (L mol ⁻¹ cm ⁻¹)	Stokes shift (eV)	$\Phi (\pm\%)$
Caffeine	C ₈ H ₁₀ N ₄ O ₂	194.19	258	—	—	15,791	—	—
Coniferyl alcohol	C ₁₀ H ₁₂ O ₃	180.2	262	337	5.2	11,860	—	—
			292		1.8	4887	0.49	0.1 (9)
Coumarin	C ₉ H ₆ O ₂	146.14	276	376	0.019	11,100	—	—
			306		0.018	6356	1.26	0.001 (5)
Cresol	C ₇ H ₈ O	108.14	279	304	1.4	1928	0.41	0.155 (28)
Ferulic acid	C ₁₀ H ₁₀ O ₄	194.18	286	414	0.062	14,425	1.33	0.002 (13)
Gallic acid	C ₇ H ₆ O ₅	170.12	252	340	0.133	8280	1.38	0.006 (4)
Indole	C ₈ H ₇ N	117.15	269	340	4.6	5240	1.01	0.335 (9)
Benzoic acid	C ₇ H ₆ O ₂	122.12	223	314	—	7772	—	—
			266		0.002	550	0.31	0.001 (17)
Phenylalanine	C ₉ H ₁₁ NO ₂	165.19	256	281	0.036	153	0.43	0.039 (7)
L-dihydroxyphenylalanine	C ₉ H ₁₁ NO ₄	197.19	279	312	1.0	2723	0.48	0.085 (25)
Salicylic acid	C ₇ H ₆ O ₃	138.12	295	407	3.8	3469	1.16	0.365 (4)
Syringic acid	C ₉ H ₁₀ O ₅	198.17	260	332	0.538	14,604	1.03	0.012 (30)
DL-Tryptophane	C ₁₁ H ₁₂ N ₂ O ₂	204.23	277	350	2.3	5368	0.96	0.162 (8)
L-Tyrosine	C ₉ H ₁₁ NO ₃	181.19	274	301	1.3	1206	0.42	0.193 (32)
Vanillic acid	C ₈ H ₈ O ₄	168.14	250	324	1.1	8832	—	—
			284		0.590	4051	0.53	0.039 (13)

Molar fluorescence and absorbance are reported for the absorbance maximum and the secondary absorbance peak if present. The quantum yield precision was estimated using the 95% confidence interval (see section 2.3) and is stated as the percentage of the estimated quantum yield.

quinine sulfate. As both 0.51 and 0.54 appear in the literature and 0.51 results in smaller errors during the cross calibration, the reference quantum yield of quinine sulfate was changed from 0.54 to **0.51**.

PAGE 5. RESULTS. OPTICAL PROPERTIES OF SAMPLES AND ORGANIC COMPOUNDS. PARAGRAPH 2.

- Molar fluorescence range changed from 0.003–38.50 (indole) to **0.002–5.2 Raman units L μmol^{-1} (coniferyl alcohol)**
- Stokes shift range changed from 0.32–1.38 eV (ferulic acid) to **0.31–1.38 eV (gallic acid)**
- Stokes shift range “group 1” changed from 0.32–0.57 eV with emission maxima of 281–339 nm to **0.32–0.49 eV and emission maxima of 281–337 nm**
- Stokes shift range group 2 changed from 0.97–1.38 eV with emission maxima of 333–413 nm to **1.01–1.38 eV and emission maxima of 340–414 nm**
- Φ of p-cresol and tyrosine changed from 0.11 and 0.13 to **0.16, and 0.19**; Stokes shift changed from 0.45 and 0.49 eV to **0.41 and 0.42 eV**
- Φ of tryptophan and indole changed from 0.15 and 0.28 to **0.16 and 0.34**

PAGE 7. RESULTS. METHOD COMPARISON: APPARENT QUANTUM YIELD CALCULATIONS.

- AQY accuracy for both approaches changed from 0.1–6% to **0.1–2.5%**
- Zero-intercept approach wavelength extent changed from 565 nm to **570 nm**
- Precision estimates of variable- and zero-intercept approach changed from $\pm 2.4\%$ and $\pm 1.3\%$ to **2.3% and 1.02%**, respectively.

PAGE 7. RESULTS. APPARENT QUANTUM YIELDS OF CDOM AND Φ OF ORGANIC COMPOUNDS. PARAGRAPH 1.

- Range of AQY₃₅₀ changed from 0.006–0.021 to **0.007–0.022**

PAGE 7. RESULTS. APPARENT QUANTUM YIELDS OF CDOM AND Φ OF ORGANIC COMPOUNDS. PARAGRAPH 2.

- Average surface water AQY changed from 0.009 to **0.010**
- Average deep-sea water AQY changed from 0.014 ± 0.003 to **0.016 ± 0.003**

TABLE 2 | Similarities between fluorescence spectra of PARAFAC components in the OpenFluor database and the spectra of organic compounds.

Organic compound	Study	Component	TCC Excitation	TCC Emission	TCC Excitation × Emission
Benzoic acid	Kauai ^a	2	0.99	0.96	0.95
	CS-Galathea ^b	3	0.95	0.90	0.86
	Recycle_StMary ^c	4	0.97	0.93	0.90
Coumarine	Swimpool ^d	1	0.95	0.95	0.90
	CS-Flocc ^e	2	1.00	0.95	0.95
p-Cresol	BWE7 ^f	1	0.98	0.98	0.96
	Recycle_WRAMS ^c	3	0.97	0.93	0.90
	FloridaKeys ^g	3	0.98	0.96	0.94
	Atlantic6AMT20 ^h	4	0.98	1.00	0.97
	CWT ⁱ	4	0.97	0.95	0.93
	Kauai	5	0.91	0.96	0.87
	LiverpoolBay ^j	6	0.95	0.97	0.92
L-DOPA	HF2005 ^k	8	0.97	0.97	0.94
	Recycle_WRAMS	3	0.95	0.99	0.94
	FloridaKeys	3	0.96	0.98	0.94
	Atlantic6AMT20	4	0.93	0.93	0.87
	CWT	4	0.96	0.98	0.94
	Beringia2005 ^l	5	0.92	0.97	0.89
	ONR ^m	6	0.96	0.97	0.93
	Kauai	6	0.95	0.94	0.90
Indole	HF2005	8	0.96	0.92	0.89
	Antarctic ⁿ	3	0.93	0.99	0.92
	Atlantic6AMT20	3	0.98	0.94	0.92
	CS-Bergen ⁿ	4	0.97	0.92	0.90
	TropicalRivers ^b	5	0.94	0.90	0.85
	LiverpoolBay	5	0.91	0.98	0.89
	CS-Bergen	6	0.92	0.94	0.87
	BWE7 ^o	6	0.96	0.95	0.91
Salicylic acid	FCE ^p	7	0.98	0.91	0.89
	Atlantic6AMT20	5	0.99	0.98	0.97
	Beringia2005	6	0.99	0.99	0.98
Syringic acid	TropicalRivers	5	0.93	0.93	0.86
	FCE	7	0.95	0.95	0.90
Tryptophan	Antarctic	3	0.98	0.94	0.92
	Atlantic6AMT20	3	0.98	0.92	0.91
	Recycle_StMary	5	0.92	0.92	0.84
	Horsens5 ^q	5	0.94	0.93	0.87
	HF2005	7	0.94	0.99	0.93
	Kauai	7	0.90	0.98	0.89
Tyrosine	BWE7	1	1.00	1.00	1.00
	FloridaKeys	3	0.97	0.93	0.90
	Atlantic6AMT20	4	1.00	1.00	0.99
	CWT	4	0.96	0.91	0.87
	Kauai	5	0.95	0.94	0.89
	Recycle_StMary	6	0.96	0.92	0.88
	LiverpoolBay	6	0.96	0.98	0.94
	HF2005	8	0.95	0.96	0.91

(Continued)

TABLE 2 | Continued

Organic compound	Study	Component	TCC Excitation	TCC Emission	TCC Excitation × Emission
Vanillic acid	Recycle_StMary	4	0.92	0.92	0.85
	DONKEY ^r	5	0.93	0.96	0.89
	FCE	7	0.97	0.95	0.92

Matches were restricted to Tucker congruence coefficients (TCC) of >0.9 and peak deviations <15 nm. ^a(Murphy et al., 2008); ^b(Jørgensen et al., 2011); ^c(Murphy et al., 2011); ^d(Seredyńska-Sobecka et al., 2011); ^e(Søndergaard et al., 2003) ^f(Murphy et al., 2006); ^g(Yamashita et al., 2013); ^h(Kowalczuk et al., 2013); ⁱ(Yamashita et al., 2011a); ^j(Yamashita et al., 2011b); ^k(Stedmon and Markager, 2005a); ^l(Walker et al., 2009); ^m(Osburn and Stedmon, 2011); ⁿ(Stedmon et al., 2011); ^o(Stedmon and Markager, 2005b); ^p(Yamashita et al., 2010); ^q(Murphy et al., 2014); ^r(Stedmon et al., 2007).

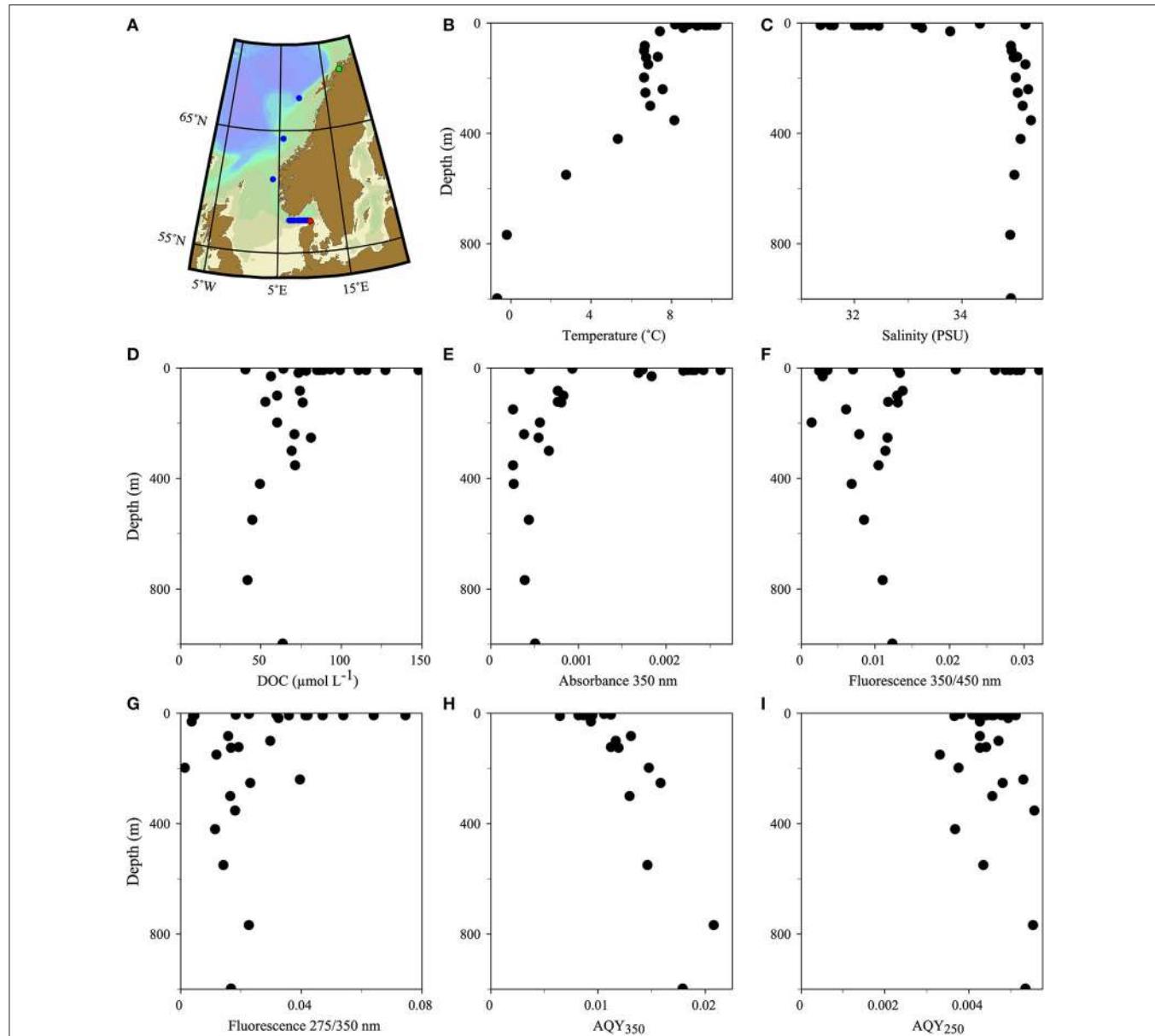


FIGURE 1 | Map (A) and vertical profiles of various biogeochemical parameters (B–I) of the transect along the Norwegian shelf and the Skagerrak. The transect direction was north (starting in Tromsø, green dot) to south (ending in Hirtshals, red dot). A total of 11 stations were sampled. Eight stations in the Skagerrak were sampled for surface waters; three stations along the Norwegian shelf included vertical profiles.

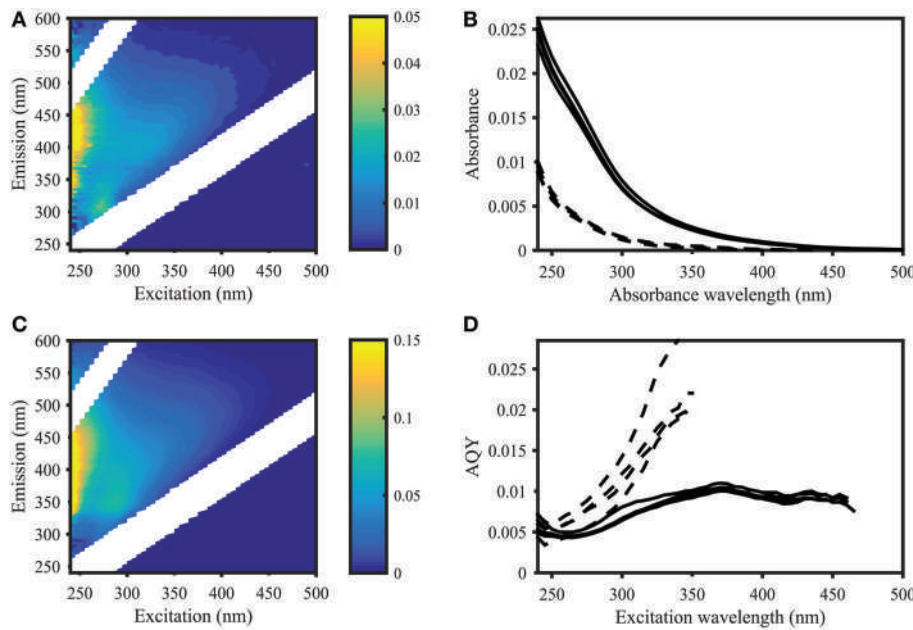


FIGURE 2 | Apparent quantum yield and fluorescence in samples from the Norwegian Sea (Station 2, deep sea) and Skagerrak (Station 14, surface water). Left panel: EEMs of deep (**A**) and surface (**C**) samples in Raman units (different scales as indicated by colorbar). Right panel: CDOM absorbance (**B**) and CDOM apparent fluorescence quantum yields (**D**) of four deep sea samples (dashed lines) and four surface water samples (solid lines), showing deep sea AQYs consistently higher than in surface waters. AQYs at wavelengths where signal to noise ratios were below 25 are missing values.

- Average AQY₂₅₀ changed from 0.004 ± 0.0006 to 0.005 ± 0.0007
- **Figure 4:** water depth changed from 30, 10, and 200 m (A–C, respectively) to **6 m, 30 m and 200 m (A–C, respectively)**.

PAGE 7. RESULTS. APPARENT QUANTUM YIELDS OF CDOM AND Φ OF ORGANIC COMPOUNDS. PARAGRAPH 3.

- Recalculation of AQYs eliminated the outlier at 197 m
- **Table 1:** Molar absorbance and fluorescence is reported for all mentioned peaks in the corrected version of the paper. Most values reported in the original version of the document have changed slightly. The correct values are reported in **Table 1**.

PAGE 7–8. RESULTS. APPARENT QUANTUM YIELDS OF CDOM AND Φ OF ORGANIC COMPOUNDS. PARAGRAPH 4.

- Range of Φ for organic compounds changed from $0.00079\text{--}0.35$ to **$0.001\text{--}0.37$**
- Wavelength dependence of Φ for salicylic acid changed from 0.35 at 295 nm and 0.15 at 250 nm to **0.37 at 295 nm and 0.18 at 250 nm** .
- Distinct minima of coniferyl alcohol changed from 300 nm: 0.06, 250 nm: 0.11, 315 nm: 0.16 to **$280\text{ nm: }0.07$, $250\text{ nm: }0.14$, $312\text{ nm: }0.17$**

- **Figure 4:** water depth changed from 30, 10, and 200 m (A–C, respectively) to **6 m, 30 m and 200 m (A–C, respectively)**.

PAGE 8. RESULTS. SPECTRAL MATCHING OF ORGANIC COMPOUNDS WITH PARAFAC SPECTRA

- List of potential matches for organic compounds changed from p-cresol, tryptophan, indole, L-dihydroxyphenylalanine, tyrosine, coumarin, salicylic acid, ferulic acid, and benzoic acid to **indole, p-cresol, L-diphenylalanine, tyrosine, tryptophan, vanillic acid, benzoic acid, syringic acid, and salicylic acid**
- Similarity of spectra changed from p-cresol and tryptophan, as well as indole and tyrosine to **p-cresol and tyrosine, as well as indole and tryptophan**

PAGE 8–9. DISCUSSION. DOM APPARENT FLUORESCENCE QUANTUM YIELDS. PARAGRAPH 1.

- Maximum Φ of organic compounds changed from 0.35 to **0.37**
- AQY of equimolar mixture of caffeine and salicylic acid changed from 0.0046 to **0.0054**
- Range of AQY of 1 mol L⁻¹ salicylic acid and 0.01 to 1 mol L⁻¹ caffeine changed from 0.15–0.0046 to **0.19–0.0054**
- AQY of mixture for mixture of caffeine and salicylic acid above 310 nm changed from 0.35 to **0.37**

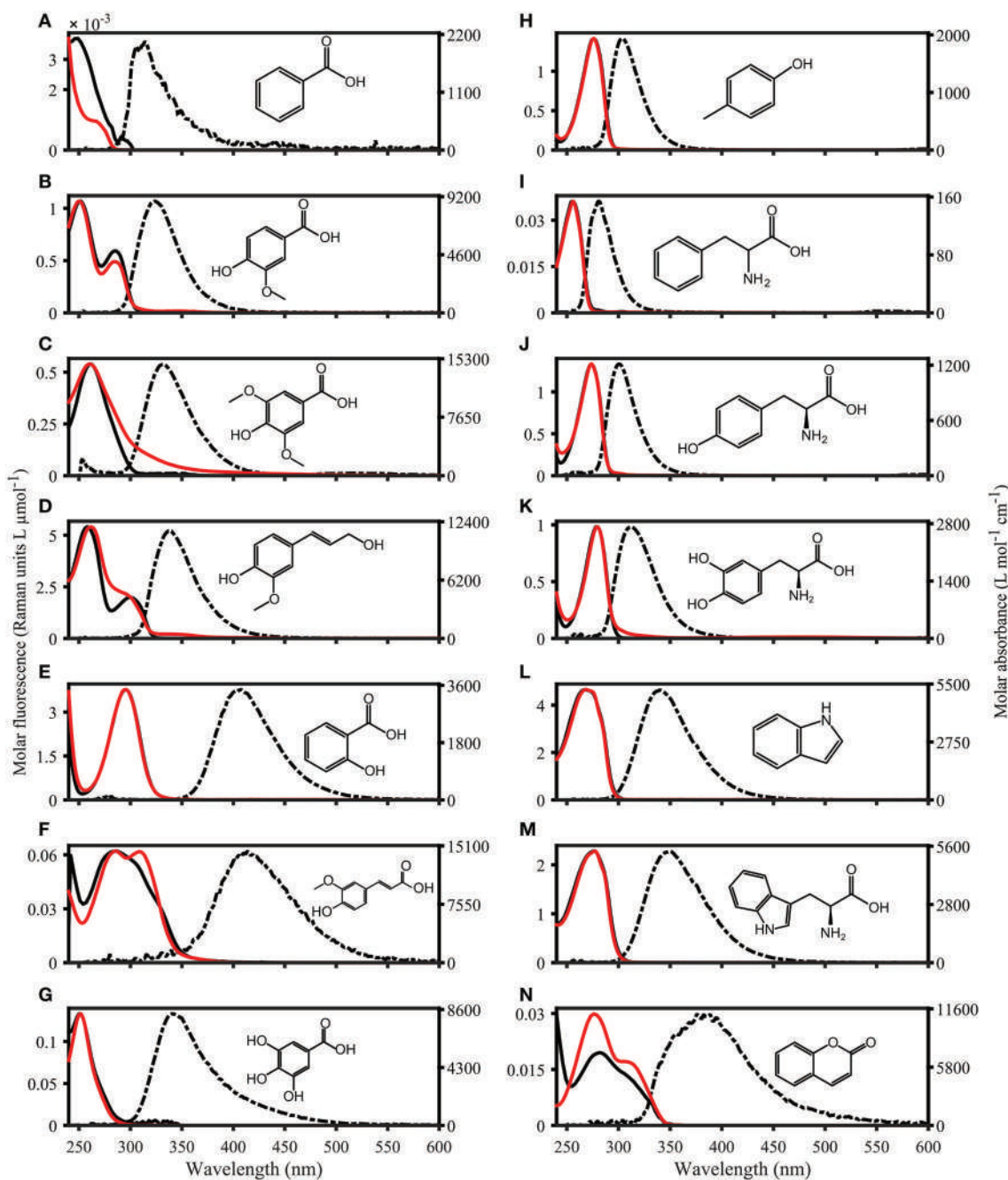


FIGURE 3 | Absorbance and Fluorescence spectra of organic compounds dissolved in water with 1 mmol L^{-1} PO_4 buffer (pH 7.5). The molar absorptivity is shown as a solid red line, excitation loadings are solid black lines, and emission loadings are dashed black lines. **(A–G)** Benzoic acid, vanillic acid, syringic acid, coniferyl alcohol, salicylic acid, ferulic acid, gallic acid. **(H–N)** p-Cresol, phenylalanine, tyrosine, dihydroxyphenylalanine, indole, tryptophan, coumarin.

PAGE 9. DISCUSSION. DOM APPARENT FLUORESCENCE QUANTUM YIELDS. PARAGRAPH 2.

- Average AQY at 350 nm changed from 0.011 ± 0.003 to 0.012 ± 0.004
- Figure 5A legend: Recalculation eliminated outlier at 197 m

PAGE 10–11. DISCUSSION. METHOD COMPARISON: QUANTUM YIELD CALCULATIONS. PARAGRAPH 4.

- %-difference between reference study and this study for optical properties of salicylic acid changed from 1.3, 2.9, and 0.4 (molar absorbance, Φ , and Stokes shift, respectively) to

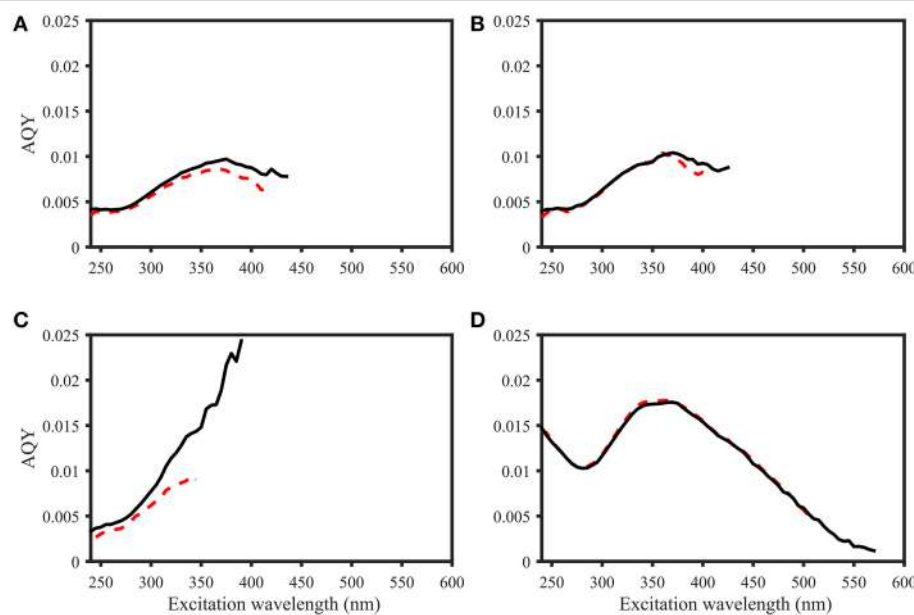


FIGURE 4 | Comparison of AQY calculations for four samples. Black line: Zero-intercept approach. Red dashed line: Variable-intercept approach. **(A–C)** Norwegian shelf DOM, water depth: 6, 30, and 200 m (**A–C**, respectively). **(D)** 2.5 mg L^{-1} Suwannee River XAD-8 fulvic acid extract. Figures do not include error bars for ease of viewing, but in all cases, AQY values of the two calculation approaches were within the precision estimates.

- 1.3, 2.7, and 0.3 (molar absorbance, Φ , and Stokes shift, respectively).**
- Φ of phenylalanine changed from 0.018 to 0.039. This matches previously published values (Feitelson, 1964). Therefore, the last three sentences of paragraph 4 are redundant.
- Table 2:** The erroneous spectral correction factors resulted in slightly inaccurate peak shapes for many organic compounds. This affected similarity scores between organic compounds such that some previously-matched PARAFAC components were excluded, while new hits were added to the table.

PAGE 13. DISCUSSION. LINKING OPTICAL AND CHEMICAL PROPERTIES. PARAGRAPH 1.

- Range of molar fluorescence and absorbance of a 1 nmol L^{-1} equivalent changed from 35×10^{-5} – 0.0036 m^{-1} , and 25×10^{-5} – 0.038 Raman units to 3.5×10^{-5} to 0.0036 m^{-1} for absorbance, and 2.1×10^{-6} to 0.0052 Raman units

- **Figure 9 legend:** AQY decrease changed from 0.15– 0.0046 changed to 0.19 – 0.0054

AUTHOR CONTRIBUTIONS

All authors (UW, KM, and CS) contributed substantially to the text of the submitted corrigendum. UW performed the data analysis and correction, CS and KM assisted during the correction process.

FUNDING

This work is supported by Technical University of Denmark and Chalmers Technical University Nordic5Tech collaboration. CS would like to acknowledge the Danish Research Council for Independent Research (DFF 1323- 00336), and KM acknowledges funding by the Swedish Research Council for Environment, Agricultural Sciences and Spatial Planning (FORMAS grant 2013-1214).

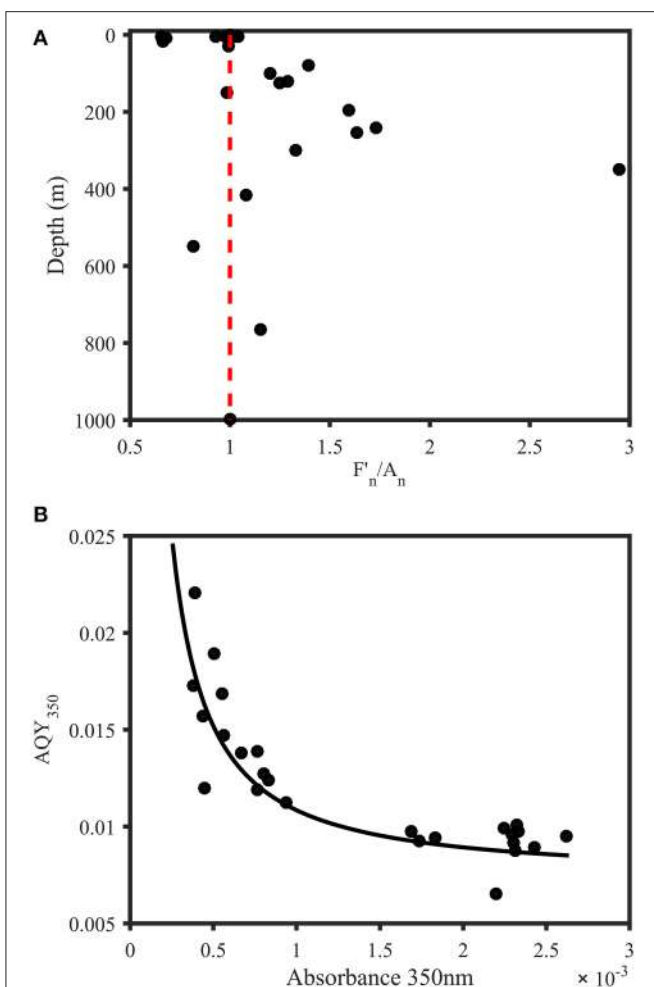


FIGURE 5 | Trends in AQYs of natural samples from the Norwegian shelf and Skagerrak. (A) Depth profile of F'_{350}/A_{350} divided by A_{350} (both normalized to station maximum) for samples from 11 stations in the Norwegian Sea and Skagerrak ($n = 28$). Red line indicates a ratio of 1 and represents equal relative contribution of fluorescence and absorbance. Subsurface waters were characterized by a strong fluorescence contribution, with the exception of one sample with abnormally high absorbance (548 m). Surface waters either showed equal FDOM and CDOM levels or dominant CDOM absorbance contribution. **(B)** AQY vs. absorbance at 350 nm. The black line represents a power fit ($a \times a_{350\text{nm}}^b + c$, $a = 9.821 \times 10^{-6}$, $b = -1.181$, $c = 0.0074$, $R^2 = 0.75$).

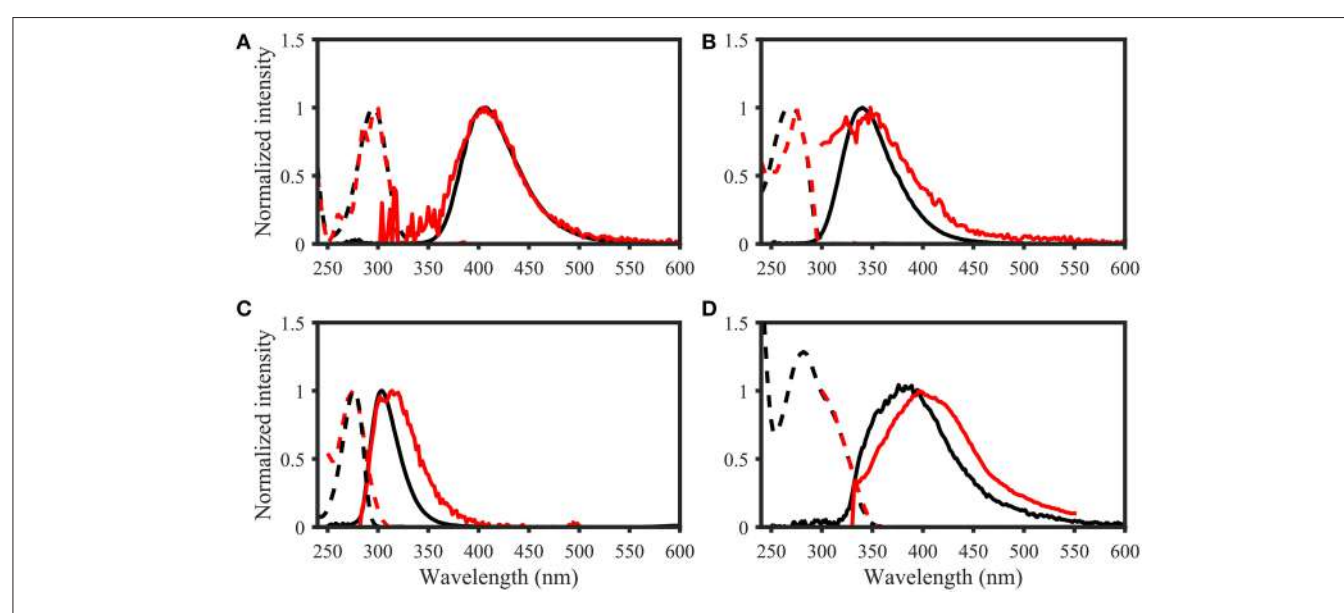
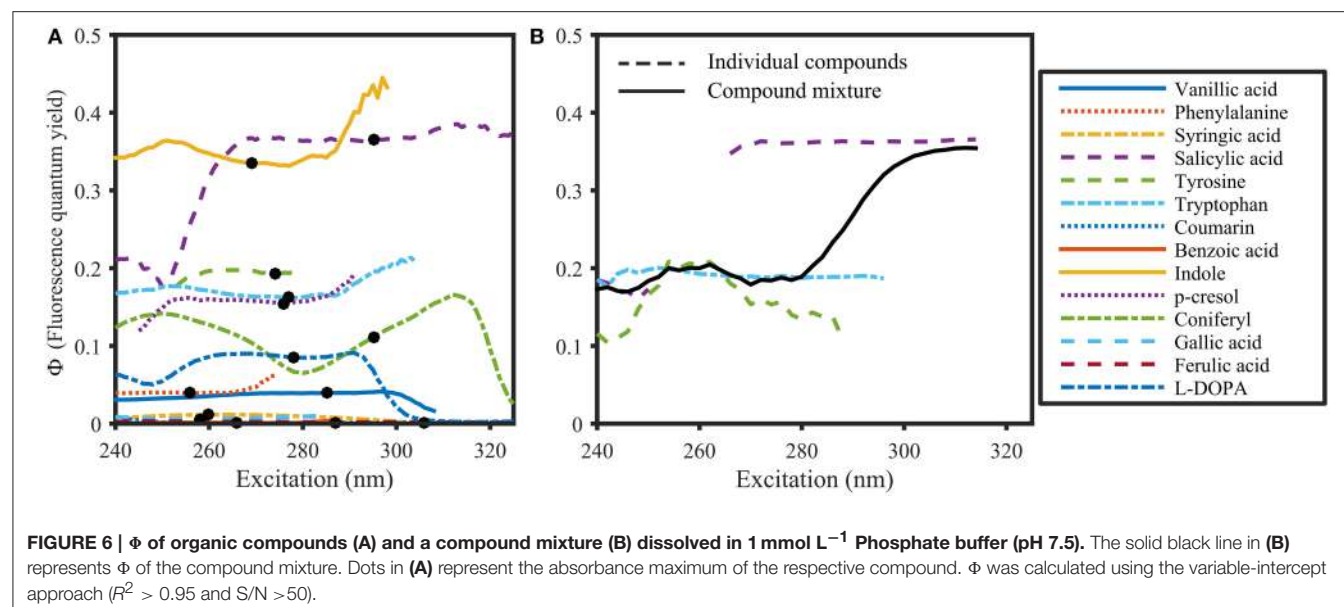


FIGURE 7 | Examples of spectral matching between PARAFAC components in the OpenFluor database with organic compounds. Dashed lines represent excitation loadings, solid lines show emission loadings. Organic compounds are shown in black, PARAFAC components in red. (A) Salicylic acid against component 5 from Kowalcuk et al. (2013), (B) Indole against component 3 from Kowalcuk et al. (2013), (C) p-cresol against component 3 from Murphy et al. (2011), (D) Coumarin against component 2 from Søndergaard et al. (2003).

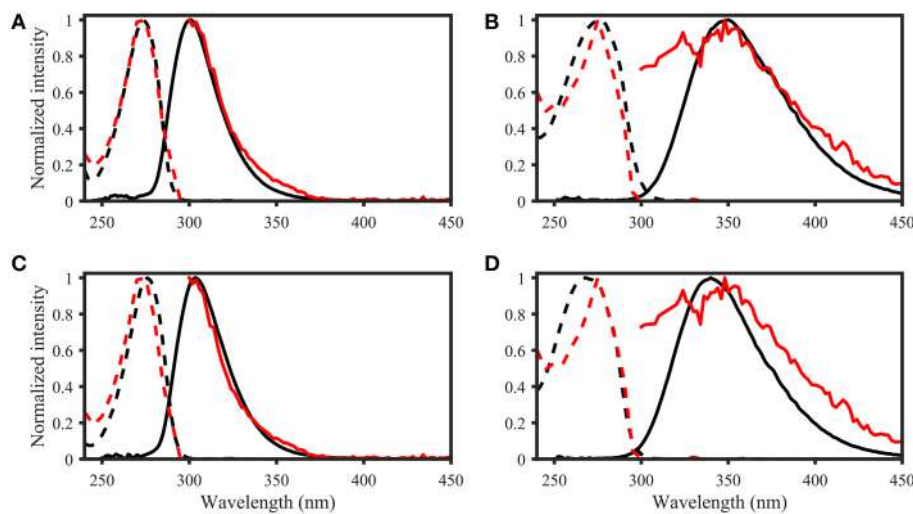


FIGURE 8 | OpenFluor matches of (A) tyrosine, (B) tryptophan, (C) p-cresol, and (D) indole (all in black) with PARAFAC components (all in red) from Kowalcuk et al. (2013). Dashed lines represent excitation loadings, solid lines show emission loadings. Tryptophan and indole, as well as tyrosine and p-cresol yield matches with the same PARAFAC component.

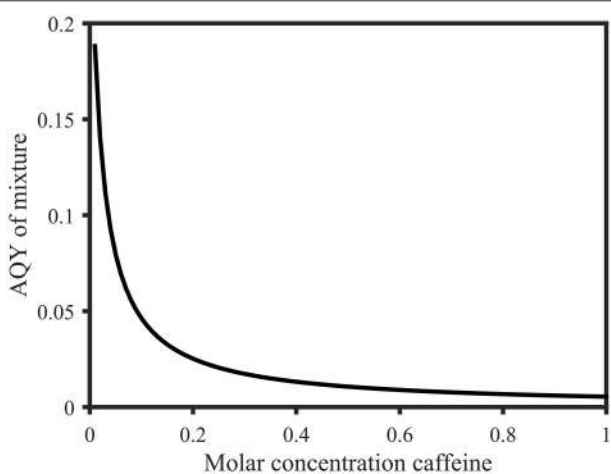


FIGURE 9 | Calculated apparent quantum yields of a mixture of 1 mol L^{-1} salicylic acid solution with variable molar parts of caffeine (0.01 mol L^{-1} to 1 mol L^{-1}) at 258 nm . The apparent quantum yield decreases from 0.19 (0.01 mol L^{-1} caffeine) to 0.0054 (1 mol L^{-1} caffeine). Calculations were based on Eq. 5 and are explained in the Supplementary Material.

REFERENCES

- Feitelson, J. (1964). On the mechanism of fluorescence quenching. Tyrosine and similar compounds. *J. Phys. Chem.* 68, 391–397. doi: 10.1021/j100784a033
- Jørgensen, L., Stedmon, C. A., Kragh, T., Markager, S., Middelboe, M., and Søndergaard, M. (2011). Global trends in the fluorescence characteristics and distribution of marine dissolved organic matter. *Mar. Chem.* 126, 139–148. doi: 10.1016/j.marchem.2011.05.002
- Kowalcuk, P., Tilstone, G. H., Zablocka, M., Röttgers, R., and Thomas, R. (2013). Composition of dissolved organic matter along an Atlantic Meridional Transect from fluorescence spectroscopy and Parallel Factor Analysis. *Mar. Chem.* 157, 170–184. doi: 10.1016/j.marchem.2013.10.004
- Murphy, K. R., Bro, R., and Stedmon, C. A. (2014). “Chemometric analysis of organic matter fluorescence,” in *Aquatic Organic Matter Fluorescence*, eds P. Coble, A. Baker, J. Lead, D. Reynolds, and R. Spencer (New York, NY: Cambridge University Press), 339–375.
- Murphy, K. R., Hamblly, A., Singh, S., Henderson, R. K., Baker, A., Stuetz, R., et al. (2011). Organic matter fluorescence in municipal water recycling schemes: Toward a unified PARAFAC model. *Environ. Sci. Technol.* 45, 2909–2916. doi: 10.1021/es103015e
- Murphy, K. R., Ruiz, G. M., Dunsmuir, W. T. M., and Waite, T. D. (2006). Optimized parameters for fluorescence-based verification of ballast water exchange by ships. *Environ. Sci. Technol.* 40, 2357–2362. doi: 10.1021/es0519381
- Murphy, K. R., Stedmon, C. A., Waite, T. D., and Ruiz, G. M. (2008). Distinguishing between terrestrial and autochthonous organic matter sources in marine environments using fluorescence spectroscopy. *Mar. Chem.* 108, 40–58. doi: 10.1016/j.marchem.2007.10.003
- Osburn, C. L., and Stedmon, C. A. (2011). Linking the chemical and optical properties of dissolved organic matter in the Baltic-North Sea transition zone to differentiate three allochthonous inputs. *Mar. Chem.* 126, 281–294. doi: 10.1016/j.marchem.2011.06.007
- Seredyńska-Sobecka, B., Stedmon, C. A., Boe-Hansen, R., Waul, C. K., and Arvin, E. (2011). Monitoring organic loading to swimming pools by fluorescence excitation-emission matrix with parallel factor analysis (PARAFAC). *Water Res.* 45, 2306–2314. doi: 10.1016/j.watres.2011.01.010
- Søndergaard, M., Stedmon, C. A., and Borch, N. H. (2003). Fate of terrigenous dissolved organic matter (DOM) in estuaries: aggregation and bioavailability. *Ophelia* 57, 161–176. doi: 10.1080/00785236.2003.10409512
- Stedmon, C. A., and Markager, S. (2005a). Resolving the variability of dissolved organic matter fluorescence in a temperate estuary and its catchment using PARAFAC analysis. *Limnol. Oceanogr.* 50, 686–697. doi: 10.4319/lo.2005.50.2.00686
- Stedmon, C. A., and Markager, S. (2005b). Tracing the production and degradation of autochthonous fractions of dissolved organic matter using fluorescence analysis. *Limnol. Oceanogr.* 50, 1415–1426. doi: 10.4319/lo.2005.50.5.1415
- Stedmon, C. A., Markager, S., Tranvik, L., Kronberg, L., Slätis, T., and Martinsen, W. (2007). Photochemical production of ammonium and transformation of dissolved organic matter in the Baltic Sea. *Mar. Chem.* 104, 227–240. doi: 10.1016/j.marchem.2006.11.005
- Stedmon, C. A., Thomas, D. N., Papadimitriou, S., Granskog, M. A., and Dieckmann, G. S. (2011). Using fluorescence to characterize dissolved organic matter in Antarctic sea ice brines. *J. Geophys. Res. Biogeosci.* 116, 1–9. doi: 10.1029/2011JG001716
- Walker, S. A., Amon, R. M. W., Stedmon, C. A., Duan, S., and Louchouarn, P. (2009). The use of PARAFAC modeling to trace terrestrial dissolved organic matter and fingerprint water masses in coastal Canadian Arctic surface waters. *J. Geophys. Res. Biogeosci.* 114, 1–12. doi: 10.1029/2009JG000990
- Yamashita, Y., Boyer, J. N., and Jaffé, R. (2013). Evaluating the distribution of terrestrial dissolved organic matter in a complex coastal ecosystem using fluorescence spectroscopy. *Cont. Shelf Res.* 66, 136–144. doi: 10.1016/j.csr.2013.06.010
- Yamashita, Y., Kloeppel, B. D., Knoepp, J., Zausen, G. L., and Jaffé, R. (2011a). Effects of Watershed History on Dissolved Organic Matter Characteristics in Headwater Streams. *Ecosystems* 14, 1110–1122. doi: 10.1007/s10021-011-9469-z
- Yamashita, Y., Panton, A., Mahaffey, C., and Jaffé, R. (2011b). Assessing the spatial and temporal variability of dissolved organic matter in Liverpool Bay using excitation-emission matrix fluorescence and parallel factor analysis. *Ocean Dyn.* 61, 569–579. doi: 10.1007/s10236-010-0365-4
- Yamashita, Y., Scinto, L. J., Maie, N., and Jaffé, R. (2010). Dissolved organic matter characteristics across a subtropical wetland's landscape: application of optical properties in the assessment of environmental dynamics. *Ecosystems* 13, 1006–1019. doi: 10.1007/s10021-010-9370-1

Conflict of Interest Statement: The authors declare that the research was conducted in the absence of any commercial or financial relationships that could be construed as a potential conflict of interest.

The Guest Associate Editor CO declares that, despite co-authoring a paper with author CAS, the review process was handled objectively and no conflict of interest exists.

Copyright © 2016 Wünsch, Murphy and Stedmon. This is an open-access article distributed under the terms of the Creative Commons Attribution License (CC BY). The use, distribution or reproduction in other forums is permitted, provided the original author(s) or licensor are credited and that the original publication in this journal is cited, in accordance with accepted academic practice. No use, distribution or reproduction is permitted which does not comply with these terms.



Studies on Hydroxyl Radical Formation and Correlated Photoflocculation Process Using Degraded Wood Leachate as a CDOM Source

Luni Sun and Kenneth Mopper *

Department of Chemistry and Biochemistry, Old Dominion University, Norfolk, VA, USA

OPEN ACCESS

Edited by:

Christopher Osburn,
North Carolina State University, USA

Reviewed by:

Cristina Sobrino,
University of Vigo, Spain

Leanne C Powers,
Skidaway Institute of Oceanography,
USA

*Correspondence:

Kenneth Mopper
kmopper@odu.edu

Specialty section:

This article was submitted to
Marine Biogeochemistry,
a section of the journal
Frontiers in Marine Science

Received: 29 September 2015

Accepted: 14 December 2015

Published: 11 January 2016

Citation:

Sun L and Mopper K (2016) Studies on Hydroxyl Radical Formation and Correlated Photoflocculation Process Using Degraded Wood Leachate as a CDOM Source. *Front. Mar. Sci.* 2:117.
doi: 10.3389/fmars.2015.00117

In this study, we examined hydroxyl radical ($\bullet\text{OH}$) formation with respect to photoreactivity of colored dissolved organic matter (CDOM), the Fenton reaction, and photoflocculation using leachate from decaying wood. The relationship between $\bullet\text{OH}$ photoproduction rate and leachate optical properties (UV-visible absorption and fluorescence excitation-emission matrices (EEMS)) was studied during irradiation using a UV solar simulator. The results showed that the $\bullet\text{OH}$ photochemical formation rate is strongly related to humic-like fluorescence as characterized by parallel factor analysis (PARAFAC), and that these fluorescence components are more photolabile than most of the other CDOM components. Fourier transform infrared spectroscopy (FT-IR) indicated the photodegradation of lignin-related structures. To examine the role of iron and $\bullet\text{OH}$ in the photoflocculation process, Fe speciation (particulate Fe, organically-complexed Fe(II), organically-complexed Fe(III), free Fe(II), and free Fe(III)) were measured in the leachate samples amended with Fe. The addition of Fe accelerated $\bullet\text{OH}$ production substantially, and Fe was photochemically cycled between Fe(II) and Fe(III). The photodegradation of iron complexing ligands appears to play an important role in DOM photoflocculation.

Keywords: hydroxyl radical, CDOM, EEMS, iron, photoflocculation

INTRODUCTION

The hydroxyl radical ($\bullet\text{OH}$) is a highly reactive oxygen species that is formed by photochemical reactions in natural waters (Buxton et al., 1988; Vaughan and Blough, 1998). It not only reacts with a variety of organic and inorganic compounds, but can also impact aquatic organisms, i.e., damaging cells and inducing excretion of protective slime (Mague et al., 1980; Zlotnik and Dubinsky, 1989; He and Häder, 2002). The photo-Fenton reaction and dissolved organic matter (DOM) photoreactions are two of its major sources (Mostafa et al., 2013). In seawater and high DOM freshwaters, DOM photoreactions appear to be the main source for $\bullet\text{OH}$. There are two known $\bullet\text{OH}$ production pathways from DOM: a H_2O_2 dependent pathway where the H_2O_2 is formed from DOM (Vione et al., 2006), and an H_2O_2 independent pathway (Page et al., 2011). In the latter pathway, the sources and mechanisms of $\bullet\text{OH}$ photoproduction from DOM are still unknown.

In the photo-Fenton reaction, Fe(II) reacts with H₂O₂ to yield •OH and Fe(III). The latter is then reduced to Fe(II), mainly through ligand to metal charge transfer (LMCT) reactions with DOM (Scott et al., 1998; Klapper et al., 2002; Barbeau, 2006), and through the reduction by HO₂/O₂⁻ (Voelker et al., 1997). Both inorganic and organically-complexed Fe(II), in which the Fe is usually bound to the phenolic and carboxyl groups (Baruah et al., 1981), take part in the Fenton reaction. Although organically-complexed Fe(II) is less reactive with H₂O₂ than inorganic Fe(II) (Miller et al., 2012), it is environmentally important because •OH may not be produced from the oxidation of inorganic Fe(II) under circum-neutral conditions (Miller et al., 2012), and the inorganic Fe(II) concentration is a small percentage of total Fe (Emmenegger et al., 2001; Shiller et al., 2006).

Several studies have shown that Fe and DOM photochemistries are involved in the photoflocculation process (Zepp et al., 1992; Gao and Zepp, 1998; Helms et al., 2013a), which may be important in transformation and transportation of DOM and particulate organic matter (POM) from rivers to the ocean (Helms et al., 2013a; Chen et al., 2014). Gao and Zepp (1998) reported that dark-colored particles formed in river samples after 3 days irradiation, and that the particles accounted for 45% of the total iron and 13% of the total organic carbon. Kopáček et al. (2005) proposed the photoflocculation pathway proceeds by iron mediated photodegradation of organic iron-binding ligands causing release of inorganic iron to form insoluble hydroxides. Chen et al. (2014) further confirmed that the DOM-associated Fe is converted to insoluble Fe(III) oxyhydroxides. Shiller et al. (2006) showed that organically-complexed Fe is released during photo-oxidation of low molecular-weight DOM, followed by precipitation of the released Fe as colloidal Fe(III) oxyhydroxides.

It is currently not known if •OH produced from DOM and Fenton reactions plays a role in photoflocculation processes. Therefore, a major goal of this study was to examine •OH formation with respect to the Fenton reaction and DOM photoreactions and to determine their potential impact on photoflocculation. We estimated time-course •OH photoformation rates in Fe-poor leachates of decayed wood using near-instantaneous •OH formation rates. We chose to study wood leachate because it can be an important source for DOM in natural waters (Kalbitz et al., 2000; Spencer et al., 2008; Sun et al., 2014), contains colored DOM (CDOM), and very low iron concentrations. The latter is important because it allowed the effects of added Fe to be readily examined. To elucidate the possible sources for •OH photochemical formation from DOM, DOM optical properties, i.e., UV-visible absorption spectra, specific UV absorption (SUVA), fluorescence excitation-emission matrices (EEMS), and Fourier transform infrared spectroscopy (FT-IR), were measured for the irradiated Fe-poor wood leachate. Furthermore, to study the role of •OH and iron in the photoflocculation process, Fe speciation (particulate Fe, organically-complexed Fe(II), organically-complexed Fe(III), free Fe(II), and free Fe(III)) was measured in the irradiated sample with Fe addition.

EXPERIMENTAL SECTION

Materials

Phenol (purity grade >99%), benzene (HPLC grade), ferrozine (97%), hydroxylamine hydrochloride (%), ammonium acetate (99%), sodium acetate (99%), and ferric chloride (99%) were obtained from Sigma-Aldrich; the iron standard solution was made from ferric nitrate in 2 % (v/v) nitric acid (1000 ppm, Certified, Fisher Chemical), and ferrous ammonium sulfate hexahydrate was obtained from Fisher; methanol (HPLC grade) was obtained from Acros; and Maxi-Clean 600 mg SCX cation solid phase extraction (SPE) cartridges were obtained from Grace. Ultra-pure water (Milli-Q water) was used for solution preparation. All glassware was acid soaked and pre-combusted (450°C).

Sample Description

The decayed wood sample was collected near Portsmouth Ditch in the Great Dismal Swamp (Chesapeake VA, USA). This area is covered by mainly maple gum (http://www.usgs.gov/climate_landuse/land_carbon/default.asp). A high S/V ratio (2.8), defined as the total mass of syringaldehyde, acetosyringone, and syringic acid divided by the total mass of vanillin, acetovanillone, and vanillic acid measured by CuO HPLC method (Sun et al., 2015a), indicated that the wood sample is angiosperm (Hedges and Mann, 1979). The sample was visually highly degraded. The sample was oven-dried at 60°C for 24 h, crushed into powder by a mortar and pestle to pass through a 600 µm sieve, then a 5.0 g sample was leached in 1.0 L Milli-Q water by continuous mixing overnight at room temperature. The particles were removed by filtration through a pre-combusted 0.7 µm GF/F filter (Whatman), followed by a 0.1 µm capsule filter (Polycap TC, Whatman). Dissolved organic carbon (DOC) and total dissolved nitrogen (TDN) were 12 ppm and 0.5 ppm, respectively. The pH of the wood leachate was 4.3. To examine the effect of iron on the •OH formation rate, 20 µM FeCl₃ (final concentration) was added to an aliquot of wood leachate, and the pH was adjusted to the original pH of 4.3. Such high iron concentrations are typical of many DOM-rich natural waters, such as found in the Satilla River and Estuary and the Great Dismal Swamp (White et al., 2003; Chen et al., 2014; Sun et al., 2014). The sample was kept in the dark for 24 h to complete organic-iron complex interaction, and then filtered with a GF/F filter.

Irradiations

The iron unamended and amended samples were placed into 500 mL round-bottom quartz flasks in duplicates. The samples were kept oxygenated by periodic shaking in air, and were irradiated at 22 ± 2°C using a solar simulator. The solar simulator provided 127% of DOM photobleaching occurring under winter mid-day natural sunlight at 36.89°N latitude, which was described elsewhere (Minor et al., 2007; Sun et al., 2014). Some flasks were wrapped in foil and kept as dark controls. At each time point, irradiated and dark control samples were subsampled. •OH formation rates, pH, absorbance, EEMS and Fe speciation (particulate Fe (PFe), organically-complexed Fe (OFe), free Fe (FFe), Fe(II), and Fe(III)) were measured immediately.

The subsamples for DOC/TDN were acidified and stored (4°C) for later analysis. The subsamples for FT-IR analysis were freeze-dried.

•OH Formation Rates

Benzene was used as the •OH probe because it has a higher selectivity than other commonly used probes, such as benzoic acid (Vione et al., 2010). The •OH formation rate at each test time point was determined by irradiating 30 mL subsamples in quartz tubes in the presence of the benzene probe (3 mM) for ≤ 2 h. This method yields a more accurate estimate of the •OH formation rate than leaving the probe in the sample for the entire irradiation period (Sun et al., 2014). DOC loss was measured in one tube with no probe in order to calibrate •OH formation rates in the tube relative to the round-bottom flask.

The •OH formation rate R was calculated as:

$$R = \frac{R_{ph} \times F}{Y}$$

Where R_{ph} is the observed photo-formation rate of phenol from the reaction of •OH with benzene, which was measured by HPLC; Y is the yield of phenol formed per benzene molecule oxidized by •OH; we used the value of $69.3 \pm 2.2\%$ (Sun et al., 2014); F is a calibration factor, which was evaluated by competition kinetics using a series of different benzene concentrations as described in detail by Zhou and Mopper (1990).

Dissolved Organic Carbon (DOC) and Total Dissolved Nitrogen (TDN)

DOC and TDN were measured using high temperature (720°C) catalytic combustion on a Shimadzu TOC-V-CPH carbon analyzer. Potassium hydrogen phthalate (KHP) and KNO_3 were used to make calibration curves to quantify the DOC and TDN concentrations respectively.

Optical Properties

UV-visible absorption spectra were measured by UV-vis absorbance (200–700 nm in 1-nm intervals) using an Agilent 8453 diode array spectrophotometer with a 1 cm quartz cuvette (Helms et al., 2008). Strongly absorbing samples were diluted prior to measurement to ensure linear response. First derivative UV-visible absorption spectra were obtained as described in Helms et al. (2014). SUVA₂₅₄, SUVA₂₈₀, and SUVA₃₀₀ were determined by dividing the absorbance at 254, 280, and 300 nm respectively by the DOC concentration.

Fluorescence EEMS were measured as described in Murphy et al. (2010). Raw EEMS were collected using a Cory Eclipse fluorometer with a 1 cm quartz cuvette at specified excitation wavelengths (λ_{ex}) of 240–450 nm in 5-nm intervals and emission wavelengths (λ_{em}) of 300–600 nm in 2-nm intervals; blank EEMS and Raman scans ($\lambda_{ex} = 350$ nm, $\lambda_{em} = 365$ –450 nm in 0.5 nm intervals) were obtained from Milli-Q water, and emission scans ($\lambda_{ex} = 350$ nm) were obtained from a quinine sulfate (QS) dilution series (0, 20, 50, 100 ppb) from a 1000 ppb working solution. Data was processed in MATLAB using the FDOMcorr toolbox (Murphy et al., 2010). EEMS were processed

by spectral correction, inner filter correction, Raman correction, and QS calibration, and then analyzed by PARAFAC using the DOMFluor toolbox (Stedmon and Bro, 2008). Fluorescence intensity is reported in Raman units (RU) (Murphy et al., 2010).

FT-IR analysis was conducted as described in Abdulla et al. (2010). One milligram sample was mixed with 100 mg pre-heated KBr and homogenized by a Wig-L-Bug grinding mill. Subsamples were then compressed by anvils to a disk. FT-IR spectra were collected using a Nicolet 370 FT-IR spectrometer equipped with purge gas generator unit. Spectra were collected with 200 scans and a resolution of 4 cm^{-1} . The FT-IR spectra were normalized to the integrated absorbance from 4000 to 500 cm^{-1} and multiplied by 1000 in order to account for minor concentration variations between samples. The FT-IR absorbance spectra were processed using OMNIC software with the second-order Savitzky-Golay method with 11 convolution points used to generate the second derivative of the spectra (Abdulla et al., 2010).

Iron Speciation

Fe speciation includes dissolved total Fe (DTFe), particulate total Fe (PTFe), dissolved strong organically-complexed Fe (OFe), and free Fe (FFe). Sub-samples were taken at different time points during the irradiation and $0.2\text{ }\mu\text{m}$ filtered (Gelman Sciences). PTFe was measured indirectly by subtracting DTFe at each time point from the initial DTFe. The FFe and OFe fractions were separated by SCX cation exchange cartridges (Tangen et al., 2002). SCX cartridges were employed because they are more convenient than loose resin (Tangen et al., 2002; Shiller et al., 2006). The cartridges were conditioned with 14 mL Milli-Q water, followed by 14 mL 0.4 M ammonium acetate buffer pH 4.5, and 4 mL of sample to rinse out the buffer. Since FFe is selectively bound to the SCX cartridges, the remaining Fe in eluate solution after SPE extraction was considered as OFe. FFe was calculated by subtracting the Fe concentration after SPE (OFe) from DTFe.

Fe(II) and Fe(III) were determined before and after SPE extraction by a modified ferrozine method (Viollier et al., 2000). Non-reduced sample absorbance for Fe(II), was measured by mixing 5.0 mL of sample, 500 μL 0.01 M ferrozine solution (prepared in 2 M ammonium acetate), 200 μL 5 M ammonium acetate, and standard addition with a range of 0–20 μM . The final pH was 5–6. DTFe was measured after reducing the sample by hydroxylamine hydrochloride (prepared in 2 M HCl). The dissolved Fe(III) concentration was calculated by subtracting Fe(II) from DTFe.

RESULTS AND DISCUSSION

•OH Formation Rates

During irradiation, the •OH formation rate was initially markedly higher in the presence of added Fe (Figure 1A). During the first hour, the •OH formation rate reached $1.3\text{ }\mu\text{M/h}$ in the Fe amended sample, which was about five times that of the original (unamended) sample ($0.25\text{ }\mu\text{M/h}$). However, in the Fe amended sample, the •OH formation rates dropped quickly with the occurrence of photoflocculation. Since each sample was run in duplicate, pooled relative standard deviation and pooled numbers (all eight time points) were used for statistical

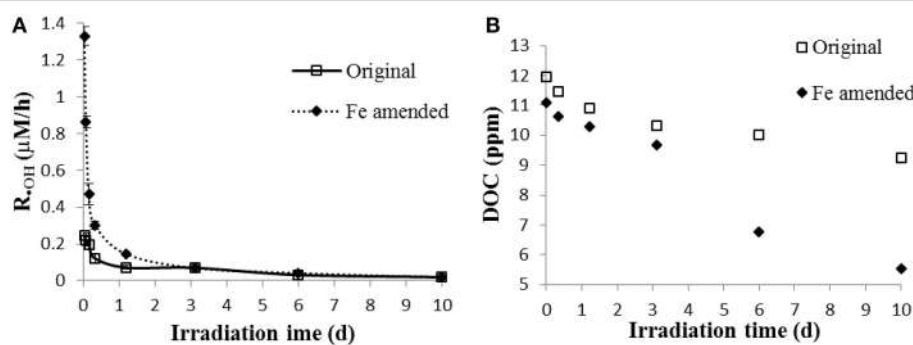


FIGURE 1 | (A) •OH formation rates; **(B)** dissolved organic carbon (DOC) in original and Fe amended aqueous leachates of degraded wood. The •OH formation rate was the mean value calculated from two measurements, and the error bars represent the range.

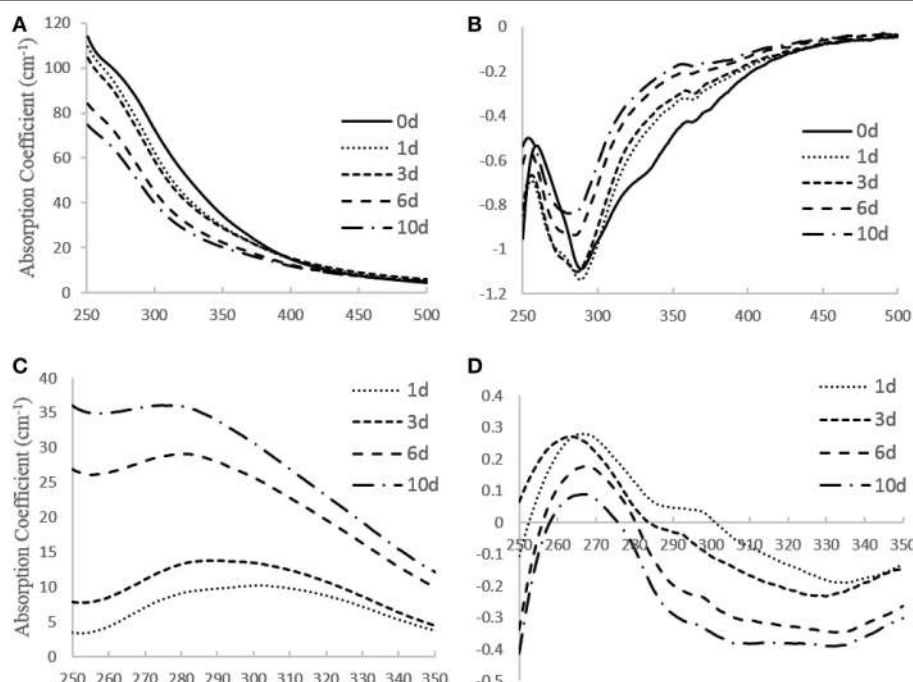


FIGURE 2 | (A) UV-visible absorption spectra, **(B)** first derivative absorption spectra, **(C)** difference spectra, **(D)** first derivative of difference spectra obtained for wood leachate during irradiation.

analysis. The difference in •OH formation rate between the Fe amended and unamended sample was significant during the first 2 days, and insignificant after day 3 (t -test, $p < 0.01$). DOC decreased faster in Fe amended sample than in the original sample. The DOC dropped by 23% in original sample, but 53% in Fe amended sample after 10 d of irradiation (Figure 1B), which indicates that Fe-associated photoreactions assist the mineralization, transformation and flocculation of DOM (Pullin et al., 2004; Molot et al., 2005).

Optical Properties of Wood Leachate

From the UV-visible absorption spectra (Figures 2A,B), the steepness of the first derivative absorption spectrum

around 280 nm decreases with increasing irradiation time (Figure 2B). This trend indicates that the short wavelength absorbing chromophores at ~ 280 nm, which are likely aromatic chromophores, are preferentially lost. This conclusion is supported by the slope ratio (S_R), which increased from 0.73 to 1.0 during the initial 8 h and stayed at ~ 1.0 for the remaining 10 days. An increase in slope ratio indicates loss of aromaticity (Helms et al., 2008). Moreover, the shift to the shorter wavelengths in the minimum in the first derivative spectrum during irradiation (Figure 2B), suggests that the degree of conjugation and/or molecular size also decreased during irradiation (Helms et al., 2008, 2013b). Difference spectra (Figure 2C) indicates that during the first day of the irradiation,

when $\cdot\text{OH}$ production was greatest (**Figure 1**), maximum photobleaching occurred at $\sim 300\text{--}310\text{ nm}$, as clearly indicated by the first derivative of the difference spectra (**Figure 2D**). Photobleaching then shifted to DOM chromophores that absorbed at $\sim 270\text{--}280\text{ nm}$ as the irradiation progressed (**Figures 2C,D**). These results suggest that chromophores

absorbing at $\sim 300\text{--}310$ are more photolabile than the remaining chromophores and that they may be mainly responsible for the initially high $\cdot\text{OH}$ production, as is supported by past studies (Vaughan and Blough, 1998; White et al., 2003) that showed the highest $\cdot\text{OH}$ apparent quantum yield is at 310 nm.

However, $\cdot\text{OH}$ formation rates normalized to DOC, SUVA₂₅₄, SUVA₂₈₀, and SUVA₃₀₀ decreased during the irradiation (**Figure 3**), indicating that $\cdot\text{OH}$ production is not simply correlated to DOC and absorbance. Also, the results indicate that the non-irradiated sample had the highest capability of photoproducing $\cdot\text{OH}$, and that the chromophoric sites within DOM responsible for $\cdot\text{OH}$ production were preferentially transformed and/or degraded (relative to the total aromaticity) during irradiation, and thus appear to be more photolabile, in agreement with the photobleaching results discussed above.

Fluorescence EEMS showed that the overall fluorescent intensity of the sample decreased markedly during irradiation (**Figure 4**). Three main fluorescent components were characterized in the sample by PARAFAC analyses (**Figure 5**): components 1 (ex/em < 250, 305/418) and 2 (ex/em 260, 340/460) are characterized as humic-like DOM (Fellman et al., 2010; Guo et al., 2011), while component 3 is characterized as tryptophan-like DOM (ex/em < 250, 280/350; Yamashita et al., 2008; Fellman et al., 2010; Guo et al., 2011). Components 1 and 2

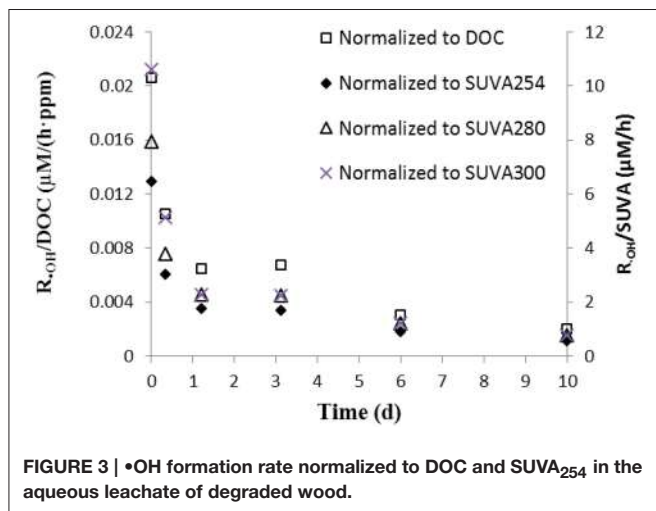


FIGURE 3 | $\cdot\text{OH}$ formation rate normalized to DOC and SUVA₂₅₄ in the aqueous leachate of degraded wood.

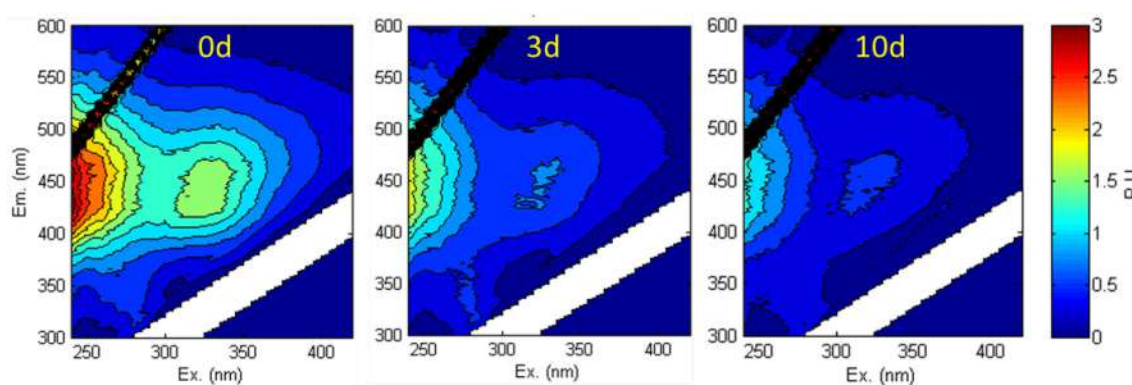


FIGURE 4 | Fluorescence EEMS of the aqueous leachate of the degraded wood sample at 0, 3, and 10 d irradiation.

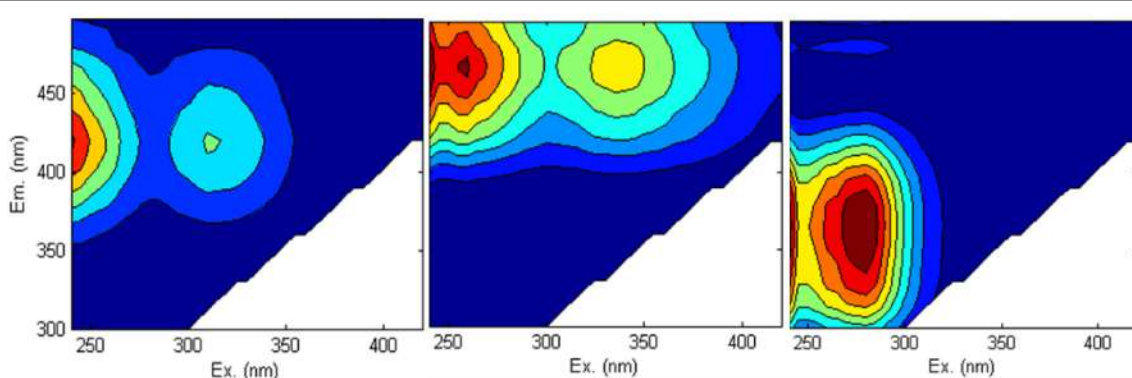


FIGURE 5 | Three components identified by PARAFAC analysis in all non-Fe-amended samples. Components 1 and 2 are humic-like DOM, and component 3 is tryptophan-like DOM.

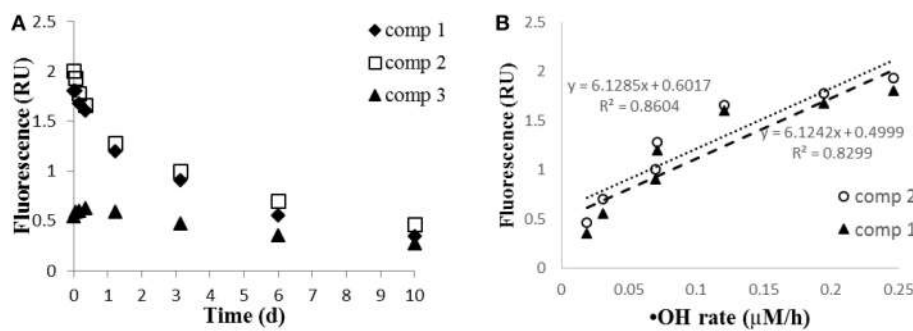


FIGURE 6 | (A) EEMS-PARAFAC components 1 and 2 (humic-like DOM), and component 3 (tryptophan-like DOM) during irradiation; **(B)** relationship of •OH formation rate ($\mu\text{M}/\text{h}$) to components 1 and 2.

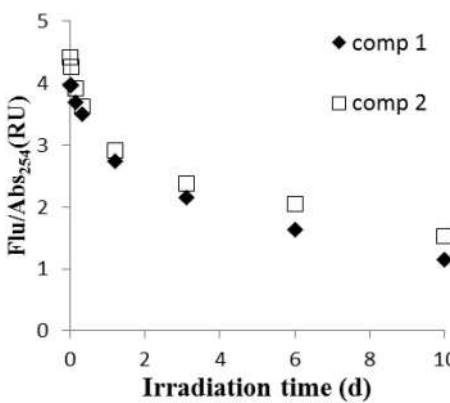


FIGURE 7 | The ratios of fluorescence (Flu) to absorbance at 254 nm (Abs_{254}) for component 1 and 2.

decreased while component 3 did not change significantly during the 10 day irradiation (Figure 6A). The decrease of humic-like components during irradiation is consistent with past studies (Ishii and Boyer, 2012; Xu and Jiang, 2013). Also, the results show that the •OH formation rate is positively correlated to humic-like components (component 1 and 2; $R^2 = \sim 0.83-0.86$; Figure 6B). The latter result is consistent with Lee et al. (2013) who showed that the •OH apparent quantum yield from the humic fraction in wastewater effluent organic matter was much higher than that from non-humic fraction.

From the ratio of fluorescence (Flu) to absorbance at 254 nm (Abs_{254}) (Figure 7), it is clear that humic fluorescence (FDOM) components (components 1 and 2) are 3–4 times more photolabile than most of the other CDOM components. In our sample, humic substances are primarily derived from lignin transformation (McDonald et al., 2004). From FT-IR spectroscopy (Figure 8), lignin-related structures, which correspond to bands are at 1518 cm^{-1} (vibration of aromatic ring) and 1242 cm^{-1} (C=O asymmetric stretching; Abdulla et al., 2010), decreased during irradiation. Also, the C=O stretching at $1720-1740\text{ cm}^{-1}$ decreased in intensity, indicating the conversion of organic acids into carboxylate and CO_2 (Rodríguez-Zúñiga et al., 2008). In a recent study (Sun et al., 2015b), we reported that simple phenolic acids and related

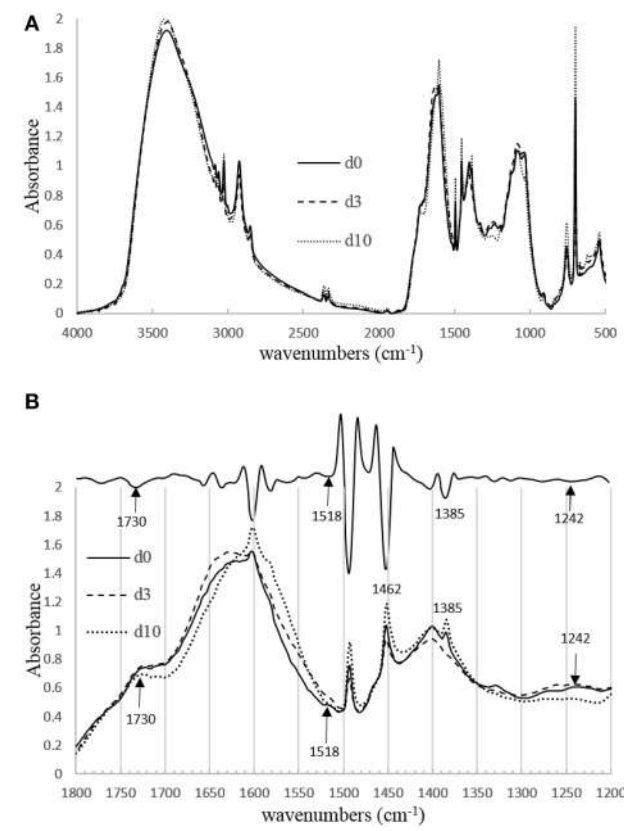


FIGURE 8 | (A) The region between 4000 and 500 cm^{-1} of the FT-IR spectra for the initial wood leachate sample and after 3 and 10 days of irradiation. **(B)** Bottom: The region between 1800 and 1200 cm^{-1} of the FT-IR spectra. Upper: second derivative FT-IR spectrum obtained from day 10 irradiation.

compounds can produce •OH radicals; these phenolic structures are widely present in lignin and humic substances and are thought to be important chromophoric sites within DOM. It should be pointed out that the DOM became progressively more aliphatic during the irradiations, as the bands at 1462 cm^{-1} (CH_3 asymmetric deformation) and 1385 cm^{-1} (CH_3 umbrella mode) increased during irradiation. The increase in aliphatic nature of the DOM will increase its tendency to flocculate during the irradiation (Helms et al., 2013a).

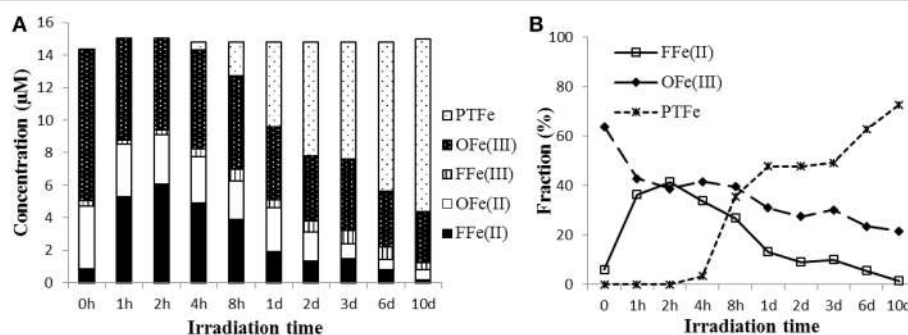


FIGURE 9 | (A) Particulate total Fe (PTFe), DOM-complexed Fe(II) (OFe(II)), DOM-complexed Fe(III) (OFe(III)), free Fe(II) (FFe(II)), free Fe(III) (FFe(III)); **(B)** FFe(II) and OFe(III), and PTFe fraction of TFe (%) in Fe amended aqueous leachate of degraded wood during irradiation. Note non-linearity of the time axis.

Fe Speciation in Fe Amended Wood Leachate

Optical properties were not determined for the Fe amended sample because Fe has a quenching effect on absorbance and fluorescence (Cabaniss, 1992; Pullin et al., 2007; Manciulea et al., 2009) and causes wavelength shifts in FT-IR absorbances (Abdulla et al., 2010). Our Fe speciation results indicate that Fe was initially present mainly as organically complexed Fe(III) in the aqueous phase (Figure 9A; Rue and Bruland, 1995; Powell and Wilson-Finelli, 2003). During the initial 2 h of the irradiation, the OFe(III) was partially converted to FFe(II), as evidenced by the drop in the OFe(III) fraction of TFe from 64 to 38%, while the FFe(II) fraction rose from 6 to 41% (Figure 9B). These results indicate a reduction of Fe(III) to Fe(II) probably via LMCT processes (Voelker et al., 1997; Klapper et al., 2002; Barbeau, 2006). Thus, Fe was rapidly cycling between Fe(II) and Fe(III) (White et al., 2003; Shiller et al., 2006). Simultaneously, the high •OH formation rate during the first hour ($\sim 1.3 \mu\text{M}/\text{h}$) and high initial H_2O_2 production (in a similar sample; Sun et al., 2014) indicate that the photo-Fenton reaction was the dominant source for the •OH radical initially.

Because the iron complexed organic ligands were continuously degraded during the irradiation, when the FFe(III) concentration exceeded the maximum soluble concentration, insoluble Fe(III) hydroxide and oxyhydroxides formed, which coprecipitated with and/or adsorbed organic matter. In addition, the Fenton reaction in the Fe amended wood leachate generated substantially more •OH than the sample without added Fe. Therefore, it is likely that •OH played a role in the precipitation of the iron. One may argue that the precipitation was mainly due to an increase of pH, which makes the Fe less soluble during the irradiation. The system initially was buffered by carboxylates but was later buffered by bicarbonate because carboxylates degraded while CO_2 accumulated during the irradiation. However, in our experiment, a pH change was not measurable during the first few hours and thus, initially, it would have had no effect on the observed flocculation. Humic substances within the sample contain high concentrations of hydroxyl and carboxyl groups (Figure 8; Sleighter and Hatcher, 2008), which can form strong complexes with Fe. The EEMS and FT-IR results suggest that these structures are preferably degraded, and it appears that the degradation of iron complexing ligands and •OH formation

are closely related. This conclusion is supported by Chen et al. (2014), who found the Fe/carbon molar ratios of DOM decreased while this ratio increased for POM using X-ray absorption spectra (XANES and EXAFS).

SUMMARY AND CONCLUSIONS

In the unamended wood leachate sample, DOM was the main source for •OH production, as other sources, such as nitrate and nitrite photolyses and the Fenton reaction, were negligible. The decrease of •OH formation rates normalized to DOC and SUVA indicates that the CDOM sites that produce •OH within DOM are more photolabile than the total DOM fraction. The difference absorbance spectra suggest that these photolabile sites absorb maximally at about 300–310 nm. These sites appear to be located within humic-substances, as supported by the finding that FDOM humic substances are more photolabile than most of the other CDOM components, and are strongly correlated to •OH formation.

In the Fe amended sample, Fe was initially present as mainly dissolved organic complexed Fe(III). During the irradiation, free Fe was released, probably through the photodegradation of Fe complexed organic ligands. When the free Fe(III) concentration exceeded the maximum soluble concentration of Fe(III)(oxy)hydroxides, flocculation occurred. In addition, •OH generated from the Fenton reaction may have played a key role in the precipitation (Waggoner et al., 2015), especially during the early part of the irradiation.

AUTHOR CONTRIBUTIONS

LS conceived, conducted the experiments, interpreted the data and co-wrote the paper. KM conceived the experiments, interpreted the data and co-wrote the paper.

ACKNOWLEDGMENTS

This research was supported by NSF grant OCE0850635 (to KM) awarded through the Chemical Oceanography Program. We thank Drs. Hongmei Chen and Abdulla Hussain for the assistance in sampling, and Anji Chen for assistance in the FT-IR measurements.

REFERENCES

- Abdulla, H. A., Minor, E. C., Dias, R. F., and Hatcher, P. G. (2010). Changes in the compound classes of dissolved organic matter along an estuarine transect: a study using FTIR and ¹³C NMR. *Geochim. Cosmochim. Acta* 74, 3815–3838. doi: 10.1016/j.gca.2010.04.006
- Barbeau, K. (2006). Photochemistry of organic iron (III) complexing ligands in oceanic systems. *Photochem. Photobiol.* 82, 1505–1516. doi: 10.1111/j.1751-1097.2006.tb09806.x
- Baruah, M. K., Upadhyay, M. C., Baishya, N. K., and Dutta, S. N. (1981). Interaction of iron with humic acid extracted from lignite. *Fuel* 60, 971–974. doi: 10.1016/0016-2361(81)90094-6
- Buxton, G. V., Greenstock, C. L., Helman, W. P., and Ross, A. B. (1988). Critical review of rate constants for reactions of hydrated electrons, hydrogen atoms and hydroxyl radicals. *Phys. Chem. Ref. Data* 17, 513–886. doi: 10.1063/1.555805
- Cabaniss, S. E. (1992). Synchronous fluorescence spectra of metal-fulvic acid complexes. *Environ. Sci. Technol.* 26, 1133–1139. doi: 10.1021/es50002a018
- Chen, H., Abdulla, H. A., Sanders, R. L., Myneni, S. C., Mopper, K., and Hatcher, P. G. (2014). Production of black carbon-like and aliphatic molecules from terrestrial dissolved organic matter in the presence of sunlight and iron. *Environ. Sci. Technol. Lett.* 1, 399–404. doi: 10.1021/ez5002598
- Emmenegger, L., Schönenberger, R., Sigg, L., and Sulzberger, B. (2001). Light-induced redox cycling of iron in circumneutral lakes. *Limnol. Oceanogr.* 46, 49–61. doi: 10.4319/lo.2001.46.1.0049
- Fellman, J. B., Hood, E., and Spencer, R. G. (2010). Fluorescence spectroscopy opens new windows into dissolved organic matter dynamics in freshwater ecosystems: a review. *Limnol. Oceanogr.* 55, 2452–2462. doi: 10.4319/lo.2010.55.6.2452
- Gao, H., and Zepp, R. G. (1998). Factors influencing photoreactions of dissolved organic matter in a coastal river of the southeastern United States. *Environ. Sci. Technol.* 32, 2940–2946. doi: 10.1021/es9803660
- Guo, W., Yang, L., Hong, H., Stedmon, C. A., Wang, F., Xu, J., et al. (2011). Assessing the dynamics of chromophoric dissolved organic matter in a subtropical estuary using parallel factor analysis. *Mar. Chem.* 124, 125–133. doi: 10.1016/j.marchem.2011.01.003
- He, Y.-Y., and Häder, D.-P. (2002). Involvement of reactive oxygen species in the UV-B damage to the cyanobacterium *Anabaena* sp. *J. Photochem. Photobiol. Biol.* 66, 73–80. doi: 10.1016/S1011-1344(01)00278-0
- Hedges, J. I., and Mann, D. C. (1979). The characterization of plant tissues by their lignin oxidation products. *Geochim. Cosmochim. Acta* 43, 1803–1807. doi: 10.1016/0016-7037(79)90028-0
- Helms, J. R., Mao, J., Schmidt-Rohr, K., Abdulla, H., and Mopper, K. (2013a). Photochemical flocculation of terrestrial dissolved organic matter and iron. *Geochim. Cosmochim. Acta* 121, 398–413. doi: 10.1016/j.gca.2013.07.025
- Helms, J. R., Mao, J., Stubbins, A., Schmidt-Rohr, K., Spencer, R. G., Hernes, P. J., et al. (2014). Loss of optical and molecular indicators of terrigenous dissolved organic matter during long-term photobleaching. *Aqua. Sci.* 76, 353–373. doi: 10.1007/s00027-014-0340-0
- Helms, J. R., Stubbins, A., Perdue, E. M., Green, N. W., Chen, H., and Mopper, K. (2013b). Photochemical bleaching of oceanic dissolved organic matter and its effect on absorption spectral slope and fluorescence. *Mar. Chem.* 155, 81–91. doi: 10.1016/j.marchem.2013.05.015
- Helms, J. R., Stubbins, A., Ritchie, J. D., Minor, E. C., Kieber, D. J., and Mopper, K. (2008). Absorption spectral slopes and slope ratios as indicators of molecular weight, source, and photobleaching of chromophoric dissolved organic matter. *Limnol. Oceanogr.* 53:955. doi: 10.4319/lo.2008.53.3.0955
- Ishii, S. K. L., and Boyer, T. H. (2012). Behavior of reoccurring PARAFAC components in fluorescent dissolved organic matter in natural and engineered systems: a critical review. *Environ. Sci. Technol.* 46, 2006–2017. doi: 10.1021/es2043504
- Kalbitz, K., Solinger, S., Park, J.-H., Michalzik, B., and Matzner, E. (2000). Controls on the dynamics of dissolved organic matter in soils: a review. *Soil Sci.* 165, 277–304. doi: 10.1097/00010694-200004000-00001
- Klapper, L., McKnight, D. M., Fulton, J. R., Blunt-Harris, E. L., Nevin, K. P., Lovley, D. R., et al. (2002). Fulvic acid oxidation state detection using fluorescence spectroscopy. *Environ. Sci. Technol.* 36, 3170–3175. doi: 10.1021/es0109702
- Kopáček, J., Klementová, Š., and Norton, S. A. (2005). Photochemical production of ionic and particulate aluminum and iron in lakes. *Environ. Sci. Technol.* 39, 3656–3662. doi: 10.1021/es048101a
- Lee, E., Glover, C. M., and Rosario-Ortiz, F. L. (2013). Photochemical formation of hydroxyl radical from effluent organic matter: role of composition. *Environ. Sci. Technol.* 47, 12073–12080. doi: 10.1021/es402491t
- Mague, T., Friberg, E., Hughes, D., and Morris, I. (1980). Extracellular release of carbon by marine phytoplankton; a physiological approach. *Limnol. Oceanogr.* 25, 262–279. doi: 10.4319/lo.1980.25.2.0262
- Manculea, A., Baker, A., and Lead, J. R. (2009). A fluorescence quenching study of the interaction of Suwannee River fulvic acid with iron oxide nanoparticles. *Chemos.* 76, 1023–1027. doi: 10.1016/j.chemosphere.2009.04.067
- McDonald, S., Bishop, A. G., Prenzler, P. D., and Robards, K. (2004). Analytical chemistry of freshwater humic substances. *Anal. Chim. Acta* 527, 105–124. doi: 10.1016/j.aca.2004.10.011
- Miller, C. J., Rose, A. L., and Waite, T. D. (2012). Hydroxyl radical production by H₂O₂-mediated oxidation of Fe (II) complexed by Suwannee River fulvic acid under circumneutral freshwater conditions. *Environ. Sci. Technol.* 47, 829–835. doi: 10.1021/es303876h
- Minor, E., Dalzell, B., Stubbins, A., and Mopper, K. (2007). Evaluating the photoalteration of estuarine dissolved organic matter using direct temperature-resolved mass spectrometry and UV-visible spectroscopy. *Aquat. Sci.* 69, 440–455. doi: 10.1007/s00027-007-0897-y
- Molot, L. A., Hudson, J. J., Dillon, P. J., and Miller, S. A. (2005). Effect of pH on photo-oxidation of dissolved organic carbon by hydroxyl radicals in a coloured, softwater stream. *Aquat. Sci.* 67, 189–195. doi: 10.1007/s00027-005-0754-9
- Mostofa, K. G., Liu, C.-Q., Sakugawa, H., Vione, D., Minakata, D., Saquib, M., et al. (2013). "Photoinduced generation of hydroxyl radical in natural waters," in *Photobiogeochemistry of Organic Matter*, eds K. M. G. Mostofa, T. Yoshioka, A. Mottaleb, and D. Vione (Berlin; Heidelberg: Springer), 209–272.
- Murphy, K. R., Butler, K. D., Spencer, R. G., Stedmon, C. A., Boehme, J. R., and Aiken, G. R. (2010). Measurement of dissolved organic matter fluorescence in aquatic environments: an interlaboratory comparison. *Environ. Sci. Technol.* 44, 9405–9412. doi: 10.1021/es102362t
- Page, S. E., Arnold, W. A., and McNeill, K. (2011). Assessing the contribution of free hydroxyl radical in organic matter-sensitized photohydroxylation reactions. *Environ. Sci. Technol.* 45, 2818–2825. doi: 10.1021/es2000694
- Powell, R. T., and Wilson-Finelli, A. (2003). Photochemical degradation of organic iron complexing ligands in seawater. *Aquat. Sci.* 65, 367–374. doi: 10.1007/s00027-003-0679-0
- Pullin, M. J., Anthony, C., and Maurice, P. A. (2007). Effects of iron on the molecular weight distribution, light absorption, and fluorescence properties of natural organic matter. *Environ. Eng. Sci.* 24, 987–997. doi: 10.1089/ees.2006.0040
- Pullin, M. J., Bertilsson, S., Goldstone, J. V., and Voelker, B. M. (2004). Effects of sunlight and hydroxyl radical on dissolved organic matter: bacterial growth efficiency and production of carboxylic acids and other substrates. *Limnol. Oceanogr.* 49, 2011–2022. doi: 10.4319/lo.2004.49.6.2011
- Rodríguez-Zúñiga, U. F., Milori, D. M. B. P., da Silva, W. T. L., Martin-Neto, L., Oliveira, L. C., and Rocha, J. C. (2008). Changes in optical properties caused by UV-Irradiation of aquatic humic substances from the amazon river basin: seasonal variability evaluation. *Environ. Sci. Technol.* 42, 1948–1953. doi: 10.1021/es702156n
- Rue, E. L., and Bruland, K. W. (1995). Complexation of iron (III) by natural organic ligands in the Central North Pacific as determined by a new competitive ligand equilibration/adsorptive cathodic stripping voltammetric method. *Mar. Chem.* 50, 117–138. doi: 10.1016/0304-4203(95)00031-L
- Scott, D. T., McKnight, D. M., Blunt-Harris, E., Kolesar, S., and Lovley, D. (1998). Quinone moieties act as electron acceptors in the reduction of humic substances by humics reducing microorganisms. *Environ. Sci. Technol.* 32, 2984–2989. doi: 10.1021/es980272q
- Shiller, A. M., Duan, S., Van Erp, P., and Bianchi, T. S. (2006). Photo-oxidation of dissolved organic matter in river water and its effect on trace element speciation. *Limnol. Oceanogr.* 51, 1716–1728. doi: 10.4319/lo.2006.51.4.1716
- Sleighter, R. L., and Hatcher, P. G. (2008). Molecular characterization of dissolved organic matter (DOM) along a river to ocean transect of the lower Chesapeake Bay by ultrahigh resolution electrospray ionization Fourier transform ion

- cyclotron resonance mass spectrometry. *Mar. Chem.* 110, 140–152. doi: 10.1016/j.marchem.2008.04.008
- Spencer, R. G., Aiken, G. R., Wickland, K. P., Striegl, R. G., and Hernes, P. J. (2008). Seasonal and spatial variability in dissolved organic matter quantity and composition from the Yukon River basin, Alaska. *Global Biogeochem. Cy.* 22:GB4002. doi: 10.1029/2008GB003231
- Stedmon, C. A., and Bro, R. (2008). Characterizing dissolved organic matter fluorescence with parallel factor analysis: a tutorial. *Limnol. Oceanogr. Met.* 6, 572–579. doi: 10.4319/lom.2008.6.572
- Sun, L., Chen, H., Abdulla, H. A., and Mopper, K. (2014). Estimating hydroxyl radical photochemical formation rates in natural waters during long-term laboratory irradiation experiments. *Env. Sci. Process. Impact* 16, 757–763. doi: 10.1039/C3EM00587A
- Sun, L., Qian, J., Blough, N. V., and Mopper, K. (2015b). Insights into the photoproduction sites of hydroxyl radicals by dissolved organic matter in natural waters. *Environ. Sci. Technol. Lett.* 2, 352–356. doi: 10.1021/acs.estlett.5b00294
- Sun, L., Spencer, R. G., Hernes, P. J., Dyda, R. Y., and Mopper, K. (2015a). A comparison of a simplified cupric oxide oxidation HPLC method with the traditional GC–MS method for characterization of lignin phenolics in environmental samples. *Limnol. Oceanogr. Met.* 13, 1–8. doi: 10.1002/lom3.10001
- Tangen, G., Wickstrøm, T., Lierhagen, S., Vogt, R., and Lund, W. (2002). Fractionation and determination of aluminum and iron in soil water samples using SPE cartridges and ICP-AES. *Environ. Sci. Technol.* 36, 5421–5425. doi: 10.1021/es020077i
- Vaughan, P. P., and Blough, N. V. (1998). Photochemical formation of hydroxyl radical by constituents of natural waters. *Environ. Sci. Technol.* 32, 2947–2953. doi: 10.1021/es9710417
- Viollier, E., Inglett, P., Hunter, K., Roychoudhury, A., and Van Cappellen, P. (2000). The ferrozine method revisited: Fe (II)/Fe (III) determination in natural waters. *App. Geochem.* 15, 785–790. doi: 10.1016/S0883-2927(99)00097-9
- Vione, D., Falletti, G., Maurino, V., Minero, C., Pelizzetti, E., Malandriano, M., et al. (2006). Sources and sinks of hydroxyl radicals upon irradiation of natural water samples. *Environ. Sci. Technol.* 40, 3775–3781. doi: 10.1021/es052206b
- Vione, D., Ponzo, M., Bagus, D., Maurino, V., Minero, C., and Carlotti, M. (2010). Comparison of different probe molecules for the quantification of hydroxyl radicals in aqueous solution. *Environ. Chem. Lett.* 8, 95–100. doi: 10.1007/s10311-008-0197-3
- Voelker, B. M., Morel, F. M., and Sulzberger, B. (1997). Iron redox cycling in surface waters: effects of humic substances and light. *Environ. Sci. Technol.* 31, 1004–1011. doi: 10.1021/es9604018
- Waggoner, D. C., Chen, H., Willoughby, A. S., and Hatcher, P. G. (2015). Formation of black carbon-like and alicyclic aliphatic compounds by hydroxyl radical initiated degradation of lignin. *Org. Geochem.* 82, 69–76. doi: 10.1016/j.orggeochem.2015.02.007
- White, E., Vaughan, P., and Zepp, R. (2003). Role of the photo-Fenton reaction in the production of hydroxyl radicals and photobleaching of colored dissolved organic matter in a coastal river of the southeastern United States. *Aquat. Sci.* 65, 402–414. doi: 10.1007/s00027-003-0675-4
- Xu, H., and Jiang, H. (2013). UV-induced photochemical heterogeneity of dissolved and attached organic matter associated with cyanobacterial blooms in a eutrophic freshwater lake. *Wat. Res.* 47, 6506–6515. doi: 10.1016/j.watres.2013.08.021
- Yamashita, Y., Jaffé, R., Maie, N., and Tanoue, E. (2008). Assessing the dynamics of dissolved organic matter (DOM) in coastal environments by excitation emission matrix fluorescence and parallel factor analysis (EEM–PARAFAC). *Limnol. Oceanogr.* 53, 1900–1908. doi: 10.4319/lo.2008.53.5.1900
- Zepp, R. G., Faust, B. C., and Hoigne, J. (1992). Hydroxyl radical formation in aqueous reactions (pH 3–8) of iron (II) with hydrogen peroxide: the photo-Fenton reaction. *Environ. Sci. Technol.* 26, 313–319. doi: 10.1021/es00026a011
- Zhou, X., and Mopper, K. (1990). Determination of photochemically produced hydroxyl radicals in seawater and freshwater. *Mar. Chem.* 30, 71–88. doi: 10.1016/0304-4203(90)90062-H
- Zlotnik, I., and Dubinsky, Z. (1989). The effect of light and temperature on DOC excretion by phytoplankton. *Limnol. Oceanogr.* 34, 831–839. doi: 10.4319/lo.1989.34.5.0831

Conflict of Interest Statement: The authors declare that the research was conducted in the absence of any commercial or financial relationships that could be construed as a potential conflict of interest.

Copyright © 2016 Sun and Mopper. This is an open-access article distributed under the terms of the Creative Commons Attribution License (CC BY). The use, distribution or reproduction in other forums is permitted, provided the original author(s) or licensor are credited and that the original publication in this journal is cited, in accordance with accepted academic practice. No use, distribution or reproduction is permitted which does not comply with these terms.



Depth-dependent photodegradation of marine dissolved organic matter

Stephen A. Timko^{1*}, Anastasia Maydanov², Sandra L. Pittelli³, Maureen H. Conte^{4,5}, William J. Cooper¹, Boris P. Koch^{6,7}, Philippe Schmitt-Kopplin^{8,9} and Michael Gonsior¹⁰

¹ Department of Civil and Environmental Engineering, University of California, Irvine, Irvine, CA, USA, ² Department of Chemistry and Chemical Biology, Northeastern University, Boston, MA, USA, ³ Department of Chemistry and Biochemistry, Georgia Institute of Technology, Atlanta, GA, USA, ⁴ Bermuda Institute of Ocean Sciences, St. George's, Bermuda, ⁵ Ecosystems Center, Marine Biological Laboratory, Woods Hole, MA, USA, ⁶ Ecological Chemistry, Alfred-Wegener-Institut Helmholtz Zentrum für Polar- und Meeresforschung, Bremerhaven, Germany, ⁷ Maritime Technology, University of Applied Sciences, Bremerhaven, Germany, ⁸ Helmholtz Zentrum München, Analytical BioGeoChemistry, Neuherberg, Germany, ⁹ Technische Universität München, Analytical Food Chemistry, Freising-Weihenstephan, Germany, ¹⁰ Chesapeake Biological Laboratory, University of Maryland Center for Environmental Science, Solomons, MD, USA

OPEN ACCESS

Edited by:

Christopher Osburn,
North Carolina State University, USA

Reviewed by:

John Robert Helms,
Old Dominion University, USA
X. Antón Álvarez-Salgado,
Consejo Superior de Investigaciones
Científicas, Spain

*Correspondence:

Stephen A. Timko,
Department of Civil and Environmental
Engineering, University of California,
Irvine, 808 Engineering Tower,
Irvine, CA 92617, USA
stimko@uci.edu

Specialty section:

This article was submitted to
Marine Biogeochemistry,
a section of the journal
Frontiers in Marine Science

Received: 03 July 2015

Accepted: 24 August 2015

Published: 09 September 2015

Citation:

Timko SA, Maydanov A, Pittelli SL, Conte MH, Cooper WJ, Koch BP, Schmitt-Kopplin P and Gonsior M (2015) Depth-dependent photodegradation of marine dissolved organic matter. *Front. Mar. Sci.* 2:66.
doi: 10.3389/fmars.2015.00066

Marine dissolved organic matter (DOM) in surface and deep waters of the eastern Atlantic Ocean and Sargasso Sea was analyzed by excitation emission matrix (EEM) fluorescence spectroscopy and parallel factor analysis (PARAFAC). Photo-degradation with semi-continuous monitoring of EEMs and absorbance spectra was used to measure the photo-degradation kinetics and changes of the PARAFAC components in a depth profile of DOM at the Bermuda Atlantic Time Series (BATS) station in the Sargasso Sea. A five component model was fit to the EEMs, which included traditional terrestrial-like, marine-like, and protein-like components. Terrestrial-like components showed the expected high photo-reactivity, but surprisingly, the traditional marine-like peak showed slight photo-production in surface waters, which may account for its prevalence in marine systems. Surface waters were depleted in photo-labile components while protein-like fluorescent components were enriched, consistent with previous studies. Ultra-high resolution mass spectrometry detected unique aliphatic compounds in the surface waters at the BATS site, which may be photo-produced or photo-stable. Principle component and canonical analysis showed strong correlations between relative contributions of unsaturated/aromatic molecular formulas and depth, with aliphatic compounds more prevalent in surface waters and aromatic compounds in deep waters. Strong correlations were seen between these aromatic compounds and humic-like fluorescent components. The rapid photo-degradation of the deep-sea fluorescent DOM in addition to the surface water relative depletion of aromatic compounds suggests that deep-sea fluorescent DOM may be too photochemically labile to survive during overturning circulation.

Keywords: marine dissolved organic matter, excitation emission matrix fluorescence, photodegradation, CDOM, PARAFAC

Introduction

Marine dissolved organic matter (DOM) is one of the largest carbon reservoirs on Earth. At 662 Pg of carbon, it contains over 200 times the amount of carbon stored as marine biomass (Hansell et al., 2009). Consequently, the composition and reactivity of marine DOM is of utmost importance in understanding the role that this material plays in the marine carbon cycle.

DOM dynamics are often studied via changes in the portion which is colored or chromophoric (CDOM). CDOM absorbs light in the UV and visible regions, and participates in a wide range of photochemical reactions, including the production of CO and dissolved inorganic carbon (Miller and Zepp, 1995; Gao and Zepp, 1998), low molecular weight organic acids (Kieber et al., 1989), and reactive intermediates (Cooper et al., 1989; Vione et al., 2014). Photochemical transformations of CDOM can also lead to either an enhancement or reduction in its bio-availability (Kieber et al., 1989; Tranvik and Bertilsson, 2001). The smaller fraction of CDOM that is fluorescent (FDOM) is the most photo-reactive, and is found throughout the ocean.

Traditionally, CDOM in the ocean has been attributed to terrestrial sources, namely lignin, and other higher plant material, while autochthonous production was only recognized on local- and short temporal scales (Coble, 2007; Andrew et al., 2013). More recently, the microbial carbon pump model for microbial production has been found to be an important oceanic source of biologically recalcitrant CDOM in the oceans (Jiao et al., 2010), and it has been suggested that autochthonous biological production may surpass terrestrial input of FDOM to the oceans (Yamashita and Tanoue, 2008; Jørgensen et al., 2011; Nelson and Siegel, 2013).

Photo-bleaching has been recognized as the most important sink for CDOM in the ocean, both through the direct mineralization as well as potential transformation of CDOM to smaller and more bio-available forms (Gonsior et al., 2014a). In the open ocean, surface waters are usually CDOM- and FDOM depleted and concentrations increase with depth (Jørgensen et al., 2011; Catalá et al., 2015). The light history and the biogeochemical origin of the CDOM affect its lability; for example, areas of upwelling, high biological productivity, and decreased irradiance have higher CDOM and FDOM content (Nelson and Siegel, 2013). Additionally, deep water DOM that has not been exposed to light for extended periods of time may be more photosensitive, degrading faster than DOM that has already undergone some photobleaching (Gonsior et al., 2013).

Excitation emission matrix (EEM) fluorescence is the most common method of investigating FDOM in the ocean. Fluorescence detection is much more sensitive than absorbance, making it more practical for analyzing low levels of FDOM (Coble, 2007). EEM spectroscopy in particular is sensitive enough to analyze low concentrations of DOM in bulk seawater and fast enough to investigate small-scale variation in composition (Coble, 1996). While direct comparisons of EEMs is an important qualitative (and semi-quantitative) tool, parallel factor (PARAFAC) analysis, which compares large datasets of EEMs and deconvolutes them into statistically independent components,

has emerged as the leading method for quantification of fluorescence signatures (Murphy et al., 2013).

Ultrahigh resolution electrospray ionization (ESI) Fourier transform ion cyclotron resonance mass spectrometry (FT-ICR-MS) has been used to characterize marine DOM (Koch et al., 2005; Hertkorn et al., 2006; D'andrilli et al., 2010; Gonsior et al., 2011, 2014a; Flerus et al., 2012; Chen et al., 2014; Lechtenfeld et al., 2014); however, the relationship between molecular composition and optical properties remains unclear. Herzsprung et al. (2012) compared humic-like fluorescence intensities of water from a German drinking water reservoir catchment area with mass peaks identified using FT-ICR-MS, and found strong correlations between unsaturated, highly oxidized compounds and this fluorescence. Studies of DOM-rich boreal rivers and lakes likewise compared EEM-PARAFAC components with molecular formulas derived from FT-ICR-MS, identifying similar relationships between longer wavelength, “humic-like” fluorescent components and oxidized aromatic compounds (Stubbins et al., 2014; Kellerman et al., 2015).

In order to better understand the processing of FDOM in the ocean, we investigated depth-related changes in abundance and photochemical reactivity of FDOM in the North Atlantic Ocean. The molecular composition of DOM from a detailed depth profile was analyzed by FT-ICR-MS and then correlated to EEM-PARAFAC components.

Materials and Methods

Sample Sites

Samples were collected on three separate cruises in the Atlantic Ocean. Seawater samples were collected during a cruise of the R/V *Polarstern*, Nov. 2008, along a transect from 50.2° N to 31.4° S in the eastern Atlantic Ocean. Samples were collected using a 24 Niskin bottle rosette CTD profiler at the surface and 200 m depth. Depth profiles (0–4525 m) of seawater were also collected at the Bermuda Atlantic Time Series (BATS) site in the northern Sargasso Sea southeast of Bermuda during cruises of the R/V *Atlantic Explorer* in June 2012 (0, 110, 750, 1500, 3000, and 4527 m) and July 2013 (every 200 m from 0 to 4400 m, and 4525 m).

All samples were solid phase extracted using a previously described method (Dittmar et al., 2007). Briefly, 5–20 L of filtered samples (0.7 μm Whatman GF/F) were acidified with hydrochloric acid (p.a. grade) to pH 2. Solid-phase extraction cartridges (Agilent Bond Elut PPL) packed with 1 g resin were conditioned with methanol, rinsed with acidified (pH 2) ultra-pure water, and the samples were gravity-fed through each cartridge. Cartridges were then rinsed with additional acidified water, dried, and the samples eluted with 5 or 10 mL methanol. Methanolic extracts were stored at –18°C prior to further analyses. Previous work has shown that for open ocean samples, DOC extraction efficiency is ~42% (Dittmar et al., 2008; Lechtenfeld et al., 2014), and that while CDOM and FDOM extraction with this method is incomplete, extracts are representative, showing similar relative changes in absorbance and fluorescence as whole water samples (Roettgers and Koch, 2012).

Photo-irradiation Experiments

Photo-irradiation experiments were conducted on extracts collected at BATS in June 2012. The volume of extract used for each sample was proportional to the volume of seawater extracted in order to keep the concentration factor constant. Methanol extracts were dried under N₂, dissolved in 25 mL NanoPure water, sonicated for 5 min, and filtered through pre-washed 0.2 µm Whatman GD/X syringe filters immediately before use. Each sample was then irradiated for 24 h with a photo-irradiation system described in detail previously (Timko et al., in press). Briefly, samples were irradiated with an Oriel® Sol2A Class ABA solar simulator (Newport Corporation, Irvine, CA) equipped with 1000 W Xe arc lamp and AM 1.5 filter. Light intensity was measured daily with a Newport 91150 V Reference Cell and adjusted to 1000 W m⁻², with an average light flux of 33 W m⁻² from 300 to 400 nm. Samples were pumped through a flow-through irradiation cell into an equilibration vial with 750 µL of volume to allow equilibration with air and to prevent oxygen starvation. Samples were then drawn through an Aqualog spectrofluorometer (Horiba Instruments) and pumped back through the irradiation cell. The short pathlength of the irradiation cell (1 mm) prevented screening effects and allowed for accurate and reproducible experiments, with at least 4-fold changes in DOC having no effect on fluorescence degradation kinetics (Timko et al., in press).

Absorbance and EEM spectra were collected simultaneously at 20 min intervals throughout the photo-irradiation experiments. Excitation scans were recorded from 600 to 220 nm in 2 nm steps. Emission spectra were collected in ~3 nm steps from 211.5 to 617.7 nm, with integration times of 1 s. Spectra were converted to Quinine Sulfate Units (QSU) by dividing fluorescence intensities by the fluorescence intensity of 1 mg L⁻¹ standard reference quinine sulfate or to Raman Units (RU) by dividing intensities by the area under the water Raman peak at 350 nm excitation (emission range 383–442 nm). Rayleigh- and Raman scattering and inner filter effects were corrected for by the Aqualog software and in MATLAB with the methods described by Zepp et al. (2004). Methanol extracts of cruise samples not used in photo-irradiation experiments were dried under N₂, dissolved in NanoPure water, and fluorescence spectra recorded as above.

Photo-degradation of PARAFAC Components C2 and C4 (see below) were modeled using a double exponential function using IGOR Pro (WaveMetrics, Inc):

$$F_t = F_L e^{-k_L t} + F_{SL} e^{-k_{SL} t} + c \quad (1)$$

where the fluorescence (F) at time t is modeled as the loss of the labile (L) and semi-labile (SL) fractions at rate constants k (Sleighter et al., 2014; Timko et al., in press). Samples were irradiated without pH adjustment or control. The pH of samples increased slightly (0.09–0.65 pH units, 0.32 pH units average) during 24 h of irradiation, with the maximum change of 0.65 pH units occurring with the 3000 m depth sample. In a previous study, rates of FDOM loss during irradiations of Suwannee River natural organic matter were shown to be not significantly different when the pH was varied by 1 pH unit; we therefore assumed that the small pH changes during irradiations in this

study had no significant impact on the reaction kinetics (Timko et al., in press).

PARAFAC Modeling

PARAFAC modeling was conducted using the drEEM toolbox (Murphy et al., 2013). A total of 611 EEMs, of which 173 were from cruise samples and 438 from photo-irradiation experiments, were visually investigated, and outliers (scans with bubbles, spectral errors, etc.) removed. Samples were normalized to unit variance to reduce concentration effects during modeling, and the normalization reversed after model completion. Excitation wavelengths <250 nm showed high leverages (deviation from average distribution), most likely due to higher relative values and/or the lower signal to noise ratio at such wavelengths (Stedmon and Bro, 2008); removal of these wavelengths improved the modeling, namely the spectral loadings of longer-wavelength components. Two separate models were fit: the East Atlantic transect (surface and 200 m depth), and the Sargasso Sea samples (including spectra collected during photo-irradiation experiments). Evaluation of spectral loadings, split-half validation, random initialization analysis, and rigorous residuals analyses were performed as described elsewhere (Stedmon and Bro, 2008; Murphy et al., 2013). Criteria for final model assignment were (1) split-half validation (2) residuals analysis and (3) spectral loadings.

Ultrahigh Resolution Mass Spectrometry

The solid-phase extracted samples from the July 2013 depth profile at BATS (26 samples total) were analyzed using the electrospray ionization (ESI) source of the Bruker Apex QE 12 Tesla FT-ICR-MS located at the Helmholtz Center for Environmental Health, Munich, Germany. Samples were diluted with methanol 1:20 before injection to avoid overloading the ion cyclotron resonance ion trap which could lead to peak splitting and inconsistent calibration across the desired mass range (147–2000 Dalton). To avoid any cross-contamination between samples, an automated cleaning procedure was implemented that used 600 µL (80% methanol, 20% pure water) at a flow rate of 300 µL min⁻¹ between samples. The sample flow rate was set to 3 µL min⁻¹, and ESI was run in negative mode at -3.6 kV. Five hundred spectra were averaged to obtain a mass accuracy better than 0.2 ppm and an average mass resolution of about 500,000 at m/z 350–400. The MS system was pre-calibrated using arginine and then post-calibrated by using known DOM m/z ions (255.08741 = C₁₂H₁₅O₆, 297.09798 = C₁₄H₁₇O₇, 367.13984 = C₁₈H₂₃O₈, 491.15589 = C₂₄H₂₇O₁₁, 553.1562 = C₂₅H₂₉O₁₄, 611.19814 = C₂₈H₃₅O₁₅, and 707.25566 = C₃₄H₄₃O₁₆) throughout the entire mass range of interest (200–800 Da). The signal to noise ratio was set to 10 and mass lists were subsequently generated.

The mass resolution and accuracy of the FT-ICR-MS system allowed molecular formula assignments to ions up to m/z 800. Not all m/z ions could be assigned, indicating that some m/z peaks were outside of the used atomic combination of ¹²C_{0–∞}, ¹H_{0–∞}, ¹⁶O_{0–∞}, ¹⁴N_{0–3}, and ³²S_{0–2}, as well as the following isotopologs ¹³C, and ³⁴S. Visualization of complex mass spectrometric data have been achieved by elemental or van

Krevelen diagrams (van Krevelen, 1950). A modified Kendrick plot was also used to visualize homologs series that are spaced only by CH₂ groups (Yekta et al., 2012).

Multivariate Statistical Analysis

All data were normalized via autoscaling by subtracting the average of a variable from the data and then dividing by the standard deviation, allowing for multivariate statistical analysis (Bro and Smilde, 2014). All generated mass lists of all FT-ICR-MS samples were then combined in a large matrix. The generation of the matrix was undertaken by searching *m/z* ions within an error of 0.2 ppm to be able to assign one *m/z* value to all intensities of all spectra. If a *m/z* was found in one sample but not in others, the missing intensity value was replaced by 0. This approach resulted in a matrix where all *m/z* ions represented the variables and the *m/z* intensities the data. Principal component analyses (PCA) were undertaken on the normalized FT-ICR-MS and EEM-PARAFAC data sets, respectively. The normalized fluorescence data was then used to create a resemblance matrix using Spearman Rank Correlations. This EEM-PARAFAC resemblance matrix was then used for the canonical analysis on principal coordinates (CAP) of the FT-ICR-MS data matrix. CAP analysis allowed to discriminate between sets of variables, in this case, between the EEM-PARAFAC Components and *m/z* molecular ions and their intensities.

Results

PARAFAC Modeling

PARAFAC analysis of the Sargasso Sea dataset (492 EEMs) produced a five component model (split-half validated, >99.8% explained variance; **Figure 1**). The components contained “humic-like” components characterized by fluorescence in the

visible region, as well as components in the UVA portion of the spectrum. This UVA fluorescence is characteristic of small aromatic molecules, including the amino acids tryptophan and tyrosine. The model components were labeled according to conventional terminology as “marine-like” C1 (*ex/em* = <250 (306)/404 nm), “terrestrial-like” C2 (<250 (360)/447), UVA component C3 (<250 (282)/332), “terrestrial-like” C4 (276(399)/497), and UVA component C5 (276/304) (Coble, 2007; Stedmon and Nelson, 2015). To examine the robustness of the model, a five component model was fit to only the East Atlantic cruise data (119 EEMs), with 99.7% explained variance. Models with more than five components could not be split-half validated. Models with less than five components showed significant peaks and troughs throughout the residuals, indicative of a poor model fit, while the residuals of the five component models only showed minor peaks along the Raman and Rayleigh scattering lines (Murphy et al., 2013). The components in both the East Atlantic and the Sargasso Sea models were very similar with regards to peak location and shape, especially for the visible fluorescent components (**Figure 2**). This similarity provides a strong validation that the modeling of the EEMs collected during photo-irradiation experiments are indicative of fluorescence changes occurring in the natural environment, even on large geographical scales. Hence, the observed results on the photochemical changes in marine FDOM are not limited to the Sargasso Sea, but can presumably generalized, at least to the greater Atlantic Ocean.

Depth Dependence of FDOM Fluorescence Intensity at BATS

All three visible fluorescence components (C1, C2, and C4) were significantly depleted in surface waters and increased with depth (**Figure 3**). The intensity of marine-like C1 was on

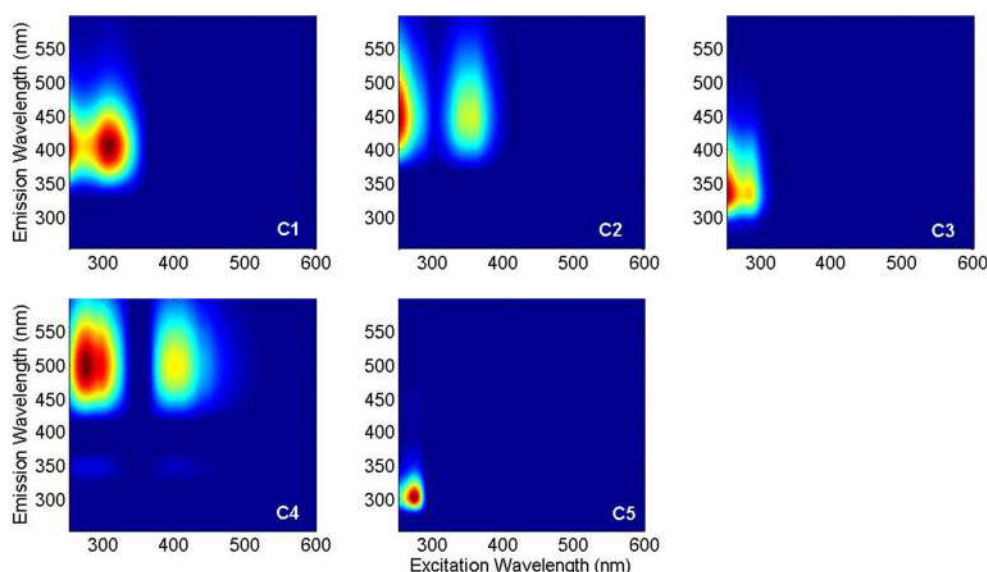


FIGURE 1 | PARAFAC components in Sargasso Sea FDOM: marine-like C1, terrestrial-like C2, UVA C3, terrestrial-like C4, and UVA C5.

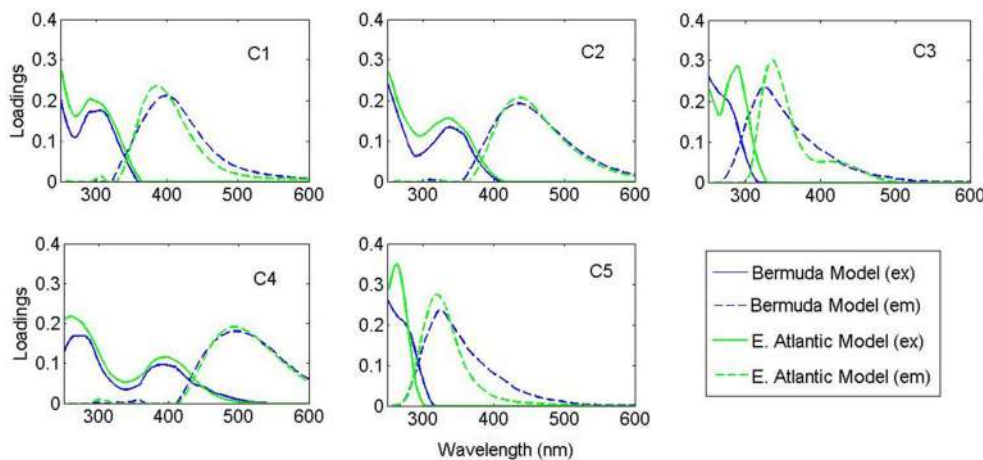


FIGURE 2 | Spectral loadings of the PARAFAC components in the Bermuda model (blue) and East Atlantic model (green).

average 3.4 times higher below 1000 m than at the surface. The intensity of “terrestrial-like” components C2 and C4 were also higher below 1000 m (5.9 and 5.6 times, respectively) than at the surface. In contrast, UVA component C5 was maximal at the surface and decreased with depth, albeit less dramatically. On average, C5 intensity was 1.5 times higher at the surface than in waters >1000 m depth. UVA component C3 showed no strong depth-dependence. No strong correlations between PARAFAC component intensity and apparent oxygen utilization (AOU) were seen, although the small dataset (two depth profiles) prevented detailed interpretation of these results.

Photo-degradation Kinetics of FDOM At BATS

EEMs before and after irradiation, and differential plots, are shown in **Figure 4**. Terrestrial-like components C2 and C4 showed significant photo-lability at all depths. The long-wavelength component C4 showed greater relative fluorescence loss (%), whereas component C2 showed greater total loss in fluorescence (**Figure 5**). The rate of loss of the semi-labile fraction, k_{SL} , showed no depth-dependent trend, with an average $0.063 \pm 0.008 \text{ h}^{-1}$ for C2 and $0.069 \pm 0.008 \text{ h}^{-1}$ for C4. The rate of loss of the labile fraction, k_L , was faster in the surface and 110 m samples ($2.2 \pm 0.2 \text{ h}^{-1}$ and $1.4 \pm 0.2 \text{ h}^{-1}$ for C2 and C4, respectively) than in the deep samples ($1.1 \pm 0.1 \text{ h}^{-1}$ and $0.89 \pm 0.08 \text{ h}^{-1}$ for C2 and C4, respectively). Loss of C2 over the 24 h irradiations was lowest in the surface sample (38%), followed by the 110 m sample (42%), while samples at depth showed extremely similar C2 loss ($50 \pm 1\%$). Loss of C4 showed a similar trend, with the least amount of fluorescence lost in the surface sample (51%), while the samples at greater depth all showed similar loss ($60 \pm 3\%$).

Marine-like component C1 showed variable, but more limited, photo-reactivity than either C2 or C4 (**Figure 5**). At the surface, C1 fluorescence decreased by 4% in the first 20 min of irradiation and then increased to a final value which was 8% higher than the initial fluorescence. Similarly, C1 fluorescence at 110 m depth (the chlorophyll fluorescence maximum) initially decreased by

3% and then increased to a final value that was 2% greater than the initial fluorescence. In deep waters, C1 fluorescence decreased over the 24 h irradiation period by 10% at 1500 m depth and by an average of 5% at other depths.

UVA fluorescent components C3 and C5 showed variable photo-lability (**Figures 5C,E**). Maximum decreases in C3 fluorescence over the 24 h irradiation period were observed at the surface (15%) and at the 110 m chlorophyll fluorescence maximum (20%). The minimum decrease in C3 fluorescence was observed at 750 m depth (<4%). Samples from 1500, 3000, and 4537 m depths showed intermediate decreases in fluorescence (12, 8, and 9%, respectively). Component C5 fluorescence intensity decreases ranged from 16 to 58% with no discernable depth trend.

Ultrahigh Resolution Mass Spectrometry

The majority of m/z peaks were shared between all samples in the 0–4525 m depth profile at the BATS site. However, direct comparison between averaged surface samples collected at BATS in 2013 and the 4525 m sample (35 m above bottom) revealed distinct characteristic and unique signatures (**Figure 6**). In surface waters, there were 165 unique CHO molecular ions at a signal to noise ratio of 10, representing largely aliphatic compounds with hydrogen to carbon ratios (H/C) between 1.5 and 2.0 and oxygen to carbon ratios (O/C) between 0.2 and 0.7, as well as 90 nitrogen-containing ions (CHNO). These occupied the same aliphatic area within the chemical space indicative of presumably labile compounds, with the exception of a distinct higher abundant group centered on H/C of 1.2 and O/C of 0.5. Interestingly, the largest unique signature was the presence of 230 high abundant sulfur-containing ions that again were localized in the aliphatic region of the van Krevelen diagram.

In contrast to surface waters, waters at 4525 m depth contained unique low abundant hydrogen deficient molecular CHO ($n = 78$) and CHNO ($n = 112$) ions that showed H/C of 0.6–1.2 and O/C of 0.2–0.6 but very few unique CHOS

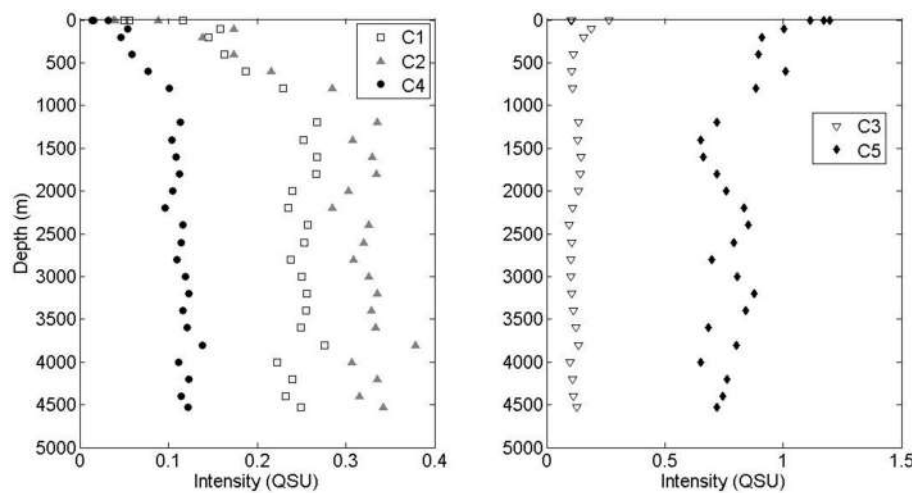


FIGURE 3 | Depth profiles of visible fluorescence components C1, C2, and C4 and UVA components C3 and C5.

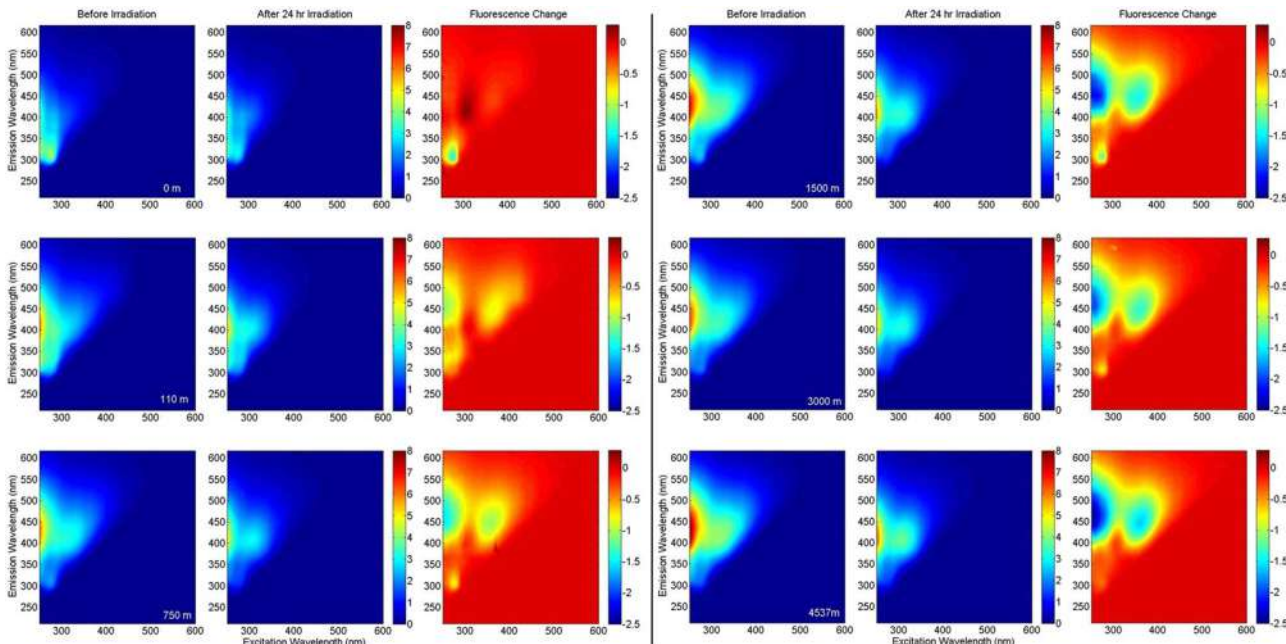


FIGURE 4 | EEM fluorescence of BATS samples at various depths before and after irradiation, and the fluorescence change. All fluorescence intensities are in Raman Units.

ions. Hence, aliphatic compounds were enriched at the surface and more aromatic compounds were present at depths. This finding agrees with the increase of FDOM with depth and the biological, and potentially photochemical, production of labile aliphatic compounds at the surface.

Statistical Evaluation of FT-MS and EEM PARAFAC Data

The PCA results from the FT-ICR-MS data clearly differentiated molecular variations in surface, mixed layer, and waters

from >800 m depth (**Figure 7B**). A Spearman Rank correlation of the variables (*m/z*) and the Principal Component 1 (indicative of depth) revealed similar patterns in the van Krevelen diagram (**Figure 8**) when compared to the unique signatures (**Figure 6**): aliphatic CHO and CHNO ions correlated well with the surface while more hydrogen-deficient ions correlated with depth. However, the region of the van Krevelen with O/C ratios between 0.5 and 0.8 and H/C ratios between 0.5 and 1.2 was much more occupied (**Figure 8, CHO plot**). This region in the van Krevelen diagram has been previously suggested to be highly correlated

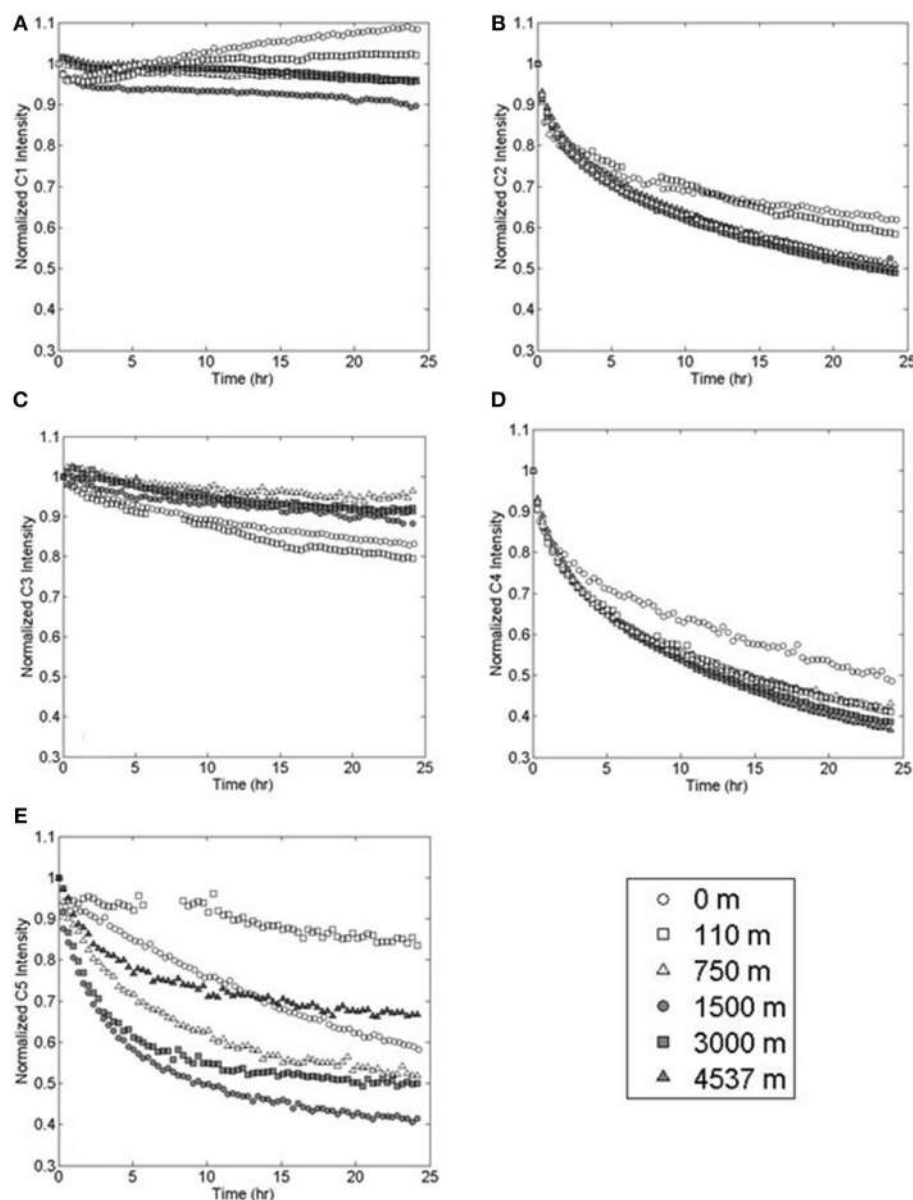


FIGURE 5 | Photo-degradation of PARAFAC components (A) marine-like C1, (B) terrestrial-like C2, (C) UVA C3, (D) terrestrial-like C4, and (E) UVA C5 at various depths in the Sargasso Sea.

with CDOM that can be flocculated by aluminum sulfate in a drinking water treatment plant (Gonsior et al., 2014b).

PCA was also carried out on the intensities of the five PARAFAC components (**Figure 7A**). Results showed a similar separation between surface and deep waters as for the FT-ICR-MS data (**Figure 7B**). Lastly, Canonical Analysis on Principal coordinates (CAP) (Anderson and Willis, 2003) was used to correlate the two independent FT-ICR-MS and EEM-PARAFAC datasets (**Figure 7C**). In this method, ordination can be constrained by using any dissimilarity measures while also incorporating the correlation structures of variables. Results of the CAP analysis of the EEM-PARAFAC data resemble

matrix (Spearman Rank correlations) with the FT-ICR-MS data also showed a clear separation between surface, mixed layer and >800 m samples (**Figure 7C**) along CAP Component 1 (CAP1). Eigenvector values of CAP1 were then used to distinguish between *m/z* ions and associated molecular formulas that were indicative of surface and mixed layer (negative values) and of the deep ocean (positive values). Results again indicate enrichment in aliphatic compounds (CHO, CHNO) and substantial sulfur-containing molecules (CHOS) in the surface waters and enrichment in more unsaturated/aromatic compounds and polyphenolic-like composition at depth (**Figure 9**).

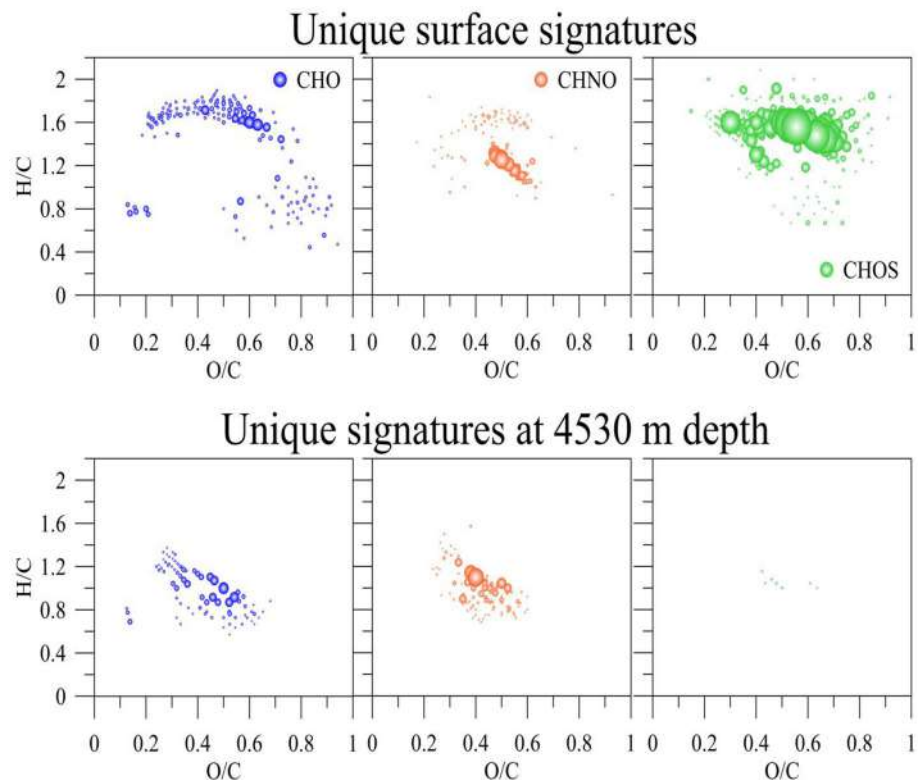


FIGURE 6 | Unique assigned molecular formulas of the SPE-DOM at 5 m and 4530 m depth collected at BATS in the Sargasso Sea, 2013.

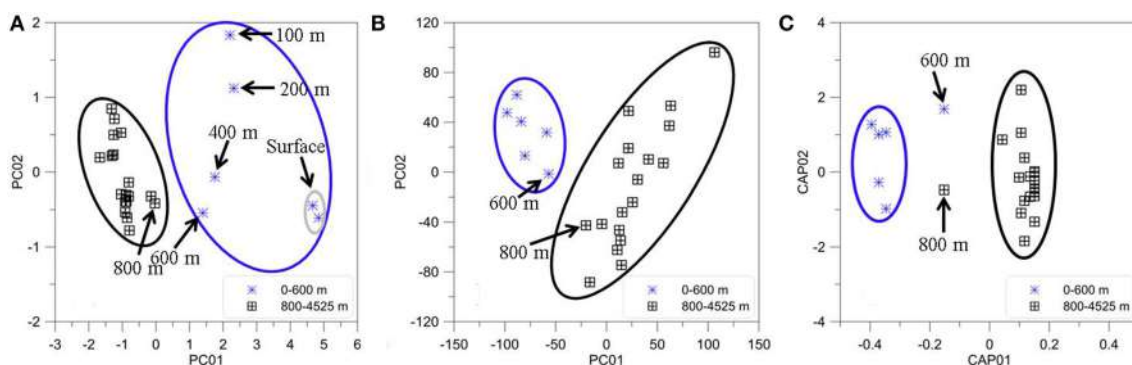


FIGURE 7 | Statistical analyses of BATS depth profile (2013). (A) Principal Components One and Two for all PARAFAC component intensities. (B) Principal Components One and Two for all FT-ICR-MS m/z molecular ions and their intensities for the same samples. (C) Canonical analysis on principal coordinates (CAP) of the normalized EEM resemblance matrix and the FT-ICR-MS data.

Discussion

Photochemical loss of fluorescence in Sargasso Sea waters was dominated by terrestrial-like components C2 and C4. The photo-reactivity of these components explains why these components were found to be depleted at the ocean surface (Jørgensen et al., 2011). The lesser degradation in the surface samples was expected, as the most photo-labile structures were already bleached from the surface water. Interestingly, the kinetic

analysis showed no depth-dependent trends in the rate of loss of the semi-labile fraction of each component, k_{SL} . This suggests that the groups of fluorophores responsible for this fraction of the fluorescence are compositionally similar at all depths, while the labile fraction, k_L , may consist of different classes of compounds that contain similar fluorescent moieties. Photo-degradation of terrestrial-like components C2 and C4 showed similar relative kinetics to Suwannee River Natural Organic Matter (IHSS standard), with C4 losing a greater percentage of

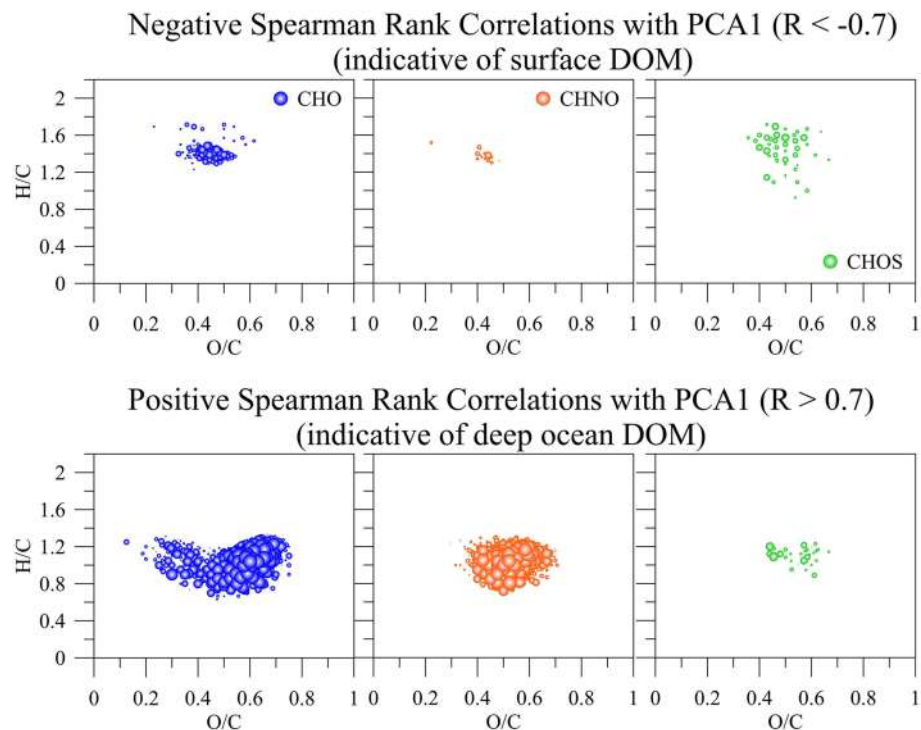


FIGURE 8 | Positive (indicative of surface DOM) and negative (indicative of deep ocean DOM) Spearman Rank correlations greater $R = 0.7$ and lower -0.7 , respectively of all common m/z ions, their intensities, and assigned molecular formulas with the first principal component (PCA1) derived from SPE-DOM samples collected at BATS in 2013 and analyzed by FT-ICR-MS. The bubble size corresponds to R -values between 0.7 and 1 and -0.7 and -1 , respectively.

its initial fluorescence, but C2 losing greater total fluorescence (Timko et al., in press). The fluorophores responsible for C4 fluorescence are believed to be high molecular weight (poly)phenolic compounds, which are some of the most reactive sites in CDOM (McNally et al., 2005; Boyle et al., 2009; Kellerman et al., 2015). The abundance and photo-lability of terrestrial-like C2 and C4 at depth could be due to the prevalence of terrestrial organic matter in Arctic waters, where this DOM is subducted before it can be extensively photo-bleached (Benner et al., 2005). Alternatively, there is growing evidence that these “terrestrial” signals may be produced *in situ* microbially (Shimotori et al., 2012; Jørgensen et al., 2014), and/or excreted by macro brown algae (Shank et al., 2010), zooplankton, and *Trichodesmium* sp. (Steinberg et al., 2004).

In contrast to the terrestrial-like FDOM signals, marine-like C1 showed limited photo-degradation, and even slight production in surface waters. Marine-like C1 production may have only been seen in the surface and 110 m samples due to lack of precursor material in deeper waters. Such materials may include tryptophan, tyrosine, and other low molecular weight aromatic structures, which have been shown to produce CDOM and “humic-like” FDOM photochemically (Biers et al., 2007; De Laurentiis et al., 2013; Bianco et al., 2014). UVA component C5 was significantly enriched in the surface and 110 m samples, and while typically are classified as “protein-like,” may also contain low molecular weight aromatics. Input of these precursors was

likely from primary producers in the photic zone (Jørgensen et al., 2011), as well as CDOM exuded by the brown macroalgae *Sargassum natans* (Shank et al., 2010), which is prevalent in the Sargasso Sea in July, when sampling occurred. Despite its lack of photo-degradation and even slight photo-production, C1 was found to be depleted in the surface ocean, which has been shown previously (Heller et al., 2013). The observed photo-products may not be photo-stable over long time periods, as photo-degradation of marine FDOM has been shown during longer irradiation experiments (Helms et al., 2013). Dried PPL extracts were reconstituted in deionized water for the photo-irradiation experiments, removing the potential impact of reactive halogen species on FDOM loss. Previous work showed that while halides had little effect on the photo-bleaching of terrestrial FDOM, an algal exudate showed enhanced FDOM loss in the C1 region when halides were present (Grebel et al., 2009). Additionally, Romera-Castillo et al., reported loss of fluorescence in the C1 region during microbial incubations (Romera-Castillo et al., 2011). Photo-bleaching via reactive halogen species or microbial degradation (all samples in this study were filter sterilized) may therefore further account for the depletion of C1 fluorescence in the surface ocean.

Protein-like compounds undergo both sunlight-induced direct photolysis and indirect photolysis via reactive intermediate species. The location of reactive sites such as tryptophan and tyrosine within the structure are a critical factor in reaction rates,

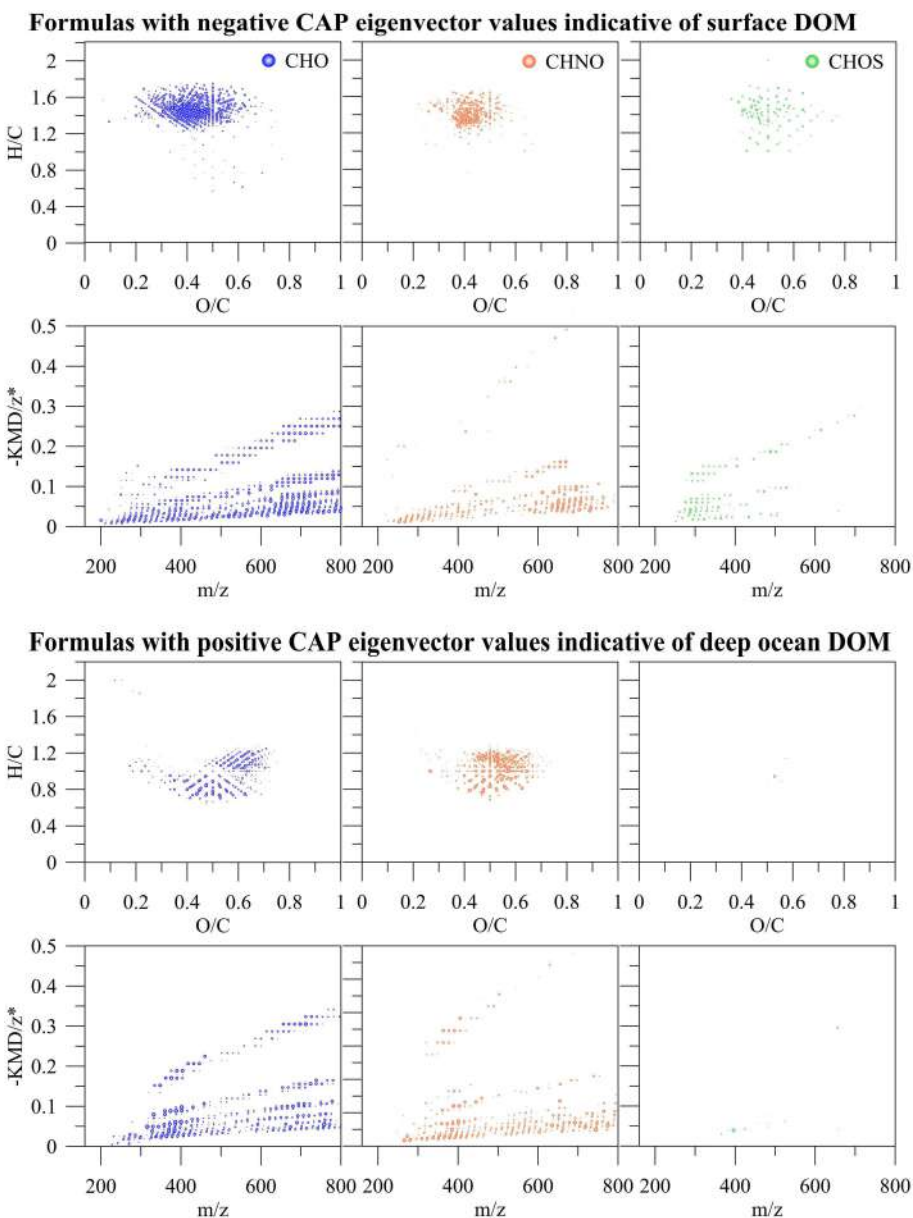


FIGURE 9 | *m/z* ions and associated molecular formulas with negative and positive eigenvector values of the canonical analysis on principal coordinate 1 (CAP1) of the EEM resemblance matrix and the FT-ICR-MS data of all SPE-DOM samples collected at BATS in 2013 (see also Figure 7C).

with steric hindrances affecting reactions with singlet oxygen and proximity to DOM sensitizers/quenchers (Janssen et al., 2014; Lundein et al., 2014). The kinetics of UVA fluorescence loss (C3 and C5) are likewise complicated by the fact that protein-like fluorescence undergoes variable quenching depending on the location of fluorescent amino acids in (or free from) the protein structure (Kronman and Holmes, 1971; Lakowicz, 2006). Additionally, protein-like fluorescence has been shown to be quenched by humic substances (Wang et al., 2015). The effects of quenching on the UVA fluorescence intensity could not be determined due to the changes in quantity and quality of the proteinaceous and humic-like materials during

irradiation. Therefore, while these components showed photolability, alternate techniques would be necessary to accurately quantify changes in proteinaceous material. Nevertheless, the photo-lability of these components is likely offset by high primary production in the surface ocean.

Ultrahigh resolution mass spectrometry showed unique aliphatic signatures in the surface waters, including a diverse group of aliphatic sulfur-containing molecular ions which may be generated by photoautotrophs or communities depending on primary production (Figure 6). The principal component analysis using the *m/z* ions and their intensities (Figure 8), as well as the correlation between the mass peaks and the fluorescence

(Figure 9) associated aliphatic compounds with surface waters and hydrogen-deficient compounds with deep water samples. The enrichment of aliphatic compounds in marine surface waters have been previously documented and is in good agreement with our data (Flerus et al., 2012). In 57 day irradiations of Congo River water, the majority of photo-resistant peaks and photo-products identified by FT-ICR-MS were aliphatic, while aromatic compounds were the most photo-reactive (Stubbins et al., 2010). NMR and FTIR spectroscopy have similarly identified aromatic sites as the most photo-labile (Thorn et al., 2010; Helms et al., 2014). These depth-dependent trends match those of the North Pacific, including an apparent homogeneity in the FT-ICR peaks below 1000 m depth (Medeiros et al., 2015). This apparent homogeneity is notable because it matched exactly the trends observed in EEM-PARAFAC components that are indicative for conjugated aromatic compounds such as polyphenols.

Fluorescence in the marine- and terrestrial-like regions of the EEM have been shown to be produced by microbes (Rochelle-Newall and Fisher, 2002; Biers et al., 2007), and correlated well with apparent oxygen utilization (AOU) at depth (Yamashita and Tanoue, 2008; Jørgensen et al., 2011; Kowalcuk et al., 2013; Catalá et al., 2015; Lønborg et al., 2015). The microbial

carbon pump is believed to produce (semi)refractory molecules, including CDOM and FDOM, in the mesopelagic zone, which are then transported to the deep ocean (Jiao et al., 2010; Flerus et al., 2012; Hansell, 2013). The fast photo kinetics shown in this study as well as the enrichment in hydrogen-deficient molecular ions at depth and depletion of these molecules at the surface highly suggests that deep-sea FDOM is very unlikely to survive overturning circulation and hence cannot be responsible for the DOM component that contributes to the very old apparent ^{14}C age of deep sea DOM of 3700–6000 years (Bauer et al., 1992).

Acknowledgments

This project was supported by the Maryland Sea Grant REU program in summer 2013 and 2014. This is contribution 5083 of the University of Maryland Center for Environmental Science. Shiptime aboard the RV Atlantic Explorer was kindly provided by the Oceanic Flux Program (OFP) time-series (NSF OCE 0927098 and OCE 1234294). This material is based upon work supported by the National Science Foundation Graduate Research Fellowship Program under Grant No. DGE-1321846 (SAT).

References

- Anderson, M. J., and Willis, T. J. (2003). Canonical analysis of principal coordinates: a useful method of constrained ordination for ecology. *Ecology* 84, 511–525. doi: 10.1890/0012-9658(2003)084[0511:CAOPCA]2.0.CO;2
- Andrew, A. A., Del Vecchio, R., Subramaniam, A., and Blough, N. V. (2013). Chromophoric dissolved organic matter (CDOM) in the Equatorial Atlantic Ocean: optical properties and their relation to CDOM structure and source. *Mar. Chem.* 148, 33–43. doi: 10.1016/j.marchem.2012.11.001
- Bauer, J. E., Williams, P. M., and Druffel, E. R. M. (1992). ^{14}C activity of dissolved organic carbon fractions in the north-central Pacific and Sargasso Sea. *Nature* 357, 667–670. doi: 10.1038/357667a0
- Benner, R., Louchouarn, P., and Amon, R. M. W. (2005). Terrigenous dissolved organic matter in the Arctic Ocean and its transport to surface and deep waters of the North Atlantic. *Global Biogeochem. Cycles* 19:GB2025. doi: 10.1029/2004GB002398
- Bianco, A., Minella, M., De Laurentiis, E., Maurino, V., Minero, C., and Vione, D. (2014). Photochemical generation of photoactive compounds with fulvic-like and humic-like fluorescence in aqueous solution. *Chemosphere* 111, 529–536. doi: 10.1016/j.chemosphere.2014.04.035
- Biers, E. J., Zepp, R. G., and Moran, M. A. (2007). The role of nitrogen in chromophoric and fluorescent dissolved organic matter formation. *Mar. Chem.* 103, 46–60. doi: 10.1016/j.marchem.2006.06.003
- Boyle, E. S., Guerriero, N., Thialet, A., Del Vecchio, R., and Blough, N. V. (2009). Optical Properties of Humic Substances and CDOM: Relation to Structure. *Environ. Sci. Technol.* 43, 2262–2268. doi: 10.1021/es803264g
- Bro, R., and Smilde, A. K. (2014). Principal component analysis. *Anal. Methods* 6, 2812–2831. doi: 10.1039/c3ay41907j
- Catalá, T. S., Reche, I., Fuentes-Lema, A., Romera-Castillo, C., Nieto-Cid, M., Ortega-Retuerta, E., et al. (2015). Turnover time of fluorescent dissolved organic matter in the dark global ocean. *Nat Commun* 6:5986. doi: 10.1038/ncomms6986
- Chen, H., Stubbins, A., Perdue, E. M., Green, N. W., Helms, J. R., Mopper, K., et al. (2014). Ultrahigh resolution mass spectrometric differentiation of dissolved organic matter isolated by coupled reverse osmosis-electrodialysis from various major oceanic water masses. *Mar. Chem.* 164, 48–59. doi: 10.1016/j.marchem.2014.06.002
- Coble, P. G. (1996). Characterization of marine and terrestrial DOM in seawater using excitation emission matrix spectroscopy. *Mar. Chem.* 51, 325–346. doi: 10.1016/0304-4203(95)00062-3
- Coble, P. G. (2007). Marine optical biogeochemistry: the chemistry of ocean color. *Chem. Rev.* 107, 402–418. doi: 10.1021/cr050350+
- Cooper, W. J., Zika Rod, G., Petasne Robert, G., and Fischer Anne, M. (1989). “Sunlight-induced photochemistry of humic substances in natural waters: major reactive species,” in *Aquatic Humic Substances*, eds I. H. Suffet, and P. MacCarthy (Washington, DC: American Chemical Society), 333–362.
- D'androlli, J., Dittmar, T., Koch, B. P., Purcell, J. M., Marshall, A. G., and Cooper, W. T. (2010). Comprehensive characterization of marine dissolved organic matter by Fourier transform ion cyclotron resonance mass spectrometry with electrospray and atmospheric pressure photoionization. *Rapid Commun. Mass Spectrom.* 24, 643–650. doi: 10.1002/rcm.4421
- De Laurentiis, E., Maurino, V., Minero, C., Vione, D., Mailhot, G., and Brigante, M. (2013). Could triplet-sensitised transformation of phenolic compounds represent a source of fulvic-like substances in natural waters? *Chemosphere* 90, 881–884. doi: 10.1016/j.chemosphere.2012.09.031
- Dittmar, T., Koch, B., Hertkorn, N., and Kattner, G. (2008). A simple and efficient method for the solid-phase extraction of dissolved organic matter (SPE-DOM) from seawater. *Limnol. Oceanogr. Methods* 6, 230–235. doi: 10.4319/lom.2008.6.230
- Dittmar, T., Whitehead, K., Minor, E. C., and Koch, B. P. (2007). Tracing terrigenous dissolved organic matter and its photochemical decay in the ocean by using liquid chromatography/mass spectrometry. *Mar. Chem.* 107, 378–387. doi: 10.1016/j.marchem.2007.04.006
- Flerus, R., Lechtenfeld, O. J., Koch, B. P., McCallister, S. L., Schmitt-Kopplin, P., Benner, R., et al. (2012). A molecular perspective on the ageing of marine dissolved organic matter. *Biogeosciences* 9, 1935–1955. doi: 10.5194/bg-9-1935-2012
- Gao, H. Z., and Zepp, R. G. (1998). Factors influencing photoreactions of dissolved organic matter in a coastal river of the southeastern United States. *Environ. Sci. Technol.* 32, 2940–2946. doi: 10.1021/es9803660
- Gonsior, M., Hertkorn, N., Conte, M. H., Cooper, W. J., Bastviken, D., Druffel, E., et al. (2014a). Photochemical production of polyols arising from significant photo-transformation of dissolved organic matter in the oligotrophic surface ocean. *Mar. Chem.* 163, 10–18. doi: 10.1016/j.marchem.2014.04.002

- Gonsior, M., Peake, B. M., Cooper, W. T., Podgorski, D. C., D'andrilli, J., Dittmar, T., et al. (2011). Characterization of dissolved organic matter across the Subtropical Convergence off the South Island, New Zealand. *Mar. Chem.* 123, 99–110. doi: 10.1016/j.marchem.2010.10.004
- Gonsior, M., Schmitt-Kopplin, P., and Bastviken, D. (2013). Depth-dependent molecular composition and photo-reactivity of dissolved organic matter in a boreal lake under winter and summer conditions. *Biogeosciences* 10, 6945–6956. doi: 10.5194/bg-10-6945-2013
- Gonsior, M., Schmitt-Kopplin, P., Stavklint, H., Richardson, S. D., Hertkorn, N., and Bastviken, D. (2014b). Changes in dissolved organic matter during the treatment processes of a drinking water plant in Sweden and formation of previously unknown disinfection byproducts. *Environ. Sci. Technol.* 48, 12714–12722. doi: 10.1021/es504349p
- Grebel, J. E., Pignatello, J. J., Song, W., Cooper, W. J., and Mitch, W. A. (2009). Impact of halides on the photobleaching of dissolved organic matter. *Mar. Chem.* 115, 134–144. doi: 10.1016/j.marchem.2009.07.009
- Hansell, D. A. (2013). Recalcitrant dissolved organic carbon fractions. *Ann. Rev. Mar. Sci.* 5, 421–445. doi: 10.1146/annurev-marine-120710-100757
- Hansell, D. A., Carlson, C. A., Repeta, D. J., and Schlitzer, R. (2009). Dissolved organic matter in the ocean: a controversy stimulates new insights. *Oceanography* 22, 202–211. doi: 10.5670/oceanog.2009.109
- Heller, M. I., Gaiero, D. M., and Croot, P. L. (2013). Basin scale survey of marine humic fluorescence in the Atlantic: Relationship to iron solubility and H₂OO₂. *Global Biogeochem. Cycles* 27, 88–100. doi: 10.1029/2012GB004427
- Helms, J. R., Mao, J., Stubbins, A., Schmidt-Rohr, K., Spencer, R. G. M., Hernes, P. J., et al. (2014). Loss of optical and molecular indicators of terrigenous dissolved organic matter during long-term photobleaching. *Aquat. Sci.* 76, 353–373. doi: 10.1007/s00027-014-0340-0
- Helms, J. R., Stubbins, A., Perdue, E. M., Green, N. W., Chen, H., and Mopper, K. (2013). Photochemical bleaching of oceanic dissolved organic matter and its effect on absorption spectral slope and fluorescence. *Mar. Chem.* 155, 81–91. doi: 10.1016/j.marchem.2013.05.015
- Hertkorn, N., Benner, R., Frommberger, M., Schmitt-Kopplin, P., Witt, M., Kaiser, K., et al. (2006). Characterization of a major refractory component of marine dissolved organic matter. *Geochim. Cosmochim. Acta* 70, 2990–3010. doi: 10.1016/j.gca.2006.03.021
- Herzsprung, P., Von Tümpeling, W., Hertkorn, N., Harir, M., Büttner, O., Bravidor, J., et al. (2012). Variations of DOM quality in inflows of a drinking water reservoir: linking of van Krevelen diagrams with EEMF spectra by rank correlation. *Environ. Sci. Technol.* 46, 5511–5518. doi: 10.1021/es300345c
- Janssen, E. M. L., Erickson, P. R., and Mcneill, K. (2014). Dual roles of dissolved organic matter as sensitizer and quencher in the photooxidation of tryptophan. *Environ. Sci. Technol.* 48, 4916–4924. doi: 10.1021/es500535a
- Jiao, N., Herndl, G. J., Hansell, D. A., Benner, R., Kattner, G., Wilhelm, S. W., et al. (2010). Microbial production of recalcitrant dissolved organic matter: long-term carbon storage in the global ocean. *Nat. Rev. Microbiol.* 8, 593–599. doi: 10.1038/nrmicro2386
- Jørgensen, L., Stedmon, C. A., Granskog, M. A., and Middelboe, M. (2014). Tracing the long-term microbial production of recalcitrant fluorescent dissolved organic matter in seawater. *Geophys. Res. Lett.* 41, 2481–2488. doi: 10.1002/2014GL059428
- Jørgensen, L., Stedmon, C. A., Kragh, T., Markager, S., Middelboe, M., and Søndergaard, M. (2011). Global trends in the fluorescence characteristics and distribution of marine dissolved organic matter. *Mar. Chem.* 126, 139–148. doi: 10.1016/j.marchem.2011.05.002
- Kellerman, A. M., Kothawala, D. N., Dittmar, T., and Tranvik, L. J. (2015). Persistence of dissolved organic matter in lakes related to its molecular characteristics. *Nature Geosci.* 8, 454–457. doi: 10.1038/ngeo2440
- Kieber, D. J., McDaniel, J., and Mopper, K. (1989). Photochemical source of biological substrates in seawater- implications for carbon cycling. *Nature* 341, 637–639. doi: 10.1038/341637a0
- Koch, B. P., Witt, M. R., Engbrodt, R., Dittmar, T., and Kattner, G. (2005). Molecular formulae of marine and terrigenous dissolved organic matter detected by electrospray ionization Fourier transform ion cyclotron resonance mass spectrometry. *Geochim. Cosmochim. Acta* 69, 3299–3308. doi: 10.1016/j.gca.2005.02.027
- Kowalcuk, P., Tilstone, G. H., Zablocka, M., Roettgers, R., and Thomas, R. (2013). Composition of dissolved organic matter along an Atlantic Meridional Transect from fluorescence spectroscopy and Parallel Factor Analysis. *Mar. Chem.* 157, 170–184. doi: 10.1016/j.marchem.2013.10.004
- Kronman, M. J., and Holmes, L. G. (1971). The fluorescence of native, denatured and reduced-denatured proteins. *Photochem. Photobiol.* 14, 113–134. doi: 10.1111/j.1751-1097.1971.tb06157.x
- Lakowicz, J. R. (2006). *Principles of Fluorescence Spectroscopy*. New York, NY: Springer.
- Lechtenfeld, O. J., Kattner, G., Flerus, R., Mccallister, S. L., Schmitt-Kopplin, P., and Koch, B. P. (2014). Molecular transformation and degradation of refractory dissolved organic matter in the Atlantic and Southern Ocean. *Geochim. Cosmochim. Acta* 126, 321–337. doi: 10.1016/j.gca.2013.11.009
- Lønborg, C., Yokokawa, T., Herndl, G. J., and Antón Alvarez-Salgado, X. (2015). Production and degradation of fluorescent dissolved organic matter in surface waters of the eastern north Atlantic ocean. *Deep Sea Res. I Oceanogr. Res Papers* 96, 28–37. doi: 10.1016/j.dsr.2014.11.001
- Lundein, R. A., Janssen, E. M. L., Chu, C., and Mcneill, K. (2014). Environmental photochemistry of Amino Acids, Peptides and Proteins. *CHIMIA Int. J. Chem.* 68, 812–817. doi: 10.2533/chimia.2014.812
- McNally, A. M., Moody, E. C., and Mcneill, K. (2005). Kinetics and mechanism of the sensitized photodegradation of lignin model compounds. *Photochem. Photobiol. Sci.* 4, 268–274. doi: 10.1039/b416956e
- Medeiros, P. M., Seidel, M., Powers, L. C., Dittmar, T., Hansell, D. A., and Miller, W. L. (2015). Dissolved organic matter composition and photochemical transformations in the Northern North Pacific Ocean. *Geophys. Res. Lett.* 42, 863–870. doi: 10.1002/2014GL062663
- Miller, W. L., and Zepp, R. G. (1995). Photochemical production of dissolved inorganic carbon from terrestrial organic matter: Significance to the oceanic organic carbon cycle. *Geophys. Res. Lett.* 22, 417–420. doi: 10.1029/94GL03344
- Murphy, K. R., Stedmon, C. A., Graeber, D., and Bro, R. (2013). Fluorescence spectroscopy and multi-way techniques. *PARAFAC. Anal. Methods* 5, 6557–6566. doi: 10.1039/c3ay41160e
- Nelson, N. B., and Siegel, D. A. (2013). “The global distribution and dynamics of chromophoric dissolved organic matter,” in *Annual Review of Marine Science*, Vol. 5, eds C. A. Carlson and S. J. Giovannoni (Palo Alto, CA: Annual Reviews), 447–476.
- Rochelle-Newall, E. J., and Fisher, T. R. (2002). Production of chromophoric dissolved organic matter fluorescence in marine and estuarine environments: an investigation into the role of phytoplankton. *Mar. Chem.* 77, 7–21. doi: 10.1016/S0304-4203(01)00072-X
- Roettgers, R., and Koch, B. P. (2012). Spectroscopic detection of a ubiquitous dissolved pigment degradation product in subsurface waters of the global ocean. *Biogeosciences* 9, 2585–2596. doi: 10.5194/bg-9-2585-2012
- Romera-Castillo, C., Sarmento, H., Álvarez-Salgado, X. A., Gasol, J. M., and Marrasé, C. (2011). Net production and consumption of fluorescent colored dissolved organic matter by natural bacterial assemblages growing on marine phytoplankton exudates. *Appl. Environ. Microbiol.* 77, 7490–7498. doi: 10.1128/AEM.00200-11
- Shank, G. C., Lee, R., Vahatalo, A., Zepp, R. G., and Bartels, E. (2010). Production of chromophoric dissolved organic matter from mangrove leaf litter and floating Sargassum colonies. *Mar. Chem.* 119, 172–181. doi: 10.1016/j.marchem.2010.02.002
- Shimotori, K., Watanabe, K., and Hama, T. (2012). Fluorescence characteristics of humic-like fluorescent dissolved organic matter produced by various taxa of marine bacteria. *Aquat. Microbiol. Ecol.* 65, 249–260. doi: 10.3354/ame01552
- Sleighter, R. L., Cory, R. M., Kaplan, L. A., Abdulla, H. A. N., and Hatcher, P. G. (2014). A coupled geochemical and biogeochemical approach to characterize the bioreactivity of dissolved organic matter from a headwater stream. *J. Geophys. Res. Biogeosci.* 119, 1520–1537. doi: 10.1002/2013JG002600
- Stedmon, C. A., and Bro, R. (2008). Characterizing dissolved organic matter fluorescence with parallel factor analysis: a tutorial. *Limnol. Oceanogr. Methods* 6, 572–579. doi: 10.4319/lom.2008.6.5.72
- Stedmon, C. A., and Nelson, N. B. (2015). “The optical properties of DOM in the Ocean,” in *Biogeochemistry of Marine Dissolved Organic Matter*, eds D. A. Hansell and C. A. Carlson (New York, NY: Academic Press), 481–508.
- Steinberg, D. K., Nelson, N. B., Carlson, C. A., and Prusak, A. (2004). Production of chromophoric dissolved organic matter (CDOM) in the open ocean by

- zooplankton and the colonial cyanobacterium *Trichodesmium* spp. *Mar. Ecol. Prog. Ser.* 267, 45–56. doi: 10.3354/meps267045
- Stubbins, A., Lapierre, J.-F., Berggren, M., Prairie, Y., Dittmar, T., and Del Giorgio, P. (2014). What's in an EEM? Molecular signatures associated with dissolved organic fluorescence in boreal Canada. *Environ. Sci. Technol.* 48, 10598–10606. doi: 10.1021/es502086e
- Stubbins, A., Spencer, R. G. M., Chen, H., Hatcher, P. G., Mopper, K., Hernes, P. J., et al. (2010). Illuminated darkness: Molecular signatures of Congo River dissolved organic matter and its photochemical alteration as revealed by ultrahigh precision mass spectrometry. *Limnol. Oceanogr.* 55, 1467–1477. doi: 10.4319/lo.2010.55.4.1467
- Thorn, K. A., Younger, S. J., and Cox, L. G. (2010). Order of functionality loss during photodegradation of aquatic humic substances. *J. Environ. Qual.* 39, 1416–1428. doi: 10.2134/jeq2009.0408
- Timko, S. A., Gonsior, M., and Cooper, W. J. (in press). Influence of pH on fluorescent dissolved organic matter photo-degradation. *Water Res.* doi: 10.1016/j.watres.2015.08.047
- Tranvik, L. J., and Bertilsson, S. (2001). Contrasting effects of solar UV radiation on dissolved organic sources for bacterial growth. *Ecol. Lett.* 4, 458–463. doi: 10.1046/j.1461-0248.2001.00245.x
- van Krevelen, D. W. (1950). Graphical-statistical method for the study of structure and reaction processes of coal. *Fuel* 29, 269–284.
- Vione, D., Minella, M., Maurino, V., and Minero, C. (2014). Indirect photochemistry in sunlit surface waters: photoinduced production of reactive transient species. *Chem. A Eur. J.* 20, 10590–10606. doi: 10.1002/chem.201400413
- Wang, Z., Cao, J., and Meng, F. (2015). Interactions between protein-like and humic-like components in dissolved organic matter revealed by fluorescence quenching. *Water Res.* 68, 404–413. doi: 10.1016/j.watres.2014.10.024
- Yamashita, Y., and Tanoue, E. (2008). Production of bio-refractory fluorescent dissolved organic matter in the ocean interior. *Nat. Geosci.* 1, 579–582. doi: 10.1038/ngeo279
- Yekta, S. S., Gonsior, M., Schmitt-Kopplin, P., and Svensson, B. H. (2012). Characterization of dissolved organic matter in full scale continuous stirred tank biogas reactors using ultrahigh resolution mass spectrometry: a qualitative overview. *Environ. Sci. Technol.* 46, 12711–12719. doi: 10.1021/es3024447
- Zepp, R. G., Sheldon, W. M., and Moran, M. A. (2004). Dissolved organic fluorophores in southeastern US coastal waters: correction method for eliminating Rayleigh and Raman scattering peaks in excitation-emission matrices. *Mar. Chem.* 89, 15–36. doi: 10.1016/j.marchem.2004.02.006

Conflict of Interest Statement: The authors declare that the research was conducted in the absence of any commercial or financial relationships that could be construed as a potential conflict of interest.

Copyright © 2015 Timko, Maydanov, Pittelli, Conte, Cooper, Koch, Schmitt-Kopplin and Gonsior. This is an open-access article distributed under the terms of the Creative Commons Attribution License (CC BY). The use, distribution or reproduction in other forums is permitted, provided the original author(s) or licensor are credited and that the original publication in this journal is cited, in accordance with accepted academic practice. No use, distribution or reproduction is permitted which does not comply with these terms.



Linking Heterotrophic Microbial Activities with Particle Characteristics in Waters of the Mississippi River Delta in the Aftermath of Hurricane Isaac

Kai Ziervogel^{1*}, Christopher Osburn², Adeline Brym², Jessica Battles³, Samantha Joye³, Nigel D'souza⁴, Joseph Montoya⁴, Uta Passow⁵ and Carol Arnosti¹

OPEN ACCESS

Edited by:

Marta Álvarez,
Instituto Español de Oceanografía,
Spain

Reviewed by:

Taichi Yokokawa,
Japan Agency for Marine-Earth
Science and Technology, Japan
Federico Baltar,
University of Otago, New Zealand

*Correspondence:

Kai Ziervogel
kai.ziervogel@unh.edu

Specialty section:

This article was submitted to
Marine Biogeochemistry,
a section of the journal
Frontiers in Marine Science

Received: 02 October 2015

Accepted: 22 January 2016

Published: 16 February 2016

Citation:

Ziervogel K, Osburn C, Brym A,
Battles J, Joye S, D'souza N,
Montoya J, Passow U and Arnosti C
(2016) Linking Heterotrophic Microbial
Activities with Particle Characteristics
in Waters of the Mississippi River Delta
in the Aftermath of Hurricane Isaac.
Front. Mar. Sci. 3:8.
doi: 10.3389/fmars.2016.00008

¹ Department of Marine Sciences, University of North Carolina at Chapel Hill, Chapel Hill, NC, USA, ² Department of Marine, Earth and Atmospheric Sciences, North Carolina State University, Raleigh, NC, USA, ³ Department of Marine Sciences, University of Georgia, Athens, GA, USA, ⁴ School of Biology, Georgia Institute of Technology, Atlanta, GA, USA, ⁵ Marine Science Institute, University of California Santa Barbara, Santa Barbara, CA, USA

Riverine runoff often triggers microbial responses in coastal marine environments, including phytoplankton blooms and enhanced bacterial biomass production that drive the transformation of dissolved and particulate organic matter (POM) on its way from land to the deep ocean. We measured concentrations and characteristics of POM, concentrations of dissolved organic carbon (DOC), and bacterial community abundance and activities in the water column at three sites near the Mississippi River Delta about 2 weeks after Hurricane Isaac made landfall in late August 2012. River plumes had salinities of >30 PSU and high levels of DOC (210–380 µM), resulting from the storm surge that pushed large quantities of marine waters upstream. Relatively high concentrations of phytoplankton POM and low levels of microbial exopolymeric particles (TEP and CSP) suggested that storm-induced riverine discharge triggered the development of phytoplankton blooms that were in their initial stages at the time of sampling. Surface water POM had C/N ratios of 5–7 and strong protein-like fluorescence signals in the base-extracted POM (BEPOM) fraction at the two sites closer to the river mouth (Stns. TE and MSP). Freshly produced POM triggered a two-fold increase in heterotrophic bacterial biomass production (³H-leucine incorporation) and a four-fold increase in bacterial peptide hydrolysis (activities of leucine-aminopeptidase). In contrast, elevated DOC concentrations coincided with only moderate bacterial community activity, suggesting that heterotrophic bacterial metabolism near the Mississippi River Delta in the aftermath of Hurricane Isaac was more closely linked with autochthonous primary production.

Keywords: hydrolytic enzyme activities, bacterial protein production, base-extracted POM, Mississippi River discharge, carbon cycle, Hurricane Isaac

INTRODUCTION

The nature and inventory of organic matter in the coastal ocean is mainly driven by heterotrophic microbial communities that process and transform organic matter from a myriad of potential sources, including riverine inputs, atmospheric deposition, and sediment resuspension, thus regulating carbon export from land to the open ocean. In the Gulf of Mexico, most of the land-sea carbon fluxes are driven by Mississippi River runoff and subsequent biogeochemical organic matter processing that occurs on the Louisiana Shelf near the bird-foot delta, where most of the riverine discharge enters the coastal ocean (e.g., Green et al., 2006). Buoyant freshwater plumes of Mississippi River water generally extend westward from the delta, following the Louisiana coastal current; however, wind-driven changes in the direction of surface water currents near the delta can also lead to an eastward offshore transport of Mississippi River plumes (Schiller et al., 2011).

The Mississippi River is the largest river in North America, draining ~40% of the continental United States. Given its important role in transport and cycling of terrestrial carbon between the land and the ocean, numerous geochemical studies have measured carbon flux from the Mississippi River into near-shore environments (e.g., Bianchi et al., 1997; Wang et al., 2004), suggesting that microbially-driven organic matter transformation could be an important sink for terrestrial carbon on the Louisiana shelf (Benner and Opsahl, 2001; Bianchi et al., 2013). Comparatively fewer studies have directly measured microbial metabolic rates on the shelf near the Mississippi River Delta, focusing on near-shore phytoplankton growth and bacterial biomass production during the high productivity season in early summer that follows highest riverine discharge in late spring (Amon and Benner, 1998; Lohrenz et al., 1999; Pakulski et al., 2000). During that time elevated rates of primary productivity and secondary production driven by high inputs of inorganic nutrients through the Mississippi River often result in the development of seasonal hypoxia on the Louisiana Shelf (Rabalais et al., 2010; Murrell et al., 2013).

In addition to seasonal inputs of riverine organic substrates, and inorganic nutrients and minerals, storm-induced perturbations can also cause elevated runoff from the Mississippi River with possible consequences for microbial growth and metabolism on the shelf. For instance, remote sensing observations revealed phytoplankton blooms near the Mississippi River Delta and on the Louisiana shelf following Tropical Storm Barry in early August, 2001, and Hurricane Lilli in late September 2002 (Yuan et al., 2004). In the aftermath of Hurricanes Katrina and Rita in August and September 2005, respectively, MODIS satellite imagery showed elevated chlorophyll *a* concentrations, suggesting increased phytoplankton biomass over large areas of the Louisiana shelf. It has been suggested that these elevations in chlorophyll may have been caused by intense deliveries of terrestrial materials into coastal waters, changes in water circulation patterns, and enhanced sediment resuspension on the Louisiana shelf (Lohrenz et al., 2008). Storm-induced sediment resuspension on

the Louisiana shelf was also observed after Hurricane George in late September 1998 (Ross et al., 2009). After Hurricane Isaac made landfall in late August 2012, lateral near-bed transport of mainly lithogenic material led to sediment resuspension and subsequent formation of bottom turbidity layers that stimulated heterotrophic bacterial biomass production and organic matter degradation in the deep Gulf of Mexico (Ziervogel et al., 2015).

The goal of the present study was to investigate the effects of Hurricane Isaac's storm-surge on microbial activities, and organic matter processing in the water column at three coastal sites near the Mississippi River Delta. Given that the extent of bacterial processing of organic matter in near-shore environments depends on the characteristics of the substrates, as well as on the capabilities and activities of heterotrophic microbial communities (see Arnosti, 2011 for a recent review), we linked measurements of bacterial activities with chemical analysis of the organic matter pool. In particular, bacterial abundance and biomass production (leucine incorporation), as well as activities of two classes of microbial hydrolytic enzymes indicative of carbohydrate and peptide hydrolysis (leucine-aminopeptidase and β -glucosidase) were measured at distinct depths throughout the water column of the three sites. In parallel we determined concentrations of dissolved and particulate organic carbon and chlorophyll *a* concentrations, abundance of transparent exopolymeric particles (TEP) and Coomassie-stainable particles (CSP), i.e., carbohydrate- and peptide-rich microparticles, respectively, which form from phytoplankton and bacterial exudates (Long and Azam, 1996; Passow, 2002), along with fluorescence properties of base-extracted particulate organic matter (BEPOM). Base-extraction of POM provides the means to compare fluorescence features indicative of sources and origin of fractions of the POM pool (Brym et al., 2014).

MATERIALS AND METHODS

Site Locations and Water Column Sampling

Water column samples were taken on September 9–10, 2012, at three sites on the Louisiana shelf, northeastern Gulf of Mexico, aboard RV *Endeavor*. The sampling occurred 12 days after Hurricane Isaac made landfall on the Louisiana coast on August 28, 2012, producing heavy rains and a storm surge that extended for more than 300 miles upriver (Berg, 2013). Two of the three sites are located to the south (Stn. MSP) and south-east (Stn. O) of the Southwest Pass; Stn. TE is located ~20 km south-east of the South Pass (**Figure 1**; **Table 1**), and near a chronic oil leakage from the sunken Taylor Energy platform. Note that in Brym et al. (2014), Stns. O, MSP, and TE are referred to as Stns. 1, 2, and 3, respectively.

Water column temperature and salinity, beam attenuation (a measure of turbidity), and chlorophyll fluorescence (a proxy for phytoplankton biomass; hereafter referred to as CTD-derived chl fluorescence) were measured by sensors attached to a CTD rosette. Water samples from distinct depths were collected by Niskin bottles attached to the rosette, and analyzed

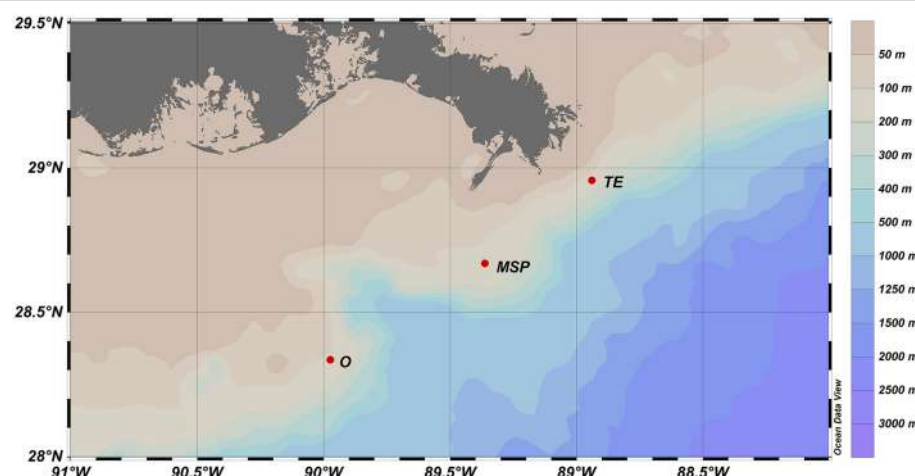


FIGURE 1 | Map of the sampling sites on the Louisiana shelf. See Table 1 for a detailed site description.

TABLE 1 | Description of sampling sites and dates of sampling.

Station	Lat (°N)	Long (°W)	Depth (m)	Sampling date/time (UTC)	Station ID
Taylor Energy (TE)	28 57.43	88 56.38	125	Sept 10, 2012/04:33	515.007.01
MS River plume (MSP)	28 40.16	89 21.80	132	Sept 09, 2012/13:53	515.005.01
Offshore (O)	28 20.14	89 58.46	111	Sept 09, 2012/08:17	515.004.01

for the parameters described below. The data presented in this study is freely available on the GRIIDC database under the Unique Dataset Identifiers (UDIs) R1.x132.134:0111 and R1.x132.134:006.

Analysis

Dissolved Organic Carbon (DOC)

Water samples were filtered through 0.2-μm surfactant-free cellulose acetate syringe filters and stored in pre-combusted glass vials at -20°C until analysis (total volume filtered per sample: 15 mL). Defrosted samples were acidified (50% phosphoric acid v/v) and injected into a Shimadzu TOC-5000 analyzer that uses high temperature catalytic oxidation. Duplicate samples per station and depth were injected; instrument settings yielded at least three repeated measurements of each sample.

Particulate Organic Carbon (POC) and Nitrogen (PON)

Water samples were vacuum filtered onto replicate pre-combusted and pre-weighed GF/F filters (total volume filtered per sample: 1000 mL) immediately after collection. The filters were stored in clean centrifuge tubes at -20°C. Prior to POC and PON analysis, the filters were dried at 40°C overnight and reweighed on a high-precision balance to determine total suspended matter (TSM). The filters were acidified with 12 M HCl for 12 h to remove inorganic carbon, followed by flash combustion to CO₂ and N₂ on a Carlo-Erba 1500 Elemental Analyzer, using acetanilide as a standard.

Chlorophyll a

Between 75 and 200 mL of seawater were filtered onto replicate 0.4 μm PC filters immediately after sampling. The filters were stored at -20°C, and soaked in 90% acetone overnight in the freezer before chlorophyll *a* (chl *a*) was measured on a fluorometer (Turner 700) according to Strickland and Parsons (1972).

Fluorescence Properties of Base-Extracted Particulate Organic Matter (BEPOM)

Samples were analyzed as described in Osburn et al. (2012) and Brym et al. (2014). In brief, base-soluble POM was extracted from each GF/F filter into 0.1 N sodium hydroxide (NaOH) for 24 h at 4°C. The basic solution was neutralized with concentrated hydrochloric acid (HCl) and filtered (0.2 μm PES filter) to remove filter particles prior to absorbance and fluorescence measurement on Varian Cary 300 and Eclipse instruments, respectively. BEPOM absorbance spectra were measured from 220 to 800 nm. Samples with raw absorbance >0.4 at 240 nm were diluted. All samples were blank-corrected against a neutralized NaOH control. Fluorescence of BEPOM samples was measured at excitation wavelengths 220–500 nm at 5 nm intervals, with 5 nm excitation slits. Emission was measured between 240 and 600 nm at 2 nm intervals with 5 nm emission slits. Fluorescence intensities were corrected for spectral variation in lamp intensities and detector response, and calibrated in quinine sulfate units (QSU). Fluorescence results are presented as

excitation-emission matrices (EEMs) and visualized as contour plots.

Transparent Exopolymeric Particles (TEP) and Coomassie Stainable Particles (CSP)

TEP and CSP are particulate components of microbial extracellular polymeric substances in the ocean. Abundance and distribution of TEP and CSP were analyzed microscopically as described in Engel (2009). In brief, 5 mL formalin-fixed water (2% final conc.) were filtered at low, constant vacuum (<200 mmHg) onto replicate 0.4- μm Nuclepore filters and stained with 0.02% Alcian Blue (pH 2.5) or 0.04% Coomassie Brilliant Blue (pH 7.4) for TEP and CSP analysis, respectively. The filters were rinsed with Milli-Q water to remove the excess dye and placed on a CytoClear slide (Sternitech Corp) with a drop of immersion oil underneath and on top of the filter, then covered with a glass cover slide. Slides were examined and photographed with an inverted microscope (Olympus CK2) equipped with a digital camera (Moticam 2500) at 200 \times magnification. Thirty pictures were taken for each filter and stained particles were analyzed using ImageJ software. The total numbers of visible particles were used to calculate particle abundance.

Bacterial Abundance

Ten milliliters of water were fixed with formalin (2% final conc.) immediately after collection and stored in the dark at 4°C until analysis. A known volume of each fixed sample was filtered onto 0.2- μm pore, black polycarbonate filter (Millipore, type GTPB) using low vacuum. The filters were transferred to clean microscope slides. Ten microliter of a freshly prepared staining solution containing 50% glycerol in 1 \times PBS at pH 7.4, ascorbic acid (1% final conc. v/v), and SYBR green I stain (0.45% final conc. v/v) was placed in the middle of a cover slip (25 \times 25 mm) and inverted onto the filter (Lunau et al., 2005). The slide was then placed in the dark at 4°C, until the weight of the cover slip dispensed the stain evenly across the filter. Bacterial cells were counted with a Nikon Labophot-2 epifluorescence microscope with blue light excitation at 1000 \times magnification, respectively. A minimum of 200 cells were enumerated within a grid of fixed dimensions across each filter.

Bacterial Biomass Production (^3H -Leucine Incorporation)

^3H -leucine incorporation measurements, a measure of bacterial protein production, were conducted onboard immediately after sampling, following the microcentrifuge tube method (Kirchman, 2001). Tritiated leucine was added at substrate saturating levels (11.4 nM final conc.) to triplicate microcentrifuge tubes containing 1.5 mL of water. Killed controls contained substrate and 100% trichloroacetic acid (TCA). Incubations were conducted in the dark at *in situ* temperature for 1–2 h. Incubations were terminated by addition of 100% TCA, followed by centrifugation of the tubes at 10,000 g for 15 min using a FlexiFuge Centrifuge (Argos). Pellets were consecutively washed with 5% ice-cold TCA and 80% ice-cold ethanol and air dried. The radioactivity of the samples, which reflected incorporation of tracer into biomass, was measured in

a scintillation counter. Assuming an isotope dilution factor of 1, bacterial biomass production was estimated by multiplying leucine incorporation rates with a carbon conversion factor of 1.5 kg C per mol (Kirchman, 2001).

Bacterial Hydrolytic Enzyme Activities

Hydrolytic enzymes are the major means for heterotrophic bacteria to access and degrade high molecular weight organic matter in the ocean (Arnosti, 2011). Enzyme activities were measured onboard immediately after sampling using L-leucine-4-methylcoumarinyl-7-amide (MCA) hydrochloride and 4-methylumbelliferon (MUF) β -D-glucopyranoside (Sigma-Aldrich) as substrate proxies for leucine-aminopeptidase (hereafter referred to as peptidase) and β -glucosidase activities (hereafter referred to as glucosidase), respectively (Hoppe, 1983). Enzymatic hydrolysis of MCA- and MUF-substrate proxies can be measured with short-term (several hour) incubations, and is generally considered to reflect activities of the *in situ* microbial community. Three milliliters of water were added to replicate disposable methacrylate cuvettes containing a single substrate at saturation levels (final concentration: 300 μM). Cuvettes were incubated in the dark at *in situ* temperature; fluorescence was measured immediately after sample addition and in subsamples from the incubation cuvette at two additional times over the course of 24 h. Because the fluorescence intensity of the tags is pH dependent, 1 ml sample was added to 1 ml 20 mM borate buffer (pH 9.2) and fluorescence was measured using a Turner Biosystems TBS-380 fluorometer (excitation/emission channels set to “UV”; 365 nm excitation, 440–470 nm emission). Fluorescence changes were calibrated using MUF and MCA standard solutions in seawater, and used to calculate hydrolysis rates. Killed controls (autoclaved seawater) showed only minor changes in fluorescence over time.

Statistical Analysis

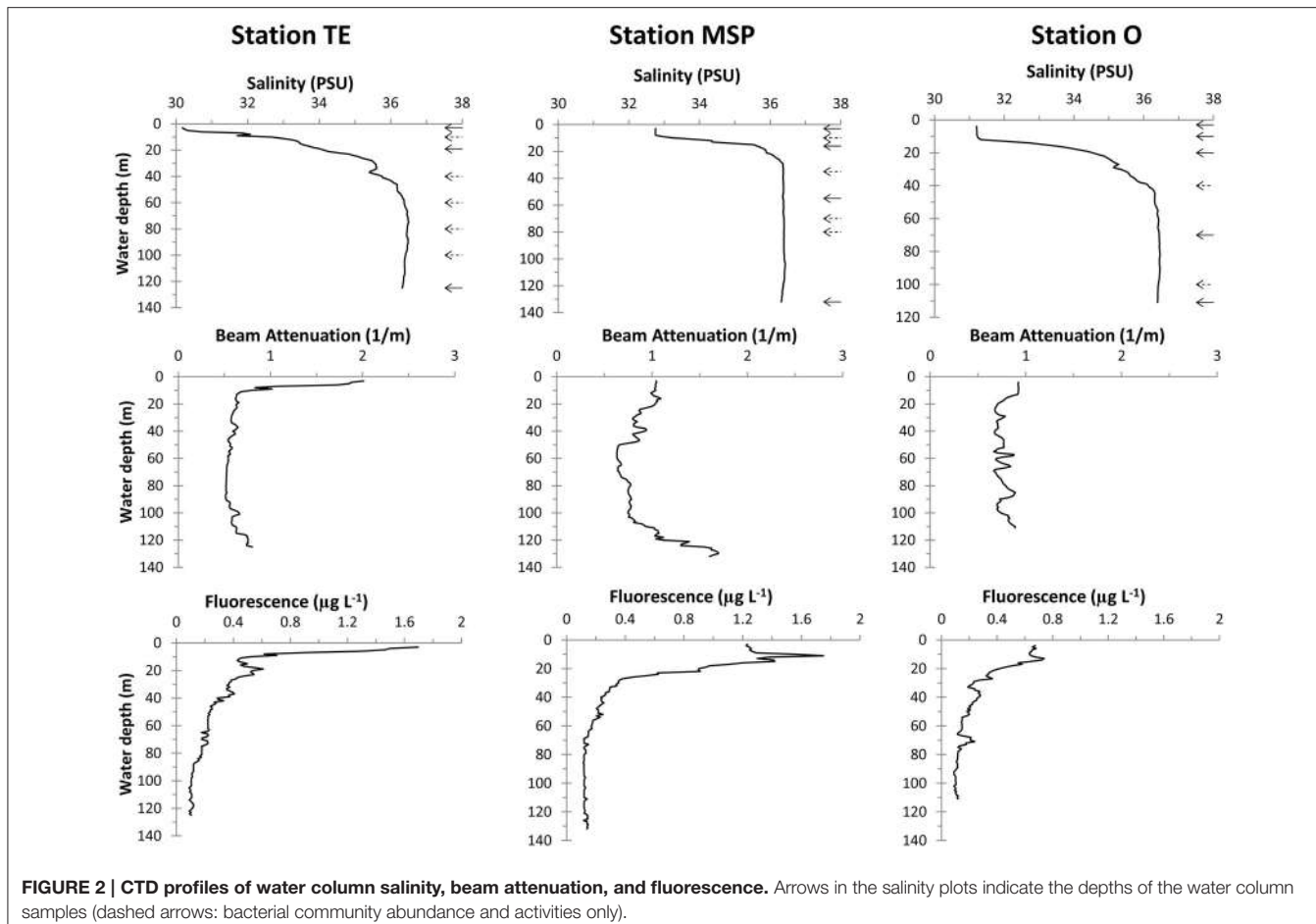
Pearson's correlation coefficients (r) between bacterial activity parameters and organic matter concentration (POC and DOC) and chl *a* were calculated in Excel® using the data analysis tool pack (open source add-in). The Student's *t*-test was used to determine the significance of the r -values.

RESULTS

Water Column Characteristics

All three stations showed freshwater influence in surface waters that reached ~30 PSU at Stn. TE, ~33 PSU at Stn. MSP, and ~31 PSU at Stn. O (Figure 2). Salinity at Stn. TE increased almost linearly in the uppermost 20 m. Stns. MSP and O, in contrast, had an upper mixed layer of ~8 and 11 m, respectively. Bottom water salinities at all three sites reached ~36 PSU.

Water column turbidity profiled by beam attenuation differed remarkably among the three sites (Figure 2). Stn. TE showed overall highest turbidity at the surface. Beam attenuation decreased sharply within the upper 10 m, and was low and invariant throughout the rest of the water column. At Stn. MSP, beam attenuation was low in surface and subsurface waters, but



increased considerably below 110 m toward the seafloor. Water column turbidity at Stn. O varied little with depth.

CTD-derived chl fluorescence profiles and chl *a* concentrations also showed site-specific differences (Figure 2; Table 2). The CTD-derived chl fluorescence profile at Stn. TE peaked at the surface, decreasing sharply within the upper 10 m and thus following similar patterns as the beam attenuation profile at this site. Stn. MSP had a distinct sub-surface CTD-derived chl fluorescence peak at 11 m water depth; Stn. O also showed a CTD-derived chl fluorescence peak at about 11 m, although much weaker than at Stn. MSP.

In accordance with the CTD-derived chl fluorescence data, chl *a* showed a surface maximum at Stn. TE, an even larger subsurface (16 m) maximum at Stn. MSP, and much lower concentrations at all depths at Stn. O (Table 2).

Dissolved Organic Carbon (DOC)

Dissolved organic carbon (DOC) concentrations were high (210–370 µM) in surface waters at all three stations, with highest concentration at Stn. O at 10 m water depth, i.e., within the upper mixed layer, followed by Stns. TE and MSP (Table 2). DOC concentration below the halocline were still somewhat elevated (ca. 64–170 µM), but were considerably lower than in the freshwater-influenced surface layers.

Particulate Organic Matter Characteristics

Total Suspended Matter (TSM)

Average TSM concentrations at Stns. TE and MSP were generally higher than at Stn. O (Table 2). Depth-related variations were minor at all three stations, except for the bottom water sample at Stn. MSP (132 m), which had the highest TSM concentrations (4.3 mg L^{-1}); between-sample variation was highest at Stn. TE, suggesting heterogeneous particle distribution at this site.

Particulate Organic Carbon (POC) and C/N Ratios

POC concentrations at all three sites were maximal at the surface and in sub-surface waters (<20 m water depths), and decreased with depth (Table 2). Stn. MSP had highest POC concentrations at 16 m, the same depth where chl *a* concentrations peaked. Bottom water POC at Stn. MSP was slightly elevated compared to the mid-water sample at 55 m. At Stn. O, POC concentration in surface waters (3 and 10 m water depth) was slightly lower compared to Stns. TE and MSP, and about a factor of 3 higher than in the mid- and bottom water sample.

The C/N ratios in surface waters were distinctly low at all three sites, ranging between 5.2 (Stn. TE) and 6.8 (Stn. O; Table 2). At Stn. MSP, C/N ratios decreased from 6.7 at the surface to 5.2 at 16 m, the depth of the chl *a* peak. C/N ratios in mid- and bottom

TABLE 2 | Water column profiles of biogeochemical parameters.

Station, sample depth	Biomass production	Peptidase	Glucosidase	TSM	POC	BEPOC	BEPOC of POC	DOC	C/N	Chl a	TEP	CSP
Stn TE												
3 m	0.74 ± 0.03	456.4 ± 59	15.1 ± 0.3	3.3 ± 1.8	216.7 ± 9.3	106.1	49	360.8 ± 1.6	5.2 ± 0.1	2.6 ± 0.2	86 ± 5	167 ± 16
10 m	0.37 ± 0.03	164.4 ± 2.1	5.5 ± 0.1	n.d.	n.d.	n.d.	n.d.	n.d.	n.d.	n.d.	n.d.	n.d.
19 m	0.23 ± 0.02	372.5 ± 21.5	18.4 ± 0.9	3.1 ± 1.3	136.7 ± 46.1	68.1	50	142.8 ± 5.2	6.7 ± 0.7	1.3 [#]	60 ± 14	94 ± 69
40 m	0.09 ± 0.0*	274.3 ± 4.6	19.6 ± 0.7	n.d.	n.d.	n.d.	n.d.	n.d.	n.d.	n.d.	n.d.	n.d.
60 m	0.07 ± 0.0*	388.6 ± 3.4	37.4 ± 0.4	n.d.	n.d.	n.d.	n.d.	n.d.	n.d.	n.d.	n.d.	n.d.
80 m	0.05 ± 0.0*	523.9 ± 23.3	37.0 ± 0.8	n.d.	n.d.	n.d.	n.d.	n.d.	n.d.	n.d.	n.d.	n.d.
100 m	0.07 ± 0.0*	493.6 ± 6.4	64.3 ± 2.7	n.d.	n.d.	n.d.	n.d.	n.d.	n.d.	n.d.	n.d.	n.d.
125 m	0.34 ± 0.03	256.5 ± 6.1	43.5 ± 1.0	2.5 ± 1	59.7 ± 2.7	15.4	26	100.3 ± 37.2	8 ± 0.4	1.1 [#]	37 ± 8	391 ± 308
Stn MSP												
3 m	0.48 ± 0.09	99.5 ± 0.6	8.5 ± 1.9	2.8 ± 0.3	172.8 ± 2.6	90.4	52	210.6 ± 2.2	6.7 ± 0.3	1.4 ± 0.0*	69 ± 15	68 ± 16
10 m	0.36 ± 0.03	83.9 ± 2.8	5.2 ± 1.2	n.d.	n.d.	n.d.	n.d.	n.d.	n.d.	n.d.	n.d.	n.d.
16 m	0.29 ± 0.03	102.1 ± 12.7	7.1 ± 0.0*	2.2 ± 0.3	214.5 ± 4.1	55.2	26	131.9 ± 2.9	5.2 ± 0.1	4.7 ± 0.3	59 ± 3	68 ± 34
35 m	0.02 ± 0.0*	48.0 ± 1.6	3.2 ± 0.3	n.d.	n.d.	n.d.	n.d.	n.d.	n.d.	n.d.	n.d.	n.d.
55 m	0.09 ± 0.01	103.3 ± 5.6	14.0 ± 1.0	2.1 ± 0.1	53.4 ± 1.1	50.5	95	111.5 ± 22.2	8.1 ± 1.5	0.2 ± 0.0*	60 ± 45	58 ± 31
70 m	0.06 ± 0.05	69.0 ± 3.2	3.4 ± 0.6	n.d.	n.d.	n.d.	n.d.	n.d.	n.d.	n.d.	n.d.	n.d.
80 m	0.04 ± 0.03	68.3 ± 0.2	3.4 ± 0.7	n.d.	n.d.	n.d.	n.d.	n.d.	n.d.	n.d.	n.d.	n.d.
110 m	n.d.	153.5 ± 2.5	7.4 ± 0.4	n.d.	n.d.	n.d.	n.d.	n.d.	n.d.	n.d.	n.d.	n.d.
132 m	0.12 ± 0.0*	243.4 ± 107.4	13.6 ± 2.6	4.3 ± 0.4	81.0 ± 8.9	70.1	87	64.4 ± 3.6	9.4 ± 1.4	0.2 ± 0.0*	107 ± 3	123 ± 36
Stn O												
3 m	0.37 ± 0.04	124.6 ± 15.3	13.5 ± 0.2	0.8 ± 0.6	149.9 ± 6.2	81.7	55	218.5 ± 44.9	6.8 ± 0.3	0.9 ± 0.2	61 ± 15	68 ± 22
10 m	0.32 ± 0.1	81.3 ± 3.8	7.0 ± 0.0*	1.2 ± 0.3	172.2 ± 9.0	80.1	47	370.2 ± 16.2	6.7 ± 0.2	0.8 ± 0.1	63 ± 9	61 ± 33
20 m	0.23 ± 0.06	84.4 ± 0.9	10.1 ± 1.1	n.d.	n.d.	n.d.	n.d.	n.d.	n.d.	n.d.	n.d.	n.d.
40 m	0.1 ± 0.01	205.0 ± 16.7	n.d.	n.d.	n.d.	n.d.	n.d.	n.d.	n.d.	n.d.	n.d.	n.d.
70 m	0.03 ± 0.01	63.6 ± 2.0	15.0 ± 3.9	1.9 ± 0.7	43.9 ± 3.2	22	50	169.5 ± 43.7	8.1 ± 0.2	0.2 ± 0.0*	19 ± 8	31 ± 3
100 m	0.02 ± 0.01	59.0 ± 5.6	3.8 ± 0.9	n.d.	n.d.	n.d.	n.d.	n.d.	n.d.	n.d.	n.d.	n.d.
111 m	0.05 ± 0.0*	55.6 ± 3.0	4.4 ± 0.8	1.7 ± 0.0	38.3 ± 1.5	14.4	38	100.9 ± 19.4	8.7 ± 0.5	0.1 ± 0.0*	46 ± 30	67 ± 32

Cell-specific biomass production (fg C cell⁻¹ h⁻¹), peptidase and β-glucosidase activities (amol cell⁻¹ h⁻¹), total suspended matter (TSM, mg L⁻¹) particulate organic carbon (POC, µg L⁻¹), dissolved organic carbon (DOC, µM), chlorophyll a (Chl a, µg L⁻¹), transparent exopolymeric particles (TEP mL⁻¹), and Coomassie-stainable particles (CSP mL⁻¹). Data are given as averages ± standard error. Values for BEPOC (base-extracted POC, µg L⁻¹) are from Brym et al. (2014). BEPOC of POC is in %. n.d., means not determined; *Value < 0.01; #only 1 filter available.

waters were higher than at the surface, ranging between 8 (Stn. O) and 9.4 (Stn. MSP).

POC constituted a variable fraction of TSM: in surface waters of Stn. O, where TSM concentrations were comparably low, POC was close to 19% of TSM. At Stn. O POC constituted over 14% of TSM at depths of 1 and 10 m, whereas POC contributed much less to TSM (2%) at deeper depths (70 and 111 m). At the other two stations, POC contributions to TSM were lower than at Stn. O and generally decreased with depth, with the exception of a comparably high contribution (almost 10%) at 16 m at Stn. MSP, where chl a concentration was also elevated.

Fluorescence Properties of Base-Extracted POM (BEPOM)

The EEM plots of the BEPOM fluorescence showed a 3-peak pattern which is characteristic for estuarine waters and distinctive of largely planktonic OM sources (Brym et al., 2014). These peaks are more representative of fluorophore molecules than the continuous longwave emission of humic substances (Ma

et al., 2010). Characteristic of this pattern is the protein-like fluorescence (excitation max 275–280 nm, emission max 340–344 nm) similar to the amino acid tryptophan (T peak) which is linked to primary production (Coble, 1996). Also prominent are two peaks at emission max 450 nm with two excitation peaks at 260 and at 365 nm. The identity of this fluorophore (or fluorophore group) is unknown but shares similarity to ubiquinone (Ubq; Li et al., 2011). The intensities of the peaks revealed depth- as well as site-specific differences. Stn. TE at the surface (3 m water depth) and Station MSP at 16 m (chl a peak) had strong protein-like signals and diminished Ubq signals (**Figure 3**). BEPOM fluorescence in surface waters at Stns. MSP (3 m) and O (3 and 10 m) revealed lower signals of protein-like fluorescence, and much stronger Ubq signals compared to Stn. TE (**Figure 3**; note the different scales). At Stn. O, a humic-like peak C was strongly evident at 70 m, and was still quite pronounced at 111 m. Note that this signal is distinct from the Ubq signal; its excitation maximum is ca. 10 nm blue-shifted from the secondary excitation peak for Ubq. Sub-surface

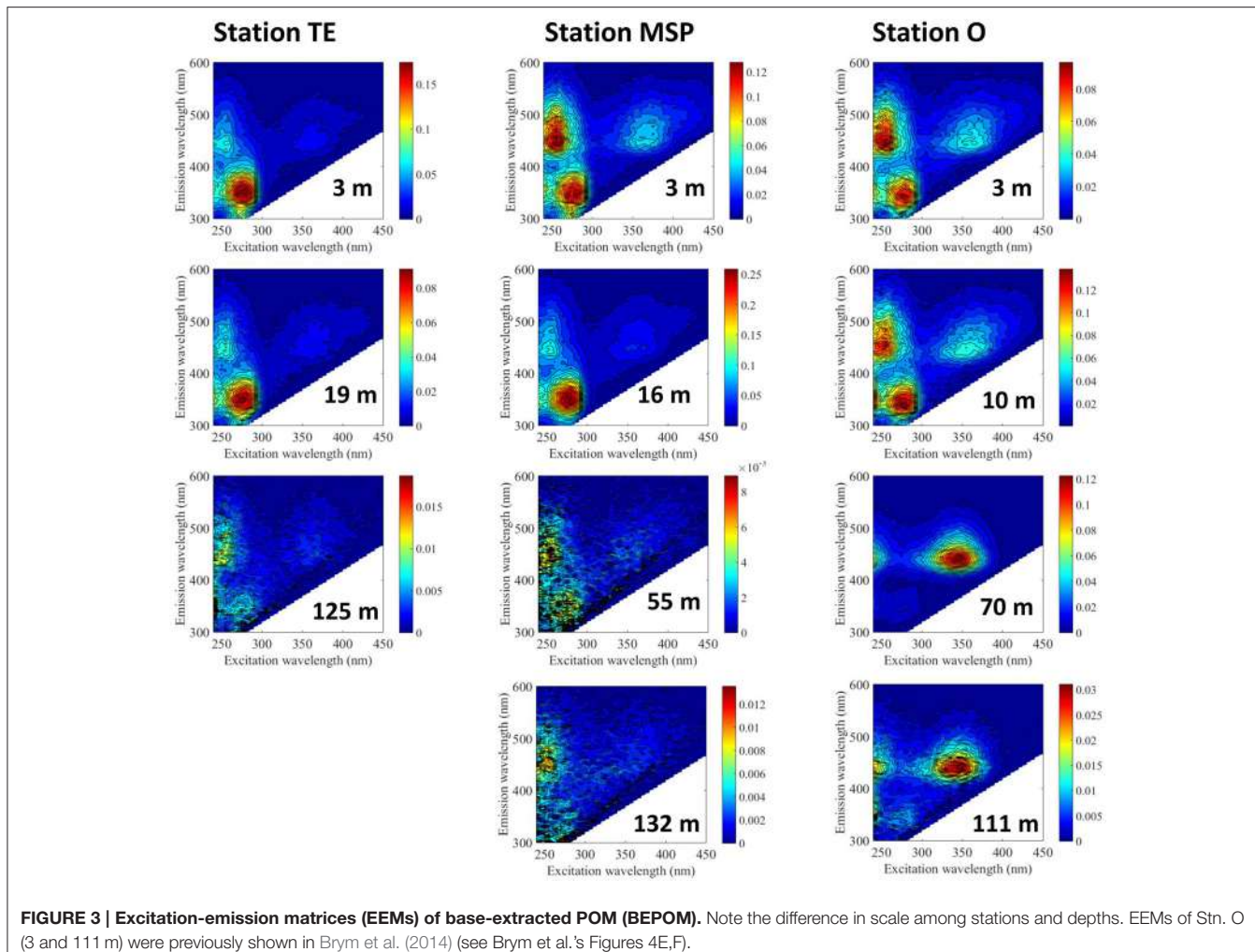


FIGURE 3 | Excitation-emission matrices (EEMs) of base-extracted POM (BEPOM). Note the difference in scale among stations and depths. EEMs of Stn. O (3 and 111 m) were previously shown in Brym et al. (2014) (see Brym et al.'s Figures 4E,F).

and bottom water BEPOM fluorescence at Stns. TE and MSP were characterized primarily by a change in peak intensity with depth.

TEP and CSP Abundance

TEP abundance at Stns. TE and O were highest at the surface and lowest at the bottom; in contrast at Stn. MSP, TEP abundance peaked near the seafloor (**Table 2**). Overall site-related differences in TEP abundance were minor, ranging between $19.4 \pm 8.1 \text{ mL}^{-1}$ (Stn. O 70 m) and $123 \pm 35.8 \text{ mL}^{-1}$ (Stn. MSP 132 m).

CSP were generally more abundant than TEP, ranging between $31.4 \pm 2.6 \text{ mL}^{-1}$ at Stn. O at 70 m and $391.4 \pm 307 \text{ mL}^{-1}$ at Stn. TE at 125 m (**Table 2**). Vertical CSP distributions were similar to those of TEP at two of the three sites (Stns. MSP and O). At Stn. TE, however, the CSP profile was different from the TEP profile with highest CSP abundance at 125 m water depth.

Bacterial Abundance and Activities

Bacterial Cell Counts

Bacterial cell numbers at all three sites were highest in surface waters ($\leq 16 \text{ m}$ water depth), ranging between $8.4 \times 10^8 \text{ cells L}^{-1}$

at Stn. MSP and $12.1 \times 10^8 \text{ cells L}^{-1}$ at Stn. O at 16 m, and coinciding with the respective chl *a* peaks (**Figure 4**). At all three stations, bacterial abundance decreased to below $5 \times 10^8 \text{ cells L}^{-1}$ at depths of 20–35 m, decreasing further to ca. $1 \times 10^8 \text{ cells L}^{-1}$ deeper in the water column. At Stn. TE, however, cell abundance increased again between 100 m and 125 m (to $2.4 \times 10^8 \text{ cells L}^{-1}$).

Bacterial Biomass Production (Leucine Incorporation)

Depth profiles of bacterial biomass production rates were generally highest in surface waters, decreasing considerably with depth (**Figure 4**). Biomass production in surface waters of Stn. TE was approximately double the rates at Stns. MSP and O. Bacterial biomass production rates at midwater depths were similar among the three sites. Bottom water rates at Stn TE, however, were one order of magnitude higher than at similar depths at the other two stations. Bacterial production on a per-cell basis (**Table 2**) showed a pattern very similar to bulk biomass production: highest rates were found at the surface of Station TE; the bottom-most depth also showed an elevated rate (**Table 2**).

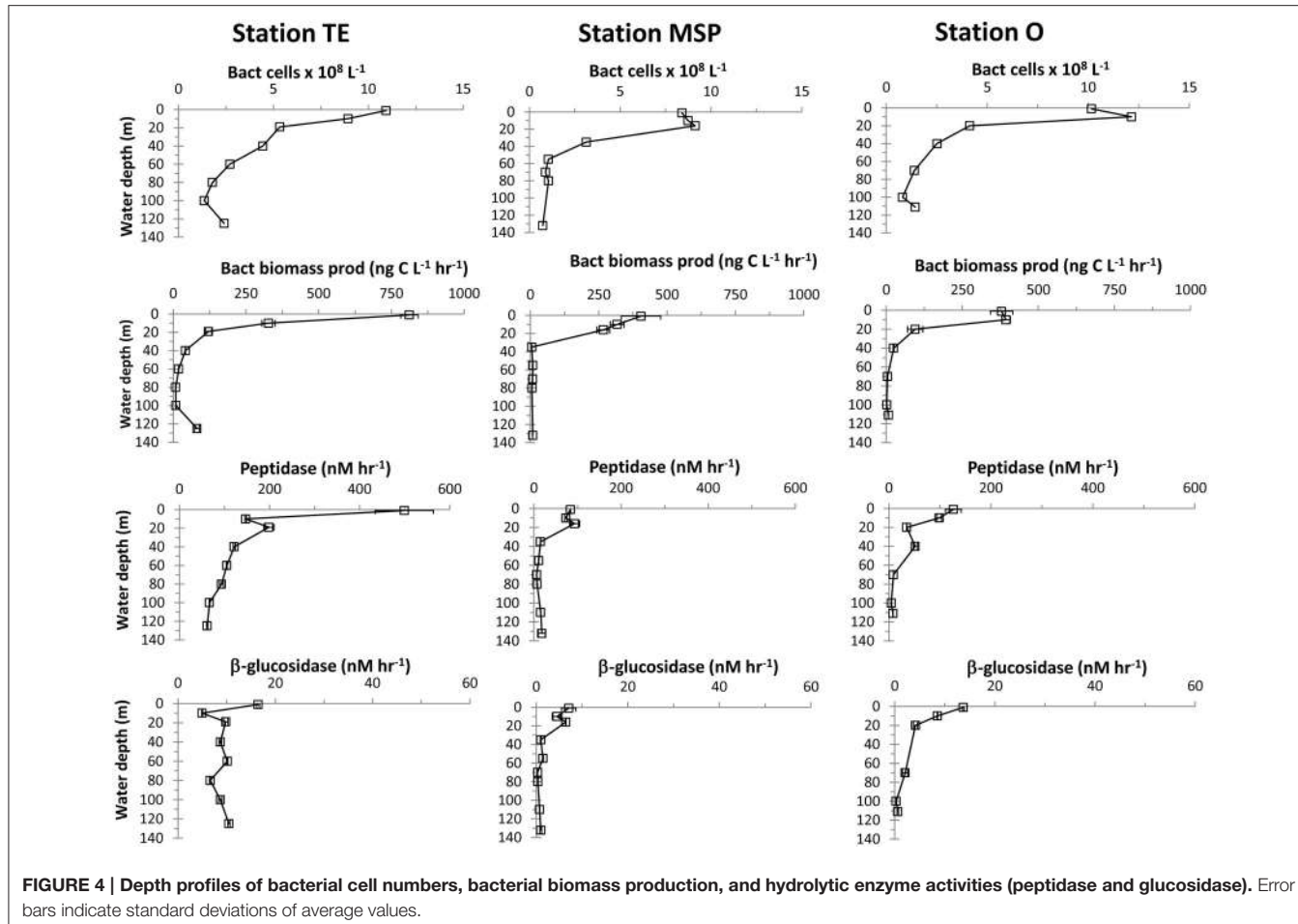


FIGURE 4 | Depth profiles of bacterial cell numbers, bacterial biomass production, and hydrolytic enzyme activities (peptidase and glucosidase). Error bars indicate standard deviations of average values.

Hydrolytic Enzymatic Activities

Peptidase and glucosidase activities were generally higher at the surface compared to subsurface waters with highest activities in Stn. TE surface waters (Figure 4). In subsurface waters at Stn. TE, peptidase and glucosidase activities were also generally more rapid than at Stns. MSP and O at the same depths. Profiles of cell-specific peptidase activities showed considerable variability with depth at Stn. TE, an increase with depth at Stn. MSP, and a comparatively constant profile with depth at Stn. O, with a single maximum at 40 m (Table 2). Cell-specific glucosidase activities at Stn. TE increased considerably with depth. Only minor variations with depth were found at Stn. MSP, while cell-specific glucosidase activities showed a decreasing trend with depth at Stn. O.

DISCUSSION

Characteristics of Organic Matter

All three sites were influenced by Mississippi River water outflow, as indicated by the presence of a strong halocline in the upper \sim 10 m of the water column (Figure 2). Surface water salinities of >30 PSU (Figure 2) are typical for a low discharge season in late summer/early fall (Walker et al., 2005;

Green et al., 2006). However, the high surface water DOC concentrations at all three sites greatly exceeded those reported from the same area at low river discharge (Biddanda et al., 1994; Benner and Opsahl, 2001), and are more typical for high riverine outflow conditions (Wang et al., 2004). The DOC concentrations generally followed surface water salinity, which also point toward input from Mississippi River outflow (Stolpe et al., 2010). Thus, high salinity/high DOC surface water at the time of sampling may have resulted in part from intense Mississippi River discharge following the landfall of Hurricane Isaac 2 weeks prior to our sampling. Hurricane Isaac pushed large volumes of marine waters upstream the Mississippi River (Berg, 2013), leading to subsequent discharge of higher salinity river plumes which carried elevated levels of terrestrial material onto the Louisiana shelf. Given the extent of the storm surge (>300 river miles; US Army Corps of Engineers, 2013), riverine discharge likely continued for over 10 days after the storm had passed, into the beginning of our sampling period.

Riverine DOC has generally higher residence times in river plumes than particulate matter from riverine outflow which rapidly flocculates and sediments near the Mississippi River mouth (Bianchi et al., 2002). Near-bed transport of riverine particulate matter onto the shelf is generally high at times of

high riverine discharge (Bianchi et al., 2006), and can explain the presence of the bottom water turbidity layer at Stn. MSP (**Figure 2**) that were also found at sites further offshore during the same cruise (Ziervogel et al., 2015).

Much of the particulate matter in surface waters at the time of sampling was derived from autochthonous primary production, as indicated by C/N ratios (**Table 2**) that were distinctly lower than those at nearby sites during high riverine discharge in late spring (Wang et al., 2004) as well as from sites sampled further offshore during the same cruise (Ziervogel et al., 2015). Following tropical storms and hurricanes, enhanced flux of inorganic nutrients from the Mississippi River often stimulate phytoplankton blooms on the Louisiana Shelf (Lohrenz et al., 2008). In the aftermath of Hurricane Lili in 2002, for instance, satellite remote sensing detected elevated chl *a* levels on the Louisiana shelf for over 14 days with varying intensity throughout the observation period (Yuan et al., 2004). We found evidence of considerable surface water phytoplankton biomass at the two sites close to the river mouth (Stns. TE and MSP, **Figure 2; Table 2**) with peak chl *a* concentrations that were double those reported from remote sensing observations during storm-induced algal blooms on the Louisiana Shelf (Yuan et al., 2004), and higher than those reported from nearby sites at >30 PSU in late summer/early fall at a time of low riverine discharge (Lohrenz et al., 1999). Strong protein-like fluorescence signals within the BEPOM fraction that were consistent with peak chl *a* levels also indicated the presence of freshly-produced POM in surface waters (**Figure 3**; note the difference in scales). Results from Stn. O showed low chl *a* and strong humic-like BEPOM fluorescence that could indicate substantial microbial processing of autochthonous primary production further away from the river mouth (Burdige et al., 2004; Shimotori et al., 2011).

TEP and CSP that often form from dissolved phytoplankton metabolites during a phytoplankton bloom (Long and Azam, 1996; Passow, 2002) were somewhat disconnected from phytoplankton biomass at all three sites (**Table 2**), and had lower abundances compared to other coastal waters during peak phytoplankton growth (e.g., Mari and Kiørboe, 1996). TEP and CSP numbers were more similar to those found during early growth stages of cultured phytoplankton (Grossart et al., 2006), suggesting that our sampling coincided with the onset of algal blooms on the Louisiana Shelf.

Microbial Biomass and Activities

Microbial community activities varied considerably among the three stations, despite generally similar cell counts (**Figure 4; Table 2**), which were in the same range as previously reported cell abundances from the northern Gulf of Mexico (Amon and Benner, 1998; Arnosti and Steen, 2013). Peak bacterial biomass production rates in surface waters at Stn. TE were double compared to Stns. MSP and O, and other near-shore sites in the Gulf of Mexico (Steen et al., 2012) that had somewhat higher cell counts (Arnosti and Steen, 2013). Surface water peptidase activities at Stn. TE were five times higher compared to Stns. MSP and O on a bulk-volume as well as on a per-cell basis. Peptidase activities in Stn TE mid- and bottom waters were also considerably higher compared to the other two sites. Glucosidase

activity followed a similar pattern with highest rates on a bulk as well as per-cell basis at Stn. TE, followed by Stn. O, and then by Stn. MSP (**Figure 4; Table 2**). Compared to previous reports from near-shore sites in the Gulf of Mexico, peak peptidase activities at Stn. TE were more than double those measured in Mississippi River plumes in the Atchafalaya Bay (Ammerman and Glover, 2000), and were more than an order of magnitude higher than at other nearby sites affected by Mississippi River plumes (Liu and Liu, 2015). In Pensacola Bay, northwestern Florida, peptidase and glucosidase activity averaged over different times of a year were 165 and 10 nM L⁻¹, respectively (Murrell, 2003), and thus also considerably lower than peak activities at Station TE. Peptidase and glucosidase activities at the offshore sites sampled during the same cruise were up to one order of magnitude lower than at Stn. TE, MSP, and O (Ziervogel et al., 2015).

Several trends emerge from these data: Bacterial biomass production decreased much more rapidly with depth relative to cell counts at all sites, a pattern in the northern Gulf of Mexico that has been attributed to subsurface communities that grow less actively than their surface counterparts (Skoog et al., 1999; Arnosti and Steen, 2013). Notably, however, cell-normalized peptidase activities decreased comparatively little with depth, and even increased with depth at specific locations, such as bottom waters of Stn. MSP and near-bottom waters of Stn. TE; cell-normalized glucosidase activities increased with depth especially at Stn. TE (**Table 2**). These data suggest that substrate acquisition was still a major focal point of heterotrophic activity, even if incorporation into cell biomass was less prevalent. Much of the glucose taken up by microbial communities in the northern Gulf of Mexico may be respired to CO₂ rather than incorporated into biomass (Arnosti and Steen, 2013); a similar situation may explain high peptidase activities and lower rates of bacterial protein production. High rates of enzyme activities thus do not necessarily correlate directly with increases in microbial biomass, an observation that has been also made in the deep North Atlantic (Baltar et al., 2009).

Patterns of Microbial Activities: Links to Organic Matter

Surface water bacterial activities at Stns. TE and MSP in part followed the patterns of POC concentrations and BEPOM fluorescence. In particular, elevated bacterial protein production and enzyme activities correspond to the depths with peak chl *a* concentrations, POC with low C/N ratios, and strong protein-like BEPOM fluorescence, and yielded significant correlations between bacterial activities and chl *a* (Stns. O and TE) and POC (Stns. O and MSP; **Table 3**). These results indicate that bacterial community activities at the Stns. TE and MSP were mainly driven by freshly produced, autochthonous POM at the time of sampling. In contrast, Stn. O had lowest surface water chl *a* and POC concentrations at relatively high C/N ratios, as well as comparatively substantial humic-like in addition to the protein-like fluorescence in the BEPOM spectra. Nonetheless, cell-specific peptidase and glucosidase activities in surface waters at Stn. O were somewhat higher compared to Stn. MSP, suggesting that bacterial communities at Stn. O were capable of degrading

TABLE 3 | Parson's correlation coefficient (*r*) between bacterial activity parameters and POC, DOC, and Chl a (*r* and *p*-values from cell-specific activities in parenthesis).

	Station	POC		DOC		Chl a	
		<i>r</i>	<i>p</i>	<i>r</i>	<i>p</i>	<i>r</i>	<i>p</i>
Biomass production	TE	0.89 (0.75)	0.30 (0.46)	0.99 (0.94)	0.07 (0.23)	0.99 (0.95)	0.04 (0.21)
	MSP	0.86 (0.78)	0.14 (0.21)	0.91 (0.91)	0.09 (0.09)	0.56 (0.43)	0.44 (0.57)
	O	0.99 (0.97)	0.006 (0.03)	0.82 (0.73)	0.18 (0.27)	0.99 (0.99)	0.01 (0.01)
Peptidase	TE	0.98 (0.93)	0.13 (0.24)	0.99 (0.74)	0.1 (0.47)	0.98 (0.72)	0.12 (0.49)
	MSP	0.99 (0.43)	0.01 (0.57)	0.71 (0.74)	0.23 (0.26)	0.83 (0.42)	0.17 (0.58)
	O	0.95 (0.73)	0.05 (0.27)	0.67 (0.37)	0.31 (0.63)	0.99 (0.87)	0.008 (0.13)
Glucosidase	TE	0.83 (0.91)	0.38 (0.27)	0.97 (0.71)	0.15 (0.5)	0.98 (0.68)	0.13 (0.52)
	MSP	0.93 (0.99)	0.07 (0.007)	0.85 (0.68)	0.15 (0.32)	0.72 (0.86)	0.28 (0.14)
	O	0.88 (0.02)	0.12 (0.98)	0.58 (0.02)	0.42 (0.98)	0.97 (0.2)	0.03 (0.8)

Values of *r* are significant at *p* < 0.05 (values in bold).

organic matter substrates that were different in their structure and possibly origin compared to the other two sites.

In contrast to the POM pool, peak DOC concentrations (Stn. O at 10 m), did not support elevated bacterial activities, perhaps a result of the mainly terrestrial origin of the DOC pool at the time of sampling. No significant correlations were found for bacterial activity parameters and DOC (Table 3), and estimates of bacterial utilization of carbon suggest that heterotrophic bacteria used a much higher fraction of the POC pool compared to the DOC pool (Table 4). Neither the DOC nor the POC concentrations, however, provide a ready explanation for the comparatively elevated microbial activities in the deeper water column at Stn. TE. The comparatively high chl *a* concentration as well as POC with relatively low C/N ratios at a depth of 125 m, however, may provide a clue. In particular, a chl *a* concentration in excess of 1 µg L⁻¹ at a depth of 125 m—four times the concentration at Stn. MSP, and more than 10 times the concentration at Stn. O—suggests that the vertical transport of freshly-produced phytoplankton material at Stn. TE is considerably greater than at the other two stations. The lack of a significant humic (terrestrially-derived) peak in the BEPOM spectrum supports the hypothesis that the POC at depth at Stn. TE is predominantly autochthonous. Moreover, the elevated CSP concentrations at depth support the hypothesis that protein-containing components are abundant in these waters. Assuming that some of this material is also metabolized during vertical sinking through the water column, microbially-driven metabolism of comparatively freshly produced marine organic matter may also drive the higher rates of bacterial biomass production as well as enzyme activities measured at intermediate depths at Stn. TE. Amon and Benner (1998) also found enhanced below-surface bacterial biomass production rates at nearby sites, suggesting that sinking of organic matter from the surface may have fueled heterotrophic activities below the pycnocline.

The site-specific differences in bacterial activities observed here may also reflect functional differences in heterotrophic bacterial communities among water masses and/or sites. Previous investigations in the Gulf of Mexico (Steen et al., 2012), as well

TABLE 4 | Estimates of carbon utilization by heterotrophic bacteria (µg C L⁻¹ d⁻¹) relative to POC and DOC (%).

Station, sample depth	Amount of C utilized	C utilization of POC	C utilization of DOC
Stn TE			
3 m	42.4	19.5	1.0
19 m	6.3	4.6	0.4
125 m	4.3	7.1	0.4
Stn MSP			
3 m	21.1	12.2	0.8
16 m	13.9	6.5	0.9
55 m	0.5	0.9	0.0*
132 m	0.5	0.6	0.1
Stn O			
3 m	19.8	13.2	0.8
10 m	20.5	11.9	0.5
70 m	0.2	0.5	0.0*
111 m	0.4	1	0.0*

Amount of carbon utilized by bacteria was calculated using bacterial biomass production divided by an average glucose utilization efficiency of 46% from Arnosti and Steen (2013) for the northern Gulf of Mexico.*Value < 0.1.

as in transects covering riverine-to-marine conditions (Ziervogel and Arnosti, 2009) have demonstrated that the capacity for pelagic microbial communities to hydrolyze a suite of complex substrates varies considerably, differences that may be correlated to differences in microbial community composition (Teske et al., 2011; D'Ambrosio et al., 2014). Factors that may drive differences in bacterial community structure and activities at the investigated sites include differences in freshwater influence due to the location of the three sites relative to the river mouth (Liu and Liu, 2015). It is also possible that bacterial community structure and function is influenced by the chronic oil leakage from the sunken Taylor Energy platform near Stn. TE. Microbial communities in the water column of the Gulf of Mexico contain members capable of degrading petroleum hydrocarbons as well

as secondary transformation products (Arnoldi et al., 2015); increased peptidase and glucosidase activities in Gulf of Mexico surface waters affected by natural oil seeps (Ziervogel et al., 2014) as well as in surface and deep waters affected by the 2010 BP oil spill (Ziervogel et al., 2012; Ziervogel and Arnoldi, 2013) have been recently documented.

CONCLUSIONS

Our results that provide a snapshot of biogeochemical processes on the Louisiana shelf following high discharge of the Mississippi River, suggest that heterotrophic microbial community activities were closely linked to phytoplankton-derived POM in the aftermath of Hurricane Isaac. DOC concentrations could only in part explain bacterial activity patterns, showing a disconnect at the station furthest away from the river mouth, where substrates from terrestrial sources may have dominated the DOC pool. The close link between POM and bacterial activities became apparent by combining activity measurements of natural heterotrophic bacterial communities with fluorescence properties of POM (BEPOM) that constituted a substantial fraction of the POC pool (**Table 2**). This study is the first that merges BEPOM fluorescence with rates of heterotrophic bacterial activities, providing a better understanding of bacterial transformation of POM especially in particle-rich coastal environments.

AUTHOR CONTRIBUTIONS

KZ measured enzyme activities, TEP and CSP abundance; ND counted bacterial cells, JB measured leucine incorporation rates;

KZ, ND, JB, and JM conducted the field sampling with JM leading the CTD operations; AB and CO conducted the BEPOM analysis; UP provided POC/PON and chl *a* data, and helped preparing TEP and CSP slides; SJ and CA helped planning the field sampling and bacterial activity analysis; KZ and CA wrote the paper with input from all authors.

ACKNOWLEDGMENTS

We thank the captain and shipboard party of RV *Endeavor* (cruise 515). We thank Dan Hoer (UNC) for DOC measurements, Julia Sweet (UCSB) for POC and chl *a* analysis, and Trent Bottoms (UNC) who helped analyzing TEP and CSP. We also thank Andrew Juhl (LDEO, Columbia University) for the use of equipment and supplies for microscopy, and Kendra Bullock (Columbia University), for assistance with microscopy. This research was made possible in part by a grant from The Gulf of Mexico Research Initiative supporting the ECOGIG (Ecosystem Impacts of Oil and Gas Inputs to the Gulf) consortium (ECOGIG contribution # 367). The data are publicly available through the Gulf of Mexico Research Initiative Information & Data Cooperative (GRIIDC) at <https://data.gulfresearchinitiative.org> (doi: R1.x132.134:0111, R1.x132.134:006). Additional funding for K.Z. came from the National Science Foundation (OCE-1335088) and for C.O. from the Strategic Environmental Research and Development Program Environmental Restoration grant and the North Carolina State University Faculty Research and Professional Development program.

REFERENCES

- Ammerman, J. W., and Glover, W. B. (2000). Continuous underway measurement of microbial ectoenzyme activities in aquatic ecosystems. *Mar. Ecol. Prog. Ser.* 201, 1–12. doi: 10.3354/meps201001
- Amon, R. M., and Benner, R. (1998). Seasonal patterns of bacterial abundance and production in the Mississippi River plume and their importance for the fate of enhanced primary production. *Microb. Ecol.* 35, 289–300. doi: 10.1007/s002489900084
- Arnoldi, C. (2011). Microbial extracellular enzymes and the marine carbon cycle. *Ann. Rev. Mar. Sci.* 3, 401–425. doi: 10.1146/annurev-marine-120709-142731
- Arnoldi, C., and Steen, A. D. (2013). Patterns of extracellular enzyme activities and microbial metabolism in an arctic fjord of Svalbard and in the northern Gulf of Mexico: contrasts in carbon processing by pelagic microbial communities. *Front. Microbiol.* 4:318. doi: 10.3389/fmicb.2013.00318
- Arnoldi, C., Ziervogel, K., Yang, T., and Teske, A. (2015). Oil-derived marine aggregates – hot spots of polysaccharide degradation by specialized bacterial communities. *Deep Sea Res. II*. doi: 10.1016/j.dsr2.2014.12.008i. [Epub ahead of print].
- Baltar, F., Arístegui, J., Sintes, E., van Aken, H. M., Gasol, J. M., and Herndl, G. J. (2009). Prokaryotic extracellular enzymatic activity in relation to biomass production and respiration in the meso- and bathypelagic waters of the (sub)tropical Atlantic. *Environ. Microbiol.* 11, 1998–2014. doi: 10.1111/j.1462-2920.2009.01922.x
- Benner, R., and Opsahl, S. (2001). Molecular indicators of the sources and transformations of dissolved organic matter in the Mississippi River plume. *Org. Geochem.* 32, 597–611. doi: 10.1016/s0146-6380(00)00197-2
- Berg, R. (2013). *Hurricane Isaac Tropical Cyclone Report*. National Hurricane Center.
- Bianchi, T., Lambert, C., Santschi, P., and Guo, L. (1997). Sources and transport of land-derived particulate and dissolved organic matter in the Gulf of Mexico (Texas shelf/slope): the use of lignin-phenols and loliolides as biomarkers. *Org. Geochem.* 27, 65–78. doi: 10.1016/S0146-6380(97)00040-5
- Bianchi, T. S., Allison, M. A., Canuel, E. A., Corbett, D. R., McKee, B. A., Sampere, T. P., et al. (2006). Rapid export of organic matter to the Mississippi canyon. *Eos Trans. Am. Geophys. Union* 87, 565–573. doi: 10.1029/2006EO500002
- Bianchi, T. S., Garcia-Tigreros, F., Yvon-Lewis, S. A., Shields, M., Mills, H. J., Butman, D., et al. (2013). Enhanced transfer of terrestrially derived carbon to the atmosphere in a flooding event. *Geophys. Res. Lett.* 40, 116–122. doi: 10.1029/2012GL054145
- Bianchi, T. S., Mitra, S., and McKee, B. A. (2002). Sources of terrestrially-derived organic carbon in lower Mississippi River and Louisiana shelf sediments: implications for differential sedimentation and transport at the coastal margin. *Mar. Chem.* 77, 211–223. doi: 10.1016/S0304-4203(01)0088-3
- Biddanda, B., Opsahl, S., and Benner, R. (1994). Plankton respiration and carbon flux through bacterioplankton on the Louisiana shelf. *Limnol. Oceanogr.* 39, 1259–1279. doi: 10.4319/lo.1994.39.6.1259
- Brym, A., Paerl, H. W., Montgomery, M. T., Handsel, L. T., Ziervogel, K., and Osburn, C. L. (2014). Optical and chemical characterization of base-extracted particulate organic matter in coastal marine environments. *Mar. Chem.* 162, 96–113. doi: 10.1016/j.marchem.2014.03.006
- Burdige, D., Kline, S., and Chen, W. (2004). Fluorescent dissolved organic matter in marine sediment pore waters. *Mar. Chem.* 89, 289–311. doi: 10.1016/j.marchem.2004.02.015
- Coble, P. G. (1996). Characterization of marine and terrestrial DOM in seawater using excitation emission matrix spectroscopy. *Mar. Chem.* 51, 325–346.

- D'Ambrosio, L., Ziervogel, K., MacGregor, B., Teske, A., and Arnosti, C. (2014). Bacterial community composition and extracellular enzymatic function in marine waters. *ISME J.* 8, 2167–2179. doi: 10.1038/ismej.2014.67
- Engel, A. (2009). "Determination of marine gel particles," in *Practical Guidelines for the Analysis of Seawater*, ed O. Wurl (Boca Raton, FL: CRC Press), 125.
- Green, R. E., Bianchi, T. S., Dagg, M. J., Walker, N. D., and Breed, G. A. (2006). An organic carbon budget for the Mississippi River turbidity plume and plume contributions to air-sea CO₂ fluxes and bottom water hypoxia. *Estuaries Coasts* 29, 579–597. doi: 10.1007/BF02784284
- Grossart, H.-P., Czub, G., and Simon, M. (2006). Algae-bacteria interactions and their effects on aggregation and organic matter flux in the sea. *Environ. Microbiol.* 8, 1074–1084. doi: 10.1111/j.1462-2920.2006.00999.x
- Hoppe, H.-G. (1983). Significance of exoenzymatic activities in the ecology of brackish water – measurements by means of methylumbelliferyl-substrates. *Mar. Ecol. Prog. Ser.* 11, 299–308. doi: 10.3354/meps01129
- Kirchman, D. L. (2001). "Measuring bacterial biomass production and growth rates from leucine incorporation from aquatic environments" in *Marine Microbiology - Methods in Microbiology*, ed J. H. Paul (San Diego, CA: Academic Press), 227–238.
- Li, W., Sheng, G., Lu, R., Yu, H., Li, Y., and Harada, H. (2011). Fluorescence spectral characteristics of the supernatants from an anaerobic hydrogen-producing bioreactor. *Appl. Microbiol. Biotechnol.* 89, 217–224. doi: 10.1007/s00253-010-2867-x
- Liu, S., and Liu, Z. (2015). Comparing extracellular enzymatic hydrolysis between plain peptides and their corresponding analogs in the northern Gulf of Mexico Mississippi River plume. *Mar. Chem.* 177, 398–407. doi: 10.1016/j.marchem.2015.06.021
- Lohrenz, S., Cai, W., Chen, X., and Tuel, M. (2008). Satellite assessment of bio-optical properties of northern Gulf of Mexico coastal waters following Hurricanes Katrina and Rita. *Sensors* 8, 4135–4150. doi: 10.3390/s8074135
- Lohrenz, S., Fahnstiel, G., Redalje, D., Lang, G., Dagg, M., Whitledge, T., et al. (1999). Nutrients, irradiance, and mixing as factors regulating primary production in coastal waters impacted by the Mississippi River plume. *Cont. Shelf Res.* 19, 1113–1141. doi: 10.1016/S0278-4343(99)00012-6
- Long, R., and Azam, F. (1996). Abundant protein-containing particles in the sea. *Aquat. Microb. Ecol.* 10, 213–221. doi: 10.3354/ame010213
- Lunau, M., Lemke, A., Walther, K., Martens-Habbena, W., and Simon, M. (2005). An improved method for counting bacteria from sediments and turbid environments by epifluorescence microscopy. *Environ. Microbiol.* 7, 961–968. doi: 10.1111/j.1462-2920.2005.00767.x
- Ma, J., Del Vecchio, R., Golanoski, K. S., Boyle, E. S., and Blough, N. V. (2010). Optical properties of humic substances and CDOM: effects of borohydride reduction. *Environ. Sci. Technol.* 44, 5395–5402. doi: 10.1021/es100880q
- Mari, X., and Kiørboe, T. (1996). Abundance, size distribution and bacterial colonization of transparent exopolymeric particles (TEP) during spring in the Kattegat. *J. Plankton Res.* 18, 969–986. doi: 10.1093/plankt/18.6.969
- Murrell, M. C. (2003). Bacterioplankton dynamics in a subtropical estuary: evidence for substrate limitation. *Aquat. Microb. Ecol.* 32, 239–250. doi: 10.3354/ame032239
- Murrell, M. C., Stanley, R. S., Lehrter, J. C., and Hagy, J. D. (2013). Plankton community respiration, net ecosystem metabolism, and oxygen dynamics on the Louisiana continental shelf: implications for hypoxia. *Cont. Shelf Res.* 52, 27–38. doi: 10.1016/j.csr.2012.10.010
- Osburn, C. L., Handzel, L. T., Mikan, M. P., Paerl, H. W., and Montgomery, M. T. (2012). Fluorescence tracking of dissolved and particulate organic matter quality in a river-dominated estuary. *Environ. Sci. Technol.* 46, 8628–8636. doi: 10.1021/es3007723
- Pakulski, J. D., Benner, R., Whitledge, T., Amon, R., Eadie, B., Cifuentes, L., et al. (2000). Microbial metabolism and nutrient cycling in the Mississippi and Atchafalaya River plumes. *Estuar. Coast. Shelf Sci.* 50, 173–184. doi: 10.1006/ecss.1999.0561
- Passow, U. (2002). Transparent exopolymer particles (TEP) in aquatic environments. *Prog. Oceanogr.* 55, 287–333. doi: 10.1016/S0079-6611(02)00138-6
- Rabalais, N. N., Diaz, R. J., Levin, L. A., Turner, R. E., Gilbert, D., and Zhang, J. (2010). Dynamics and distribution of natural and human-caused hypoxia. *Biogeosciences* 7, 585–619. doi: 10.5194/bg-7-585-2010
- Ross, C. B., Gardner, W. D., Richardson, M. J., and Asper, V. L. (2009). Currents and sediment transport in the Mississippi Canyon and effects of Hurricane Georges. *Cont. Shelf Res.* 29, 1384–1396. doi: 10.1016/j.csr.2009.03.002
- Schiller, R. V., Kourafalou, V. H., Hogan, P., and Walker, N. D. (2011). The dynamics of the Mississippi River plume: impact of topography, wind and offshore forcing on the fate of plume waters. *J. Geophys. Res.* 116, C06029. doi: 10.1029/2010JC006883
- Shimotori, K., Watanabe, K., and Hama, T. (2011). Fluorescence characteristics of humic-like fluorescent dissolved organic matter produced by various taxa of marine bacteria. *Aquat. Microb. Ecol.* 65, 249–260. doi: 10.3354/ame01552
- Strickland, J. D. H., and Parsons, T. R. (1972). *A Practical Handbook of Seawater Analysis*. Ottawa, ON: Fisheries Research Board of Canada.
- Skoog, A., Biddanda, B., and Benner, R. (1999). Bacterial utilization of dissolved glucose in the upper water column of the Gulf of Mexico. *Limnol. Oceanogr.* 44, 1625–1633. doi: 10.4319/lo.1999.44.7.1625
- Steen, A. D., Ziervogel, K., Ghobrial, S., and Arnosti, C. (2012). Functional variation among polysaccharide-hydrolyzing microbial communities in the Gulf of Mexico. *Mar. Chem.* 138, 13–20. doi: 10.1016/j.marchem.2012.06.001
- Stolpe, B., Guo, L., Shiller, A. M., and Hassellöv, M. (2010). Size and composition of colloidal organic matter and trace elements in the Mississippi River, Pearl River and the northern Gulf of Mexico, as characterized by flow field-flow fractionation. *Mar. Chem.* 118, 119–128. doi: 10.1016/j.marchem.2009.11.007
- Teske, A., Durbin, A., Ziervogel, K., Cox, C., and Arnosti, C. (2011). Microbial community composition and function in permanently cold seawater and sediments from an arctic fjord of Svalbard. *Appl. Environ. Microbiol.* 77, 2008–2018. doi: 10.1128/AEM.01507-10
- US Army Corps of Engineers (2013). *Hurricane Isaac with and without 2012 100-year HSDRRS Evaluation*. Final Report, US Army Corps of Engineers.
- Wang, X. C., Chen, R. F., and Gardner, G. B. (2004). Sources and transport of dissolved and particulate organic carbon in the Mississippi River estuary and adjacent coastal waters of the northern Gulf of Mexico. *Mar. Chem.* 89, 241–256. doi: 10.1016/j.marchem.2004.02.014
- Walker, N. D., Wiseman, W. J., Rouse, L. J., and Babin, A. (2005). Effects of river discharge, wind stress, and slope eddies on circulation and the satellite-observed structure of the Mississippi River Plume. *J. Coast. Res.* 21, 1228–1244. doi: 10.2112/04-0347.1
- Yuan, J., Miller, R., Powell, R., and Dagg, M. (2004). Storm-induced injection of the Mississippi River plume into the open Gulf of Mexico. *Geophys. Res. Lett.* 31, L09312. doi: 10.1029/2003GL019335
- Ziervogel, K., and Arnosti, C. (2009). Enzyme activities in the Delaware estuary affected by elevated suspended sediment load. *Estuar. Coast. Shelf Sci.* 84, 253–258. doi: 10.1016/j.ecss.2009.06.022
- Ziervogel, K., and Arnosti, C. (2013). Enhanced protein and carbohydrate hydrolyses in plume-associated deepwaters initially sampled during the early stages of the Deepwater Horizon oil spill. *Deep Sea Res. II*. doi: 10.1016/j.dsr2.2013.09.003. [Epub ahead of print].
- Ziervogel, K., Dike, C., Asper, V., Montoya, J., Battles, J., D'souza, N., et al. (2015). Enhanced particle fluxes and heterotrophic bacterial activities in gulf of mexico bottom waters following storm-induced sediment resuspension. *Deep Sea Res. II*. doi: 10.1016/j.dsr2.2015.06.017. [Epub ahead of print].
- Ziervogel, K., D'souza, N., Sweet, J., Yan, B., and Passow, U. (2014). Natural oil slicks fuel surface water microbial activities in the Gulf of Mexico. *Front. Aquat. Microbiol.* 5:188. doi: 10.3389/fmicb.2014.00188
- Ziervogel, K., McKay, L., Rhodes, B., Osburn, C. L., Dickson-Brown, J., Arnosti, C., et al. (2012). Microbial activities and dissolved organic matter dynamics in oil-contaminated surface seawater from the Deepwater Horizon oil spill site. *PLoS ONE* 7:e34816. doi: 10.1371/journal.pone.0034816
- Conflict of Interest Statement:** The authors declare that the research was conducted in the absence of any commercial or financial relationships that could be construed as a potential conflict of interest.
- Copyright © 2016 Ziervogel, Osburn, Brym, Battles, Joye, D'souza, Montoya, Passow and Arnosti. This is an open-access article distributed under the terms of the Creative Commons Attribution License (CC BY). The use, distribution or reproduction in other forums is permitted, provided the original author(s) or licensor are credited and that the original publication in this journal is cited, in accordance with accepted academic practice. No use, distribution or reproduction is permitted which does not comply with these terms.



Microbially-Mediated Fluorescent Organic Matter Transformations in the Deep Ocean. Do the Chemical Precursors Matter?

Fran L. Aparicio^{1*}, Mar Nieto-Cid², Encarna Borrull¹, Estela Romero^{1,3}, Colin A. Stedmon⁴, Maria M. Sala¹, Josep M. Gasol¹, Aida F. Ríos² and Cèlia Marrasé¹

¹ Institut de Ciències del Mar-CSIC, Barcelona, Spain, ² Instituto de Investigaciones Marinas-CSIC, Vigo, Spain, ³ Metis UMR 7619, Université Pierre et Marie Curie, Paris, France, ⁴ Section for Marine Ecology and Oceanography, National Institute for Aquatic Resources, Technical University of Denmark, Charlottenlund, Denmark

OPEN ACCESS

Edited by:

Thomas S. Bianchi,
University of Florida, USA

Reviewed by:

Karin M. Björkman,
University of Hawaii, USA

Nicholas David Ward,
University of Florida, USA

*Correspondence:

Fran L. Aparicio
franciscoluis.aparicio@icm.csic.es

Specialty section:

This article was submitted to
Marine Biogeochemistry,
a section of the journal
Frontiers in Marine Science

Received: 29 September 2015

Accepted: 18 November 2015

Published: 08 December 2015

Citation:

Aparicio FL, Nieto-Cid M, Borrull E, Romero E, Stedmon CA, Sala MM, Gasol JM, Ríos AF and Marrasé C (2015) Microbially-Mediated Fluorescent Organic Matter Transformations in the Deep Ocean. Do the Chemical Precursors Matter? *Front. Mar. Sci.* 2:106.
doi: 10.3389/fmars.2015.00106

The refractory nature of marine dissolved organic matter (DOM) increases while it travels from surface waters to the deep ocean. This resistant fraction is in part composed of fluorescent humic-like material, which is relatively difficult to metabolize by deep water prokaryotes, and it can also be generated by microbial activity. It has been recently argued that microbial production of new fluorescent DOM (FDOM) requires the presence of humic precursors in the surrounding environment. In order to experimentally test how the chemical quality of the available organic compounds influences the production of new FDOM, three experiments were performed with bathypelagic Atlantic waters. Microbial communities were incubated in three treatments which differed in the quality of the organic compounds added: (i) glucose and acetate; (ii) glucose, acetate, essential amino acids, and humic acids; and (iii) humic acids alone. The response of the prokaryotes and the production of FDOM were simultaneously monitored. Prokaryotic abundance was highest in treatments where labile compounds were added. The rate of humic-like fluorescence production, scaled to prokaryotic abundance, varied depending on the quality of the additions. The precursor compounds affected the generation of new humic-like FDOM, and the cell-specific production of this material was higher in the incubations amended with humic precursors. Furthermore, we observed that the protein-like fluorescence decreased only when fresh amino acids were added. These findings contribute to the understanding of FDOM variability in deep waters and provide valuable information for studies where fluorescent compounds are used in order to track water masses and/or microbial processes.

Keywords: Atlantic Ocean, deep sea, DOC, FDOM, PARAFAC, EEMs, precursors, organic matter

INTRODUCTION

An important issue to be considered when exploring the role of the ocean in carbon sequestration is the biogeochemical fate of the organic matter. Conventionally, it is known that the biological and solubility pumps combined are important for the transfer of carbon (C) from the atmosphere to the ocean interior, resulting in the temporary or permanent storage of carbon (Volk and Hoffert, 1985;

Honjo et al., 2014; Legendre et al., 2015). The recently introduced concept of the microbial carbon pump (MCP) postulates mechanisms by which dissolved refractory organic matter is produced and accumulated in the ocean through microbial activity, underlying the role that this refractory pool plays in carbon sequestration in marine systems (Jiao et al., 2010).

The mechanisms that produce dissolved organic matter (DOM) are, among others: phytoplankton exudation (Hopkinson et al., 2002; Romera-Castillo et al., 2011; Sarmento et al., 2013), release by viral lysis (Brussaard, 2004; Motegi et al., 2009), sloppy feeding and the solubilisation of particulate organic matter (POM) by bacterial and archaeal hydrolases (Nagata et al., 2000; Sala and Güde, 2004). These various mechanisms condition not only DOM production but also its quality, and consequently its ultimate fate.

The study of DOM in the ocean interior has been in the spotlight for several years. A fraction of this pool, called chromophoric dissolved organic matter (CDOM; Coble, 1996), absorbs light at both ultraviolet (UV) and visible wavelengths. A sub-fraction of this CDOM, the fluorescent DOM (FDOM; Coble, 1996, 2007), fluoresces when irradiated with UV light. In 1961, Weber described a technique to elucidate the main fluorescing groups of compounds, i.e., fluorophores, by varying the excitation and emission wavelengths and constructing a matrix of the resulting intensities (Weber, 1961). This technique generates the so-called fluorescence excitation-emission matrix (EEM) which was first applied by Coble et al. (1990) to characterize marine FDOM. This technique, however, does not permit the quantification of specific molecules. A better understanding of specific molecules has become possible with the recently developed Fourier transform ion cyclotron resonance mass spectrometry (FT-ICR-MS), a methodology that offers novel insights for molecular-level characterization of the complex composition and structure of DOM (Kim et al., 2003; Koch et al., 2005; Koprivnjak et al., 2009; Stubbins et al., 2014; Repeta, 2015). Nevertheless, the most exhaustive analysis that has been performed to date (Hertkorn et al., 2006) could only identify 8% of the molecules composing the DOM pool. These authors combined multidimensional nuclear magnetic resonance (NMR) with FT-ICR-MS on solid phase extracted dissolved organic matter (SPE-DOM), and their results indicate that carboxylic-rich alicyclic molecules (CRAM) are the major component of DOM. Great efforts are being performed in recent years to relate molecular formulas to the optical measurements of DOM in order to associate fluorescent signatures to single molecules (Stubbins et al., 2014; Reader et al., 2015). Nevertheless, the challenge of identifying and revealing the composition of DOM remains still incomplete. With that said, fluorescence spectroscopy methods, being rapid and inexpensive, are convenient for certain studies focused on humic- and protein like compounds that require large coverage, spatial or temporal.

Marine DOM is composed of a large variety of substances owning different turnover rates and residence times. The turnover times of some FDOM components have been estimated to be, on average, higher than the deep ocean water renewal, and thus the fluorescence measurements have been proposed as a

proxy to study the cycling of DOM that is resistant at centennial time scales (Catalá et al., 2015). In water masses exhausted in labile or semi-labile fractions of DOM, bacteria could “prime” the recalcitrant compounds decomposition if labile compounds are added to the media (Carlson et al., 2002; Bianchi, 2012). The “priming effect” (PE), bacterial remineralization of unreactive organic carbon substrates when labile sources are available, was described for the first time in soil sciences in 1926 by Löhnis (Löhnis, 1926). The PE has been experimentally observed in a variety of environments and with additions of different carbon compounds: in soils (Kuzyakov, 2002; Fontaine et al., 2004); fresh water ecosystems (De Haan, 1977; Shimp and Pfaender, 1985; Bianchi et al., 2015; Catalán et al., 2015); and also in marine ecosystems, mainly using mesocosm experiments (Carlson et al., 2002; Fonte et al., 2013; Guenet et al., 2014). However, as it was mentioned before, the mechanisms that hinder the complete remineralization of DOM, causing the relative permanence of part of this pool, from months to millennia, are not really well understood.

Despite the several studies conducted during the last years to assess the spatial and temporal variability of DOM quality (Yamashita et al., 2011; Koehler et al., 2012; Gontikaki et al., 2013; Kothawala et al., 2014), little is known about how the reactivity of DOM varies across landscapes (rivers, lakes, estuaries, coastal ocean, deep ocean). Most of these studies have recognized that DOM reactivity is not only inherently linked to its chemical composition, but also depends on ecosystem properties (Dittmar, 2015). A better understanding of microbial FDOM transformations in the deep ocean is required before FDOM can be consistently applied as a water mass tracer or as a proxy for a fraction of the DOM.

Recent studies have found a high correlation between apparent oxygen utilization (AOU) and the generation of humic-like compounds, indicating that humic-DOM in the dark ocean could originate from in situ microbial respiration (Yamashita and Tanoue, 2008; De La Fuente et al., 2014; Jørgensen et al., 2014b), which agrees with the MCP concept proposed by Jiao et al. (2010). Furthermore, Andrew et al. (2013) suggested that the production of humic-like fluorescence signal is favored when terrestrial chemical precursors are present. In order to gain insight into the microbially-mediated FDOM variability, the present study examines how the quality and quantity of the organic substrates influence simultaneously the generation of humic fluorescence signal and the microbial activity. This was carried out by performing incubation experiments using water samples from the deep Atlantic Ocean. These calculations are key to understand the particularities of deep waters C storage and the functioning of the MCP.

MATERIALS AND METHODS

Sample Collection and Experimental Strategy

We conducted three experiments (DEEP I, DEEP II, and DEEP III) with natural prokaryotic communities from deep waters of the South Atlantic Ocean. Seawater was taken during the

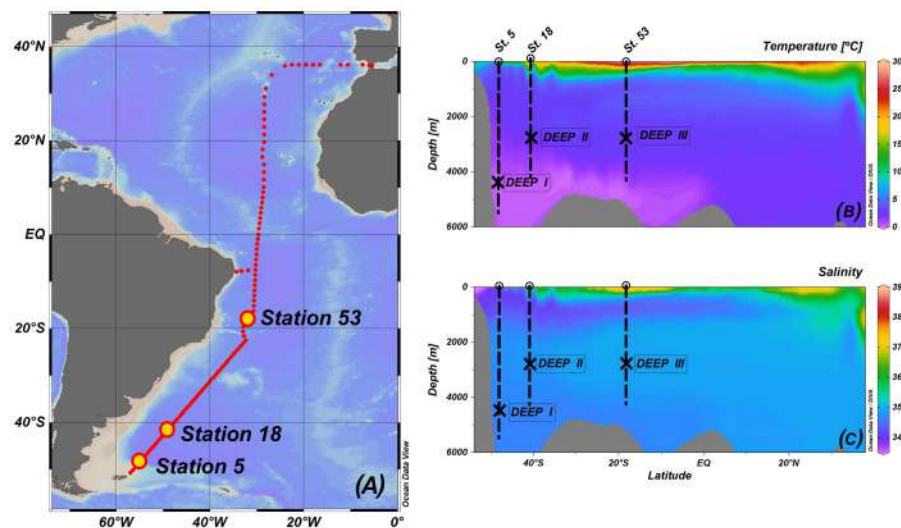


FIGURE 1 | Graphic summary of the XIVth FICARAM cruise: cruise track followed on board the Spanish R/V *Hespérides* (A), contour plot of temperature expressed in °C (B), and contour plot of salinity (C). Panels include information about the sampling station and depths for each experiment. Ocean data View is used for mapping (Schlitzer, 2015).

TABLE 1 | A list of the compounds added to each experimental treatment (Sigma-Aldrich Co. LLC.).

Compound	Molecular formulae	Final estimated concentration ($\mu\text{mol C L}^{-1}$) per treatment		
		CL	CM	CR
D-glucose	C ₆ H ₁₂ O ₆	15	3.33	
Sodium acetate	C ₂ H ₃ O ₂ Na	15	3.33	
Sodium pyruvate	C ₃ H ₃ NaO ₃		3.33	
Humic acids	Unknown		3.33	30
Cellulose	(C ₆ H ₁₀ O ₅) _n		3.33	
Chitin	(C ₈ H ₁₅ NO ₆) _n		3.33	
D-aspartic	C ₄ H ₇ NO ₄		3.33	
N-acetyl-D-glucosamine	C ₈ H ₁₅ NO ₆		3.33	
L-arginine hydrochloride	C ₆ H ₁₄ N ₄ O ₂		0.33	
L-histidine hydrochloride	C ₆ H ₉ N ₃ O ₂ ·HCl		0.33	
L-isoleucine	C ₆ H ₁₃ NO ₂		0.33	
L-leucine	C ₆ H ₁₃ NO ₂		0.33	
L-lysine hydrochloride	C ₆ H ₁₄ N ₂ O ₂		0.33	
L-methionine	C ₅ H ₁₁ NO ₂ S		0.33	
L-phenylalanine	C ₉ H ₁₁ NO ₂		0.33	
L-threonine	C ₄ H ₉ NO ₃		0.33	
L-tryptophan	C ₁₁ H ₁₂ N ₂ O ₂		0.33	
L-valine	C ₅ H ₁₁ NO ₂		0.33	

FICARAM-15 cruise, carried out from the 20th of March to the 22nd of May 2013, following a track from Punta Arenas (Chile) to Cartagena (Spain). Experiment DEEP I was performed with water taken from station 5 ($48^{\circ} 18' 18.6''$ S; $54^{\circ} 54' 35.4''$ W) at 4500 m while in experiments DEEP II and DEEP III we used 3000 m water from stations 18 ($40^{\circ} 30' 0''$ S; $48^{\circ}, 5' 28''$ W) and 53 ($17^{\circ} 50' 1.21''$ S; $31^{\circ} 38' 2.4''$ W), respectively (Figure 1).

In each experiment, sample filtration through 0.6 μm pore-size polycarbonate filters started within 20 min after collection. Then, the water was distributed into four 20 L fluorinated polyethylene carboys. The first container was kept as a control (K). Acetate and glucose (both had been found to be very labile compounds with turnover times of hours to days in marine waters (Azam and Hodson, 1981; Ho et al., 2002), were added to the second container (CL). A combination of carbon-based substances was added to the third container (CM). In this case, not only glucose and acetate were added, but also a mixture of compounds of different lability, including terrestrial humic acids and amino acids, which are known to be essential for prokaryotic metabolism, (see Table 1). In the last carboy (CR), Suwannee River humic acids (Ref. 2R101N) provided by the International Humic Substances Society (IHSS) was added. All the organic carbon (OC) substrates were dissolved in 50 mL of Milli-Q water prior to the addition into the carboys. In the case of Suwannee River humic acids, a pH of 12 was needed to favor the dilution, thus we previously added the material in a solution of NaOH and later we compensate the pH adding HCO₃⁻. All carbon amendments were calculated to result in an approximately 30 $\mu\text{mol C}$ increase in dissolved organic carbon (DOC) concentration. After the additions, the containers were manually shaken and kept 1 h at 4°C before sampling the initial point (t_0) in order to assure homogenization. At t_0 , water from each of the experimental conditions was distributed among 72 acid clean 250 mL glass bottles (18 bottles per treatment). Three glass bottles per experimental condition were harvested at every sampling date, and the three bottles were considered experimental replicates. The experiments were conducted on board in a dark temperature-controlled chamber at 4°C and monitored for a total of 35 days. Intensive samplings were scheduled for days: 0, 5, 10, 15, 25, and 35, where the variables

measured were: prokaryotic abundance, FDOM, and CDOM. Furthermore, after day 3 (t_3), one bottle of each condition was sampled daily to monitor prokaryote abundances. This subsampled bottle was then considered replicate number 1 in the following intensive sampling.

Measurements

The ship's rosette was equipped with a SBE11plus (Sea-Bird Electronics) CTD probe, recording, at each station, profiles of temperature, conductivity, and oxygen. Analyses of dissolved inorganic nutrient concentrations, nitrate (NO_3^-), phosphate (PO_4^{3-}), and silicate (SiO_2), were done on board by standard segmented flow analyses with colorimetric detection (Hansen and Grasshoff, 1983) using a Skalar Autoanalyser. Precisions were $\pm 0.01 \mu\text{mol kg}^{-1}$ NO_3^- , $\pm 0.02 \mu\text{mol kg}^{-1}$ PO_4^{3-} , and $\pm 0.01 \mu\text{mol kg}^{-1}$ SiO_2 . DOC samples were collected in 10 mL precombusted (450°C , 24 h) glass ampoules. After acidification with 50 μL of 25% H_3PO_4 to $\text{pH} < 2$, the ampoules were heat-sealed and stored in the dark at 4°C until examination. Analyses were carried out in a Shimadzu TOC-CSV organic carbon analyser. Three to five injections of 150 μL were performed per replicate. DOC concentration in each replicate was calculated by first subtracting a Milli-Q blank and then dividing by the slope of a daily standard curve made from potassium hydrogen phthalate. The precision of measurements was $\pm 0.7 \mu\text{mol L}^{-1}$. All samples were checked against deep Sargasso Sea reference water (2600 m) provided by D. Hansell (U. of Miami).

FDOM was measured using a Perkin Elmer LS55 luminescence spectrometer equipped with a xenon discharge lamp (20 kW/8 μs). A red sensitive R928 photodiode multiplier worked as a reference detector. The running parameters for the instrument were set as follows: scan speed at 250 nm min^{-1} and slit widths (for excitation and emission wavelengths) at 10 nm, at a constant room temperature of 20°C in a 1 cm quartz fluorescence cell. Excitation-emission matrices were performed by concatenating 21 excitation/emission spectra of the sample, obtained at a constant offset of 10 nm between the excitation and emission wavelengths. The spectra were collected starting from the highest excitation wavelength, to minimize the exposure of the sample to low-wavelength radiation and thereby minimize photodegradation. Following Lawaetz and Stedmon (2009), fluorescence measurements were expressed in Raman Units (R.U.) by normalization to the integrated water Raman scattering band of Milli-Q water freshly generated on board every day. Our results can be compared with quinine sulfate units (QSU) having in account that 1 QSU is equivalent to 86 ± 1 R.U.

To better characterize the dynamics of the FDOM, PARAFAC modeling of the EEM datasets was conducted using the drEEM toolbox (Murphy et al., 2013) in the Matlab® software package. The dataset for PARAFAC modeling was composed of 289 samples collected during the cruise to increase the consistency of the model, 64 of them belonging to the DEEP water experiments. In order to organize the data for the modeling process, regions of no fluorescence or scatter were removed. By doing so, our EEMs ranged from 250 to 450 nm along the excitation axis, and from 350 to 550 nm along the emission axis. The model was run

with non-negativity constraints. A series of PARAFAC models were tested with 3–7 components fitted to the data. Split-half validation was used to divide the data into six random halves of equal size and the model run independently on the halves. A four-component PARAFAC model was validated. According to the residual analyses, we could confirm that less than 10% of the fluorescence was left unexplained (subtraction of the modeled from the measured spectra yielded a residual fluorescence an order of magnitude lower than the measured EEMs). The characteristics of the four components of the PARAFAC model are shown in Figure 2. Their excitation and emission maxima are specified in Table 2 and they are associated to components already detected in previous studies. Three out of the four components identified (FIC1, FIC2, and FIC4) are placed in humic-like fluorescence regions and one of them (FIC3) in the protein-like area.

Heterotrophic prokaryotes were enumerated with a FACSCalibur (Becton Dickinson) flow cytometer equipped with a 15 mW argon-ion laser (488 nm emission) as described by (Gasol and Del Giorgio, 2000). Samples (1.8 mL) were immediately fixed with 1% paraformaldehyde plus 0.05% glutaraldehyde (final concentrations), incubated for 10 min at room temperature, frozen in liquid nitrogen and stored at -80°C . Before analysis, samples were unfrozen, stained with SYBRGreen I (Molecular Probes) at a final concentration of 10 μM and left in the dark for about 15 min. Each sample was then run at low speed ($\sim 12 \mu\text{L min}^{-1}$) for 2 min with Milli-Q water as a sheath fluid. We added 10 μL per sample of a solution of yellow-green 0.92 μm Polysciences latex beads (10^6 beads mL^{-1}) as an internal standard. Bacteria were detected by their signature in a plot of side scatter vs. FL1 (green fluorescence). Data analysis was performed with the Paint-A-Gate software (Becton Dickinson).

Statistical Analyses

The software SigmaPlot v11.0 (Systat Software Inc.) was used to perform the statistical analyses applied in this work. Two-way ANOVA was carried out to test if differences between conditions and experiments were significant and *t*-tests to discriminate if the temporal evolution of the different variables measured in an experiment could be considered significant. For both types of tests, significance was set to $p < 0.05$.

RESULTS

Initial Conditions

The physical and chemical signatures of the water masses used in each experiment, Antarctic Bottom Water (AABW) in experiment DEEP I, Circumpolar Deep Water (CDW) in experiment DEEP II and North Atlantic Deep Water (NADW) in experiment DEEP III, are listed in Table 3. AABW presented the lowest temperature and highest concentration of nutrients. As shown in Figure 1, the temperature and salinity of the deep Atlantic Ocean increased as latitude decreased, whereas DOC decrease values ranging from 40 to 45 $\mu\text{mol L}^{-1}$, in agreement with previous observations of deep ocean DOC (Hansell et al., 2009).

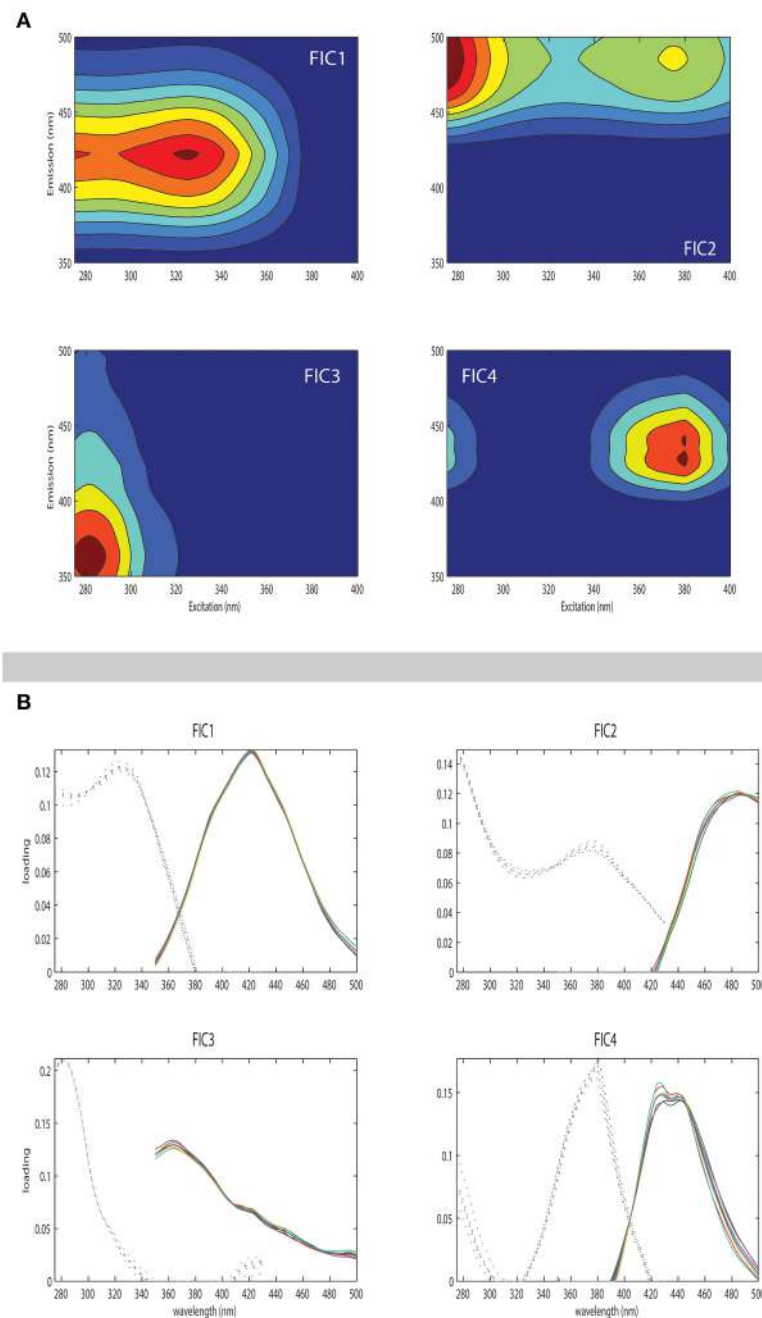


FIGURE 2 | Fluorescence signatures of the four PARAFAC components (FIC1 to FIC4) identified during the experiments are shown in panel (A). Values expressed in R.U. (B) Line plots showing split-half validations in which each component's excitation (left) and emission (right) spectra are estimated from independent halves of the dataset.

A compilation of excitation-emission matrices acquired at the beginning of each experiment (t_0) is presented in **Figure 3**. Clearly different patterns, depending on the treatment, are apparent. When comparing the EEMs for the control (K, no carbon addition, **Figures 3A–C**) among experiments, the starting points for the different water samples are similar, reflecting the limited range in DOC values between sites. High fluorescence

values (>0.01 R.U.) were located around the FIC2 maxima at Ex/Em wavelengths (275 nm/468 nm) while the other humic-like fluorophores (325 nm/423 nm and 380 nm/428 nm) had lower intensities (0.006 – 0.008 R.U.). Signals for protein-like material (281 nm/363 nm) were even lower (~ 0.004 R.U.). Likewise, the fluorescence intensities for the labile carbon treatments (CL) at t_0 (**Figures 3D–F**) did not reach values higher than 0.01 R.U.,

TABLE 2 | Optical characteristics of five components derived from the PARAFAC and their comparison with the results from previous studies available in the OpenFluor database (Murphy et al., 2014).

Compound	Ex. max (nm)	Em. max (nm)	Assignment					
			Murphy et al., 2008	Walker et al., 2009	Yamashita et al., 2010a	Kothawala et al., 2012	Graeber et al., 2012	Brym et al., 2014
FIC1	325	423	C3	BERC3*	C1			C1*/C4
FIC2	275	468	C2/C4*			C _X		
FIC3	<281	363			C6*	C _T	C5	C1*
FIC4	380	428	P3*					C3

For all comparisons Tucker's Congruence Coefficient (TCC) was >0.95.

*Component does not completely match.

TABLE 3 | Physical and chemical signatures of the water masses used in each of the three DEEP experiments.

Station (experiment)	Depth (m)	Water mass	Temperature (°C)	Salinity	Nitrate (μmol kg ⁻¹)	Phosphate (μmol kg ⁻¹)	Silicate (μmol kg ⁻¹)	Oxygen (μmol kg ⁻¹)	DOC (μmol L ⁻¹)
5 (DEEP I)	4500	Antarctic Bottom Water (AABW)	0.27	34.673	32.82	2.27	128.37	221.3	47.5
18 (DEEP II)	3000	Circumpolar Deep Water (CDW)	1.84	34.764	29.28	1.98	90.75	204.9	45.8
53 (DEP III)	3000	North Atlantic Deep Water (NADW)	2.78	34.917	20.51	1.21	32.51	250.4	41.8

indicating that the added compounds did not influence the initial fluorescence signal. As expected, in the mixed substrate treatment (CM, **Figures 3G–I**), the addition of amino acids and humic acids increased remarkably the initial fluorescence values. The addition of pure amino acids was the main reason behind the high values observed within the protein-like region (~ 0.03 R.U.), while the addition of Suwannee River natural organic matter caused higher values within the humic-like regions of the EEM, e.g., up to ~ 0.021 R.U. at the FIC2 maximum area and around 0.018 R.U. for the rest of the humic-like fluorophores. Finally, the initial EEMs of the CR treatments (refractory carbon, **Figures 3J–L**) also showed a similar trend for the three experiments. The Suwannee River humics additions altered only the visible wavelength emission enhancing humic-like intensities (up to ~ 0.06 R.U.), a reflection of the terrestrial nature of the added compounds.

Responses to Treatments

Dynamics of the Prokaryotic Community

Prokaryotic abundance increased throughout the first 5 days of the incubation following the same trend in the three experiments (**Figure 4**). Prokaryotic abundance at t_0 was about $8.0 \cdot 10^3$, $2.3 \cdot 10^4$, and $1.1 \cdot 10^4$ cells mL⁻¹ for experiments DEEP I, DEEP II, and DEEP III, respectively. The stationary phase was reached after 10 days of incubation in all experiments. Prokaryote concentration at the end of the exponential growth phase ranged from $6.9 \cdot 10^4$ to $8.0 \cdot 10^4$ cells mL⁻¹ in the K treatments, from $7.8 \cdot 10^5$ to $9.2 \cdot 10^5$ cells mL⁻¹ in the CL conditions, from $5.8 \cdot 10^5$ to $6.1 \cdot 10^5$ cells mL⁻¹ in the CM incubations and from $6.5 \cdot 10^4$ to $1.3 \cdot 10^5$ cells mL⁻¹ in the CR conditions. During the first days of experiment the slopes of the curves indicated faster growth rates for the CM treatments than for the rest of them, although the number of cells in the CL treatment reached the

highest values at the end of the exponential-growth phase. After t_{10} , the prokaryotic communities in all the experiments entered stationary phase. This lasted until the end of the experimental period.

Fluorescence Characterization

To easily visualize the net change in the humic-like and the protein-like fractions of the FDOM during the exponential-growth and stationary phases of the experiments, we subtracted the fluorescence intensities at t_0 from those measured at t_{10} and also the values at t_{10} from those measured at t_{final} . We also divided the resultant values by the number of days each phase lasted. The bar charts in **Figure 5** show fluorescence intensity increases/decreases for each humic-like component in each experiment. The resultant fluorescence intensities during the exponential-growth phase and the stationary phase were similar for experiments DEEP II and DEEP III, but DEEP I presented divergent patterns. In DEEP I, FIC1, FIC2, and FIC4 intensities decreased for all treatments during the exponential-growth phase (**Figures 5A,D,G**). The largest decreases during this phase were observed in the CR conditions followed by the decreases in the CM conditions. On the contrary, we found increases during the same time period in DEEP II and DEEP III, the highest being again detected in the CR and CM conditions, with the exception of the FIC4 signal in the CM and CL conditions in DEEP III, which decreased (**Figures 5B,C,E,F,H,I**). During the stationary phase of the three experiments the fluorescence signals tended to increase in all treatments. The values of this increase were always the highest for the CR conditions, regardless of the experiment, except in one case, for the FIC4 component.

A different temporal dynamic was observed for protein-like substances, FIC3 (**Figure 6**). All the experiments showed similar trends in K, CL, and CR treatments. The FIC3 component signal

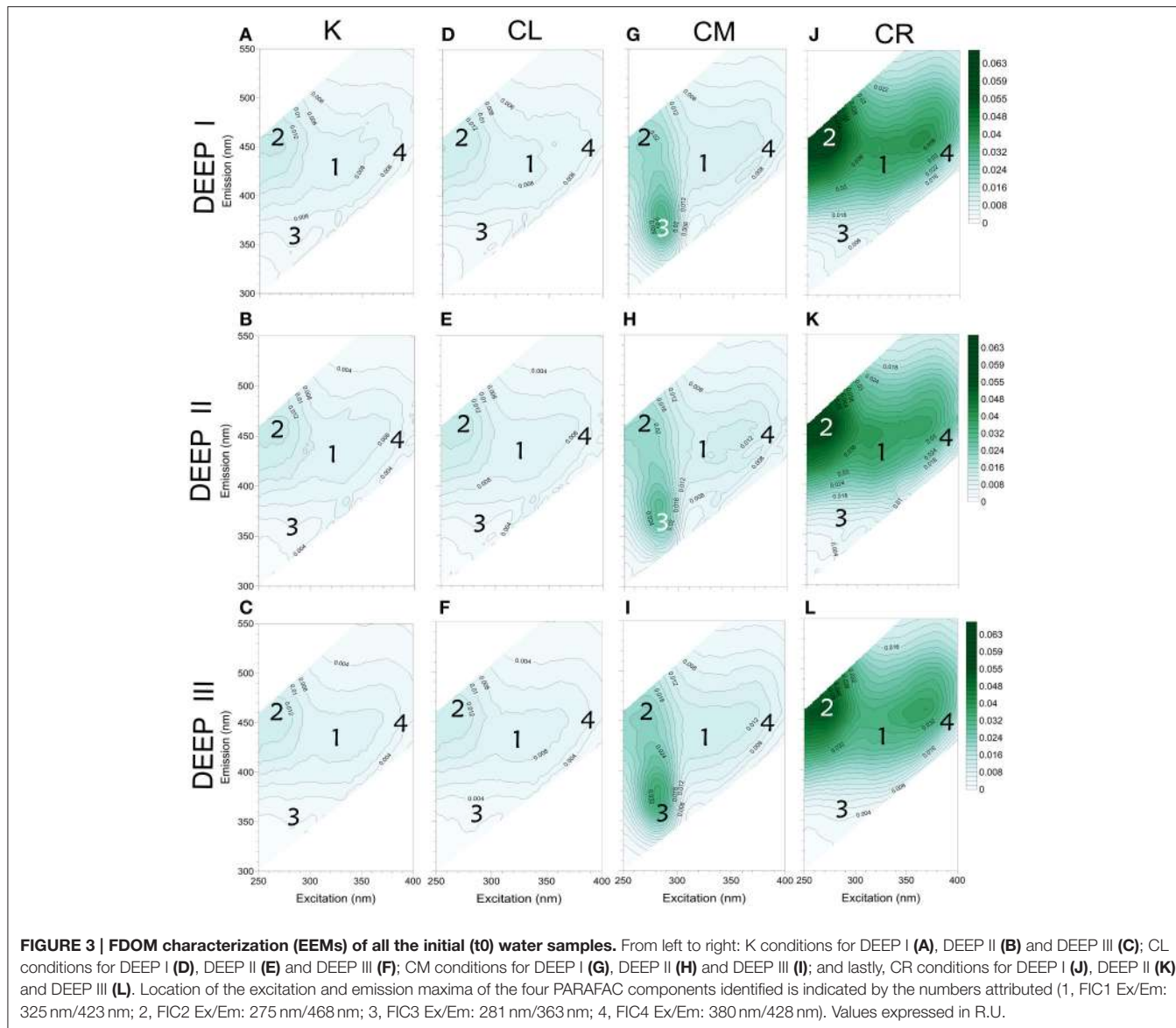


FIGURE 3 | FDOM characterization (EEMs) of all the initial (t0) water samples. From left to right: K conditions for DEEP I (**A**), DEEP II (**B**) and DEEP III (**C**); CL conditions for DEEP I (**D**), DEEP II (**E**) and DEEP III (**F**); CM conditions for DEEP I (**G**), DEEP II (**H**) and DEEP III (**I**); and lastly, CR conditions for DEEP I (**J**), DEEP II (**K**) and DEEP III (**L**). Location of the excitation and emission maxima of the four PARAFAC components identified is indicated by the numbers attributed (1, FIC1 Ex/Em: 325 nm/423 nm; 2, FIC2 Ex/Em: 275 nm/468 nm; 3, FIC3 Ex/Em: 281 nm/363 nm; 4, FIC4 Ex/Em: 380 nm/428 nm). Values expressed in R.U.

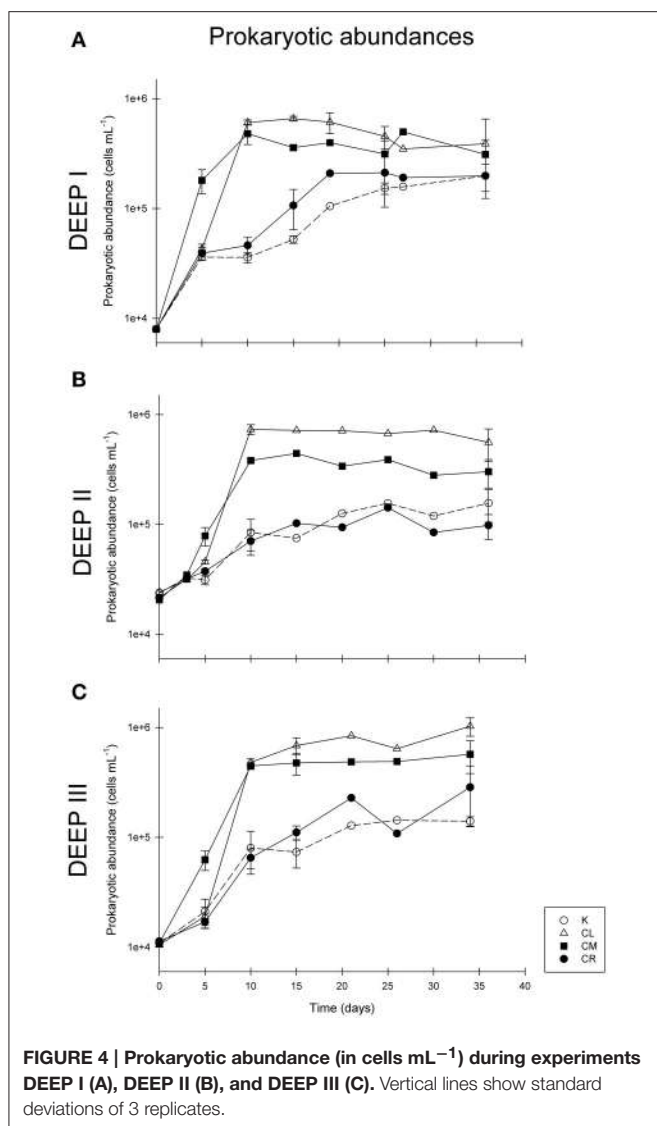
was very low at the beginning of the experiments for the K, CL, and CR treatments, while in the CM condition the added amino acids induced elevated values of protein-like fluorescence (Figure 6). FIC3 intensity coupled to prokaryotic abundance in all treatments except in that amended with protein-like precursors (CM). The decay of FIC3 signal in DEEP II and DEEP III experiments was higher than the decrease detected for this component in DEEP I. We hypothesized that the FIC3 increase in K, CL, and CR is due to bacterial growth while in the CM treatment, the consumption of the added fluorescent protein-like substances overcame FIC3 production. To examine the relative importance of FIC3 consumption with respect to FIC3 generation in CM, we estimated the production in this treatment using an empirical model based on the relationship between FIC3 fluorescence and prokaryotic abundance (Figure 7). The model was constructed with the data pooled from the treatments

with no amino acid amendments (K, CL, and CR) and where FIC3 fluorescence increased with time, as prokaryotes grew (Figure 6). Using the equation described by this empirical model (Figure 7; $R^2 \sim 0.75$, $N = 41$), we have estimated the protein-like fluorescence (eFIC3) due to prokaryotic growth for each sampling day of the CM condition. Comparing these values with the observed FIC3 intensity, we could estimate the fraction of the signal due to the original amino acids amended to this condition (aaFIC3), which decreased with time (Figure 8).

DISCUSSION

PARAFAC Component Source Identification

The OpenFluor spectral database (Murphy et al., 2014), was used to identify the different PARAFAC components present



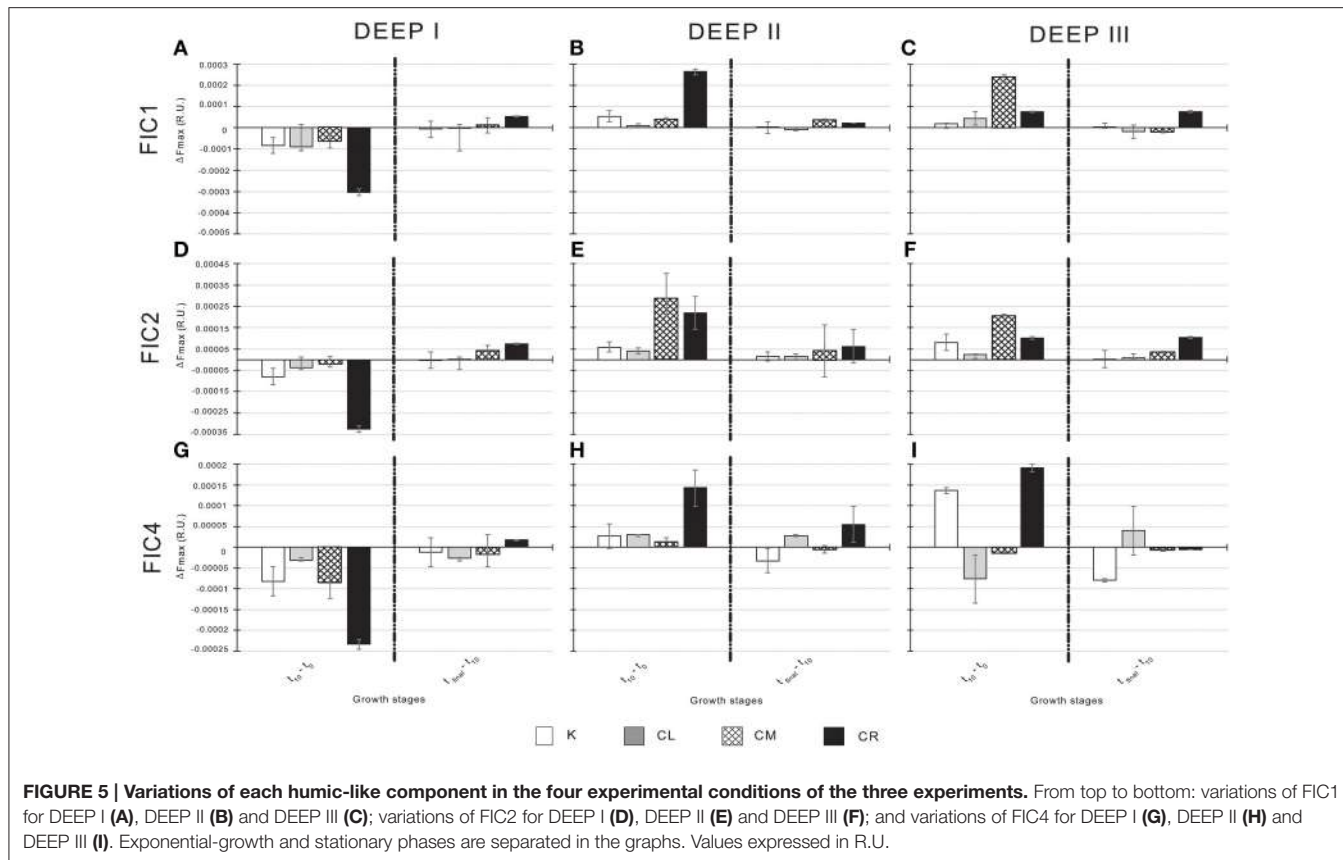
in our incubations. Two out of four components (FIC1 and FIC2) were clearly placed in areas traditionally related to humic-like fluorescence (Coble, 1996). FIC1 has recently been reported as a constituent of terrestrial and aquatic fulvic acids. Different studies devoted to track the origin of the organic compounds using their optical properties have found it in coastal areas around the globe, from Florida (Yamashita et al., 2010b; Brym et al., 2014) to Australia (Cawley et al., 2012), including Arctic rivers estuaries (Walker et al., 2013), the Bay of Liverpool (Yamashita et al., 2011), and even the ballast water of different commercial ships (Murphy et al., 2006). The fluorescent intensity of FIC2 is very similar to the traditional peak-A (Coble, 1996) a humic-like material found in rivers and sensitive to photodegradation (Søndergaard et al., 2003; Stedmon et al., 2007; Walker et al., 2009; Lapierre and del Giorgio, 2014). The FIC3 component showed characteristics of tryptophan-like fluorescence and was similar to other previously

reported PARAFAC components, which have been associated to tryptophan-like, protein-bound and free amino acids (Yamashita and Tanoue, 2003; Stedmon and Markager, 2005b; Murphy et al., 2008; Kothawala et al., 2012; Kowalcuk et al., 2013). The spectral characteristics of FIC4 have not been traditionally defined (Coble, 1996) but it occupies a region very close to those of the humic-like substances. Other studies that have found this component, mainly in the watershed of tropical rivers (Yamashita et al., 2010a) and its estuaries (Brym et al., 2014), have assigned it to a microbial reduced quinone-like substance (Ariese et al., 2004; Cory and McKnight, 2005).

Dynamics of Humic-Like Fluorescence in Response to Different Types of Organic Matter Additions

Since the incubations were performed in the dark, thus preventing photo bleaching, the changes in concentration and quality of FDOM humic-like compounds should exclusively be induced by prokaryotic metabolism, abiotic condensation or viral life cycles. With the exception of the exponential-growth phase in DEEP I, we observed an accumulation of the humic-like fraction across all treatments in the three experiments (Figure 5). In general, the increase in humic-like substances was higher in the conditions where humic precursors were added. These results would be in accordance with the hypothesis postulated by Andrew et al. (2013) about the requirement of polyphenolic terrestrial precursor material to generate additional humic fluorescence signal. The overall picture fits with the expectations that the quality of the precursor material is a significant factor determining the characteristics of the generated DOM. It is remarkable that, in CM and CR conditions, a production of humic-like substances in the stationary phase was recorded in the three experiments. These results agree with the trends observed in earlier studies that reported the accumulation of humic-like fluorescence during the development of incubation experiments. Most of these experiments were performed with the addition of different C sources to the media as phytoplankton exudates added to sea water tanks (Rochelle-Newall and Fisher, 2002; Stedmon and Markager, 2005a; Romera-Castillo et al., 2011). Our results also agree with other studies that found a positive correlation between in-situ microbial respiration and humic-like FDOM generation in the deep (De La Fuente et al., 2014; Guerrero-Feijóo et al., 2014; Jørgensen et al., 2014b; Lønborg and Alvarez-Salgado, 2014) as the three humic-like components showed an increase of intensity during the stationary phase.

In two out of the three experiments (DEEP II and III), the main trend of the humic-like compounds showed the same pattern for the total extent ($t_{\text{final}} - t_0$). Yet, when we related these FDOM increases to prokaryotic abundance, the cell-specific production of FDOM components (Table 4) differed depending on the available source of organic matter. This result indicates that the quality of the precursor material is a significant factor determining the characteristics of the generated DOM and also modifies the organisms' activity. In fact, in the CR condition, where lower prokaryotic abundances were observed, the humic



FDOM production per cell turned out to be significantly higher than in the other treatments.

Our results (Figure 5 and Table 4) allow us: (i) to reinforce Andrew et al. (2013) theory (previously stated), and (ii) to demonstrate the (Jørgensen et al., 2014b) hypothesis, who highlighted the idea that the less labile the precursor material is, the more humic fluorescence is generated. In addition, these results emphasize the appropriateness of distinguishing between different growth stages to better understand the dynamics of produced/consumed DOM.

Concerning humic FDOM dynamics, some discrepancies were observed between the DEEP I and the other two experiments, i.e., an assimilation of the humic-like components in DEEP I vs. an accumulation in DEEP II and III. We are aware that the characteristics of the water masses differed, and that this is perhaps the main reason behind the different responses. Seawater temperature for experiment DEEP I was 0.27°C while the temperatures for the DEEP II and DEEP III experiments were 1.84 and 2.78°C, respectively. Although all three temperatures were low, the DEEP I samples suffered the most substantial change when located at the temperature control chamber, set to 4°C. This fact could explain the steepest slope detected in the prokaryotes' growth curves for all conditions in the DEEP I experiment during the first 10 days of incubation (Figure 4). The prokaryotic growth rate turned out to be approximately two times higher during the first days in DEEP

I compared to DEEP II and III. The relevance of temperature in controlling the degradation of organic matter by microbes has been highlighted many times before (Leahy and Colwell, 1990; Delille, 2004; Vázquez-Domínguez et al., 2007). It is known that the metabolism of cold tolerant prokaryotes is adapted to regulate cellular activities at low temperatures (Feller et al., 1996), however a sudden relatively relevant increase of temperature combined with the availability of DOM sources in excess, and the nature of the DOM already present in the media may cause differences in the behavior of cells while incorporating nutrients (Pomeroy and Wiebe, 2001). In DEEP I experiment, this change in the metabolism could have promoted a fast growth of the bacteria, supporting the use of the humic-like substances instead of its production. We are also aware that the prokaryotic diversity found in AABW differed from those present in NADW and CDW (M. Sebastián, personal communication). For that reason, we cannot reject the hypothesis that the different groups of microorganisms present in the water could have experienced a faster growth in DEEP I, and thus changing the consumption/production ratio of the humic-like substances.

Dynamics of Protein-Like Fluorescence in Response to Different Types of Organic Matter Additions

The large initial drop detected in FIC3 fluorescence in the CM treatments is likely due to the utilization of the added

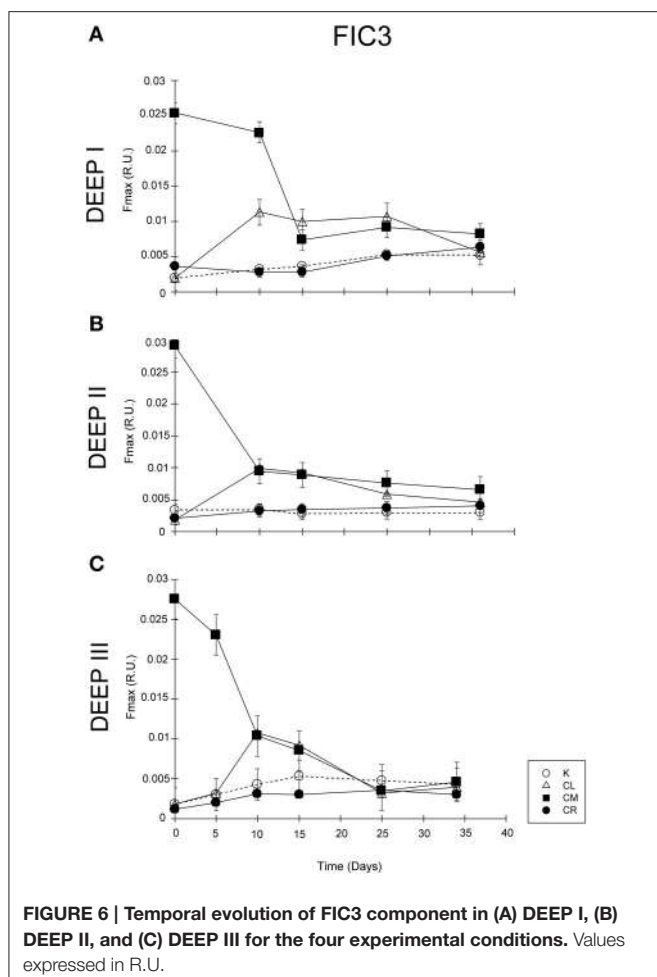


FIGURE 6 | Temporal evolution of FIC3 component in (A) DEEP I, (B) DEEP II, and (C) DEEP III for the four experimental conditions. Values expressed in R.U.

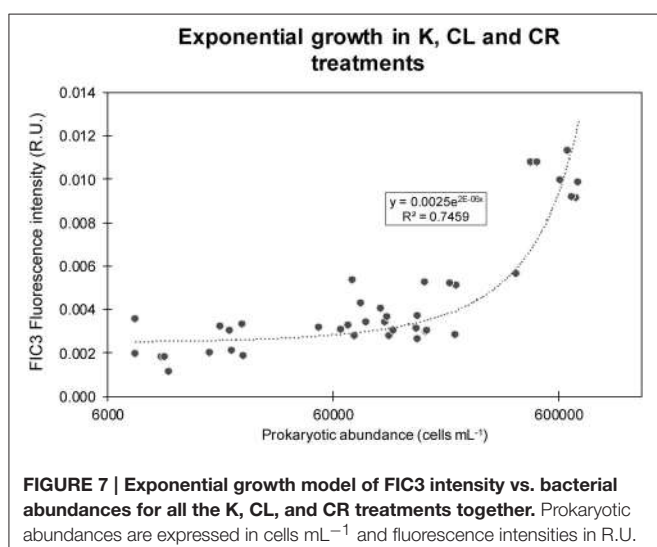


FIGURE 7 | Exponential growth model of FIC3 intensity vs. bacterial abundances for all the K, CL, and CR treatments together. Prokaryotic abundances are expressed in cells mL⁻¹ and fluorescence intensities in R.U.

amino acids by prokaryotes, while the signal increase in the K, CL, and CR conditions could be attributed: (i) to an increase in prokaryotic biomass, as microbial cells have protein-like fluorescence themselves (Determann et al., 1998) or (ii) to

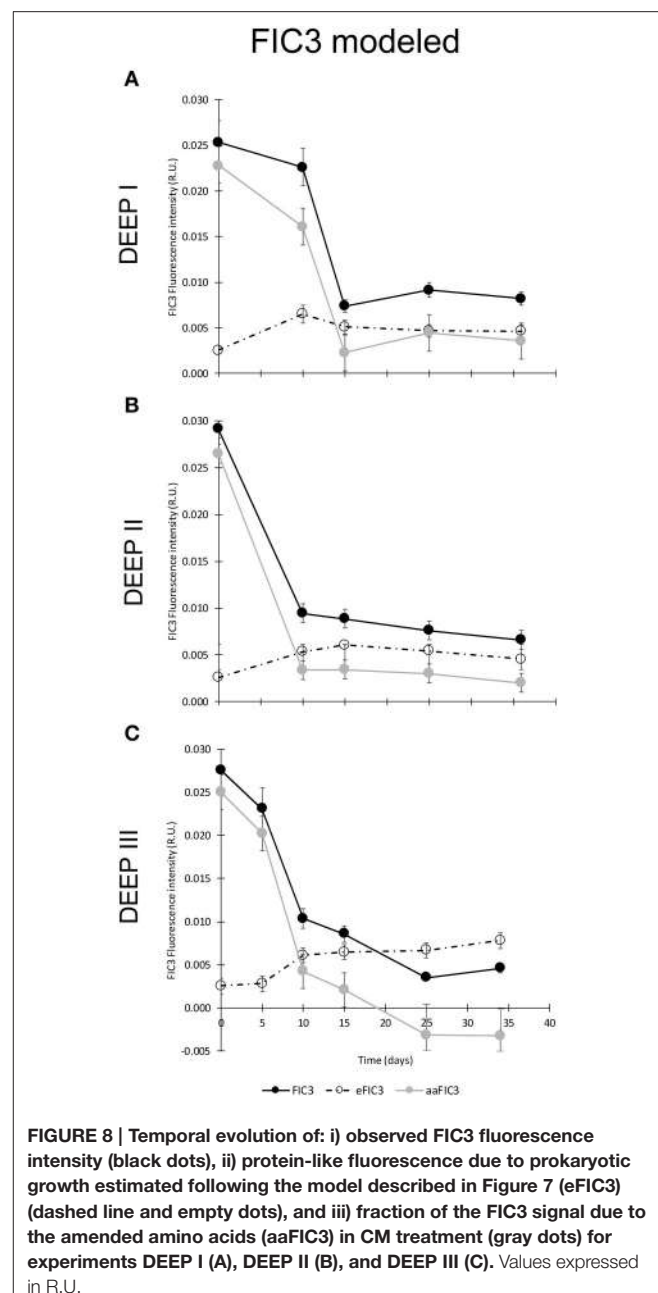


FIGURE 8 | Temporal evolution of: i) observed FIC3 fluorescence intensity (black dots), ii) protein-like fluorescence due to prokaryotic growth estimated following the model described in Figure 7 (eFIC3) (dashed line and empty dots), and iii) fraction of the FIC3 signal due to the amended amino acids (aaFIC3) in CM treatment (gray dots) for experiments DEEP I (A), DEEP II (B), and DEEP III (C). Values expressed in R.U.

prokaryotic by-products that fluoresce in the protein-like region (Yamashita and Tanoue, 2003). The differences between the CM and the other conditions were caused by the different origin of the carbon sources available for prokaryotic consumption. In previous experiments where the only source of carbon was glucose, a selective release of amino acids (D-alanine) and an increase of other components (glucosamine and muramic acid) was observed, associated to prokaryotic growth (Kawasaki and Benner, 2006; Azúa et al., 2014; Jørgensen et al., 2014a). These findings concur with the increase of protein-like fluorescence observed in the K, CL, and CR treatments in our experiments.

TABLE 4 | Overall production/consumption of humic-like fluorescence per cell [(FDOM at t_{final} –FDOM at t_0)·(prokaryotes at t_{final} –prokaryotes at t_0) $^{-1}$] for all the different treatments during the experiments (in R.U.-cells $^{-1}$ d $^{-1}$).

		K	CL	CM	CR
DEEP I	FIC1	$-5.22 \pm 0.02 \cdot 10^{-9}$	$-2.34 \pm 0.06 \cdot 10^{-9}$	$-1.16 \pm 0.03 \cdot 10^{-9}$	$-8.90 \pm 0.05 \cdot 10^{-9}$
	FIC2	$-4.48 \pm 3.02 \cdot 10^{-9}$	$-8.56 \pm 0.11 \cdot 10^{-10}$	$3.18 \pm 0.01 \cdot 10^{-9}$	$-7.42 \pm 0.02 \cdot 10^{-9}$
	FIC4	$-6.05 \pm 3.06 \cdot 10^{-9}$	$-2.59 \pm 0.02 \cdot 10^{-9}$	$-3.55 \pm 0.11 \cdot 10^{-9}$	$-1.00 \pm 0.05 \cdot 10^{-8}$
DEEP II	FIC1	$4.17 \pm 2.10 \cdot 10^{-9}$	$-1.48 \pm 0.01 \cdot 10^{-10}$	$4.88 \pm 1.01 \cdot 10^{-9}$	$4.17 \pm 1.03 \cdot 10^{-8}$
	FIC2	$7.39 \pm 3.06 \cdot 10^{-9}$	$1.44 \pm 0.04 \cdot 10^{-9}$	$1.37 \pm 0.02 \cdot 10^{-8}$	$4.94 \pm 2.05 \cdot 10^{-8}$
	FIC4	$-4.15 \pm 1.02 \cdot 10^{-9}$	$1.84 \pm 0.33 \cdot 10^{-9}$	$2.16 \pm 0.12 \cdot 10^{-11}$	$3.65 \pm 0.02 \cdot 10^{-8}$
DEEP III	FIC1	$2.01 \pm 0.11 \cdot 10^{-9}$	$-4.28 \pm 2.00 \cdot 10^{-9}$	$3.72 \pm 0.01 \cdot 10^{-9}$	$9.75 \pm 3.03 \cdot 10^{-9}$
	FIC2	$-1.13 \pm 0.00 \cdot 10^{-9}$	$4.60 \pm 0.001 \cdot 10^{-9}$	$3.44 \pm 0.02 \cdot 10^{-9}$	$1.32 \pm 0.02 \cdot 10^{-8}$
	FIC4	$-4.81 \pm 1.45 \cdot 10^{-9}$	$2.24 \pm 0.00 \cdot 10^{-10}$	$-2.80 \pm 0.06 \cdot 10^{-9}$	$1.48 \pm 0.07 \cdot 10^{-8}$

On the other hand, using data from Bermuda (BATS) and Hawaii (HOT) time series, Kaiser and Benner (2009) found that carbohydrates and amino acids were preferentially used during microbial decomposition of marine organic matter.

We suggest that, in our CM conditions, prokaryotes may have been using the available amino acids for growth. Thus, the drop in the fluorescence signal would correspond to the balance between production and assimilation microbial processes. In order to evaluate the relative importance of these two processes, we estimated the FIC3 signal produced by prokaryotes in the CM condition by applying an exponential model (Figure 7).

According to the model calculations, approximately 90% of the fluorescence detected at t_0 was due to the added amino acids in the CM treatment, while this percentage decreased down to about 2% of the total fluorescence detected at t_{10} or t_{15} (Figure 8), implying that bacteria used the amino acids added to supply their metabolic requirements until they reached the end of the exponential growth phase. This is in accordance with prior results obtained in degradation experiments (Nieto-Cid et al., 2006) where they observed a rapid consumption of recently produced dissolved protein-like material which was accumulated in the water column only when gross primary production exceeded a threshold value. Nevertheless, during the stationary phase, values of eFIC3 remained practically unaltered, suggesting that the prokaryotic community would have entered in a low-anabolic activity stage. In this regard, our results indicate that prokaryotic heterotrophic activity participates in both consumption and production of protein-like fluorescent substances, although production tends to surpass consumption during the exponential phase when labile/refractory substances are present.

CONCLUSIONS

Recently, Arrieta et al. (2015) found that deep sea prokaryotic growth was stimulated when organisms were exposed to increasing concentrations of autochthonous DOM. Our results demonstrated that the quality also influences prokaryotic activity.

In addition, we found that both the quality of organic matter added, and the initial biotic and abiotic conditions can modify the

microbial net production and consumption of FDOM. A clear FDOM net consumption was only observed in the experiment with Antarctic Bottom Water (AABW). To better understand the final fate of organic matter, further experiments should include analyses of organic matter at molecular levels (e.g., with spectrometry methods) and microbial gene diversity.

Based on our findings we conclude that, although mechanisms that hinder DOC total remineralization in deep waters are still poorly understood, the sequestration of OC in the deep ocean can significantly be reduced when labile substrates become available.

AUTHOR CONTRIBUTIONS

FA—Participated in the development of the experimental design, the sampling strategy, the acquisition of data, the treatment of data, and the writing procedure of the manuscript. MN—Participated in the acquisition of data, the interpretation of data, and the final approval of the manuscript version to be submitted. EB—Participated in the development of the experimental design, the sampling strategy, and the acquisition of data. ER—Participated in the sampling strategy, the acquisition of data, and the writing procedure of the manuscript. CS—Participated in the interpretation of data, and the final approval of the manuscript version to be submitted. MS—Participated in the final approval of the manuscript version to be submitted. JG—Participated in the interpretation of data and the final approval of the manuscript version to be submitted. AR—Participated in the interpretation of data and the final approval of the manuscript version to be submitted. CM—Participated in the development of the experimental design, the sampling strategy, the acquisition of data, the treatment of data, and the writing procedure of the manuscript.

ACKNOWLEDGMENTS

The authors would like to acknowledge the captain, crew, technicians of the R/V Hespérides and the team mates of the FICARAM cruise for their valuable help (C. R. Giner, V. Balagué, C. Cardelús, C. Antequera, and F. Alonso). The

experiments have been possible thanks to the funding of projects STORM (Structure of Organic Matter: Biogeochemical and Ecological Implications, CTM2009-09352) and DOREMI (Dissolved Organic Matter Remineralization in the Ocean: Microbial and Biogeochemical Constraints, CTM2012-342949) from the Spanish Ministerio de Economía y Competitividad.

REFERENCES

- Andrew, A. A., Del Vecchio, R., Subramaniam, A., and Blough, N. V. (2013). Chromophoric dissolved organic matter (CDOM) in the Equatorial Atlantic Ocean: optical properties and their relation to CDOM structure and source. *Mar. Chem.* 148, 33–43. doi: 10.1016/j.marchem.2012.11.001
- Ariese, F., Van Assema, S., Gooijer, C., Brucolieri, A. G., and Langford, C. H. (2004). Comparison of Laurentian Fulvic Acid luminescence with that of the hydroquinone/quinone model system: evidence from low temperature fluorescence studies and EPR spectroscopy. *Aquat. Sci.* 66, 86–94. doi: 10.1007/s00027-003-0647-8
- Arrieta, J. M., Mayol, E., Hansman, R. L., Herndl, G. J., Dittmar, T., and Duarte, C. M. (2015). Dilution limits dissolved organic carbon utilization in the deep ocean. *Science* 348, 331–333. doi: 10.1126/science.1258955
- Azam, F., and Hodson, R. E. (1981). Multiphasic kinetics for D-glucose uptake by assemblages of natural marine bacteria. *Mar. Ecol. Prog. Ser.* 6, 213–222. doi: 10.3354/meps006213
- Azúa, I., Goiriena, I., Baña, Z., Iribarri, J., and Unanue, M. (2014). Release and consumption of D-amino acids during growth of marine prokaryotes. *Microbiol. Ecol.* 67, 1–12. doi: 10.1007/s00248-013-0294-0
- Bianchi, T. S. (2012). Correction. The role of terrestrially derived organic carbon in the coastal ocean: a changing paradigm and the priming effect. *Proc. Natl. Acad. Sci. U.S.A.* 109, 5134–5134. doi: 10.1073/pnas.1202757109
- Bianchi, T. S., Thornton, D. C. O., Yvon-Lewis, S. A., King, G. M., Eglington, T. I., Shields, M. R., et al. (2015). Positive priming of terrestrially derived dissolved organic matter in a freshwater microcosm system. *Geophys. Res. Lett.* 42, 5460–5467. doi: 10.1002/2015GL064765
- Brussard, C. P. D. (2004). Viral control of phytoplankton - a review. *J. Eukaryot. Microbiol.* 51, 125–138. doi: 10.1111/j.1550-7408.2004.tb00537.x
- Brym, A., Paerl, H. W., Montgomery, M. T., Hansel, L. T., Ziervogel, K., and Osburn, C. L. (2014). Optical and chemical characterization of base-extracted particulate organic matter in coastal marine environments. *Mar. Chem.* 162, 96–113. doi: 10.1016/j.marchem.2014.03.006
- Carlson, C. A., Giovannoni, S. J., Hansell, D. A., Goldberg, S. J., Parsons, R., Otero, M. P., et al. (2002). The effect of nutrient amendments on bacterioplankton growth, DOC utilization, and community structure in the northwestern Sargasso Sea. *Aquat. Microb. Ecol.* 30, 19–36. doi: 10.3354/ame030019
- Catalá, T. S., Reche, I., Fuentes-Lema, A., Romera-Castillo, C., Nieto-Cid, M., Ortega-Retuerta, E., et al. (2015). Turnover time of fluorescent dissolved organic matter in the dark global ocean. *Nat. Commun.* 6, 1–8. doi: 10.1038/ncomms6986
- Catalán, N., Kellerman, A. M., Peter, H., Carmona, F., and Tranvik, L. J. (2015). Absence of a priming effect on dissolved organic carbon degradation in lake water. *Limnol. Oceanogr.* 60, 159–168. doi: 10.1002/lno.10016
- Cawley, K. M., Ding, Y., Fourqurean, J., and Jaffé, R. (2012). Characterising the sources and fate of dissolved organic matter in Shark Bay, Australia: a preliminary study using optical properties and stable carbon isotopes. *Mar. Freshw. Res.* 63, 1098–1107. doi: 10.1071/MF12028
- Coble, P. G. (1996). Characterization of marine and terrestrial DOM in seawater using excitation-emission matrix spectroscopy. *Mar. Chem.* 51, 325–346. doi: 10.1016/0304-4204(95)00062-3
- Coble, P. G. (2007). Marine optical biogeochemistry: the chemistry of ocean color. *Chem. Rev.* 107, 402–418. doi: 10.1021/cr050350+
- Coble, P. G., Green, S. A., Blough, N. V., and Gagosian, R. B. (1990). Characterization of dissolved organic matter in the Black Sea by fluorescence spectroscopy. *Nature* 348, 432–435. doi: 10.1038/348432a0
- FA, benefited of a JAE-pre pre-doctoral fellowship from the Consejo Superior de Investigaciones Científicas (CSIC). MN-C was funded by the CSIC Program “Junta para la Ampliación de Estudios” co-financed by the ESF. CS acknowledges funding from the Danish Research Council for Independent Research (DFF 1323-00336).
- Cory, R. M., and McKnight, D. M. (2005). Fluorescence spectroscopy reveals ubiquitous presence of oxidized and reduced quinones in dissolved organic matter. *Environ. Sci. Technol.* 39, 8142–8149. doi: 10.1021/es0506962
- De Haan, H. (1977). Effect of benzoate on microbial decomposition of fulvic acids in Tjeukemeer (the Netherlands). *Limnol. Oceanogr.* 22, 38–44. doi: 10.4319/lo.1977.22.1.00038
- De La Fuente, P., Marrasé, C., Canepa, A., and Álvarez-Salgado, X. A. (2014). Does a general relationship exist between fluorescent dissolved organic matter and microbial respiration? — The case of the dark equatorial Atlantic Ocean. *Deep Sea Res. Part I Oceanogr. Res. Pap.* 89, 44–55. doi: 10.1016/j.dsri.2014.03.007
- Delille, D. (2004). Abundance and function of bacteria in the Southern Ocean. *Cell. Mol. Biol.* 50, 543–551.
- Determann, S., Llobes, J. M., Reuter, R., and Rullkötter, J. (1998). Ultraviolet fluorescence excitation and emission spectroscopy of marine algae and bacteria. *Mar. Chem.* 62, 137–156. doi: 10.1016/S0304-4203(98)00026-7
- Dittmar, T. (2015). “Reasons behind the long-term stability of dissolved organic matter,” in *Biogeochemistry of Marine Dissolved Organic Matter*, eds D. A. Hansell and C. A. Carlson (San Diego, CA: Elsevier Inc.), 369–388. doi: 10.1016/B978-0-12-405940-5.00007-8
- Feller, G., Narinx, E., Arpigny, J. L., Aittaleb, M., Baise, E., Genicot, S., et al. (1996). Enzymes from psychrophilic organisms. *FEMS Microbiol. Rev.* 18, 189–202. doi: 10.1111/j.1574-6976.1996.tb00236.x
- Fontaine, S., Bardoux, G., Abbadie, L., and Mariotti, A. (2004). Carbon input to soil may decrease soil carbon content. *Ecol. Lett.* 7, 314–320. doi: 10.1111/j.1461-0248.2004.00579.x
- Fonse, E. S., Amado, A. M., Meirelles-Pereira, F., Esteves, F. A., Rosado, A. S., and Farjalla, V. F. (2013). The combination of different carbon sources enhances bacterial growth efficiency in aquatic ecosystems. *Microb. Ecol.* 66, 871–878. doi: 10.1007/s00248-013-0277-1
- Gasol, J. M., and Del Giorgio, P. A. (2000). Using flow cytometry for counting natural planktonic bacteria and understanding the structure of planktonic bacterial communities. *Sci. Mar.* 64, 197–224. doi: 10.3989/scimar.2000.64n2197
- Gontikaki, E., Thornton, B., Huvenne, V. A. I., and Witte, U. (2013). Negative priming effect on organic matter mineralisation in NE Atlantic slope sediments. *PLoS ONE* 8:e67722. doi: 10.1371/journal.pone.0067722
- Graeber, D., Gelbrecht, J., Pusch, M. T., Anlanger, C., and von Schiller, D. (2012). Agriculture has changed the amount and composition of dissolved organic matter in Central European headwater streams. *Sci. Total Environ.* 438, 435–446. doi: 10.1016/j.scitotenv.2012.08.087
- Guenet, B., Danger, M., Harrault, L., Allard, B., Jausset-Alcalá, M., Bardoux, G., et al. (2014). Fast mineralization of land-born C in inland waters: first experimental evidences of aquatic priming effect. *Hydrobiologia* 721, 35–44. doi: 10.1007/s10750-013-1635-1
- Guerrero-Feijóo, E., Nieto-Cid, M., Álvarez, M., and Álvarez-Salgado, X. A. (2014). Dissolved organic matter cycling in the confluence of the Atlantic and Indian oceans south of Africa. *Deep Sea Res. Part I Oceanogr. Res. Pap.* 83, 12–23. doi: 10.1016/j.dsri.2013.08.008
- Hansell, D. A., Carlson, C. A., Repeta, D. J., and Schlitzer, R. (2009). Dissolved organic matter in the ocean. A controversy stimulates new insights. *Oceanography* 22, 202–211. doi: 10.5670/oceanog.2009.109
- Hansen, H. P., and Grasshoff, K. (1983). “Automatic chemical analysis,” in *Methods of Seawater Analysis*, eds K. Grasshoff, M. Ehrhardt, and K. Kremling (Weinheim: Verlag Chemie), 368–376.
- Hertkorn, N., Benner, R., Frommberger, M., Schmitt-Kopplin, P., Witt, M., Kaiser, K., et al. (2006). Characterization of a major refractory component of marine dissolved organic matter. *Geochim. Cosmochim. Acta* 70, 2990–3010. doi: 10.1016/j.gca.2006.03.021

- Ho, T.-Y., Scranton, M. I., Taylor, G. T., Varela, R., Thunell, R. C., and Muller-Karger, F. (2002). Acetate cycling in the water column of the Cariaco Basin: seasonal and vertical variability and implication for carbon cycling. *Limnol. Oceanogr.* 47, 1119–1128. doi: 10.4319/lo.2002.47.4.1119
- Honjo, S., Eglington, T. I., Taylor, C. D., Ulmer, K. M., Sievert, S. M., Bracher, A., et al. (2014). Understanding the role of the biological pump in the global carbon cycle. An imperative for ocean science. *Oceanography* 27, 10–16. doi: 10.5670/oceanog.2014.78
- Hopkinson, C. S., Vallino, J. J., and Nolin, A. (2002). Decomposition of dissolved organic matter from the continental margin. *Deep. Res. II* 49, 4461–4478. doi: 10.1016/S0967-0645(02)00125-X
- Jiao, N., Herndl, G. J., Hansell, D. A., Benner, R., Kattner, G., Wilhelm, S. W., et al. (2010). Microbial production of recalcitrant dissolved organic matter: long-term carbon storage in the global ocean. *Nat. Rev. Microbiol.* 8, 593–599. doi: 10.1038/nrmicro2386
- Jørgensen, L., Lechtenfeld, O. J., Benner, R., Middelboe, M., and Stedmon, C. A. (2014a). Bacterial production and transformation of dissolved neutral sugars and amino acids in seawater. *Biogeosciences Discuss* 11, 6151–6184. doi: 10.5194/bgd-11-6151-2014
- Jørgensen, L., Stedmon, C. A., Granskog, M. A., and Middelboe, M. (2014b). Tracing the long-term microbial production of recalcitrant fluorescent dissolved organic matter in seawater. *Geophys. Res. Lett.* 41, 2481–2488. doi: 10.1002/2014GL059428
- Kaiser, K., and Benner, R. (2009). Biochemical composition and size distribution of organic matter at the Pacific and Atlantic time-series stations. *Mar. Chem.* 113, 63–77. doi: 10.1016/j.marchem.2008.12.004
- Kawasaki, N., and Benner, R. (2006). Bacterial release of dissolved organic matter during cell growth and decline: origin and composition. *Limnol. Oceanogr.* 51, 2170–2180. doi: 10.4319/lo.2006.51.5.2170
- Kim, S., Kramer, R. W., and Hatcher, P. G. (2003). Graphical method for analysis of ultrahigh-resolution broadband mass spectra of natural organic matter, the van Krevelen diagram. *Anal. Chem.* 75, 5336–5344. doi: 10.1021/ac034415p
- Koch, B. P., Witt, M., Engbrodt, R., Dittmar, T., and Kattner, G. (2005). Molecular formulae of marine and terrigenous dissolved organic matter detected by electrospray ionization Fourier transform ion cyclotron resonance mass spectrometry. *Geochim. Cosmochim. Acta* 69, 3299–3308. doi: 10.1016/j.gca.2005.02.027
- Koehler, B., von Wachenfeldt, E., Kothawala, D. N., and Tranvik, L. J. (2012). Reactivity continuum of dissolved organic carbon decomposition in lake water. *J. Geophys. Res. Biogeosciences* 117, 1–14. doi: 10.1029/2011JG001793
- Koprivnjak, J. F., Pfromm, P. H., Ingall, E., Vetter, T. A., Schmitt-Kopplin, P., Hertkorn, N., et al. (2009). Chemical and spectroscopic characterization of marine dissolved organic matter isolated using coupled reverse osmosis-electrodialysis. *Geochim. Cosmochim. Acta* 73, 4215–4231. doi: 10.1016/j.gca.2009.04.010
- Kothawala, D. N., Stedmon, C. A., Müller, R. A., Weyhenmeyer, G. A., Köhler, S. J., and Tranvik, L. J. (2014). Controls of dissolved organic matter quality: evidence from a large-scale boreal lake survey. *Glob. Chang. Biol.* 20, 1101–1114. doi: 10.1111/gcb.12488
- Kothawala, D. N., von Wachenfeldt, E., Koehler, B., and Tranvik, L. J. (2012). Selective loss and preservation of lake water dissolved organic matter fluorescence during long-term dark incubations. *Sci. Total Environ.* 433, 238–246. doi: 10.1016/j.scitotenv.2012.06.029
- Kowalcuk, P., Tilstone, G. H., Zablocka, M., Röttgers, R., and Thomas, R. (2013). Composition of dissolved organic matter along an Atlantic Meridional Transect from fluorescence spectroscopy and Parallel Factor Analysis. *Mar. Chem.* 157, 170–184. doi: 10.1016/j.marchem.2013.10.004
- Kuzyakov, Y. (2002). Separating microbial respiration of exudates from root respiration in non-sterile soils: a comparison of four methods. *Soil Biol. Biochem.* 34, 1621–1631. doi: 10.1016/S0038-0717(02)00146-3
- Lapiere, J.-F., and del Giorgio, P. A. (2014). Partial coupling and differential regulation of biologically and photo-chemically labile dissolved organic carbon across boreal aquatic networks. *Biogeosciences* 11, 5969–5985. doi: 10.5194/bg-11-5969-2014
- Lawaetz, A. J., and Stedmon, C. A. (2009). Fluorescence intensity calibration using the raman scatter peak of water fluorescence intensity calibration using the raman scatter peak of water. *Appl. Spectrosc.* 63, 936–940. doi: 10.1366/000370209788964548
- Leahy, J. G., and Colwell, R. R. (1990). Microbial degradation of hydrocarbons in the environment. *Microbiol. Rev.* 54, 305–315.
- Legendre, L., Rivkin, R. B., Weinbauer, M., Guidi, L., and Uitz, J. (2015). The microbial carbon pump concept: potential biogeochemical significance in the globally changing ocean. *Prog. Oceanogr. Press* 134, 432–450. doi: 10.1016/j.pocean.2015.01.008
- Löhnis, F. (1926). Nitrogen availability of green manures. *Soil Sci.* 22, 253–290. doi: 10.1097/00010694-192610000-00001
- Lønborg, C., and Alvarez-Salgado, X. A. (2014). Tracing dissolved organic matter cycling in the eastern boundary of the temperate North Atlantic using absorption and fluorescence spectroscopy. *Deep Sea Res. Part I Oceanogr. Res. Pap.* 85, 35–46. doi: 10.1016/j.dsr.2013.11.002
- Motegi, C., Nagata, T., Miki, T., Weinbauer, M. G., Legendre, L., and Rassoulzadegan, F. (2009). Viral control of bacterial growth efficiency in marine pelagic environments. *Limnol. Oceanogr.* 54, 1901–1910. doi: 10.4319/lo.2009.54.6.1901
- Murphy, K. R., Ruiz, G. M., Dunsmuir, W. T. M., and Waite, T. D. (2006). Optimized parameters for fluorescence-based verification of ballast water exchange by ships. *Environ. Sci. Technol.* 40, 2357–62. doi: 10.1021/es0519381
- Murphy, K. R., Stedmon, C. A., Graeber, D., and Bro, R. (2013). Fluorescence spectroscopy and multi-way techniques. *PARAFAC. Anal. Methods* 5, 6557–6566. doi: 10.1039/c3ay41160e
- Murphy, K. R., Stedmon, C. A., Waite, T. D., and Ruiz, G. M. (2008). Distinguishing between terrestrial and autochthonous organic matter sources in marine environments using fluorescence spectroscopy. *Mar. Chem.* 108, 40–58. doi: 10.1016/j.marchem.2007.10.003
- Murphy, K. R., Stedmon, C. A., Wenig, P., and Bro, R. (2014). OpenFluor—an online spectral library of auto-fluorescence by organic compounds in the environment. *Anal. Methods* 6, 658–661. doi: 10.1039/C3AY41935E
- Nagata, T., Fukuda, H., Fukuda, R., and Koike, I. (2000). Bacterioplankton distribution and production in deep Pacific waters: Large-scale geographic variations and possible coupling with sinking particle fluxes. *Limnol. Oceanogr.* 45, 426–435. doi: 10.4319/lo.2000.45.2.00426
- Nieto-Cid, M., Alvarez-Salgado, X. A., and Pérez, F. F. (2006). Microbial and photochemical reactivity of fluorescent dissolved organic matter in a coastal upwelling system. *Limnol. Oceanogr.* 51, 1391–1400. doi: 10.4319/lo.2006.51.3.1391
- Pomeroy, L. R., and Wiebe, W. J. (2001). Temperature and substrates as interactive limiting factors for marine heterotrophic bacteria. *Aquat. Microb. Ecol.* 23, 187–204. doi: 10.3354/ame023187
- Reader, H. E., Stedmon, C. A., Nielsen, N. J., and Kritzberg, E. S. (2015). Mass and UV-visible spectral fingerprints of dissolved organic matter: sources and reactivity. *Front. Mar. Sci.* 2, 1–10. doi: 10.3389/fmars.2015.00088
- Repeta, D. J. (2015). “Chemical characterization and cycling of dissolved organic matter,” in *Biogeochemistry of Marine Dissolved Organic Matter*, eds D. A. Hansell and C. A. Carlson (San Diego, CA: Elsevier Inc.), 21–63. doi: 10.1016/B978-0-12-405940-5.00002-9
- Rochelle-Newall, E. J., and Fisher, T. R. (2002). Production of chromophoric dissolved organic matter fluorescence in marine and estuarine environments: an investigation into the role of phytoplankton. *Mar. Chem.* 77, 7–21. doi: 10.1016/S0304-4203(01)00072-X
- Romera-Castillo, C., Sarmento, H., Alvarez-Salgado, X. A., Gasol, J. M., and Marrasé, C. (2011). Net production and consumption of fluorescent colored dissolved organic matter by natural bacterial assemblages growing on marine phytoplankton exudates. *Appl. Environ. Microbiol.* 77, 7490–7498. doi: 10.1128/AEM.00200-11
- Sala, M. M., and Güde, H. (2004). Ectoenzymatic activities and heterotrophic bacteria decomposing detritus. *Arch. Hydrobiol.* 160, 289–303. doi: 10.1127/0003-9136/2004/0160-0289
- Sarmento, H., Romera-Castillo, C., Lindh, M., Pinhassi, J., Sala, M. M., Gasol, J. M., et al. (2013). Phytoplankton species-specific release of dissolved free amino acids and their selective consumption by bacteria. *Limnol. Oceanogr.* 58, 1123–1135. doi: 10.4319/lo.2013.58.3.1123
- Schlitzer, R. (2015). *Ocean Data View*. Available online at: <http://odv.awi.de>
- Shimp, R. J., and Pfaender, F. K. (1985). Influence of easily degradable naturally occurring carbon substrates on biodegradation of monosubstituted phenols by aquatic bacteria. *Appl. Environ. Microbiol.* 49, 394–401.

- Søndergaard, M., Stedmon, C. A., and Borch, N. H. (2003). Fate of terrigenous dissolved organic matter (DOM) in estuaries: aggregation and bioavailability. *Ophelia* 57, 161–176. doi: 10.1080/00785236.2003.10409512
- Stedmon, C. A., and Markager, S. (2005a). Resolving the variability in dissolved organic matter fluorescence in a temperate estuary and its catchment using PARAFAC analysis. *Limnol. Oceanogr.* 50, 686–697. doi: 10.4319/lo.2005.50.2.0686
- Stedmon, C. A., and Markager, S. (2005b). Tracing the production and degradation of autochthonous fractions of dissolved organic matter using fluorescence analysis. *Limnol. Oceanogr.* 50, 1415–1426. doi: 10.4319/lo.2005.50.5.1415
- Stedmon, C. A., Thomas, D. N., Granskog, M. A., Kaartokallio, H., Papadimitriou, S., and Kuosa, H. (2007). Characteristics of dissolved organic matter in baltic Coastal Sea ice: allochthonous or autochthonous origins? *Environ. Sci. Technol.* 41, 7273–7279. doi: 10.1021/es071210f
- Stubbins, A., Lapierre, J. F., Berggren, M., Prairie, Y. T., Dittmar, T., and Del Giorgio, P. A. (2014). What's in an EEM? Molecular signatures associated with dissolved organic fluorescence in boreal Canada. *Environ. Sci. Technol.* 48, 10598–10606. doi: 10.1021/es502086e
- Vázquez-Domínguez, E., Vaqué, D., and Gasol, J. M. (2007). Ocean warming enhances respiration and carbon demand of coastal microbial plankton. *Glob. Chang. Biol.* 13, 1327–1334. doi: 10.1111/j.1365-2486.2007.01377.x
- Volk, T., and Hoffert, M. I. (1985). “Ocean Carbon pumps: analysis of relative strengths and efficiencies in ocean-driven atmospheric CO₂ changes,” in *The Carbon Cycle and Atmospheric CO₂: Natural Variations Archean to Present*, eds E. T. Sundquist and W. S. Broecker (Washington, DC: AGU Monograph 32; American Geophysical Union), 99–110.
- Walker, S. A., Amon, R. M. W., and Stedmon, C. A. (2013). Variations in high-latitude riverine fluorescent dissolved organic matter: a comparison of large Arctic rivers. *J. Geophys. Res. Biogeosciences* 118, 1689–1702. doi: 10.1002/2013JG002320
- Walker, S. A., Amon, R. M. W., Stedmon, C. A., Duan, S., and Loucheourn, P. (2009). The use of PARAFAC modeling to trace terrestrial dissolved organic matter and fingerprint water masses in coastal Canadian Arctic surface waters. *J. Geophys. Res.* 114, G00F06. doi: 10.1029/2009jg000990
- Weber, G. (1961). Enumeration of components in complex systems by fluorescence spectrophotometry. *Nature* 90, 27–29. doi: 10.1038/190027a0
- Yamashita, Y., Maie, N., Briceño, H., and Jaffé, R. (2010a). Optical characterization of dissolved organic matter in tropical rivers of the Guayana Shield, Venezuela. *J. Geophys. Res.* 115, 1–15. doi: 10.1029/2009jg000987
- Yamashita, Y., Panton, A., Mahaffey, C., and Jaffé, R. (2011). Assessing the spatial and temporal variability of dissolved organic matter in Liverpool Bay using excitation-emission matrix fluorescence and parallel factor analysis. *Ocean Dyn.* 61, 569–579. doi: 10.1007/s10236-010-0365-4
- Yamashita, Y., Scinto, L. J., Maie, N., and Jaffé, R. (2010b). Dissolved organic matter characteristics across a subtropical wetland's landscape: application of optical properties in the assessment of environmental dynamics. *Ecosystems* 13, 1006–1019. doi: 10.1007/s10021-010-9370-1
- Yamashita, Y., and Tanoue, E. (2003). Chemical characterization of protein-like fluorophores in DOM in relation to aromatic amino acids. *Mar. Chem.* 82, 255–271. doi: 10.1016/S0304-4203(03)00073-2
- Yamashita, Y., and Tanoue, E. (2008). Production of bio-refractory fluorescent dissolved organic matter in the ocean interior. *Nat. Geosci.* 1, 579–582. doi: 10.1038/ngeo279

Conflict of Interest Statement: The authors declare that the research was conducted in the absence of any commercial or financial relationships that could be construed as a potential conflict of interest.

Copyright © 2015 Aparicio, Nieto-Cid, Borrull, Romero, Stedmon, Sala, Gasol, Ríos and Marrasé. This is an open-access article distributed under the terms of the Creative Commons Attribution License (CC BY). The use, distribution or reproduction in other forums is permitted, provided the original author(s) or licensor are credited and that the original publication in this journal is cited, in accordance with accepted academic practice. No use, distribution or reproduction is permitted which does not comply with these terms.

Advantages of publishing in Frontiers



OPEN ACCESS

Articles are free to read,
for greatest visibility



COLLABORATIVE PEER-REVIEW

Designed to be rigorous
– yet also collaborative,
fair and constructive



FAST PUBLICATION

Average 85 days from
submission to publication
(across all journals)



COPYRIGHT TO AUTHORS

No limit to article
distribution and re-use



TRANSPARENT

Editors and reviewers
acknowledged by name
on published articles



SUPPORT

By our Swiss-based
editorial team



IMPACT METRICS

Advanced metrics
track your article's impact



GLOBAL SPREAD

5'100'000+ monthly
article views
and downloads



LOOP RESEARCH NETWORK

Our network
increases readership
for your article

Frontiers

EPFL Innovation Park, Building I • 1015 Lausanne • Switzerland
Tel +41 21 510 17 00 • Fax +41 21 510 17 01 • info@frontiersin.org
www.frontiersin.org

Find us on

